PROCEEDINGS OF THE EIGHTEENTH WORKSHOP ON GENERAL RELATIVITY AND GRAVITATION IN JAPAN

FACULTY CLUB, HIROSHIMA UNIVERSITY,
HIGASHI-HIROSHIMA, JAPAN
NOVEMBER 17-21, 2008

Edited by
Yasufumi Kojima, Kazuhiro Yamamoto, Ryo Yamazaki, Misao Sasaki

Preface

The eighteenth workshop on General Relativity and Gravitation (the 18th JGRG meeting) was held at the faculty club in the campus of Hiroshima University from 17 to 21 November 2008.

There has been impressive progress in astrophysical/cosmological observations in recent years. Cosmology has entered an era of precision science. Astrophysical black holes have been observed in many frequency bands with better resolutions and sensitivities. Observations of gamma-ray bursts have added a new mystery to relativistic astrophysics. And, a new frontier is waiting to be explored by gravitational wave interferometers. On the theoretical side, motivated by unified theories of fundamental interactions, especially string theory, many efforts have been made for studies of physics in 5-dimensional or higher dimensional spacetimes, and there is a growing interest in experimental verifications of extra dimensions. There have been also important and interesting developments in various other areas, including alternative theories of gravity, quantum gravity, and spacetime singularities, to mention a few.

This year, we invited eight speakers from various countries, who gave us clear overviews of recent developments and future perspectives. We witnessed active discussions among the participants during the meeting. We would like to thank all the participants for their earnest participation. This workshop was supported in part by JSPS Grant-in-Aid for Scientific Research (B) No. 17340075, JSPS Grant-in-Aid for Creative Scientific Research No. 19GS0219, and Satake memorial foundation.

Yasufumi Kojima, Kazuhiro Yamamoto, Ryo Yamazaki, Misao Sasaki March 2009

Organizing Committee

Hideki Asada (Hirosaki Univ.), Takeshi Chiba (Nihon Univ.), Akio Hosoya (Tokyo Inst. Univ.), Kunihito Ioka (KEK), Hideki Ishihara (Osaka City Univ.), Hideo Kodama (KEK), Yasufumi Kojima (Hiroshima Univ.), Kei-ichi Maeda (Waseda Univ.), Shinji Mukohyama (IPMU), Takashi Nakamura (Kyoto Univ.), Ken'ichi Nakao (Osaka City Univ.), Yasusada Nambu (Nagoya Univ.), Ken-ichi Oohara (Niigata Univ.), Misao Sasaki (YITP), Masaru Shibata (Univ. of Tokyo), Tetsuya Shiromizu (Kyoto Univ.), Jiro Soda (Kyoto Univ.), Naoshi Sugiyama (Nagoya Univ.), Takahiro Tanaka (YITP), Jun'ichi Yokoyama (Univ. of Tokyo)

TABLE OF CONTENTS[1]

Invited talks

*Markus Ackermann (SLAC, USA)
"First results and future prospects of the Fermi Large Area Telescope"

Roverto Emparan (Barcelona Spain)
"New phases of black holes in higher dimensions"

*Yasushi Fukazawa (Hiroshima Univ.)
"Current status of Fermi Gamma-ray Space Telescope"

*Kazunori Kohri (Lancaster, UK)
"Long-lived particles and cosmology in supergravity"

Kazuya Koyama (Portsmouth, UK)
"Modified gravity as an alternative to dark energy"

*Luciano Rezzolla (AEI, Germany)
"Modeling black holes and neutron stars as sources of gravitational waves"

*Gary Shiu (Wisconsin-Madison, USA)
"String Inflation: an Update"

*Koji Yoshimura (KEK, Japan)
"Cosmic-ray antiparticles as a probe of early universe"

Oral Presentation

Hideki Asada (Hirosaki University)
"Perturbation theory of N point-mass gravitational lens"

*Luca Baiotti (University of Tokyo)
"Inspiralling neutron-star binaries"

Antonino Flachi (YITP, Kyoto University)
"Signatures of spinning evaporating micro black holes"

Jakob Hansen (Waseda University)
"Numerical performance of the parabolized ADM (PADM) formulation in general relativity"

Tomohiro Harada (Rikkyo University)
"Gravitational collapse of a dust ball from the perspective of loop quantum gravity: an application"

Kenta Hioki (Waseda University)
"Measuring the spin parameter of Kerr black holes and naked singularities"

Takashi Hiramatsu (ICRR, University of Tokyo)
"Non-linear evolution of density power spectrum in a closure theory"

*Peter Hogan (Tohoku University)
"On The Motion of a Small Charged Black Hole in General Relativity"

Takamitsu Horiguchi (Nagoya University)
"Particle acceleration in force-free magnetospheres around rotating black holes – the outer gap models –"

[1]The asterisk (*) denotes not being contained in this proceedings

*Takahisa Igata (Osaka City University)
"Killing Tensors and Constants of Motion of a Charged Particle"

Akihiro Ishibashi (KEK)
"Extremal Black Holes in Higher Dimensions and Symmetries"

Keisuke Izumi (Kyoto University)
"Massive spin-2 ghost in de Sitter spacetime"

Kohei Kamada (RESCEU, The University of Tokyo)
"Can dissipative effects help the MSSM inflation?"

*Masumi Kasai (Hirosaki University)
"Inhomogeneous Interpretation on The Supernova Legacy Survey Data"

*Kazumi Kashiyama (Kyoto University)
"Analytic approach to the Hawking Page transition"

Masashi Kimura (Osaka City University)
"Anisotropic inflation from vector impurity"

Shunichiro Kinoshita (The University of Tokyo)
"Thermodynamic and dynamical stability of Freund-Rubin compactification"

Kenta Kiuchi (Waseda University)
"Long term simulation of binary neutron star merger"

Taichi Kobayashi (Nagoya University)
"Super-radiance of electromagnetic radiation from disk surface around Kerr black hole"

Takeshi Kobayashi (The University of Tokyo)
"Conformal Inflation, Modulated Reheating, and WMAP5"

Tsutomu Kobayashi (Waseda University)
"Relativistic stars in $f(R)$ gravity, and absence thereof"

Hideo Kodama (IPNS, KEK)
"Repulsons in the 5D Myers-Perry family"

*Tatsuhiko Koike (Keio University)
"Systematic construction of classical string solutions"

*Roman Konoplya (Kyoto University)
"Particles motion near the magnetized black hole surrounded by a toroidal distribution of matter"

*Amitabha Lahiri (S.N.Bose National Centre for Basic Sciences)
"Black hole no-hair theorems for positive Lambda"

Wonwoo Lee (CQUeST, Sogang University)
"The vacuum bubble and black hole pair creation"

Shuntaro Mizuno (RESCEU)
"Non-gaussianity from the bispectrum in general multiple field inflation"

Keiju Murata (Kyoto University)
"Phase Transitions of Charged Kerr-AdS Black Holes from Gauge Theories"

Masahiro Nakashima (RESCEU)
"WMAP-5yr Constraint on the Varying Fine Structure Constant"

Kazunori Nakayama (ICRR, University of Tokyo)
"Non-Gaussianity from Isocurvature Perturbations"

Atsushi Naruko (Kyoto University)
"Large non-Gaussianity from multi-brid inflation"

Ishwaree Neupane (University of Canterbury)
"Viscosity and Entropy Bounds from Black Hole Physics"

*Masashi Oasa (Waseda University)
"Post-Newtonian parameters and constraints on TeVeS theory"

Hiromi Saida (Daido Inst. of Tech.)
"Does the Entropy-Area law hold for Schwarzschild-de Sitter spacetime ? "

Motoyuki Saijo (Rikkyo University)
"Faraday Resonance in Dynamically Bar Unstable Stars"

Ryo Saito (RESCEU)
"Gravitational-Wave Constraints on Abundance of Primordial Black Holes"

Masakazu Sano (Hokkaido University)
"Moduli fixing in Brane gas cosmology"

Masaki Satoh (Kyoto University)
"Higher Curvature Corrections to Primordial Fluctuations in Slow-roll Inflation"

Shintaro Sawayama (Sawayama Cram School of Physics)
"Entanglement of universe"

Fabio Scardigli (National Taiwan University)
"Invariances of generalized uncertainty principles"

Yuichiro Sekiguchi (National Astronomical Observatory of Japan)
"Towards clarifying the central engine of long gamma-ray bursts"

*Naoki Seto (NAOJ)
"Science with space gravitational wave detectors"

Masahiro Shimano (Rikkyo University)
"The scalar field potential of the super-inflation in Loop Quantum Cosmology"

*Ryotaku Suzuki (Kyoto University)
"Phase transition on AdS Kerr-Newman Black holes"

Tomo Takahashi (Saga University)
"Non-Gaussianity in the Curvaton Scenario"

Yuichi Takamizu (Waseda University)
"Nonlinear superhorizon perturbations of non-canonical scalar"

*Yosuke Takamori (Osaka City University)
"Can the Blandford-Znajek monopole solution extend beyond the inner light surface?"

Takashi Tamaki (Waseda University)
"Gravitating Q-balls and their stabilities"

Makoto Tanabe (Waseda University)
"Non-BPS Rotating Black Hole and Black String by Intersecting M-branes"

Norihiro Tanahashi (Kyoto University)
"Initial data of black hole localized on Karch-Randall brane"

Tomo Tanaka (Waseda University)
"Black hole entropy for the general area spectrum"

*Yuji Torigoe (Hirosaki University)
"Gravitational radiation by celestial bodies in various orbits"

Motomu Tsuda (Saitama Institute of Technology)
"Nonlinear supersymmetric general relativity and origin of mass"

Yuko Urakawa (Waseda University)
"Solution to IR divergence problem of interacting inflaton field"

Kunihito Uzawa (Osaka City University)
"Classification of dynamical intersecting brane solutions"

Babak Vakili (IAU, Iran)
"Deformed phase space and canonical quantum cosmology"

Kent Yagi (Kyoto University)
"Stringent Constraints on Brans-Dicke Parameter using 0.1Hz Gravitational Wave Interferometers"

Daisuke Yamauchi (YITP, Kyoto University)
"Open inflation in string landscape"

*Shuichiro Yokoyama (Nagoya University)
"Primordial Trispectrum in Multi-Scalar Inflation"

Chul-Moon Yoo (Asia Pacific Center for Theoretical Physics)
"Solving the Inverse Problem with Inhomogeneous Universes
—Toward a test of the Copernican principle—"

Olexandr Zhydenko (Universidade de Sao Paulo)
"Black string perturbations and the Gregory-Laflamme instability"

Poster Presentation

*Masaru Adachi (Hirosaki University)
"Inhomogeneous interpretation on the m-z relation of the type Ia supernovae"

Fumitoshi Amemiya (Keio University)
"Deparametrised quantum cosmology with Phantom dust"

Hideyoshi Arakida (Waseda University)
"Influence of Dark Matter on Light Propagation in Solar System Experiment"

*Frederico Arroja (University of Portsmouth)
"Second order gravitational waves"

Ryuichi Fujita (Raman Research Institute)
"Bound geodesics in Kerr space time"

Teruki Hanada (Yamaguchi University)
"Cosmology of multigravity"

Kazuhiro Iwata (Nagoya University)
"The distance-redshift relation for the inhomogeneous and anisotropic universe"

Nahomi Kan (Yamaguchi Junior College)
"Cancellation of long-range forces in Einstein-Maxwell-dilaton system"

Shota Kisaka (Hiroshima University)
"The correlation of black hole mass with metallicity index of host spheroid"

Hiroshi Kozaki (Ishikawa National College of Technology)
"Integrability of strings with a symmetry in the Minkowski spacetime"

Satoshi Maeda (Tokyo Institute of Technology)
"Primordial magnetic fields from second-order cosmological perturbations: Tight coupling approximation"

Takuya Maki (Japan Woman's College of Physical Education)
"Dilatonic Universe in Arbitrary Dimensions"

Masato Minamitsuji (CQUeST, Sogang University)
"Thick de Sitter brane solutions in higher dimensions"

Yoshiyuki Morisawa (Osaka University of Economics and Law)
"Informational interpretation on volume operator and physical bound on information"

Kouji Nakamura (the Grad. Univ. for Adv. Studies, NAOJ)
"Second-order gauge-invariant cosmological perturbation theory 3 : — Consistency of equations —"

Hiroyuki Nakano (Rochester Institute of Technology)
"Comparison of Post-Newtonian and Numerical Evolutions of Black-Hole Binaries"

Hidenori Nomura (Hiroshima University)
"Damping of the baryon acoustic oscillations in the matter power spectrum as a probe of the growth factor"

Masato Nozawa (Waseda University)
"Quasinormal modes of black holes localized on the Randall-Sundrum 2-branes"

Yuji Ohsumi (Nagoya University)
"Classicality of the stochastic approach to inflation"

Takahiro Sato (Hiroshima University)
"Testing general relativity on the scales of cosmology using the redshift-space distortion"

Yuuiti Sendouda (YITP, Kyoto University)
"Higher curvature theories of gravity in the ADM canonical formalism"

Hisa-aki Shinkai (Osaka Institute of Technology)
"Towards the dynamics in Einstein-Gauss-Bonnet gravity: Initial Value Problem"

*Takeshi Suehiro (Keio University)
"Gravitational radiation from a stationary cosmic string"

*Hideyuki Tagoshi (Osaka University)
"Detecting gravitational waves from inspiraling binaries with a network of geographically separated detectors"

Takashi Tamaki (Waseda University)
"Revisiting chameleon gravity–thin-shells and no-shells with appropriate boundary conditions"

Shinya Tomizawa (KEK)
"Kaluza-Klein-Kerr-Gödel Black Holes"

Takashi Torii (Osaka Institute of Technology)
"Dilatonic Black Holes in Gauss-Bonnet Gravity in Various Dimensions"

Yuta Yamada (Osaka Institute of Technology)
"Apparent horizon formation in higher dimensional spacetime"

New phases of black holes in higher dimensions

Roberto Emparan[1]

Institució Catalana de Recerca i Estudis Avançats (ICREA), and
Departament de Física Fonamental, Universitat de Barcelona
Marti i Franquès 1, E-08028 Barcelona, Spain

Abstract

I review recent progress in understanding black hole solutions of higher-dimensional vacuum gravity.

1 Introduction

Classical General Relativity in more than four spacetime dimensions has been the subject of increasing attention in recent years. Reasons for this interest include its application to string/M-theory, the AdS/CFT correspondence (and its recent derivatives: AdS/QGP, AdS/cond-mat etc), the possible production of higher-dimensional black holes in future colliders, and the mathematics of Lorentzian Ricci-flat manifolds.

But higher-dimensional gravity is also of intrinsic interest. Just like we study quantum field theories with a field content different than what might be directly relevant to Nature (e.g., $SU(N)$ gauge theories with large N), we may gain insight into the General Theory of Relativity, and its most fundamental solutions: black holes, by studying it at different values of some adjustable parameter. The equations of General Relativity in vacuum, $R_{\mu\nu} = 0$, appear to possess only one such tunable parameter: the number of spacetime dimensions D. Thus, we would like to know which properties of black holes are peculiar to four-dimensions, and which hold more generally. At the very least, this study will lead to a deeper understanding of classical black holes and of what spacetime can do at its most extreme.

This contribution to the proceedings of the JGRG18 workshop consists mostly of excerpts from an extensive review on the subject written in collaboration with Harvey Reall [1], to which interested readers are directed for a more complete coverage.

2 Frequently asked questions

I will begin by trying to give simple answers to two frequently asked questions: 1) why should one expect any interesting new dynamics in higher-dimensional General Relativity, and 2) what are the main obstacles to a direct generalization of the four-dimensional techniques and results. A straightforward answer to both questions is to simply say that as the number of dimensions grows, the number of degrees of freedom of the gravitational field also increases, but more specific yet intuitive answers are possible.

2.1 Why gravity is richer in $d > 4$

The novel features of higher-dimensional black holes that have been identified so far can be understood in physical terms as due to the combination of two main ingredients: different rotation dynamics, and the appearance of extended black objects.

There are two aspects of rotation that change significantly when spacetime has more than four dimensions. First, there is the possibility of rotation in several independent rotation planes [2]. The rotation group $SO(d-1)$ has Cartan subgroup $U(1)^N$, with

$$N \equiv \left\lfloor \frac{d-1}{2} \right\rfloor , \tag{1}$$

[1]E-mail: emparan@ub.edu

hence there is the possibility of N independent angular momenta. In simpler and more explicit terms, group the $d-1$ spatial dimensions (say, at asymptotically flat infinity) in pairs (x_1, x_2), (x_3, x_4),..., each pair defining a plane, and choose polar coordinates in each plane, (r_1, ϕ_1), (r_2, ϕ_2),.... Here we see the possibility of having N independent (commuting) rotations associated to the vectors ∂_{ϕ_1}, ∂_{ϕ_2} .... To each of these rotations we associate an angular momentum component J_i.

The other aspect of rotation that changes qualitatively as the number of dimensions increases is the relative competition between the gravitational and centrifugal potentials. The radial fall-off of the Newtonian potential

$$-\frac{GM}{r^{d-3}} \tag{2}$$

depends on the number of dimensions, whereas the centrifugal barrier

$$\frac{J^2}{M^2 r^2} \tag{3}$$

does not, since rotation is confined to a plane. We see that the competition between (2) and (3) is different in $d = 4$, $d = 5$, and $d \geq 6$. In Newtonian physics this is well-known to result in a different stability of Keplerian orbits, but this precise effect is not directly relevant to the black hole dynamics we are interested in. Still, the same kind of dimension-dependence will have rather dramatic consequences for the behavior of black holes.

The other novel ingredient that appears in $d > 4$ but is absent in lower dimensions (at least in vacuum gravity) is the presence of black objects with extended horizons, i.e., black strings and in general black p-branes. Although these are not asymptotically flat solutions, they provide the basic intuition for understanding novel kinds of asymptotically flat black holes.

Let us begin from the simple observation that, given a black hole solution of the vacuum Einstein equations in d dimensions, with horizon geometry Σ_H, then we can immediately construct a vacuum solution in $d+1$ dimensions by simply adding a flat spatial direction[2]. The new horizon geometry is then a *black string* with horizon $\Sigma_H \times \mathbf{R}$. Since the Schwarzschild solution is easily generalized to any $d \geq 4$, it follows that black strings exist in any $d \geq 5$. In general, adding p flat directions we find that black p-branes with horizon $S^q \times \mathbf{R}^p$ (with $q \geq 2$) exist in any $d \geq 6 + p - q$.

How are these related to new kinds of asymptotically flat black holes? Heuristically, take a piece of black string, with $S^q \times \mathbf{R}$ horizon, and curve it to form a *black ring* with horizon topology $S^q \times S^1$. Since the black string has a tension, then the S^1, being contractible, will tend to collapse. But we may try to set the ring into rotation and in this way provide a centrifugal repulsion that balances the tension. This turns out to be possible in any $d \geq 5$, so we expect that non-spherical horizon topologies are a generic feature of higher-dimensional General Relativity.

It is also natural to try to apply this heuristic construction to black p-branes with $p > 1$, namely, to bend the worldvolume spatial directions into a compact manifold, and balance the tension by introducing suitable rotations. The possibilities are still under investigation, but it is clear that an increasing variety of black holes should be expected as d grows. Observe again that the underlying reason is a combination of extended horizons with rotation.

Horizon topologies other than spherical are forbidden in $d = 4$ by well-known theorems [3]. These are rigorous, but also rather technical and formal results. Can we find a simple, intuitive explanation for the *absence* of vacuum black rings in $d = 4$? The previous argument would trace this fact back to the absence of asymptotically flat vacuum black holes in $d = 3$. This is often attributed to the absence of propagating degrees of freedom for the three-dimensional graviton (or one of its paraphrases: $2+1$-gravity is topological, the Weyl tensor vanishes identically, etc), but here we shall use the simple observation that the quantity GM is dimensionless in $d = 3$. Hence, given any amount of mass, there is no length scale to tell us where the black hole horizon could be[3]. So we would attribute the absence of black strings in $d = 4$ to the lack of such a scale. This observation goes some way towards understanding the absence of vacuum black rings with horizon topology $S^1 \times S^1$ in four dimensions: it implies that there cannot

[2]This is no longer true if the field equations involve not only the Ricci tensor but also the Weyl tensor, such as in Lovelock theories.

[3]It follows that the introduction of a length scale, for instance in the form of a (negative) cosmological constant, is a necessary condition for the existence of a black hole in $2 + 1$ dimensions. But gravity may still remain topological.

exist black ring solutions with different scales for each of the two circles, and in particular one could not make one radius arbitrarily larger than the other. This argument, though, could still allow for black rings where the radii of the two S^1 are set by the same scale, i.e., the black rings should be plump. The horizon topology theorems then tell us that plump black rings do not exist: they would actually be within a spherical horizon.

Extended horizons also introduce a feature absent in $d = 4$: dynamical horizon instabilities [4]. Again, this is to some extent an issue of scales. Black brane horizons can be much larger in some of their directions than in others, and so perturbations with wavelength of the order of the 'short' horizon length can fit several times along the 'long' extended directions. Since the horizon area tends to increase by dividing up the extended horizon into black holes of roughly the same size in all its dimensions, this provides grounds to expect an instability of the extended horizon (however, when other scales are present, as in charged solutions, the situation can become quite more complicated). It turns out that higher-dimensional rotation can make the horizon much more extended in some directions than in others, which is expected to trigger this kind of instability [5]. At the threshold of the instability, a zero-mode deformation of the horizon has been conjectured to lead to new 'pinched' black holes that do not have four-dimensional counterparts.

Finally, an important question raised in higher dimensions refers to the rigidity of the horizon. In four dimensions, stationarity implies the existence of a $U(1)$ rotational isometry [3]. In higher dimensions stationarity has been proven to imply one rigid rotation symmetry too [6], but not (yet?) more than one. However, all *known* higher-dimensional black holes have multiple rotational symmetries. Are there stationary black holes with less symmetry, for example just the single $U(1)$ isometry guaranteed in general? Or are black holes always as rigid as can be? This is, in our opinion, the main unsolved problem on the way to a complete classification of five-dimensional black holes, and an important issue in understanding the possibilities for black holes in higher dimensions.

2.2 Why gravity is more difficult in $d > 4$

Again, the simple answer to this question is the larger number of degrees of freedom. However, this can not be an entirely satisfactory reply, since one often restricts to solutions with a large degree of symmetry for which the number of actual degrees of freedom may not depend on the dimensionality of spacetime. A more satisfying answer should explain why the methods that are so successful in $d = 4$ become harder, less useful, or even inapplicable, in higher dimensions.

Still, the larger number of metric components and of equations determining them is the main reason for the failure so far to find a useful extension of the Newman-Penrose (NP) formalism to $d > 4$. This formalism, in which all the Einstein equations and Bianchi identities are written out explicitly, was instrumental in deriving the Kerr solution and analyzing its perturbations. The formalism is tailored to deal with algebraically special solutions, but even if algebraic classifications have been developed for higher dimensions [7], and applied to known black hole solutions, no practical extension of the NP formalism has appeared yet that can be used to derive the solutions nor to study their perturbations.

Then, it seems natural to restrict to solutions with a high degree of symmetry. Spherical symmetry yields easily by force of Birkhoff's theorem. The next simplest possibility is to impose stationarity and axial symmetry. In four dimensions this implies the existence of two commuting abelian isometries– time translation and axial rotation–, which is extremely powerful: by integrating out the two isometries from the theory we obtain an integrable two-dimensional $GL(2, \mathbf{R})$ sigma-model. The literature on these theories is enormous and many solution-generating techniques are available, which provide a variety of derivations of the Kerr solution.

There are two natural ways of extending axial symmetry to higher dimensions. We may look for solutions invariant under the group $O(d-2)$ of spatial rotations around a given line axis, where the orbits of $O(d-2)$ are $(d-3)$-spheres. However, in more than four dimensions these orbits have non-zero curvature. As a consequence, after dimensional reduction on these orbits, the sigma-model acquires terms (of exponential type) that prevent a straightforward integration of the equations (see [8, 9] for an investigation of these equations).

This suggests looking for a different higher-dimensional extension of the four-dimensional axial symmetry. Instead of rotations around a line, consider rotations around (spatial) codimension-2 hypersurfaces.

These are $U(1)$ symmetries. If we assume $d-3$ commuting $U(1)$ symmetries, so that we have a spatial $U(1)^{d-3}$ symmetry in addition to the timelike symmetry $\mathbf{R}$, then the vacuum Einstein equations again reduce to an integrable two-dimensional $GL(d-2,\mathbf{R})$ sigma-model with powerful solution-generating techniques.

However, there is an important limitation: only in $d=4,5$ can these geometries be globally asymptotically flat. Global asymptotic flatness implies an asymptotic factor S^{d-2} in the spatial geometry, whose isometry group $O(d-1)$ has a Cartan subgroup $U(1)^N$. If, as above, we demand $d-3$ axial isometries, then, asymptotically, these symmetries must approach elements of $O(d-1)$, so we need $U(1)^{d-3} \subset U(1)^N$, i.e.,

$$d-3 \leq N = \left\lfloor \frac{d-1}{2} \right\rfloor , \tag{4}$$

which is only possible in $d=4,5$. This is the main reason for the recent great progress in the construction of exact five-dimensional black holes, and the failure to extend it to $d>5$.

Finally, the classification of possible horizon topologies becomes increasingly complicated in higher dimensions [10]. In four spacetime dimensions the (spatial section of the) horizon is a two-dimensional surface, so the possible topologies can be easily characterized and restricted. Much less restriction is possible as d is increased.

3 The Schwarzschild-Tangherlini solution and black p-branes

The linearized approximation to the field of a static pointlike source in higher-dimensions is easily found to be

$$ds^2_{(lin)} = -\left(1-\frac{\mu}{r^{d-3}}\right)dt^2 + \left(1+\frac{\mu}{r^{d-3}}\right)dr^2 + r^2 d\Omega^2_{d-2}, \tag{5}$$

where, to lighten the notation, we have introduced the 'mass parameter'

$$\mu = \frac{16\pi GM}{(d-2)\Omega_{d-2}}. \tag{6}$$

This suggests that the Schwarzschild solution generalizes to higher dimensions in the form

$$ds^2 = -\left(1-\frac{\mu}{r^{d-3}}\right)dt^2 + \frac{dr^2}{1-\frac{\mu}{r^{d-3}}} + r^2 d\Omega^2_{d-2}\,. \tag{7}$$

In essence, all we have done is change the radial fall-off $1/r$ of the Newtonian potential to the d-dimensional one, $1/r^{d-3}$. As Tangherlini found in 1963 [11], this turns out to give the correct solution: it is straightforward to check that this metric is indeed Ricci-flat. It is apparent that there is an event horizon at $r_0 = \mu^{1/(d-3)}$.

Having this elementary class of black hole solutions, it is easy to construct other vacuum solutions with event horizons in $d \geq 5$. The direct product of two Ricci-flat manifolds is itself a Ricci-flat manifold. So, given any vacuum black hole solution $\mathcal{B}$ of the Einstein equations in d dimensions, the metric

$$ds^2_{d+p} = ds^2_d(\mathcal{B}) + \sum_{i=1}^{p} dx^i dx^i \tag{8}$$

describes a black p-brane, in which the black hole horizon $\mathcal{H} \subset \mathcal{B}$ is extended to a horizon $\mathcal{H} \times \mathbf{R}^p$, or $\mathcal{H} \times \mathbf{T}^p$ if we identify periodically $x^i \sim x^i + L_i$. A simple way of obtaining another kind of vacuum solutions is the following: unwrap one of the directions x^i; perform a boost $t \to \cosh\alpha t + \sinh\alpha x^i$, $x^i \to \sinh\alpha t + \cosh\alpha x^i$, and re-identify points periodically along the new coordinate x^i. Although locally equivalent to the static black brane, the new boosted black brane solution is globally different from it.

4 Myers-Perry solutions

The generalization of the Schwarzschild solution to $d>4$ is, as we have seen, a rather straightforward problem. However, in General Relativity it is often very difficult to extend a solution from the static

case to the stationary one (as exemplified by the Kerr solution). Impressively, in 1986 Myers and Perry (MP) managed to find exact solutions for black holes in any dimension $d > 4$, rotating in all possible independent rotation planes [2]. The feat was possible since the solutions belong in the Kerr-Schild class

$$g_{\mu\nu} = \eta_{\mu\nu} + 2H(x^\rho)k_\mu k_\nu \tag{9}$$

where k_μ is a null vector with respect to both $g_{\mu\nu}$ and the Minkowski metric $\eta_{\mu\nu}$. This entails a sort of linearization of the problem, which facilitates greatly the resolution of the equations. Of all known vacuum black holes in $d > 4$, only the Myers-Perry solutions seem to have this property.

In this section I review these solutions and their properties, focusing on black holes with a single rotation. The existence of ultra-spinning regimes in $d \geq 6$ is emphasized.

4.1 Rotation in a single plane

Black holes that rotate in a single plane are not only simpler, but they also exhibit more clearly the qualitatively new physics afforded by the additional dimensions.

The metric takes the form

$$\begin{aligned} ds^2 &= -dt^2 + \frac{\mu}{r^{d-5}\Sigma}\left(dt - a\sin^2\theta\, d\phi\right)^2 + \frac{\Sigma}{\Delta}dr^2 + \Sigma d\theta^2 + (r^2+a^2)\sin^2\theta\, d\phi^2 \\ &\quad + r^2\cos^2\theta\, d\Omega^2_{(d-4)}\,, \end{aligned} \tag{10}$$

where

$$\Sigma = r^2 + a^2\cos^2\theta\,, \qquad \Delta = r^2 + a^2 - \frac{\mu}{r^{d-5}}\,. \tag{11}$$

The physical mass and angular momentum are easily obtained and are given in terms of the parameters μ and a by

$$M = \frac{(d-2)\Omega_{d-2}}{16\pi G}\mu\,, \qquad J = \frac{2}{d-2}Ma\,. \tag{12}$$

Hence one can think of a as essentially the angular momentum per unit mass. We can choose $a \geq 0$ without loss of generality.[4]

As in Tangherlini's solution, this metric seems to follow from a rather straightforward extension of the Kerr solution, which is recovered when $d = 4$. The first line in eq. (10) looks indeed like the Kerr solution, with the $1/r$ fall-off replaced, in appropriate places, by $1/r^{d-3}$. The second line contains the line element on a $(d-4)$-sphere which accounts for the additional spatial dimensions. It might therefore seem that, again, the properties of these black holes should not differ much from their four-dimensional counterparts.

However, this is not the case. Heuristically, we can see the competition between gravitational attraction and centrifugal repulsion in the expression

$$\frac{\Delta}{r^2} - 1 = -\frac{\mu}{r^{d-3}} + \frac{a^2}{r^2}\,. \tag{13}$$

Roughly, the first term on the right-hand side corresponds to the attractive gravitational potential and falls off in a dimension-dependent fashion. In contrast, the repulsive centrifugal barrier described by the second term does not depend on the total number of dimensions, since rotations always refer to motions in a plane.

Given the similarities between (10) and the Kerr solution it is clear that the outer event horizon lies at the largest (real) root r_0 of $g_{rr}^{-1} = 0$, i.e., $\Delta(r) = 0$. Thus, we expect that the features of the event horizons will be strongly dimension-dependent, and this is indeed the case. If there is an event horizon at $r = r_0$,

$$r_0^2 + a^2 - \frac{\mu}{r_0^{d-5}} = 0\,, \tag{14}$$

its area will be

$$\mathcal{A}_H = r_0^{d-4}(r_0^2 + a^2)\Omega_{d-2}\,. \tag{15}$$

[4] This choice corresponds to rotation in the positive sense (i.e. increasing ϕ). The solution presented in [2] is obtained by $\phi \to -\phi$, which gives rotation in a negative sense.

For $d = 4$, a regular horizon is present for values of the spin parameter a up to the Kerr bound: $a = \mu/2$ (or $a = GM$), which corresponds to an extremal black hole with a single degenerate horizon (with vanishing surface gravity). Solutions with $a > GM$ correspond to naked singularities. In $d = 5$, the situation is apparently quite similar since the real root at $r_0 = \sqrt{\mu - a^2}$ exists only up to the extremal limit $\mu = a^2$. However, this extremal solution has zero area, and in fact, has a naked ring singularity.

For $d \geq 6$, $\Delta(r)$ is always positive at large values of r, but the term $-\mu/r^{d-5}$ makes it negative at small r (we are assuming positive mass). Therefore Δ always has a (single) positive real root independently of the value of a. Hence regular black hole solutions exist with arbitrarily large a. Solutions with large angular momentum per unit mass are referred to as "ultra-spinning".

An analysis of the shape of the horizon in the ultra-spinning regime $a \gg r_0$ shows that the black holes flatten along the plane of rotation [5]: the extent of the horizon along this plane is $\sim a$, while in directions transverse to this plane its size is $\sim r_0$. In fact, a limit can be taken in which the ultraspinning black hole becomes a black membrane with horizon geometry $\mathbf{R}^2 \times S^{d-4}$. This turns out to have important consequences for black holes in $d \geq 6$, as we will discuss later. The transition between the regime in which the black hole behaves like a fairly compact, Kerr-like object, and the regime in which it is better characterized as a membrane, is most clearly seen by analyzing the black hole temperature

$$T_H = \frac{1}{4\pi}\left(\frac{2r_0}{r_0^2 + a^2} + \frac{d-5}{r_0}\right) . \tag{16}$$

At

$$\left(\frac{a}{r_0}\right)_{\rm mem} = \sqrt{\frac{d-3}{d-5}} , \tag{17}$$

this temperature reaches a minimum. For a/r_0 smaller than this value, quantities like T_H and $\mathcal{A}_H$ decrease, in a manner similar to the Kerr solution. However, past this point they rapidly approach the black membrane results in which $T_H \sim 1/r_0$ and $\mathcal{A}_H \sim a^2 r_0^{d-4}$, with a^2 characterizing the area of the membrane worldvolume.

The properties of the solutions are conveniently encoded using the dimensionless variables a_H, j introduced in [12]. For the solutions (10) the curve $a_H(j)$ can be found in parametric form, in terms of the dimensionless 'shape' parameter $\nu = \frac{r_0}{a}$, as

$$j^{d-3} = \frac{\pi}{(d-3)^{\frac{d-3}{2}}} \frac{\Omega_{d-3}}{\Omega_{d-2}} \frac{\nu^{5-d}}{1+\nu^2} , \tag{18}$$

$$a_H^{d-3} = 8\pi \left(\frac{d-4}{d-3}\right)^{\frac{d-3}{2}} \frac{\Omega_{d-3}}{\Omega_{d-2}} \frac{\nu^2}{1+\nu^2} . \tag{19}$$

The static and ultra-spinning limits correspond to $\nu \to \infty$ and $\nu \to 0$, respectively. The inflection point where $d^2 a_H/dj^2$ changes sign when $d \geq 6$, occurs at the value (17).

5 Black rings

Five-dimensional black rings are black holes with horizon topology $S^1 \times S^2$ in asymptotically flat spacetime. The S^1 describes a contractible circle, not stabilized by topology but by the centrifugal force provided by rotation. An exact solution for a black ring with rotation along this S^1 was presented in [13]. Its most convenient form was given in [14] as[5]

$$\begin{aligned} ds^2 = & -\frac{F(y)}{F(x)}\left(dt - C\,R\,\frac{1+y}{F(y)}\,d\psi\right)^2 \\ & + \frac{R^2}{(x-y)^2}\,F(x)\left[-\frac{G(y)}{F(y)}d\psi^2 - \frac{dy^2}{G(y)} + \frac{dx^2}{G(x)} + \frac{G(x)}{F(x)}d\phi^2\right] , \end{aligned} \tag{20}$$

[5] An alternative form was found in [15, 16]. The relation between the two is given in [17].

where

$$F(\xi) = 1 + \lambda\xi, \qquad G(\xi) = (1-\xi^2)(1+\nu\xi)\,, \tag{21}$$

and

$$C = \sqrt{\lambda(\lambda-\nu)\frac{1+\lambda}{1-\lambda}}\,. \tag{22}$$

The dimensionless parameters λ and ν must lie in the range

$$0 < \nu \leq \lambda < 1\,. \tag{23}$$

The coordinates vary in the ranges $-\infty \leq y \leq -1$ and $-1 \leq x \leq 1$, with asymptotic infinity recovered as $x \to y \to -1$. The axis of rotation around the ψ direction is at $y = -1$, and the axis of rotation around ϕ is divided into two pieces: $x = 1$ is the disk bounded by the ring, and $x = -1$ is its complement from the ring to infinity. The horizon lies at $y = -1/\nu$. Outside it, at $y = -1/\lambda$, lies an ergosurface. A detailed analysis of this solution and its properties can be found in [17] and [18], so we shall only discuss it briefly.

In the form given above the solution possesses three independent parameters: λ, ν, and R. Physically, this sounds like one too many: given a ring with mass M and angular momentum J, we expect its radius to be dynamically fixed by the balance between the centrifugal and tensional forces. This is also the case for the black ring (20): in general it has a conical defect on the plane of the ring, $x = \pm 1$. In order to avoid it, the angular variables must be identified with periodicity

$$\Delta\psi = \Delta\phi = 4\pi\frac{\sqrt{F(-1)}}{|G'(-1)|} = 2\pi\frac{\sqrt{1-\lambda}}{1-\nu} \tag{24}$$

and the two parameters λ, ν must satisfy

$$\lambda = \frac{2\nu}{1+\nu^2}\,. \tag{25}$$

This eliminates one parameter, and leaves the expected two-parameter (ν, R) family of solutions. The mechanical interpretation of this balance of forces for thin rings is discussed in [12]. The Myers-Perry solution with a single rotation is obtained as a limit of the general solution (20) [14], but cannot be recovered if λ is eliminated through (25).

The physical parameters of the solution (mass, angular momentum, area, angular velocity, surface gravity) in terms of ν and R can be found in [17]. It can be seen that while R provides a measure of the radius of the ring's S^1, the parameter ν can be interpreted as a 'thickness' parameter characterizing its shape, corresponding roughly to the ratio between the S^2 radius and the S^1 radius.

More precisely, one finds two branches of solutions, whose physical differences are seen most clearly in terms of the dimensionless variables j and a_H introduced above. For a black ring in equilibrium, the phase curve $a_H(j)$ can be expressed in parametric form as

$$a_H = 2\sqrt{\nu(1-\nu)}\,, \qquad j = \sqrt{\frac{(1+\nu)^3}{8\nu}}\,. \tag{26}$$

This curve is easily seen to have a cusp at $\nu = 1/2$, which corresponds to a minimum value of $j = \sqrt{27/32}$ and a maximum $a_H = 1$. Branching off from this cusp, the *thin black ring* solutions ($0 < \nu < 1/2$) extend to $j \to \infty$ as $\nu \to 0$, with asymptotic $a_H \to 0$. The *fat black ring* branch ($1/2 \leq \nu < 1$) has lower area and extends only to $j \to 1$, ending at $\nu \to 1$ at the same zero-area singularity as the MP solution. This implies that in the range $\sqrt{27/32} \leq j < 1$ there exist three different solutions (thin and fat black rings, and MP black hole) with the same value of j. The notion of black hole uniqueness that was proven to hold in four dimensions does not extend to five dimensions.

A remarkable vacuum black ring solution with rotation along both the S^1 and the S^2 was presented in [19].

6 Vacuum solutions in more than five dimensions

With no available techniques to construct asymptotically flat exact solutions beyond those found by Myers and Perry, the situation in $d \geq 6$ is much less developed than in $d = 5$.

However, despite the paucity of exact solutions, there are strong indications that the variety of black holes that populate General Relativity in $d \geq 6$ is vastly larger than in $d = 4, 5$. A first indication came from the conjecture in ref. [5] about the existence of black holes with spherical horizon topology but with axially symmetric 'ripples' (or 'pinches'). The plausible existence of black rings in any $d \geq 5$ was argued in [20, 18]. More recently, ref. [12] has constructed approximate solutions for black rings in any $d \geq 5$ and then exploited the conjecture of [5] to try to draw a phase diagram with connections and mergers between the different expected phases. In the following I summarize these results.

6.1 Approximate solutions from curved thin branes

In the absence of exact techniques, ref. [12] resorted to approximate constructions, in particular to the method of matched asymptotic expansions previously used in the context of black holes localized in Kaluza-Klein circles in [21, 22, 23, 24][6]. The basic idea is to find two widely separated scales in the problem, call them R_1 and R_2, with $R_2 \ll R_1$. Then try to solve the equations in two limits: first, as a perturbative expansion for small R_2, and then in an expansion in $1/R_1$. The former solves the equations in the far-region $r \gg R_2$, in which the boundary conditions, e.g., asymptotic flatness, fix the integration constants. The second expansion is valid in a near-region $r \ll R_1$. In order to fix the integration constants in this case, one matches the two expansions in the overlap region $R_2 \ll r \ll R_1$ in which both approximations are valid. The process can then be iterated to higher orders in the expansion, see [22] for an explanation of the systematics involved.

In order to construct a black ring with horizon topology $S^1 \times S^{d-3}$, we take the scales R_1, R_2 to be the radii of the S^1 and S^{d-3} respectively[7]. To implement the above procedure, we take $R_2 = r_0$, the horizon radius of the S^{d-3} of a straight boosted black string, and $R_1 = R$ the large circle radius of a very thin circular string. Thus, in effect, to first order in the expansion what one does is: (i) find the solution within linearized approximation, i.e., for small r_0/r, around a Minkowski background for an infinitely thin circular string with momentum along the circle; (ii) perturb a straight boosted black string so as to bend it into an arc of circle of very large radius $1/R$. The latter step not only requires matching to the previous solution in order to provide boundary conditions for the homogeneous differential equations: one also needs to check that the perturbations can be made compatible with regularity of the horizon.

It is worth noting that the form of the solution thus found exhibits a considerable increase in complexity when going from $d = 5$, where an exact solution is available, to $d > 5$: simple linear functions of r in $d = 5$ change to hypergeometric functions in $d > 5$. We take this as an indication that exact closed analytical forms for these solutions may not exist in $d > 5$.

We will not dwell here on the details of the perturbative construction of the solution –see [12] for this–, but instead we shall emphasize that adopting the view that a black object is approximated by a certain very thin black brane curved into a given shape can easily yield non-trivial information about new kinds of black holes. Eventually, of course, the assumption that the horizon remains regular after curving needs to be checked.

Consider then a stationary black brane, possibly with some momentum along its worldvolume, with horizon topology $\mathbf{R}^{p+1} \times S^q$, with $q = d-p-2$. When viewed at distances much larger than the size r_0 of the S^q, we can approximate the metric of the black brane spacetime by the gravitational field created by an 'equivalent source' with distributional energy tensor $T^\nu_\mu \propto r_0^{q-1}\delta^{(q+1)}(r)$, with non-zero components only along directions tangent to the worldvolume, and where $r = 0$ corresponds to the location of the brane. Now we want to put this same source on a curved, compact p-dimensional spatial surface in a given background spacetime (e.g., Minkowski, but possibly (Anti-)deSitter or others, too). In principle we can obtain the mass M and angular momenta J_i of the new object by integrating T^t_t and T^i_t over the entire spatial section of the brane worldvolume. Moreover, the total area $\mathcal{A}_H$ is similarly obtained by replacing the volume of $\mathbf{R}^p$ with the volume of the new surface. Thus, it appears that we can easily obtain the relation $\mathcal{A}_H(M, J_i)$ in this manner.

There is, however, the problem that having changed the embedding geometry of the brane, it is not guaranteed that the brane will remain stationary. Moreover, $\mathcal{A}_H$ will be a function not only of (M, J_i),

[6] The classical effective field theory of [25, 26] is an alternative to matched asymptotic expansions which presumably should be useful as well in the context discussed in this section.

[7] The S^{d-3} is not round for known solutions, but one can define an effective scale R_2 as the radius of a round S^{d-3} with the same area.

but it will also depend explicitly on geometrical parameters of the surface. However, we would expect than in a situation of equilibrium some of these geometrical parameters should be fixed dynamically by the mechanical parameters (M, J_i) of the brane. For instance, take a boosted string and curve it into a circular ring so the linear velocity turns into angular rotation. If we fix the mass and the radius then the ring will *not* be in equilibrium for every value of the boost, i.e., of the angular momentum, so there must exist a fixed relation $R = f(M, J)$. This is reflected in the fact that in the new situation the stress-energy tensor is in general not conserved, $\nabla_\mu T^{\mu\nu} \neq 0$: additional stresses would be required to keep the brane in place. An efficient way of imposing the brane equations of motion is in fact to demand conservation of the stress-energy tensor. In the absence of external forces, the classical equations of motion of the brane derived in this way are [27]

$$K^\rho{}_{\mu\nu} T^{\mu\nu} = 0\,, \tag{27}$$

where $K^\rho{}_{\mu\nu}$ is the second-fundamental tensor, characterizing the extrinsic curvature of the embedding surface spanned by the brane worldvolume. For a string on a circle of radius R in flat space, parametrized by a coordinate $z \sim z + 2\pi R$, this equation becomes

$$\frac{T_{zz}}{R} = 0\,. \tag{28}$$

In $d = 5$, this can be seen to correspond to the condition of absence of conical singularities in the solution (20), in the limit of a very thin black ring [16]. Ref. [12] showed that this condition is also required in $d \geq 6$ in order to avoid curvature singularities on the plane of the ring.

In general, eq. (27) constrains the allowed values of parameters of a black brane that can be put on a given surface. Ref. [12] easily derived, for any $d \geq 5$, that the radius R of thin rotating black rings of given M and J is fixed to

$$R = \frac{d-2}{\sqrt{d-3}} \frac{J}{M} \tag{29}$$

so large R corresponds to large spin for fixed mass. The horizon area of these thin black rings goes like

$$\mathcal{A}_H(M, J) \propto J^{-\frac{1}{d-4}}\, M^{\frac{d-2}{d-4}}\,. \tag{30}$$

This is to be compared to the value for ultra-spinning MP black holes in $d \geq 6$ (cf. eqs. (18), (19) as $\nu \to 0$),

$$\mathcal{A}_H(M, J) \propto J^{-\frac{2}{d-5}}\, M^{\frac{d-2}{d-5}}\,. \tag{31}$$

This shows that in the ultra-spinning regime the rotating black ring has larger area than the MP black hole.

6.2 Phase diagram

Equation (30) allows to compute the asymptotic form of the curve $a_H(j)$ in the phase diagram at large j for black rings. However, when j is of order one the approximations in the matched asymptotic expansion break down, and the gravitational interaction of the ring with itself becomes important. At present we have no analytical tools to deal with this regime for generic solutions. In most cases, numerical analysis may be needed to obtain precise information.

Nevertheless, ref. [12] has advanced heuristic arguments to propose a completion of the curves that is qualitatively consistent with all the information available at present. A basic ingredient is the observation in [5], discussed in section 4.1, that in the ultraspinning regime in $d \geq 6$, MP black holes approach the geometry of a black membrane $\approx \mathbf{R}^2 \times S^{d-4}$ spread out along the plane of rotation.

We already discussed how using this analogy, ref. [5] argued that ultra-spinning MP black holes should exhibit a Gregory-Laflamme-type of instability [28]. Since the threshold mode of the GL instability gives rise to a new branch of static non-uniform black strings and branes [29, 30, 31], ref. [5] argued that it is natural to conjecture the existence of new branches of axisymmetric 'lumpy' (or 'pinched') black holes, branching off from the MP solutions along the stationary axisymmetric zero-mode perturbation of the GL-like instability.

Ref. [12] developed further this analogy, and drew a correspondence between the phases of black membranes and the phases of higher-dimensional black holes. Although the analogy has several limitations,

it allows to propose a phase diagram in $d \geq 6$, see [12], which should be compared to the much simpler diagram in five dimensions. It includes the presence of an infinite number of black holes with spherical topology, connected via merger transitions to MP black holes, black rings, and black Saturns. Of all multi-black hole configurations, the diagram only includes those phases in which all components of the horizon have the same surface gravity and angular velocity: presumably, these are the only ones that can merge to a phase with connected horizon. Even within this class of solutions, the diagram is not expected to contain all possible phases with a single angular momentum: blackfolds with other topologies must likely be included too. The extension to phases with several angular momenta also remains to be done.

Indirect evidence for the existence of black holes with pinched horizons is provided by the results of [32], which finds 'pinched plasma ball' solutions of fluid dynamics that are CFT duals of pinched black holes in six-dimensional AdS space. The approximations involved in the construction require that the horizon size of the dual black holes be larger than the AdS curvature radius, so they do not admit a limit to flat space space. Nevertheless, their existence provides an example, if indirect, that pinched horizons make appearance in $d = 6$ (and not in $d = 5$).

Acknowledgements

I would like to express my gratitude to the organizers of the JGRG18 workshop for their invitation to deliver this talk, and for their successful efforts at running an estimulating and enjoyable conference. I would like to thank Harvey Reall for his collaboration in the review article that this contribution is based on. This work has been supported in part by DURSI 2005 SGR 00082 and CICYT FPA 2004-04582-C02-02 and FPA 2007-66665C02-02.

References

[1] R. Emparan and H. S. Reall, "Black Holes in Higher Dimensions," submitted to Living Rev. Rel. arXiv:0801.3471 [hep-th].

[2] R. C. Myers and M. J. Perry, "Black Holes In Higher Dimensional Space-Times," Annals Phys. **172**, 304 (1986).

[3] S. W. Hawking and G. F. R. Ellis, "The Large scale structure of space-time," *Cambridge University Press, Cambridge, 1973*

[4] R. Gregory and R. Laflamme, "Black strings and p-branes are unstable," Phys. Rev. Lett. **70** (1993) 2837 [arXiv:hep-th/9301052].

[5] R. Emparan and R. C. Myers, "Instability of ultra-spinning black holes," JHEP **0309**, 025 (2003) [arXiv:hep-th/0308056].

[6] S. Hollands, A. Ishibashi and R. M. Wald, "A higher dimensional stationary rotating black hole must be axisymmetric," Commun. Math. Phys. **271**, 699 (2007) [arXiv:gr-qc/0605106].

[7] A. A. Coley, "Classification of the Weyl Tensor in Higher Dimensions and Applications," arXiv:0710.1598 [gr-qc].

[8] C. Charmousis and R. Gregory, "Axisymmetric metrics in arbitrary dimensions," Class. Quant. Grav. **21** (2004) 527 [arXiv:gr-qc/0306069].

[9] C. Charmousis, D. Langlois, D. Steer and R. Zegers, "Rotating spacetimes with a cosmological constant," JHEP **0702** (2007) 064 [arXiv:gr-qc/0610091].

[10] G. J. Galloway and R. Schoen, "A generalization of Hawking's black hole topology theorem to higher dimensions," Commun. Math. Phys. **266**, 571 (2006) [arXiv:gr-qc/0509107].

[11] F. R. Tangherlini, "Schwarzschild field in n dimensions and the dimensionality of space problem," Nuovo Cim. **27**, 636 (1963).

[12] R. Emparan, T. Harmark, V. Niarchos, N. A. Obers and M. J. Rodriguez, "The Phase Structure of Higher-Dimensional Black Rings and Black Holes," JHEP **0710** (2007) 110 [arXiv:0708.2181 [hep-th]].

[13] R. Emparan and H. S. Reall, "A rotating black ring in five dimensions," Phys. Rev. Lett. **88** (2002) 101101 [arXiv:hep-th/0110260].

[14] R. Emparan, "Rotating circular strings, and infinite non-uniqueness of black rings," JHEP **0403** (2004) 064 [arXiv:hep-th/0402149].

[15] K. Hong and E. Teo, "A new form of the C-metric," Class. Quant. Grav. **20** (2003) 3269 [arXiv:gr-qc/0305089].

[16] H. Elvang and R. Emparan, "Black rings, supertubes, and a stringy resolution of black hole non-uniqueness," JHEP **0311**, 035 (2003) [arXiv:hep-th/0310008].

[17] R. Emparan and H. S. Reall, "Black rings," Class. Quant. Grav. **23** (2006) R169 [arXiv:hep-th/0608012].

[18] H. Elvang, R. Emparan and A. Virmani, "Dynamics and stability of black rings," JHEP **0612** (2006) 074 [arXiv:hep-th/0608076].

[19] A. A. Pomeransky and R. A. Sen'kov, "Black ring with two angular momenta," arXiv:hep-th/0612005.

[20] J. L. Hovdebo and R. C. Myers, "Black rings, boosted strings and Gregory-Laflamme," Phys. Rev. D **73**, 084013 (2006) [arXiv:hep-th/0601079].

[21] T. Harmark, "Small black holes on cylinders," Phys. Rev. D **69**, 104015 (2004) [arXiv:hep-th/0310259].

[22] D. Gorbonos and B. Kol, "A dialogue of multipoles: Matched asymptotic expansion for caged black holes," JHEP **0406**, 053 (2004) [arXiv:hep-th/0406002].

[23] D. Karasik, C. Sahabandu, P. Suranyi and L. C. R. Wijewardhana, "Analytic approximation to 5 dimensional black holes with one compact dimension," Phys. Rev. D **71**, 024024 (2005) [arXiv:hep-th/0410078].

[24] D. Gorbonos and B. Kol, "Matched asymptotic expansion for caged black holes: Regularization of the post-Newtonian order," Class. Quant. Grav. **22**, 3935 (2005) [arXiv:hep-th/0505009].

[25] Y. Z. Chu, W. D. Goldberger and I. Z. Rothstein, "Asymptotics of d-dimensional Kaluza-Klein black holes: Beyond the newtonian approximation," JHEP **0603** (2006) 013 [arXiv:hep-th/0602016].

[26] B. Kol and M. Smolkin, "Classical Effective Field Theory and Caged Black Holes," arXiv:0712.2822 [hep-th].

[27] B. Carter, "Essentials of classical brane dynamics," Int. J. Theor. Phys. **40**, 2099 (2001) [arXiv:gr-qc/0012036].

[28] R. Gregory and R. Laflamme, "The Instability of charged black strings and p-branes," Nucl. Phys. B **428** (1994) 399 [arXiv:hep-th/9404071].

[29] R. Gregory and R. Laflamme, "Hypercylindrical black holes," Phys. Rev. D **37** (1988) 305.

[30] S. S. Gubser, "On non-uniform black branes," Class. Quant. Grav. **19**, 4825 (2002) [arXiv:hep-th/0110193].

[31] T. Wiseman, "Static axisymmetric vacuum solutions and non-uniform black strings," Class. Quant. Grav. **20** (2003) 1137 [arXiv:hep-th/0209051].

[32] S. Lahiri and S. Minwalla, "Plasmarings as dual black rings," arXiv:0705.3404 [hep-th].

Modified Gravity as an Alternative to Dark Energy

Kazuya Koyama[1]

[1] *Institute of Cosmology & Gravitation, University of Portsmouth, Portsmouth, Hampshire, PO1 3FX, UK*

Abstract

The late time accelerated expansion of the Universe may indicate that General Relativity (GR) fails on cosmological scales. In this review, we study structure formation in modified gravity models and explain how large scale structure of the Universe can be used to distinguish between modified gravity models and dark energy models in GR. An emphasize is made on the necessity to obtain the non-linear power spectrum of dark matter perturbations by properly taking into a mechanism to recover GR on small scales, which is essential to evade stringent constraints on deviations from GR at solar system scales.

1 Introduction

The late-time acceleration of the Universe is surely the most challenging problem in cosmology. Within the framework of general relativity (GR), the acceleration originates from dark energy. The simplest option is the cosmological constat. However, in order to explain the current acceleration of the Universe, the required value of the cosmological constant must be incredibly small. Alternatively, there could be no dark energy, but a large distance modification of GR may account for the late-time acceleration of the Unverse. Recently considerable efforts have been made to construct models for modified gravity as an alternative to dark energy and distinguish them from dark energy models by observations (see [1–4] for reviews). Although fully consistent models have not been constructed yet, some indications of the nature of the modified gravity models have been obtained. In general, there are three regimes of gravity in modified gravity models [2, 5]. On the largest scales, gravity must be modified significantly in order to explain the late time acceleration without introducing dark energy. On the smallest scales, the theory must approach GR because there exist stringent constraints on the deviation from GR at solar system scales. On intermediate scales between the cosmological horizon scales and the solar system scales, there can be still a deviation from GR. In fact, it is a very common feature in modified gravity models that there is a significant deviation from GR on large scale structure scales. This is due to the fact that, once we modify GR, there arises a new scalar degree of freedom in gravity. This scalar mode changes gravity even below the length scale where the modification of the tensor sector of gravity becomes significant, which causes the cosmic acceleration.

Therefore, large scale structure of the Universe offers the best opportunity to distinguish between modified gravity models and dark energy models in GR. [6–19]. The expansion history of the Universe determined by the Friedman equation can be completely the same in modified gravity models and dark energy models. In fact, it is always possible to find a dark energy model that can mimic the expansion history of the Universe in a given modified gravity model by tuning the equation of state of dark energy. However, this degeneracy can be broken by the growth rate of structure formation. This is because the scalar degree of freedom in modified gravity models changes the strength of gravity on sub-horizon scales and thus changes the growth rate of structure formation. Thus combining the geometrical test and structure formation test, one can distinguish between dark energy models and modified gravity models.

However, there is a subtlety in testing modified gravity models using large scale structure of the Universe. In any successful modified gravity models, we should recover GR on small scales. Indeed, unless there is an additional mechanism to screen the scalar interaction which changes the growth rate of structure formation, the modification of gravity contradicts to the stringent constraints on the deviation from GR at solar system scales. This mechanism affects the non-linear clustering of dark matter. We

[1] E-mail:Kazuya.Koyama@port.ac.uk

expect that the power-spectrum of dark matter perturbations approaches the one in the GR dark energy model with the same expansion history of the Universe because the modification of gravity disappears on small scales. Then the difference between a modified gravity model and a dark energy model with the same expansion history becomes smaller on smaller scales. This recovery of GR has important implications for weak lensing measurements because the strongest signals in weak lensing measurements come from non-linear scales.

In this review, we use two examples, branewrold models and $f(R)$ gravity models to explain how large scale structure of the Universe can be used to distinguish between modified gravity models from dark energy models in GR. For this purpose, a general framework based on Brans-Dicke (BD) gravity is introduced to describe inhomogeneities under horizon scales. The two examples are included in this general framework. Then the mechanisms to recover GR is introduced and we study their effects on the non-linear clustering of dark matter.

2 Quasi-static perturbations in modified gravity models

We consider perturbations around the Friedman-Robertson-Walker universe described in the Newtonian gauge:

$$ds^2 = -(1+2\psi)dt^2 + a^2(1+2\phi)\delta_{ij}dx^i dx^j. \tag{1}$$

We will work on the evolution of matter fluctuations inside the Hubble horizon. Then we can use the quasi-static approximation and neglect the time derivatives of the perturbed quantities compared with the spatial derivatives. As mentioned in the introduction, the large distance modification of gravity which is necessary to explain the late-time acceleration generally modifies gravity even on sub-horizon scales due to the introduction of a new scalar degree of freedom. This modification of gravity due to the scalar mode can be described by the Brans-Dicke (BD) gravity. The action of the BD theory is given by

$$S = \frac{1}{16\pi}\int d^4x\sqrt{-g_4}\left(\varphi R - \frac{\omega_{\rm BD}}{\varphi}(\nabla\varphi)^2\right). \tag{2}$$

Under the quasi-static approximations, perturbed modified Einstein equations give

$$\phi + \psi = -\varphi, \tag{3}$$

$$\frac{1}{a^2}\nabla^2\psi = 4\pi G\rho_m\delta - \frac{1}{2a^2}\nabla^2\varphi, \tag{4}$$

$$(3+2\omega_{\rm BD})\frac{1}{a^2}\nabla^2\varphi = -8\pi G\rho_m\delta, \tag{5}$$

where we expanded the BD scalar as $\varphi = \varphi_0 + \varphi(x,t)$, $G = 1/\varphi_0$, ρ_m is the background dark matter energy density and δ is dark matter density perturbations. In general, modified gravity models that explain the late time acceleration have $\omega_{\rm BD} \sim O(1)$ on sub-horizon scales today. This would contradict to the solar system constraints which require $\omega_{\rm BD} > 40000$. However, this constraint can be applied only when the BD scalar has no potential and no self-interactions. Thus, in order to avoid this constraint, the BD scalar should acquire some interaction terms on small scales. In general we expect that the BD scalar field equation is given by

$$(3+2\omega_{\rm BD})\frac{1}{a^2}k^2\varphi = 8\pi G\rho_m\delta - \mathcal{I}(\varphi), \tag{6}$$

in a Fourier space. Here the interaction term $\mathcal{I}$ can be expanded as

$$\begin{aligned}\mathcal{I}(\varphi) &= M_1(k)\varphi + \frac{1}{2}\int\frac{d^3\boldsymbol{k}_1 d^3\boldsymbol{k}_2}{(2\pi)^3}\delta_D(\boldsymbol{k}-\boldsymbol{k}_{12})M_2(\boldsymbol{k}_1,\boldsymbol{k}_2)\varphi(\boldsymbol{k}_1)\varphi(\boldsymbol{k}_2)\\ &\quad + \frac{1}{6}\int\frac{d^3\boldsymbol{k}_1 d^3\boldsymbol{k}_2 d^3\boldsymbol{k}_3}{(2\pi)^6}\delta_D(\boldsymbol{k}-\boldsymbol{k}_{123})M_3(\boldsymbol{k}_1,\boldsymbol{k}_2,\boldsymbol{k}_3)\varphi(\boldsymbol{k}_1)\varphi(\boldsymbol{k}_2)\varphi(\boldsymbol{k}_3) + ...,\end{aligned} \tag{7}$$

where $\boldsymbol{k}_{ij} = \boldsymbol{k}_i + \boldsymbol{k}_j$ and $\boldsymbol{k}_{ijk} = \boldsymbol{k}_i + \boldsymbol{k}_j + \boldsymbol{k}_k$.

There are two known mechanisms where the non-linear interaction terms $\mathcal{I}$ are responsible for the recovery of GR on small scales. One is the chameleon mechanism [20]. In this case, the BD scalar has a non-trivial potential. The potential gives a mass to the BD scalar. Then the BD scalar mediates the Yukawa-type force and the interaction decays exponentially beyond the length scale determined by the inverse of mass, the compton wavelength. Then the scalar interaction is hidden beyond the compton wavelength and GR is recovered. The BD scalar is coupled to the trace of the energy momentum tensor. Thus the effective potential depends on the energy density of the environment. The potential is tuned so that the mass of the BD scalar becomes large for a dense environment such as the solar system. Then the compton wavelength becomes very short for a dense environment and the scalar mode is effectively hidden. In this paper, we deal with this mechanism perturbatively. M_1 determines the mass term in the cosmological background. The higher order terms $M_i, (i > 1)$ describe the change of the mass term due to the change of the energy density. If the chameleon mechanism is at work, the effective mass becomes larger when the density fluctuations become non-linear.

The other mechanism relies on the existence of the non-linear derivative interactions. A typical example is the Dvali-Gabadadze-Porratti (DGP) model where we are supposed to be living on a 4D brane in a 5D Minkowski spacetime [21]. In this model, the BD scalar is identified as the brane bending mode which describes the deformation of the 4D brane in the 5D bulk spacetime. The brane bending mode has a large second-order term in the equation of motion which cannot be neglected even when the metric perturbations remain linear [22–24]. This corresponds to the existence of a large $M_2(k)$ term. it has been shown that once this second order term dominates over the linear term, the scalar mode is hidden and the solutions for metric perturbations approach GR solutions. For a static spherically symmetric source, we can identify the length scale below which the second order interaction becomes important. This length scale is known as the Vainshtein radius [25]. In the cosmological situation, it is expected that once the density perturbations become non-linear, the second order term becomes important and we recover GR. In the next section, we apply the perturbation theory to solve the equations. Thus we only keep up to the third order in the expansion of $\mathcal{I}$ which is necessary to calculate the quasi non-linear power spectrum.

The evolution equations for matter perturbations are obtained from the conservation of energy momentum tensor, the continuity equation and the Euler equation:

$$\frac{\partial \delta}{\partial t} + \frac{1}{a}\nabla \cdot [(1+\delta)\boldsymbol{v}] = 0, \tag{8}$$

$$\frac{\partial \boldsymbol{v}}{\partial t} + H\boldsymbol{v} + \frac{1}{a}(\boldsymbol{v}\cdot\nabla)\boldsymbol{v} = -\frac{1}{a}\nabla\psi. \tag{9}$$

Eqs. (4), (6), (8) and (9) are the basic equations that have to be solved.

3 Linear regime

In this section, we study the behaviour of perturbations on linear scales under horizon. First we study two explicit examples and then discuss the possibility to distinguish between modified gravity models and dark energy models.

3.1 Linear growth rate

By linearizing Eqs. (4), (6), the solutions for metric perturbations are given by

$$\frac{k^2}{a^2}\Phi = 4\pi G\left(\frac{2(1+\omega_{\rm BD}) + M_1 a^2/k^2}{3+2\omega_{\rm BD}+M_1 a^2/k^2}\right)\rho_m \delta_m, \tag{10}$$

$$\frac{k^2}{a^2}\Psi = -4\pi G\left(\frac{2(2+\omega_{\rm BD}) + M_1 a^2/k^2}{3+2\omega_{\rm BD}+M_1 a^2/k^2}\right)\rho_m \delta_m, \tag{11}$$

where we only keep the linear order in $\mathcal{I}$. There are two ways to recover GR solutions at linearized level. One is to take $\omega_{\rm BD} \to \infty$. The other is to consider a large mass for the BD scalar which satisfies $M_1 \gg k/a$. However, modified gravity models that explain the late time acceleration do not satisfy

these conditions in general and linearized gravity under horizon scales deviates from GR. The evolution equation for density perturbations is obtained by Eq. (8) and (9) using the solutions (10) and (11):

$$\widehat{\mathcal{L}}\delta_m = 0, \tag{12}$$

where the linear operator $\widehat{\mathcal{L}}$ is given by

$$\widehat{\mathcal{L}} \equiv \frac{d^2}{dt^2} + 2H\frac{d}{dt} - \frac{\kappa^2}{2}\rho_{\rm m}\left(\frac{2(2+\omega_{\rm BD}) + M_1 a^2/k^2}{3+2\omega_{\rm BD}+M_1 a^2/k^2}\right), \tag{13}$$

and we assumed the irrotationality of the fluid. In the following, we consider two explicit examples and study the behaviour of density perturbations.

3.2 DGP models

In DGP models, we are supposed to be living in a 4D brane in a 5D spacetime. The model is described by the action given by

$$S = \frac{1}{4\kappa^2 r_c}\int d^4x\sqrt{-g_5}R_5 + \frac{1}{2\kappa^2}\int d^4x\sqrt{-g}(R+L_{\rm m}), \tag{14}$$

where $\kappa^2 = 8\pi G$, R_5 is the Ricci scalar in 5D and $L_{\rm m}$ stands for the matter lagrangian confined to a brane. The cross over scale r_c is the parameter in this model which is a ratio between the 5D Newton constant and the 4D Newton constant. The modified Friedman equation is given by

$$\epsilon\frac{H}{r_c} = H^2 - \frac{\kappa^2}{3}\rho, \tag{15}$$

where $\epsilon = \pm 1$ represents two distinct branches of the solutions [26]. From this modified Friedman equation, we find that the cross-over scale r_c must be fine-tuned to be the present-day horizon scales in order to modify gravity only at late times. The solution with $\epsilon = +1$ is known as the self-accelerating branch because even without the cosmological constant, the expansion of the Universe is accelerating as the Hubble parameter is constant, $H = 1/r_c$. On the other hand $\epsilon = -1$ corresponds to the normal branch. In this branch, we need a cosmological constant to realize the cosmic acceleration. However, due to the modified gravity effects, the Universe behaves as if it were filled with the Phantom dark energy with the equation of state w smaller than -1. It is known that the self-accelerating solution is plagued by the ghost instabilities (see [27] for a review). Also it gives a poor fit to the observations such as supernovae and cosmic microwave background anisotropies [28]. However, as we will see later, this model is the simplest modified gravity model where the mechanism of the recovery of GR on small scales is naturally encoded and it can be used to get insights into the effect of this mechanism on the non-linear power spectrum.

In this model, gravity becomes 5D on large scales larger than r_c. On small scales, gravity becomes 4D but it is not described by GR. The quasi-static perturbations are described by the BD theory where the BD parameter is given by

$$\omega_{\rm BD}(t) = \frac{3}{2}\Big(\beta(t)-1\Big), \quad \beta(t) = 1 - 2\epsilon H r_c\left(1+\frac{\dot{H}}{3H^2}\right), \tag{16}$$

where $\dot{H}$ is a cosmic time derivative of the Hubble parameter H. Note that the BD parameter depends on time in this model. The BD scalar is massless $M_1 = 0$. Then the solutions for the metric perturbations are given by [29,30]

$$\frac{k^2}{a^2}\Phi = 4\pi G\left(1-\frac{1}{3\beta}\right)\rho_m\delta_m, \tag{17}$$

$$\frac{k^2}{a^2}\Psi = 4\pi G\left(1+\frac{1}{3\beta}\right)\rho_m\delta_m, \tag{18}$$

and the linear growth rate is determined as

$$\widehat{\mathcal{L}}\delta_m = 0, \quad \widehat{\mathcal{L}} \equiv \frac{d^2}{dt^2} + 2H\frac{d}{dt} - \frac{\kappa^2}{2}\rho_m\left(1 - \frac{1}{3\beta}\right). \tag{19}$$

In the self-accelerating branch, $\beta < 0$ and the BD parameter is negative which makes the Newton constant effectively smaller than GR. Thus the growth rate receives additional suppressions compared with dark energy models in GR. On the other hand, in the normal branch, $\beta > 0$ and the BD parameter is positive which makes the Newton constant larger than GR. Then the growth rate is enhanced. In order to demonstrate the effect of this modification, it is instructive to consider a dark energy model in GR which follows the same expansion history of the Universe in the self-accelerating universe:

$$H^2 = \frac{8\pi G}{3}(\rho_m + \rho_{de}), \tag{20}$$

where $\rho_{de} = H/r_c$. The equation of state of dark energy $w_{de} = p_{de}/\rho_{de}$ is given by $w_{de} = -1/(1+\Omega_m)$ where $\Omega_m = 8\pi G\rho_m/3H^2$ [29]. Now let us consider the linear growth rate in this dark energy mode. Since gravity is not modified, the linear growth rate is given by

$$\widehat{\mathcal{L}}\delta_m = 0, \quad \widehat{\mathcal{L}} \equiv \frac{d^2}{dt^2} + 2H\frac{d}{dt} - \frac{\kappa^2}{2}\rho_m. \tag{21}$$

Fig. 1 shows the comoving distance in the self-accelerating universe, the dark energy model and ΛCDM model. Clearly, we cannot distinguish between the dark energy model and the self-accelerating universe. However, if we look at the linear growth rate of density perturbations, this degeneracy is broken.

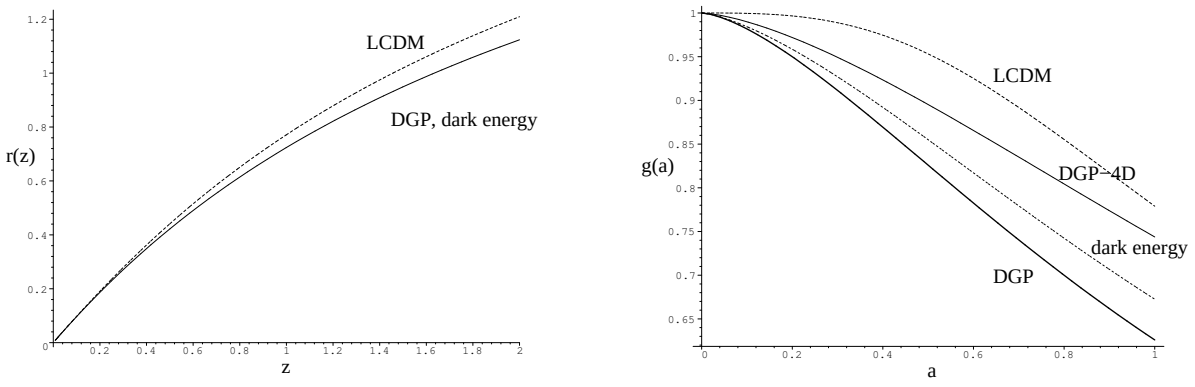

Figure 1: The comoving distance $r(z)$ and the growth rate $g(a) = \delta_m(a)/a$ are shown for the standard LCDM (long dashed), DGP (solid, thick) and the equivalent GR dark energy model. From [30].

3.3 $f(R)$ gravity models

We consider another class of modified theory of gravity that generalizes the Einstein-Hilbert action to include an arbitrary function of the scalar curvature R:

$$S = \int d^4x\sqrt{-g}\left[\frac{R + f(R)}{2\kappa^2} + L_{\rm m}\right], \tag{22}$$

where $\kappa^2 = 8\pi\, G$ and $L_{\rm m}$ is the Lagrangian of the ordinary matter. This theory is equivalent to the BD theory with $\omega_{\rm BD} = 0$ but there is a non-trivial potential [31]. This can be seen from the trace of modified Einstein equations:

$$3\Box f_R - R + f_R R - 2f = -\kappa^2\rho, \tag{23}$$

where $f_R = df/dR$ and $\Box$ is a Laplacian operator and we assumed matter dominated universe. We can identify f_R as the BD scalar field and its perturbations are defined as

$$\varphi = \delta f_R \equiv f_R - \overline{f}_R, \tag{24}$$

where the bar indicates that the quantity is evaluated on the cosmological background. In this paper, we assume $|f_R| \ll 1$ and $|f/R| \ll 1$. These conditions are necessary to have the background which is close to ΛCDM cosmology. Then the BD scalar perturbations satisfy

$$3\frac{1}{a^2}\nabla^2\varphi = -\kappa^2\bar{\rho}_m\delta + \delta R, \quad \delta R \equiv R(f_R) - R(\overline{f}_R). \tag{25}$$

This is noting but the equation for the BD scalar perturbations with $\omega_{\rm BD} = 0$ and the potential gives the non-linear interaction term

$$\mathcal{I}(\varphi) = \delta R(\varphi). \tag{26}$$

By linearizing the potential we find

$$M_1 = \overline{R}_f(t) \equiv \frac{d\overline{R}(f_R)}{df_R}. \tag{27}$$

The solutions for the metric perturbations are then given by

$$\frac{k^2}{a^2}\Phi = 4\pi G\left(\frac{2 + M_1a^2/k^2}{3 + M_1a^2/k^2}\right)\rho_m\delta_m, \tag{28}$$

$$\frac{k^2}{a^2}\Psi = 4\pi G\left(\frac{4 + M_1a^2/k^2}{3 + M_1a^2/k^2}\right)\rho_m\delta_m, \tag{29}$$

and the liner growth rate is given by

$$\widehat{\mathcal{L}}\delta_m = 0, \quad \widehat{\mathcal{L}} \equiv \frac{d^2}{dt^2} + 2H\frac{d}{dt} - \frac{\kappa^2}{2}\left(\frac{4 + M_1a^2/k^2}{3 + M_1a^2/k^2}\right)\rho_m. \tag{30}$$

In this paper, we consider a function $f(R)$ of the form [32]

$$f(R) \propto \frac{R^n}{AR^n + 1}, \tag{31}$$

where A is a constant with dimensions of length squared and n is an integer. In the following we take $n = 1$. In the limit $R \to 0$, $f(R) \to 0$ and there is no cosmological constant. For high curvature $AR \gg 1$, $f(R)$ can be expanded as

$$f(R) = -2\kappa^2\rho_\Lambda - f_{R0}\frac{\bar{R}_0}{R}, \tag{32}$$

where ρ_Λ is determined by A, $\bar{R}_0$ is the background curvature today and we defined f_{R0} as $f_{R0} = \bar{f}_R(R_0)$. As we mentioned before, we take $|f_{R0}| \ll 1$ and assume that the background expansion follows the ΛCDM history with the same ρ_Λ. The M_1 term determines the mass of the BD field $m_{\rm BD} = (M_1/3)^{1/2}$ as

$$m_{\rm BD}(t) \equiv \sqrt{\frac{R_f}{3}} = \left(\frac{R_0}{6|\bar{f}_R|}\sqrt{\frac{f_{R0}}{\bar{f}_R}}\right)^{1/2}. \tag{33}$$

Above the compton length $m_{\rm BD}^{-1}$, the BD scalar interaction decays exponentially and we recover GR. On small scales, we recover the BD theory with $\omega_{\rm BD} = 0$. Then the Newton constant is $4/3$ times large than GR. Thus the linear power spectrum acquires a scale dependent enhancement on small scales (Fig. 2).

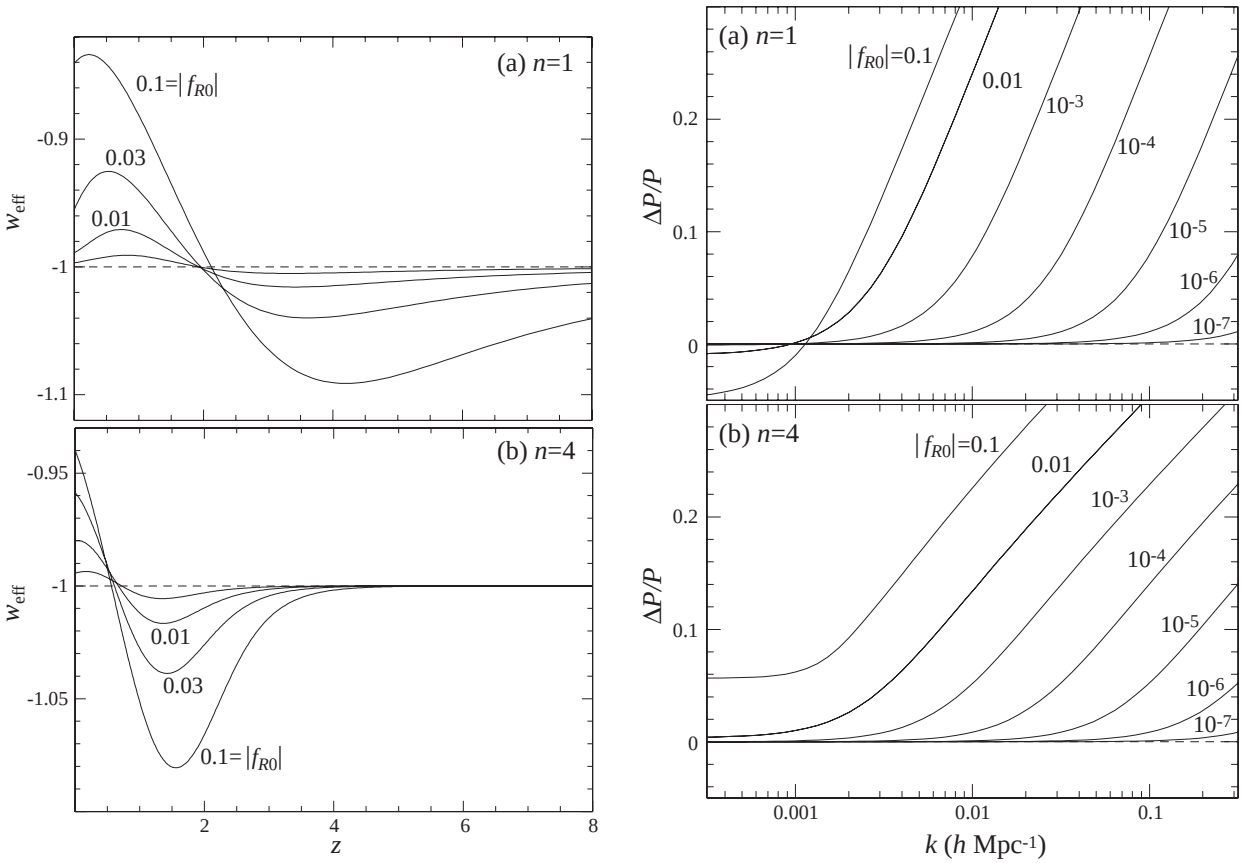

Figure 2: Left: Evolution of the effective equation of state w_{de} for $n = 1, 4$ for several values of the cosmological field amplitude today, f_{R0}. Right: Fractional change in the matter power spectrum $P(k)$ relative to ΛCDM for a series of the cosmological field amplitude today, f_{R0}, for $n = 1, 4$ models. For scales that are below the cosmological Compton wavelength during the acceleration epoch $k/a \gg M_1$ perturbation dynamics transition to the low-curvature regime where $\omega_{\rm BD} = 0$ and density growth is enhanced. From [32].

3.4 Distinguish between modified gravity and dark energy models

Fig.3 illustrates how one can detect the failure of GR from future observations. Suppose that our Universe is described by the DGP model. However, astronomers still try to fit the data by dark energy models in GR. For example, they use the parametrization of the equation of state of dark energy

$$w = w_0 + w_1 z. \tag{34}$$

Combining SN observations, CMB shift parameter and weak lensing, there appears an inconsistency. This is because weak lensing probes the growth of structure and the growth rate in the DGP model cannot be fitted by the growth rate in GR models given the same expansion history.

However, there is a subtlety in testing modified gravity models using large scale structure of the Universe. In any successful modified gravity models, we should recover GR on small scales. Indeed, unless there is an additional mechanism to screen the scalar interaction which changes the growth rate of structure formation, the modification of gravity contradicts to the stringent constraints on the deviation from GR at solar system scales. This mechanism affects the non-linear clustering of dark matter. We expect that the power-spectrum of dark matter perturbations approaches the one in the GR dark energy model with the same expansion history of the Universe because the modification of gravity disappears on small scales. Then the difference between a modified gravity model and a dark energy model with the same expansion history becomes smaller on smaller scales. This recovery of GR has important implications

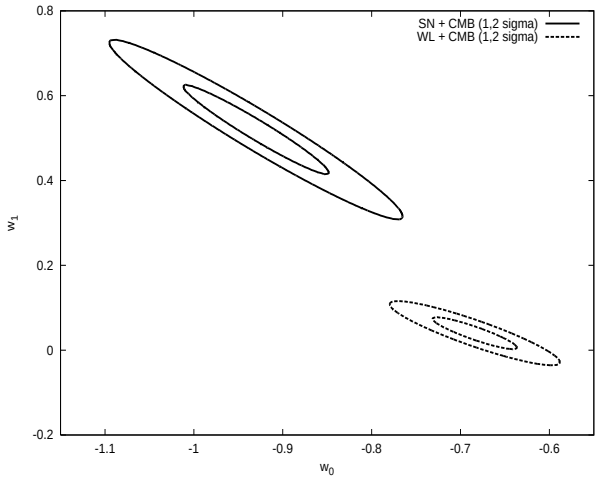

Figure 3: Equations of state found using two different combinations of data sets. Solid contours are for fits to SN Ia and CMB data, while dashed contours are for fits to weak lensing and CMB data. The significant difference (inconsistency) between the equations of state found using these two combinations is a signature of the DGP model. The inconsistency is an observational detection of the underlying modified gravity DGP model (assumed here to generate the data). From [8].

for weak lensing measurements because the strongest signals in weak lensing measurements come from non-linear scales.

In almost all of the literature including the result in Fig. 3, the non-linear power spectrum in modified gravity models was derived using the mapping formula between the linear power spectrum and the non-linear power spectrum. This is equivalent to assume that gravity is modified down to small scales in the same way as in the linear regime which contradicts to the solar system constraints. Thus this approach overestimates the difference between modified gravity models and dark energy models. This was explicitly shown by N-body simulations in the context of $f(R)$ gravity [33–35]. By tuning the function f, it is possible to make the Compton wavelength of the BD scalar short at solar system scales and screen the BD scalar interaction [32,36,37]. N-body simulations show that, due to this mechanism, the deviation of the non-linear power spectrum from GR is suppressed on small scales. It was shown that the mapping formula failed to describe this recovery of GR and it overestimated the deviation from GR.

4 Non-linear clustering in modified gravity models

In the section, we develop a formalism to treat the quasi non-linear evolution of the power spectrum in modified gravity models by properly taking into account the mechanism to recover GR on small scales [38]. Our formalism is based on the closure approximation which gives a closed set of evolution equations for the matter power spectrum [39]. These evolution equations reproduce the one-loop results of the standard perturbation theory (SPT) by replacing the quantities in the non-linear terms with linear-order ones. The SPT in GR is tested against N-body simulations extensively recently and it has been shown that, at the quasi non-linear regime, it can predict the power-spectrum with a sub-percent accuracy [40]. Although the validity regime of the perturbation theory is limited, it is the most relevant regime to distinguish between modified gravity models and dark energy models in GR because the difference in the two models is large in the linear and quasi-non-linear regime.

4.1 Evolution equations for perturbations

The Fourier transform of the fluid equations (8) and (9) become

$$H^{-1}\frac{\partial\delta(\boldsymbol{k})}{\partial t}+\theta(\boldsymbol{k})=-\int\frac{d^3\boldsymbol{k}_1d^3\boldsymbol{k}_2}{(2\pi)^3}\delta_{\rm D}(\boldsymbol{k}-\boldsymbol{k}_1-\boldsymbol{k}_2)\alpha(\boldsymbol{k}_1,\boldsymbol{k}_2)\,\theta(\boldsymbol{k}_1)\delta(\boldsymbol{k}_2), \tag{35}$$

$$H^{-1}\frac{\partial\theta(\boldsymbol{k})}{\partial t}+\left(2+\frac{\dot H}{H^2}\right)\theta(\boldsymbol{k})-\left(\frac{k}{a\,H}\right)^2\psi(\boldsymbol{k})=-\frac{1}{2}\int\frac{d^3\boldsymbol{k}_1d^3\boldsymbol{k}_2}{(2\pi)^3}\delta_{\rm D}(\boldsymbol{k}-\boldsymbol{k}_1-\boldsymbol{k}_2)\beta(\boldsymbol{k}_1,\boldsymbol{k}_2)\,\theta(\boldsymbol{k}_1)\theta(\boldsymbol{k}_2), \tag{36}$$

where the kernels in the Fourier integrals, α and β, are given by

$$\alpha(\boldsymbol{k}_1,\boldsymbol{k}_2)=1+\frac{\boldsymbol{k}_1\cdot\boldsymbol{k}_2}{|\boldsymbol{k}_1|^2},\qquad\beta(\boldsymbol{k}_1,\boldsymbol{k}_2)=\frac{(\boldsymbol{k}_1\cdot\boldsymbol{k}_2)\,|\boldsymbol{k}_1+\boldsymbol{k}_2|^2}{|\boldsymbol{k}_1|^2|\boldsymbol{k}_2|^2}. \tag{37}$$

We take into account the non-linear interaction terms $\mathcal{I}$ in the BD scalar equation. Due to the non-linear interactions, the potential ψ is couples to δ through the BD scalar φ in a fully non-linear way. To derive closed equations for δ and θ, we must employ the perturbative approach to Eq. (6). By solving Eq. (6) perturbatively assuming $\varphi<1$, ψ can be expressed in terms of δ as

$$-\left(\frac{k}{a}\right)^2\psi=\frac{1}{2}\,\kappa^2\,\overline{\rho}_{\rm m}\left[1+\frac{1}{3}\frac{(k/a)^2}{\Pi(k)}\right]\delta(\boldsymbol{k})+\frac{1}{2}\left(\frac{k}{a}\right)^2S(\boldsymbol{k}), \tag{38}$$

where

$$\Pi(k)=\frac{1}{3}\left((3+2\omega_{BD})\frac{k^2}{a^2}+M_1\right), \tag{39}$$

and $\kappa^2=8\pi G$. The function $S(\boldsymbol{k})$ is the non-linear source term which is obtained perturbatively using (4) as

$$\begin{aligned}S(\boldsymbol{k}) &= -\frac{1}{6\Pi(\boldsymbol{k})}\left(\frac{\kappa^2\,\overline{\rho}_{\rm m}}{3}\right)^2\int\frac{d^3\boldsymbol{k}_1d^3\boldsymbol{k}_2}{(2\pi)^3}\,\delta_{\rm D}(\boldsymbol{k}-\boldsymbol{k}_{12})M_2(\boldsymbol{k}_1,\boldsymbol{k}_2)\frac{\delta(\boldsymbol{k}_1)\,\delta(\boldsymbol{k}_2)}{\Pi(\boldsymbol{k}_1)\Pi(\boldsymbol{k}_2)}\\ &\quad-\frac{1}{18\,\Pi(\boldsymbol{k})}\left(\frac{\kappa^2\,\overline{\rho}_{\rm m}}{3}\right)^3\int\frac{d^3\boldsymbol{k}_1d^3\boldsymbol{k}_2d^3\boldsymbol{k}_3}{(2\pi)^6}\delta_{\rm D}(\boldsymbol{k}-\boldsymbol{k}_{123})\left\{M_3(\boldsymbol{k}_1,\boldsymbol{k}_2,\boldsymbol{k}_3)-\frac{M_2(\boldsymbol{k}_1,\boldsymbol{k}_2+\boldsymbol{k}_3)M_2(\boldsymbol{k}_2,\boldsymbol{k}_3)}{\Pi(\boldsymbol{k}_{23})}\right\}\\ &\quad\times\frac{\delta(\boldsymbol{k}_1)\,\delta(\boldsymbol{k}_2),\delta(\boldsymbol{k}_3)}{\Pi(\boldsymbol{k}_1)\Pi(\boldsymbol{k}_2)\Pi(\boldsymbol{k}_3)},\end{aligned} \tag{40}$$

The expression (40) is valid up to the third-order in δ.

The perturbation equations (35), (36) and (40) can be further reduced to a compact form by introducing the following quantity:

$$\Phi_a(\boldsymbol{k})=\begin{pmatrix}\delta(\boldsymbol{k})\\ -\theta(\boldsymbol{k})\end{pmatrix}. \tag{41}$$

We can write down the basic equations in a single form as

$$\begin{aligned}\frac{\partial\Phi_a(\boldsymbol{k};\eta)}{\partial\eta}+\Omega_{ab}(k;\eta)\,\Phi_b(\boldsymbol{k};\eta) &= \int\frac{d^3\boldsymbol{k}_1d^3\boldsymbol{k}_2}{(2\pi)^3}\,\delta_{\rm D}(\boldsymbol{k}-\boldsymbol{k}_{12})\,\gamma_{abc}(\boldsymbol{k}_1,\boldsymbol{k}_2;\eta)\,\Phi_b(\boldsymbol{k}_1;\eta)\Phi_c(\boldsymbol{k}_2;\eta)\\ &\quad+\int\frac{d^3\boldsymbol{k}_1d^3\boldsymbol{k}_2d^3\boldsymbol{k}_3}{(2\pi)^6}\,\delta_{\rm D}(\boldsymbol{k}-\boldsymbol{k}_{123})\,\sigma_{abcd}(\boldsymbol{k}_1,\boldsymbol{k}_2,\boldsymbol{k}_3;\eta)\,\Phi_b(\boldsymbol{k}_1;\eta)\Phi_c(\boldsymbol{k}_2\eta)\Phi_d(\boldsymbol{k}_3;\eta),\end{aligned} \tag{42}$$

where the time variable η is defined by $\eta=\ln a(t)$. The matrix Ω_{ab} is given by

$$\Omega_{ab}(k;\eta)=\begin{pmatrix}0 & -1\\ -\dfrac{\kappa^2}{2}\dfrac{\overline{\rho}_{\rm m}}{H^2}\left[1+\dfrac{1}{3}\dfrac{(k/a)^2}{\Pi(k)}\right] & 2+\dfrac{\dot H}{H^2}\end{pmatrix}. \tag{43}$$

From the $(2,1)$ component of Ω_{ab}, we can define the effective Newton constant as

$$G_{\rm eff} = G\left[1 + \frac{1}{3}\frac{(k/a)^2}{\Pi(k)}\right]. \tag{44}$$

If M_1=0, the effective Newton constant is given by

$$G_{\rm eff} = \frac{2(2+\omega_{\rm BD})}{3+2\omega_{\rm BD}}G. \tag{45}$$

For a positive $\omega_{\rm BD} > 0$, the effective gravitational constant is larger than GR and the gravitational force is enhanced. On the other hand, if $M_1 \gg k^2/a^2$, $G_{\rm eff}$ becomes G. The quantity γ_{abc} is the vertex function as in the GR case, but new non-vanishing components arise in the case of modified gravity:

$$\gamma_{abc}(\boldsymbol{k}_1,\boldsymbol{k}_2;\eta) = \begin{cases} \dfrac{1}{2}\,\alpha(\boldsymbol{k}_2,\boldsymbol{k}_1) & ; \quad (a,b,c)=(1,1,2), \\ \dfrac{1}{2}\,\alpha(\boldsymbol{k}_1,\boldsymbol{k}_2) & ; \quad (a,b,c)=(1,2,1), \\ -\dfrac{1}{12H^2}\left(\dfrac{\kappa\overline{\rho}_{\rm m}}{3}\right)^2\left(\dfrac{k_{12}^2}{a^2}\right)\dfrac{M_2(\boldsymbol{k}_1,\boldsymbol{k}_2)}{\Pi(\boldsymbol{k}_{12})\Pi(\boldsymbol{k}_1)\Pi(\boldsymbol{k}_2)} & ; \quad (a,b,c)=(2,1,1), \\ \dfrac{1}{2}\,\beta(\boldsymbol{k}_1,\boldsymbol{k}_2) & ; \quad (a,b,c)=(2,2,2), \\ 0 & ; \quad \text{otherwise.} \end{cases} \tag{46}$$

Here γ_{211} is absent in GR. Note that the symmetric properties of the vertex function, $\gamma_{abc}(\boldsymbol{k}_1,\boldsymbol{k}_2) = \gamma_{acb}(\boldsymbol{k}_2,\boldsymbol{k}_1)$, still hold in the modified theory of gravity. In Eq. (42), there appears another vertex function coming from the non-linearity of Poisson equation. The explicit form of the higher-order vertex function σ_{abcd} is given by

$$\sigma_{abcd}(\boldsymbol{k}_1,\boldsymbol{k}_2,\boldsymbol{k}_3;\eta) = \begin{cases} -\dfrac{1}{36H^2}\left(\dfrac{\kappa\overline{\rho}_{\rm m}}{3}\right)^3\left(\dfrac{k_{123}^2}{a^2}\right)\dfrac{M_3(\boldsymbol{k}_1,\boldsymbol{k}_2,\boldsymbol{k}_3)}{\Pi(\boldsymbol{k}_{123})\Pi(\boldsymbol{k}_1)\Pi(\boldsymbol{k}_2)\Pi(\boldsymbol{k}_3)} & \\ \times\left[1-\dfrac{1}{3}\dfrac{1}{M_3(\boldsymbol{k}_1,\boldsymbol{k}_2,\boldsymbol{k}_3)}\left\{\dfrac{M_2(\boldsymbol{k}_1,\boldsymbol{k}_2+\boldsymbol{k}_3)M_2(\boldsymbol{k}_2,\boldsymbol{k}_3)}{\Pi(\boldsymbol{k}_{23})}+\text{perm.}\right\}\right] & ; \quad (a,b,c,d)=(2,1,1,1), \\ 0 & ; \quad \text{otherwise.} \end{cases}$$

Again this term is absent in GR. The vertex function $\sigma_{abcd}(\boldsymbol{k}_1,\boldsymbol{k}_2,\boldsymbol{k}_3;\eta)$ defined above is invariant under the permutation of $b \leftrightarrow c \leftrightarrow d$ or $\boldsymbol{k}_1 \leftrightarrow \boldsymbol{k}_2 \leftrightarrow \boldsymbol{k}_3$.

4.2 Evolution equations for power spectrum

In this paper, we are especially concerned with the evolution of the matter power spectrum, defined by

$$\left\langle \Phi_a(\boldsymbol{k};\eta)\Phi_b(\boldsymbol{k}';\eta)\right\rangle = (2\pi)^3\,\delta_{\rm D}(\boldsymbol{k}+\boldsymbol{k}')\,P_{ab}(|\boldsymbol{k}|;\eta). \tag{47}$$

Here the bracket $\langle\cdot\rangle$ stands for the ensemble average. Note that we obtain the three different power spectra: $P_{\delta\delta}$ from $(a,b)=(1,1)$, $-P_{\delta\theta}$ from $(a,b)=(1,2)$ and $(2,1)$, and $P_{\theta\theta}$ from $(a,b)=(2,2)$.

Let us consider how to compute the power spectrum. In the standard treatment of perturbation theory, we first solve Eq.(42) by expanding the quantity Φ_a as $\Phi_a = \Phi_a^{(1)} + \Phi_a^{(2)} + \cdots$. Substituting the perturbative solutions into the definition (47), we obtain the weakly non-linear corrections to the power spectrum. This treatment is straightforward, but it is not suited for numerical calculations. Furthermore, successive higher-order corrections generally converge poorly and SPT will be soon inapplicable at late-time stage of the non-linear evolution. Here in order to deal with modified gravity models in which

analytical calculations are intractable in many cases, we take another approach. Our approach is based on the closure approximation proposed by Ref. [39], in which the evolution of power spectrum is obtained numerically by solving a closed set of evolution equations.

Provided the basic equation (42), the evolution equation for power spectrum can be derived by truncating the infinite chain of the moment equations with a help of perturbative calculation, called closure approximation. We skip the details of the derivation and present the final results. Readers interested in the derivation can refer to Ref. [39]. The resultant evolution equations are the coupled equations characterized by the three statistical quantities including the power spectrum. We define

$$\begin{aligned}
&\Big\langle \Phi_a(\boldsymbol{k};\eta)\Phi_b(\boldsymbol{k}';\eta')\Big\rangle = (2\pi)^3\,\delta_{\rm D}(\boldsymbol{k}+\boldsymbol{k}')\,R_{ab}(|\boldsymbol{k}|;\eta,\eta') \quad ; \qquad \eta>\eta', \\
&\Big\langle \frac{\delta\Phi_a(\boldsymbol{k};\eta)}{\delta\Phi_b(\boldsymbol{k}';\eta')}\Big\rangle = \delta_{\rm D}(\boldsymbol{k}-\boldsymbol{k}')\,G_{ab}(|\boldsymbol{k}|;\eta,\eta') \quad ; \qquad \eta\geq\eta'.
\end{aligned} \tag{48}$$

The quantities R_{ab} and G_{ab} respectively denote the cross spectra between different times and the non-linear propagator. Note that $R_{ab}\neq R_{ba}$, in general. Then, the closure equations become

$$\begin{aligned}
\widehat{\Sigma}_{abcd}(k;\eta)\,P_{cd}(k;\eta) &= \int\frac{d^3\boldsymbol{q}}{(2\pi)^3}\Big[\gamma_{apq}(\boldsymbol{q},\boldsymbol{k}-\boldsymbol{q};\eta)\,F_{bpq}(-\boldsymbol{k},\boldsymbol{q},\boldsymbol{k}-\boldsymbol{q};\eta)+\gamma_{bpq}(\boldsymbol{q},-\boldsymbol{k}-\boldsymbol{q};\eta)\,F_{apq}(\boldsymbol{k},\boldsymbol{q},-\boldsymbol{k}-\boldsymbol{q};\eta)\Big] \\
&\quad +3\int\frac{d^3\boldsymbol{q}}{(2\pi)^3}\Big[\sigma_{apqr}(\boldsymbol{q},-\boldsymbol{q},\boldsymbol{k};\eta)P_{pq}(q;\eta)P_{rb}(k;\eta)+\sigma_{bpqr}(\boldsymbol{q},-\boldsymbol{q},-\boldsymbol{k};\eta)\,P_{pq}(q;\eta)P_{ra}(k;\eta)\Big],
\end{aligned} \tag{49}$$

$$\begin{aligned}
\widehat{\Lambda}_{ab}(k;\eta)\,R_{bc}(k;\eta,\eta') &= \int\frac{d^3\boldsymbol{q}}{(2\pi)^3}\gamma_{apq}(\boldsymbol{q},\boldsymbol{k}-\boldsymbol{q};\eta)\,K_{cpq}(-\boldsymbol{k},\boldsymbol{q},\boldsymbol{k}-\boldsymbol{q};\eta,\eta') \\
&\quad +3\int\frac{d^3\boldsymbol{q}}{(2\pi)^3}\sigma_{apqr}(\boldsymbol{q},-\boldsymbol{q},\boldsymbol{k};\eta)P_{pq}(q;\eta)R_{rc}(k;\eta,\eta'),
\end{aligned} \tag{50}$$

$$\begin{aligned}
\widehat{\Lambda}_{ab}(k;\eta)\,G_{bc}(k|\eta,\eta') &= 4\int_{\eta'}^{\eta}d\eta''\int\frac{d^3\boldsymbol{q}}{(2\pi)^3}\gamma_{apq}(\boldsymbol{q},\boldsymbol{k}-\boldsymbol{q};\eta)\,\gamma_{lrs}(-\boldsymbol{q},\boldsymbol{k};\eta'')G_{ql}(|\boldsymbol{k}-\boldsymbol{q}||\eta,\eta'')R_{pr}(q;\eta,\eta'')G_{sc}(k|\eta'',\eta'), \\
&\quad +3\int\frac{d^3\boldsymbol{q}}{(2\pi)^3}\sigma_{apqr}(\boldsymbol{q},-\boldsymbol{q},\boldsymbol{k};\eta)P_{pq}(q;\eta)G_{rc}(k|\eta,\eta'),
\end{aligned} \tag{51}$$

where the operators $\widehat{\Sigma}_{abcd}$ and $\widehat{\Lambda}_{ab}$ are defined as

$$\widehat{\Sigma}_{abcd}(k;\eta)=\delta_{ac}\delta_{bd}\frac{\partial}{\partial\eta}+\delta_{ac}\Omega_{bd}(k;\eta)+\delta_{bd}\Omega_{ac}(k;\eta),\quad \widehat{\Lambda}_{ab}(k;\eta)=\delta_{ab}\frac{\partial}{\partial\eta}+\Omega_{ab}(k;\eta), \tag{52}$$

The explicit expressions for the kernels F_{apq} and K_{cpq} are summarized as

$$\begin{aligned}
F_{apq}(\boldsymbol{k},\boldsymbol{p},\boldsymbol{q};\eta) &= 2\int_{\eta_0}^{\eta}d\eta''\,\Big[\,2\,G_{ql}(q|\eta,\eta'')\,\gamma_{lrs}(\boldsymbol{k},\boldsymbol{p};\eta'')\,R_{ar}(k;\eta,\eta'')R_{ps}(p;\eta,\eta'') \\
&\qquad +\;G_{al}(k|\eta,\eta'')\,\gamma_{lrs}(\boldsymbol{p},\boldsymbol{q};\eta'')\,R_{pr}(p;\eta,\eta'')\,R_{qs}(q;\eta,\eta'')\,\Big],
\end{aligned} \tag{53}$$

$$\begin{aligned}
&K_{cpq}(\boldsymbol{k}',\boldsymbol{p},\boldsymbol{q};\eta,\eta') \\
&\quad = \;4\int_{\eta_0}^{\eta}d\eta''\;G_{ql}(q|\eta,\eta'')\,\gamma_{lrs}(\boldsymbol{k}',\boldsymbol{p};\eta'')\,R_{ps}(p;\eta,\eta'') \\
&\qquad\qquad \times\Big\{R_{cr}(k';\eta',\eta'')\Theta(\eta'-\eta'')+R_{rc}(k';\eta'',\eta')\Theta(\eta''-\eta')\Big\} \\
&\quad +\;2\int_{\eta_0}^{\eta'}d\eta''\,G_{cl}(k'|\eta',\eta'')\,\gamma_{lrs}(\boldsymbol{p},\boldsymbol{q};\eta'')\,R_{pr}(p;\eta,\eta'')\,R_{qs}(q;\eta,\eta'').
\end{aligned} \tag{54}$$

The closure equations (50)–(51) are the integro-differential equations involving several non-linear terms, in which the information of the higher-order corrections in SPT is encoded. Thus, replacing all statistical quantities in these non-linear terms with linear-order ones, the solutions of closure equations automatically reproduce the leading-order results of SPT, called one-loop power spectra. Further, fully

non-linear treatment of the closure equations is a non-perturbative description of the power spectra, and have an ability to predict the matter power spectra accurately, beyond one-loop SPT. Strictly speaking, the non-linear terms in the right-hand side of Eqs. (50)–(51) have only the information of the one-loop corrections. However, it has been shown in Ref. [39] that the present formulation is equivalent to the one-loop level of renormalized perturbation theory [41], and even the leading-order approximation still contain some non-perturbative effects. The application of the closure approximation, together with the detailed comparison with N-body simulations, is presented in Refs. [40, 42].

In this paper, we mainly use the closure equations for the purpose of computing the one-loop power spectra. The results for fully non-linear treatment of the closure equations will be presented elsewhere. The numerical scheme to solve the closure equations is basically the same as described in Ref. [39]. In Appendix A, we briefly review the numerical scheme and summarize several modifications.

Before closing this section, we note here that the resultant equations (50)–(51) contain the additional non-linear terms originating from the modification of the Poisson equation (see Eq.(38)). In particular, for the terms containing the higher-order vertex function σ_{abcd} can be effectively absorbed into the matrix Ω_{ab}. Since the non-vanishing contribution of the higher-order vertex function only comes from σ_{2111}, this means that the effective Newton constant $G_{\rm eff}$ defined by (44) is renormalized as $G_{\rm eff} \to G_{\rm eff} + \delta G_{\rm eff}$, with $\delta G_{\rm eff}$ given by

$$\delta G_{\rm eff} = \frac{3H^2}{4\pi\,\rho_m} \int \frac{d^3\boldsymbol{q}}{(2\pi)^3}\, \sigma_{2111}(\boldsymbol{q}, -\boldsymbol{q}, \boldsymbol{k}; \eta)\, P_{11}(q;\eta). \tag{55}$$

This is a clear manifestation of the mechanism that non-linear clustering does generically alter the growth rate of the structure formation through the renormalisation of the Newton constant and, due to this mechanism, successful modified gravity models are expected to recover GR on small scales.

5 Non-linear power spectrum in modified gravity models

In this section, we show solutions for the non-lienar power spectrum in two examples, DGP models and $f(R)$ gravity models. We also extend these results to fully non-linear scales using the so-called Parametrized Post Friedmann (PPF) framework.

5.1 PPF formalism

Sawicki and Hu proposed a fitting formula for the non-linear power spectrum in modified gravity models [5]. The fitting formula based on the observation that the non-linear power spectrum should approach the one in the GR model that follows the same expansion history of the Universe due to the recovery of GR on small scales. They postulate that the full non-linear power spectrum in a modified gravity model is given by the formula

$$P(k,z) = \frac{P_{\rm non-GR}(k,z) + c_{\rm nl}\Sigma^2(k,z) P_{\rm GR}(k,z)}{1 + c_{\rm nl}\Sigma^2(k,z)}, \tag{56}$$

where z is a red-shift. Here $P_{\rm non-GR}(k,z)$ is the non-linear power spectrum which is obtained without the non-linear interactions that are responsible for the recovery of GR. This is equivalent to assume that gravity is modified down to the small scales in the same way as in the linear regime. $P_{\rm GR}(k,z)$ is the non-linear power spectrum obtained in the GR dark energy model that follows the same expansion history of the Universe as in the modified gravity model. The function $\Sigma^2(k,z)$ determines the degree of non-linearity at a relevant wavenumber k. They propose to take $\Sigma^2(k) = k^3 P_{\rm lin}(k,z)/2\pi^2$, where $P_{\rm lin}(k,z)$ is the linear power spectrum in the modified gravity model. Finally, $c_{\rm nl}$ is a parameter in this framework which controls the scale at which the theory approaches GR.

Once we obtain the quasi non-linear power spectrum, we can check whether the PPF framework works and determines $c_{\rm nl}$ in the quasi non-linear regime. In our formalism, $P_{\rm non-GR}(k,z)$ is obtained by neglecting the non-linear interaction $\mathcal{I}$. $P_{\rm GR}(k,z)$ can be obtained by taking $\omega_{BD} \to \infty$ limit and also neglecting $\mathcal{I}$. We again consider two explicit examples.

5.2 DGP models

In DGP models, the BD scalar acquires a large second order interaction given by

$$\mathcal{I}(\varphi) = \frac{r_c^2}{a^4}\Big[(\nabla^2\varphi)^2 - (\nabla_i\nabla_j\varphi)^2\Big]. \tag{57}$$

Note that r_c is tuned to be the present-day horizon scale. Thus this second order term has a large effect. The higher order terms than the second order are suppressed by the additional powers of the 4D Planck scale and, in the Newtonian limit, we can safely ignore them. Therefore, in this model, we have

$$M_1 = 0, \quad M_2(\boldsymbol{k}_1, \boldsymbol{k}_2) = 2\frac{r_c^2}{a^4}\Big[k_1^2k_2^2 - (\boldsymbol{k}_1\cdot\boldsymbol{k}_2)^2\Big], \quad M_3 = 0, \tag{58}$$

$$\Pi(k,\eta) = \beta(\eta)\frac{k^2}{a^2}. \tag{59}$$

In this paper, we only consider the self-accelerating branch solutions and use the best-fit cosmological parameters for the flat self-accelerating universe: $\Omega_m = 0.257, \Omega_b = 0.0544, h = 0.66, n_s = 0.998$ [28]. In the left panel of Fig. 4, the solid (black) line shows the fractional difference between the power spectrum in DGP models and dark energy models that follow the same expansion history obtained by solving the linearized closure equation numerically. The dashed (red) line shows the result obtained by neglecting the non-linear term M_2, $P_{\rm non-GR}$. we can see that the non-linear interaction enhances the non-linear power spectrum. This is natural because in the self-accelerating branch, the linear growth rate is suppressed compared to the GR model that follows the same expansion history due to the negative BD parameter $\omega_{\rm BD} < 0$ which makes the Newton constant smaller than GR. This is closely related to the fact that the BD scalar becomes a ghost in this model. Classically, the ghost mediates a repulsive force and suppresses the gravitational collapse. The non-linear interaction makes the theory approach GR. Thus it effectively increases the Newton constant by screening the BD scalar. Then the power-spectrum receives an enhancement compared with the case without the non-linear interaction.

For DGP models, we find that the PPF formalism with

$$\Sigma^2(k,z) = \frac{k^3}{2\pi^2}P_{\rm lin}(k,z) \tag{60}$$

as proposed by Sawicki and Hu gives a nice fit to the results obtained in the perturbation theory. We find that by allowing the time dependence in $c_{\rm nl}$, it is possible to recover the solutions for t he non-linear power spectrum very well within the validity regime of the perturbation theory. At $z = 0$, $c_{\rm nl}$ is given by 0.3 and there is a slight redshift dependence (the dotted (blue) line in the left panel of Fig. 4).

Armed with this result, it is tempting to extend our analysis to the fully non-linear regime. In GR, there are several fitting formulae which provide the mapping between the linear power spectrum and non-linear power spectrum. It is impossible to apply these mapping formulae to modified gravity models as the mapping does not take into account the non-linear interaction terms in the Poisson equation $\mathcal{I}$. If we apply the GR mapping formula to the linear power spectrum, we would get the non-linear power spectrum without $\mathcal{I}$, $P_{\rm non-GR}(k)$. In fact, there exist N-body simulations in DGP models performed by neglecting the non-linear interaction terms [43]. It was shown that the power spectrum obtained in these N-body simulations can be fitted well by the mapping formulae in GR. The mapping formulae should be valid in GR models, so we can also predict $P_{\rm GR}(k)$. Then using the PPF formalism (56), we can predict the non-linear power spectrum if $c_{\rm nl}$ is known. In the right panel of Fig. 4, we plotted the fractional difference between the power spectrum in the DGP model and the GR model with the same expansion history. We used the fitting formula developed by Smith et.al. [44]. If we could extrapolate the result in the quasi non-linear regime, we would have $c_{\rm nl} = 0.3$ at $z = 0$. If this is correct, we find that even at $k = 10{\rm Mpc\ h^{-1}}$, the difference between the power spectrum in DGP and that in the equivalent GR model remains at 7% level. This is crucial to distinguish between the two models using weak lensing as the signal to noise ratio is larger on smaller scales. Of course, we should emphasize that there is no guarantee that $c_{\rm nl}$ measured in the quasi non-linear regime is valid down to the fully non-linear scales and this should be tested using N-body simulations. Still there is no N-body simulation available in DGP models and it would be important to test the prediction against N-body simulations.

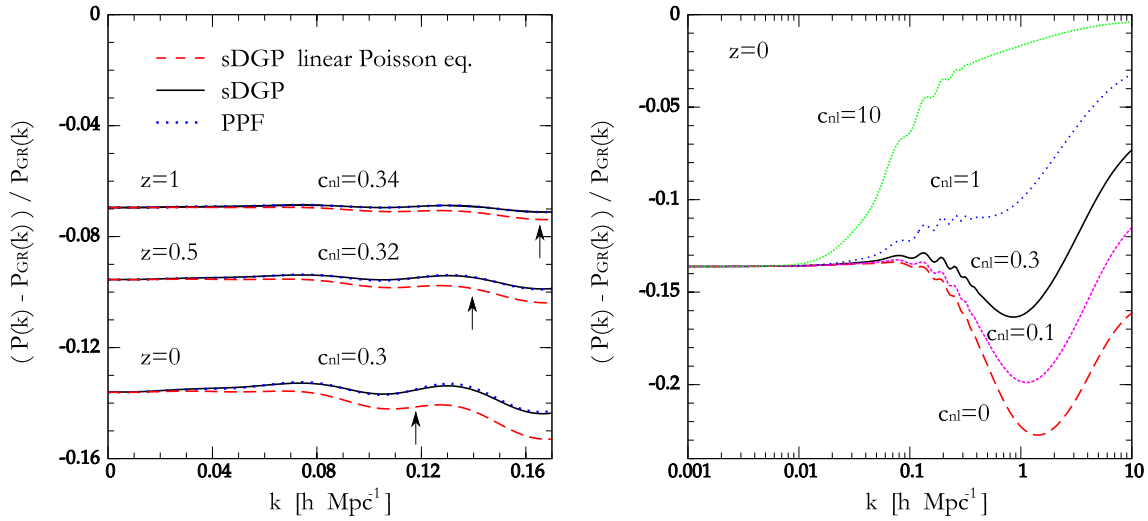

Figure 4: The fractional difference between the power spectrum in the DGP model and the one in the GR model which has the same expansion history as the DGP. The solid (black) line shows the perturbation theory solution and the dashed (red) line shows the perturbation theory solution without the non-linear interaction terms in the Poisson equation. The dotted (blue) line shows the PPF fitting. By allowing the redshift dependence of $c_{\rm nl}$, we can fit the power spectrum very well within the validity regime of the perturbation theory indicated by arrows. The right panel shows the results at $z = 0$ obtained from the fitting formula by Smith et.al. for $P_{\rm non-GR}$ and $P_{\rm GR}$. If $c_{\rm nl} = 0.3$ obtained by the perturbation theory is applicable, the the solid (black) line is the prediction on non-linear scales. The cosmological parameters are the same as in Fig 1.

5.3 $f(R)$ gravity models

Next, we consider $f(R)$ gravity models. In these models the potential gives the non-linear interaction term

$$\mathcal{I}(\varphi) = \delta R(\varphi). \tag{61}$$

Then we find

$$M_1 = \overline{R}_f(\eta) \equiv \frac{d\overline{R}(f_R)}{df_R}, \quad M_2 = \overline{R}_{ff}(\eta) \equiv \frac{d^2\overline{R}(f_R)}{df_R^2}, \quad M_3 = \overline{R}_{fff}(\eta) \equiv \frac{d^3\overline{R}(f_R)}{df_R^3},$$
$$\Pi(k,\eta) = \left(\frac{k}{a}\right)^2 + \frac{\overline{R}_f(\eta)}{3}.$$

In this paper, we consider the model described in section 3.3 where $f(R)$ is given by Eq. (31). We adopt the cosmological parameters given by $f_{R0} = 10^{-4}, n_s = 0.958, \Omega_m = 0.24, \Omega_b = 0.046, \Omega_\Lambda = 0.76, h = 0.73$. In this model, the solar system constraints are satisfied but it has been pointed that the chameleon mechanism does not work for strong gravity and Neutron stars cannot exist [45, 46]. A fine-tuned higher curvature corrections to $f(R)$ are needed to cure the problem [47]. In this paper, we perturbatively take into account the chameleon mechanism in the cosmological background and the quasi non-linear power spectrum would be insensitive to the high curvature corrections.

The left panel of Fig. 5, the solid (black) line shows the fractional difference between the power spectrum in $f(R)$ models and ΛCDM by solving the linearized closure equation numerically. The dashed (red) line shows the result obtained by neglecting the non-linear terms, $P_{\rm non-GR}$. The linear power spectrum acquires a scale dependent enhancement on small scales due to the larger effective Newton constant $G_{\rm eff} = 4G/3$. The higher order terms $M_i (i > 1)$ are responsible for the suppression of this modification of gravity on small scales. Thus the non-linear interaction terms $\mathcal{I}$ suppress the non-linear power spectrum.

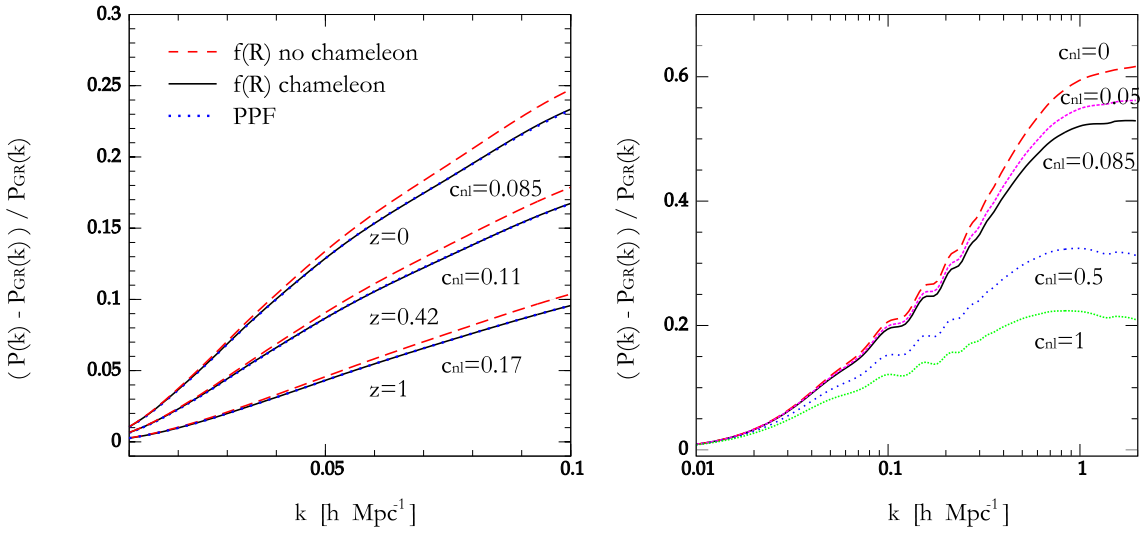

Figure 5: The same as Fig. 4 in $f(R)$ gravity models

As in the DGP model, we first check if we can reproduce the perturbation theory results by the PPF fitting. We find that the fitting is not very good if we adopt $\Sigma(k,z)$ as is proposed by Hu and Sawicki. Instead, if we choose $\Sigma(k,z)$ as

$$\Sigma^2(k,z) = \left(\frac{k^3}{2\pi^2}P_{\rm lin}(k,z)\right)^{1/3}, \tag{62}$$

the solutions in the perturbation theory are fitted by the PPF formula very well by allowing the redshift dependence in $c_{\rm nl}$. At $z=0$, $c_{\rm nl}=0.085$ gives an excellent fitting to the power spectrum within the validity regime of the perturbation theory. In Fig. 5, we also show the prediction for the fractional difference between the power spectrum in $f(R)$ theory and that in ΛCDM model in fully non-linear regime for several $c_{\rm nl}$.

In $f(R)$ gravity models, it is possible to check our predictions against the No-body simulations. Fig. 6 shows the comparison between the PPF prediction and N-body simulations. The dashed line corresponds to non-Chameleon case with $c_{\rm nl}=0$. The corresponding N-body results are shown by triangles. We again used the fitting formula by Smith et.al. to derive the non-linear power spectrum from the linear power spectrum. Compared with the N-body results, the formula by Smith et.al. slightly underestimates the power spectrum around $0.03h{\rm Mpc}^{-1} < k < 0.5h{\rm Mpc}^{-1}$ and overestimates the power at $k > 0.5h{\rm Mpc}^{-1}$ though N-body simulations have large errors in this regime. The solid line shows the case with the chameleon mechanism. Again the PPF formula underestimates the power spectrum in the same region as the non-chameleon case. If we take the ratio between the non-chameleon case and chameleon case, the PPF formalism nicely recovers the N-body results up to $k\sim 0.5h{\rm Mpc}^{-1}$.Beyond that, N-body simulations have large errors. We should emphasize that the perturbation theory is valid only up to $k=0.08h{\rm Mpc}^{-1}$ at $z=0$. Thus the PPF formula using $c_{\rm nl}$ derived by the perturbation theory describe the effect of the chameleon mechanism on non-linear scales beyond the validity regime of the perturbation theory.

This observation suggests that an improvement of the PPF formalism can be made by getting a more accurate power spectrum without the chameleon mechanism because the PPF formalism describes the effect of the chameleon mechanism very well. In order to demonstrate this fact, we derive the power spectrum without the chameleon mechanism $P_{\rm non-GR}$ by interpolating the N-body results. Using this power spectrum as the non-chameleon power spectrum in the PPF formula, we find that the power spectrum with the chameleon mechanism can be very well described by the PPF formula where $c_{\rm nl}$ is derived by the perturbation theory. We should emphasize that the ratio between the power spectra with and without the chameleon mechanism is insensitive to the non-chameleon power spectrum. This also indicates that the PPF formalism with $c_{\rm nl}$ determined by the perturbation theory describes the effect of the chameleon mechanism very well at least up to $k\sim 0.5h{\rm Mpc}^{-1}$. For larger k, N-body simulations also do not have enough resolutions and it is difficult to tell whether this extrapolation is good or not. More

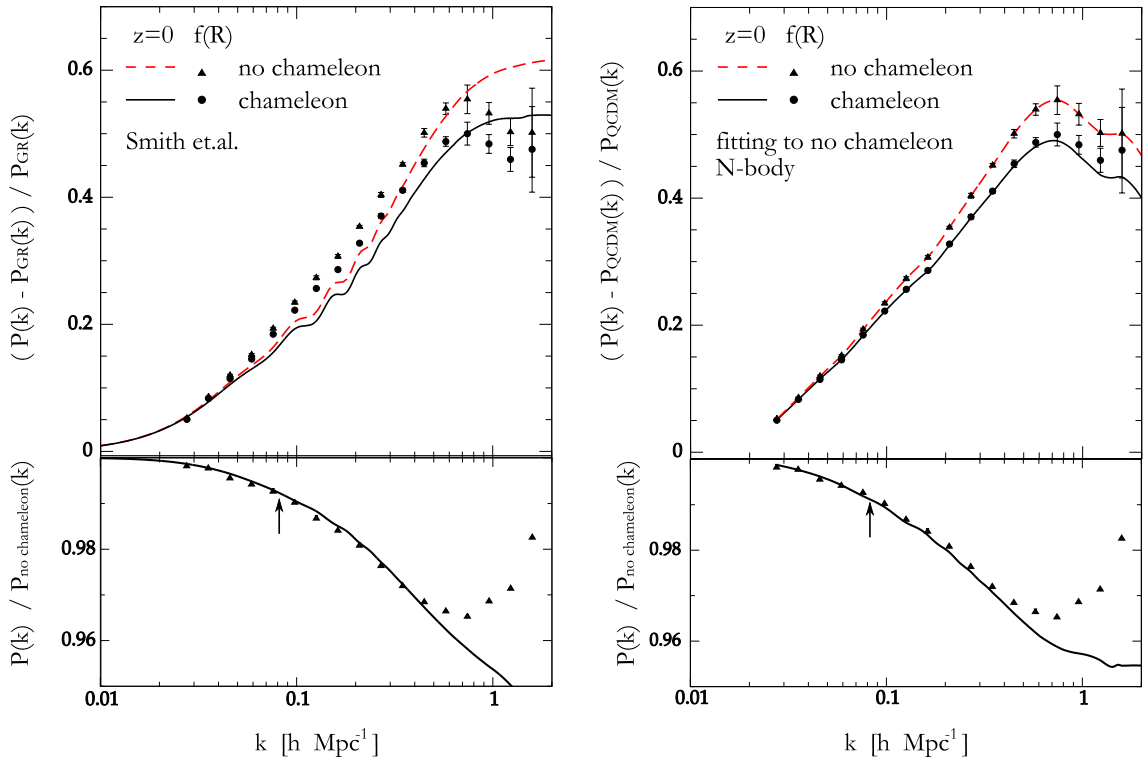

Figure 6: Comparison between the PPF prediction and N-body simulations. In the left panel, Smith et.al. fitting formula is used to predict $P_{\rm non}$ and $P_{\rm GR}$. We used $c_{\rm nl}$ determined by the perturbation theory $c_{\rm nl} = 0.085$ at $z = 0$. In the left panel, we fitted N-body results without the chameleon mechanism to derive $P_{\rm non}$.

detailed study is needed to address the power spectrum at larger k, but the PPF formalism is likely to give a promising way to develop a fitting formula for the non-linear power spectrum in modified gravity models.

6 Conclusion

Modified gravity models are still under developments and still no fully consistent models are developed. Although DGP models and $f(R)$ models provide us interesting indications of the nature of modified gravity models, these models face severe problems. However, the general feature of these models that large scale structure of the Universe is affected by the modification of gravity would be valid in many modified gravity models. This feature can be used to distinguish modified gravity models from dark energy models in GR. In the study of large scale structure in modified gravity models, an emphasis should be made on the recovery of GR on small scales which is essential to evade the stringent constraints on the deviation from GR at solar system scales. Any successful modified gravity models should have a mechanism to recover GR at solar system scales and this mechanism affects the non-linear power spectrum of dark matter perturbations. The study of non-linear clustering of dark matter has just started but the perturbations theory and N-body simulations begin to reveal the nature of non-linear clustering in modified gravity models. Cosmology is now experiencing a golden age of discovery driven by on-going and future massive new surveys of the sky. Rapid progress in cosmological observations will enable us to distinguish modified gravity models from dark energy models in general relativity, and to provide a test of general relativity on cosmological scales

Acknowledgement

I would like to thank my collaborators in this subject. This review is mainly based on a paper with Takashi Hiramatsu and Atsushi Taruya [38]. KK is supported by ERC, RCUK and STFC.

References

[1] S. Nojiri and S. D. Odintsov, ECONF **C0602061**, 06 (2006), hep-th/0601213.

[2] K. Koyama, Gen. Rel. Grav. **40**, 421 (2008), 0706.1557.

[3] R. Durrer and R. Maartens, (2008), 0811.4132.

[4] R. Durrer and R. Maartens, Gen. Rel. Grav. **40**, 301 (2008), 0711.0077.

[5] W. Hu and I. Sawicki, (2007), arXiv:0708.1190 [astro-ph].

[6] J.-P. Uzan and F. Bernardeau, Phys. Rev. **D64**, 083004 (2001), hep-ph/0012011.

[7] A. Lue, R. Scoccimarro, and G. Starkman, Phys. Rev. **D69**, 044005 (2004), astro-ph/0307034.

[8] M. Ishak, A. Upadhye, and D. N. Spergel, Phys. Rev. **D74**, 043513 (2006), astro-ph/0507184.

[9] L. Knox, Y.-S. Song, and J. A. Tyson, Phys. Rev. **D74**, 023512 (2006).

[10] K. Koyama, JCAP **0603**, 017 (2006), astro-ph/0601220.

[11] T. Chiba and R. Takahashi, Phys. Rev. **D75**, 101301 (2007), astro-ph/0703347.

[12] L. Amendola, M. Kunz, and D. Sapone, JCAP **0804**, 013 (2008), 0704.2421.

[13] K. Yamamoto, D. Parkinson, T. Hamana, R. C. Nichol, and Y. Suto, Phys. Rev. **D76**, 023504 (2007), 0704.2949.

[14] K. Yamamoto, T. Sato, and G. Huetsi, Prog. Theor. Phys. **120**, 609 (2008), 0805.4789.

[15] Y.-S. Song and W. J. Percival, (2008), 0807.0810.

[16] M. Kunz and D. Sapone, Phys. Rev. Lett. **98**, 121301 (2007), astro-ph/0612452.

[17] B. Jain and P. Zhang, (2007), 0709.2375.

[18] Y.-S. Song and K. Koyama, JCAP **01**, 048 (2009), 0802.3897.

[19] Y.-S. Song and O. Dore, (2008), 0812.0002.

[20] J. Khoury and A. Weltman, Phys. Rev. **D69**, 044026 (2004), astro-ph/0309411.

[21] G. R. Dvali, G. Gabadadze, and M. Porrati, Phys. Lett. **B485**, 208 (2000), hep-th/0005016.

[22] M. A. Luty, M. Porrati, and R. Rattazzi, JHEP **09**, 029 (2003), hep-th/0303116.

[23] T. Tanaka, Phys. Rev. **D69**, 024001 (2004), gr-qc/0305031.

[24] K. Koyama and F. P. Silva, Phys. Rev. **D75**, 084040 (2007), hep-th/0702169.

[25] C. Deffayet, G. R. Dvali, G. Gabadadze, and A. I. Vainshtein, Phys. Rev. **D65**, 044026 (2002), hep-th/0106001.

[26] C. Deffayet, Phys. Lett. **B502**, 199 (2001), hep-th/0010186.

[27] K. Koyama, Class. Quant. Grav. **24**, R231 (2007), 0709.2399.

[28] W. Fang *et al.*, Phys. Rev. **D78**, 103509 (2008), 0808.2208.

[29] A. Lue, R. Scoccimarro, and G. D. Starkman, Phys. Rev. **D69**, 124015 (2004), astro-ph/0401515.

[30] K. Koyama and R. Maartens, JCAP **0601**, 016 (2006), astro-ph/0511634.

[31] T. Chiba, Phys. Lett. **B575**, 1 (2003), astro-ph/0307338.

[32] W. Hu and I. Sawicki, Phys. Rev. **D76**, 064004 (2007), 0705.1158.

[33] H. Oyaizu, Phys. Rev. **D78**, 123523 (2008), 0807.2449.

[34] H. Oyaizu, M. Lima, and W. Hu, Phys. Rev. **D78**, 123524 (2008), 0807.2462.

[35] F. Schmidt, M. V. Lima, H. Oyaizu, and W. Hu, (2008), 0812.0545.

[36] A. A. Starobinsky, JETP Lett. **86**, 157 (2007), 0706.2041.

[37] S. A. Appleby and R. A. Battye, Phys. Lett. **B654**, 7 (2007), 0705.3199.

[38] K. Koyama, A. Taruya, and T. Hiramatsu, (2009), in preparation.

[39] A. Taruya and T. Hiramatsu, (2007), 0708.1367.

[40] T. Nishimichi *et al.*, (2008), 0810.0813.

[41] M. Crocce and R. Scoccimarro, Phys. Rev. **D73**, 063519 (2006), astro-ph/0509418.

[42] A. Taruya, T. Nishimichi, S. Saito, and T. Hiramatsu, (2009), in preparation.

[43] I. Laszlo and R. Bean, Phys. Rev. **D77**, 024048 (2008), 0709.0307.

[44] The Virgo Consortium, R. E. Smith *et al.*, Mon. Not. Roy. Astron. Soc. **341**, 1311 (2003), astro-ph/0207664.

[45] A. V. Frolov, Phys. Rev. Lett. **101**, 061103 (2008), 0803.2500.

[46] T. Kobayashi and K.-i. Maeda, (2008), 0807.2503.

[47] T. Kobayashi and K.-i. Maeda, Phys. Rev. **D79**, 024009 (2009), 0810.5664.

Perturbation theory of N point mass gravitational lens

Hideki Asada[1]

Faculty of Science and Technology, Hirosaki University, Hirosaki 036-8561, Japan

Abstract

We make the first systematic attempt to determine using perturbation theory the positions of images by gravitational lensing due to arbitrary number of coplanar masses without any symmetry on a plane, as a function of lens and source parameters. We present a method of Taylor-series expansion to solve the lens equation under a small mass-ratio approximation. The advantage of our method is that it allows a systematic iterative analysis. We determine image positions for binary lens systems up to the third order in mass ratios and for arbitrary N point masses up to the second order. The number of the images that admit a small mass-ratio limit is less than the maximum number. It is suggested that positions of extra images could not be expressed as Maclaurin series in mass ratios. Magnifications are finally discussed.

1 Introduction

Gravitational lensing has become one of important subjects in modern astronomy and cosmology. It plays crucial roles as gravitational telescopes in various fields ranging from extra-solar planets to dark matter and dark energy at cosmological scales. This work focuses on gravitational lensing due to a N-point mass system. Definitely it is a challenging problem to express the image positions as functions of lens and source parameters.

There are several motivations for this work. One is that gravitational lensing offers a tool of discoveries and measurements of planetary systems (Schneider and Weiss 1986, Mao and Paczynski 1991, Gould and Loeb 1992, Bond et al. 2004, Beaulieu et al. 2006), compact stars, or a cluster of dark objects, which are difficult to probe with other methods. Gaudi et al. (2008) have recently found an analogy of the Sun-Jupiter-Saturn system by lensing. Efficient methods for producing light curves beyond binary cases are preferred.

Another motivation is to pursue a transit between a particle method and a fluid (mean field) one. For microlensing studies, particle methods are employed, because the systems consist of stars, planets or MACHOs. In cosmological lensing, on the other hand, light propagation is considered for the gravitational field produced by inhomogeneities of cosmic fluids, say galaxies or large scale structures of our Universe. It seems natural, though no explicit proof has been given, that observed quantities computed by continuum fluid methods will agree with those by discrete particle ones in the limit $N \to \infty$, at least on average, where N is the number of particles.

Galois showed that the fifth-order and higher polynomials cannot be solved algebraically. Hence, no formula for quintic equations is known.

In this work, we present a method of Taylor-series expansion to solve the lens equation under a small mass-ratio approximation.

2 Complex Formalism

We consider a lens system with N point masses. The mass and two-dimensional location of each body is denoted as M_i and the vector $\boldsymbol{E}_i$, respectively. For the later convenience, let us define the angular size of the Einstein ring as

$$\theta_E = \sqrt{\frac{4GM_{tot}D_{\rm LS}}{c^2 D_{\rm L} D_{\rm S}}}, \tag{1}$$

[1]E-mail: asada@phys.hirosaki-u.ac.jp

where G is the gravitational constant, c is the light speed, M_{tot} is the total mass $\sum_{i=1}^{N} M_i$ and $D_{\rm L}$, $D_{\rm S}$ and $D_{\rm LS}$ denote distances between the observer and the lens, between the observer and the source, and between the lens and the source, respectively. In the unit normalised by the angular size of the Einstein ring, the lens equation becomes

$$\boldsymbol{\beta} = \boldsymbol{\theta} - \sum_{i}^{N} \nu_i \frac{\boldsymbol{\theta} - \boldsymbol{e}_i}{|\boldsymbol{\theta} - \boldsymbol{e}_i|^2}, \tag{2}$$

where $\boldsymbol{\beta} = (\beta_x, \beta_y)$ and $\boldsymbol{\theta} = (\theta_x, \theta_y)$ denote the vectors for the position of the source and image, respectively and we defined the mass ratio and the angular separation vector as $\nu_i = M_i/M_{tot}$ and $\boldsymbol{e}_i = \boldsymbol{E}_i/\theta_E = (e_{ix}, e_{iy})$.

Bourassa, Kantowski and Norton (1973), Bourassa and Kantowski (1975) introduced a complex notation to describe gravitational lensing. In a formalism based on complex variables, two-dimensional vectors for the source, lens and image positions are denoted as $w = \beta_x + i\beta_y$, $z = \theta_x + i\theta_y$, and $\epsilon_i = e_{ix} + ie_{iy}$, respectively. By employing this formalism, the lens equation is rewritten as

$$w = z - \sum_{i}^{N} \frac{\nu_i}{z^* - \epsilon_i^*}, \tag{3}$$

where the asterisk $*$ means the complex conjugate. The lens equation is non-analytic because it contains both z and z^*.

3 Perturbation

The lens equation is written as

$$C(z, z^*) = \sum_{k=2}^{N} \nu_k D_k(z^*), \tag{4}$$

where $C(z, z^*)$ was defined by Eq. (5) and we defined

$$C(z, z^*) = w - z + \frac{1}{z^*}, \tag{5}$$

$$D_k(z^*) = \frac{1}{z^*} - \frac{1}{z^* - \epsilon_k^*}. \tag{6}$$

We seek a solution in expansion series as

$$z = \sum_{p_2=0}^{\infty} \sum_{p_3=0}^{\infty} \cdots \sum_{p_N=0}^{\infty} (\nu_2)^{p_2} (\nu_3)^{p_3} \cdots (\nu_N)^{p_N} z_{(p_2)(p_3)\cdots(p_N)}, \tag{7}$$

where $z_{(p_2)(p_3)\cdots(p_N)}$ is a constant to be determined iteratively.

It is convenient to normalise the perturbed roots in the units of the zeroth-order one as

$$\sigma_{(p_2)(p_3)\cdots(p_N)} = \frac{z_{(p_2)(p_3)\cdots(p_N)}}{z_{(0)\cdots(0)}}. \tag{8}$$

Here, we shall give perturbative roots when the zeroth order roots are not located at the lens position. Please see Asada (2009) for the special case when the zeroth order roots are located at the lens position.

3.1 0th order ($z_{(0)\cdots(0)} \neq \epsilon_i$ for $i = 1, \cdots, N$)

Zeroth-order solution is given as

$$z_{(0)\cdots(0)} = Aw, \tag{9}$$

where, we defined

$$A = \frac{1}{2}\left(1 \pm \sqrt{1 + \frac{4}{ww^*}}\right). \tag{10}$$

3.2 1st order ($z_{(0)\cdots(0)} \neq \epsilon_i$ for $i = 1, \cdots, N$)

We obtain the first order solution as

$$z_{(0)\cdots(1_k)\cdots(0)} = \frac{b_{(0)\cdots(1_k)\cdots(0)} - a_{(0)\cdots(1_k)\cdots(0)} b^*_{(0)\cdots(1_k)\cdots(0)}}{1 - a_{(0)\cdots(1_k)\cdots(0)} a^*_{(0)\cdots(1_k)\cdots(0)}}. \tag{11}$$

Here, we defined

$$a_{(0)\cdots(1_k)\cdots(0)} = \frac{1}{(z^*_{(0)\cdots(0)})^2}, \tag{12}$$

$$b_{(0)\cdots(1_k)\cdots(0)} = \frac{\epsilon^*_k}{z^*_{(0)\cdots(0)}(z^*_{(0)\cdots(0)} - \epsilon^*_k)}. \tag{13}$$

3.3 2nd order ($z_{(0)\cdots(0)} \neq \epsilon_i$ for $i = 1, \cdots, N$)

There are two types of second-order solutions as shown below. First, we obtain

$$z_{(0)\cdots(2_k)\cdots(0)} = \frac{b_{(0)\cdots(2_k)\cdots(0)} - a_{(0)\cdots(2_k)\cdots(0)} b^*_{(0)\cdots(2_k)\cdots(0)}}{1 - a_{(0)\cdots(2_k)\cdots(0)} a^*_{(0)\cdots(2_k)\cdots(0)}}. \tag{14}$$

Here, we defined

$$a_{(0)\cdots(2_k)\cdots(0)} = \frac{1}{(z^*_{(0)\cdots(0)})^2}, \tag{15}$$

$$b_{(0)\cdots(2_k)\cdots(0)} = -D_{k(0)\cdots(1_k)\cdots(0)} + \frac{(\sigma^*_{(0)\cdots(1_k)\cdots(0)})^2}{z^*_{(0)\cdots(0)}}. \tag{16}$$

Next, let us assume $k < \ell$. We obtain

$$z_{(0)\cdots(1_k)\cdots(1_\ell)\cdots(0)} = \frac{b_{(0)\cdots(1_k)\cdots(1_\ell)\cdots(0)} - a_{(0)\cdots(1_k)\cdots(1_\ell)\cdots(0)} b^*_{(0)\cdots(1_k)\cdots(1_\ell)\cdots(0)}}{1 - a_{(0)\cdots(1_k)\cdots(1_\ell)\cdots(0)} a^*_{(0)\cdots(1_k)\cdots(1_\ell)\cdots(0)}}. \tag{17}$$

Here, we defined

$$a_{(0)\cdots(1_k)\cdots(1_\ell)\cdots(0)} = \frac{1}{(z^*_{(0)\cdots(0)})^2}, \tag{18}$$

$$b_{(0)\cdots(1_k)\cdots(1_\ell)\cdots(0)} = -D_{k(0)\cdots(1_\ell)\cdots(0)} - D_{\ell(0)\cdots(1_k)\cdots(0)} + \frac{2\sigma^*_{(0)\cdots(1_k)\cdots(0)} \sigma^*_{(0)\cdots(1_\ell)\cdots(0)}}{z^*_{(0)\cdots(0)}}. \tag{19}$$

4 Conclusion

Under a small mass-ratio approximation, we have developed a perturbation theory of N coplanar (in the thin lens approximation) point-mass gravitational lens systems without symmetries on a plane. The system can be separated into a single mass lens as a background and its perturbation due to the remaining point masses.

The number of the images that admit the small mass-ratio limit is less than the maximum number. This suggests that the other images do not have the small mass limit. Therefore, it is conjectured that

positions of the extra images could not be expressed as Maclaurin series in mass ratios. This is a topic of future work.

There are possible applications along the course of the perturbation theory of N point-mass gravitational lens systems. For instance, it will be interesting to study lensing properties such as magnifications by using the functional form of image positions. Furthermore, the validity of the present result may be limited in the weak field regions. It is important also to extend the perturbation theory to a domain near the strong field.

References

[1] Asada H., 2009, MNRAS, *in press* (ArXiv:0809.4122)

[2] Beaulieu J. P., et al., 2006, Nature, 439, 437

[3] Bond I. A., et al., 2004, ApJ, 606, L155

[4] Bourassa R. R., Kantowski R., Norton T. D., 1973, ApJ, 185, 747

[5] Bourassa R. R., Kantowski R., 1975, ApJ, 195, 13

[6] Gaudi B. S., et al., 2008, Science, 319, 927

[7] Gould A., Loeb A., 1992, ApJ, 396, 104

[8] Mao S., Paczynski B., 1991, ApJ, 374, 37L

[9] Schneider P., Weiss A., 1986, A&A. 164, 237

Signatures of spinning evaporating micro black holes

Antonino Flachi, Misao Sasaki, Takahiro Tanaka

Yukawa Institute for Theoretical Physics, Kyoto University, Kyoto 606–8502, Japan

Abstract

We consider the evaporation of rotating micro black holes produced in highly energetic particle collisions, taking into account the polarization due to the coupling between the spin of the emitted particles and the angular momentum of the black hole. The effect of rotation shows up in the helicity dependent angular distribution significantly. By using this effect, there is a possibility to determine the axis of rotation for each black hole formed, suggesting a way to improve the statistics. Deviation from thermal spectrum is also a signature of rotation. This deviation is due to the fact that rapidly rotating holes have an effective temperature $T_{\rm eff}$ significantly higher than the Hawking temperature T_H. The deformation of the spectral shape becomes evident only for very rapidly rotating cases. We show that, since the spectrum follows a blackbody profile with an effective temperature, it is difficult to determine both the number of extra-dimensions and the rotation parameter from the energy spectrum alone. We argue that the helicity dependent angular distribution may provide a way to resolve this degeneracy. We illustrate the above results for the case of fermions.

In this paper, we consider micro black holes resulting from the collision of two particles at energies much higher than the higher dimensional Planck mass M_P [1, 2, 3, 4]. We have in mind models with M_P of order of a few TeV and the standard model confined on a 3-brane, embedded in a $(4+n)$-dimensional bulk [5, 6]. These black holes have horizon radius smaller than the size of the extra dimensions, and are expected to follow balding, spin-down, Schwarzschild, and Planck phases. Micro black hole formation has been studied both analytically [7] and numerically [8], and their evaporation has also been the subject of considerable attention (see for example [9, 10]). Previous work suggests that micro black holes mostly evaporate into brane modes [12].

We analyze the fermion emission from spinning evaporating micro black holes, whose geometry can be approximated by a vacuum higher dimensional Kerr [13]:

$$\begin{aligned} ds^2 &= \left(1-\frac{M}{\Sigma r^{n-1}}\right)dt^2+\frac{2aM\sin^2\theta}{\Sigma r^{n-1}}dtd\varphi-\frac{\Sigma}{\Delta}dr^2-\Sigma d\theta^2-\left(r^2+a^2+\frac{a^2M\sin^2\theta}{\Sigma r^{n-1}}\right)\sin^2\theta d\varphi^2 \\ &\quad -r^2\cos^2\theta d\Omega_n^2 \ , \end{aligned}$$

where $\Delta\equiv r^2+a^2-Mr^{1-n}$ and $\Sigma\equiv r^2+a^2\cos^2\theta$. M_P is normalized to one. Since we are interested in the visible brane modes, the background spacetime will be given by the projection of the above metric on the brane. Massless fermions emitted by the black hole are described by the Dirac equation:

$$e_a^\mu\gamma^a\left(\partial_\mu+\Gamma_\mu\right)\psi=0 \ ,$$

where ψ is the Dirac spinor wave function, e_a^μ a set of tetrads, Γ_μ the spin-affine connections determined by $\Gamma_\mu=\gamma^a\gamma^b\omega_{ab\mu}/4$, with $\omega_{ab\mu}$ being the Ricci rotation coefficients. The matrices $\gamma^\mu=e_a^\mu\gamma^a$ are chosen to satisfy the relation $\gamma^\mu\gamma^\nu+\gamma^\nu\gamma^\mu=g^{\mu\nu}$, with $g^{\mu\nu}$ being the metric on the brane.

Due to the symmetries of the Kerr spacetime, the spinor wave function factorizes as [14]

$$\psi=\mathcal{N}e^{i(m\varphi-\omega t)}\begin{pmatrix}\vec{\phi}\\ \pm\vec{\phi}\end{pmatrix} \ ,$$

where the + and − signs refer to negative and positive helicities, respectively. We illustrate the results for the case of negative helicity. The positive helicity case can be obtained by a trivial chirality transformation. The field $\vec{\phi}$ takes the form

$$\vec{\phi}=\begin{pmatrix}R_-(r)S_-(\theta)\\ R_+(r)S_+(\theta)\end{pmatrix} \ ,$$

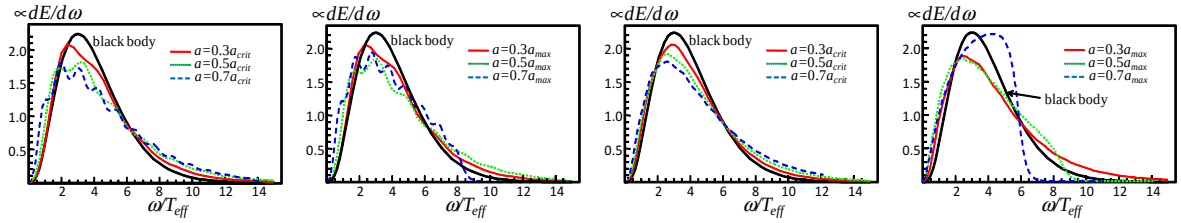

Figure 1: Energy spectrum of the emitted fermions. The horizontal axis is rescaled by the effective temperature determined by fitting the data by a black body profile. The overall amplitude is normalized since the absolute magnitude is not observable. The first (last) two panels from left refer to $n = 2$ ($n = 4$).

and the normalization factor is $\mathcal{N}^{-1} = \Delta^{1/4}(r + ia\cos\theta)^{1/2}\sin^{1/2}\theta$. The angular and radial modes obey

$$\left(\frac{d}{d\theta} \pm \omega a \sin\theta \mp \frac{m}{\sin\theta}\right) S_{\mp}(\theta) = \pm\kappa S_{\pm}(\theta) \ ,$$
$$\left(\frac{d}{dr} \mp \frac{i}{\Delta}\left(\omega(r^2+a^2) - ma\right)\right) R_{\mp}(r) = \kappa\Delta^{-1/2} R_{\pm}(r) \ ,$$

where κ is a separation constant. Supplemented with regularity conditions at $\theta = 0$ and π, the set of angular equations provides an eigenvalue problem, which determines κ [16]. In order to compute the particle flux, we impose ingoing boundary conditions at the horizon. The number of (negative helicity) particles emitted, for fixed frequency ω, is distributed according to the Hawking radiation formula:

$$\frac{dN}{d\omega d\cos\theta} = \frac{1}{2\pi\sin\theta}\sum_{l,m} |S_-(\theta)|^2 \frac{\sigma_{l,m}}{e^{\tilde{\omega}/T_H}+1} \ , \tag{1}$$

where $\tilde{\omega} = \omega - ma/(r_h^2+a^2)$, $T_H = \frac{1}{4\pi r_h}\frac{(n+1)r_h^2+(n-1)a^2}{r_h^2+a^2}$ is the Hawking temperature, and $\sigma_{l,m}$ the grey-body factor (see Ref. [17]). The initial angular momentum of the produced black holes $J = 2aM/(n+2)$ is restricted by requiring the impact parameter $b = J/M$ to be smaller than the horizon radius r_h, determined by $\Delta(r_h) = 0$. Then, the maximum value of the rotation parameter a turns out to be $a_{max} = \frac{n+2}{2} r_h$ [9]. The upper bound on J might be even lower for $n \geq 2$. In fact, there exists a critical value for a, $a_{crit} \equiv (n+1)(n-1)^{-1} r_h^2$, where $|\partial(T, \Omega_h)/\partial(M, J)|$ vanishes. If the same argument as in the case of black branes applies, black holes with $a > a_{crit}$ suffer from the Gregory Laflamme instability (See also Ref. [18]). Then, a_{crit} represents the maximal value below which the higher dimensional Kerr solution is adequate. Interestingly $a_{crit} < a_{max}$ (for $n = 2,\ 3,\ 4$ extra dimensions, $a_{crit} = 1.09,\ 1.07,\ 1.06$, whereas $a_{max} = 1.25,\ 1.89,\ 2.46$). Although it is widely believed that a dynamical instability exists, the value of a_{crit} obtained above is only heuristic. Thus, we consider two possible cases: the maximal value allowed for a is a_{crit} or a_{max}. A set of representative values for the parameter a is chosen as $a/a_{max} =$ 0.3, 0.5, 0.7, and $a/a_{crit} =$ 0.3, 0.5, 0.7. M is set to unity. Having fixed a in the above way, we compute the energy spectrum, shown in Fig. 1. We normalize the horizontal axis by using an effective temperature $T_{\rm eff}$ determined by fitting the data by a blackbody spectrum profile. The effective temperature $T_{\rm eff}$ is much higher than the Hawking temperature as shown in Fig. 2. However, the spectral shape is not so different from the thermal one except for the cases with $a \approx a_{max}$ (Fig. 1).

The renormalized spectra are enhanced for both lower and higher frequencies compared with the black body spectrum at $T = T_{\rm eff}$ (thick line). Except for very large values of a, the obtained spectra can be fit well by superpositions of black body profiles with width of about $2\Omega_H \times T_{\rm eff}$. The motion of the hypothetical emitting surface on the rotating black hole, relative to observers at infinity, causes the additional blueshift factor which varies from place to place. However, because of the change in the temperature and the rotation parameter during the evaporation, the broadening of the spectrum due to the rotation will not be identified straightforwardly. Wiggles can be seen in the spectrum for a small number of extra-dimensions, however, they are likely to disappear as T and a change during the evaporation. For high rotation velocity, the deviation from the thermal spectrum is much clearer. As a

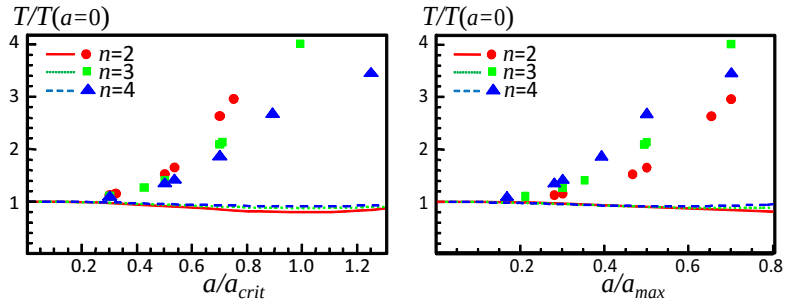

Figure 2: Effective Hawking temperature normalized by the temperature at $a = 0$ versus the rotation parameter a normalized by a_{crit} (left) and a_{max} (right).

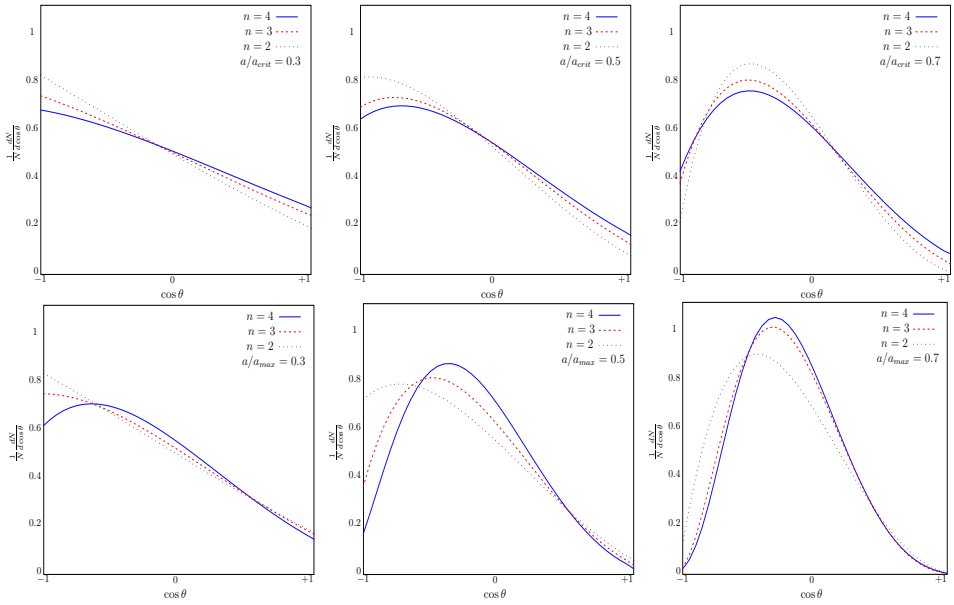

Figure 3: Angular distribution of emitted negative helicity fermions.

novel signature, we find that the spectrum is sharply cut off at high-frequencies for rapid rotation. This signature may survive even after taking into account the superposition of spectra along the evolutionary track of an evaporating micro black hole. This highly spinning regime is realized for $a > a_{crit}$.

In Fig. 3, the angular distribution of negative helicity particles is displayed for various parameters, setting ω to a representative frequency $\bar{\omega}$. The value $\bar{\omega}$ is chosen by requiring that the fraction of particles emitted with frequency below $\bar{\omega}$, $N(\bar{\omega}) = \int_0^{\bar{\omega}} dN$, to be 0.5.

The emission is suppressed in the direction anti-parallel to the black hole angular momentum. For rapid rotation, the particles tend to be emitted towards the equatorial plane. This concentration in the rapidly rotating case can also be seen in the helicity independent angular distribution [9]. The emission around both poles looks suppressed, but the observed apparent suppression is simply due to the large enhancement of emission in the directions close to the equatorial plane. The asymmetry in the helicity dependent angular distribution is visible even for relatively slow rotation and becomes evident as a increases. For very fast rotation, the concentration of the emitted particles around the equatorial plane may affect the features of cosmic ray air showers mediated by black holes.

For slow (rapid) rotation, the asymmetry decreases (increases) as n grows. This tendency may be used as an indicator to discriminate scenarios with different number of extra-dimensions. For a/a_{crit} fixed the peak position of the helicity dependent angular distribution is almost independent of n as shown in upper panel, Fig. 3. If we can align the direction of the axis of rotation of the black hole for various

events even approximately, we can collectively use the experimental data to achieve high statistics for the angular distribution of emitted particles. The LHC may allow to perform such measurements and for this reason it is important to estimate the error in the determination of the axis of rotation. A simple estimation can be perfomed by identifying the direction of the black hole angular momentum with the $l = 1$ (dipole) and $l = 2$ (quadrupole) moments (a more sophisticated statistical analyses may reduce the error). Assuming that the angular distribution shown in Fig. 3, the error δ in degrees, for 100 particles emitted, is summarized in Table 1.

a/a_{max}	0.3	0.5	0.7	a/a_{crit}	0.3	0.5	0.7
$n = 2$	18.20	15.17	9.47	$n = 2$	20.68	16.20	13.17
$n = 3$	19.93	13.43	8.19	$n = 3$	25.47	19.32	15.34
$n = 4$	20.03	10.97	7.50	$n = 4$	29.84	21.75	17.14

Table 1: Estimate of δ in degrees for the curves of fig. 3.

Acknowledgements. We acknowledge the support of the JSPS through Grants Nos. 19GS0219, 20740133, 17340075, 19540285 and 18204024, and Grant-in-Aid for the Global COE Program "The Next Generation of Physics, Spun from Universality and Emergence" from the Ministry of Education, Culture, Sports, Science and Technology (MEXT) of Japan. We thank Y. Sendouda for help with the numerics.

References

[1] T. Banks, W. Fischler, hep-th/9906038.

[2] S. Dimopoulos, G. Landsberg, Phys. Rev. Lett. **87** (2001) 161602.

[3] S. B. Giddings, S. Thomas, Phys. Rev. D**65** (2002) 056010.

[4] P.C. Argyres, S. Dimopoulos, J. March-Russell, Phys. Lett. B**441** (1998) 96.

[5] N. Arkani-Hamed, S. Dimopoulos, G. Dvali, Phys. Lett. B**429** (1998) 263.

[6] L. Randall, R. Sundrum, Phys. Rev. Lett. **83** (1999) 3370.

[7] D.M. Eardley, S.B. Giddings, Phys. Rev. D**66** (2002) 044011.

[8] H. Yoshino, Y. Nambu, Phys. Rev. D**66** (2002) 065004; Phys. Rev. D**67** (2003) 024009.

[9] D. Ida, K. Oda, S.C. Park, Phys. Rev. D**67** (2003) 064025; erratum *ibid.* D**69** (2004) 049901; Phys. Rev. D**71** (2005) 104039; Phys. Rev. D**73** (2006) 124022.

[10] G. Duffy, C. Harris, P. Kanti, E. Winstanley, JHEP **09** (2005) 049.

[11] M. Casals, S. Dolan, P. Kanti, E. Winstanley, JHEP **03** (2007) 019.

[12] R. Emparan, G.T. Horowitz, R.C. Myers, Phys. Rev. Lett. **85** (2000) 499.

[13] R. C. Myers and M. J. Perry, Ann. Phys. **172** (1986) 304.

[14] W. Unruh, Phys. Rev. Lett. **31** (1973) 1265; Phys. Rev. D**10** (1974) 3194.

[15] A. Vilenkin, Phys. Rev. Lett. **41** (1978) 1575; erratum *ibid.* **42** (1979) 195.

[16] W.H. Press, S.A. Teukolsky, The Astrophysical J. **185** (1973) 649.

[17] D. Page, Phys. Rev. D**14** (1976) 3260.

[18] R. Emparan, R.C. Myers, JHEP **09** (2003) 025.

Numerical performance of the Parabolized ADM (PADM) formulation of General Relativity

Jakob Hansen[22]

[1]*Department of Physics, Waseda University, 55N-307, Okubo 3-4-1, Shinjuku-ku, Tokyo 169-8555, Japan*

Abstract

A new parabolic extension (PADM) of the standard 3+1 Arnowitt, Deser, Misner (ADM) formulation of the equations of general relativity is presented. By parabolizing first-order ADM in a certain way, the PADM formulation turns it into a mixed hyperbolic - second-order parabolic, well-posed system. The surface of constraints of PADM becomes a local attractor for all solutions and all possible well-posed gauge conditions. Numerical properties of PADM are compared with those of standard ADM and its hyperbolic Kidder, Scheel, Teukolsky (KST) extension in a series of standard tests. The PADM scheme is numerically stable, convergent and second-order accurate. The new formulation has better control of the constraint-violating modes than ADM and KST. Full details can be found in [1] and [2].

I. INTRODUCTION

For years people have tried to obtain analytic solutions of the complex field equations of Einstein's general theory of relativity (GR). Approximation methods have been developed over the course of time, but the most promising tool for tackling problems such as gravitational waves arising from binary black hole (BBH) or binary neutron star mergers, gravitational collapse etc., is numerical relativity.

The numerical integration of the Einstein equations is not an easy task because the computations can become unstable and an exponential blow up of the numerical error may occur, even when the formulation employed admits a well-posed initial value problem. If the numerical techniques employed and gauge and boundary conditions chosen do not suffer from pathologies, perhaps the most important source that can potentially lead to instabilities during a free evolution is the growth of the constraint violating modes. Over the years, several methods have been proposed to deal with this type of instability [3–15].

The approach which has attracted most attention in recent years takes advantage of the fact that in the ideal case where the constraint equations are satisfied, one has the freedom to add combinations of the constraint equations to the right-hand-side (RHS) of the evolution equations of a given formulation. By virtue of this freedom, it is also possible to introduce in the system of evolution equations terms which act as "constraint drivers" and turn the constraint surface into an attractor. This technique is usually termed as "constraint damping".

One way to achieve efficient damping is to construct formulations of GR that under free evolution force all constraint violating modes to evolve according to parabolic equations, which are known for their damping and smoothing properties [16]. In [1] this goal was achieved by the construction of an evolution system based on the first-order form of the standard Arnowitt, Deser, Misner (ADM) formulation [17], through the addition of appropriate combinations of the derivatives of the constraints and the constraints themselves at the RHS of the ADM evolution equations. We call this evolution system the Parabolized ADM (PADM) formulation throughout this work. It was shown in [1] that the evolution of the constraint equations with the PADM formulation are second-order parabolic, independently of the gauge conditions employed. This in turn implies that the constraint surface becomes a local attractor. Finally, it was proved, that the PADM system satisfies the necessary conditions for well-posedness and based on the results of [18] an argument, which indicates strong evidence that the PADM system admits a well-posed initial value problem, was given.

The purpose of this work is to test the numerical accuracy and stability of the PADM system, and compare the PADM formulation with the first-order ADM and the Kidder, Scheel, Teukolsky (KST) [19] formulations. The comparison between the three formulations is carried out in a series of standard one- and two-dimensional tests, usually referred to as the "Apples with Apples" tests or the "Mexico City" tests [20].

II. THE PADM FORMULATION

The PADM system is obtained from the first-order ADM formulation [17] by addition of constraints and their derivatives to the RHS of the ADM evolution equations. The PADM formulation is given by (see [18] for details):

$$\partial_t \gamma_{ij} = (ADM) + \lambda \gamma^{ab} \partial_b \mathcal{C}_{aij}, \tag{1}$$

$$\partial_t K_{ij} = (ADM) + \phi \gamma_{ij} \gamma^{ab} \partial_a \mathcal{M}_b + \theta \partial_{(i} \mathcal{M}_{j)}, \tag{2}$$

$$\partial_t D_{kij} = (ADM) + \epsilon \gamma^{ab} \partial_a \mathcal{C}_{bkij} + \xi \gamma_{ij} \partial_k \mathcal{H} + \zeta \mathcal{C}_{kij}, \tag{3}$$

where $\lambda, \phi, \theta, \epsilon, \xi, \zeta$ are the six parameters of the formulation and where $\mathcal{H}, \mathcal{M}_b, \mathcal{C}_{aij}$ and $\mathcal{C}_{bkij}$ are the constraint equations of the first order ADM formulation. We refer to the added terms of the PADM formulation as the constraint driver. It was shown in [1] that for gauges which do not introduce second-order derivatives of the dynamical variables in the evolution equations the PADM system satisfies the Petrovskii condition for well-posedness [21], provided that

$$\lambda > 0, \epsilon > 0, \xi < 0, \phi < 0, \theta > 0. \tag{4}$$

Therefore, in this work we use the PADM equations in conjunction with the algebraic gauge condition $\alpha = \alpha(\gamma), \beta_i = 0$.

When the aforementioned conditions are satisfied, the PADM system has the following properties:

a) The PADM evolution equations can be classified as a set of mixed hyperbolic - second-order parabolic quasi-linear partial differential equations.

b) The evolution equations of the constraint variables become second-order parabolic partial differential equations (PDEs) independently of the spacetime geometry and the gauge conditions employed. Therefore, the constraint propagation equations admit a well-posed Cauchy problem themselves.

c) Because of the parabolic structure of the evolution equations of the constraints, the constraint surface becomes a local attractor. All small amplitude, high-frequency constraint-violating perturbations are exponentially damped in time as $\exp(-\lambda\kappa^2 t)$, where κ is the magnitude of the wavevector of the perturbations. This in turn implies that the hazardous high frequency perturbations will be damped very efficiently. This is espcially of importance in numerical simulations since it is most often the high frequency perturbations that kills a simulation.

III. NUMERICAL TESTS

To test the numerical performance of the PADM formulation, we used the so-called "Apples With Apples" [20] tests, which were designed to provide the numerical relativity community with a set of standard tests that could be use to, quantitatively, compare different numerical implementations of different formulations of GR.

The tests are briefly described below, for in-detail descriptions of the tests and their results, see [2]. The tests include both one- and two-dimensional solutions. For 1D tests the simulations are run for 1000 light crossings (or until the code crash) and for 2D tests, the simulations are run for 100 light crossings (or until the code crash). Note that the dimensionality of the tests refers to the dimensionalty of the solutions, not the grid, i.e. for a 1D test, the wave travels parallel to the computational mesh, for a 2D test, the solution wave travels diagonally. However, *all* tests are carried out in a 3 dimensional computational mesh, such that all cross derivatives are evaluated and the *full* Einstein equations are thus evolved. The tests are :

- **Standard Robust Stability Test :** The standard robust stability test is based on small random perturbations about Minkowski spacetime. In this test, all the dynamic variables are set equal to their Minkowski space values and the initial data are then perturbed by random noise of sufficiently small amplitude such that the evolution remains in the linearized regime unless any instabilities arise. The perturbed initial data is then evolved for 1000 light crossing (or until the simulation

crashes) Although being a very simple test, it is naturally a very important one since all codes will experience such random perturbations due to numerical roundoff and truncation errors, hence all codes must be able to pass this test sucessfully.

The main outcome of this test was that 1) ADM fails miserably due to the illposed nature of this formulation, 2) KST pass this test, but the constraint violations are seen to grow linearly in time since this formulation has no mechanism of dissipating constraint violations. 3) In strong contrast to this, the PADM formulation not only pass this test perfectly, but the constraint violations are seen to be quickly damped away. In particular, it is shown that high frequency perturbations are damped away extremely quickly.

- **Strong Robust Stability Test :** Another version of the robust test (not included in the standard "Apples With Apples" testbed) requires perturbation by random noise not only at the initial time-step, but at *every* time-step throughout the entire simulation. We call this test the "strong" robust stability test. This test is much more challenging than the standard robust test and is much closer to reality because in numerical simulations, truncation and round-off errors will unavoidably be introduced into the solution of the PDE system at every time-step.

  The result of this test is again that 1) ADM fails, 2) KST pass this test if the amplitude of the noise is sufficiently small or if the simulation is run for only a short time. But since KST has no way of dissipating the introduced noise, eventually KST will crash. 3) In contrast to this, PADM pass this test for even high amplitude noise and show no indications of any instabilities or growth of the constraint violations due to the PADM formulations unique ability to damp constraint violations.

- **Gauge Wave Test :** In the gauge wave test, a gauge wave is evolved in both a one-dimensional and two-dimensional form. Both 1D and 2D tests are carried out for gauge waves with different amplitudes. The gauge wave stability test has proven to be one of the most challenging tests for most evolution schemes mainly due to the existence of a one-parameter family of exponential, harmonic gauge solutions that is excited by truncation errors during numerical solutions. This eventually causes the numerical solution to veer off the analytic one.

  The result of this test is that PADM performs better than both ADM and KST. In particular it is shown that PADM can pass the two-dimensional, high amplitude gauge wave test. We know of no other formulations which can do this, including BSSN.

- **Linear Weak Wave Test :** The linear wave test evolves a traveling gravitational wave of amplitude small enough so the evolution remains in the linear regime. This test is carried out in both a one-dimensional and two-dimensional form.

  This test pose no particular problems for most formulations and both ADM, KST and PADM can pass this test. However, PADM is still seen to have better control of the constraint violations than the other two formulations.

- **Gowdy Wave Test :** The polarized Gowdy T3 spacetimes are solutions of the Einstein equations which describe an expanding (or contracting) universe containing plane polarized gravitational waves, see for example [20] and references therein. The previous tests can be considered as perturbations about flat spacetime, so they probe the weak field limit of the Einstein equations, whereas the Gowdy test probes the strong field regime of GR.

  - **The expanding Gowdy wave test** has proved to be one of the most challenging problems in numerical relativity. This is because the metric components grow exponentially with time and hence the truncation errors introduced in the numerical solution grow with time, if the resolution is fixed. Consequently, the numerical solution soon veers off the analytical one. Another result of the exponential growth is that the dynamical variables eventually grow so large that the computations cannot be handled by using standard 64-bit floating-point arithmetic. Therefore, all simulations of the expanding Gowdy solution will eventually terminate [20].

    Our results for the expanding Gowdy wave test is that KST performs particularly bad in this test and crash after just 20 lightcrossing times. The ADM formulation performs suprisingly well and can do roughly 260 light crossings before accuracy is completely lost, but the winner is still the PADM formulation which does not terminate until 275 light crossing times has

passed. The reason why ADM performs relatively well in this test is that the solution is one-dimensional and in the particular case of one-dimensional solutions, the ADM formulation can be shown to be well posed [1].

– **The collapsing Gowdy wave test** is less challenging and all the formulations are able to pass this test. However, still we see that PADM performs (marinally) better than the other two formulations.

For all tests we thus find that PADM behaves better than the ADM and KST formulations. In particular, PADM can pass the high amplitude gauge wave test and performs better in the expanding gowdy wave test than any other formulations know to the authors.

The most important feature of the PADM formulation is that it damps away constraint violating perturbations and thus drive the solution back to the surface of constraints. High frequency constraint violations are damped away the most effectively, which is important for ensuring the numerical stability of PADM implementations.

IV. CONCLUSIONS

In [1] is presented the PADM formulation of GR and in [2] we have described a stable, convergent and second-order accurate numerical scheme for solving the equations of the PADM system. Also in [2] we have tested the accuracy and stability of the PADM system and compared it with the first-order ADM and KST evolution systems using the "Apples with Apples" tests.

For all tests we find that PADM behaves significantly better than the ADM and KST formulations. In particular, the PADM formulation damps away constraint violating perturbations and thus drive the solution back to the surface of constraints. High frequency violations are damped away most effectively.

We conclude that PADM successfully passes the standard tests of numerical relativity and works equally well with a variety of algebraic gauges. Via the comparison of the numerical performance of the PADM formulation and those of the ADM and the KST formulations, we conclude that PADM has better control of the constraint violations than both ADM and KST. This leads to hope that the PADM formulation can lead to new advances in numerical relativity.

[1] V. Paschalidis, Phys.Rev.D **78**, 024002 (2008), gr-qc/0704.2861.
[2] V. Paschalidis, J. Hansen, and A. Khokhlow, Phys. Rev. D **78**, 064048 (2008), gr-qc/0712.1258.
[3] R. F. Stark and T. Piran, Phys. Rev. Lett **55**, 891 (1985).
[4] A. M. Abrahams and C. R. Evans, Phys. Rev. D **46**, R4117 (1992).
[5] M. W. Choptuik, Phys. Rev. Lett. **70**, 9 (1993).
[6] A. M. Abrahams and C. R. Evans, Phys. Rev. Lett **70**, 2980 (1993).
[7] A. M. A. et al., Phys. Rev. D **49**, 5153 (1994).
[8] M. W. C. et al., Class. Quantum Grav. **20**, 1857 (2003).
[9] M. W. C. et al., Phys. Rev. D2 **68**, 044007 (2003).
[10] O. Brodbeck, S. Frittelli, P. Haubner, and O. A. Reula, J. Math. Phys. **40**, 909 (1999).
[11] C. Gundlach, G. Calabrese, I. Hinder, and J. M. Martín-García, Class. Quantum Grav. **22**, 3767 (2005).
[12] G. Yoneda and H. aki Shinkai (2001).
[13] M. H. et al., Phys. Rev. D, (2004).
[14] M. Anderson and R. A. Matzner, Found. Phys **35**, 1477 (2005).
[15] D. R. Fiske, Phys. Rev. D **69**, 047501 (2004).
[16] H.-O. Kreiss and J. Lorenz, *Initial-Boundary Value Problems and the Navier-Stokes Equations* (Academic Press Inc., 1989).
[17] R. Arnowitt, S. Deser, and C. W. Misner, *Gravitation: An Introduction to Current research* (Wiley, 1962), gr-qc/0405109.
[18] V. Paschalidis, A. M. Khokhlov, and I. D. Novikov, Phys. Rev. D **75**, 024026 (2007).
[19] L. E. Kidder, M. A. Scheel, and S. A. Teukolsky, Phys. Rev. D **64**, 064017 (2001).
[20] M. A. et al., Class. Quant. Grav. **21**, 589 (2004).
[21] B. Gustafsson, H. Kreiss, and J. Oliger, *Time dependent problems and difference methods* (John Willey & Sons, 1995).

[22] E-mail:jakob@jakobonline.dk

Gravitational collapse of a dust ball from the perspective of loop quantum gravity: an application

Tomohiro Harada[1]

Department of Physics, Rikkyo University, Toshima, Tokyo 171–8501, Japan

Abstract

At an effective level, consistent versions of dynamics with corrections from loop quantum gravity are presented which implement the conditions together with the dynamical constraints of gravity in an anomaly-free manner. These are then used for analytical as well as numerical investigations of the fate of classical singularities, including non-spacelike ones, as they generically develop in these models. None of the corrections used here resolve those singularities by regular effective geometries. However, there are numerical indications that the collapse ends in a tamer shell-crossing singularity prior to the formation of central singularities for mass functions giving a regular conserved mass density. Moreover, we find quantum gravitational obstructions to the existence of exactly homogeneous solutions within this class of models. This indicates that homogeneous models must be seen in a wider context of inhomogeneous solutions and their reduction in order to provide reliable dynamical conclusions.

1 Introduction

Quantum gravity is supposed to solve the problems, such as, how we can deal with spacetime singularities which appear in big bang and in gravitational collapse in classical general relativity, how black hole entropy is related to the microscopic degrees of freedom, whether a black hole evaporates away completely or leaves a Planck mass relic and how gravitational force behaves from low-energy scale to the Planck scale? We here focus on the problem how loop quantum gravity (LQG) affects the scenario of spacetime singularities in gravitational collapse. LQG is nonperturbative, background-independent quantum gravity with no ultraviolet divergence. This is based on a canonical quantisation approach. LQG has inspired loop quantum cosmology (LQC), which successfully avoids big bang singularity and predicts a bouncing universe

This article is based on the collaboration with M. Bojowald and R. Tibrewala. Details of the present analysis is given in Ref [1]. We use the unit in which $c = 1$.

2 Lemaitre-Tolman-Bondi spacetime in classical theory

The Lemaitre-Tolman-Bondi (LTB) solution is an exact solution to Einstein's field equations, which describes the evolution of a spherically symmetric inhomogeneous dust cloud. Here, we focus on the marginally bound case, in which the energy function, which is the sum of kinetic energy and potential energy, vanishes identically. The line element in this solution is given by

$$ds^2 = -dt^2 + R'^2 dx^2 + R^2(d\theta^2 + \sin^2\theta d\phi^2), \tag{1}$$

$$R(t,x) = \left(x^{3/2} - \frac{3}{2}\sqrt{F(x)}t\right)^{2/3}, \tag{2}$$

where $F(x)$ is an arbitrary function, which is twice the conserved dust mass, and the prime denotes the derivative with respect to x. The density of the dust is given by

$$\epsilon = \frac{F'}{8\pi G R^2 R'}, \tag{3}$$

[1]E-mail:harada@rikkyo.ac.jp

where G is the gravitational constant.

LQG is formulated in terms of the densitised triad E^i and the Ashtekar connection A^i, where $i = 1, 2, 3$ is the index for internal gauge. In a spherically symmetric spacetime, we can choose the following canonical pairs given by

$$\{A_x(x), E^x(y)\} = 2\gamma G\delta(x, y), \tag{4}$$
$$\{\gamma K_\varphi(x), E^\varphi(y)\} = \gamma G\delta(x, y), \tag{5}$$

where the brackets are the Poisson brackets and γ is a nondimensional constant called the Immirzi parameter.

The spatial metric components can be expressed in terms of the densitised triad. Because of the metric form (1), the densitised triad must satisfy the following relations:

$$R^2 = |E^x(x)|, \quad E^\varphi(x) = \frac{1}{2}|E^x(x)|', \quad K'_\varphi = K_x \mathrm{sgn} E^x, \tag{6}$$

where K_i denotes the extrinsic curvature and we call the last two relations the LTB relations.

The Hamiltonian for this classical system is given by $H = H_{\rm grav} + H_{\rm dust}$, where

$$H_{\rm grav} = -\frac{1}{2G}\left(\frac{K_\varphi^2 E^\varphi}{\sqrt{|E^x|}} + 2K_\varphi K_x\sqrt{|E^x|}\right), \tag{7}$$
$$H_{\rm dust} = \frac{F'(x)}{2G}, \tag{8}$$

in terms of the triad and the connection.

3 Effects of LQG in LTB system: formulation

For the moment, we need to recall the treatment for getting a finite Hamiltonian in full theory of LQG [2]. The classical gravitational Hamiltonian can be written in terms of the volume V of a three dimensional region and the curvature F^i and then the inverse factor of the determinant of the triad in the Hamiltonian disappears apparently.

In LQG, the Hilbert space is spanned by spin-network states. The basic operator corresponding to the connection is the holonomy

$$\hat{h}_\gamma = \mathcal{P}\exp\int_\gamma A, \tag{9}$$

where γ is a link of a spin network. The volume operator is also defined on the Hilbert space and spin-network states are its eigenstates. We can construct a finite Hamiltonian in terms of the holonomy and the volume operator which has an appropriate classical limit.

In this approach, we can expect semiclassical effects from the regularisation of the factor of the inverse of the triad determinant and from the introduction of the holonomy in place of the connection. The former is called the inverse triad effects, while the latter is called the holonomy effects. We focus on the inverse triad effects in this article.

The inverse triad correction can be incorporated by considering the effective Hamiltonian

$$H^{\rm eff}_{\rm grav} = -\frac{1}{2G}\left(\frac{\alpha(E^x)}{\sqrt{|E^x|}}K_\varphi^2 E^\varphi + 2K_\varphi K_x\sqrt{|E^x|}\right), \tag{10}$$

where α is a function given by

$$\alpha(E^x) := 2\frac{\sqrt{|E^x + \gamma\ell_{\rm P}^2/2|} - \sqrt{|E^x - \gamma\ell_{\rm P}^2/2|}}{\gamma\ell_{\rm P}^2}\sqrt{|E^x|}, \tag{11}$$

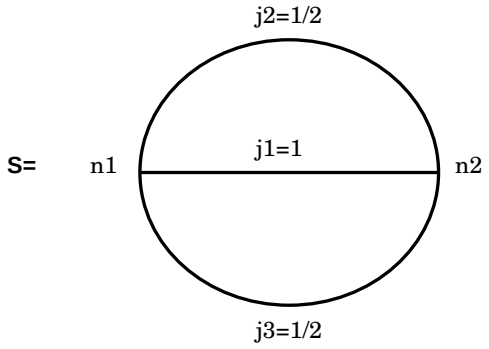

Figure 1: A spin network

where $\ell_{\rm P} = \sqrt{G\hbar}$ is the Planck length. To get the LTB relation consistent with the time evolution generated by the above effective Hamiltonian, we also take into account the correction to the LTB relation such as

$$(E^x)' = 2f(E^x)E^\varphi, \quad K'_\varphi = f(E^x)K_x. \tag{12}$$

With the above correction effects, we can derive the following field equations for this system. The Hamiltonian constraint and the evolution equation are respectively given by

$$\dot{R}^2 R'(\alpha(R)-1) + 2R\dot{R}\dot{R}' + \dot{R}^2 R' = f(R)F' \tag{13}$$

$$2R\ddot{R} + \dot{R}^2 + (\alpha(R)-1)\dot{R}^2 = 0\,, \tag{14}$$

where

$$\alpha(R) = 2\frac{\sqrt{|R^2+\gamma\ell_{\rm P}^2/2|} - \sqrt{|R^2-\gamma\ell_{\rm P}^2/2|}}{\gamma\ell_{\rm P}^2}R. \tag{15}$$

Another correction function f must satisfy

$$\frac{df(R)}{dR} = (1-\alpha(R))\frac{f}{R}. \tag{16}$$

The correction functions are plotted in Fig. 2. In this figure, we can see that the the classical value is recovered for $R \gg R_*$ and the deviation becomes significant for $R \lesssim R_*$.

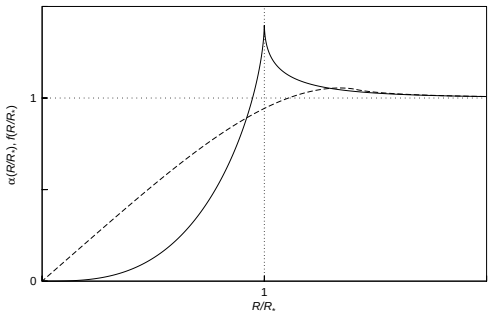

Figure 2: $\alpha(R)$ (solid) and $f(R)$ (dashed), where $R_* := \sqrt{\gamma/2}\ell_{\rm P}$.

4 Effects of LQG in LTB system: analysis

The field equations of the effective theory are so complicated that we cannot expect to get an exact solution in general. Nevertheless, we can find interesting results analytically.

Even for a vacuum static solution with vanishing mass, we find that the Minkowski spacetime is not a solution but is replaced by a unique nontrivial geometry given by

$$ds^2 = -dt^2 + f(R)^{-2}dR^2 + R^2(d\theta^2 + \sin^2\theta d\phi^2). \tag{17}$$

In this spacetime, there is a singularity at $R = 0$. We can also show that there is no bounce because $\dot{R} = 0$ is impossible. We can also show that there is no Friedmann solution, i.e, the system does not allow a homogeneous solution and that there is no Oppenheimer-Snyder-like solution with a homogeneous interior and a vacuum exterior. For a regular initial dust density, the central density remains constant in time as long as the Taylor-series expansion is applicable.

We have also obtained numerical solutions of the field equations by the technique of numerical simulations. In classical general relativity, the endstate of generic inhomogeneous spherical dust collapse is a naked singularity formation at the centre. We have chosen the function $F(x)$ so that the collapse ends in the naked singularity formation in classical general relativity. The result of the numerical simulation with the inverse triad correction is plotted in Fig. 3. In (a), the dashed lines denote the conserved dust density defined by Eq. (3). As we can see in the figure, the gravitational collapse is strongly slowed down for $R \lesssim R_*$ There appears a density spike for $0 < R \lesssim R_*$. This will correspond to shell-crossing singularity, which is gravitationally weak. The slow down near the centre implies repulsive effects of quantum gravity but this is not so strong that the collapse may turn to expand. We have also studied a different version formulation of the inverse triad correction and/or different initial density profiles and found that the result is qualitatively the same.

5 Summary

LQG is a promising candidate for successful quantum gravity. We have considered the inverse triad correction effects in the marginally bound LTB spacetime. We have formulated a consistent semiclassical

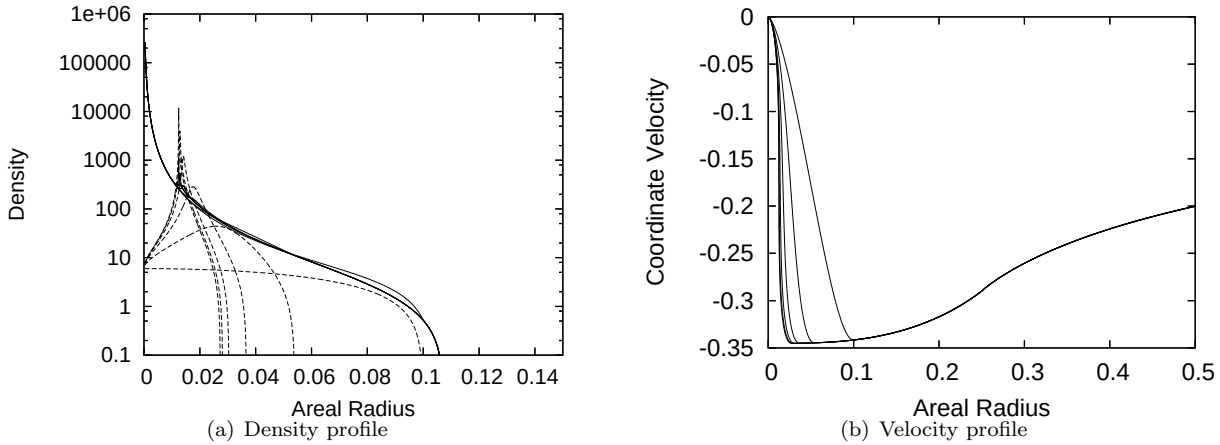

(a) Density profile (b) Velocity profile

Figure 3: The collapse of the quadratic density profile model with the initial dust radius and the mass are given $R_s = 0.1$ and $M = 0.01$, respectively. $R_* = \sqrt{\gamma/2}\ell_{\rm P} \sim 0.25$ in the present unit. In (a), the dashed lines denote the conserved dust density and the solid lines denote the effective density.

effective theory for this purpose. There is no bounce, no Friedmann solution or no self-similar solution in this system. The Minkowski spacetime in classical general relativity is replaced with a nontrivial geometry which is singular at the centre. The collapse in the central region is strongly slowed down and shell-crossing singularity is generically appears. The present result will be a caution to LQC which is based on purely homogeneous models because there is no tendency for bounce in the spherical inhomogeneous system while there is bounce in the effective theory for the homogeneous system. However, it should be noted that there are so many ambiguities in the interpretation of the present result. The present effective theory would not be a unique one even for the inverse triad effects. The present model is spherically symmetric with marginally bound dust fluid and may not be sufficiently generic. There will be other effects from loop quantum gravity. From this point of view, it is interesting to see nonmarginally bound cases, non spherically symmetric cases and different matter fields free from shell-crossing singularity.

References

[1] M. Bojowald, T. Harada and R. Tibrewala, Phys. Rev. D**78**, 064057 (2008).

[2] C. Rovelli, *Quantum Gravity*, (Cambridge University Press, Cambridge, 2004)

Measuring the spin parameter of Kerr black holes and naked singularities

Kenta Hioki[A,1] and Kei-ichi Maeda[A,B,2]

[A] *Department of Physics, Waseda University, Okubo 3-4-1, Tokyo 169–8555, Japan*
[B] *Advanced Research Institute for Science and Engineering, Waseda University, Okubo 3-4-1, Tokyo 169–8555, Japan*

Abstract

The possibility that the existence of black holes as compact objects at the cores of galaxies has become high. The black hole is said to cast an apparent shape (or a shadow) as an optical appearance because of the strong gravitational field in the black hole itself. The apparent shape is of varied forms mainly depending on the spin parameter and the inclination angle of the object. In this paper, we investigate whether it is possible to determine the spin parameter and the inclination angle by observing the apparent shape, on the assumption that the intended compact object is the Kerr space-time. In particular, we define observables which definitely characterize the apparent shape. We find that one can estimate the spin parameter and the inclination angle of the Kerr black hole even when it is naked singularity, by measuring the observables. As a prerequisite, one needs only information of the mass of the object to say so. The result will become a realistic method which come a step closer to probe the Galactic centre using future advanced interferometers.

1 Introduction

It is widely believed that there exist black holes at the cores of many galaxies. Sagittarius A*, which is the ultra compact radio source at the centre of the Milky Way, is highly likely to be a black hole. The possibility of direct observation of black holes by the future interferometers is becoming higher. However, the research of the observation of black holes in a theoretical approach is still lacking.

The theory of gravitational lensing has been developed in the weak field approximation and has been succeed to explain many physical and astronomical observations. The influence of the strong gravity of the black hole appears when the photon passes the vicinity of the origin of the gravity. In order to obtain a physical information of black holes holding the strong gravity, the direct imaging of the apparent shapes are important to be investigated [1, 2, 3, 4, 5, 6].

As a final state of a realistic gravitational collapse, the solutions of Einstein equations with strong gravity generally possess a space-time singularity. If the space-time singularity has appeared from physically reasonable initial conditions, the space-time singularity is hidden within the event horizon, so-called the cosmic censorship hypothesis, which was proposed by Penrose. It implies that a naked singularity which is a space-time singularity which is uncovered by event horizon does not existed. However, the proof for the hypothesis have not been successful up to the present date. So it is still one of the most important problem in general relativity. There is a possibility that the candidate of the black hole could be a naked singularity [7, 8].

To reach the information of the black holes such as the spin parameter and the inclination angle, we have to construct a method for a measurement of parameters with the flexibility to meet the case that the compact object is not to be a black hole but to be a naked singularity. The detail calculations of the following contents will be displayed in [9].

[1] E-mail:hioki@gravity.phys.waseda.ac.jp
[2] E-mail:maeda@waseda.jp

2 Equations of geodesic motion

The Kerr space-time in Boyer-Lindquist coordinates [10] is given by

$$ds^2 = -\left(1-\frac{2Mr}{\rho^2}\right)dt^2+\frac{\rho^2}{\Delta}dr^2+\rho^2 d\theta^2-\frac{4Mra\sin^2\theta}{\rho^2}dtd\phi+\frac{A\sin^2\theta}{\rho^2}d\phi^2 \ , \tag{1}$$

where $\Delta := r^2-2Mr+a^2$, $\rho^2 := r^2+a^2\cos^2\theta$, and $A := \left(r^2+a^2\right)^2-\Delta a^2\sin^2\theta$. M and a are the mass and the spin parameter of the Kerr space-time, respectively. The regular horizon condition for Kerr space-time to be a black hole is $|a|\leq M$. In this paper, we deal with both cases that regular horizon condition is satisfied and not satisfied $M<|a|$, which the latter case is to be a naked singularity.

We can have the general solution of geodesic motion in the following first-order form [11],

$$\begin{aligned}
\rho^2\frac{dr}{d\lambda} &= \sigma_r\sqrt{R} \ , \quad R := \left[\left(r^2+a^2\right)E-aL_z\right]^2-\Delta[(L_z-aE)^2+mr^2+\mathcal{Q}] \ , \\
\rho^2\frac{d\theta}{d\lambda} &= \sigma_\theta\sqrt{\Theta} \ , \quad \Theta := \mathcal{Q}-[a^2(m^2-E^2)+L_z^2\csc^2\theta]\cos^2\theta \\
\rho^2\frac{dt}{d\lambda} &= \frac{1}{\Delta}(AE-2MraL_z) \ , \\
\rho^2\frac{d\phi}{d\lambda} &= \frac{1}{\Delta}[2MarE+L_z\csc^2\theta(\rho^2-2Mr)] \ .
\end{aligned} \tag{2}$$

λ is the affine paramater and m is the mass of the particle. σ_r and σ_θ are sign functions, which changes the signs independently at the turning point of the geodesic. E and L_z represent the energy and the angular momentum with respect to rotation axis of the space-time of the particle, respectively. $\mathcal{Q}$ is Carter constant, which is the additional conserved quantity. For considering null geodesics $m=0$, E can be gauged away by rescaling of the affine parameter λ as

$$\tilde{R} := R/E^2 \ , \ \tilde{\Theta} := \Theta/E^2 \ , \ \xi := L_z/E \ , \ \eta := \mathcal{Q}/E^2 \ .$$

The conserved quantities ξ and η completely identify the null geodesic.

3 Measurement of the parameters

The strong gravitational field of the Kerr space-time are said to cast an apparent shape as an optical appearance. The apparent shapes of Kerr-Newman space-times were mutually complementary analyzed in [3, 6]. We would like to investigate, whether it is possible to estimate the spin parameter and the inclination angle by observing the apparent shape.

We assume that the observer is at the infinity of positive value r with inclination angle i. The celestial coordinates (α,β) of the observer are defined as the apparent perpendicular distance of the image from the rotational axis and the apparent perpendicular distance of the image from its projection on the equatorial plane, respectively. The celestial coordinates have relations with conserved quantities ξ, η and the inclination angle i as,

$$\begin{aligned}
\alpha(\xi,\eta;i) &:= \lim_{r\to\infty}\frac{rp^{(\varphi)}}{p^{(r)}} = -\xi\csc i \ , \\
\beta(\xi,\eta;i) &:= \lim_{r\to\infty}\frac{rp^{(\theta)}}{p^{(r)}} = \sqrt{\eta+a^2\cos^2 i-\xi^2\cot^2 i} \ ,
\end{aligned} \tag{3}$$

where $\left(p^{(t)},p^{(r)},p^{(\theta)},p^{(\phi)}\right)$ are the tetrad components of the momentum of null geodesics with respect to locally nonrotating reference frames [12]. We define the apparent shape of the space-time as the region in the celestial coordinates which is the set of points coincide to the null geodesics that were launch from the infinity of positive value r toward the singularity and can not come back to the infinity of positive value r again. We assume that the light sources are at the infinity of positive value r with an abundant angular size.

(a) BHs (b) NSs

Figure 1: Part (a) The contour map of the distorted rate $\hat{d}$ (the green dashed curves) and the radius $\hat{r}$ (the red solid curves). From this figure, we can estimate the spin parameter a of the Kerr black hole and the inclination angle i of the observer. Part (b) The contour map of the central angle $\hat{c}$ (the green dashed curves) and the radius $\hat{r}$ (the red solid curves). From this figure, we can estimate the spin parameter a of the Kerr naked singularity and the inclination angle i of the observer.

In the case of the Kerr black holes, we propose two observables that characterize the apparent shape, precisely. First we approximate the contour of the apparent shape by the circle passing through the three points which are at the extreme right, the upper limit, and the lower limit of the apparent shape in celestial coordinates. We define the radius $\hat{r}$ of the apparent shape as the radius of the circle which we used for approximation. Calling into account the hollow of the extreme left of the apparent shape $\triangle\hat{r}$ which is the maximal distance of the difference between the circle and the apparent shape, we define the distortion rate $\hat{d}$ of the apparent shape as $\hat{d} := \triangle\hat{r}/\hat{r}$.

We can obtain the contour maps of the radius and the distortion rate and get them together to a single Fig. 1(a). If we can measure the radius $\hat{r}$ and the distortion rate $\hat{d}$ by observation, the spin parameter a and the inclination angle i could be restricted by putting Fig. 1(a) to practical use.

In the case of the Kerr naked singularities, the apparent shape is not always a single object. It consists of two isolated parts, at most. We have to consider which part of the apparent shape is important for observation. Based on this standpoint, the "arc" is one of an interesting object. In the sense of the capture region the "arc" is 1-dimensional object, which is measure zero, but in the realistic observation the neighborhood of the "arc" can be dark enough to be observed as a black "lunate surface". We suppose a circle that passes both ends and the center of the "arc", and prepare to define observables.

We propose here the radius $\hat{r}$ and the central angle $\hat{c}$ of the "arc". The radius $\hat{r}$ is defined as the radius of the circle which we supposed. The central angle $\hat{c}$ is defined as the angular distance of the arc segment on the circle. The radius and the central angle feature the shape of the "arc", which continuously changes by the spin parameter and the inclination angle. Fig. 1(b) is the contour map of the radius and the central angle, which enable one to estimate the spin parameter and the inclination angle by observing the two observables $\hat{r}$ and $\hat{c}$.

4 Conclusion

We defined new observables and proposed a method for the estimation of the parameters of the Kerr space-time as the compact object. In fact, we have shown that one can estimate the spin parameter and the inclination angle of the Kerr space-time by measuring the observables of the apparent shape without degeneracy. However, the resolution capability of an observation equipment at present age makes a limitation for the measurement. We must hold up a hope for further progress in technology of future advanced interferometers.

References

[1] P. J. Young, Phys. Rev. D **14**, 3281 (1976).

[2] H. Falcke, F. Melia and E. Agol, Astrophys. J. **528**, L13 (2000) arXiv:astro-ph/9912263.

[3] A. de Vries, Class. Quant. Grav. **17**, 123 (2000).

[4] R. Takahashi, J. Korean Phys. Soc. **45**, S1808 (2004) [Astrophys. J. **611**, 996 (2004)] [arXiv:astro-ph/0405099].

[5] A. E. Broderick and R. Narayan, Astrophys. J. **638**, L21 (2006) [arXiv:astro-ph/0512211].

[6] K. Hioki and U. Miyamoto, Phys. Rev. D **78**, 044007 (2008) [arXiv:0805.3146 [gr-qc]].

[7] K. i. Nakao, N. Kobayashi and H. Ishihara, Phys. Rev. D **67**, 084002 (2003) [arXiv:gr-qc/0211061].

[8] K. S. Virbhadra and G. F. R. Ellis, Phys. Rev. D **65**, 103004 (2002).

[9] K. Hioki and K. Maeda, (in preparation).

[10] R. P. Kerr, Phys. Rev. Lett. **11**, 237 (1963).

[11] B. Carter, Phys. Rev. **174**, 1559 (1968).

[12] J. M. Bardeen, W. H. Press and S. A. Teukolsky, Astrophys. J. **178**, 347 (1972).

Non-linear evolution of matter power spectrum in a closure theory

Takashi Hiramatsu[1], Kazuya Koyama[2] and Atsushi Taruya[3]

[1]*Institute for Cosmic Ray Research (ICRR), The University of Tokyo, Chiba 277–8582, Japan*
[2]*Institute of Cosmology & Gravitation, University of Portsmouth, Portsmouth, Hampshire, PO1 2EG, UK*
[3]*Research Center for the Early Universe (RESCEU), The University of Tokyo, Tokyo 113–0033, Japan*

Abstract

We study the non-linear evolution of cosmological power spectra in a closure theory. Governing equations for matter power spectra have been previously derived by a non-perturbative technique with closure approximation. Solutions of the resultant closure equations just correspond to the resummation of an infinite class of perturbation corrections, and they consistently reproduce the one-loop results of standard perturbation theory. We develop a numerical algorithm to solve closure evolutions in both perturbative and non-perturbative regimes. The present numerical scheme is particularly suited for examining non-linear matter power spectrum in general cosmological models, including modified theory of gravity. As a demonstration, we apply our numerical scheme to the Dvali-Gabadadze-Porrati braneworld model.

1 Introduction

Probing the nature of dark energy, accelerating the late-time universe, is one of the most tough issues in cosmology and astrophysics. So far it remains to be clarified what the dark energy really is. A simple solution is that it is the cosmological constant, or described by dynamics of unknown scalar fields. Another solution may lie in the sector of gravity. The attention has been focused on the test of general relativity (GR) in both solar system experiments and cosmological contexts. Several modified theories of gravity beyond GR have passed these tests and been viable. A key to distinguish these possibilities is to precisely predict the matter power spectrum considering non-linear dynamics of matter perturbations. This situation motivates to develop a framework to compute the non-linear matter power spectrum in a variety of cosmological models.

The naive perturbative approach (see [1] for a review) has been frequently used for predictions of the power spectra, as well as fully numerical approach such as N-body simulations. Recently, alternative to perturbation theory, several authors have recently proposed the renormalisation/resummation technique for the infinite series of the loop calculation appeared in the naive expansion of the perturbative quantities. In those treatments, the fundamental quantities are not the density/velocity perturbations but propagators, power spectra and vertex functions of density and velocity divergence [2]. In our previous paper [3], we have derived evolution equations of the non-perturbative quantities, power spectra and propagators of matter fluctuations on the basis of the closure approximation used in the statistical theory of turbulence [4]. This approach is suited for numerical purpose where we set the initial conditions and track the time evolution of those quantities.

In this paper, we demonstrate the closure equations in the case of Dvali-Gabadadze-Poratti (DGP) braneworld model. For the numerical scheme, please see [5] and, for the numerical analysis, [6].

2 Evolution equations for perturbations

We consider the cold dark matter plus baryon system as a pressureless perfect (irrotational) fluid neglecting the contribution from massive neutrinos. The density contrast, $\delta \equiv \delta\rho/\rho$, and the velocity divergence,

[1]E-mail:hiramatz@icrr.u-tokyo.ac.jp
[2]E-mail:kazuya.koyama@port.ac.uk
[3]E-mail:ataruya@utap.phys.s.u-tokyo.ac.jp

$\theta \equiv \nabla \cdot \mathbf{u}$, are governed by the Euler and the continuity equations. The Newton potential, ϕ, satisfies the Poisson equation with non-linear source terms, if exists,

$$-\frac{k^2}{a^2}\phi(\mathbf{k},\tau) = 4\pi G_{\rm eff}(\mathbf{k},\tau)\rho_m\widetilde{\delta}(\mathbf{k},\tau) + (\text{nonlinear terms}), \quad G_{\rm eff} = G\left[1+\frac{1}{3}\frac{(k/a)^2}{\Pi(k)}\right], \tag{1}$$

where we take the time coordinate as $\tau = \log(a/a_0)$, and $G_{\rm eff}$ represents the effective gravity constant generalising the Newton constant G in GR with a model-dependent function, $\Pi(k)$.

For the purpose of quantitative estimation of the density/velocity perturbations, we consider their statistical quantities, namely, power spectra. The perturbations are recasted in a vector form, $\Phi_a(\mathbf{k},\tau) = (\widetilde{\delta}(\mathbf{k},\tau), -\widetilde{\theta}(\mathbf{k},\tau))^{\rm T}$. The standard approach of perturbative estimation of power spectra is then to expand $\Phi_a = \Phi_a^{(0)} + \Phi_a^{(1)} + \cdots$, where $\Phi_a^{(i\geq 1)}$ is iteratively obtained from the Euler and the continuity equations, and to substitute it into the definition of the power spectra,

$$\langle \Phi_a(\mathbf{k},\tau)\Phi_b(\mathbf{k}',\tau)\rangle = (2\pi)^3\delta_D(\mathbf{k}+\mathbf{k}')P_{ab}(|\mathbf{k}|;\tau). \tag{2}$$

In addition to this quantity, we here introduce the propagator, $G_{ab}(\mathbf{k}|\tau,\tau')$, and the power spectra between different times, $R_{ab}(\mathbf{k};\tau,\tau')$, defined as [2, 3]

$$\left\langle \frac{\delta\Phi_a(\mathbf{k},\tau)}{\delta\Phi_b(\mathbf{k}',\tau')}\right\rangle = G_{ab}(\mathbf{k}|\tau,\tau')\delta_D(\mathbf{k}-\mathbf{k}'), \quad \langle \Phi_a(\mathbf{k},\tau)\Phi_b(\mathbf{k}',\tau')\rangle = (2\pi)^3\delta_D(\mathbf{k}+\mathbf{k}')R_{ab}(|\mathbf{k}|;\tau,\tau'), \quad (\tau>\tau'). \tag{3}$$

Then using those quantities, the above naïve expansion is re-organised in a non-perturbative way.

In the closure theory, we truncate the non-perturbative expansions of the power spectra and the propagator up to the one-loop level, and make them close. The resultant equations are [3, 5, 6]

$$\hat{\Lambda}_{ab}G_{bc}(k|\tau,\tau') = \int_{\tau'}^{\tau} d\tau''\, M_{as}(k;\tau,\tau'')G_{sc}(k|\tau'',\tau') + S_{ar}(k;\tau)G_{rc}(k|\tau,\tau'), \tag{4}$$

$$\hat{\Lambda}_{ab}R_{bc}(k;\tau,\tau') = \int_{\tau_0}^{\tau} d\tau''\, M_{as}(k;\tau,\tau'')R_{\overline{sc}}(k;\tau'',\tau') + \int_{\tau_0}^{\tau'} d\tau''\, N_{a\ell}(k;\tau,\tau'')G_{c\ell}(k|\tau',\tau'') + S_{ar}(k;\tau)R_{rc}(k;\tau,\tau'), \tag{5}$$

where we defined $k = |\mathbf{k}|$ and $k' = |\mathbf{k}'|$, and

$$M_{as}(k;\tau,\tau'') = 4\int\frac{d^3\mathbf{k}'}{(2\pi)^3}\gamma_{apq}(\mathbf{k}-\mathbf{k}',\mathbf{k}')\gamma_{\ell rs}(\mathbf{k}'-\mathbf{k},\mathbf{k})G_{q\ell}(k'|\tau,\tau'')R_{pr}(|\mathbf{k}-\mathbf{k}'|;\tau,\tau''), \tag{6}$$

$$N_{a\ell}(k;\tau,\tau'') = 2\int\frac{d^3\mathbf{k}'}{(2\pi)^3}\gamma_{apq}(\mathbf{k}-\mathbf{k}',\mathbf{k}')\gamma_{\ell rs}(\mathbf{k}-\mathbf{k}',\mathbf{k}')R_{qs}(k';\tau,\tau'')R_{pr}(|\mathbf{k}-\mathbf{k}'|;\tau,\tau''), \tag{7}$$

$$S_{ar}(k;\tau) = 3\int\frac{d^3\mathbf{k}'}{(2\pi)^3}\sigma_{apqr}(\mathbf{k}',-\mathbf{k}',\mathbf{k};\tau)P_{pq}(k';\tau). \tag{8}$$

Here the functions γ_{acd} and σ_{abcd} are called as the vertex functions described as a simple function of wavenumber. The non-linear terms in the Euler and continuity equations give rise to three non-vanishing components, $\gamma_{112}, \gamma_{121}$ and γ_{222}. In the case where the Poisson equation has non-linear source terms, the components, γ_{211} and σ_{2111}, become non-zero, while the other components remain to be zero. The operator $\hat{\Lambda}_{ab}$ is defined by

$$\hat{\Lambda}_{ab} = \delta_{ab}\frac{\partial}{\partial\tau} + \Omega_{ab}(\tau), \quad \Omega_{ab}(\tau) = \begin{pmatrix} 0 & -1 \\ -4\pi G_{\rm eff}\frac{\rho_{\rm m}}{H^2} & 2+\frac{\dot{H}}{H^2}\end{pmatrix}. \tag{9}$$

Eqs. (4)(5) contain the non-linear quantities in those source terms. Since we truncated at the one-loop level when the equations were derived, it is easy to see the recovery of the one-loop power spectrum in the SPT by replacing all power spectra, R_{ab}, and propagators, G_{ab}, in the source terms with those calculated in the linear theory, $R^{\rm L}_{ab}$, and $G^{\rm L}_{ab}$ [3]. Here the linear quantities are given by Eqs. (4)(5) with neglecting all of right-hand sides. Furthermore, it needs to be emphasised that, the formal solution of the closure equations has been confirmed to coincide with the renormalised one-loop results presented by Crocce and Scoccimarro apart from the vertex renormalisation [2]. Hence, the closure equation is basically equivalent to the RPT truncated at the one-loop level.

3 Results

3.1 Non-linear solution : ΛCDM model

We first present the results of closure equations (4)(5) in the flat ΛCDM model with the cosmological parameters : $\Delta^2_R(k_0) = 2.457 \times 10^{-9}$, $n_s = 0.960$, $\Omega_{M0} = 0.279$, $h = 0.701$. In this case, $\gamma_{211} = \sigma_{2111} = 0$, and $\Pi(\mathbf{k}) = (k/a)^2/3$, resulting in $G_{\rm eff} = G$.

In the left panel of Fig. 1, the ratio of the non-linear power spectrum to the linear one at $z = 3$ is plotted. We found that the non-linear effects of the closure equations suppress the amplitude on small scales in comparison with the SPT (dashed line, see [1]). The dotted and the dotted-dashed lines are the power spectra analytically obtained with the 1st and 2nd Born approximation, respectively, [3]. We confirmed that the higher order approximation tends to agree with the result of the closure equations.

The behaviour of the propagators in the closure equations is shown in the middle panel where we define $\widetilde{G}_1 \equiv G_{11} + G_{12}$. The amplitude is normalised to unity on large scales by multiplying the linear growth rate. While the propagator computed in SPT goes negative infinity shown as the dotted line, the numerical solution in the closure equations tends to converge to zero on small scales. This damping feature is caused by the non-linear effects as a result of taking into account the higher-order corrections neglected in the SPT, leading to the suppression of the power on small scales.

As we mentioned in [3], in the small-scale limit, the propagator behaves as the Bessel function of the first kind. On the other hand, in the large-scale limit, the propagator should coincide with the one-loop result in the SPT. The dashed line in the right panel is the approximate solution matching the both limits obtained in [3]. We found that the approximate solution agrees well with the numerical solution of the closure equations even on intermediate scales between the limits.

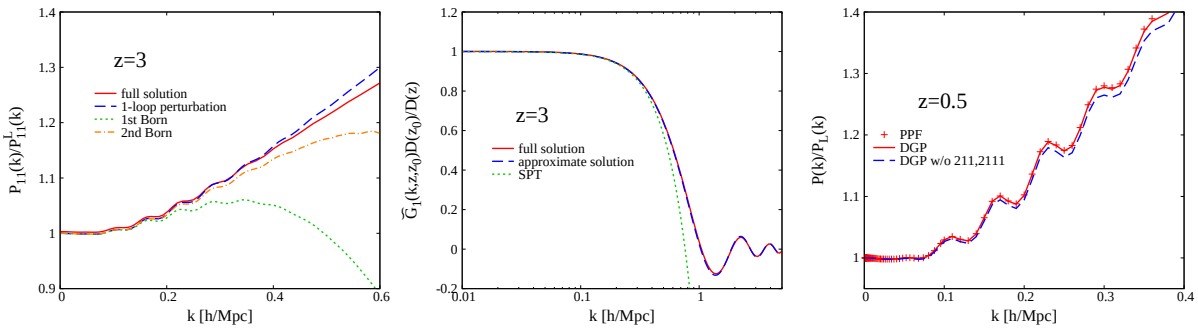

Figure 1: [*Left*] The resultant power spectra divided by the linear power spectra at $z = 3$, [*Middle*] the propagators $\widetilde{G}_1(k, z, z_0) \equiv G_{11} + G_{12}$ evaluated at $z = 3$, and [*Right*] the perturbative solution normalised by the linear power spectrum in the DGP model at $z = 0.5$ (next subsection). 'PPF' is obtained from the fitting formula proposed by [8] with $c_{nl} \approx 0.36$.

3.2 Perturbative solution : DGP model

As an application of our formalism, we apply it to the DGP braneworld model to compute the power spectrum in the SPT. The perturbative solution, namely, the calculation in the SPT, can be done by a simple replacement of G_{ab} and R_{ab} in the right-hand sides of the closure equations (4)(5) with the linear propagator and power spectra, $G^{\rm L}_{ab}$ and $R^{\rm L}_{ab}$, as discussed in the end of Sec.2.

The modified Friedman equation in the self-accelerating branch is given by

$$\frac{H}{r_c} = H^2 - \frac{\kappa^2}{3}\rho, \tag{10}$$

where r_c is the parameter in this model which is a ratio between the 5D Newton constant and the 4D Newton constant.

In this model, gravity becomes 5D on large scales larger than r_c. On small scales, gravity becomes 4D but it is not described by GR. According to the quasi-static perturbations [7], the brane-bending mode couples to the Newton potential on the brane. Therefore we have

$$\gamma_{211}(\mathbf{k}_1,\mathbf{k}_2;\tau) = -\frac{1}{12H^2}\left(\frac{8\pi G\rho_{\rm m}}{3}\right)^2\left(\frac{k_{12}^2}{a^2}\right)\frac{M(\mathbf{k}_1,\mathbf{k}_2)}{\Pi(\mathbf{k}_{12})\Pi(\mathbf{k}_1)\Pi(\mathbf{k}_2)} \tag{11}$$

$$\sigma_{2111}(\mathbf{k}_1,\mathbf{k}_2,\mathbf{k}_3;\tau) = \frac{8\pi G\rho_{\rm m}}{324H^2}\left(\frac{k_{123}^2/a^2}{\Pi(\mathbf{k}_{123})\Pi(\mathbf{k}_1)\Pi(\mathbf{k}_2)\Pi(\mathbf{k}_3)}\right)\left(\frac{M(\mathbf{k}_1,\mathbf{k}_2+\mathbf{k}_3)M(\mathbf{k}_2,\mathbf{k}_3)}{\Pi(\mathbf{k}_{23})}+\text{perm.}\right) \tag{12}$$

where

$$M(\mathbf{k}_1,\mathbf{k}_2) = 2\frac{r_c^2}{a^4}[k_1^2k_2^2-(\mathbf{k}_1\cdot\mathbf{k}_2)^2],\quad \beta(\tau) = 1-2Hr_c\left(1+\frac{\dot{H}}{3H^2}\right) \tag{13}$$

For the numerical calculation, we use the best fit parameters for the flat self-accelerating universe $\Omega_m = 0.257, \Omega_r = 0.138, h = 0.66, n_s = 0.998$. The resultant power spectrum normalised by the linear one is presented as the solid line in the right panel of Fig. (1). The dashed line is the same calculation neglecting the extra functions, γ_{211} and σ_{2111}. From this figure, we found that γ_{211} gives a positive contribution to the mode coupling, while σ_{2111} gives a negative and smaller contribution. Therefore the resultant power is enhanced on small scales.

We also plotted the prediction in the Parameterised Post-Friedmann (PPF) framework proposed in [8] as 'PPF' in the right panel. It is possible to recover the numerical solution for the non-linear power spectrum very well with the non-linear parameter $c_{nl} \approx 0.36$ introduced in [8].

4 Summary

In this paper, we showed the non-linear matter power spectra as a demonstration of our numerical scheme for the closure equations derived in [3]. From the calculation in the ΛCDM model, we observed the extra suppression of the power on small scales due to the non-linear effects which are neglected in the SPT, as shown in the left panel of Fig (1). Moreover, the middle panel shows that the resultant propagator converges to zero on small scales, and coincides with the approximate solution obtained in an analytic way in [3]. These facts confirm that the closure equations contain non-linear contributions more than the SPT, and that our numerical scheme works well from the qualitative viewpoint.

As an application, we applied the closure equations to compute the perturbative prediction of the matter power spectrum in the DGP model. The perturbative calculation, namely, the calculation in the SPT can be performed by the replacement of the right-hand sides of the closure equations (4)(5) with the linear propagator and power spectra, $G_{ab}^{\rm L}$ and $R_{ab}^{\rm L}$. As as result, the extra vertex function, γ_{211}, gives a positive, and large, contribution to the mode coupling, enhancing the power on small scales.

More detailed analysis can be seen in [6] together with the application to a $f(R)$ gravity model.

References

[1] F. Bernardeau, S. Colombi, E. Gaztanaga and R. Scoccimarro, Phys. Rept. **367** (2002) 1

[2] M. Crocce and R. Scoccimarro, Phys. Rev. D **73**, 063519 (2006) [arXiv:astro-ph/0509418] ;M. Crocce and R. Scoccimarro, Phys. Rev. D **73**, 063520 (2006) [arXiv:astro-ph/0509419].

[3] A. Taruya and T. Hiramatsu, arXiv:0708.1367 [astro-ph].

[4] R. H. Kraichnan, J. of Fluid Mechanics **5**, 497 (1959)

[5] T. Hiramatsu and A. Taruya, in preparation.

[6] K. Koyama, A. Taruya and T. Hiramatsu, in preparation.

[7] K. Koyama and F. P. Silva, Phys. Rev. D **75**, 084040 (2007) [arXiv:hep-th/0702169].

[8] W. Hu, Phys. Rev. D **77**, 103524 (2008) [arXiv:0801.2433 [astro-ph]].

Particle acceleration in force-free magnetospheres around rotating black holes - the outer gap models -

Takamitsu Horiguchi[1], Taichi Kobayashi[2], Kohei Onda[3] and Akira Tomimatsu[4]

[1,2,3,4] *Department of Physics, Nagoya University, Chikusa-Ku, Nagoya, 464–8602, Japan*

Abstract

We consider the position of the outer gap in a disk-hole system without solving the Grad-Shafranov equation for the force-free magnetosphere. It is believed that the magnetosphere around the rotating black hole surrounded by the accretion disk, such as active galactic nuclei, mainly causes high energy phenomena. In the force-free magnetospheres of pulsars, it is known that the accelerating electric field arises in a charge depletion region from the so-called Goldreich-Julian charge density and can influence to produce high energy gamma-rays, as the outer gap and polar-cap models. We focus on the magnetosphere of the closed-field configuration in which the magnetic field lines directly connect the hole to the disk, and apply outer gap models of a pulsar to it. As a result, it is shown that gaps can arise in the region with both the closed field from the hole to the disk and the open field from the disk to infinity. We also estimate the size of the gap, the energy of a particle accelerated in the gap, and the energy of gamma rays emitted from the gap.

1 Introduction

Recent observations show that the central engines of active galactic nuclei (AGN), the supermassive black holes, most probably operate as powerful particle accelerators. Also, AGN are possible candidate sites of high energy cosmic ray acceleration, which is supported by Auger observations [1] although there also are arguments against it [2]. At the least, it's considered that particles, such as electrons and protons are accelerated to high energy in AGN. As the way to reveal it, it has been considered that the black hole magnetosphere which is formed by a supermassive black hole in AGN operates on the particle acceleration. Blandford-Znajek process in the force-free black hole magnetospheric model which is the model of a stationary, plasma-filled magnetosphere around a rotating black hole is used to explain extracting the energy from a black hole [3]. It's well known as explanation for the energy of the jet. But, it cannot show the concrete way to accelerate particles. So, as one model, we show that an "outer gap" in the force-free magnetosphere effectively operate particle acceleration.

2 Outer gap and force-free magnetospheric model

The outer gap model is known as a model of γ-ray emission in pulsar magnetospheres and is successful in explaining the observation [4, 5, 6]. This is a strong electric field sustained along a magnetic field line in force-free magnetospheres. In force-free magnetospheres, the charge density should keep the Goldreich-Julian charge density:

$$\rho_{\rm GJ} = -\frac{1}{4\pi}\boldsymbol{\nabla}\cdot\left(\frac{\delta\Omega}{\alpha}\boldsymbol{\nabla}\Psi\right), \tag{1}$$

where $\delta\Omega \equiv \Omega_F - \omega$, $\Omega_F = \Omega_F(\Psi)$ is angular velocity of the field line, $\Psi(r,\theta)$ is poloidal magnetic flux function, and α and ω are the lapse function and the angular velocity of zero angular momentum

[1]E-mail:horiguchi@gravity.phys.nagoya-u.ac.jp
[2]E-mail:kobayashi@gravity.phys.nagoya-u.ac.jp
[3]E-mail:onda@gravity.phys.nagoya-u.ac.jp
[4]E-mail:atomi@gravity.phys.nagoya-u.ac.jp

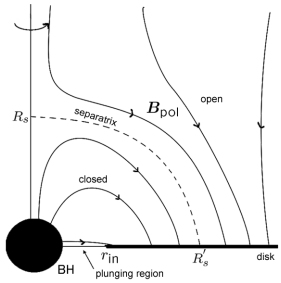

Figure 1: Schematic drawing of a magnetically coupled configuration. The magnetic flux connects from the disk to the black hole inside the separatrix and from the disk to infinity outside the separatrix. The separatrix arrives at the point $r = R_s$ above the pole from the point $r = R_s^{'}$ in the equator.

observers, respectively, and the charge-separated plasma cannot be accelerated. But, the "null charge surface" (or simply "null surface") where $\rho_{\rm GJ}$ vanishes could be regions with a strong electric field $E_\parallel$ sustained along a magnetic field line. Although the emerging $E_\parallel$ would act to move available charge into (from) the charge deficient (excess) region if the charge density ρ_e differed significantly from $\rho_{\rm GJ}$ in any region, there is not enough available charge to redistribute near this surface. So, this carge deficit leads to the emergence of the stationary gap. $E_\parallel$ is given by the Poisson equation:

$$\boldsymbol{\nabla} \cdot \boldsymbol{E}_\parallel = 4\pi \left(\rho_e - \rho_{\rm GJ}\right), \tag{2}$$

where $\rho_e \equiv e(N_+ - N_-)$ is the charge density defined by the difference between positive and negative charges.

Application of the outer gap to black hole magnetospheres was originally examined by Beskin *et al.* [7] and the more quantitative study was developed by Hirotani & Okamoto [8]. However, we regard the outer gap as the particle accelerator for the γ-rays and cosmic rays emission. Since it's considered that the accretion disk is the source of protons and heavy nuclei which are charged particles of cosmic rays, we hope to consider a model that the charged particles flow from the disk to the outer gap and are accelerated there. But this cannot be realized in the black hole magnetospheres with uniform or monopole fields which the past study showed because no magnetic field line connected from the disk to the gap exists in it. Neronov *et al.* showed that it's possible to accelerate the particle flowing from the disk in the gap of the polar region by absence of alignment of the magnetic field with the black hole rotation axis [9]. However, since the magnetosphere which they assumed isn't force-free magnetospheres but vacuum ones, it was inadequate for the plasma-filled ones.

So, we focus on the particle acceleration in the gap and the paricle flow from the disk to infinity in the force-free black hole magnetosphere. This is realized by the magnetically coupled configuration of which the most simple model is that all magnetic field lines from the black hole connect to the disk and the magnetic field line outside the separatrix which is the boundary between open field lines and closed field lines connect from the disk to infinity (see Figure.1). Its one model is numerically solved by Uzdensky [10]. We research the position of the outer gap in this topology and consider if it can accelerate the particle from the disk. Also, we roughly estimate the gap width and the voltage drop.

3 The position of the outer gap

Since the outer gap emerges around the null charge surface, we search the position of null charge surface. Although we need to solve the generally relativistic Grad-Shafranov equation for force-free magnetospheres in order to solve $\rho_{\rm GJ} = 0$ (for need of magnetic flux Ψ), we don't solve it exactly. Instead, we use such equation as the second-order derivatives Ψ in the Grad-Shafranov equation is substituted for (1):

$$\rho_{\rm GJ} = \frac{1}{D}\left[\frac{\alpha^3}{4\pi\varpi^2}\frac{\delta\Omega^2\varpi^4}{\alpha^4}\boldsymbol{\nabla}\left(\frac{\alpha^2}{\delta\Omega\varpi^2} + \omega\right)\cdot\boldsymbol{\nabla}\Psi + \frac{1}{4\pi\alpha}\delta\Omega I\frac{dI}{d\Psi}\right], \tag{3}$$

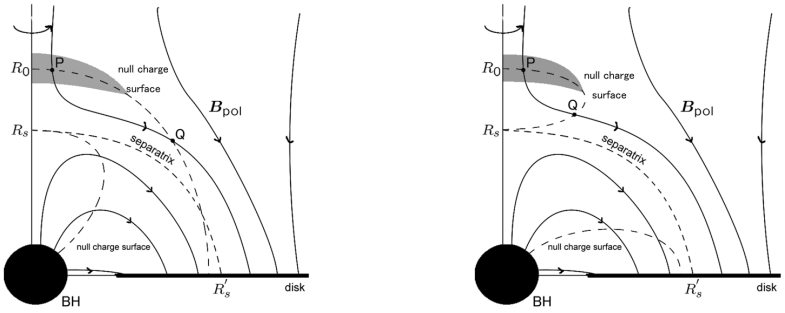

(a) (b)

Figure 2: The possible configuration of null charge surfaces to eject from the disk to infinity. Both configurations can accelerate the charged particle flowing along the field to infinity in polar region. Directing our attention to the magnetic flux right outside the separatrix, the region of the gap is the gray region.

where $D \equiv \alpha^2 - \delta\Omega^2\varpi^2$, $\varpi \equiv \sqrt{g_{\varphi\varphi}}$ in Boyer-Lindquist coordinate and $I = I(\Psi)$ is $2/c$ times the poloidal electric current flowing through the circular loop $r = \text{const}$, $\theta = \text{const}$. Of cource, it is difficult to solve this equation. So, we expect the position of $\rho_{\rm GJ} = 0$ by finding it in the polar region, on the equator, and on the vent horizon.

As a result, we found that two surfaces are in the polar region, one surface is near the horizon and one surface is on the equator. One surface in the polar region is on the separatrix and the other is on the corotation point ($\delta\Omega = 0$). The surface on the horizon is on the magnetic field line with the maximal current ($I(dI/d\Psi) = 0$). And, The surface on the equator is on the corotation surface if its surface is on the plunging region which is between the black hole and the disk or between the magnetic field line with the maximal current and the separatrix ($r = R_s'$ in Figure.1) if the corotation surface is on the disk. We can expect the configuration of the null charge surface by connecting their four boundaries. In the expected configurations, the model where particles flowing from the disk are accelerated to infinity is realized in the case where the gap emerges in the open field region near the polar axis (Figure.2). The condition of this model is that the corotation surface in the polar region is outside the separatrix. The difference between two configurations of Figure.2 is a difference of the position between the corotation surface $r = R_0$ and the separatrix $r = R_s$ on the polar axis. They tend to select (b) in Figure.2 if there is the corotation surface near the separatrix or the configuration of the separatrix is oblate ($R_s < R_s'$). Since the inner null charge surface in (a) in Figure.2 always crosses to the inner light surface (which is the surface of $D = 0$ and the singular surface of the Grad-Shafranov equation), appropriate regularity conditions may be selected on this light surface in order to select (a).

Directing our attention to the magnetic field line in the open field region near the separatrix, charged particles moving along this can be accelerated in the gap near the polar axis (gray color region in Figure.2) and can be ejected to infinity. This field line crosses the null charge surface twice, but it's thought that the gap cannot grow around the inside null charge surface (around the point Q), because the direction of the electric field is opposite and the global electric current is interfered. Such region is filled to the Goldreich-Julian charge density with the charge from the disk or the other gap.

4 Rough estimation of the gap width and the voltage drop

We roughly estimate the gap width and the voltage drop by using one-dimensional equations along the magnetic field lines. In particular, high energy γ-rays are observed not only from luminous AGN, such as quasars and blazars (its luminosity is $\gtrsim 10^{43}$ [ergs s^{-1}]), but also from low luminosity AGN, such as weak Seyfert (its luminosity is 10^{40}-10^{43} [ergs s^{-1}]). So, we show the luminosity dependence of them.

The following static physical process is considered in the gap. First, the electric field emerges around the null charge surface because of the charge depletions. Secondly, it accelerates the charged particles in the gap and they emits the γ-ray photons by the curvature radiation or the inverse Compton scattering. Finally, the emitted photons generate electrons & positrons with soft background photons by the pair production and are reduced, whereas the charged particles increase. These processes is showed by self-consistently solving the Poisson equation (2), the kinetic equation with the reaction force for γ-ray emission, and the Boltzmann equation of particles and photons. We roughly estimate these equation and get the gap width H and the voltage drop $V_{\rm gap}$:

$$H \approx 10^{11} \left(\frac{M}{10^8 M_\odot}\right)^{0.79} \left(\frac{L}{L_{\rm Edd}}\right)^{-0.07} \ [\rm cm], \tag{4}$$

$$V_{\rm gap} \approx 10^{12} \left(\frac{M}{10^8 M_\odot}\right)^{0.36} \left(\frac{L}{L_{\rm Edd}}\right)^{-0.21} \ [\rm V], \tag{5}$$

in the case where curvature radiation is dominant and

$$H \approx 10^{9} \left(\frac{M}{10^8 M_\odot}\right)^{0.80} \left(\frac{L}{L_{\rm Edd}}\right)^{-0.40} \ [\rm cm], \tag{6}$$

$$V_{\rm gap} \approx 10^{7} \left(\frac{M}{10^8 M_\odot}\right)^{0.40} \left(\frac{L}{L_{\rm Edd}}\right)^{-1.20} \ [\rm V], \tag{7}$$

in the case where inverse Compton is dominant. Here, M is the black hole mass, and L is the luminosity of the soft background photon emitted from the disk and is represented by the ratio of the Eddington luminosity. We found that the curvature radiation is dominant because of the gap width being shorter than the width by inverse Compton scattering if L is less than $10^{-5} - 10^{-6} L_{\rm Edd}$. Its width is 10^{12} [cm] and the energy gained the proton, electron and so on is 10^{15} [eV]. Also, we found that the more luminosity lowers, the more energy is high.

5 Summary

We considered the outer gap in the force-free magnetosphere with separatrix. We showed the configuration of the outer gap in it and found that the separatrix formed the gap in the polar retion which can eject the particle flowing from the disk to infinity. Also, we estimated the gap width and the energy gained particles by roughly estimation. We found that curvature radiation is dominant and the high energy over TeV is got if the Eddington ratio for accretion is low. So, it's thought that the outer gap is expected as the source of the high energy γ-ray and cosmic ray emission.

References

[1] Abraham, J., *et al.* 2007, Science, 318, 939

[2] Gorbunov, D. S., Tinyakov, P. G., Tkachev, I. I., & Troitsky, S. V. 2008, arXiv:astro-ph/08041088

[3] Blandford, R. D., & Znajek, R. L. 1977, MNRAS, 179, 433

[4] Hirotani, K., & Shibata, S. 1999a, MNRAS, 308, 54

[5] Hirotani, K., & Shibata, S. 1999b, MNRAS, 308, 67

[6] Romani, R. W., & Yadigaroglu, I. -A. 1995, ApJ, 438, 314

[7] Beskin, V. S., Istomin, Ya. N., & Par'ev, V. I. 1992, Soviet Ast., 36, 642

[8] Hirotani, K., & Okamoto, I. 1998, ApJ, 497, 563

[9] Neronov, A. Yu., Semikoz, D. V., & Tkachev, I. I. 2007, arXiv:astro-ph/0712.1737v1

[10] Uzdensky, D. A. 2005, ApJ, 620, 889

Extremal Black Holes in Higher Dimensions and Symmetries

Akihiro Ishibashi[1]

Cosmophysics Group, Institute of Particle and Nuclear Studies
KEK, Tsukuba, Ibaraki, 305-0801, Japan

Abstract

This is a brief introduction of the recent paper "On the 'Stationary Implies Axisymmetric' Theorem for Extremal Black Holes in Higher Dimensions" by S. Hollands and the present author arXiv:0809.2659 [gr-qc]. Main focus is on illustrating—using a simple model—the key ideas of our proof of the black hole rigidity theorem that applies to both extremal and non-extremal black holes in higher dimensions.

1 Introduction

It is known that in four-dimensional general relativity, a stationary rotating black hole must be axisymmetric. More precisely, one can show under certain conditions that (i) the event horizon of an asymptotically flat, stationary black hole must be a Killing horizon, and (ii) if the black hole is rotating, then the spacetime must also be axisymmetric as well as stationary. This assertion—called the *rigidity theorem*—provides a firm basis of the black hole thermodynamics, guaranteeing that the notion of the surface gravity/temperature is well-defined, and in particular, plays an essential role in the proof of the black hole uniqueness theorem. However, it is now known that in higher dimensions, the black hole uniqueness theorem no longer holds as it stands, and there is a much richer variety of exact black hole solutions, the classification of which is a major open problem in higher dimensional general relativity. In view of this, it is of great interest to study whether the rigidity property also holds in higher dimensions since (if holds) one may be able to place restrictions on possible exact black hole solutions from the view point of spacetime symmetry.

The rigidity theorem for four-dimensional stationary black holes was first shown by Hawking long time ago. In his original proof, a key role is played by the fact that the horizon cross section is topologically two-sphere. For this reason, it would not appear to be obvious whether the rigidity property also holds true in higher dimensions. Recently, Hollands, Wald, and the present author was able to generalise the rigidity theorem to higher dimensions [1], by invoking the *ergodic theorem*. Our theorem [1] apply to non-spherical black holes, which can occur in higher dimensions. However, the proof does not apply to extremal black holes with degenerate event horizon. Since extremal black holes play an important role in string theory, it is desirable to generalise the higher dimensional rigidity theorem to include extremal black holes in higher dimensions. This has recently been done by Hollands and the present author [2] by imposing seemingly artificial restrictive condition on the vector of horizon angular velocities. Although it is unclear whether this additional condition is really needed or just an artefact of the proof, it has also been shown in [2] that this condition is only violated by a measure zero set of the space of angular velocity parameters. The purpose of this paper is to illustrate what the main difficulties are in generalising the proof of the rigidity theorem to higher dimensions, and briefly sketch the key idea of our rigidity proof by considering a simple, toy model.

2 Main issues and the key idea

Since the stationary Killing vector field t^a generates a one-parameter group of isometries, it must be tangent to the event horizon, $\mathcal{H}$. Then, when t^a is not normal to $\mathcal{H}$ (i.e., not tangent to the null geodesic generators of $\mathcal{H}$), the black hole is said to be *rotating*. We first show that there exists an additional Killing vector field, K^a, that is normal to $\mathcal{H}$ on $\mathcal{H}$, besides t^a. Then, having the desired K^a, (a linear

[1]E-mail:akihiro.ishibashi@kek.jp

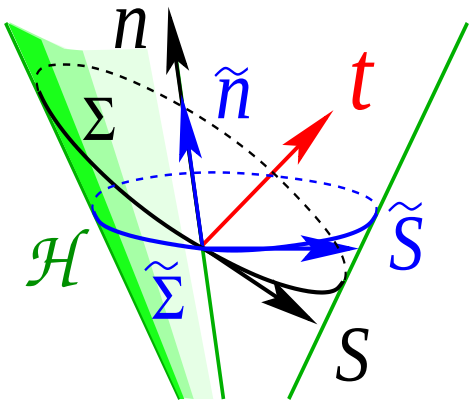

Figure 1: The decomposition $t^a = n^a + s^a$ depends on the choice of foliation Σ. We wish to find a 'correct' foliation $\tilde{\Sigma}$ so that the corresponding $\tilde{n}^a = K^a$ satisfies—as a candidate Killing field—the desired properties (i)–(iii).

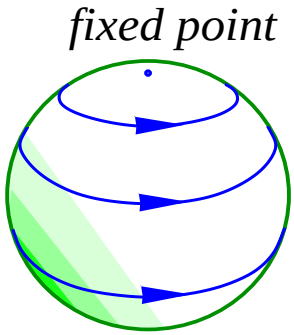

Figure 2: A horizon cross-section Σ for a 4-dimensional black hole. The blue lines denote the flow of s^a, which has a fixed point on $\Sigma \approx S^2$ and closed orbits.

combination of) rotational symmetries may be expressed by $S^a = t^a - K^a$. Such a desired Killing vector field is (I) first to be constructed locally in a neighbourhood of $\mathcal{H}$, and (II) then to be extended to the domain of outer communication by invoking the assumption that all relevant fields, e.g., spacetime metric components, are real, analytic. In the following we focus on Step (I): Find a candidate K^a on the horizon. The properties that the desired candidate Killing field K^a should possess are: (i) $K^a K_a = 0$, $\pounds_t K^a = 0$, (ii) $\pounds_K \Phi = 0$, where Φ collectively denotes all relevant physical fields, such as the metric, and (iii) $K^c \nabla_c K^a = \alpha K^a$ with α being constant that is to be identified with the surface gravity. Now let us choose a foliation of the event horizon $\mathcal{H}$ by compact cross-sections Σ and decompose the vector t^a on $\mathcal{H}$ with respect to Σ as $t^a = n^a + s^a$, where n^a is null and s^a spacelike, tangent to Σ. (One can construct a well-behaved foliation by first choosing a single cross-section Σ_0, and then Lie-dragging Σ_0 over $\mathcal{H}$ by the isometry of t^a. Here and in the following, we use Σ to denote a single cross-section and foliation, interchangeably.) Then, it is straightforward to check that n^a satisfies (i) and (ii). However, there is a prior no reason that α with respect to n^a need be constant, since the decomposition $n^a = t^a - s^a$ depends on the choice of Σ. (See fig. 1.) Therefore our task is, starting from an arbitrary chosen Σ, to find the correct foliation $\tilde{\Sigma}$ that gives rise to $\tilde{n}^a = K^a$ with $\tilde{\alpha}$ being constant, satisfying the property (iii). It turns out that to find such a correct foliation $\tilde{\Sigma}$, one has to solve the following type of differential equations defined on a compact Σ,

$$s^a D_a \Psi = J \,, \tag{1}$$

where J is some analytic function on Σ. Now when solving this equation, the spacetime dimension and the topology of Σ play a role. For four-dimensions, it can be shown that the horizon cross-section must be topologically two-sphere. Then, it immediately follows from this fact that the orbits of s^a on Σ must be closed (see fig. 2). Then, by integrating eq. (1) along a closed orbit of s^a one can always find a well-defined solution Ψ which gives our desired $\tilde{\Sigma}$ and $K^a = \tilde{n}^a$. However, in higher dimensions, the

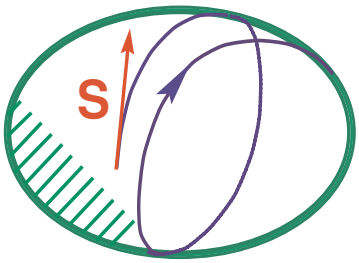

Figure 3: We wish to integrate eq. (1) along a *non-closed* orbit of s^a on Σ.

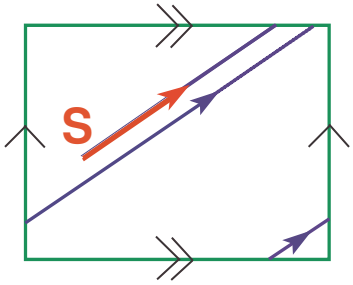

Figure 4: The fundamental region of two-dimensional torus. Two-dimensional flat torus admits two Killing fields, each of which has closed orbits, but their linear combination s^a does not necessarily have closed orbits.

orbits of s^a are *not necessarily* closed. (This would be the case even in four-dimensions if the horizon topology were non-spherical, e.g., torus). Therefore, in general, there is no guarantee that one can find a well-defined solution, Ψ, for higher dimensional black hole case.

The problem may be nicely illustrated by considering the following simple, lower-dimensional case: Consider the case in which Σ is two-dimensional flat torus and solve the same type of equation, eq. (1), on Σ along a non-closed orbit of s^a on Σ. Two-dimensional flat torus Σ has two Killing fields $\tau_1^a = (\partial/\partial\tau_1)^a$ and $\tau_2^a = (\partial/\partial\tau_2)^a$, each of which has closed orbits on Σ. Then, s^a with non-closed orbits can be expressed as a linear combination

$$s^a = \Omega_1\tau_1^a - \Omega_2\tau_2^a\,, \tag{2}$$

with the ratio, Ω_1/Ω_2, of the two coefficients being an irrational number. Then, it immediately follows that in terms of Fourier transform $\widehat{J}(\mathbf{x}, m_1, m_2)$ of $J(\mathbf{x}, \tau_1, \tau_2)$, a *formal* solution Ψ is given by

$$\Psi(\mathbf{x}) = i\sum_{m_1,m_2}\frac{\widehat{J}(\mathbf{x}, m_1, m_2)}{m_1\Omega_1 - m_2\Omega_2} = i\sum_{m_1,m_2}\frac{\widehat{J}(\mathbf{x}, m_1, m_2)}{m_1\Omega_2}\cdot\left|\frac{\Omega_1}{\Omega_2} - \frac{m_2}{m_1}\right|^{-1}. \tag{3}$$

Now recall that any irrational number, $\Omega_1/\Omega_2 \notin \mathbb{Q}$, can be approximated by some rational number $m_2/m_1 \in \mathbb{Q}$ as close as possible, by taking $m_1,\ m_2, \to \infty$ in a certain way. This implies that the denominator of the right side of the above equation can become arbitrarily small and therefore that Ψ need not be convergent. However, if we impose the following additional condition

$$\text{There exists } q > 0 \text{ such that } \quad \left|\frac{\Omega_1}{\Omega_2} - \frac{m_2}{m_1}\right| > \frac{1}{m_1^q}\,,$$

then we can show that the formal solution, Ψ, becomes convergent and well-defined. This condition—called the *Diophantine condition*—does *not* hold when Ω_1/Ω_2 is a Liouville number. However, such a number is known to be in a set of *measure zero*. Therefore we can essentially always solve eq. (1).

Now applying this idea of imposing the Diophantine condition to the higher dimensional black hole rigidity problem, we can show the following theorem [2]

Theorem. Let all relevant fields be *real, analytic*. Suppose vector fields $\underline{\Omega} = (\Omega_1, \ldots, \Omega_N)$ locally defined on cross-sections Σ of $\mathcal{H}$ satisfy

$$\forall \underline{m} \in \mathbb{Z}^N, \ \exists\, q > 0 \ \text{ such that } \quad |\underline{\Omega} \cdot \underline{m}| > |\underline{\Omega}| \cdot |\underline{m}|^{-q}\,.$$

Then, there exists a Killing field K^a which is *normal* to $\mathcal{H}$. Therefore $\mathcal{H}$ is a Killing horizon. Furthermore, there is an *axial Killing field*, $\phi^a_{(i)}$, such that $K^a = t^a - \sum_i \Omega_{(i)} \phi^a_{(i)}$.

Remarks: (i) $\Omega_{(i)}$'s turn out to be the angular velocities of $\mathcal{H}$ with respect to infinity. (ii) The proof applies to both extremal and non-extremal black holes. (iii) For non-extremal (finite-temperature) case、we do not need to impose the Diophantine condition [1].

References

[1] Hollands, S. Ishibashi, A. and Wald, R.M.: *A Higher dimensional stationary rotating black hole must be axisymmetric*, Commun. Math. Phys. 271: 699-722 (2007)

[2] Hollands, S. and Ishibashi, A.: *On the 'Stationary Implies Axisymmetric' Theorem for Extremal Black Holes in Higher Dimensions*, arXiv:0809.2659v1 [gr-qc]

Massive spin-2 ghost in de Sitter spacetime

Keisuke Izumi[1], Kazuya Koyama[2], Oriol Pujolàs[3] and Takahiro Tanaka[4]

[1] *Department of Physics, Kyoto University, Kyoto 606-8502, Japan*
[2] *Institute of Cosmology and Gravitation, University of Portsmouth, Portsmouth PO1 2EG,UK*
[3] *Center for Cosmology and Particle Physics, New York University New York, NY, 10003, USA*
[4] *Yukawa Institute for Theoretical Physics, Kyoto University, Kyoto 606–8502, Japan*

Abstract

We study the ghost of massive graviton in de Sitter space. In de Sitter space with Hubble constant H, if a mass of a spin-2 mode m satisfies $m^2 < 2H^2$, the helicity-0 mode becomes ghost. In order to explain the dark energy problem by a modification of gravity theory, the low energy effective theory becomes massive gravity theory. Then, the mass of the graviton naively becomes the present Hubble parameter and the ghost mode appears. First, we attempt to construct a ghost-free model by a modification of DGP braneworld model. We study the possibility of avoiding the appearance of the ghost by slightly modifying the model via the introduction of a second brane. By changing the separation between the branes, we find that we can erase the spin-2 ghost. However, this can be done only at the expense of the appearance of a spin-0 ghost instead. Secondly, we revisit the ghost problem. In general, the presence of a ghost particle, which has negative energy, drives the vacuum to be unstable through pair production of ghost particles and ordinary particles. Explicitly estimating the number density and the energy density of particles created by the pair production of two conformal scalar particles and one helicity-0 ghost graviton, we find that these densities both diverge. However, since we show that models with helicity-0 ghost graviton have no de Sitter invariant vacuum state, it is rather natural to consider a UV cutoff scale in the three-dimensional momentum space. Then, even if we take the cutoff scale as large as the Planck scale, the created number density and energy density are well suppressed. In many models the cutoff scale is smaller than the Planck scale. In such models the created number density and the energy density are negligibly small as long as only the physics below the cutoff scale is concerned.

1 Introduction

In late twentieth century, from the observation of Type Ia supernova [1, 2] we got to know that the expansion of the universe is accelerated at the present day. This is the so-called dark energy problem and the hottest topic in cosmology. There are two aspects in this issue: The first problem is to explain the late-time accelerated expansion of the universe, and the second is to explain why the accelerated expansion began only recently. There have been many attempts to modify standard model of cosmology in order to address these problems. As far as we know, none of these give a natural solution to the second problem. To give a solution to the second problem, one may need to combine ideas which solve the first problem with the anthropic principle [3].

Our interest is in the first problem. Most of ideas that partly solve the first problem are modifications of the scalar (spin-0) sector of the cosmological model, such as introduction of a cosmological constant [4] or quintessence [5, 6]. But there is another direction which has not been explored much so far. That is modifying the gravity theory in the spin-2 sector.

The simplest model with a modified spin-2 involves massive gravity [7]. Since models which have terms quadratic in metric perturbations can be regarded as a massive gravity theories, most of modifications of gravity in spin-2 sector fall into this category. If we introduce the mass of the graviton to explain

[1] E-mail:ksuke@tap.scphys.kyoto-u.ac.jp
[2] E-mail:kazuya.koyama@port.ac.uk
[3] E-mail:pujolas@ccpp.nyu.edu
[4] E-mail:tanaka@yukawa.kyoto-u.ac.jp

the accelerated expansion of the universe, its value would be the same order as the present value of the Hubble parameter, $m_g \simeq H$. However, it is known that a spin-2 graviton with mass in the range $0 < m^2 < 2H^2$ in de Sitter background has a ghost excitation in its helicity-0 component [8]. The Hubble parameter is larger in an earlier epoch of the universe. Hence it seems difficult to avoid the appearance of a ghost throughout the evolution of the universe in simple models that attempt to explain the present-day accelerated expansion. Here we would like to raise simple two questions. One question is "Can we build a model, incorporating modification of the spin-2 sector, that explains the accelerated cosmic acceleration and is ghost-free?" The other question is "Is the ghost really harmful?"

2 Building a ghost-free model

In order to answer the first question, we attempt to improve Dvali-Gabadadze-Porrati (DGP) braneworld model [9]. In braneworld models, in the five dimensional spacetime which is called bulk there is a four dimensional object which is called brane. Particles of the standard model of the field theory are trapped on the brane, whereas gravity can propagate in the bulk. The feature of the DGP braneworld model is that the action has the four dimensional Einstein Hilbert term on the brane. The DGP braneworld model is one of the most studied examples of a modified gravity model. In this model, there are two branches of solutions [10]. One is called conventional branch which has a Minkowski brane without tension in the Minkowski bulk. The other is called self accelerating branch in which the brane undergoes an exponential expansion without introducing a cosmological constant [10]. This branch attracted attention as a novel alternative to the dark energy. However, this branch contains a ghost in the spectrum at the quadratic order [11, 12, 13, 14, 15, 16, 17] as mentioned above. In the analysis of the ghost of the DGP braneworld model, Kaluza-Klein tower of massive gravitons in the four dimensional effective theory is obtained. One of these Kaluza-Klein masses satisfies $m^2 \leq 2H^2$ where we have equality in the case of tensionless brane. A detailed analysis showed that there is a ghost in tensionless case, too [18]. In order to avoid the appearance of the ghost, it seems that we have only to increase the Kaluza-Klein masses. Since the values of Kaluza-Klein masses are determined by the size of the extra dimension, we put another brane, and the size of the extra dimension is made small. By this modification, we can remove the ghost of the Kaluza-Klein graviton. However, the moduli mode, which represents the distance between two branes, becomes a ghost mode instead. Although we attempt to stabilize the moduli mode by introducing a scalar field in the bulk, we find that we cannot remove the ghost mode.

If the self accelerating branch contains a ghost instability at non-perturbative level, then we are naturally lead to ask what this solutions decays? One of the possibilities is that it decays to the conventional branch. We consider the nucreation of the bubble of the conventional branch in the environment of the self accelerating branch [19]. In the thin wall approximation, such a solution exists. However, in the model where the wall separating two phases is made of a scalar field, a corresponding solution cannot be obtained.

3 Is the ghost really harmful?

Next, we address the second question. If a ghost mode is quantized in the usual manner, a negative norm state emerges. In order to avoid the negative norm state, one possible prescription is to exchange the mode functions attached to the creation and annihilation operators [20, 21]. As a result, the excitations of ghost particles have negative energy. Excitations with negative energy are not unusual in cosmology, e.g. tachyon. A distinguishing feature of the ghost, however, is in that a ghost mode has negative energy even for the high momentum states, which is thought to lead the model to a disaster. In the Minkowski spacetime, if a ghost mode couples to normal particles, whose excitation energy is positive, pair-creation from the vacuum is not prohibited by the energy conservation because the total energy of the ghost and the normal particles can be zero. The probability of the reaction that is obtained by boosting the original one by a Lorentz transformation is the same. The total number density and the total energy density of the created normal particles are given by integrals over the whole three dimensional momentum space. When we calculate the number density created in the finite time, we must set the time direction to that of observed frame. Therefore, the integrand is proportional to the inverse of three dimensional

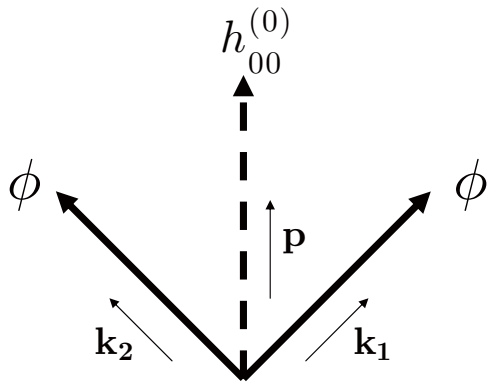

Figure 1: the lowest order coupling; $h^{(0)}_{00}$ is the helicity-0 mode of the massive graviton (ghost mode) and ϕ is a normal particle.

momentum. As a result, The total number density and the total energy density instantaneously become infinite due to the divergent UV-contribution, as long as the pair-creation process for given momenta has a finite probability no matter how small it is. When the model has the Lorentz symmetry, it is natural that the UV-cutoff scale (if it exists) is to be imposed in the Lorentz invariant manner in the four dimensional momentum space. Then, the three dimensional integrals mentioned above have no chance to have a natural cutoff, and the UV-divergence cannot be avoided. This means that such a model should be rejected.

However, the same story does not apply to the massive spin-2 field with a ghost mode in de Sitter background. We show that, in the massive gravity theory with a ghost mode, a de Sitter invariant vacuum does not exist [21]. Thus, any vacuum state necessarily breaks the de Sitter symmetry. Therefore, we estimate the number density and energy density of the created normal particles [22] (See Fig. 1). The obtained values are diverge as we send the three dimensional cutoff to infinity. However, the break of the de Sitter symmetry leads to an interesting possibility that a cutoff in three dimensional momentum space may naturally arise as a consequence of the symmetry breaking. Under the assumption that the model has a cutoff at a finite magnitude of the three dimensional momentum, the total number density and the total energy density of created normal particles remain finite, and the model may escape from being discarded immediately.

4 Summary

Although we cannot construct a ghost-free model with acceleration, there is a possibility that the ghost of the massive spin-2 field in de Sitter space does not lead models to disaster. However, besides the issue of ghost, these models of massive gravity bear a common obstacle; vDVZ discontinuity. To avoid this discontinuity in the massless limit, non-linear effects should play an important role on a relatively large distance scale, which in turn means that the models are strongly coupled on a relatively low energy scale. Main difficulty in pursuing the possibility of modification of spin-2 sector of gravity in explaining the present-day accelerating expansion of the universe is not due to the presence of ghost but to the lack of our knowledge about how to handle the strong coupling regime of the models of modified gravity.

References

[1] A. G. Riess et al., Astron. J. **116**, 1009 (1998),

[2] A. G. Riess et al., Astron. J. **607**, 665 (2004),

[3] B. J. Carr and M. J. Rees, Nature **278**, 605 (1979),

[4] S. Weinberg, Rev. Mod. Phys. **61**, 1 (1989),

[5] C. Wetterich, Nucl. Phys. B **302**, 668 (1988),

[6] B. Ratra and P. J. E. Peebles, Phys. Rev. D **37**, 3406 (1988),

[7] M. Fierz and W. Pauli, Proc. Roy. Soc. Lond. A **173**, 211 (1939),

[8] A. Higuchi, Nucl. Phys. B **282**,397 (1987),

[9] G. R. Dvali, G. Gabadadze and M. Porrati, Phys. Lett. B **484**, 112 (2000),

[10] C. Deffayet, Phys. Lett. B **502**, 199 (2001),

[11] M. A. Luty, M. Porrati and R. Rattazzi, JHEP **0309**, 029 (2003),

[12] A. Nicolis and R. Rattazzi, JHEP **0406**, 059 (2004),

[13] K. Koyama and K. Koyama, Phys. Rev. D **72**, 043511 (2005),

[14] K. Koyama, Phys. Rev. D **72**, 123511 (2005),

[15] C. Charmousis, R. Gregory, N. Kaloper and A. Padilla, JHEP **0610**, 066 (2006),

[16] M. Carena, J. Lykken, M. Park and J. Santiago, Phys. Rev. D **75**, 026009 (2007),

[17] K. Izumi, K. Koyama and T. Tanaka, JHEP **0704**, 053 (2007),

[18] D. Gorbunov, K. Koyama and S. Sibiryakov, Phys. Rev. D **73** 044016 (2006),

[19] K. Izumi, K. Koyama, O. Pujolas and T. Tanaka Phys. Rev. D **76**, 104041 (2007),

[20] J. M. Cline, S. Jeon, G. D. Moore , Phys. Rev. D **70**, 043543 (2004),

[21] K. Izumi and T. Tanaka, Prog. Theor. Phys. *to be published*, arXiv:0709.0199,

[22] K. Izumi and T. Tanaka, Prog. Theor. Phys. *to be published*, arXiv:0810.4811,

Can dissipative effects help the MSSM inflation?

Kohei Kamada[1,2] and Jun'ichi Yokoyama[2,3]

[1] *Department of Physics, Graduate School of Science, The University of Tokyo, Tokyo 113-0033, Japan*
[2] *Research Center for the Early Universe (RESCEU), Graduate School of Science, The University of Tokyo, Tokyo 113-0033, Japan*
[3] *Institute for the Physics and Mathematics of the Universe, The University of Tokyo, Chiba 277-8582, Japan*

Abstract

We study the dissipative effects on the MSSM inflation, which suffers from severe fine-tuning problems on potential parameters and initial conditions. Dissipative effects appear as a consequence of interactions between an inflaton and other fields and they act as a friction term in its equation of motion. Of course it also can emerge in the case of MSSM inflation. However, we find that in the inflationary stage it can neither overwhelm the friction term that is due to the cosmic expansion nor affect the primordial fluctuations. Therefore it cannot relax the fine-tuning problem of the MSSM inflation.

1 Introduction

MSSM inflation [1] is a model of inflation that is based on an extension of the Standard Model (SM) that is motivated by the supersymmetry (SUSY), the Minimal Supersymmetric Standard Model (MSSM). In this model, the inflaton is the flat direction in the MSSM, a gauge invariant combination of either squark or slepton fields. Flat directions can be lifted by the SUSY-breaking effect and the non-renormalizable potential. If a fine-tuning of the potential parameters is realized, the potential for the flat direction has a saddle point and inflation can occur near the point. If we take the inflaton as the $\bar{u}\bar{d}\bar{d}$ or the $LL\bar{e}$ flat direction, the saddle point locates at $\varphi \sim 10^{14}$ GeV and the Hubble parameter during inflation is about $1 - 10$ GeV. Here φ is the inflaton. Its most interesting feature is that the inflaton couplings to particles in the SM are known and, at least in principle, measurable in laboratory experiments such as the Large Hadron Collider or a future Linear Collider. We do not need new physics beyond the MSSM.

Despite these attractive features described above, the MSSM inflation has some drawbacks, such as the fine-tuning of the potential parameters and worse, the fine-tuning of the initial condition. In particular, the latter is a very difficult problem. Because the slow-roll region for the MSSM inflation is extremely narrow, if the former is solved by some mechanism, the inflaton must reach the slow-roll region with an extremely small velocity in order to expand the Universe exponentially.

However, previous analyses have been neglected the interactions between the inflaton and other MSSM particles, which we know well, when they consider the dynamics of the inflaton. In general, interactions of the scalar fields with other fields can cause the dissipative effect. This phenomenon has been discussed in the high temperature regime [2, 3], in particular, in the context of the warm inflation [4]. It acts as a friction term in the equation of motion of the inflaton and can affects its dynamics. Therefore it has a possibility of relaxation of the fine-tuning of the MSSM inflation.

We investigate the interaction between the MSSM inflaton and other fields and the resultant dissipative effect carefully. As a consequence, dissipative effects arise but cannot change the dynamics of the MSSM inflaton in the inflationary stage. Moreover, it does not affect the primordial fluctuations. Therefore dissipative effects cannot relax the fine-tuning problem of the MSSM inflation.

2 MSSM inflation

Let us summarize the main features of the MSSM inflation [1] briefly. We adopt a non-renormalizable superpotential of the form

$$W_{\rm non} = \frac{\lambda}{6M_G^3}\Phi^6. \tag{1}$$

Here M_G is the reduced Planck mass and Φ is a supermultuplet whose scalar component ϕ parameterizes the flat direction. in the case where the $\bar{u}\bar{d}\bar{d}$ flat direction acts as an inflaton, ϕ represents the following field configuration.

$$\tilde{\bar{u}}_i^{\alpha} = \tilde{\bar{d}}_j^{\beta} = \tilde{\bar{d}}_k^{\gamma} = \frac{1}{\sqrt{3}}\phi, \quad (j \neq k, \alpha \neq \beta \neq \gamma), \tag{2}$$

where i, j and k are the family indices and α, β and γ are the color indices. We assume that λ is parameter of order unity. The flat direction is lifted by the superpotential (1). Hereafter we consider the case when the scalar component of ϕ acquires a large expectation value.

Including the SUSY breaking effect from the hidden sector, the scalar potential is found to be

$$V(\varphi) = \frac{1}{2}m_\phi^2\varphi^2 - \frac{A\lambda}{24M_G^3}\varphi^6 + \frac{\lambda^2}{32M_G^6}\varphi^{10}, \tag{3}$$

where m_ϕ ~100 GeV - 1 TeV is the soft-breaking mass of ϕ and A is a parameter whose amplitude is also $|a| \simeq \mathcal{O}(100)$ GeV - 1 TeV. This is justified when SUSY-breaking is gravity-mediated. Here we minimized the potential along the angular direction of ϕ, and rewriting the flat direction as $\phi = \frac{1}{\sqrt{2}}\varphi e^{i\theta}$, with φ being a real quantity,

If A is fine-tuned as $A^2 = 20m_\phi^2(1 + \alpha^2/4)$, with $\alpha^2 \ll 1$, $V(\varphi)$ has a inflection point φ_0 at

$$\varphi_0 = \left(\frac{2AM_G^3}{5\lambda}\right)^{1/4}(1 + \mathcal{O}(\alpha^2)), \quad V''(\varphi_0) = 0, \tag{4}$$

where

$$V(\varphi_0) = \frac{4}{15}m_\phi^2\varphi_0^2(1 + \mathcal{O}(\alpha^2)). \quad V'(\varphi_0) = m_\phi^2\varphi_0 \times \mathcal{O}(\alpha^2), \tag{5}$$

Therefore inflation can occur near the inflection point and its Hubble parameter is

$$H_{\rm MSSM} \simeq \frac{2m_\phi}{3\sqrt{5}M_G}\varphi_0 \simeq 10^{-16}\left(\frac{m_\phi}{10^3{\rm GeV}}\right)\varphi_0. \tag{6}$$

The potential for MSSM inflation $V(\varphi)$ can be expanded around the inflection point as

$$V(\varphi) = \frac{4}{15}m_\phi^2\varphi_0^2 + \frac{8}{3}\frac{m_\phi^2}{\varphi_0}(\varphi - \varphi_0)^3. \tag{7}$$

The slow-roll parameters, $\epsilon \equiv (M_G^2/2)(V'/V)^2$ and $\eta \equiv M_G^2(V''/V)$, can be calculated from Eq. (7). We find that the required degree of fine-tuning is

$$|\alpha| \ll 10^{-9} \tag{8}$$

in order to generate the correct primordial perturbations [1].

Moreover we find that slow roll region is very narrow, $|\varphi - \varphi_0|/\varphi_0 \ll 10^{-10}$ even if the above fine-tuning is accomplished by some unknown mechanism. Therefore the inflaton must reach the slow-roll region with an extremely small velocity, $H^{-1}d(\log\varphi)/dt|_{\varphi=\varphi_{c+}} < \varphi_0^2/20M_G^2$. Otherwise the inflaton passes through the slow-roll region within a time interval of H^{-1} because the time interval of passing is shorter than the time scale of deceleration of the inflaton. If the above condition is accomplished, the Universe goes through the self-reproducing regime when exactly $\varphi = \varphi_0$ and we have enough number of e-folds and correct primordial perturbations.

3 Dissipative effect

Next, we consider the dissipative effects. So far, we have not considered the interactions between the inflaton and other fields, which might cause dissipative effects and modify the dynamics of the inflaton. As a consequence, the narrowness of the slow-roll region could be relaxed if dissipative effects turned out to be strong enough. Here, we see whether it can relax the problems of the MSSM inflation or not.

3.1 Modification to inflation

When an inflaton ϕ has interaction with other fields, especially when they are in thermal bath, a dissipative phenomenon takes place and the inflaton feels a damping force. Although often a thermal correction to the potential also causes and might affect the slow-roll conditions, in the context of the MSSM inflation, it is difficult to consider such a case. For the fields that couple to the inflaton acquire large mass from the vacuum expectation value of the inflaton. Such fields are hard to be in thermal bath. Moreover, if they are in thermal bath, their energy density will overwhelm that of the inflaton. Consequently, inflaton does not occur. Instead, we consider the case where the inflaton couples to the radiation catalyzed by heavy fields [5]. In such a case, we do not have to worry about the thermal correction to the potential.

According to the discussion above, we take into account dissipative effects and write down the equation of motion for the inflaton ϕ approximately as

$$\ddot{\phi} + (3H + F_r)\dot{\phi} + \frac{\partial V}{\partial \phi} = 0. \tag{9}$$

Here F_r is the dissipative coefficient representing the dissipative effect, which may enhance inflation [6]and depends on ϕ and the temperature of radiation T. We estimate the value of F_r in the next subsection. The relative strength of the dissipative effect compared to the friction term from the expansion can be described by a parameter r,

$$r \equiv \frac{F_r}{H}. \tag{10}$$

If r is much larger than unity, the dynamics of inflaton would be modified. In order to estimate it quantitatively, we evaluate the dynamics of the inflaton and other components of the Universe further.

Other equations that governs the universe are,

$$3M_G^2 H^2 = V(\phi) + \rho_\gamma, \tag{11}$$

$$\dot{\rho}_\gamma + 4H\rho_\gamma = F_r \dot{\phi}^2, \tag{12}$$

where ρ_γ is the energy density of the radiation, that is, $\rho_\gamma = (\pi^2/30) g_* T^4$. Here g_* is the effective number of relativistic degree of freedom. (11) is the Friedman equation and (12) is the Boltzmann equation for the radiation.

The slow-roll conditions in this case are, then, the conditions that the time variations of H, $\dot{\phi}$ and T is negligible in comparison to the time scale of the cosmic expansion. Using equations (9), (11) and (12), if $r \gg 1$, the slow-roll condition changes as [7]

$$\epsilon \ll r, \quad \eta \ll r, \quad \beta \ll r. \tag{13}$$

Here β is the new slow-roll parameter introduced in order to take into account the time variation of F_r,

$$\beta \equiv M_G^2 \left(\frac{V_{,\phi} F_{r,\phi}}{V F_r} \right). \tag{14}$$

We can see from (13) that slow-roll condition is relaxed by the factor of r. [1]

If we apply this effect to the MSSM inflation, the slow-roll region is determined by the condition $\eta \ll r$. As a consequence, the slow-roll region will be enhanced,

$$\frac{|\varphi - \varphi_0|}{\varphi_0} \ll 10^{-10} r. \tag{15}$$

3.2 Dissipative coefficients for the MSSM inflaton

Then, we estimate the dissipative coefficients of the MSSM inflaton. The relevant part of the potential is, then,

$$\begin{aligned} V_{\rm int} =& h_1^2(|\phi|^2|\chi_1|^2 + |\phi|^2|\chi_2|^2 + |\chi_1|^2|\chi_2|^2) + h_1 h_2(\phi \chi_2 y_1^* y_2^* + \text{H.c.}) \\ &+ h_2(|\chi_1|^2|y_1|^2 + |\chi_1|^2|y_2|^2 + |y_1|^2|y_2|^2) \\ &+ h_1\left(\phi \bar{\psi}_\chi P_L \psi_\chi + \phi^* \bar{\psi}_\chi P_R \psi_\chi\right) + h_2\left(\chi_1 \bar{\psi}_y P_L \psi_y + \chi_1^* \bar{\psi}_y P_R \psi_y\right), \end{aligned} \tag{16}$$

[1] Strictly speaking, the degree of relaxation is dependent on the form of the potential V and the dissipative coefficient F_r.

Here ϕ, χ and y are the scalar fields. $P_L(P_R) = 1 - \gamma_5(1+\gamma_5)$ is left-(right-)handed projection operators. ψ_χ and ψ_y are the four-component Dirac spinor . As derived in [2], the dissipative coefficients are calculated using the in-in or the closed time-path formalism,

$$F_r = h_1^4 \varphi_c(t)^2 \int_{-\infty}^{t} dt'(t'-t) \int \frac{d^3q}{(2\pi)^3} \mathrm{Im}\left[G_{\chi_i}^{++}(\boldsymbol{q}, t-t') G_{\chi_i}^{++}(\boldsymbol{q}, t'-t)\right], \tag{17}$$

where $G_\chi^{++}(\boldsymbol{k}, t)$ is the Fourier transform of the Feynman propagator of χ [2]

In order to include the dissipative process, we dress the χ propagator with ψ loop. The imaginary part of its self energy generate non-zero value of F_r. At zero temperature, although there exists an imaginary part of its self energy, its contribution cancels out. At non-zero temperature non-zero value of the dissipative coefficient appears[5],

$$F_r = C g_* \frac{T^3}{\varphi^2}. \tag{18}$$

Here C is a numerical constant of $\mathcal{O}(10)$ and $g_* \simeq \mathcal{O}(10^2)$ is the relativistic degree of freedom. However, the radiation must not overwhelm the vacuum energy, $(\pi^2/30) g_* T^4 < (4/15) m_\phi^2 \varphi_0^2$. As a result, the dissipative coefficient F_r is smaller than $3H$, the friction coefficient from cosmic expansion unless g_* is extremely large. [2] Therefore, dissipative effects cannot relax the fine-tuning problem or the problem of narrowness of the slow-roll region.

4 Conclusion

We have studied the effect of the interaction of the MSSM inflaton. The interaction between the MSSM inflaton and the other fields can cause the dissipative effect. However, this effect is very weak and cannot change the dynamics of the MSSM inflaton. It also does not change the primordial perturbations that the MSSM inflaton generates. Therefore, there still remains the problem of the narrowness of the slow-roll region of the MSSM inflaton. The fine-tuning problem of the MSSM inflation must be solved by other mechanisms.

References

[1] R. Allahverdi, K. Enqvist, J. Garcia-Bellido and A. Mazumdar, Phys. Rev. Lett. **97**, 191304 (2006) [arXiv:hep-ph/0605035]; R. Allahverdi, K. Enqvist, J. Garcia-Bellido, A. Jokinen and A. Mazumdar, JCAP **0706**, 019 (2007) [arXiv:hep-ph/0610134]; J. C. Bueno Sanchez, K. Dimopoulos and D. H. Lyth, JCAP **0701**, 015 (2007) [arXiv:hep-ph/0608299].

[2] M. Gleiser and R. O. Ramos, Phys. Rev. D **50**, 2441 (1994) [arXiv:hep-ph/9311278];

[3] M. Morikawa and M. Sasaki, Prog. Theor. Phys. **72**, 782 (1984). A. Hosoya and M. a. Sakagami, Phys. Rev. D **29**, 2228 (1984); M. Morikawa, Phys. Rev. D **33**, 3607 (1986); J. Yokoyama, Phys. Rev. D **70**, 103511 (2004) [arXiv:hep-ph/0406072];

[4] A. Berera, Phys. Rev. Lett. **75**, 3218 (1995) [arXiv:astro-ph/9509049]; J. Yokoyama and A. D. Linde, Phys. Rev. D **60**, 083509 (1999) [arXiv:hep-ph/9809409].

[5] I. G. Moss and C. Xiong, arXiv:hep-ph/0603266; A. Berera, I. G. Moss and R. O. Ramos, arXiv:0808.1855 [hep-ph].

[6] J. Yokoyama and K. Maeda, Phys. Lett. B **207**, 31 (1988).

[7] L. M. H. Hall, I. G. Moss and A. Berera, Phys. Rev. D **69**, 083525 (2004) [arXiv:astro-ph/0305015].

[2] Even if g_* is extremely large, the warm inflationary solution requires extremely small temperature, which is inconsistent with the assumption that g_* is large.

Anisotropic Inflation from Vector Impurity

Masashi Kimura[1], Sugumi Kanno[2], Jiro Soda[3], and Shuichiro Yokoyama[4]

[1]*Department of Mathematics and Physics, Graduate School of Science, Osaka City University, Osaka, 558-8585, Japan*
[2]*Department of Mathematical Sciences, University of Durham, Durham DH1 3LE, United Kingdom*
[3]*Department of Physics, Kyoto University, Kyoto, 606-8501, Japan*
[4]*Department of Physics and Astrophysics, Nagoya University, Aichi, 464-8602, Japan*

Abstract

We study an anisotropic inflationary scenario. We show that the universe undergoes anisotropic inflationary expansion due to a preferred direction determined by a vector. In particular, it is stressed that primordial gravitational waves can be induced from curvature perturbations. Hence, even in low scale inflation, a sizable amount of primordial gravitational waves may be produced during inflation. To verify this expectation, we study perturbations in the anisotropic inflationary background.

1 Introduction

It is often mentioned that cosmology has entered into a new stage, so-called precision cosmology. Of course, it is referring to developments of observational side. From theoretical point of view, however, we have not yet exhausted possible phenomenology on the order of a few percent. Clearly, it is important to explore qualitatively new scenarios at the percent level. Here, above all, we would like to point out that an inflationary model with a few percent of anisotropy yields significant consequences. Indeed, a few percent does not mean the consequent effects are negligible. Rather, it provides the leading component of the primordial gravitational waves in low scale inflationary models which are preferred by recent model construction in string theory [1].

In this talk, we propose an anisotropic inflation model with the vector impurity [2]. It is expected that the anisotropic inflation yields the statistical anisotropy in fluctuations. More importantly, the primordial gravitational waves could be induced from curvature perturbations through the anisotropic background. In order to verify this expectation, we need to study perturbations around the anisotropic background. This is a status report of the study in this direction.

2 Anisotropic Inflation

We consider the following action for the background gravitational field, the scalar field ϕ and the non-minimally coupled massive vector field A_μ [3]:

$$S = \int d^4x\sqrt{-g}\left[\ \frac{1}{2\kappa^2}R - \frac{1}{2}\left(\partial_\mu\phi\right)^2 - V(\phi) - \frac{1}{4}F_{\mu\nu}F^{\mu\nu} - \frac{1}{2}\left(m^2 - \frac{R}{6}\right)A_\mu A^\mu\ \right]\ , \tag{1}$$

where g is the determinant of the metric, R is the Ricci scalar, $V(\phi)$ is the scalar potential, m is the mass of the vector field, and we have defined $F_{\mu\nu} = \partial_\mu A_\nu - \partial_\nu A_\mu$. The equation of motion for A_μ from above action:

$$\frac{1}{\sqrt{-g}}\partial_\mu\left(\ \sqrt{-g}F^{\mu\nu}\ \right) = \left(m^2 - \frac{R}{6}\right)A^\nu \tag{2}$$

reduces $A_0(t) = 0$ in the case of $\nu = 0$ because of antisymmetry of $F^{\mu\nu}$. As we find the vector field has only spatial components, we take x-axis in the direction of the vector,

$$A_\mu = (\ 0,\ A_x(t),\ 0,\ 0\ ), \qquad \phi = \phi(t)\,. \tag{3}$$

Now, we will take the metric to be homogeneous but anisotropic Bianchi type-I, i.e.

$$ds^2 = -dt^2 + e^{2\alpha(t)} \left[e^{-4\sigma_+(t)} dx^2 + e^{2\sigma_+(t)} \left(e^{2\sqrt{3}\sigma_-(t)} dy^2 + e^{-2\sqrt{3}\sigma_-(t)} dz^2 \right) \right]. \tag{4}$$

With this ansatz, equations of motion become:

$$\frac{3}{\kappa^2}\left(-\dot{\alpha}^2 + \dot{\sigma}_+^2 + \dot{\sigma}_-^2\right) + \frac{1}{2}\dot{\phi}^2 + V + \frac{1}{2}\left(\dot{X} - 2\dot{\sigma}_+ X\right)^2 + \frac{m^2}{2}X^2 + \left(\frac{1}{2}\dot{\sigma}_+^2 + \frac{1}{2}\dot{\sigma}_-^2 - 2\dot{\alpha}\dot{\sigma}_+\right)X^2 = 0\,, \tag{5}$$

$$\ddot{\phi} + 3\dot{\alpha}\dot{\phi} + V_{,\phi} = 0\,, \tag{6}$$

$$\ddot{X} + 3\dot{\alpha}\dot{X} + \left(m^2 - 2\ddot{\sigma}_+ - 2\dot{\alpha}\dot{\sigma}_+ - 5\dot{\sigma}_+^2 - \dot{\sigma}_-^2\right)X = 0\,, \tag{7}$$

$$\left[e^{3\alpha}\left(\frac{6}{\kappa^2} + X^2\right)\dot{\sigma}_- \right]^{\cdot} = 0\,, \tag{8}$$

$$\left[e^{3\alpha}\left\{ \left(\frac{6}{\kappa^2} + 5X^2\right)\dot{\sigma}_+ - 2X\dot{X} - 2\dot{\alpha}X^2 \right\} \right]^{\cdot} = 0\,, \tag{9}$$

$$\ddot{\alpha} + 3\dot{\alpha}^2 - \kappa^2 V + \frac{2}{3}\kappa^2\dot{\sigma}_+ X\dot{X} + \kappa^2\left(\frac{1}{3}\ddot{\sigma}_+ + \dot{\alpha}\dot{\sigma}_+ - \frac{1}{2}m^2\right)X^2 = 0\,. \tag{10}$$

where $X \equiv \exp(-\alpha + 2\sigma_+)A_x$ and $V_{,\phi} \equiv \frac{dV}{d\phi}$. Note that if the effective mass squared of X in Eq. (7) is negative, the system will be tachyonic. To avoid this, we require the effective mass squared is positive, $m^2 - 2\ddot{\sigma}_+ - 2\dot{\alpha}\dot{\sigma}_+ - 5\dot{\sigma}_+^2 - \dot{\sigma}_-^2 > 0$, that is, $m \neq 0$ and $\dot{\sigma}_\pm$ has to be sufficiently small. In fact, this latter condition implies the amplitude of the vector field X should be small [2]. In this sense, the vector field is a kind of impurity.

Let us consider the universe after a sufficient expansion, $\alpha \to \infty$. It is straightforward in this limit to integrate Eqs. (8) and (9) to find

$$\dot{\sigma}_- = 0\,, \qquad \dot{\sigma}_+ = \frac{1}{6/\kappa^2 + 5X^2}\left(2X\dot{X} + 2\dot{\alpha}X^2\right). \tag{11}$$

We find that the anisotropy in y-z plane, $\dot{\sigma}_-$, will disappear. This is reminiscent of the comic no-hair theorem by Wald [4]. However, as long as the vector field exists $X \neq 0$, the anisotropy in x direction, $\dot{\sigma}_+$, will still remain even if the universe undergoes a period of inflation. In the proof of the cosmic no-hair theorem for Bianchi models, the strong and dominant energy conditions are assumed. The reason why the anisotropy does not disappear in our model is that the non-minimal coupling breaks the strong energy condition. Thus, we can restrict our metric to the following form:

$$ds^2 = -dt^2 + e^{2\alpha(t)} \left[e^{-4\sigma_+(t)} dx^2 + e^{2\sigma_+(t)} \left(dy^2 + dz^2 \right) \right]. \tag{12}$$

Now, we numerically solve Eqs. (5)-(10) by setting $\sigma_- = 0$. We will use new variables $H = \dot{\alpha}$ and $\Sigma = \dot{\sigma}_+$ below. We take $V = 1/2\mu^2\phi^2$ as the potential for the inflaton ϕ. The parameter of the system is the ratio m/μ. For this calculation, we set $\kappa = 1$, $\mu = 10^{-5}$ and $m = 2\sqrt{2} \times 10^{-5}$. And, we took the initial values $\phi_0 = 10$ and $H_0 = 3 \times 10^{-4}$ for all figures. In Fig. 1, we depicted the phase flow in X-$\dot{X}$ plane. We set the initial value $\Sigma_0 = 0$ and determined $\dot{\phi}_0$ using the constraint equation (5). We see that slow-roll phase of the vector field is an attractor when the amplitude of the vector field is sufficiently small. For the appropriate parameter m/μ, the small value such as $X^2 \sim 0.1$ is easily attainable. In Fig. 2, the phase flow in ϕ - $\dot{\phi}$ is plotted with the same initial conditions as Fig. 1. The trajectories are almost same irrespective of the initial conditions for X, and show the slow-roll phase. After slow-rolling, the inflaton field gets its damped oscillations. Therefore, the anisotropic inflation ends with reheating as in the standard inflation. In Fig. 3, we have plotted H as a function of e-folding number $N \equiv \alpha - \alpha_0$. Actually, we plotted four lines for different initial conditions $\Sigma_0/H_0 = 0,\ 0.05,\ 0.1,\ 0.15$ with fixed initial conditions $X_0 = 0.5$ and $\dot{X}_0 = 1.5 \times 10^{-5}$. In the Fig. 3, all lines are degenerated. Irrespective of the initial conditions, we see the slow-roll phase from this figure. In Fig.4, we have plotted Σ/H as a function of the e-folding number with the same initial conditions as Fig. 3. We see the anisotropy remains sizable for some period and then dumped down to zero around $N \sim 20$ irrespective of its initial condition.

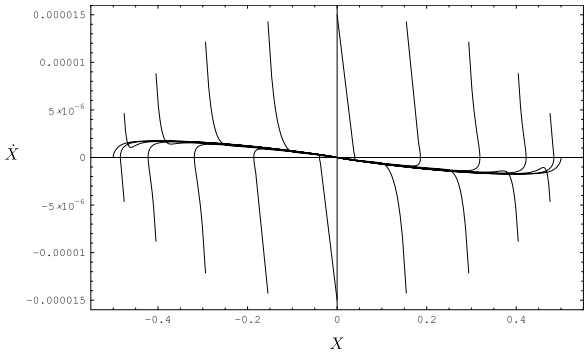

Figure 1: The phase flow in X-$\dot{X}$ plane is depicted. For various initial conditions with small amplitude of X, we have plotted the trajectories. Every trajectory converges to the slow roll attractor.

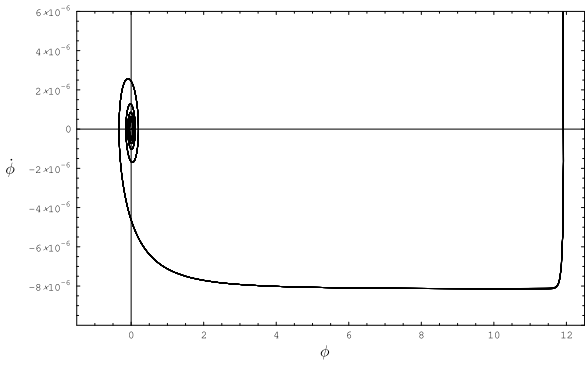

Figure 2: The phase flow in ϕ-$\dot{\phi}$ plane is depicted. Every trajectory is degenerated irrespective of the initial conditions for X.

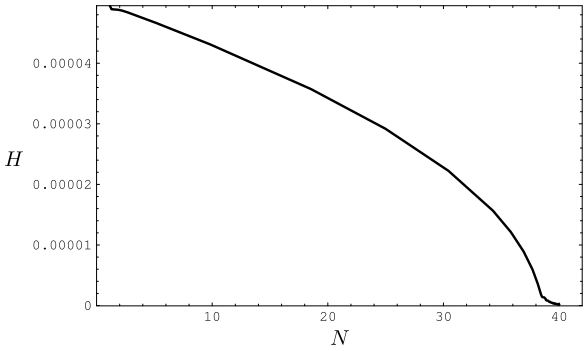

Figure 3: The Hubble parameter H is plotted as a function of e-folding number N. We see a slow-roll phase clearly. We have e-folding number $N \sim 40$ for this case.

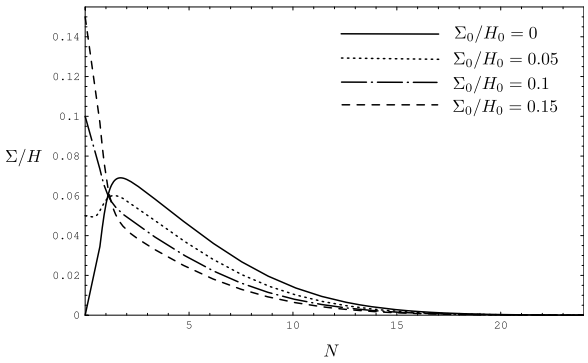

Figure 4: The ratio Σ/H is plotted as a function of e-folding number. In spite of the rapid expansion of universe, the anisotropy remains sizable for some period relevant to observations.

Since we succeeded to construct the anisotropic inflation model in which $\dot{\sigma}_+/\dot{\alpha} \sim 0.01$ at the early stage of inflation, we expect that this scenario provide: statistical anisotropy of spectrum, source of gravitational wave, linear polarization of gravitational wave. To see this explicitly, we need to calculate perturbation on anisotropic inflation background.

3 Liner Perturbations

The metric (12) has the symmetry of two dimensional Euclidean space $\mathbb{E}^2$, so we can decompose perturbed quantities to scalar and vector modes with respect to the symmetry as

$$h_{\mu\nu}dx^\mu dx^\nu = h^{(S)}_{AB}\mathbb{S}dx^A dx^B + 2dx^A\left[h^{(S)}_{AL}(\partial_i\mathbb{S})dx^i + h^{(V)}_{AT}\mathbb{V}_i dx^i\right] + \left[h^{(S)}_L\delta_{ij}\mathbb{S} + h^{(S)}_T\left(\partial_i\partial_j - \frac{\delta_{ij}}{2}\partial^\ell\partial_\ell\right)\mathbb{S} + h^{(V)}_T(\partial_i\mathbb{V}_j + \partial_j\mathbb{V}_i)\right]dx^i dx^j \tag{13}$$

$$\delta A_\mu dx^\mu = \delta A^{(S)}_A\mathbb{S}dx^A + \left[\delta A^{(S)}_L\partial_i\mathbb{S} + \delta A^{(V)}_L\mathbb{V}_i\right]dx^i \tag{14}$$

$$\delta\phi = \delta\phi^{(S)}\mathbb{S} \tag{15}$$

where $A, B = t, x$, $i, j = y, z$ and $\mathbb{S}$, $\mathbb{V}_i$ are scalar and vector harmonics on $\mathbb{E}^2$ given by

$$\triangle_{\mathbb{E}^2}\mathbb{S} = Q_S\mathbb{S}, \qquad \triangle_{\mathbb{E}^2}\mathbb{V}_i = Q_V\mathbb{V}_i \ \text{ s.t. } \ \partial^i\mathbb{V}_i = 0 \tag{16}$$

In this talk, as a first step, we focus on vector mode perturbations. We leave analysis of scalar mode perturbations for future work[1]. After some calculation and gauge fixing, we get two coupled equations for vector mode perturbations as

$$\ddot{\tilde{h}}_T^{(V)} + 3H\dot{\tilde{h}}_T^{(V)} + e^{-2\alpha}k^2\tilde{h}_T^{(V)} = O(\kappa^2X^2)\dot{\tilde{h}}_T^{(V)} + O(\kappa^2X^2)\tilde{h}_T^{(V)} + O(\kappa^2X^2)\delta\dot{X}_L^{(V)} + O(\kappa^2X^2)\delta X_L^{(V)} \tag{17}$$

$$\delta\ddot{X}_L^{(V)} + 3H\delta\dot{X}_L^{(V)} + (e^{-2\alpha}k^2 + m_X^2)\delta X_L^{(V)} = O(\kappa^2X^2)\delta\dot{X}_L^{(V)} + O(\kappa^2X^2)\delta X_L^{(V)} + O(\kappa^2X^2)\dot{\tilde{h}}_T^{(V)} \tag{18}$$

where $\tilde{h}_T^{(V)} \equiv \exp(-2\alpha - 2\sigma_+)h_T^{(V)}$, $\delta X_L^{(V)} \equiv \exp(-\alpha - \sigma_+)\delta A_L^{(V)}$. Here, the right-hand side should be

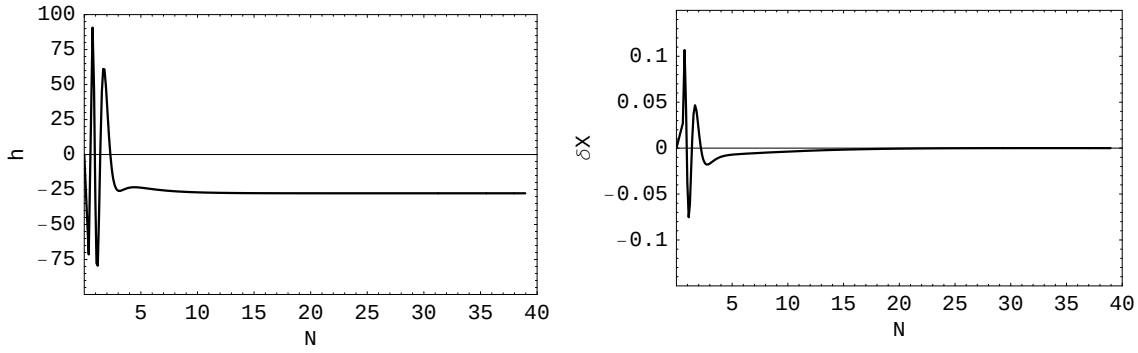

Figure 5: Typical behavior of $\tilde{h}_T^{(V)}$ and $\delta X_L^{(V)}$.

understood schematically. We can numerically integrate the above equations for some initial conditions. Typical behavior of $\tilde{h}_T^{(V)}$ and $\delta X_L^{(V)}$ is depicted in Fig.5 Since perturbative quantities does not diverge for various initial conditions, we expect vector modes are stable. We have to quantize this system and make a prediction for the spectrum. However, it is still under investigation.

4 Conclusion

We have shown the anisotropic inflationary scenario is viable. There are many attractive phenomenological consequences in this scenario such as the conversion of the gravitational waves from curvature perturbations. Admittedly, our understanding of perturbations in the anisotropic inflationary background is poor due to the complexity of perturbed equations. Surely, further investigations are necessary.

References

[1] R. Kallosh and A. Linde, JHEP **0412**, 004 (2004) [arXiv:hep-th/0411011].

[2] S. Kanno, M. Kimura, J. Soda and S. Yokoyama, JCAP **0808**, 034 (2008) [arXiv:0806.2422 [hep-ph]].

[3] A. Golovnev, V. Mukhanov and V. Vanchurin, arXiv:0802.2068 [astro-ph].

[4] R. W. Wald, Phys. Rev. D **28** (1983) 2118.

[5] B. Himmetoglu, C. R. Contaldi and M. Peloso, arXiv:0809.2779 [astro-ph].

[1] In [5], it is stressed that there exist unstable modes in scalar mode perturbation. However, they did not show that explicitly by the caluculation of the perturbation. so whether their argument is really true is unknown yet.

Thermodynamic and dynamical stability of Freund–Rubin compactification

Shunichiro Kinoshita[1] and Shinji Mukohyama[2]

[1] *Department of Physics, The University of Tokyo, Hongo 7-3-1, Bunkyo-ku, Tokyo 113-0033, Japan*
[2] *Institute for the Physics and Mathematics of the Universe (IPMU), The University of Tokyo, 5-1-5 Kashiwanoha, Kashiwa, Chiba 277-8582, Japan*

Abstract

We investigate stability of Freund–Rubin compacti cation from both thermodynamic and dynamical perspectives. Freund–Rubin compacti cation not only has trivial Freund–Rubin solutions but also deformed solutions which are described as warped product of external de Sitter space and internal deformed sphere. We study dynamical stability by analyzing linear perturbations around the deformed solutions. Also we study thermodynamic stability between the Freund–Rubin solutions and the deformed solutions based on de Sitter entropy. We show close relations between thermodynamic and dynamical stability exist in this system.

1 Introduction

The Freund–Rubin compacti cation is a simple model with a stabilization mechanism by ux [1]. In this model, considering $(p+q)$-dimensional spacetime, there is a q-form ux eld for stabilizing the q-dimensional compact space. Moreover, introducing a bulk cosmological constant allows an external de Sitter space and an internal manifold with positive curvature. We obtain a $(p+q)$-dimensional product spacetime of p-dimensional de Sitter space dS_p and q-dimensional sphere S^q.

It has been shown that the Freund–Rubin solution has dynamical instabilities that are divided into two classes [3, 4]; one is attributed to homogeneous excitation ($l = 0$ mode) in the internal space, which corresponds to a change of the radius of the extra dimensions, and the other is inhomogeneous excitation with quadrupole moment and higher multi-pole moments ($l \geq 2$ modes), which represents the deformation of the internal space. The $l = 0$ mode is a so-called volume modulus or radion, and becomes tachyonic when the Hubble parameter of the external de Sitter space is too large (in other words, the ux density on the internal space is small). This fact implies that if the energy scale of the in ationary external spacetime is su ciently larger than the compacti cation scale of the internal space, stabilization by ux will be broken. In order to avoid the emergence of this instability, con gurations with small Hubble parameters would be preferable. On the other hand, instabilities arising from inhomogeneous excitations will emerge only if the number of extra dimensions is larger than or equal to four. In the unstable region, in which the $l \geq 2$ modes are tachyonic, the external spacetime has small Hubble parameters including the Minkowski spacetime. It means that the ux densities are very large. It should also be added that for more than four extra dimensions, the two unstable regions overlap so that stable con gurations for the FR solution no longer exist.

Little has been known about the non-perturbative nature of the instability from higher multi-pole modes; how it turns out after the onset of this instability and whether any stable con guration as a possible end-state exists in this model, and so on. In [2] we have shown that in the Freund–Rubin compacti cation there is a new branch of di erent solutions other than the FR solutions. Those solutions are described as the warped product of an external de Sitter space and an internal deformed sphere. It has been found that the branch of the FR solutions and that of the deformed solutions intersect at one point where the FR solution becomes marginally stable for the $l = 2$ mode. Although we have seen existence of solution other than the FR solution, its stability remains unanswered.

[1] E-mail:kinoshita@utap.phys.s.u-tokyo.ac.jp
[2] E-mail:shinji.mukohyama@ipmu.jp

Here we are particularly concerned with the close connection between dynamical stability and thermodynamic stability for revealing nature. The interesting relationship between dynamical and thermodynamic stability, which is well known as the correlated stability conjecture (or the Gubser–Mitra conjecture), has been suggested and ensured for some black objects (strings, branes and so on) by many authors. It is signi cant to examine whether such connections will exist and whether the idea can be extended to systems such as spacetimes with de Sitter horizons other than black objects.

Consequently, the aim of this study is to examine the stability of the new branch of deformed solutions from both dynamical and thermodynamic perspectives. This opens up new possibilities of the applicability of close connection between dynamical and thermodynamic stabilities.

2 Dynamical stability

We investigate dynamical stability of deformed solution by considering perturbation around background solution. We will concentrate on scalar-type perturbation with respect to the external de Sitter space because in the case of the FR solution instability arises from this type perturbation.

We suppose that the background $(p+q)$-dimensional metric and q-form eld strength are given by

$$\mathrm{d}s^2 = A^2(y) g_{\mu\nu}(x)\mathrm{d}x^\mu \mathrm{d}x^\nu + \mathrm{d}y^2 + B^2(y)\mathrm{d}\,{}^{2}_{q\ 1}, \quad F_{(q)} = b\frac{B^{q\ 1}}{A^p}\mathrm{d}y \wedge \mathrm{d}\,{}_{q\ 1}, \tag{1}$$

where $g_{\mu\nu}$ is the metric of p-dimensional de Sitter space with a Hubble parameter h and $\mathrm{d}\,{}^{2}_{q\ 1}$ is the metric of the unit round $(q\ \ 1)$-sphere. Here b is a ux density.

All we need to consider are perturbations which are scalar-type quantities with respect to not only p-dimensional de Sitter symmetry of the external space but also $SO(q)$ symmetry of the internal space. For simplicity we assume that the perturbations have $SO(q)$ symmetry on the internal space. By choosing an appropriate gauge, we can write the perturbed metric and eld strength as follows:

$$\mathrm{d}s^2 = (1+\ \ \mathsf{Y})\, A^2(y) g_{\mu\nu}\mathrm{d}x^\mu \mathrm{d}x^\nu + [1+(\qquad)\mathsf{Y}]\,\mathrm{d}y^2 + \ \ 1+\ \ \frac{}{q\ \ 1}\ \ \frac{p\ \ 1}{q\ \ 1}\ \ \mathsf{Y}\ \ B^2(y)\mathrm{d}\,{}^{2}_{q\ 1}, \tag{2}$$

and

$$F_{(q)} = b\frac{B^{q\ 1}}{A^p}\mathrm{d}y \wedge \mathrm{d}\,{}_{q\ 1} + \mathrm{d}\,(\varphi\mathsf{Y}) \wedge \mathrm{d}\,{}_{q\ 1} \tag{3}$$

where $\mathsf{Y}(x)$ is scalar harmonics on the de Sitter space with the Hubble parameter h and perturbed variables , and φ depend on only y-coordinate due to $SO(q)$-symmetry.

From the linearized Einstein equation and Maxwell equation, we obtain a set of two perturbation equations in terms of two variables and :

$$\begin{aligned}
&(p+q\ \ 2)\ \ '' + (q\ \ 2)\ \ '' + (p+q\ \ 2)\ \ p\frac{A'}{A}\ \ \ (q\ \ 1)\frac{B'}{B}\ \ \ ' + (q\ \ 2)\ \ p\frac{A'}{A} + (q\ \ 1)\frac{B'}{B}\ \ \ ' \\
&\qquad + \ \ \frac{\mu^2}{A^2} + \frac{2(q\ \ 2)}{B^2}\ \ [(p+q\ \ 2)\qquad q\ \ ] = 0, \\
&''+\ \ (3p\ \ 2)\frac{A'}{A} + 3(q\ \ 1)\frac{B'}{B}\ \ \ ' \ \ \ \frac{2(p+q\ \ 2)(q\ \ 2)}{B^2}\ \ \ 4 \\
&\qquad + \ \ \frac{\mu^2 + 2h^2(p\ \ 1)^2}{A^2} + \frac{2q(q\ \ 2)}{B^2}\ \ \ 4\qquad = 0,
\end{aligned} \tag{4}$$

where μ^2 is the KK mass squared which is de ned by $\nabla^2\mathsf{Y}(x) = \mu^2\mathsf{Y}(x)$. Thus the perturbation equations are reduced to eigenvalue problems with eigenvalue μ^2. If the spectrum of μ^2 is non-negative, we can conclude that the background spacetime is dynamically stable.

For the deformed solution we will numerically solve the eigenvalue problem for a set of di erential equations (4) in order to nd the mass spectrum μ^2. In Fig 1, we present numerical result of the mass spectrum of the deformed branch for $p = 4$ and $q = 4$. The solid lines represent μ^2 for the deformed branch and the dashed lines for the FR branch. We will focus our attention on the $l = 2$ mode because

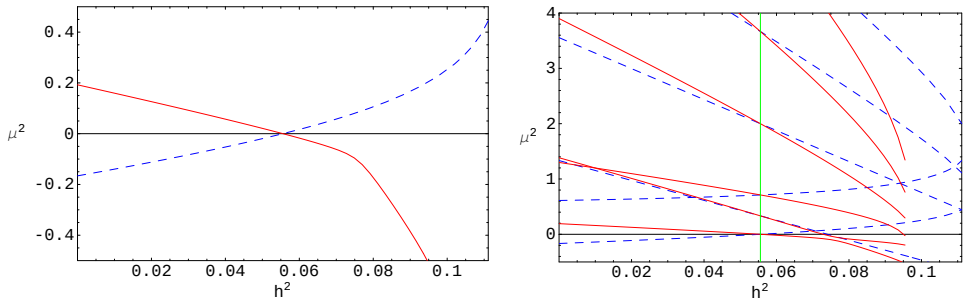

Figure 1: The mass spectrum for scalar perturbations. Solid lines and dashed lines indicate the deformed branch and the FR branch, respectively. The vertical line indicates the critical value at which two branches merge. In the low Hubble region where the FR branch is unstable, the deformed branch is stable.

it is the rst unstable mode for inhomogeneous perturbations on the FR branch. It turns out that, for the Hubble parameters h^2 below the critical value, μ^2 of the deformed branch is positive, while the $l = 2$ mode of the FR branch becomes tachyonic. Thus the deformed branch is stable con guration in the low Hubble region, in which the FR branch is unstable.

The mass squared for some modes with other multi-pole moments than $l = 2$ is shown in Fig 1, also. As the mass spectrum, the deformed branch has no unstable mode in the low Hubble region. In addition we nd that μ^2 of the deformed branch tends to lift up at the side of lower h^2 solutions. Deformation will stabilize the internal space for the low Hubble region.

3 Thermodynamic stability

Assuming $SO(p+1)$ $SO(q)$ isometry, we can take the metric and the q-form eld strength as

$$\mathrm{d}s_{\mathrm{E}}^2 = e^{2\phi(r)} h^{2}\mathrm{d}\,{}^{2}_{p} + e^{\frac{2p}{q-2}\phi(r)}[\mathrm{d}r^2 + a^2(r)\mathrm{d}\,{}^{2}_{q\ 1}], \quad F_{(q)} = A'(r)\mathrm{d}r \wedge \mathrm{d}\,{}_{q\ 1}, \tag{5}$$

where $\mathrm{d}\,{}^{2}_{p}$ and $\mathrm{d}\,{}^{2}_{q\ 1}$ denote the metrics of the unit round p and $(q\ \ 1)$-sphere, respectively. The Euclidean action is given by

$$\begin{aligned} I_{\mathrm{E}}[a,\ ,A] = &\ \frac{1}{16}\int \mathrm{d}^{p+q}x_{\mathrm{E}}\sqrt{g_{\mathrm{E}}}\ \ R\ \ \ 2\ \ \ \frac{1}{q!}F_{(q)}^2 \\ = &\ \frac{p\ \ q\ \ 1}{16\ \ h^p}\int_{r_-}^{r_+}\mathrm{d}r\Bigg[(q\ \ 1)(q\ \ 2)\frac{a'^2+1}{a^2}\ \ \frac{p(p+q\ \ 2)}{q\ \ 2}\ {}'^2 + p(p\ \ 1)h^2 e^{\frac{2(p+q-2)}{q-2}\phi} \\ &\ 2\ e^{\frac{2p}{q-2}\phi}\ \ \frac{e^{\frac{2p(q-1)}{q-2}\phi}}{a^{2(q\ \ 1)}}A'^2\Bigg]a^{q\ \ 1}, \end{aligned} \tag{6}$$

where the boundary terms have vanished since the boundary conditions require $a(r_\pm) = 0$, $|a'(r_\pm)| = 1$ and $'(r_\pm) = 0$ at the boundaries $r = r_\pm$.

Here we de ne an entropy as one quarter of the total area $\mathcal{A}$ which is that of de Sitter horizon integrated over the internal space:

$$S\ \ \frac{\mathcal{A}}{4} = \frac{p\ \ 2\ \ q\ \ 1}{4h^p\ \ 2}\int_{r_-}^{r_+}\mathrm{d}r\, e^{\frac{2(p+q-2)}{q-2}\phi}a^{q\ \ 1}. \tag{7}$$

Using the equations of motion, we evaluate the Euclidean action I_{E} on shell and it turns out $I_{\mathrm{E}} = \ \ S$. The total ux of the form eld, which is de ned as $\oint F_{(q)}$, is given by

$$= \ _{q\ \ 1}[A(r_+)\ \ \ A(r\ \ )] = b\ _{q\ \ 1}\int_{r_-}^{r_+}\mathrm{d}r\, e^{\frac{2p(q-1)}{q-2}\phi}a^{q\ \ 1}, \tag{8}$$

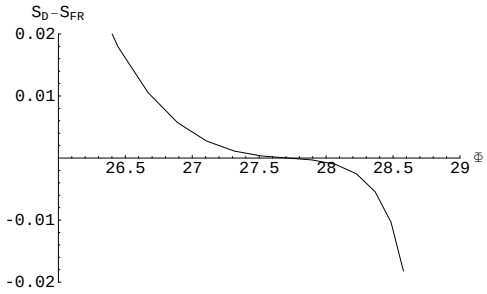

Figure 2: The di erence between the entropy of the deformed branch $S_{\rm D}$ and that of the FR branch $S_{\rm FR}$.

where b is an integration constant which is de ned by $A' = be^{\frac{2p(q-1)}{q-2}\phi} a^{q-1}$ from the equation of motion for the form eld.

We now proceed to discuss the di erential thermodynamic relation such as the rst law of thermodynamics. We consider the rst variation of the action $I_{\rm E}[a, , A]$ with respect to a, and A. Suppose both $\{a, , A\}$ and $\{a + a, + , A + A\}$ are di erent sets of solutions satisfying the equations of motion, the rst variation of the action $I_{\rm E}$ is given by

$$I_{\rm E} = \frac{p q 1}{8 h^p} \frac{e^{\frac{2p(q-1)}{q-2}\phi}}{a^{q-1}} A' A \Big|_{r_-}^{r_+} + \int_{r_-}^{r_+} {\rm d}r \,(\text{EOM for } a, \text{ and } A)\,. \tag{9}$$

Integrand functions in the last term will vanish because of the equations of motion for a, and A. Only the boundary term contributes to the rst variation of the action. Thus the rst law can be derived as

$${\rm d}S = \frac{p 2b}{4(p 1)h^p} {\rm d} . \tag{10}$$

This implies that the entropy is described by a function of the total ux. Hence the entropy S is a thermodynamic potential with respect to the total ux as a natural thermodynamic variable. We shall call a sequence of solutions which satis es the rst law a "branch" of solutions.

We will discuss thermodynamic stability for the FR branch and the deformed branch of solutions. As we have seen the entropy S is the thermodynamic potential when we choose the total ux as a natural variable. Therefore, the second law of thermodynamics states that, if the total ux is given, a con guration with larger entropy is thermodynamically favored. We shall now proceed to the issue of the deformed branch and focus on the case for $p = 4$ and $q = 4$ as a explicit example. We denote the entropy of the FR branch and that of the deformed branch as $S_{\rm FR}$ and $S_{\rm D}$, respectively. A di erence of entropy between $S_{\rm D}$ and $S_{\rm FR}$ for xed uxes is shown in Fig. 2. It turns out that in the lower side for the total ux , in which the Hubble parameter become small, the di erence is positive and the deformed branch is stable. On the other hand, in the higher side the di erence is negative and the FR branch is stable. At the critical point where two branches merge it is marginally stable. It is worth noting that the FR branch has dynamical instability arising from inhomogeneous excitation where the deformed branch is favored thermodynamically.

References

[1] P. G. O. Freund and M. A. Rubin, Phys. Lett. B **97**, 233 (1980).

[2] S. Kinoshita, Phys. Rev. D **76**, 124003 (2007) [arXiv:0710.0707 [hep-th]].

[3] R. Bousso, O. DeWolfe and R. C. Myers, Found. Phys. **33**, 297 (2003) [arXiv:hep-th/0205080].

[4] J. U. Martin, JCAP **0504**, 010 (2005) [arXiv:hep-th/0412111].

Long term simulation of binary neutron star merger

Kenta Kiuchi[1] Yuichiro Sekiguchi[2] Masaru Shibata[3] and Keisuke Taniguchi[4]

[1]*Department of Physics, Waseda University, 3-4-1 Okubo, Shinjuku-ku, Tokyo 169-8555, Japan*
[2]*Division of Theoretical Astronomy/Center for Computational Astrophysics, National Astronomical Observatory of Japan, 2-21-1, Osawa, Mitaka, Tokyo, 181-8588, Japan*
[3]*Graduate School of Arts and Sciences, University of Tokyo, Komaba, Meguro, Tokyo 153-8902, Japan*
[4] *Department of Physics, University of Wisconsin-Milwaukee, P.O. Box 413, Milwaukee, Wisconsin 53201 USA*

Abstract

General relativistic simulation for the merger of binary neutron stars is performed in a modified method, as an extension of a previous work [1]. We prepare binary neutron stars with a large initial orbital separation and employ the moving-puncture formulation, which enables to follow merger and ringdown phases for a long time, even after black hole formation. Three equal-mass binaries with each mass $1.4M_\odot, 1.45M_\odot, 1.5M_\odot$ and two unequal-mass binaries with mass 1.3–$1.6M_\odot$, 1.35–$1.65M_\odot$ are prepared. We focus primarily on the black hole formation case, and explore mass and spin of the black hole, mass of disks which surround the black hole, and gravitational waves emitted during the black hole formation.

1 Introduction

Coalescence of binary neutron stars is one of the most promising sources for kilometer-size laser interferometric detectors such as the LIGO, GEO,VIRGO, and TAMA. Latest statistical estimate indicates that detection rate of gravitational waves from binary neutron stars will be 1 event per 4–100 years for the first-generation interferometric detectors and 10–500 events per year for the advanced detectors. This suggests that gravitational waves from binary neutron stars will be detected within the next decade.

For theoretically studying the late inspiral, merger, and ringdown phases of the binary neutron stars, numerical relativity is the unique approach. Until quite recently, there has been no general relativistic simulation that quantitatively clarifies the inspiral and merger phases because of limitation of the computational resources or difficulty in simulating a black-hole spacetime, although a number of simulations have been done for a qualitative study. The most crucial drawbacks in the previous works were summarized as follows ; (i) the simulation were not able to be continued for a long time after formation of a black hole and/or (ii) the simulations were short-term for the inspiral phase; the inspiral motion of the binary neutron stars is followed only for $\sim$ 1–2 orbits.

In the present work, we perform an improved simulation overcoming these drawbacks; (i) we adopt the moving-puncture approach [2], which enables to evolve black hole spacetimes for an arbitrarily long time; (ii) we prepare binary neutron stars in quasicircular orbits of a large separation as the initial condition. In the chosen initial data, the binary neutron stars spend in the inspiral phase for 3–4 orbits before the onset of merger, and hence, approximately correct non-zero approaching velocity and nearly zero eccentricity will be results. We focus in particular on quantitatively clarifying formation process of a black hole for the case that it is formed promptly (i.e., in the dynamical time scale $\sim$ 1–2 ms) after the onset of merger. More specifically, the primary purpose of this paper is (1) to determine the final mass and spin of the black hole formed after the merger, (3) to clarify quantitative features of gravitational waves emitted in the merger and ringdown phases.

[1]E-mail:kiuchi@gravity.phys.waseda.ac.jp
[2]E-mail:sekig@th.nao.ac.jp

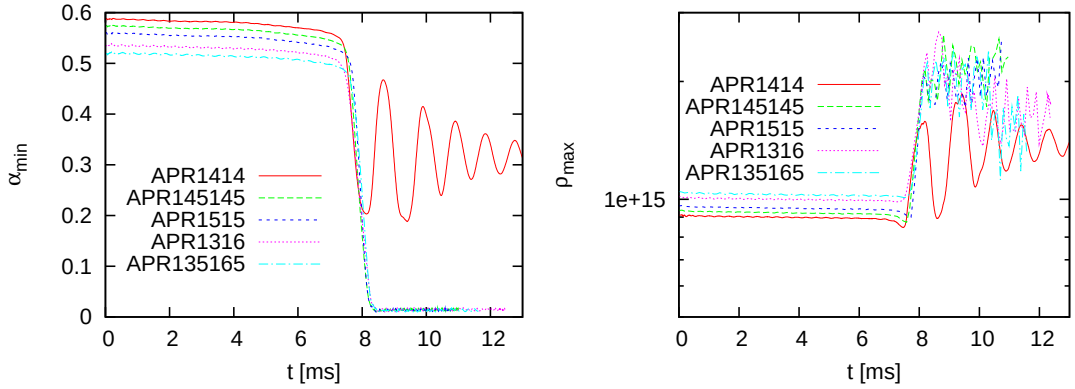

Figure 1: Evolution of the minimum value of the lapse function, $\alpha_{\rm min}$, and the maximum rest-mass density $\rho_{\rm max}$ for models APR1414, APR145145, APR1515, APR1316, and APR135165.

2 Summary of basic equation and numerical issue

For solving the Einstein evolution equation, we use the original version of the Baumgarte-Shapiro-Shibata-Nakamura formulation [3]: The numerical code for solving the Einstein equation and for the hydrodynamics is the same as that in Ref. [4].

3 Result

3.1 General feature for merger process

We have already performed the simulation for binary neutron stars with realistic EOSs [1]. Although the qualitative feature for the merger process found in the present work is the same as in the previous works, we here summarize generic feature of the merger again.

Figure 1 plots the evolution of the minimum lapse function, $\alpha_{\rm min}$, and maximum baryon rest-mass density, $\rho_{\rm max}$, for all the models studied in this paper. For models APR145145, APR1515, APR1316, and APR135165 for which a black hole is formed soon after the onset of the merger, $\alpha_{\rm min}$ ($\rho_{\rm max}$) decreases (increases) monotonically. For these runs, two neutron stars come into the first contact at $t \sim 7.5$ ms. For all the cases, apparent horizon is formed when $\alpha_{\rm min}$ reaches ~ 0.03. For model APR1414, $\alpha_{\rm min}$ ($\rho_{\rm max}$) steeply decreases (increases) after the onset of the merger, but then, they start oscillation and eventually settle down to relaxed values. This indicates that a hypermassive neutron star is the outcome.

In the unequal-mass case, less massive neutron star is tidally deformed ~ 1 orbit before the onset of merger. Then, mass shedding occurs, and as a result, the material in the less massive neutron star acrretes onto the massive companion. During the merger, it is highly tidally deformed, and thus, an efficient angular momentum transport occurs. Due to this, the material in the outer region of the less massive neutron star spreads outward to form a spiral arm. This process helps formation of accretion disks around the formed black hole.

3.2 Black hole mass and spin

As mentioned in the previous subsections, the final outcome after the merger for models APR145145, APR1515, APR1316, and APR135165 is a rotating black hole. We here determine the black-hole mass, $M_{\rm BH,f}$, and spin, $a_{\rm f}$, using the same method as those used in Refs. [1]. All the results for the black-hole mass and spin are summarized in Table 1. We find that $M_{\rm BH,f}$ and $C_e/4\pi$ agree within 0.2% error for all

Table 1: Black-hole mass $M_{\rm BH,f}$ and nondimensional spin parameter $a_{\rm f}$ for models APR145145, APR1515, APR1316, and APR135165. ΔE, ΔJ, $M_{r>r_{\rm AH}}$, $J_{r>\rm AH}$, C_p, C_e, and $f_{\rm QNM}$ denote energy and angular momentum carried by gravitational waves, rest mass and angular momentum of the material located outside apparent horizon, and polar and equatorial circumferential radii of the apparent horizon, respectively. $M_{r>r_{\rm AH}}$ and $J_{r>r_{\rm AH}}$, are given in units of M_0 and J_0, respectively.

Model	$\Delta E/M_0$	$\Delta J/J_0$	$M_{r>r_{\rm AH}}$	$J_{r>r_{\rm AH}}$	$M_{\rm BH,f}/M_0$	$C_e/4\pi M_0$	C_p/C_e	$a_{\rm f1}$	$a_{\rm f2}$
APR145145	1.15%	16.7%	–	–	0.988	0.9880	0.8628	0.77	0.77
APR1515	1.19%	16.9%	0.004%	–	0.988	0.9864	0.8576	0.79	0.78
APR1316	1.14%	16.8%	1.13%	2.69%	0.977	0.9768	0.8692	0.75	0.75
APR135165	1.10%	16.4%	0.26%	0.58%	0.986	0.9859	0.8625	0.77	0.77

the models. This indicates that both quantities at least approximately denote the black-hole mass and that we obtain the black-hole mass within $\sim 0.2\%$ error.

The spin parameters $a_{\rm f1}$ and $a_{\rm f2}$, which are determined from the aparent horizon area $\hat{A}_{\rm AH}$ and horizon shape C_p and C_e, respectively, agree within 2% error for all the models. We find that C_p/C_e and $\hat{A}_{\rm AH}$ depend weakly on the grid resolution, and so do $a_{\rm f1}$ and $a_{\rm f2}$. This suggests that the convergent value of the black-hole spin is close to $a_{\rm f1}$ and $a_{\rm f2}$, and for all the models, we estimate the black-hole spin as $a_{\rm f} \approx 0.77 \pm 0.03$.

In the merger of equal-mass, nonspinning binary black holes, $a_{\rm f}$ is ≈ 0.69, which is by about 0.1 smaller than that for the merger of binary neutron stars. This difference arises primarily from the magnitude of ΔJ in the final phase of coalescence. In the merger of binary black holes, a significant fraction of angular momentum is dissipated by gravitational radiation during the last inspiral, merger, and ringdown phases, because a highly nonaxisymmetric state is accompanied with a highly compact state from the last orbit due to the high compactness of black holes. By contrast, compactness of the neutron stars is by a factor of ~ 5 smaller, and as a result, such a highly nonaxisymmetric and compact state is not achieved for the binary neutron stars. Indeed, angular momentum loss rate by gravitational waves during the last phases is much smaller than that of binary black holes.

3.2.1 Merger and ringdown gravitational waves

The waveforms in the ringdown phase are primarily characterized by the fundamental quasinormal mode of the formed black holes for models APR145145, APR1515, APR1316, and APR135165. To clarify this fact, Fig. 2 plots Ψ_4 together with a fitting formula in the form

$$A{\rm e}^{-t/t_d}\sin(2\pi f_{\rm QNM}t+\delta) \tag{1}$$

where A and δ are constants, and the frequency and damping time scale are predicted by a linear perturbation analysis as

$$f_{\rm QNM} \approx 10.7\left(\frac{M_{\rm BH,f}}{3.0M_\odot}\right)^{-1}[1-0.63(1-a_{\rm f})^{0.3}]\ {\rm kHz}, \quad t_d \approx \frac{2(1-a_{\rm f})^{-0.45}}{\pi f_{\rm QNM}}. \tag{2}$$

Figure 2 (a) shows that gravitational waves for model APR1515 are well fitted by the hypothetical waveforms given by Eq. (1) for $t_{\rm ret} \gtrsim 8.4$ ms. [Here, we set $a_{\rm f} = a_{\rm f1}$ for the fitting (cf. Sec. 3.2)]. This is reasonable because the final outcome for model APR1515 is a stationary rotating black hole with negligible disk mass, and hence, the black-hole perturbation theory (i.e., Eq. (1)) should work well. This is also the case for the gravitational waveforms for model APR145145, for which the merger proceeds in essentially the same manner as that for model APR1515.

3.2.2 Fourier spectrum

We define Fourier power spectrum of gravitational waves by

$$h(f) \equiv \frac{D}{M_0}\sqrt{\frac{|h_+(f)|^2+|h_\times(f)|^2}{2}}, \quad h_+(f)=\int e^{2i\pi ft}h_+(t)dt, \quad h_\times(f)=\int e^{2i\pi ft}h_\times(t)dt. \tag{3}$$

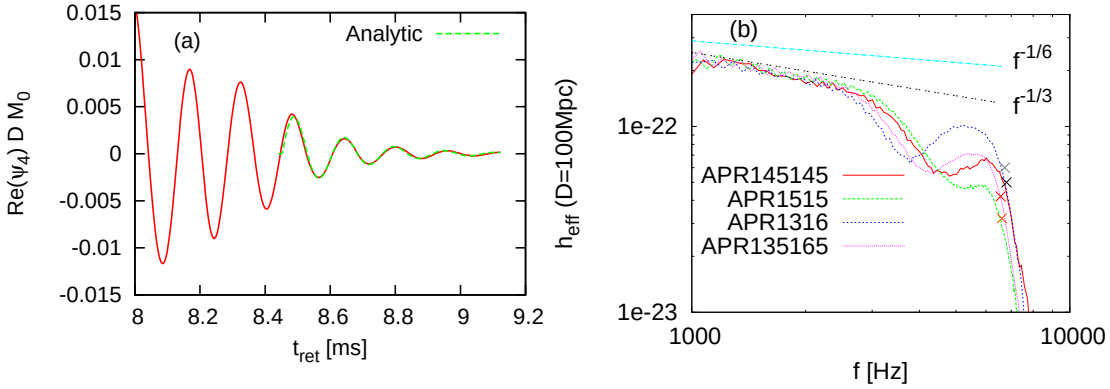

Figure 2: Ringdown waveforms associated primarily with the fundamental quasinormal mode for model APR1515. We plot the real part of Ψ_4. For the figure(a), the dashed curves denote the fitting curves calculated by Eq. (1). (b) Spectrum of gravitational waves for all the black hole formation models.

Here, h_+ and $h_\times$ denote the + and $\times$ modes of gravitational waves of $l = |m| = 2$. From $h(f)$, we define a nondimensional spectrum (or effective amplitude) as $h_{\rm eff}(f) \equiv h(f) f M_0/D$.

In Fig. 2, we show the spectrum ($h_{\rm eff}$) of gravitational waves for models APR1414, APR1515, APR1316, and APR13516. To plot Fig. 2, we assume $D = 100$ Mpc. The Fourier spectrum shows universal features, irrespective of the total mass and mass ratio of the binary neutron stars. We quantitatively summarized as follows: (i) For $f \le f_{\rm cut} \approx 2.5$–3 kHz, the spectrum amplitude gradually decreases according to the relation $\propto f^{-n}$ where n is a slowly varying function of f; $n = 1/6$ for $f \to 0$, and $n \sim 1/3$ for $f \to f_{\rm cut}$. $f_{\rm cut}$ is much larger than the frequency at the ISCO. This is due to the fact that even after the onset of the merger, the merged object has two high-density peaks, and emits gravitational waves for which the waveform is similar to the inspiral one. (ii) For $f \ge f_{\rm cut}$, the spectrum amplitude steeply decreases. This seems to reflect the fact that at such frequency, two density peaks disappear duering the collapse to a black hole. (iii) For $f = f_{\rm peak} \approx 5$–6 kHz, which is slightly smaller than $f_{\rm QNM} \sim 6.7$–6.9 kHz, a broad peak appears. Because the frequency is always smaller than $f_{\rm QNM}$, this peak is not associated with the ringdown gravitational waveform but with the merger waveform. (iv) For $f > f_{\rm fin} \approx f_{\rm QNM}$, the amplitude damps in an exponential manner.

Although the features (i)–(iv) are qualitatively universal, the values of $f_{\rm cut}$, $f_{\rm peak}$, $f_{\rm QNM}$, and $f_{\rm fin}$, and the height and width of the peak at $f = f_{\rm peak}$ depend on the total mass and mass ratio of binary neutron stars, i.e., merger and black hole formation processes. This indicates that if we can detect gravitational waves of high frequency $f = 2$–8 kHz, we will be able to get information about merger and black hole formation precesses.

References

[1] M. Shibata and K. Taniguchi, Phys. Rev. D **73**, 064027 (2006).

[2] M. Campanelli, C. O. Lousto, P. Marronetti and Y. Zlochower, Phys. Rev. Lett. **96**, 111101 (2006); J. G. Baker, J. Centrella, D.-I. Choi, M. Koppitz, and J. van Meter, Phys. Rev. Lett. **96**, 111102 (2006).

[3] M. Shibata and T. Nakamura, Phys. Rev. D **52** (1995) 5428. see also, T. W. Baumgarte and S. L. Shapiro, Phys. Rev. D **59**, 024007 (1999)

[4] M. Shibata and K. Taniguchi, Phys. Rev. D **77**, 084015 (2008).

Super-radiance of electromagnetic radiation from disk surface around Kerr black hole

Taichi Kobayashi[1], Kohei Onda[2] and Akira Tomimatsu[3]

Department of Physics, Nagoya University, Nagoya , 464-8602, Japan

Abstract

According to recent observation, it is possible to see the event-horizon-scale structure in the supermassive black hole candidate at the Galactic Centre. Therefore, it is important to consider the electromagnetic waves emitted by disk surface near the black hole horizon. In general, the electromagnetic waves are essentially influenced by gravitation around the black hole (cf. doppler shift, lensing effects, and super-radiance). Using ray-tracing, there is the study of black hole shadow, which is the image of disk configuration influenced by black hole. However, in ray-tracing, the influence of waves (cf. superradiance) is not treated. We focus on the superradiance of electromagnetic waves emitted from disk surface around Kerr black hole. Then it is interesting to see the amplification of disk radiation, and estimate the energy radiated away to infinity.

1 Introduction

It is widely believed that there exists a rotating black hole surrounded by a disk in the central region of highly energetic astrophysical objects, such as active galactic nuclei (AGNs), x-ray binary systems, and gamma-ray bursts (GRBs). Because the electromagnetic waves cannot be emitted from horizon of black hole, the electromagnetic waves emitted from disk surface are observed in the observation of black hole candidates. Then the electromagnetic waves near the horizon are influenced by strong gravitational field. Furthermore, according to recent observation, it is possible to see the event-horizon-scale structure in the supermassive black hole candidate at the galactic centre[1]. In these situations, it is important to consider the behavior of electromagnetic waves around Kerr black holes.

On the other hand, there is the study of radiation from disk around Kerr black holes, called by "Ray-tracing" method[2]. In this method, the effects of gravitation, such as the bending of light and gravitational red shift, are considered. However, the interaction between wave and black hole, is not treated. One of effect is super-radiance which is energy extraction process from black hole due to electromagnetic waves.

In a previous study of well-known super-radiance scattering[3], an disk boundary condition is not considered. Therefore we consider the vacuum electromagnetic fields with a disk boundary condition on the equatorial plane around Kerr black holes. Then we focus on super-radiance and energy transport due to electromagnetic waves.

2 Formalism

To treat vacuum electromagnetic fields in the disk-black hole system, it is convenient to use the Kerr-Schild formalism for solving the Einstein-Maxwell equation[4]. If this formalism is applied to obtain electromagnetic perturbations on Kerr background, it is known that all the field components are simply derived by two arbitrary complex functions ψ and ϕ, which can be appropriately chosen according to the disk boundary condition. Here, we put a branch cut in arbitrary complex function ψ on the equatorial plane. Then, the component of $F_{t\theta}$, $F_{\theta\varphi}$ and $F_{r\theta}$ become discontinuous at $\theta = \pi/2$. This discontinuties correspond to the existence of disk current on the equator[5].

[1]E-mail:kobayashi@gravity.phys.nagoya-u.ac.jp
[2]E-mail:onda@gravity.phys.nagoya-u.ac.jp
[3]E-mail:atomi@gravity.phys.nagoya-u.ac.jp

Using Newman-Penrose formalism[6], the electromagnetic fields derived from Kerr-Schild formalism (called by KS solution) are described as

$$\begin{aligned}
\phi_0^{\rm KS} &= 0, && (1)\\
(r-ia\cos\theta)^2\phi_1^{\rm KS} &= \psi(X)/2, && (2)\\
(r-ia\cos\theta)\phi_2^{\rm KS} &= \frac{e^{i\tilde{\varphi}}\phi(Y,\tau)}{2\sqrt{2}\cos^2(\theta/2)} + \frac{X\psi_X}{\sqrt{2}(r+ia\cos\theta)\sin\theta}\left[(r-ia)2i\sigma\cos^2(\theta/2)-1\right]. && (3)
\end{aligned}$$

Here, $Y = e^{i\tilde{\varphi}}\tan(\theta/2)$, $\tau = -\tilde{t}+r+ia\cos\theta$, $X = e^{i\sigma\tau}Y$, σ is corresponding to frequency, and $\tilde{t}$ and $\tilde{\varphi}$ are Kerr-Schild coordinates which remain finite even on the horizon. Here we consider the expansion of arbitrary complex function ψ. By using the expansion form, for example, we obtain

$$X\psi_{,X} = \sum_m m a_m X^m. \tag{4}$$

As a result, we choose an azimuthal mode m. Then the electromagnetic field is described as

$$\begin{aligned}
\phi_{0\ m}^{\rm KS} &= 0, && (5)\\
(r-ia\cos\theta)^2\phi_{1\ m}^{\rm KS} &= a_m e^{-i\omega t+im\varphi}e^{i\omega r_*+i\int\frac{ma}{r^2+a^2}{\rm d}r_*}\tan^m(\theta/2)/2, && (6)\\
(r-ia\cos\theta)\phi_{2\ m}^{\rm KS} &= \frac{e^{i\tilde{\varphi}}\phi(Y,\tau)}{2\sqrt{2}\cos^2(\theta/2)}\\
&\quad + \frac{a_m e^{-i\omega t+im\varphi}e^{i\omega r_*+i\int\frac{ma}{r^2+a^2}{\rm d}r_*}\tan^m(\theta/2)}{\sqrt{2}(r+ia\cos\theta)\sin\theta}\left[(r-ia)2i\omega\cos^2(\theta/2)-m\right], && (7)
\end{aligned}$$

in Boyer-Lindquist coordinates, where we define $\omega \equiv m\sigma$ and ${\rm d}r_*/{\rm d}r = 2mr/(r^2+a^2)$. However, if the Kerr-Schild formalism is applied to the radiation from disk, the pure outgoing waves are emitted on the horizon. Therefore to require the elimination of outgoing wave on the horizon, we consider the superposition between Kerr-Schild solution and well-known electromagnetic perturbations (called by TP solution)[3]. The electromagnetic fields are described as

$$\phi_a = \phi_a^{\rm KS} + \phi_a^{\rm TP}, \quad [a = 0,\ 1,\ 2]. \tag{8}$$

Then, we consider the boundary conditions as follows: ingoing waves on the horizon and outgoing waves at infinity. Our model differ from the "well-known" perturbations, such as analysis of quasi-normal mode, because on the disk boundary there are emission and absorption of electromagnetic waves.

3 Energy flux in each regions

In this section, we consider the distribution of the energy flux. The energy flux is written by

$$\mathcal{E} = -T_{\ t}, \tag{9}$$

where

$$\begin{aligned}
T &= \frac{1}{4\pi}\left[\phi_0\bar{\phi}_0 n\ \ n\ \ + \phi_2\bar{\phi}_2 l\ \ l\ \ 2\phi_1\bar{\phi}_1(l_{(}\ \ n\ \ _{)} + m_{(}\ \ \bar{m}\ \ _{)})\right.\\
&\quad \left. -4\bar{\phi}_0\phi_1 n_{(}\ \ m\ \ _{)} - 4\bar{\phi}_1\phi_2 l_{(}\ \ m\ \ _{)} + 2\phi_2\bar{\phi}_0 m\ \ m\ \ \right] + \text{C.C.}, && (10)
\end{aligned}$$

and, l , n and m are Kinnersley's tetrad written by

$$\begin{aligned}
l &= \left[1,\ -\Sigma/\Delta,\ 0,\ -a\sin^2\theta\right], && (11)\\
n &= (\Delta/2\Sigma)\left[1,\ \Sigma/\Delta,\ 0,\ -a\sin^2\theta\right], && (12)\\
m &= \left[ia\sin\theta,\ 0,\ -\Sigma,\ -i(r^2+a^2)\sin\theta\right]/\sqrt{2}(r+ia\cos\theta), && (13)
\end{aligned}$$

in Boyer-Lindquist coordinates. In particular, the radial and angular components of energy flux are described as

$$\mathcal{E}^r = \frac{1}{4\pi}\left[-\frac{\Delta^2}{4\Sigma^2}\phi_0\bar{\phi}_0 + \phi_2\bar{\phi}_2 + \frac{ia\sin\theta}{\sqrt{2}(r+ia\cos\theta)}\frac{\Delta}{\Sigma}\bar{\phi}_0\phi_1 - \frac{2ia\sin\theta}{\sqrt{2}(r+ia\cos\theta)}\bar{\phi}_1\phi_2\right] + \text{C.C.}, \quad (14)$$

$$\mathcal{E}^\theta = -\frac{1}{4\pi\Sigma}\left[\frac{\Delta}{\sqrt{2}(r+ia\cos\theta)}\bar{\phi}_0\phi_1 + \frac{2\Sigma}{\sqrt{2}(r+ia\cos\theta)}\bar{\phi}_1\phi_2 - \frac{\Sigma ia\sin\theta}{(r+ia\cos\theta)^2}\bar{\phi}_0\phi_2\right] + \text{C.C.}, \quad (15)$$

where $\Delta = r^2 + a^2 - 2Mr$, $\Sigma = r^2 + a^2\cos^2\theta$.

First we see the total energy on the horizon written by

$$E_{\rm H} = \int_0^\pi \mathcal{E}^r_{\rm H}\Sigma_{\rm H}\sin\theta {\rm d}\theta. \quad (16)$$

Using Maxwell equations, the total energy is described as

$$E_{\rm H} \propto -\left(\frac{\omega}{k}A + \frac{\omega_{\rm H}}{k}B\right), \quad (17)$$

where ω and $\omega_{\rm H}$ are frequency of wave and angular velocity of black hole, respectively, and $k = \omega - m\omega_{\rm H}$. Here, if superradiant condition ($0 < \omega < \omega_{\rm H}$) is filled, the rotational energy is extracted due to the electromagnetic waves.

Secondly, to see the energy transport, we consider the low-frequency limit ($a\omega \ll 1$). In this limit, we can solve the radial equation of electromagnetic field. As a result, we get the relations between each coefficients of waves, which is corresponding to amplitude. This relations are written by

$$\frac{({\rm out})^\infty_s}{({\rm out})^{\rm H}_s} = (-1)^{-l}(r_1-r_2)^{2s+1}(2\kappa)^{l-s}\frac{(l+s)!(l-s)!}{(2l)!(2l+1)!}\frac{\Gamma(l+1+2iQ)}{\Gamma(-s+2iQ)}, \quad (18)$$

$$\frac{({\rm In})^{\rm H}_s}{({\rm out})^{\rm H}_s} = \frac{(-1)^{-s+1}}{(r_1-r_2)^{-2s}}\frac{(l-s)!}{(l+s)!}\frac{\Gamma(s+1-2iQ)\Gamma(l+1+2iQ)}{\Gamma(l+1-2iQ)(\Gamma(1-s+2iQ)}, \quad (19)$$

where $\kappa = -i(r_1-r_2)\omega$, $Q = ({r_1}^2+a^2)(\omega_{\rm H}-\omega)/(r_1-r_2)$, r_1 and r_2 are distance of outer and inner horizon, respectively, the electromagnetic field is described as $s = \pm 1$, and $s = 1$ and $s = -1$ are corresponding to coefficients of ϕ_0 and ϕ_2, respectively. Then we can see the dependence on frequency in the energy fluxes. As a result, it is easy to see that the extracted energy is transported to disk region.

4 Summary

We consider the electromagnetic perturbations considered by disk boundary. Then we put the boundary conditions as follows: ingoing waves on the horizon and outgoing waves at infinity. However, because the source of radiation exist, Our model differ from the "well-known" perturbations, such as analysis of quasi-normal mode. As a result, we find the energy extracted from black hole due to super-radiance, and the extracted energy is transported to disk regions.

References

[1] S. S. Doelema et al., "Event-horizon-scale structure in the supermassive black hole candidate at the Galactic Centre", Nature, 455, 78 (2008)

[2] A. Müler, & M. Camenzind, "Relativistic emission lines from accretion black holes: The effect of disk truncation on line profiles", A&A, 413, 861(2004)

[3] W. H. Press, & S. A. Teukolsky, Perturbations of Rotating Black hole. III. Interaction of the Hole with Gravitational and Electromagnetic Radiation", ApJ, 193, 443(1974)

[4] G. C. Debney, R. P. Kerr, & A. Schild, "Solutions of the Einstein and Einstein-Maxwell Equations", J. Math. Phys., 10, 1842(1969)

[5] T. Kobayashi et al., "Disk illumination by black hole superradiance of electromagnetic perturbations", Phys. Rev. D, 77, 064011(2008)

[6] E. T. Newman & R. Penrose, "An Approach to Gravitational Radiation by a Method of Spin Coefficients". J. Math. Phys., 6, 566(1962)

Conformal Inflation, Modulated Reheating, and WMAP5

Takeshi Kobayashi[1] and Shinji Mukohyama[2]

[1]*Department of Physics, School of Science, The University of Tokyo, Hongo 7-3-1, Bunkyo-ku, Tokyo 113-0033, Japan*
[2]*Institute for the Physics and Mathematics of the Universe (IPMU), The University of Tokyo, 5-1-5 Kashiwanoha, Kashiwa, Chiba 277-8582, Japan*

Abstract

We investigate density perturbations generated through modulated reheating while inflation is driven by a conformally coupled scalar field. A large running of the spectral index is obtained, which reflects the basic nature of conformal inflation that higher-order time derivatives of the Hubble parameter during inflation are not necessarily small. This feature may allow us to distinguish between conformal inflation models and standard minimally coupled ones. We also investigate how the resulting fluctuations are modified when there is a deviation from an exact conformal coupling between the inflaton and gravity. Finally, we apply our results to the warped brane inflation model and see that observational bounds from the WMAP5 data suggest a blue tilted density perturbation spectrum. The discussion here is based on the paper [1].

1 Introduction

Ever since the idea of cosmic inflation was proposed, inflationary model building has largely focused on slow-rolling scalar fields minimally coupled to gravity as candidate inflatons. However, recently it was pointed out in [2] that conformally coupled scalar fields are also capable of accelerating the universe. Since the existence of such conformally coupled fields are rather common in models from string theory, it is of great interest to explore the possibility of conformally coupled fields driving inflation. In this light, we also come up with a new question of how we can distinguish between these "conformal inflation" models and standard minimally coupled ones.

The aim of our work is to focus on density perturbations and seek for distinctive features conformal inflation might have left. A conformally coupled inflaton itself cannot be responsible for generating primordial fluctuations, but instead string theory suggests alternative scenarios such as modulated reheating [3, 4]. Thence, we consider the case where modulated reheating generates density perturbations while inflation is driven by an almost conformally coupled inflaton. We study the scale dependence of the generated density perturbations.

We also investigate how the resulting density perturbations are modified when there is a deviation from an exact conformal coupling between the inflaton and gravity. The result will allow us to impose constraints on the inflaton's coupling from observational data. As a concrete example, our generic results are applied to the well-studied warped brane inflation model [5].

2 Review of Conformal Inflation

Here we give a brief review of conformal inflation. Consider the action

$$S = \int dx^4 \sqrt{-g} \left[\frac{M_p^2}{2} \mathcal{R} - \frac{1}{2} g^{\mu\nu} \partial_\mu \phi \partial_\nu \phi - V(\phi) - \frac{\xi}{2} \mathcal{R} \phi^2 \right] \tag{1}$$

[1]E-mailptkobayashi@utap.phys.s.u-tokyo.ac.jp
[2]E-mail:shinji.mukohyama@ipmu.jp

where $\mathcal{R}$ is the scalar curvature and ξ is the non-minimal coupling to gravity. Choosing a flat FRW background $ds^2 = -dt^2 + a(t)^2 d\mathbf{x}^2$ and also introducing $\pi \equiv \dot{\phi} + H\phi$, the Friedmann equation is

$$M_p^2 H^2 = \frac{1}{3}V + \frac{1}{6}\pi^2 + \left(\xi - \frac{1}{6}\right)(2H\phi\pi - H^2\phi^2), \tag{2}$$

and the equation of motion of ϕ is

$$\dot{\pi} + 2H\pi + V' + 6\left(\xi - \frac{1}{6}\right)(\dot{H} + 2H^2)\phi = 0. \tag{3}$$

The conformal case $\xi = 1/6$ was investigated in [2], where inflation was realized while the equations (2) and (3) could be approximated to

$$M_p^2 H^2 \simeq \frac{1}{3}V, \qquad cH\pi \simeq -V'. \tag{4}$$

Here, c is a dimensionless constant[3]. Let us define three "flatness parameters" as

$$\epsilon \equiv \frac{M_p^2}{2}\left(\frac{V'}{V}\right)^2, \qquad \tilde{\epsilon} \equiv \frac{\phi V'}{2V}, \qquad \eta_c \equiv \eta + \frac{c}{3}\left(\frac{V''\phi}{V'} + c - 2\right), \tag{5}$$

where $\eta \equiv M_p^2 V''/V$. When $|c| \sim \mathcal{O}(1)$, one can check that the necessary conditions for (4) and $|\dot{H}/H^2| \ll 1$ are simply

$$\epsilon \ll 1, \quad |\tilde{\epsilon}| \ll 1, \quad |\eta_c| \ll 1. \tag{6}$$

The proportionality constant c is chosen such that it is the largest constant to minimize $|\eta_c|/c^2$ [1].

It is clear from (2) and (4) that π^2/V is small during inflation. Especially when the potential is flat enough to satisfy $|M_p^2 V'| \ll |c\phi V|$, then $\dot{\phi} \approx -H\phi$, which suggests that the inflaton is rapidly rolling towards its origin.

3 Density Perturbations from Modulated Reheating

We analyze the case where density perturbations are generated through modulated reheating [3, 4] after conformal inflation. The scale dependence of the perturbations can be expressed by expansion in terms of the flatness parameters. Furthermore, we take account of the inflaton's slight deviation from a conformal coupling ($\xi - 1/6$). This procedure allows us to deal with a wide variety of situations, e.g., when there exists additional corrections to the action which ruins the exact conformal coupling, when the frame where the inflaton ϕ is conformally coupled to gravity differs from the frame where the light modulus χ is minimally coupled. In [1] the resulting spectral index and its running were shown to take the form,

$$\begin{aligned} n_s - 1 = \frac{d\ln H^2}{d\ln k} &= 2\frac{\dot{H}}{H^2}\left(1 + \frac{\dot{H}}{H^2}\right)^{-1} \\ &= -2\tilde{\epsilon} - \left(\frac{12}{c^2} + \kappa^2\right)\epsilon + \mathcal{O}(\epsilon^{3/2}, \epsilon\eta_c) + \left(\xi - \frac{1}{6}\right)\left\{2\kappa^2 + \mathcal{O}(\epsilon^{1/2})\right\} + \mathcal{O}\left(\left(\xi - \frac{1}{6}\right)^2\right), \end{aligned} \tag{7}$$

$$\begin{aligned} \frac{dn_s}{d\ln k} &= 2\left(1 + \frac{\dot{H}}{H^2}\right)^{-3}\frac{1}{H}\left(\frac{\dot{H}}{H^2}\right)^{\cdot} \\ &= 2\left(3 - c + \frac{3}{c}\eta_c\right)\tilde{\epsilon} + \left(\frac{6(8-3c)}{c^2} + (7-3c)\kappa^2\right)\epsilon + \mathcal{O}(\epsilon^{3/2}, \epsilon\eta_c) \\ &\quad + \left(\xi - \frac{1}{6}\right)\left\{-4\kappa^2 + \mathcal{O}(\epsilon^{1/2})\right\} + \mathcal{O}\left(\left(\xi - \frac{1}{6}\right)^2\right), \end{aligned} \tag{8}$$

[3]Our parameterization of c differs from that of [2] by $c_{\text{ours}} = c_{[2]} + 2$.

where the right hand sides should be estimated at the moment of horizon crossing $k = aH$. We immediately see that $|dn_s/d\ln k|$ can become large, comparable to $|n_s - 1|$. This is due to the fact that the derivatives of the flatness parameters do not necessarily become smaller than the parameters themselves. Since this is a generic feature of conformal inflation, a large running is expected even if we consider mechanisms other than modulated reheating for generating fluctuations (e.g. curvaton models). Also, our results indicate that $(\xi - 1/6)$-corrections can dominantly determine the values of the cosmological observables unless $|\xi - 1/6|$ is smaller than the flatness parameters.

4 Application to Warped Brane Inflation

Let us now apply the results obtained in the previous section to a specific model. Here we consider the warped brane inflation model [5], where the universe experiences inflation while a D3-brane moves towards the tip of a flux compactified warped throat. The D3-brane is pulled by a stack of $\overline{\text{D3}}$-branes sitting at the tip. If the position of the D3-brane is a conformally coupled scalar (for a discussion on this issue, see e.g. [7]), then this model serves as a realization of conformal inflation.

Considering a throat whose geometry is $AdS_5 \times X_5$, the potential of the inflaton takes the form

$$V(\phi) = 2ph_0^4 T_3 \left(1 - \frac{h_0^4 T_3^2 R^4}{N\phi^4}\right). \tag{9}$$

Here, the inflaton is related to the radial position ρ of the D3 through $\phi = \sqrt{T_3}\rho$, p is the number of $\overline{\text{D3}}$s at the tip, $h_0 = \rho_0/R$ is the warping at the tip, $T_3 = 1/(2\pi)^3 g_s(\alpha')^2$ is the D3 tension, $R^4 = 2^2\pi^4 g_s(\alpha')^2 N/\text{Vol}(X_5)$ is the AdS radius of the throat, $\text{Vol}(X_5)$ is the dimensionless volume of the base space X_5, and $N(>1)$ is the 5-form charge.

The conformally coupled inflaton satisfies $\dot{\phi} \approx -\phi H$ during inflation, hence the number of e-foldings generated is $\mathcal{N} \approx \log(\rho_i/\rho_f) \approx -\log(h_0/\lambda_i)$, where we have set the initial position of the D3 by a dimensionless constant λ_i as $\rho_i = \lambda_i R$, and assumed inflation to end when the D3 approaches the tip $\rho_f \approx \rho_0$. This shows that in order to obtain enough e-foldings, the throat should be strongly warped $h_0/\lambda_i \ll 1$.

The scale dependence of the perturbations can be computed by (7) and (8). We parametrize the position of the D3 when the CMB scale was originally produced by $\rho_{\text{CMB}} = \lambda R$. Furthermore, for simplicity, we ignore the compactified bulk to which the throat is glued, hence $M_p^2 \simeq \frac{2}{(2\pi)^7 g_s^2(\alpha')^4}\int_{\rho_0}^{R} d\rho\, \text{Vol}(X_5)\frac{\rho^5}{h^4} \simeq \frac{\text{Vol}(X_5)R^6}{(2\pi)^7 g_s^2(\alpha')^4}$. Then under the assumption $h_0/\lambda \ll 1$, the flatness parameters and κ can be calculated (note that $c = 7$)

$$\epsilon \simeq \frac{2h_0^8}{\lambda^{10}N}, \quad \tilde{\epsilon} \simeq \frac{2h_0^4}{\lambda^4 N}, \quad \eta_c = \eta \simeq -\frac{5h_0^4}{\lambda^6}, \quad \kappa^2 \simeq \frac{4\lambda^2}{N}. \tag{10}$$

Since ϵ is extremely small compared to the other flatness parameters, the cosmological observables can be estimated as follows:

$$n_s - 1 \simeq -\frac{4}{N}\left\{\frac{h_0^4}{\lambda^4} - 2\lambda^2\left(\xi - \frac{1}{6}\right)\right\}, \qquad \frac{dn_s}{d\ln k} \simeq -\frac{16}{N}\left\{\frac{h_0^4}{\lambda^4} + \lambda^2\left(\xi - \frac{1}{6}\right)\right\}. \tag{11}$$

The 5-year WMAP+BAO+SN data gives bounds $n_s = 1.022^{+0.043}_{-0.042}$ (68% CL) and $dn_s/d\ln k = -0.032^{+0.021}_{-0.020}$ (68% CL) when tensor mode perturbations are negligible [6]. Since the h_0^4/λ^4 terms are too small to be constrained by the observational bounds, we ignore them. Then the observables are determined only by the inflaton's deviation from an exact conformal coupling,

$$n_s - 1 \simeq 8\frac{\lambda^2}{N}\left(\xi - \frac{1}{6}\right), \qquad \frac{dn_s}{d\ln k} \simeq -16\frac{\lambda^2}{N}\left(\xi - \frac{1}{6}\right). \tag{12}$$

It is easy to see that the spectral index and its running are related by

$$\frac{dn_s}{d\ln k} \simeq -2(n_s - 1). \tag{13}$$

Using the observational bound on $dn_s/d\ln k$ to constrain $\lambda^2(\xi-1/6)/N$,

$$0.001 \lesssim \frac{\lambda^2}{N}\left(\xi - \frac{1}{6}\right) \lesssim 0.003. \tag{14}$$

If we further make use of this bound to constrain the spectral index, we obtain

$$0.006 \lesssim n_s - 1 \lesssim 0.026. \tag{15}$$

Thus the 1σ observational bound on the running allows us to predict a blue tilt for the warped brane inflation model. Moreover, the values of the observables were dominantly determined by the inflaton's deviation from a conformal coupling. The bound (14) suggests that this deviation can be fairly large, e.g., $(\xi-1/6) \sim 10^{-1}$ when $\lambda \sim 1$, $N \sim 10^2$.

5 Conclusion

We have investigated the scale dependence of the density perturbations that are generated through modulated reheating after conformal inflation. We have written down the spectral index and its running in terms of the flatness parameters and the inflaton's deviation from an exact conformal coupling. The general results we have obtained are that (i) modulated reheating together with conformal inflation can produce a nearly scale-invariant spectrum, (ii) the running of the spectral index $|dn_s/d\ln k|$ turns out to be as large as $|n_s - 1|$. The latter result reflects the nonexistence of hierarchy among higher-order time derivatives of the Hubble parameter $d^n \ln H^2/dt^n H^n$ during conformal inflation. This is in strong contrast to standard minimal models where higher-order derivatives are suppressed by higher orders of the slow-roll parameters (and their derivatives). Hence this feature offers a chance of obtaining a smoking-gun signal for non-minimally coupled inflation models.

We also applied our results to the warped brane inflation model, where it was shown that observables were dominantly determined by the deviation from the conformal coupling. We have shown that the spectral index and its running are related by (13) for this model. Since the running is highly constrained by the WMAP5 data, a stringent bound on the coupling of the inflaton to gravity was obtained. Also, comparison with the WMAP5 data suggested a blue tilt of the spectrum.

While our analysis focused on general aspects of modulated reheating after conformal inflation, we have not presented the light modulus responsible for generating fluctuations in a concrete setup. In the warped brane inflation case, potential candidates for such light fields are angular positions of the D3($\overline{\text{D3}}$)-branes sitting in throats with angular isometries, and/or axions associated with shift symmetries of the Kähler potential. For further study, it is important to come up with an explicit realization of our mechanism based on fundamental theories. We leave this for future work.

One of the general lessons of our work is that a non-minimal coupling with gravity can drastically change the behavior of inflation. Large values for higher-order time derivatives of the Hubble parameter is a special nature of conformal inflation. Cosmological observations are imposing (not necessarily direct but) important constraints on such features even at the present stage.

References

[1] T. Kobayashi and S. Mukohyama, arXiv:0810.0810 [hep-th].

[2] L. Kofman and S. Mukohyama, Phys. Rev. D **77**, 043519 (2008) [arXiv:0709.1952 [hep-th]].

[3] G. Dvali, A. Gruzinov and M. Zaldarriaga, Phys. Rev. D **69**, 023505 (2004) [arXiv:astro-ph/0303591].

[4] L. Kofman, arXiv:astro-ph/0303614.

[5] S. Kachru, R. Kallosh, A. Linde, J. M. Maldacena, L. P. McAllister and S. P. Trivedi, JCAP **0310**, 013 (2003) [arXiv:hep-th/0308055].

[6] E. Komatsu *et al.* [WMAP Collaboration], arXiv:0803.0547 [astro-ph].

[7] N. Seiberg and E. Witten, JHEP **9904**, 017 (1999) [arXiv:hep-th/9903224].

Relativistic stars in $f(R)$ gravity, and absence thereof

Tsutomu Kobayashi[1] and Kei-ichi Maeda[2]

[1,2] *Department of Physics, Waseda University, Okubo 3-4-1, Shinjuku, Tokyo 169-8555, Japan*
[2] *Advanced Research Institute for Science and Engineering, Waseda University, Okubo 3-4-1, Shinjuku, Tokyo 169-8555, Japan*

Abstract

Several $f(R)$ modified gravity models have been proposed which realize the correct cosmological evolution and satisfy solar system and laboratory tests. Although non-relativistic stellar configurations can be constructed, we argue that relativistic stars cannot be present in such $f(R)$ theories. This problem appears due to the dynamics of the effective scalar degree of freedom in the strong gravity regime. Our claim thus raises doubts on the viability of $f(R)$ models.

1 Introduction

The accelerating expansion of the present universe is one of the deepest mysteries in cosmology. This acceleration may be due to some unknown energy-momentum component having the equation of state $p/\rho \approx -1$, or may be due to a modification of general relativity. We are interested in the latter possibility.

Any modified theories of gravity must account for the late time cosmology which is well established by observations, and at the same time must be consistent with solar system and laboratory tests of gravity. However, since $f(R)$ gravity has the equivalent description in terms of the Brans-Dicke theory with the Brans-Dicke parameter $\omega = 0$, naively constructed models would result in violation of the above requirements. The most successful class of $f(R)$ models [1, 2, 3] incorporates the Chameleon mechanism to evade local gravity tests.

In this paper, we consider the strong gravity regime of the carefully constructed models of [1, 2, 3]. Recently, Frolov suggested that such $f(R)$ models generically suffer from the problem of curvature singularities which can be easily accessed by the field dynamics *in the presence of matter* [4]. In other words, a curvature singularity may be caused not by diverging gravitational potential depth, $|\Phi| = \infty$, but rather by a slightly large gravitational field, $|\Phi| \lesssim 1/2$. This motivate us to study relativistic stars in the context of $f(R)$ gravity. We shall show that stellar solutions with relatively strong gravitational fields cannot be constructed [5, 6].

2 $f(R)$ gravity as a scalar-tensor theory

2.1 Field equations

The action we consider has the form of

$$S = \int d^4x\sqrt{-g}\left[\frac{f(R)}{16\pi G} + \mathcal{L}_{\rm m}\right], \tag{1}$$

where $f(R)$ is a function of the Ricci scalar R, and $\mathcal{L}_{\rm m}$ is the Lagrangian of matter fields. Variation with respect to metric leads to the field equations

$$f_R R_{\mu\nu} - \nabla_\mu\nabla_\nu f_R + \left(\nabla^2 f_R - \frac{1}{2}f\right)g_{\mu\nu} = 8\pi G T_{\mu\nu}, \tag{2}$$

[1] E-mail:tsutomu@gravity.phys.waseda.ac.jp
[2] E-mail:maeda@waseda.jp

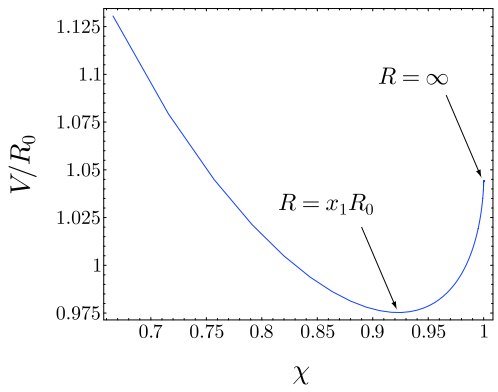

Figure 1: The potential $V(\chi)$ for $n = 1$ and $x_1 = 3.6$.

where $f_R := df/dR$ and $T_{\mu\nu} := -2\delta\mathcal{L}_{\rm m}/\delta g^{\mu\nu} + g_{\mu\nu}\mathcal{L}_{\rm m}$. The trace of Eq. (2) reduces to

$$\nabla^2 f_R = \frac{8\pi G}{3}T + \frac{1}{3}(2f - f_R R). \tag{3}$$

We now introduce an effective scalar degree of freedom, which sometimes is dubbed "scalaron," by defining $\chi := f_R$. Inverting this relation, the Ricci scalar can be expressed in terms of χ: $R = Q(\chi)$. In this way Eqs. (2) and (3) are equivalently rewritten as

$$\chi G_\mu{}^\nu = 8\pi G T_\mu{}^\nu + \left(\nabla_\mu\nabla^\nu - \delta_\mu{}^\nu\nabla^2\right)\chi - \chi^2 V(\chi)\delta_\mu{}^\nu, \tag{4}$$

$$\nabla^2\chi = \frac{8\pi G}{3}T + \frac{2\chi^3}{3}\frac{dV}{d\chi}, \tag{5}$$

where the potential V is given by

$$V(\chi) := \frac{1}{2\chi^2}\left[\chi Q(\chi) - f(Q(\chi))\right], \tag{6}$$

and $dV/d\chi = \left[2f(Q(\chi)) - \chi Q(\chi)\right]/(2\chi^3)$.

In order to be explicit, we take $f(R)$ in the following form [1]:

$$f(R) = R + \lambda R_0\left[\left(1 + \frac{R^2}{R_0^2}\right)^{-n} - 1\right], \tag{7}$$

where $n, \lambda\,(> 0)$, and $R_0\,(> 0)$ are parameters. This model is carefully constructed so that it gives viable cosmology and satisfies solar system and laboratory tests. Suppose that the de Sitter solution in this theory is expressed as $R = R_1 = \text{constant} = x_1 R_0$. We may define the "cosmological constant" as $\Lambda_{\rm eff} := R_1/4$.

The scalar field χ is written in terms of R as

$$\chi = 1 - 2n\lambda\frac{R}{R_0}\left(1 + \frac{R^2}{R_0^2}\right)^{-n-1}. \tag{8}$$

One sees that $\chi \to 1$ as $R \to \pm\infty$ and $R \to 0$. Note that curvature singularities, $R = \pm\infty$, is mapped to the finite value of $\chi = 1$. The value of χ at the de Sitter minimum is given by $\chi = \chi_1(x_1) < 1$. An example of the potential $V(\chi)$ around the de Sitter minimum is shown in Fig. 1.

2.2 Classical mechanical analogy

We are going to investigate static, spherically symmetric stellar solutions with constant densities (i.e., a generalization of the Schwarzschild interior solution) in the above system. We shall work along the lines of our papers [5, 6]. The basic equations are found there.

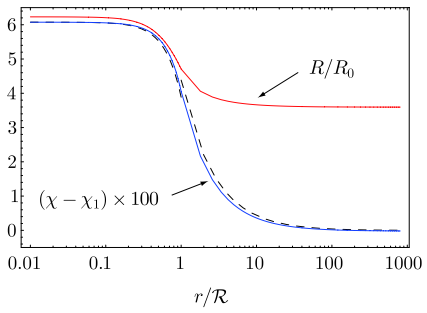

Figure 2: Numerical solutions of the Ricci scalar and χ for a nonrelativistic star. Dashed line is a plot of the analytic approximation.

To study the radial profile of χ through Eq. (5), it is useful to note that the equation can be written as

$$\frac{d^2\chi}{dr^2}+\frac{2}{r}\frac{d\chi}{dr}=-\frac{dU}{d\chi}+\mathcal{F}, \tag{9}$$

where

$$\frac{dU}{d\chi}=-\frac{2\chi^3}{3}\frac{dV}{d\chi} \tag{10}$$

and $\mathcal{F}=(8\pi G/3)T$. Here we have ignored the effect of the metric for simplicity. (Later we will solve the full set of the field equations numerically.) Now, by identifying r as a time coordinate, Eq. (9) can be regarded as the equation of motion in classical mechanics. One can understand the radial profile of χ intuitively as the motion of a particle in the potential U under the time-dependent force $\mathcal{F}$ (and the frictional force corresponding to the second term in the left hand side). The mechanical analogy is particularly useful to comprehend the essential point of the nonexistence statement for relativistic stars in $f(R)$ gravity [5, 6].

Given a density ρ_0 and the central values of the pressure p_c and the scalar field χ_c (or, equivalently, the central curvature R_c), we can integrate relevant equations numerically from the regular center $r=0$ to the surface of the star, $r=\mathcal{R}$, defined by $p(\mathcal{R})=0$. (The boundary condition at the center is also given in Refs. [5, 6].) Then, imposing the continuity of the metric functions, the scalar field χ, and its derivative $d\chi/dr$ at the stellar surface, we integrate the vacuum field equations to find the exterior geometry. We are looking for a solution such that it is asymptotic to de Sitter with $\Lambda_{\rm eff}=R_1/4$ (and hence $\chi\to\chi_1$). For fixed ρ_0 and p_c, we can find the desired solution (if it exists) by carefully tuning the initial value $\chi_c=\chi_{\rm crit}$. In the mechanical analogy, this solution corresponds to the situation where the particle starts at rest and reaches the top of the potential ($\chi=\chi_1$) in the limit of $r\to\infty$. The particle overshoots the top of the potential for $\chi_c<\chi_{\rm crit}$, while it turns around before it reaches the top and falls into the singularity for $\chi_c>\chi_{\rm crit}$. One can show that $\chi_{\rm crit}$ becomes larger as the gravitational potential of the star increases, getting eventually at χ_s, above which the slope of the potential $dU/d\chi$ is greater than the force term and so the particle cannot climb up the potential. Thus, if the gravitational potential is larger than a certain value, the desired solution described above does not exist, and we only have two types of singular solutions, i.e., a "falling-down" type and a "overshooting" one.

3 Numerical results

The model parameters we use are: $n=1$ and $x_1=3.6$ ($\lambda=2.088$), for which $\chi_1=0.9228$. For numerical solutions we shall take $4\pi G\rho_0=10^6\Lambda_{\rm eff}$. This is not a realistic value, e.g., for neutron stars, but we do not have to concern about this point because the properties of stellar solutions which we are interested in are basically characterized by the gravitational potential rather than the energy density itself, provided

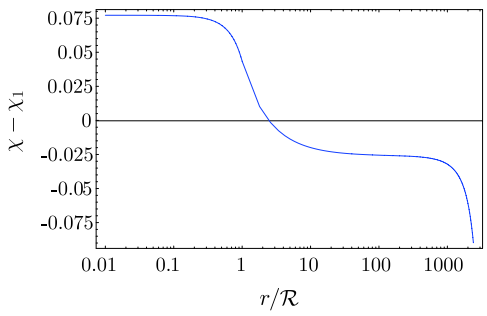

Figure 3: A rolling-down solution for a would-be relativistic star.

that $G\rho_0 \gg \Lambda_{\rm eff}$. This is expected from the analytic result, and we have confirmed that it is indeed true for our numerical solutions.

Taking $4\pi G\rho_0 = 10^6\Lambda_{\rm eff}$ and $p_c = 10^{-4}\rho_0$, we found an asymptotically de Sitter solution of a star for $R_c = 2.001 \times 10^{-6} \times 8\pi G\rho_0$, and confirmed that the solution agrees well with the analytic approximation.

A numerical calculation was performed also in the case of $4\pi G\rho_0 = 10^6\Lambda_{\rm eff}$ and $p_c = 5 \times 10^{-2}\rho_0$. We have found a solution by tuning $R_c = 3.462 \times 10^{-6} \times 8\pi G\rho_0$ ($\chi_c = 0.9836$), for which $\hat{G}M/\mathcal{R} \simeq 0.06687$. Our numerical result is shown in Figs. 2 and 3. One can see from Fig. 2 that $R \to x_1 R_0$ and $\chi \to \chi_1$ as $r \to \infty$.

To explore stars with larger $\hat{G}M/\mathcal{R}$, we tried to find numerical solutions for $4\pi G\rho_0 = 10^6\Lambda_{\rm eff}$ and $p_c = 0.1 \times \rho_0$. A solution which is regular inside the star is obtained, e.g., for $R_c = 0.7000 \times 8\pi G\rho_0$, but this is the rolling-down solution (see Fig. 3) and hence is unphysical ($N(r) \to 0$ and $B(r) \to \infty$ as $r \to \infty$). In this case, the gravitational potential is as "large" as $\hat{G}M/\mathcal{R} \simeq 0.1203$. Taking a slightly larger value of the central curvature, $R_c = 0.7001 \times 8\pi G\rho_0$, the Ricci scalar rapidly diverges inside the star. This corresponds to the case in which χ starts to move to the right toward the curvature singularity, $\chi = 1$.

4 Conclusions

In this paper, we have studied the strong gravity aspect of $f(R)$ modified gravity models that reproduce the conventional cosmological evolution and evade solar system and laboratory tests [1, 2, 3]. We have explored uniform density, spherically symmetric stars and their exterior geometry in the $f(R)$ model of [1]. The main result of the present paper is summarized as follows: given model parameters, there is a maximum value of the gravitational potential produced by a star, above which no asymptotically de Sitter stellar configurations can be constructed. We show this both analytically and numerically. For example, the model with $n = 1$ and $\lambda \approx 2$ gives $\Phi_{\rm max} \approx 0.1$. This raises a warning sign for a class of $f(R)$ theories, because neutron stars cannot be present in such gravity models.

References

[1] A. A. Starobinsky, JETP Lett. **86**, 157 (2007) [arXiv:0706.2041 [astro-ph]].

[2] W. Hu and I. Sawicki, Phys. Rev. D **76**, 064004 (2007) [arXiv:0705.1158 [astro-ph]].

[3] S. A. Appleby and R. A. Battye, Phys. Lett. B **654**, 7 (2007) [arXiv:0705.3199 [astro-ph]].

[4] A. V. Frolov, Phys. Rev. Lett. **101**, 061103 (2008) [arXiv:0803.2500 [astro-ph]].

[5] T. Kobayashi and K. i. Maeda, Phys. Rev. D **78**, 064019 (2008) [arXiv:0807.2503 [astro-ph]].

[6] T. Kobayashi and K. i. Maeda, Phys. Rev. D **79**, 024009 (2009) [arXiv:0810.5664 [astro-ph]].

Repulsons in the 5D Myers-Perry Family

Hideo Kodama[1]

IPNS, KEK and the Graduate University of Advanced Studies,
1-1 Oho, Tsukuba 305-0801, Japan

Abstract

In this talk, we point out that curvature-regular asymptotically flat solitons with negative mass are contained in the Myers-Perry family in five dimensions. These solitons do not have horizon, but instead a conical NUT singularity of quasi-regular nature surrounded by naked CTCs. We show that this quasi-regular singularity can be made regular for a set of discrete values of angular momentum by introducing some periodic identifications, at least in the case in which two angular momentum parameters are equal. Although the spatial infinity of the solitons is diffeomorphic to $S^1 \times S^3/\mathbb{Z}_n$ ($n \geq 3$), the corresponding spacetime is simply connected and asymptotically flat.

1 Introduction

In four dimensions, there are some asymptotically flat regular black hole solutions with CTCs inside horizon. However, no asymptotically flat regular simply-connected vacuum solution with naked CTCs has been found so far. For example, the Kerr and the Kerr-Newman solutions have CTCs, but they become naked only in the superextreme case with naked ring singularity. Similarly, the Tomimatsu-Sato solution with $\delta = 2$[1] has double horizons and circles generated by the rotational Killing vector become time-like near the z-axis segment connecting two horizons, but the spacetime has the well-know naked ring singularity and a conical singularity along the segment[2](see Fig. 1). Here, the asymptotically flatness is a crucial condition, because we have the Taub-NUT solution and the Gödel solution as famous examples of curvature-regular vacuum solutions that have CTCs but are not asymptotically flat.

In higher dimensions, the situation changes. For example, the BMPV solution[3, 4] in a five-dimensional gauged supergravity theory represents a rotating charged BPS black hole for slow rotations, while when its angular velocity exceeds some critical value, the horizon turns to a surface called a repulson which is surrounded by CTCs and cannot be penetrated[5]. Similar BPS solutions were found in other supergravity theories in five dimensions[6, 7].

These BPS solutions show that the existence of CTCs and regularity and asymptotically flatness can coexist in higher dimensions. The main purpose of this talk is to point out that another set of examples of such spacetimes are contained in the five dimensional Myers-Perry solution[8]. They are asymptotically flat regular spacetimes with negative mass and naked CTCs.

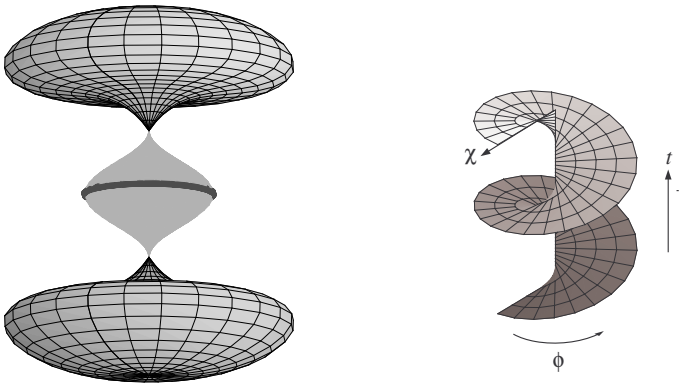

Figure 1: TS2 solution. The left panel show the two horizons connected by a region where the angular Killing vector becomes time-like and the ring singularity on its boundary. The right panel show the helical structure of the time coordinate on the z-axis connecting the two horizons[2].

[1]E-mail: Hideo.Kodama@kek.jp

2 Internal Structure of the 5D Myers-Perry Solution

2.1 Metric and regularity

In terms of the Boyer-Lindquist coordinates $(t, \phi_1, \phi_2, r, \theta)$, the 5D Myers-Perry solution can be written as[8]

$$\begin{aligned} ds^2 &= \frac{r^2\rho^2}{\Delta}dr^2 + \rho^2 d\theta^2 + (r^2+a^2)\sin^2\theta d{\phi_1}^2 + (r^2+b^2)\cos^2\theta d{\phi_2}^2 \\ &\quad -dt^2 + \frac{}{\rho^2}\left[dt + a\sin^2\theta d\phi_1 + b\cos^2\theta d\phi_2\right]^2, \end{aligned} \tag{1}$$

where $\Delta := (r^2+a^2)(r^2+b^2) - \ r^2$.

Because the determinant of the metric is given by $-g = r^2\rho^4\sin^2\theta\cos^2\theta$, apart from the angular coordinate singularities at $\theta = 0, \pi/2$, the metric (1) is apparently singular at $r = 0$ and at $\Delta = 0$ in addition to $\rho = 0$, which is curvature singularity from the expression for the Kretchman invariant,

$$R\ \ {}_{\lambda\sigma}R\ \ {}^{\lambda\sigma} = 24\ \ {}^2\frac{(3r^2 - a^2\cos^2\theta - b^2\sin^2\theta)(r^2 - 3a^2\cos^2\theta - 3b^2\sin^2\theta)}{\rho^{12}}. \tag{2}$$

Among these apparent singularities, we can confirm that the points with $r = 0$ are not real singularity by expressing the metric in terms of $x = r^2$ as[8]

$$\begin{aligned} ds^2 &= \frac{\rho^2}{4\Delta}dx^2 + \rho^2 d\theta^2 + (x+a^2)\sin^2\theta d{\phi_1}^2 + (x+b^2)\cos^2\theta d{\phi_2}^2 \\ &\quad -dt^2 + \frac{}{\rho^2}\left[dt + a\sin^2\theta d\phi_1 + b\cos^2\theta d\phi_2\right]^2. \end{aligned} \tag{3}$$

Now, Δ and ρ^2 become polynomials in x as

$$\Delta = (x+a^2)(x+b^2) - \ x, \quad \rho^2 = x + a^2\cos^2\theta + b^2\sin^2\theta, \tag{4}$$

and $-g$ is expressed as $-g = \rho^4\sin^2\theta\cos^2\theta/4$.

2.2 Structure of Killing orbits

On a Killing horizon, the induced metric on the orbit space of the Killing vectors $\partial_t, \partial_{\ 1}$ and $\partial_{\ 2}$ becomes degenerate. From $|g_{ab}|_{a,b=t,\ 2,\ 1} = -\Delta\sin^2\theta\cos^2\theta$, this condition can be written $\Delta = 0$. When $ab \neq 0$ and $\ > 0$, this equation for x has a root in the region $\rho^2 > 0$ iff $\ > (|a| + |b|)^2$. In this case, there actually exist two positive roots, which are both regular horizons.

In contrast, when $\ < 0$, we have only negative roots, but one of them, $x = x_h$, is larger than $-b^2$ and in the region with $\rho^2 > 0$. This apparently indicates that even in the negative mass case, the spacetime has a regular horizon and a regular domain of outer communication. However, this is not the case. In fact, the spacetime has pathological features around $x = x_h$, when $x_h \neq 0$. For example, the Killing vector k whose norm vanishes at $x = x_h$ becomes spacelike outside the horizon. Further, the norm of the Killing vector ∂_t is negative definite for $x \quad x_h$.

2.3 CTCs

Let Φ be the symmetric matrix of degree 2 defined by $\Phi := (g_{ij})_{i,j=\ 1.\ 2}$. Then, we can show that $\det\Phi = D_1\sin^2\theta\cos^2\theta/\rho^2$ is non-negative in $x > 0$ for $\ > 0$, and therefore that there occurs no causality violation at or outside the outer horizon for $\ > (|a| + |b|)^2$.

In contrast, for $\ < 0$, causality violation occurs in the region $x \quad x_h$. In fact, D_1 can be written as

$$D_1 = \Delta(x + a^2\sin^2\theta + b^2\cos^2\theta + \ ) + \ \ {}^2x. \tag{5}$$

From this, around $x = x_h$ at which $\Delta = 0$, the sign of D_1 is determined by the sign of x_h. Hence, when $x_h < 0$, 2-tori generated by $\partial_{\ 1}$ and $\partial_{\ 2}$ become timelike surfaces around $x = x_h$, which always contain

CTCs. As we show in the next section, this feature together with the fact that g_{tt} is netative and Φ has a finite non-degenerate limit at $x = x_h$ implies that $x = x_h$ is not a horizon but rather something like a repulson, which was first found by Gibbons and Herdeiro for supersymmetric rotating black holes in five dimensions[5, 6].

3 Repulson

3.1 U(2) MP solution

In the case $a = b \neq 0$, the metric in the Boyer-Lindquist coordinates reads

$$ds^2 = \frac{ydy^2}{4(y^2 - \quad y + a^2 \quad)} + yds^2(S^3) - dt^2 + \frac{}{y}\left(dt + a\chi^3\right)^2, \tag{6}$$

where $y = \rho^2 = x + a^2$, and χ^3 is the 1-form on S^3 invariant under the action of SU(2)

$$\chi^3 = \sin^2\theta d\phi_1 + \cos^2\theta d\phi_2. \tag{7}$$

3.2 Negative mass soliton

Now, we show that the surface corresponding to the root $x = x_h(> -a^2)$ of $\Delta = 0$ for $\quad < 0$, which is intrinsically S^2, is not a regular submanifold of the spacetime, but rather a quasi-regular singularity. For that purpose, let us introduce the coordinate

$$\xi = \left(\frac{a^2 - y_h}{2a^2 - y_h}(y - y_h)\right)^{1/2}, \tag{8}$$

where $y_h = x_h + a^2 > 0$. Then, in terms of the 1-forms

$$\tilde{\tau} = -\frac{a}{y_h}dt + \chi_3, \quad \tilde{\chi} = \chi_3 + \frac{y_h}{2a^2 - y_h}\tilde{\tau}, \tag{9}$$

the metric can be written near the locus $y = y_h$ as

$$ds^2 \simeq -\frac{y_h^2}{(a^2 - y_h)}\tilde{\tau}^2 + d\xi^2 + c^2\xi^2\tilde{\chi}_3^2 + y_h ds^2(S^2), \tag{10}$$

where

$$c = \frac{2a}{(a^2 - y_h)^{1/2}}\left(1 - \frac{y_h}{2a^2}\right). \tag{11}$$

The curvature tensor of this metric is bounded everywhere. However, it has a kind of conical singularity at $\xi = 0$ because $c > 2$ and t is not a periodic coordinate. This conical singularity cannot be removed even by a periodic identification of t in general. For some discrete values of y_h, however, the spacetime can be made regular by such an identification. To see this, we utilise the local charts, (z_+, w_+, t_+) for $\theta \neq \pi/2$ and (z_-, w_-, t_-) for $\theta \neq 0$ defined by

$$z \quad := (\tan\theta) \quad {}^1e \quad {}^i, \quad w \quad := \xi e^{ic(\psi \quad)/2}, \quad t \quad := t - \frac{y_h}{4a}(\psi \pm \phi). \tag{12}$$

It is easy to see that in each of these coordinate system, the metric (10) has regular expressions.

In the region $0 < \theta < \pi/2$ covered by both charts, the two set of coordinates are related by

$$z_- = \frac{1}{z_+}, \quad w_- = w_+\left(\frac{z_+}{|z_+|}\right)^{-c}, \quad t_- = t_+ + i\frac{y_h}{a}\ln\frac{z_+}{|z_+|}. \tag{13}$$

From the relation for w , we find that c must be an integer $n > 2$ for the coordinate transformation to be well-defined. Further, because the ln-term in the relation for t produces ambiguity in the values of

t written as an integer multiple of $2\pi y_h/a$, these two charts are consistent only when we identify t periodically with a period $2\pi y_h/(ma)$ where m is some positive integer.

For $\xi \neq 0$, by this identification, each $\xi =$ const surface becomes a S^1 bundle over $S^3/\mathbb{Z}_n$. However, since we can easily show that the regular manifold constructed above from the region around $\xi = 0$ is simply connected for $m = 1$, the whole spacetime is also simply connected for $m = 1$. In that case, CTCs along S^1 produced by the above identification at $\xi \neq 0$ cannot be removed by taking a covering space.

4 Summary and Discussion

In the present paper, we have shown that the five-dimensional Myers-Perry solution with negative mass describes an asymptotically flat rotating spacetime with naked CTCs, no horizon and no curvature singularity. We further pointed out that we can construct a regular repulson-type asymptotically flat soliton from them for a discrete set of values of the angular momentum for a fixed mass parameter .

Although the structure of the original metric when the repulson appears is similar to that of BPS solutions with repulsons, there exist several big differences between our family and the BPS families. In particular, our solutions are non-BPS solution to the purely vacuum Einstein equations, and the repulson is a regular submanifold of the whole spacetime. This should be contrasted to the BPS case in which the repulson is at spatially infinite distance. Further, the soliton spacetime obtained after regularisation is not asymptotically flat in the standard sense because it has some time periodicity at spatial infinity and its spatial infinity is $S^3/\mathbb{Z}_n$ with n 3, although it is topologically simply connected. Finally, the repulson appears only for negative mass. This is rather striking because a regular soliton spacetime with negative mass can exist in higher dimensions.

Finally, we note that our analysis can be extended to the U(N) symmetry Myers-Perry solutions in $2N+1$ dimensions[9]. It can be also extended to the rotating black-hole type solutions with cosmological constant[10] and to the black holes with generic angular momentum parameters. These extensions are under investigation.

Acknowledgement

This talk is based on the work in collaboration with G.W. Gibbons. The author would like to thank Hideki Maeda, Akihiro Ishibashi, Shinya Tomizawa and Andres Anabalon for discussions and useful comments. This work was supported in part by Grants-in-Aids for Scientific Research from JSPS (No. 18540265) and for the Japan-U.K. Research Cooperative Program.

References

[1] Tomimatsu, A. and Sato, H.: *Phys. Rev. Lett.* **29**, 1344 (1972).

[2] Kodama, H. and Hikida, W.: *Class. Quant. Grav.* **20**, 5121–40 (2003).

[3] Breckenridge, J., Myers, R., Peet, A. and Vafa, C.: *Phys. Lett. B* **391**, 93–98 (1997).

[4] Kallosh, R., Rajaraman, A. and Wong, W.: *Phys. Rev. D* **55**, R3246–9 (1997).

[5] Gibbons, G. and Herdeiro, C.: *Class. Quantum Grav.* **16**, 3619–52 (1999).

[6] Cvetic, M., Gibbons, G., Lü, H. and Pope, C.: *hep-th0504080* (2005).

[7] Gauntlett, J., Gutowski, J., Hull, C., Pakis, S. and Reall, H.: *Class. Quant. Grav.* **20**, 4587–4634 (2003).

[8] Myers, R. and Perry, M.: *Ann. Phys.* **172**, 304–347 (1986).

[9] Gibbons, G. and Kodama, H.: *arXiv:0910.1203* (2009).

[10] Gibbons, G. W., Lü, H., Page, D. N. and Pope, C. N.: *J. Geom. Phys.* **53**, 49–73 (2005).

Vacuum Bubble Nucleation and Black Hole Pair Creation

Bum-Hoon Lee[1] and Wonwoo Lee[2]

[1] *Department of Physics and Center for Quantum Spacetime, Sogang University, Seoul 121-742, Korea*
[2] *Center for Quantum Spacetime, Sogang University, Seoul 121-742, Korea*

Abstract

We study the nucleation of a vacuum bubble in the presence of gravity and consider the pair production of blak holes in the background of bubble solutions. This article is prepared for the proceedings of The 18th Workshop on General Relativity and Gravitation in Japan (JGRG18) in Hiroshima, Japan, 17-21 Nov 2008.

1 Introduction

Recently, we have investigated the possible types of the nucleation of vacuum bubbles [1]. We classified true vacuum bubbles in de Sitter background and present some numerical solutions. The nucleation rate and the radius of true and false vacuum bubbles are analytically computed using the thin-wall approximation. We obtained static bubble wall solutions of junction equation with black hole pair. In this article, we will summarize our results.

It has been shown that the first-order vacuum phase transitions occur via the nucleation of true vacuum bubble at zero temperature both in the absence of gravity [2] and in the presence of gravity [3]. This result was extended by Parke [4] to the case of arbitrary vacuum energy densities. An extension of this theory to the case of non-zero temperatures has been found by Linde [5] in the absence of gravity, where one should look for the $O(3)$-symmetric solution due to periodicity in the time direction β with period T^{-1} unlike the $O(4)$-symmetric solution in the zero temperature. These processes as cosmological applications of false vacuum decay have been applied to various inflationary universe scenarios by many authors [6]. The Hawking-Moss transition describes the scalar field jumping simultaneously at the top of the potential barrier [7]. A new method to calculate the tunneling wave function that describes vacuum decay was studied by Gen and Sasaki [8]. The effect of the Gauss-Bonnet term on vacuum decay was also studied [9]. Marvel and Wesley studied thin-wall instanton with negative tension wall and its relation to Witten's bubble of nothing [10]. In Ref. [11], the authors discussed the possible four different instantons in Euclidean de Sitter space.

As for the false vacuum bubble formation, Lee and Weinberg [12] have shown that if the vacuum energies are greater than zero, gravitational effects make it possible for bubbles of a higher-energy false vacuum to nucleate and expand within the true vacuum bubble in the de Sitter space which has a topology of 4-sphere. The false vacuum bubble nucleation is described as the inverse process of the true vacuum bubble nucleation. However, their solution is larger than the true vacuum horizon [13]. The oscillating bounce solutions, another type of Euclidean solutions, have been studied in detail by Hackworth and Weinberg [14]. On the other hand Kim *et al.* [15] have shown that false vacuum region may nucleate within the true vacuum bubble as global monopole bubble in the high temperature limit.

Next, we will consider black hole pair creation. Caldwell *et al.* studied black hole pair creation in the presence of a domain wall [16] using the cut-and-paste procedure, where the background has vanishing cosmological constant and the probability was obtained. The repulsive property of the domain wall give rise to black hole pair creation. However, our solutions give rise to the background for the black hole pair creation with a bubble wall more naturally.

[1] E-mail:bhl@sogang.ac.kr
[2] E-mail:warrior@sogang.ac.kr

2 The vacuum bubble

The bubble nucleation rate or the decay rate of background vacuum is semiclassically given by

$$\Gamma/V = Ae^{-B/\hbar}, \tag{1}$$

where B is the difference between Euclidean action corresponding to bubble solution and that of the background and the prefactor A is discussed in Ref. [17], that with some gravitational corrections in Ref. [18]. We are interested in finding the coefficient B.

Let us consider the action

$$S = \int_{\mathcal{M}} \sqrt{-g} d^4x \left[\frac{R}{2\kappa} - \frac{1}{2}\nabla^\alpha\Phi\nabla_\alpha\Phi - U(\Phi)\right] + \oint_{\partial\mathcal{M}} \sqrt{-h} d^3x \frac{K}{\kappa}, \tag{2}$$

where $\kappa \equiv 8\pi G$, $g \equiv detg_{\mu\nu}$, and the second term on the right-hand side is the boundary term. $U(\Phi)$ is the scalar field potential with two non-degenerate minima with lower minima at Φ_T and higher minima at Φ_F, R denotes the Ricci curvature of spacetime $\mathcal{M}$, and K is the trace of the extrinsic curvature of the boundary $\partial\mathcal{M}$.

We will take $O(4)$ symmetry for both Φ and the spacetime metric $g_{\mu\nu}$, expecting its dominant contribution [19].

The Euclidean field equations for Φ and ρ have the form

$$\Phi'' + \frac{3\rho'}{\rho}\Phi' = \frac{dU}{d\Phi}, \tag{3}$$

$$\rho'' = -\frac{\kappa}{3}\rho(\Phi'^2 + U), \tag{4}$$

respectively and the Hamiltonian constraint is given by

$$\rho'^2 - 1 - \frac{\kappa\rho^2}{3}\left(\frac{1}{2}\Phi'^2 - U\right) = 0. \tag{5}$$

We will consider only the case with initial de Sitter space. The boundary conditions for the bounce are

$$\left.\frac{d\Phi}{d\eta}\right|_{\eta=0} = 0, \quad \left.\frac{d\Phi}{d\eta}\right|_{\eta=\eta_{max}} = 0, \quad \rho_{\eta=0} = 0, \quad \text{and } \rho_{\eta=\eta_{max}} = 0, \tag{6}$$

where η_{max} is a finite value in Euclidean de Sitter space.

In this article, we consider only several cases including true, false, and degenerate vacua. Firstly, we consider the large true anti-de Sitter bubble with small false de Sitter background. The size of the bubble and the nucleation rate are evaluated to be

$$\bar{\rho}^2 = \frac{\bar{\rho}_o^2}{D} \quad \text{and} \quad B = \frac{2B_o(\frac{\lambda_2}{\lambda_1})^2[\{1 + (\frac{\lambda_1}{\lambda_2})^2(\frac{\bar{\rho}_o}{2\lambda_2})^2\} - (\frac{\lambda_1}{\lambda_2})^2 D^{1/2} + E]}{[(\frac{\bar{\rho}_o}{2\lambda_2})^4\{(\frac{\lambda_2}{\lambda_1})^4 - 1\}D^{1/2}]}, \tag{7}$$

where $D = \left[1 + 2(\frac{\bar{\rho}_o}{2\lambda_1})^2 + (\frac{\bar{\rho}_o}{2\lambda_2})^4\right]$, $\lambda_1^2 = [3/\kappa(U_F + U_T)]$, $\lambda_2^2 = [3/\kappa(U_F - U_T)]$, $U_T < 0$, and $E = 2\{(\frac{\lambda_2}{\lambda_1})^4 - 1\}(\frac{\bar{\rho}_o}{2\lambda_1})^2[1 - (\frac{\bar{\rho}_o}{2\lambda_2})^2]D^{-1}$.

Secondly, we consider the large false de Sitter bubble with the small true de Sitter background. The size of the bubble has the same as above case. The nucleation rate is given by

$$B = \frac{2B_o[\{1 + (\frac{\bar{\rho}_o}{2\lambda_1})^2\} + \{1 + 2(\frac{\bar{\rho}_o}{2\lambda_1})^2 + (\frac{\bar{\rho}_o}{2\lambda_2})^4\}^{1/2}]}{[(\frac{\bar{\rho}_o}{2\lambda_2})^4\{(\frac{\lambda_2}{\lambda_1})^4 - 1\}\{1 + 2(\frac{\bar{\rho}_o}{2\lambda_1})^2 + (\frac{\bar{\rho}_o}{2\lambda_2})^4\}^{1/2}]}. \tag{8}$$

Thirdly, we consider the transition between degenerate vacua in de Sitter space. The critical radius of the wall is given by

$$\bar{\rho} = \frac{2}{\kappa\sqrt{\frac{S_o^2}{4} + \frac{4}{3\kappa}U_o}}. \tag{9}$$

The nucleation rate is given by

$$B = \frac{12\pi^2 S_o}{\kappa^2 U_o\sqrt{\frac{S_o^2}{4} + \frac{4}{3\kappa}U_o}}. \tag{10}$$

3 Black hole pair creation

We consider several types of the configuration as the background space for black hole pair creation. In this work the general Euclidean junction condition becomes

$$\sqrt{1-\frac{2GM}{r}\pm\frac{\Lambda_-}{3}r^2-\dot{r}^2}+\sqrt{1-\frac{2GM}{r}-\frac{\Lambda_+}{3}r^2-\dot{r}^2}=4\pi G\sigma r, \tag{11}$$

where $S_o=\sigma$ and $\cdot$ denotes the differentiation with respect to the proper time measured by the observer moving along with the wall. The signs $(-)$ and $(+)$ as a subscript of Λ represent left and right spacetime, respectively. After squaring twice, we define the effective potential for Euclidean junction equation to be

$$V_{eff}=\frac{1}{2}-\frac{1}{2}\left[\left(2\pi G\sigma+\frac{(\Lambda_+-\Lambda_-)}{24\pi G\sigma}\right)^2+\frac{\Lambda_-}{3}\right]r^2-\frac{GM}{r}, \tag{12}$$

with total energy is 0. The static bubble wall solution satisfies the following conditions

$$V_{eff}(r_b)=0,\quad \text{and}\quad \frac{dV_{eff}}{dr}\Big|_{r_b}=0. \tag{13}$$

The solution can exist at $r_b=3GM$. The masses of created black holes are uniquely determined by the given cosmological constant and surface tension on the wall:

$$M=\frac{1}{3G\sqrt{3\left[\left(2\pi G\sigma+\frac{(\Lambda_+-\Lambda_-)}{24\pi G\sigma}\right)^2+\frac{\Lambda_-}{3}\right]}}. \tag{14}$$

In this process the location of the wall with black holes is given by

$$r_b=3GM\quad\text{or}\quad r_b=\frac{1}{\sqrt{3\left[\left(2\pi G\sigma+\frac{(\Lambda_+-\Lambda_-)}{24\pi G\sigma}\right)^2+\frac{\Lambda_-}{3}\right]}}. \tag{15}$$

This case is that the left of the wall corresponds to flat space and the right corresponds to de Sitter space. The action turns out to be

$$\begin{aligned}
S_E &= S_E^C-\frac{\sigma}{4}\left(\sqrt{1-\frac{2GM}{r}}\int_0^{\tau_-}d\tau_-+\sqrt{1-\frac{2GM}{r}-\frac{\Lambda_+}{3}r^2}\int_0^{\tau_+}d\tau_+\right)\int_0^{\pi}d\theta\int_0^{2\pi}d\phi r^2\sin\theta\\
&- S_E(bulk)-S_E^B\\
&= S_E^C-\pi\sigma r_b^2\left(\frac{8\pi GM}{\sqrt{3}}+\left(4\pi G\sigma r_b-\frac{1}{\sqrt{3}}\right)\frac{2\pi r_h\sqrt{1-(9\Lambda_+G^2M^2)^{1/3}}}{1-\Lambda_+r_h^2}\right)\\
&- \frac{2\pi U_+}{3}r_b^3\left(\frac{2\pi r_h\sqrt{1-(9\Lambda_+G^2M^2)^{1/3}}}{1-\Lambda_+r_h^2}\right)+\frac{2\pi^2U_+}{\sqrt{3\Lambda_+}}r_{wob}^3\\
&+ \sigma\pi r_{wob}^2\left(\frac{\pi r}{2}+2\sqrt{\frac{3}{\Lambda_+}}(4\pi G\sigma r-1)\right),
\end{aligned} \tag{16}$$

where $U_+>0$ and we use the Bousso-Hawking normalization for Schwarzschild-de Sitter space.

4 Summary and Discussions

In this paper we classified the possible types of vacuum bubbles and calculated the radius and the nucleation rate. We present analytic computation using the thin-wall approximation. There are nine types of true vacuum bubbles, three false vacuum bubbles, and Hawking-Moss transition in which the

thin-wall approximation is not considered. Our results, including the half sized and the large bubble for true vacuum bubbles, false vacuum bubbles, and degenerate case, extend Parke's results. We considered the pair creation of black holes in some of these vacuum bubble backgrounds. These solutions give rise to the background for the black hole pair creation more naturally.

Our solutions, even if it has simple structure, can be used to understand the mechanism how the complicated spacetime structure could be created in the early universe as well as tunneling phenomena occur in the string landscape and eternal inflation.

Acknowledgements

We would like to thank Misao Sasaki for his hospitality at the 18th Workshop on General Relativity and Gravitation in Japan (JGRG18) in Hiroshima. We would like to thank Kei-ichi Maeda for helpful discussions. This work was supported by the Korea Science and Engineering Foundation (KOSEF) grant funded by the Korea government(MEST) through the Center for Quantum Spacetime(CQUeST) of Sogang University with grant number R11 - 2005 - 021. W.L. was supported by the Korea Research Foundation Grant funded by the Korean Government(MOEHRD)(KRF-2007-355-C00014).

References

[1] B.-H. Lee and W. Lee, arXiv:0809.4907.

[2] S. Coleman, Phys. Rev. D **15**, 2929 (1977); *ibid.* D **16**, 1248(E) (1977).

[3] S. Coleman and F. De Luccia, Phys. Rev. D **21**, 3305 (1980).

[4] S. Parke, Phys. Lett. B **121**, 313 (1983).

[5] A. D. Linde, Phys. Lett. B **100**, 37 (1981); Nucl. Phys. B **216**, 421 (1983).

[6] A. H. Guth, Phys. Rev. D **23**, 347 (1981); K. Sato, Mon. Not. R. Astron. Soc. **195**, 467 (1981); J. R. Gott, Nature **295**, 304 (1982); J. R. Gott and T. S. Statler, Phys. Lett. B **136**, 157 (1984); M. Bucher, A. S. Goldhaber, and N. Turok, Phys. Rev. D **52**, 3314 (1995).

[7] S. W. Hawking and I. G. Moss, Phys. Lett. B **110**, 35 (1982).

[8] U. Gen and M. Sasaki, Phys. Rev. D **61**, 103508 (2000).

[9] R.-G. Cai, B. Hu, and S. Koh, arXiv:0806.2508.

[10] K. Marvel and D. Wesley, arXiv:0808.3186.

[11] K. Marvel and N. Turok, arXiv:0712.2719.

[12] K. Lee and E. J. Weinberg, Phys. Rev. D **36**, 1088 (1987).

[13] R. Basu, A. H. Guth, and A. Vilenkin, Phys. Rev. D **44**, 340 (1991); J. Garriga, Phys. Rev. D **49**, 6327 (1994).

[14] J. C. Hackworth and E. J. Weinberg, Phys. Rev. D **71**, 044014 (2005).

[15] Y. Kim, K. Maeda, and N. Sakai, Nucl. Phys. B **481**, 453 (1996); Y. Kim, S. J. Lee, K. Maeda, and N. Sakai, Phys. Lett. B **452**, 214 (1999).

[16] R. R. Caldwell, H. A. Chamblin, and G. W. Gibbons, Phys. Rev. D **53**, 7103 (1996).

[17] C. G. Callan and S. Coleman, Phys. Rev. D **16**, 1762 (1977); E. J. Weinberg, Phys. Rev. D **47**, 4614 (1993); G. V. Dunne and H. Min, Phys. Rev. D **72**, 125004 (2005).

[18] D. Metaxas, arXiv:0804.1045.

[19] S. Coleman, V. Glaser, and A. Martin, Commun. Math. Phys. **58**, 211 (1978).

Non-gaussianity from the bispectrum in general multiple field inflation

Shuntaro Mizuno[1] , Frederico Arroja[2] and Kazuya Koyama[3]

[1] *Research Center for the Early Universe (RESCEU), School of Science, University of Tokyo, 7-3-1 Hongo, Bunkyo, Tokyo 113-0033, Japan*
[2,3] *Institute of Cosmology and Gravitation, University of Portsmouth, Portsmouth PO1 2EG, UK*

Abstract

We study the non-gaussianity from the bispectrum in multi-field inflation models with a general kinetic term. The models include the multi-field K-inflation and the multi-field Dirac-Born-Infeld (DBI) inflation as special cases. We derive the three point function for the curvature perturbation which depends on both adiabatic and entropy perturbations, in the small sound speed limit and at leading order in the slow-roll expansion. The contribution from the entropy perturbations has a different momentum dependence if the sound speed for the entropy perturbations is different from the adiabatic one, which provides a possibility to distinguish the multi-field models from single field models.

1 Introduction

The non-gaussianity of the primordial fluctuations will provide powerful ways to constrain models (see e.g. [1] for a review). The simplest single field inflation models predict that the non-gaussianity of the fluctuations should be very difficult to be detected even in the future experiments such as Planck. If we detect large non-gaussianity, this means that the simplest model of inflation would be rejected.

There are a few models where the primordial fluctuations generated during inflation have a large non-gaussianity. One way to obtain the large primordial non-gaussianity is to consider Multi-field inflation models where the curvature perturbation is modified on large scales due to the entropy perturbations [2]. Since it is shown that in the case of the standard kinetic term, it is not easy to generate large non-gaussianity from multi-field dynamics, it is interesting to consider the multi-field generalization to the models with non-canonical kinetic term like K-inflation [3, 4] and Dirac-Born-Infeld (DBI) inflation [5, 6], motivated by string theory. Especially, since in the DBI-inflation, the inflaton is identified with the position of a moving D3 brane where each compact direction is described by a scalar field, the DBI-inflation is naturally a multi-field model [7].

In this paper, based on [8], we study a fairly general class of multi-field inflation models with a general kinetic term which includes K-inflation [9] and DBI-inflation [10, 11]. We study the sound speeds of the adiabatic perturbations and entropy perturbations and clarify the difference between K-inflation and DBI-inflation. Then we calculate the third order action by properly taking into account the effect of gravity. Then three point functions at the leading order in slow-roll and in the small sound speed limit are obtained. We can recover the results for K-inflation and DBI-inflation easily from this general result.

2 The model

We consider a very general class of models described by the following action

$$S = \frac{1}{2}\int d^4x\sqrt{-g}\left[M_{Pl}^2 R + 2P(X^{IJ},\phi^I)\right], \tag{1}$$

[1] E-mail:mizuno@resceu.s.u-tokyo.ac.jp
[2] E-mail:Frederico.Arroja@port.ac.uk
[3] E-mail:Kazuya.Koyama@port.ac.uk

where ϕ^I are the scalar fields ($I = 1, 2, ..., N$), M_{Pl} is the Planck mass that we will set to unity hereafter, R is the Ricci scalar and

$$X^{IJ} \equiv -\frac{1}{2} g^{\mu\nu} \partial_\mu \phi^I \partial_\nu \phi^J, \tag{2}$$

is the kinetic term, $g_{\mu\nu}$ is the metric tensor. We label the fields' Lagrangian by P and we assume that it is a well behaved function. Greek indices run from 0 to 3. Lower case Latin letters denote spatial indices. Upper case Latin letters denote field indices.

In the background, we are interested in flat, homogeneous and isotropic Friedmann-Robertson-Walker universes. For this background, we consider perturbations beyond linear order. For this purpose, we will construct the action at second and third order in the perturbations and it is convenient to use the ADM metric formalism where the ADM line element reads

$$ds^2 = -N^2 dt^2 + h_{ij} \left(dx^i + N^i dt\right) \left(dx^j + N^j dt\right), \tag{3}$$

where N is the lapse function, N^i is the shift vector and h_{ij} is the 3D metric. For convenience, we define background scalar fields ϕ_0^I and scalar field perturbations Q^I in the flat hypersurface as

$$\phi^I(x,t) = \phi_0^I(t) + Q^I(x,t). \tag{4}$$

Furthermore, we decompose the perturbations into the instantaneous adiabatic and entropy perturbations, where the adiabatic direction corresponds to the direction of the background fields' evolution while the entropy directions are orthogonal to this. Similar to [8], we introduce an orthogonal basis $e_n^I (n = 1, 2, ..., N)$ in the field space so that the orthonormalily condition and the adiabatic basis are given by

$$P_{,X^{IJ}} e_n^I e_m^J = \delta_{nm}\,, \quad e_1^I = \frac{\dot\phi^I}{\sqrt{P_{,X^{JK}} \dot\phi^J \dot\phi^K}}\,. \tag{5}$$

Furthermore, for simplicity, let us consider models described by

$$P(X^{IJ}, \phi^I) = \tilde P(Y, \phi^I)\,, \quad \text{where} \quad Y = G_{IJ}(\phi^K) X^{IJ} + \frac{b(\phi^K)}{2} (X^2 - X_I^J X_J^I)\,. \tag{6}$$

The functional form of Y is chosen so that $Y = X \equiv G_{IJ} X^{IJ}$ in the background as in the DBI-inflation model. This model includes as particular cases the K-inflation model for $b = 0$ and the DBI-inflation for $b = -2f$ and if $\tilde P$ has the DBI form. This might be surprising as the DBI action contains additional terms of order f^2, f^3 and f^4, but it turn out that these terms do not contribute to the leading order third order action.

3 Second and Third-order actions

The second order action can be written in terms of the decomposed perturbations as

$$\begin{aligned} S_{(2)} \;=\; & \frac{1}{2} \int dt d^3x a^3 \Bigg[\left\{ \delta_{mn} + \frac{2X\tilde P_{,YY}}{\tilde P_{,Y}} \delta_{1m}\delta_{1n} + \frac{bX}{1+bX} (\delta_{n1}\delta_{m1} - \delta_{mn}) \right\} (D_t Q_m)(D_t Q_n) \\ & - \frac{1}{a^2} \delta_{mn} \partial_i Q_m \partial^i Q_n - \tilde{\mathcal{M}}_{mn} Q_m Q_n + \tilde{\mathcal{N}}_{mn} Q_n (D_t Q_m) \Bigg]\,, \end{aligned} \tag{7}$$

From this, we can see that the sound speed for adiabatic perturbations c_{ad}^2 and for entropy perturbations c_{en}^2 are given by

$$c_{ad}^2 = \frac{\tilde P_{,Y}}{\tilde P_{,Y} + 2X\tilde P_{,YY}}\,, \quad c_{en}^2 = 1 + bX\,. \tag{8}$$

Similarly, at the leading order in slow-roll approximation where the following parameters are small,

$$\epsilon = -\frac{\dot H}{H^2} = \frac{X\tilde P_{,Y}}{H^2}, \quad \eta = \frac{\dot\epsilon}{\epsilon H}, \quad \chi_{ad} = \frac{\dot c_{ad}}{c_{ad} H}, \quad \chi_{en} = \frac{\dot c_{en}}{c_{en} H}, \tag{9}$$

the third-order action can be written as

$$S_{(3)} = \int dx^3 dt a^3 \left[\frac{1}{2} \Xi_{nml} \dot{Q}_n \dot{Q}_m \dot{Q}_l - \frac{1}{2a^2} \Upsilon_{nml} \dot{Q}_n (\partial_i Q_m)(\partial^i Q_l) \right], \tag{10}$$

where we define the coefficients Ξ_{nml} and Υ_{nml} as

$$\Xi_{nml} = (2X\tilde{P}_{,Y})^{-\frac{1}{2}} \left[\frac{(1-c_{ad}^2)}{c_{ad}^2 c_{en}^2} \delta_{1(n}\delta_{ml)} + \left(\frac{4}{3} \frac{X^2 \tilde{P}_{,YYY}}{\tilde{P}_{,Y}} - \frac{(1-c_{ad}^2)(1-c_{en}^2)}{c_{ad}^2 c_{en}^2} \right) \delta_{n1}\delta_{m1}\delta_{l1} \right], \tag{11}$$

$$\Upsilon_{nml} = (2X\tilde{P}_{,Y})^{-\frac{1}{2}} \left(\frac{1-c_{ad}^2}{c_{ad}^2} \delta_{n1}\delta_{ml} - \frac{2(1-c_{en}^2)}{c_{en}^2} \left(\delta_{n1}\delta_{ml} - \delta_{n(m}\delta_{l)1} \right) \right), \tag{12}$$

and it is obvious that the DBI-inflation is a specific case of the general model with $c_{ad}^2 = c_{en}^2 = c_s^2$.

4 Three-point functions

We derive the three point functions of the adiabatic and entropy fields in the generalized case and at leading order in slow-roll and in the small sound speeds limit. We consider the two-field case with the adiabatic field σ and the entropy field s.

The vacuum expectation value of the three point operator in the interaction picture is

$$\langle \Omega | Q_l(t, \mathbf{k_1}) Q_m(t, \mathbf{k_2}) Q_n(t, \mathbf{k_3}) | \Omega \rangle = -i \int_{t_0}^{t} d\tilde{t} \langle 0 | \left[Q_l(t, \mathbf{k_1}) Q_m(t, \mathbf{k_2}) Q_n(t, \mathbf{k_3}), H_I(\tilde{t}) \right] | 0 \rangle, \tag{13}$$

where t_0 is some early time during inflation when the field's vacuum fluctuation are deep inside the horizons, t is some time after horizon exit. $|\Omega\rangle$ is the interacting vacuum which is different from the free theory vacuum $|0\rangle$. At this order, the only non-zero three point functions are

$$\begin{aligned} &\langle \Omega | Q_\sigma(0, \mathbf{k_1}) Q_\sigma(0, \mathbf{k_2}) Q_\sigma(0, \mathbf{k_3}) | \Omega \rangle = (2\pi)^3 \delta^{(3)}(\mathbf{k_1} + \mathbf{k_2} + \mathbf{k_3}) \frac{2c_{ad}|A_\sigma|^6}{H} \frac{1}{\Pi_{i=1}^3 k_i^3} \frac{1}{K} \\ &\times \left[6c_{ad}^2 (C_3 + C_4) \frac{k_1^2 k_2^2 k_3^2}{K^2} - C_1 k_1^2 \mathbf{k_2} \cdot \mathbf{k_3} \left(1 + \frac{k_2 + k_3}{K} + 2\frac{k_2 k_3}{K^2} \right) + 2 \text{ cyclic terms} \right], \end{aligned} \tag{14}$$

$$\begin{aligned} &\langle \Omega | Q_\sigma(0, \mathbf{k_1}) Q_s(0, \mathbf{k_2}) Q_s(0, \mathbf{k_3}) | \Omega \rangle = (2\pi)^3 \delta^{(3)}(\mathbf{k_1} + \mathbf{k_2} + \mathbf{k_3}) \frac{|A_\sigma|^2 |A_s|^4}{H} \frac{1}{\Pi_{i=1}^3 k_i^3} \frac{1}{\tilde{K}} \\ &\times \left[C_2 c_{en}^2 k_3^2 \mathbf{k_1} \cdot \mathbf{k_2} \left(1 + \frac{c_{ad} k_1 + c_{en} k_2}{\tilde{K}} + \frac{2 c_{ad} c_{en} k_1 k_2}{\tilde{K}^2} \right) + (k_2 \leftrightarrow k_3) \right. \\ &\left. + 4 C_3 c_{ad}^2 c_{en}^4 \frac{k_1^2 k_2^2 k_3^2}{\tilde{K}^2} - 2(C_1 + C_2) c_{ad}^2 k_1^2 \mathbf{k_2} \cdot \mathbf{k_3} \left(1 + c_{en} \frac{k_2 + k_3}{\tilde{K}} + 2 c_{en}^2 \frac{k_2 k_3}{\tilde{K}^2} \right) \right], \end{aligned} \tag{15}$$

where $K = k_1 + k_2 + k_3$, $\tilde{K} = c_{ad} k_1 + c_{en}(k_2 + k_3)$, cyclic terms means cyclic permutations of the three wave vectors and $(k_2 \leftrightarrow k_3)$ denotes a term like the preceding one but with k_2 and k_3 interchanged.

Then, we calculate the leading order in slow-roll three point function of the comoving curvature perturbation. In this work we will ignore the possibility that the entropy perturbations during inflation can lead to primordial entropy perturbations that could be observable in the CMB. But we shall consider the effect of entropy perturbations on the final curvature perturbation. We will follow the analysis, where it has been shown that even on large scales the curvature perturbation can change in time because of the presence of entropy perturbations. The way the entropy perturbations are converted to curvature perturbations is model dependent but it was shown that this model dependence can be parameterized by a transfer coefficient $T_{\mathcal{RS}}$ like

$$\mathcal{R} = \mathcal{A}_\sigma Q_{\sigma *} + T_{\mathcal{RS}} \mathcal{A}_s Q_{s*}, \tag{16}$$

with

$$\mathcal{A}_\sigma = \left(\frac{H}{\dot{\sigma}\sqrt{\tilde{P}_{,Y}}} \right)_*, \quad \mathcal{A}_s = \left(\frac{H}{\dot{\sigma}\sqrt{\tilde{P}_{,Y}}} \sqrt{\frac{c_{en}}{c_{ad}}} \right)_*. \tag{17}$$

Using the previous expressions we can now relate the three point function of the curvature perturbation to the three point functions of the fields obtained in the previous subsection. The three point function of the curvature perturbation is given by

$$\langle \mathcal{R}(\mathbf{k_1})\mathcal{R}(\mathbf{k_2})\mathcal{R}(\mathbf{k_3})\rangle = \mathcal{A}_\sigma^3\langle Q_\sigma(\mathbf{k_1})Q_\sigma(\mathbf{k_2})Q_\sigma(\mathbf{k_3})\rangle + \mathcal{A}_\sigma\mathcal{A}_s^2\left(\langle Q_\sigma(\mathbf{k_1})Q_s(\mathbf{k_2})Q_s(\mathbf{k_3})\rangle + 2\,perms.\right). \quad (18)$$

For the DBI-inflation case the previous equation can be simplified and the total momentum dependence of the three point function of the comoving curvature perturbation is the same as in single field DBI. For our general model this is no longer the case, i.e., the different terms of the previous equation have different momentum dependence. Once again one can see that DBI-inflation is a very particular case and more importantly it provides a distinct signature that enables us to distinguish it from other more general models.

5 Conclusions

In this paper, we studied the non-gaussianity from the bispectrum in general multi-field inflation models with a generic kinetic term. We derived the second and third order action for the perturbations including the effect of gravity. The second order action is written in terms of adiabatic and entropy perturbations. It was shown that the sound speeds for these perturbations are in general different. The K-inflation and the DBI-inflation are special cases where the sound speed for entropy perturbations is one and the same as the adiabatic perturbations, respectively.

Then we derive the three point function in the small sound speeds limit at the leading order in slow-roll expansion. In these approximations there exists a three point function between adiabatic perturbations Q_σ and entropy perturbations Q_s, $\langle Q_\sigma(k_1)Q_s(k_2)Q_s(k_3)\rangle$, in addition to the pure adiabatic three point function. This mixed contribution has a different momentum dependence if the sound speed for the entropy perturbations is different from the adiabatic one. This provides a possibility to distinguish between the multi-field models and the single field models. Unfortunately, in the multi-field DBI case, the sound speed for the entropy perturbation is the same as the adiabatic one and the mixed contribution only changes the amplitude of the three point function. This could help to ease the constraints on DBI-inflation. For the specialty of the DBI inflation model, we can see that the trispectrum can distinguish the multi-field inflation from the single field DBI inflation model [12].

References

[1] N. Bartolo, E. Komatsu, S. Matarrese and A. Riotto, Phys. Rept. **402**, 103 (2004).

[2] A. A. Starobinsky and J. Yokoyama, arXiv:gr-qc/9502002.

[3] C. Armendariz-Picon, T. Damour and V. F. Mukhanov, Phys. Lett. B **458** (1999) 209.

[4] J. Garriga and V. F. Mukhanov, Phys. Lett. B **458** (1999) 219.

[5] E. Silverstein and D. Tong, Phys. Rev. D **70** (2004) 103505.

[6] M. Alishahiha, E. Silverstein and D. Tong, Phys. Rev. D **70** (2004) 123505.

[7] D. A. Easson, R. Gregory, D. F. Mota, G. Tasinato and I. Zavala, JCAP **0802** (2008) 010.

[8] F. Arroja, S. Mizuno and K. Koyama, JCAP **0808**, 015 (2008).

[9] D. Langlois and S. Renaux-Petel, JCAP **0804** (2008) 017.

[10] D. Langlois, S. Renaux-Petel, D. A. Steer and T. Tanaka, Phys. Rev. Lett. **101**, 061301 (2008).

[11] D. Langlois, S. Renaux-Petel, D. A. Steer and T. Tanaka, Phys. Rev. D **78**, 063523 (2008).

[12] S. Mizuno, F. Arroja and K. Koyama, in preparation

Phase Transitions of Charged Kerr-AdS Black Holes from Large-N Gauge Theories

Keiju Murata[1], Tatsuma Nishioka[2], Norihiro Tanahashi[3] and Hikaru Yumisaki[4]

Department of Physics, Kyoto University, Kyoto 606-8502, Japan

Abstract

We study $\mathcal{N} = 4$ super Yang-Mills theories on a three-sphere with two types of chemical potential. One is associated with the R-symmetry and the other with the rotational symmetry of S^3 ($SO(4)$ symmetry). These correspond to charged Kerr-AdS black holes via AdS/CFT. The exact partition functions at zero coupling are computed and the thermodynamical properties are studied. We find a nontrivial gap between the confinement/deconfinement transition line and the boundary of the phase diagram when we include more than four chemical potentials. In dual gravity, we find such a gap in the phase diagram by studying the thermodynamics of the charged Kerr-AdS black hole. This shows that the qualitative phase structures agree between both theories.

1 Introduction

The AdS/CFT correspondence has played a central role for about ten years in the study of the strongly coupled region of $\mathcal{N} = 4$ super Yang-Mills theory with $SU(N)$ gauge group because it is simply described by type IIB supergravity on $AdS_5 \quad S^5$. In the AdS space, there is a phase transition between the thermal AdS space and the AdS-Schwarzschild black hole, the so-called Hawking-Page transition. As the dual picture of the Hawking-Page transition, the confinement/deconfinement transition was found even at zero coupling by studying large-N gauge theories. [1–3]

In this paper, we study $\mathcal{N} = 4$ SYM theory on a three-sphere with general (R- and $SO(4)$ symmetry) chemical potentials. In gravity theory, we study the thermodynamics of the charged Kerr-AdS black hole [4] and compare the result with that of the gauge theory. This paper is based on [5].

2 Large-N gauge theory

2.1 Symmetry of $\mathcal{N} = 4$ super Yang-Mills theory and chemical potentials

The AdS boundary of a charged Kerr-AdS black hole has S^3 topology in global coordinates. Therefore, we need to study $\mathcal{N} = 4$ SYM on S^3. The action is given by

$$S = \int d^4x\sqrt{\quad g}\,\mathrm{tr}\ \frac{1}{2}(F_{\mu\nu})^2 + (D_\mu \quad _m)^2 + l \quad ^2 \quad ^2_m + i\lambda^A \quad ^\mu D_\mu \lambda_A \quad \frac{g^2}{2}[\quad _m,\quad _n]^2 \quad g\lambda^A \quad ^m[\quad _m, \lambda_A]\ , \quad (1)$$

and the background metric is

$$ds^2 = g_{\mu\nu}dx^\mu dx^\nu = \quad dt^2 + l^2 d\quad ^2_3\ , \quad (2)$$

where $\mu = 0, 1, 2, 3,\ m = 1, 2, \ldots, 6,\ A = 1, \ldots, 4,\ F_{\mu\nu} = \partial_\mu A_\nu \quad \partial_\nu A_\mu + ig[A_\mu, A_\nu]$, A_μ is the gauge field of $U(N)$. $\quad _m$ is a scalar field and λ_A is a four-dimensional spinor in the $(\mathbf{2}, \bar{\mathbf{4}}) + (\bar{\mathbf{2}}, \mathbf{4})$ representation under $SO(1,3) \quad SU(4)$. All fields are adjoint representation of $U(N)$. l is the radius of S^3 and we set $l = 1$ for simplicity. The mass term of the scalar field $(\mathcal{R}/6)\ ^2_m = l \quad ^2 \quad ^2_m$ is needed to make the theory conformal invariant, where $\mathcal{R}$ is the Ricci scalar in (2). This action has two types of global symmetry. One of them is $R_t \quad SO(4)$, which arises from the symmetry of the background spacetime (2), where R_t

[1] e-mail:murata@tap.scphys.kyoto-u.ac.jp
[2] e-mail:nishioka@gauge.scphys.kyoto-u.ac.jp
[3] e-mail:tanahashi@tap.scphys.kyoto-u.ac.jp
[4] e-mail:yumisak@scphys.kyoto-u.ac.jp

represents the time translation invariance. The other one is $SO(6) \simeq SU(4)$, which originates from the R-symmetry of $\mathcal{N} = 4$ supersymmetry.

The conserved charges are associated with commutative (Cartan) subgroups of global symmetry R_t $SO(4)$ $SU(4)$. Due to the time translation symmetry R_t, the Hamiltonian $\hat{H}$ is conserved. The $SO(4)$ group contains a $U(1)^2$ Cartan subgroup and we denote the associated charges as $\hat{J}_1$ and $\hat{J}_2$. These charges represent angular momenta on S^3. The $SU(4)$ group also contains a $U(1)^3$ Cartan subgroup and we will denote the associated charges as $\hat{Q}_a$ $(a = 1, 2, 3)$. Therefore, we can consider a grand canonical ensemble with five chemical potentials in SYM at a finite temperature. The grand canonical partition function is given by

$$Z(\ ) = \mathrm{Tr}\left[e^{\ \beta(\hat{H}\ \ \sum_{a=1}^{3}\mu_a\hat{Q}_a\ \ \Omega_1\hat{J}_1\ \ \Omega_2\hat{J}_2)}\right] \tag{3}$$

where μ_a, $_1$ and $_2$ are the chemical potentials conjugate to $\hat{Q}_a$, $\hat{J}_1$ and $\hat{J}_2$, respectively. We study the thermodynamics of $\mathcal{N} = 4$ SYM theory using the partition function (3).

2.2 Phase structure

We can find the confinement/deconfinement transition in SYM theory and depict the transition lines on the phase space. The phase space is the six-dimensional space of $(T,\ _1,\ _2, \mu_1, \mu_2, \mu_3)$ and we cannot cover the whole phase space. We thus focus on several slices, which are $(\mu_1, \mu_2, \mu_3) = (\mu, 0, 0), (\mu, \mu, 0), (\mu, \mu, \mu)$ and $\mu,\ _1,\ _2 > 0$. The confinement/deconfinement phase transition lines of these slices are depicted in Fig. 1.

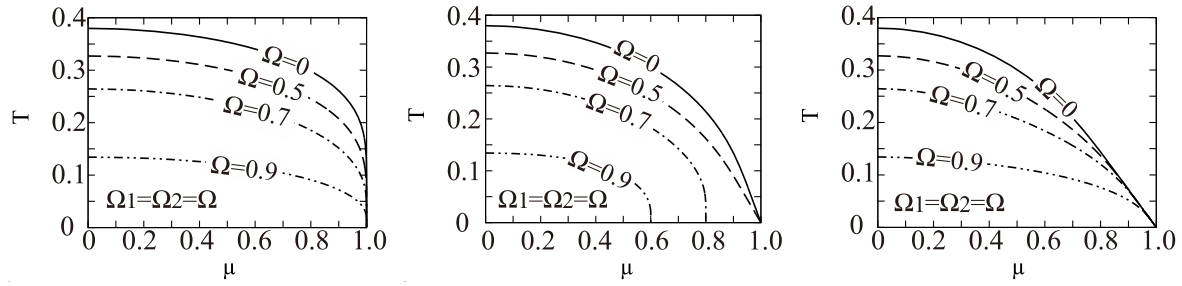

(a) $\mu_1 \equiv \mu, \mu_2 = \mu_3 = 0$ (b) $\mu_1 = \mu_2 \equiv \mu, \mu_3 = 0$ (c) $\mu_1 = \mu_2 = \mu_3 \equiv \mu$

Figure 1: Phase diagrams of $\mathcal{N} = 4$ large-N SYM theory with R-symmetry and $SO(4)$-symmetry chemical potentials. We plot the critical temperature T_H for nonzero R-charge chemical potentials (μ_1, μ_2, μ_3) in the cases of $_1 = \ _2$ and $= 0, 0.5, 0.7$ and 0.9 in (a), (b) and (c). The confinement phase is below the line and the deconfinement phase is above it. We set the R-charge chemical potentials as (a) $(\mu, 0, 0)$, (b) $(\mu, \mu, 0)$ and (c) (μ, μ, μ).

Fig. 1 shows that the critical line becomes lower as the $SO(4)$ chemical potential increases irrespective of the values of the R-symmetry chemical potentials. Almost all lines converge to the point where $T = 0$ and $\mu = 1$ for $(\mu, 0, 0)$ and (μ, μ, μ) (Fig. 1(a) and 1(c)), while the lines for $(\mu, \mu, 0)$ with large end at some maximal chemical potential $\mu_{\max}(\ )$ (Fig. 1(b)).

2.3 Unitarity line

We determine the unitarity line where the phase diagram is bounded. In the presence of the chemical potentials, the time derivative in the Lagrangian shifts as $\partial_0 \to \partial_0\ \ i(\sum_{a=1}^{3}\mu_a Q_a + \sum_{i=1}^{2}\ _i J_i)$. Then, the Hamiltonian is shifted as $H \to H\ \ \sum_{a=1}^{3}\mu_a Q_a\ \ \sum_{i=1}^{2}\ _i J_i$, and the chemical potentials are introduced into the path integral. By the replacement of the time derivative, the mass of the scalar with the representation $(E_s = 2j + 1, m_L, m_R, Q_1 = 1, Q_2 = 0, Q_3 = 0)$, $|m_L| \le j, |m_R| \le j$ shifts as

$$m^2_{\mathrm{scalar}} = E_s^2 = (2j+1)^2 \quad \to \quad m^2_{\mathrm{scalar}} = E_s^2 \quad (\mu_1 + (\ _1 + \ _2)m_L + (\ _1 \ \ _2)m_R)^2 . \tag{4}$$

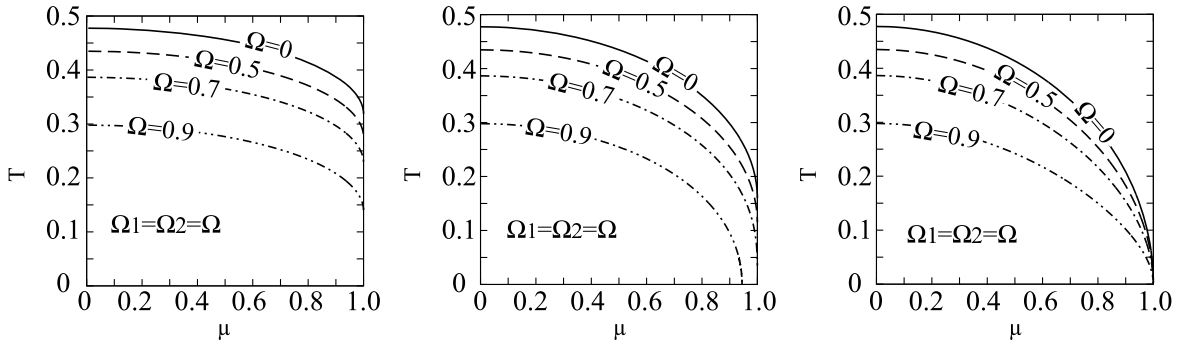

(a) $\mu_1 \equiv \mu, \mu_2 = \mu_3 = 0$ (b) $\mu_1 = \mu_2 \equiv \mu, \mu_3 = 0$ (c) $\mu_1 = \mu_2 = \mu_3 \equiv \mu$

Figure 2: Phase diagrams for charged Kerr-AdS black holes with two equal rotations and three independent R-charges: (J, J, Q_1, Q_2, Q_3). We plot the transition lines for the R-symmetry chemical potentials (a) $(\mu, 0, 0)$, (b) $(\mu, \mu, 0)$ and (c) (μ, μ, μ), varying the angular velocities $\quad = \quad_1 = \quad_2$. The thermal AdS space is preferentially realized below the lines, and the black hole is preferentially formed above the lines. These figures are drawn in the same scale as the phase diagrams for the gauge theory in Fig. 1.

The $j = 0$ mode first becomes tachyonic as the chemical potentials increase, and this gives the bound $\mu_1 = 1$ above which the theory breaks down. The scalar modes with $(Q_1, Q_2, Q_3) = (0, 1, 0)$ and $(0, 0, 1)$ also give the bounds $\mu_2 = 1$ and $\mu_3 = 1$, respectively. Similarly, the $j = \infty$ mode also requires the upper bound $\quad_i = 1$. The $j = \infty$ mode of the vector field also becomes tachyonic for $\quad_i > 1$, and thus it imposes the same upper bound on $\quad_i$.

This unitarity line meets to the transition line at $T = 0$ for many cases as shown in Fig. 1, while in general a gap appears between these two lines when there are more than four. chemical potentials. we will provide a dual description of this unitarity line, which we think is the line representing the black hole instability, and we find remarkable agreement between their behaviors.

3 Comparison with dual gravity

3.1 Phase structure

The dual gravity theory is given by $U(1)^3$-gauged $\mathcal{N} = 2$ five-dimensional supergravity. These $U(1)^3$ charges correspond to the R-charges in dual gauge theory. In general, the solution of the $U(1)^3$-gauged supergravity can have two independent rotations and three independent charges. Unfortunately such a general solution has not yet been discovered and we concentrate on one of the currently known charged Kerr-AdS solution $(J_1, J_1, Q_1, Q_2, Q_3)$ [4].

Now let us consider the phase structure of the charged Kerr-AdS black hole. The transition temperature is determined by the condition that the free energy of the black hole is zero. We plot the diagrams numerically, which are shown in Fig. 2. The phase diagrams of the charged Kerr-AdS black hole (Figs. 2) are similar to the phase diagrams for the dual gauge theory (Figs. 1). In particular, we can see the strong agreement between Fig. 1(b) and Fig. 2(b). In this case, for $\quad \gtrsim 0.9$, the transition line ends at $(\mu, T) = (\mu_{\max}, 0)$, where $\mu_{\max} < 1$. This appearance of $\mu_{\max}$ also occurs in the gauge theory for $\quad > 0.5$ (see Fig. 1(b)). These similarities show that a global phase structure such as a confinement/ deconfinement transition does not depend on the coupling constant if we regard the gravity theory to be the strongly coupled gauge theory via AdS/CFT.

3.2 Instability of charged Kerr-AdS black hole

In §2.3, we studied the unitarity line for gauge theory. This unitarity line in the gauge theory corresponds to the local thermodynamical instability line in dual gravity theory. The local thermodynamical

instability means that the Hessian matrix of second derivatives of the mass with respect to the entropy and the conserved charges has a negative eigenvalue. Fig. 3 shows the resultant instability lines on which the Hessian matrix has zero eigenvalue, along with the Hawking-Page transition lines. We also depict the confinement/deconfinement transition lines and the unitarity lines of the dual gauge theory.

In Fig. 3, we can see qualitative similarities between the instability line of the gravity theory and the unitarity line of the dual gauge theory. In particular, in Fig. 3(b) for the case $(\mu_1, \mu_2, \mu_3) = (\mu, \mu, 0)$, a gap appeared between the Hawking-Page line and the instability line. We found such a gap in the dual gauge theory in §2.3.

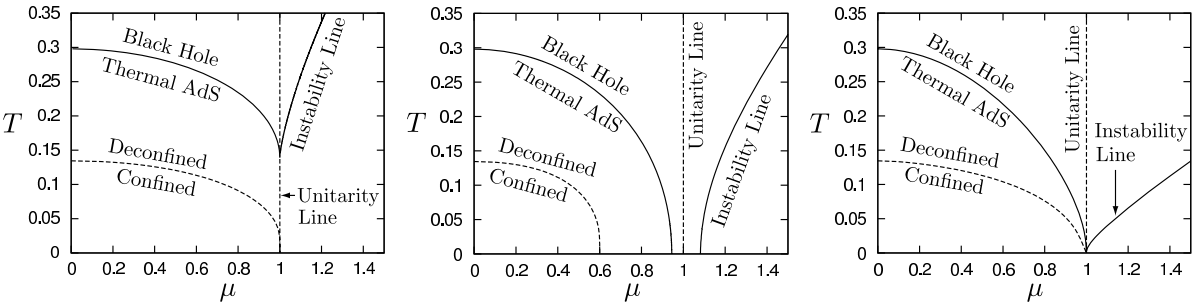

(a) $\mu_1 \equiv \mu, \mu_2 = \mu_3 = 0$ (b) $\mu_1 = \mu_2 \equiv \mu, \mu_3 = 0$ (c) $\mu_1 = \mu_2 = \mu_3 \equiv \mu$

Figure 3: Phase diagrams for $= 0.9$ including the unitarity lines. The solid lines are the Hawking-Page transition line and the instability line of a charged Kerr-AdS black hole. The dashed lines are the confinement/deconfinement transition line and the unitarity line of the dual gauge theory.

4 Conclusion

We have studied the free $\mathcal{N} = 4$ SYM theory dual to the charged Kerr-AdS black hole. We found the confinement/deconfinement transition and specified the unitarity bound for this theory. In the dual gravity theory, the Hawking-Page transition and the thermodynamical instability of charged Kerr-AdS black holes have been investigated. The resulting phase diagrams for gauge theory and charged Kerr-AdS black holes resemble each other, and, in particular, we have found that the confinement/deconfinement transition line and the unitarity line of gauge theory correspond to the Hawking-Page transition line and the instability line in dual gravity theory, respectively.

References

[1] B. Sundborg, Nucl. Phys. B **573**, 349 (2000) [arXiv:hep-th/9908001].

[2] O. Aharony, J. Marsano, S. Minwalla, K. Papadodimas and M. Van Raamsdonk, Adv. Theor. Math. Phys. **8**, 603 (2004) [arXiv:hep-th/0310285].

[3] D. Yamada and L. G. Yaffe, JHEP **0609**, 027 (2006) [arXiv:hep-th/0602074].

[4] M. Cvetic, H. Lu and C. N. Pope, Phys. Rev. D **70**, 081502 (2004) [arXiv:hep-th/0407058].

[5] K. Murata, T. Nishioka, N. Tanahashi and H. Yumisaki, Prog. Theor. Phys. **120**, 473 (2008) [arXiv:0806.2314 [hep-th]].

WMAP-5yr Constraint on the Varying Fine Structure Constant

Masahiro Nakashima,[1,2] Ryo Nagata[2] and Jun'Ichi Yokoyama[2,3]

[1] *Department of Physics, Graduate School of Science, The University of Tokyo, Tokyo 113-0033, Japan*
[2] *Research Center for the Early Universe (RESCEU), Graduate School of Science, The University of Tokyo, Tokyo 113-0033, Japan*
[3] *Institute for the Physics and Mathematics of the Universe (IPMU), The University of Tokyo, Kashiwa, Chiba 277-8568, Japan*

Abstract

The constraints on the time variation of the fine structure constant at recombination epoch relative to its present value,$\Delta\alpha/\alpha \equiv (\alpha_{\rm rec} - \alpha_{\rm now})/\alpha_{\rm now}$, are obtained from the analysis of the 5-year WMAP cosmic microwave background data. As a result of Markov-Chain Monte-Carlo analysis, it is found that, contrary to the analysis based on the previous WMAP data, the mean value of $\Delta\alpha/\alpha = -0.0009$ does not change significantly whether we use the Hubble Space Telescope (HST) measurement of the Hubble parameter as a prior or not. The resultant 95% confidence ranges of $\Delta\alpha/\alpha$ are $-0.028 < \Delta\alpha/\alpha < 0.026$ with HST prior and $-0.050 < \Delta\alpha/\alpha < 0.042$ without HST prior.

1 Introduction

The variation of the fundamental physical constants is a long-standing issue. Dirac first considered such a possibility [1] and proposed that the Newton constant should be inversely proportional to time. While his claim is not compatible with the current observations, recent unification theories such as superstring theories naturally predict the variation of the fundamental constants [2]. Because of these theoretical motivations, it is important to measure their possible time variation observationally.

Among various fundamental constants, the time variation of the fine structure constant α has been most extensively discussed in observational contexts. We briefly summarize those terrestrial and celestial limits on α as follows.

- $\dot{\alpha}/\alpha = (-1.6 \pm 2.3) \times 10^{-17}$ yr^{-1} from the measurement of the frequency ratio of aluminium and mercury single-ion optical clocks[3].
- $\Delta\alpha/\alpha = (-0.8 \pm 1.0) \times 10^{-8}$ or $\Delta\alpha/\alpha = (0.88 \pm 0.07) \times 10^{-7}$ from the Oklo natural reactor in Gabon ($z \sim 0.1$)[4].
- $\Delta\alpha/\alpha = (-0.57 \pm 0.11) \times 10^{-5}$ ($z \sim 0.2 - 4.2$) [5] and $\Delta\alpha/\alpha = (-0.64 \pm 0.36) \times 10^{-5}$ ($z \sim 0.4 - 2.3$) [6] from spectra of quasars.
- $-5.0 \times 10^{-2} < \Delta\alpha/\alpha < 1.0 \times 10^{-2}$ (95%C.L.) from big bang nucleosynthesis (BBN, $z \sim 10^9 - 10^{10}$)[7].
- $-0.048 < \Delta\alpha/\alpha < 0.032$,[8] $-0.06 < \Delta\alpha/\alpha < 0.01$ [9] or $-0.039 < \Delta\alpha/\alpha < 0.010$ [10] (95%C.L.) from the cosmic microwave background (CMB, $z \sim 10^3$), the former two of which are based on the analysis of the 1-year WMAP data and the last one on the 3-year WMAP data.

Here, we focus on the CMB constraint on α from 5-year WMAP data, finding new limits on its value at the recombination epoch[11]. While the other physical constants may vary in time simultaneously, they are so model-dependent that we consider only the variation of α.

Both CMB and BBN are useful for obtaining the constraints of the variation of α over a cosmological time scale. Although BBN is superior in the sense that it can probe a longer timespan, it has a drawback that the effect of α in Helium abundance Y_p is model-dependent so that we cannot obtain a robust result from BBN analysis. On the other hand, the physics of the CMB is much simpler and well understood with high-precision data, so we can obtain a meaningful limit on the variation of α from the CMB data.

2 CMB and varying ne structure constant

As is well known, changing the value of the fine structure constant affects the CMB power spectrum mainly through the change of the recombination time[12]. Hence, CMB probes the value of α in this particular epoch.

The recombination process is well approximated by the evolutions of three variables: the proton fraction, the fraction of the singly ionized Helium, and the matter temperature. Their evolution equations are so complicated that we solve them numerically by public RECFAST code[13]. Incorporating the α-dependence into RECFAST code and calculating the ionization fraction (or visibility function), we can find two charastrictic signatures of changing α: the higher redshift of the last scattering surface and the narrower width of the visibility function due to the larger value of *alpha* at the recombination epoch.

Then, increasing α results in three features in the angular power spectrum of the temperature anisotropy, namely, shift of the peaks to higher multipoles, increase in the height of the peaks due to the enhanced early integrated Sachs Wolfe effect, and decrease in the small-scale diffusion damping effect.

3 Results

We constrain the variation of α using three types of CMB anisotropy spectra, namely, angular power spectrum of temperature anisotropy, C_ℓ^{TT}, that of E-mode polarization, C_ℓ^{EE}, and cross correlation of temperature and E-mode polarization C_l^{TE} of the 5-year WMAP data[14]. For this purpose, we have modified the CAMB code [15] including the RECFAST code to calculate the theoretical anisotropy spectra for different values of α at recombination and we performed the parameter estimation using Markov-Chain Monte-Carlo (MCMC) techniques implemented in the CosmoMC code[16].

We have run the CosmoMC code on four Markov chains. To check the convergence, we used the "variance of chain means"/"mean of chain variances" R statistic and adopted the condition $R-1<0.03$.

First, we consider the modified version of the flat ΛCDM model, that is, as for cosmological parameters, we take $(\Omega_B h^2, \Omega_{DM} h^2, H_0, n_s, A_s, \tau, \Delta\alpha/\alpha)$, where $\Omega_B h^2$ is the normalized baryon density, $\Omega_{DM} h^2$ is the normalized cold-dark-matter density, $H_0 \equiv 100h \left[\mathrm{km\ sec^{-1}\ Mpc^{-1}}\right]$ is the Hubble constant, n_s is the spectral index of the primordial curvature perturbation, A_s is its amplitude, and $\Delta\alpha/\alpha \equiv (\alpha_{\rm rec} - \alpha_{\rm now})/\alpha_{\rm now}$ is the variation of the fine structure constant at recombination relative to its present value. We have also analyzed the standard flat ΛCDM model without $\Delta\alpha/\alpha$ and compared the other parameter values between these two models.

The results obtained from MCMC calculations are given in Fig. 1, which shows the one-dimensional marginalized posterior distributions of the parameters. From the result, it can be seen that the effect of the additional parameter $\Delta\alpha/\alpha$ is only to increase the errors of the other parameters, and the mean values of the other parameters in modified flat ΛCDM are practically the same as in the standard flat ΛCDM. The marginalized distributions of H_0 and Ω_B in Fig. 1 suggest the degeneracy of these parameters with $\Delta\alpha/\alpha$.

Actually, in the above calcutions, we have incorporated the result of the Hubble Key Project of the Hubble Space Telescope (HST) on the Hubble parameter H_0,[17] that is, we have imposed a prior that H_0 is a Gaussian with the mean 72 $\left[\mathrm{km\ sec^{-1}\ Mpc^{-1}}\right]$ and the variance 8 $\left[\mathrm{km\ sec^{-1}\ Mpc^{-1}}\right]$. If we do not use the HST prior, we can only obtain weaker constraints on the parameter values because of projection degeneracy. To check the effect of the HST prior, we show one-dimensional distributions in Fig. 2. It is confirmed that the HST prior is very important to realistically constrain the time varition of α.

The 95% confidence interval and the mean value of $\Delta\alpha/\alpha$ from 5-year WMAP data with HST prior are

$$-0.028 < \Delta\alpha/\alpha < 0.026 \quad \text{and} \quad \Delta\alpha/\alpha = -0.000894, \tag{1}$$

respectively. Without the HST prior, they read

$$-0.050 < \Delta\alpha/\alpha < 0.042 \quad \text{and} \quad \Delta\alpha/\alpha = -0.00181, \tag{2}$$

respectively. Previous results from 1-year WMAP data are $-0.048 < \Delta\alpha/\alpha < 0.032$ and $-0.107 < \Delta\alpha/\alpha < 0.043$, with and without HST prior, respectively[8], so our results from 5-year WMAP data are

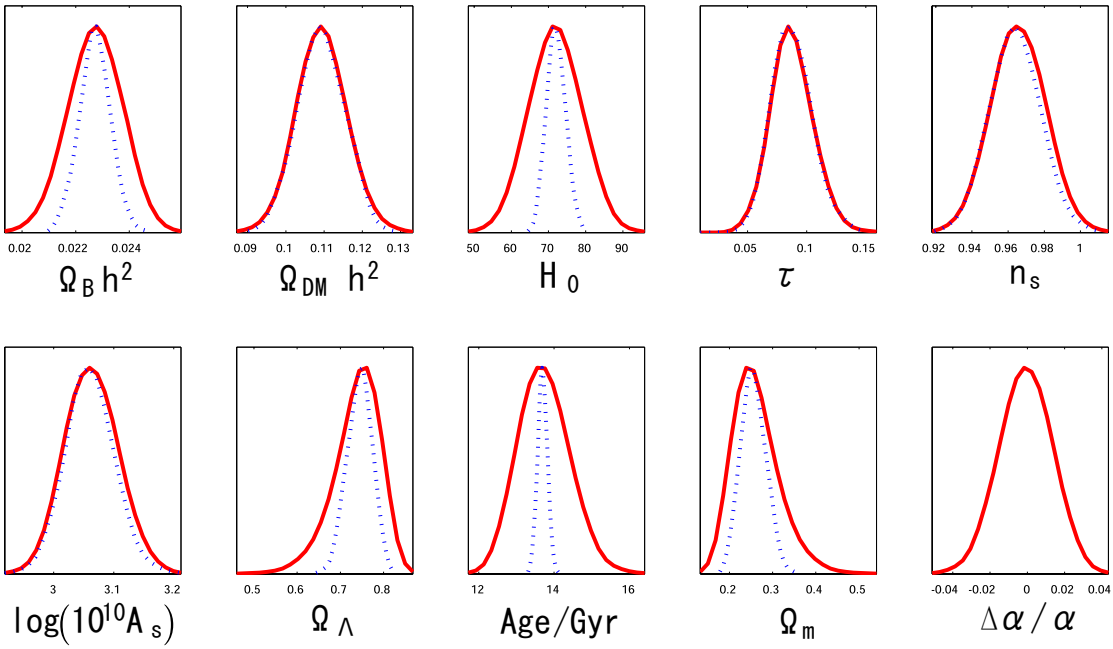

Figure 1: (colour online) One-dimensional marginalized posterior distributions for the parameters of the modified flat ΛCDM model (solid red curve), and for the standard flat ΛCDM model (dotted blue curve).

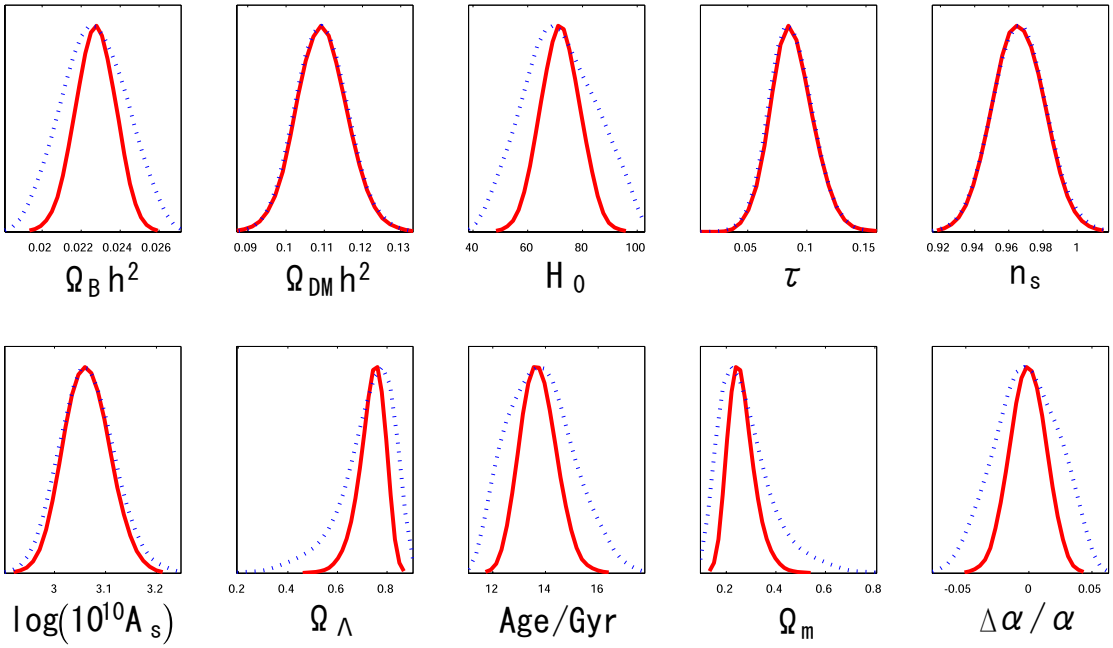

Figure 2: One-dimensional marginalized posterior distributions for the results with HST prior (solid red curve), and without it (dotted blue curve).

about 30% tighter than those from the 1-year WMAP data. We also note that for the 1-year data, the mean value of $\Delta\alpha/\alpha$ was found to be $\Delta\alpha/\alpha = -0.04$ without the HST prior although it was practically equal to 0 with it. For the 5-year data, we have found that the mean value remains practically intact whether we use the HST prior or not. This may be interpreted as an indication that the observational cosmology has made a step forward to the concordance at an even higher level.

4 Conclusion

In terms of the MCMC analysis using CosmoMC code, we have updated constraints on the time variation of the fine structure constant α based on 5-year WMAP data. We obtained tighter constraints compared with previous results from 1-year WMAP data owing to the inclusion of the polarization data and the decrease in the statistical errors. Compared with the result based on the 3-year WMAP data[10], where no comparison between the cases with and without HST prior has been made, the resultant limit is almost of the same order of magnitude but the mean value of ours is closer to 0. We have verified that the null result is favored concerning the variation of α, and the addition of this new parameter $\Delta\alpha/\alpha$ does not essentially affect the determinations of the other standard parameters contrary to the case of the analysis based on the 1-year WMAP data[8].

References

[1] P. A. M. Dirac, Nature **139** (1937), 323 , P. A. M. Dirac, Proc. R. Soc. London A **165** (1938), 199.

[2] J. P. Uzan, Rev. Mod. Phys. **75** (2003), 403, hep-ph/0205340.

[3] T. Rosenband et al., Science **319** (2008), 1808.

[4] Y. Fujii et al., in Proc. Int. Conf. on Nuclear Data for Science and Technology, 2001, hep-ph/0205206.

[5] M. T. Murphy et al., Lecture Notes in Phys., **131** (2004), 648.

[6] M. T. Murphy, J. K. Webb and V. V. Flambaum, Mon. Not. R. Astron. Soc. **384** (2008), 1053, astro-ph/0612407.

[7] K. Ichikawa and M. Kawasaki, Phys. Rev. D **65** (2002), 123511, hep-ph/0203006.

[8] K. Ichikawa, T. Kanzaki and M. Kawasaki, Phys. Rev. D **74** (2006), 023515, astro-ph/0602577.

[9] G. Rocha, R. Trotta, C. J. A. Martins, A. Melchiorri, P. P. Avelino, R. Bean and P. T. P. Viana, Mon. Not. R. Astron. Soc. **352** (2004), 20, astro-ph/0309211.

[10] P. Stefanescu, New Astron. **12** (2007), 635, arXiv:0707.0190.

[11] M. Nakashima, R. Nagata and J. Yokoyama, Prog. Theor. Phys. **120**, 1207 (2008) [arXiv:0810.1098 [astro-ph]].

[12] S. Hannestad, Phys. Rev. D **60** (1999), 023515, astro-ph/9810102 , M. Kaplinghat, R. J. Scherrer and M. S. Turner, Phys. Rev. D **60** (1999), 023516, astro-ph/9810133.

[13] `http://www.astro.ubc.ca/people/scott/recfast.html`

[14] M. R. Nolta et al. (WMAP Collaboration), arXiv:0803.0593, J. Dunkley et al. (WMAP Collaboration), arXiv:0803.0586, E. Komatsu et al. (WMAP Collaboration), arXiv:0803.0547.

[15] A. Lewis, A. Challinor and A. Lasenby, Astrophys. J. **538** (2000), 473, astro-ph/9911177 , `http://camb.info/`

[16] A. Lewis and S. Bridle, Phys. Rev. D **66** (2002), 103511, astro-ph/0205436, `http://cosmologist.info/cosmomc/`

[17] W. L. Freedman et al. (HST Collaboration), Astrophys. J. **553** (2001), 47, astro-ph/0012376.

Non-Gaussianity from Isocurvature Perturbations

Kazunori Nakayama[1]

Institute for Cosmic Ray Research, University of Tokyo, Kashiwa, Chiba 277-8582, Japan

Abstract

We develop a formalism to study non-Gaussianity in both curvature and isocurvature perturbations. It is shown that non-Gaussianity in the CDM/baryonic isocurvature perturbation leaves distinct signatures in the CMB temperature fluctuations, which may be confirmed in future experiments, or possibly, even in the currently available observational data. As an explicit example, we consider the QCD axion and show that it can actually induce sizable non-Gaussianity.

1 Introduction

Non-Gaussianity in the cosmological perturbation is currently a hot topic since simple slow-roll inflation models predict negligible non-Gaussian fluctuations, and a large non-Gaussianity, if detected, means that there is a need for some modifications on a standard scenario where the curvature perturbation on the Universe comes from quantum fluctuation of the inflaton. Yadav and Wandelt reported a detection of non-zero non-Gaussianity using WMAP3 year data [1], but WMAP5 results were consistent with vanishing non-Gaussianity [2]. Although it is not settled yet a large non-Gaussianity exists or not, it is important to know in which situation a non-Gaussianity can be significantly large.

Recently we have pointed out that large non-Gaussian fluctuation can exist in the CDM/baryonic isocurvature perturbation [3, 4, 5]. This point was missed in the previous literature except for a few works [6]. We have developed a formalism for studying non-Gaussianity of both adiabatic and isocurvature type systematically and also studied their characteristic effects on CMB bispectrum [3, 5]. It is found that non-Gaussian fluctuations in the isocurvature perturbations have distinct signatures on CMB anisotropy and can be detected in future experiments.

2 Non-Gaussianity from isocurvature perturbations

We are interested in the case where the (CDM) isocurvature perturbation S exists in addition to the usual curvature perturbation ζ generated during inflation. For the long wavelength limit, the curvature perturbation in the matter dominated era can be written as

$$\zeta^{\rm MD} = \zeta + \frac{1}{3}S. \tag{1}$$

In the most literature, only the case where the non-Gaussian fluctuation resides in the primordial curvature perturbation (ζ) was studied. However, the isocurvature perturbation (S) can also have significant non-Gaussianity. The bispectrum is a useful tool for characterizing the non-Gaussianity. Thus, in order to see this, we define the bispectrum of $\zeta^{\rm MD}$, $B_\zeta^{\rm MD}$ by the following equation [3, 5],

$$\langle \zeta^{\rm MD}_{\vec{k}_1}\zeta^{\rm MD}_{\vec{k}_2}\zeta^{\rm MD}_{\vec{k}_3}\rangle \equiv (2\pi)^3\delta(\vec{k}_1+\vec{k}_2+\vec{k}_3)\ B_\zeta^{\rm MD}(k_1,k_2,k_3). \tag{2}$$

This contains four kind of terms, like $\langle\zeta\zeta\zeta\rangle, \langle\zeta\zeta S\rangle, \langle\zeta SS\rangle$ and $\langle SSS\rangle$. Performing the integration, we can express $B_\zeta^{\rm MD}$ in terms of the four combinations of the bispectrum of ζ and S,

$$B_\zeta^{\rm MD}(k_1,k_2,k_3) \simeq \left(\beta_{\zeta\zeta\zeta} + \frac{1}{3}\beta_{\zeta\zeta S} + \frac{1}{9}\beta_{\zeta SS} + \frac{1}{27}\beta_{SSS}\right)\left[P_\delta\ (k_1)P_\delta\ (k_2) + 2 \text{ perms.}\right], \tag{3}$$

[1]E-mail:nakayama@icrr.u-tokyo.ac.jp

where each term on the right hand side (RHS) is given by

$$\beta_{\zeta\zeta\zeta} = N_a N_b N_{ab} + N_{ab} N_{bc} N_{ca} \Delta_\delta^2 \ \ln(k_b L), \tag{4}$$

$$\beta_{\zeta\zeta S} = N_a N_b S_{ab} + 2 N_{ab} N_a S_b + 3 N_{ab} N_{bc} S_{ca} \Delta_\delta^2 \ \ln(k_b L), \tag{5}$$

$$\beta_{\zeta S S} = S_a S_b N_{ab} + 2 S_{ab} S_a N_b + 3 S_{ab} S_{bc} N_{ca} \Delta_\delta^2 \ \ln(k_b L), \tag{6}$$

$$\beta_{SSS} = S_a S_b S_{ab} + S_{ab} S_{bc} S_{ca} \Delta_\delta^2 \ \ln(k_b L), \tag{7}$$

in a squeezed configuration that one of the three wave vectors is much smaller than the other two (e.g. $k_1 \ll k_2, k_3$), where $k_b \equiv \min\{k_1, k_2, k_3\}$, $\Delta_\delta = H_{\rm inf}/2\pi$ and L is taken to be a few times larger than the present Hubble scale. These terms except for the first one exist when the isocurvature perturbation has non-Gaussian fluctuation. Here we have used a δN expansion such that $\zeta = N_a \delta\phi^a + \dots$ and also $S = S_a \delta\phi^a + \dots$. Since a single parameter is not enough to parametrize the non-Gaussianity in the presence of both the adiabatic and isocurvature perturbations because of their different effects on matter spectrum or temperature anisotropy of the CMB (see below), we define four types of non-linerity parameters as following [5],

$$\frac{6}{5} f_{\rm NL}^{\rm (adi)} = \frac{\beta_{\zeta\zeta\zeta}}{\alpha_\zeta^2}, \quad \frac{6}{5} f_{\rm NL}^{\rm (cor1)} = \frac{1}{3}\frac{\beta_{\zeta\zeta S}}{\alpha_\zeta^2}, \quad \frac{6}{5} f_{\rm NL}^{\rm (cor2)} = \frac{1}{9}\frac{\beta_{\zeta S S}}{\alpha_\zeta^2}, \quad \frac{6}{5} f_{\rm NL}^{\rm (iso)} = \frac{1}{27}\frac{\beta_{SSS}}{\alpha_\zeta^2}, \tag{8}$$

where $\alpha_\zeta = N_a N^a$. The first one, $f_{\rm NL}^{\rm (adi)}$, is the "well-known" $f_{\rm NL}$ often used in many literature. However, in general, all the four non-linearity parameters can be concomitant and their effects on the temperature anisotropy have not been investigated in the previous literatures.

Now let us move to their effects on the bispectrum of the CMB anisotropy [3, 5]. From temperature anisotropies originated from the adiabatic and isocurvature perturbations $\Delta T^{\rm (adi)}(\vec{n})$ and $\Delta T^{\rm (iso)}(\vec{n})$ for a given direction $\vec{n}$, we define $a_{\ell m}$ by

$$a_{\ell m} \ = \ \int d\vec{n} \ \left[\frac{\Delta T^{\rm (adi)}(\vec{n})}{T} + \frac{\Delta T^{\rm (iso)}(\vec{n})}{T} \right] Y^*_{\ell m}(\vec{n}). \tag{9}$$

Transfer functions, which connect the curvature perturbation ζ and isocurvature perturbation S to the temperature fluctuation, are defined as $\Theta_\ell^{\rm (adi)}(\vec{k}) \ \equiv \ g_{T\ell}^{\rm (adi)}(k)\zeta_{\vec{k}}$ and $\Theta_\ell^{\rm (iso)}(\vec{k}) \ \equiv \ g_{T\ell}^{\rm (iso)}(k) S_{\vec{k}}$, where $\Theta_\ell^{\rm (adi/iso)}(\vec{k})$ is the multipole moment of CMB temperature anisotropy from the adiabatic/isocurvature perturbation. The angular bispectrum of $a_{\ell m}$, given by

$$\langle a_{\ell_1 m_1} a_{\ell_2 m_2} a_{\ell_3 m_3} \rangle \equiv \ \mathcal{G}^{m_1 m_2 m_3}_{\ell_1 \ell_2 \ell_3} b_{\ell_1 \ell_2 \ell_3}, \tag{10}$$

where $\mathcal{G}^{m_1 m_2 m_3}_{\ell_1 \ell_2 \ell_3} \equiv \int d\vec{n} \ Y_{\ell_1 m_1}(\vec{n}) Y_{\ell_2 m_2}(\vec{n}) Y_{\ell_3 m_3}(\vec{n})$ (Gaunt integral), $b_{\ell_1 \ell_2 \ell_3}$ can be expressed in terms of $f_{\rm NL}$'s defined above and transfer functions. In general $b_{\ell_1 \ell_2 \ell_3}$ has complicated form, and here we focus on the following two terms, which are relevant when the isocurvature perturbation is uncorrelated with the curvature perturbation,

$$b^{\rm (adi)}_{\ell_1 \ell_2 \ell_3} = \frac{48}{5\pi^3} \int_0^\infty dr \ r^2 \int_0^\infty dk_1 \ k_1^2 g^{\rm (adi)}_{T\ell_1}(k_1) j_{\ell_1}(k_1 r) P_\zeta(k_1) \int_0^\infty dk_2 \ k_2^2 g^{\rm (adi)}_{T\ell_2}(k_2) j_{\ell_2}(k_2 r) P_\zeta(k_2)$$
$$\times \int_0^\infty dk_3 \ k_3^2 g^{\rm (adi)}_{T\ell_3}(k_3) j_{\ell_3}(k_3 r) \ f_{\rm NL}^{\rm (adi)} + (2 \text{ perms}), \tag{11}$$

$$b^{\rm (iso)}_{\ell_1 \ell_2 \ell_3} = \frac{1296}{5\pi^3} \int_0^\infty dr \ r^2 \int_0^\infty dk_1 \ k_1^2 g^{\rm (iso)}_{T\ell_1}(k_1) j_{\ell_1}(k_1 r) P_\zeta(k_1) \int_0^\infty dk_2 \ k_2^2 g^{\rm (iso)}_{T\ell_2}(k_2) j_{\ell_2}(k_2 r) P_\zeta(k_2)$$
$$\times \int_0^\infty dk_3 \ k_3^2 g^{\rm (iso)}_{T\ell_3}(k_3) j_{\ell_3}(k_3 r) \ f_{\rm NL}^{\rm (iso)} + (2 \text{ perms}). \tag{12}$$

Total bispectrum in this case is $b_{\ell_1 \ell_2 \ell_3} = b^{\rm (adi)}_{\ell_1 \ell_2 \ell_3} + b^{\rm (iso)}_{\ell_1 \ell_2 \ell_3}$. Expressing these terms as

$$b^{\rm (adi/iso)}_{\ell_1 \ell_2 \ell_3} = b^{\rm L,\,L,\,NL(adi/iso)}_{\ell_1 \ell_2 \ell_3} + b^{\rm L,\,NL,\,L(adi/iso)}_{\ell_1 \ell_2 \ell_3} + b^{\rm NL,\,L,\,L(adi/iso)}_{\ell_1 \ell_2 \ell_3}, \tag{13}$$

we plot the bispectrum of the CMB anisotropy $b^{\rm L,\,L,\,NL}_{\ell_1 \ell_2 \ell_3}$ and $b^{\rm NL,\,L,\,L}_{\ell_1 \ell_2 \ell_3}$ in Fig. 1, for both adiabatic and isocurvature cases with $(6/5) f_{\rm NL}^{\rm (adi)} = 1$ and $(6/5) f_{\rm NL}^{\rm (iso)} = 1/27$, respectively.

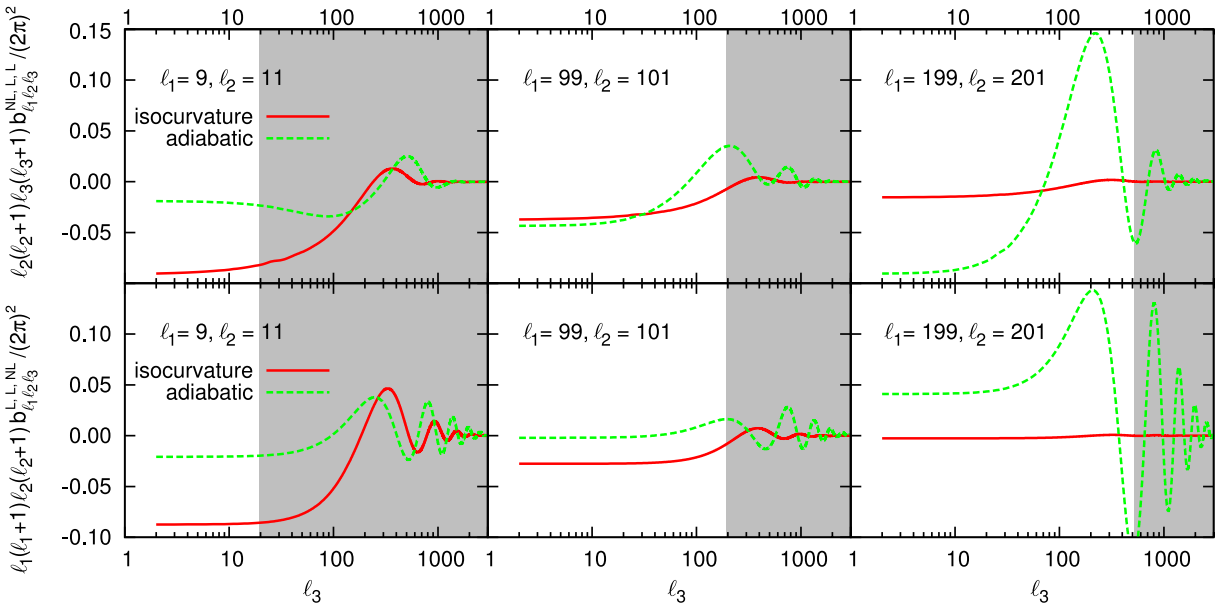

Figure 1: Bispectrum of the CMB anisotropy $b^{\rm NL,\,L,\,L}_{\ell_1\ell_2\ell_3}$ and $b^{\rm L,\,L,\,NL}_{\ell_1\ell_2\ell_3}$ for $(6/5)f^{\rm (adi)}_{\rm NL} = 1$ and $(6/5)f^{\rm (iso)}_{\rm NL} = 1/27$. Shaded regions are unphysical. (Courtesy of T. Sekiguchi.)

3 Application to the axion

In this section we apply our formulation to the axion as a concrete example [3]. The axion, a, is a pseudo Nambu-Goldstone boson associated with the spontaneous breaking of the PQ symmetry. The existence of the axion is strongly motivated, since it naturally solves the strong CP problem in QCD. Let us denote the breaking scale by F_a, whose magnitude is constrained from various experiments, astrophysical and cosmological considerations. The most strict lower bound on F_a comes from the observation of 1987A. In order to prevent too fast cooling by the axion emission, $F_a \gtrsim 10^{10}$ GeV is required. On the other hand, the upper bound is provided by the cosmological argument. The axion obtains a tiny mass after the QCD phase transition due to the anomaly effect which explicitly breaks the PQ symmetry. The axion begins to oscillate coherently after that. Since the lifetime of the axion is very long, it survives until now and contributes to DM of the universe. The abundance is estimated as

$$\Omega_a h^2 \simeq 0.2 \left(\frac{F_a}{10^{12}\ {\rm GeV}}\right)^{-0.82} \left(\frac{a_*}{10^{12}\ {\rm GeV}}\right)^2, \tag{14}$$

where $a_* = \max\{F_a\theta,\ H_{\rm inf}/2\pi\}$ and θ denotes the initial misalignment angle of the axion.

If the PQ symmetry is already broken before or during inflation and if it is never restored after inflation, the axion has unsuppressed quantum fluctuations during inflation because it remains practically massless during inflation. Since the axion contributes to some fraction of DM, such an axionic isocurvature fluctuation is converted to the CDM isocurvature fluctuation. Thus the axion is a plausible candidate for generating the non-Gaussianity from the isocurvature perturbation. The isocurvature perturbation is given by

$$S \simeq \left(\frac{\Omega_a}{\Omega_{\rm CDM}}\right)\left[\frac{2a_i\delta a}{a_*^2} + \left(\frac{\delta a}{a_*}\right)^2\right], \tag{15}$$

where $a_i = F_a\theta$. The second term denotes the non-Gaussian isocurvature fluctuation. In Fig. 2, $f^{\rm (iso)}_{\rm NL}$ is shown for $F_a = 10^{12}$ GeV. Constraint on the uncorrelated isocurvaure perturbation from CMB power spectrum [2] is also shown. Thus we can see that large enough $f^{\rm (iso)}_{\rm NL}$ can be obtained with satisfying the isocurvature constraint.[2]

[2]In the case where the axion rolls down from the top of the cosine-type potential, see Ref. [7].

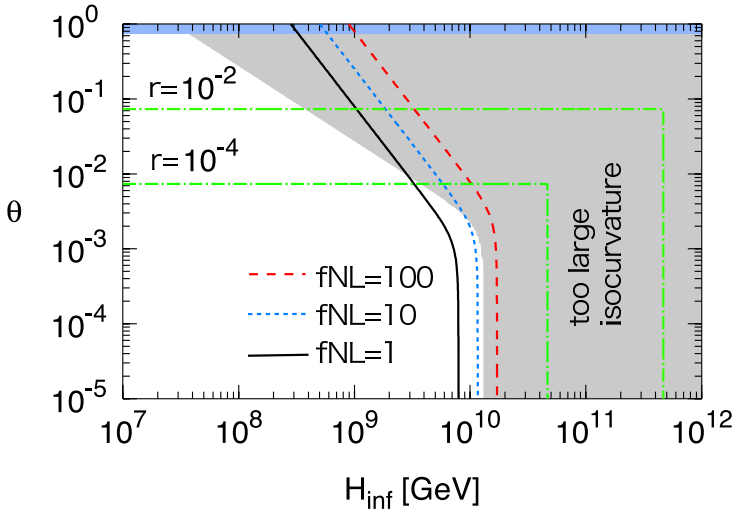

Figure 2: Contours of $f_{\rm NL}^{(\rm iso)}(= 1, 10 \text{ and } 100)$ and $r \equiv \Omega_a/\Omega_{\rm CDM}$ for $F_a = 10^{12}$ GeV.

4 Conclusions

We have investigated a possibility that large non-Gaussianity is generated by isocurvature fluctuations. One interesting feature of this scenario is that the bispectrum and the power spectrum of the CMB temperature fluctuations exhibit characteristic scale dependence. Furthermore, our results indicate that large non-Gaussianity may be accompanied with an observable fraction of the isocurvature perturbation. If future observations confirm both large non-Gaussianity and a certain amount of isocurvature fluctuation component, our scenario will become very attractive. Although we have restricted ourselves to the CDM isocurvature perturbation, the baryonic isocurvature perturbation can also generate large non-Gaussianity in a similar fashion [4]. Another example is a curvaton scenario with correlated CDM (baryonic) isocurvature perturbations [5]. For some recent related works see Refs. [8, 9, 10].

References

[1] A. P. S. Yadav and B. D. Wandelt, Phys. Rev. Lett. **100**, 181301 (2008) [arXiv:0712.1148 [astro-ph]].

[2] E. Komatsu *et al.* [WMAP Collaboration], arXiv:0803.0547 [astro-ph].

[3] M. Kawasaki, K. Nakayama, T. Sekiguchi, T. Suyama and F. Takahashi, JCAP **0811**, 019 (2008) [arXiv:0808.0009 [astro-ph]].

[4] M. Kawasaki, K. Nakayama and F. Takahashi, JCAP **0901**, 002 (2009) [arXiv:0809.2242 [hep-ph]].

[5] M. Kawasaki, K. Nakayama, T. Sekiguchi, T. Suyama and F. Takahashi, arXiv:0810.0208 [astro-ph], to appear in JCAP.

[6] A. D. Linde and V. F. Mukhanov, Phys. Rev. D **56**, 535 (1997) [arXiv:astro-ph/9610219]; N. Bartolo, S. Matarrese and A. Riotto, Phys. Rev. D **65**, 103505 (2002) [arXiv:hep-ph/0112261]; L. Boubekeur and D. H. Lyth, Phys. Rev. D **73**, 021301 (2006) [arXiv:astro-ph/0504046].

[7] M. Kawasaki, K. Nakayama and F. Takahashi, JCAP **0901**, 026 (2009) [arXiv:0810.1585 [hep-ph]].

[8] D. Langlois, F. Vernizzi and D. Wands, JCAP **0812**, 004 (2008) [arXiv:0809.4646 [astro-ph]].

[9] T. Moroi and T. Takahashi, arXiv:0810.0189 [hep-ph].

[10] C. Hikage, K. Koyama, T. Matsubara, T. Takahashi and M. Yamaguchi, arXiv:0812.3500 [astro-ph].

Large non-Gaussianity from multi-brid in ation

Atsushi Naruko [1] and Misao Sasaki[2]

Yukawa Institute for Theoretical Physics, Kyoto University, Kyoto 606–8502, Japan

Abstract

A model of multi-component hybrid in ation, dubbed multi-brid in ation, which may yield a large non-Gaussian paramter f_{NL}, was proposed recently. In particular, for a two-brid in ation model with an exponential potential and the condition that the end of in ation is an ellipse in the eld space, it was found that, while keeping the other observational quantities within the range consistent with observations, large non-Gaussianity is possible for certain in ationary trajectories. In this talk, in order to see if this result is a general feature of multi-brid in ation, we consider a model with a potential with an exponent quadratic in the scalar eld components. We also consider a more general class of ellipses for the end of in ation. Focusing on the case of two-brid in ation, we nd that large non-Gaussianity is also possible in the present model. Then by tuning the model parameters, we nd that there exist models for which both the non-Gaussianity and the tensor-to-scalar ratio are large enough to be detected in the very near future.

1 Introduction

The primordial non-Gaussianity has been one of the hottest topics in cosmology in recent years. The conventional, single- eld slow-roll in ation predicts that the curvature perturbation is Gaussian to an extremely high accuracy. In other words, if any primordial non-Gaussianity is detected, it strongly indicates that the dynamics of in ation is not as simple as we thought it to be.

The primordial non-Gaussianity is conveniently represented by a parameter denoted by f_{NL} [1]. Roughly, it is the ratio of the 3-point correlation function (or the bispectrum) to the square of the 2-point correlation function (or the square of the spectrum). It is expected that near-future experiments such as those of PLANCK will be able to detect f_{NL} at a level as small as 5 [2].

Finding even a small deviation from Gaussianity will have profound implications on the theory of the early universe. Consequently, numerous types of in ationary models that produce detectable non-Gaussianity have been proposed and studied. In terms of the nature of non-Gaussianities, most of these models can be classi ed into two categories; those with non-Gaussianities arising intrinsically from the quantum uctuations, and those with non-Gaussianities due to nontrivial classical dynamics on superhorizon scales. A typical example of the former is the DBI in ation, in which the slow-roll condition can be fully violated. In this case, the equilateral f_{NL} (denoted by $f_{NL}^{\rm equil}$) representing the amplitude of the bispectrum of the equilateral con gurations, is found to play an important role. On the other hand, in the latter case where non-Gaussianities are produced on superhorizon scales, by causality the local f_{NL} (denoted by $f_{NL}^{\rm local}$) characterizes the level of the non-Gaussianity. It is de ned in terms of the coe cient in front of the second order curvature perturbation [1],

$$= \ _L + f_{NL}^{\rm local} \ ^2_L \, , \tag{1}$$

where is the curvature perturbation on the Newtonian slice and $_L$ is its linear, Gaussian part.

In this paper, we focus on the latter case, that is, we consider models that may produce a large value of $f_{NL}^{\rm local}$, for example 10–100. More speci cally, we consider hybrid in ation with multiple in aton elds, dubbed multi-brid in ation [3]. The in aton elds are assumed to follow the slow-roll equations of motion, and their uctuations are assumed to be Gaussian. In this case, the N formalism is most useful for the evaluation of the curvature perturbation and non-Gaussianity [4].

[1]E-mail:naruko@yukawa.kyoto-u.ac.jp
[2]E-mail:misao@yukawa.kyoto-u.ac.jp

As in the conventional hybrid in ation, the in aton elds are coupled to a water-fall eld, and in ation ends when the in aton elds satisfy a certain condition that triggers the instability of the water-fall eld. However, unlike the case of a single in aton eld in which there is essentially no degree of freedom in the condition for the end of in ation, there is a substantial increase in the degree of freedom at the end of in ation in multi-brid in ation and it widens the viable range of the parameter space considerably and leads to the possibility of generating large non-Gaussianity.

As a model of multi-brid in ation, an analytically solvable two-brid in ation model was recently investigated in detail [3], where the potential was assumed to be exponential with the exponent given by a linear combination of the in aton elds. In this paper, we consider a two-brid model with again an exponential potential but with the exponent given by a quadratic function of the in aton elds. The potential has point symmetry about the origin of the eld space, in contrast to the case of the linear exponent which has no symmetry. Thus by investigating the quadratic case, we will be able to see if the generation of large non-Gaussianity is a generic feature of multi-brid in ation or if it is due to the lack of symmetry that leads to large non-Gaussianity in the linear exponent case.

2 Two-brid in ation

We consider a two-component scalar eld whose action is given by

$$S = \int d^4x\sqrt{\ g}\left[\frac{1}{2}g^{\mu\nu}\sum_{A=1,2}\partial_\mu\ \ _A\partial_\nu\ \ _A + V(\ \ )\right], \tag{2}$$

where the potential is given by

$$V = V_0(\ \ ,\ \ _1,\ \ _2)\exp\ \ \frac{1}{2}\ \ m_1^2\ \ _1^2 + m_2^2\ \ _2^2\ \ \ , \tag{3}$$

with V_0 being a function of a water-fall eld as well as of $_1$ and $_2$, but is assumed to be constant in time during in ation.

The slow-roll equations of motion are obtained by neglecting the kinetic term in the Friedmann equation and the second time derivative in the eld equations. Thus the slow-roll equations of motion are

$$3H^2 = V\,, \quad \frac{d\ \ _A}{dN} = \frac{1}{V}\frac{\partial V}{\partial\ \ _A} = m_A^2\ \ _A\,, \tag{4}$$

where $H = \dot{a}/a$ and the dot $\dot{}$ denotes a derivative with respect to the cosmic proper time. The number of e-folds counted backwards in time, $dN = \ \ Hdt$, is used as the time variable for later convenience. Hence we immediately obtain

$$N = \frac{1}{2}\ln\left[\ \ {}^{2/m_1^2}_{1} + \ \ {}^{2/m_2^2}_{2}\right]\ \ \ \frac{1}{2}\ln\left[\ \ {}^{2/m_1^2}_{1,f} + \ \ {}^{2/m_2^2}_{2,f}\right], \tag{5}$$

where the number of e-folds is set to zero at the end of in ation and $_{A,f}$ is the nal value of the in aton elds.

We assume that in ation ends at

$$^2 = G(\ \ _1,\ \ _2)\ \ \ g_1^2(\ \ _1\cos\ \ +\ \ _2\sin\ \ )^2 + g_2^2(\ \ \ _1\sin\ \ +\ \ _2\cos\ \ )^2\,, \tag{6}$$

which is realized by the potential V_0 given by

$$V_0 = \frac{1}{2}G(\ \ _1,\ \ _2)\ \ ^2 + \frac{\lambda}{4}\ \ \ ^2\ \ \ \frac{^2}{\lambda}\ \ ^2\,. \tag{7}$$

We parametrize the scalar elds at the end of in ation as

$$\frac{}{g_1}\cos\ \ =\ \ _{1,f}\cos\ \ +\ \ _{2,f}\sin\ \ \ ,\ \ \ \frac{}{g_2}\sin\ \ =\ \ \ _{1,f}\sin\ \ +\ \ _{2,f}\cos\ \ \ , \tag{8}$$

The angle describes the amount of rotation of the ellipse relative to the $_1$ and $_2$ axes. The angle describes the position of the in aton trajectory at the end of in ation.

Since there is a constant of motion from Eq.(4), we have

$$\frac{\ln\ _1}{m_1^2}\quad\frac{\ln\ _2}{m_2^2}=\frac{1}{m_1^2}\ln\frac{}{g_1g_2}(g_2\cos\quad\cos\qquad g_1\sin\quad\sin\ )\quad\frac{1}{m_2^2}\ln\frac{}{g_1g_2}(g_2\sin\quad\cos\qquad g_1\cos\quad\sin\ ). \tag{9}$$

This equation determines the parameter in terms of $_1$ and $_2$: $=(\ _1,\ _2)$. Hence, from Eq. (8), $_{1,f}$ and $_{2,f}$ become functions of $_1$ and $_2$,

$$_{1,f}=\ _{1,f}(\ _1,\ _2)\,,\qquad _{2,f}=\ _{2,f}(\ _1,\ _2)\,. \tag{10}$$

With this understanding, the number of e-folds given by Eq. (5) becomes a function of $(\ _1,\ _2)$. It is then straightforward to obtain N to full nonlinear order. It can be straightforwardly calculated as

$$N=N(\ _1+\quad_1,\ _2+\quad_2)\quad N(\ _1,\ _2)\,. \tag{11}$$

3 Case for large non-Gaussianity

In this section, we compute the curvature perturbation of our model explicitly, and evaluate the curvature perturbation spectrum $\mathcal{P}_S$, the spectral index n_S, the tensor-to-scalar ratio r, and the non-Gaussianity parameter $f_{NL}^{\rm local}$. But, because these expressions are very complicated, it is not easy to study all possible cases in detail. However, there are some limiting cases in which we have a substantially simpli ed expression for $\mathcal{P}_S, n_S, r$ and $f_{NL}^{\rm local}$, but which are yet su ciently of interest.

One case of interest is when the two masses are equal, $m_1=m_2$. In this case, the potential during in ation is $O(2)$ symmetric. This symmetry is broken at the end of in ation because of condition (6), unless $g_1=g_2$. This model was discussed by Alabidi and Lyth [5] as a new mechanism of generating curvature perturbations. Another case of interest is when the ratio of the mass parameters are large, for example, $m_1\gg m_2$.

Using N-formalism, the expressions of $\mathcal{P}_S, n_S, r$ and $f_{NL}^{\rm local}$ are given. In equal mass case, the formulas simplify considerably to

$$\mathcal{P}_S\quad=\quad\frac{g}{m^2e^{m^2N_k}}\ ^2\frac{1+\cos2\quad\cos2}{2}\quad\frac{H}{2}\ ^2_{t_k}=\frac{8}{r}\quad\frac{H}{2}\ ^2_{t_k}\,, \tag{12}$$

$$n_S\quad1\quad=\quad2m^2\quad2\quad\frac{m^2e^{m^2N_k}}{g}\Bigg)^2\frac{1\quad\cos2\quad\cos2}{\sin^2 2}=2m^2\quad\frac{r}{8}\frac{1\quad\cos^2 2\quad\cos^2 2}{\sin^2 2}\,, \tag{13}$$

$$r\quad=\quad8\quad\frac{m^2e^{m^2N_k}}{g}\Bigg)^2\frac{2}{1+\cos2\quad\cos2}\,, \tag{14}$$

$$f_{NL}^{\rm local}\quad=\quad\frac{5m^2}{6}\left\{\quad\frac{\cos2\quad\sin2}{1+\cos2\quad\cos2}\ ^2\qquad1\right\}\,, \tag{15}$$

here g and is giben by $g=\sqrt{g_1^2+g_2^2}$ and $\tan\ =g_2/g_1$ respectively. Note that the -dependence has disappeared because of the symmetry.

As is clear from Eq. (15) for $f_{NL}^{\rm local}$, in order to obtain large non-Gaussianity, it is necessary for the factor in the curly brackets to become large, that is, $\cos2\quad\sin2\ /(1+\cos2\quad\cos2\ )\gg1$. This is possible either in the limit $(\ ,\ )\to(0,\ /2)$ or $(\ ,\ )\to(\ /2,0)$. Since these two limits are equivalent, let us take the limit $(\ ,\ )\to(0,\ /2)$. This corresponds to the situation in which the ellipse is highly elongated and the in aton trajectory hits the ellipse close to one of the tips of the majoraxis.

To investigate in more detail the theoretical predictions of this model, let us derive expressions for r and $f_{NL}^{\rm local}$ in terms of the observational data as much as possible. We x the amplitude of the spectrum $\mathcal{P}_S$ and the spectral index n_S. The WMAP normalization at the present Hubble horizon scale and the

WMAP 5-year analysis [6] gives

$$\mathcal{P}_S = \frac{8}{r}\left(\frac{H}{2}\right)^2_{t_k} = 2.5 \quad 10^{-9}, \qquad n_S = 0.96^{+0.014}_{-0.015}. \tag{16}$$

Below we replace $\mathcal{P}_S$ and n_S by these observed values.

The useful expression may be obtained by combining the two expressions of r and $f_{NL}^{\rm local}$:

$$f_{NL}^{\rm local} \quad 52\left(\frac{r}{0.1}\right)\left(\frac{10^{-4}}{2}\right)\left(\frac{m^2}{m^2+0.02}\right). \tag{17}$$

This tells us that for $m^2 > 0.02$, in the very near future, both r and $f_{NL}^{\rm local}$ may be large enough to be detected upon tuning the model parameters to some extent. As we can see, although the values of $f_{NL}^{\rm local}$ and r are relatively sensitive to the values of m^2 and , there indeed exist models with large $f_{NL}^{\rm local}$ and r simultaneously.

4 conclusion

We analytically investigated the curvature perturbation and its non-Gaussianity in a model of multi- eld hybrid in ation, dubbed *multi-brid* in ation. The model we considered is a two- eld hybrid in ation (two-brid in ation) model with the potential mimicking conventional quadratic potentials. The new ingredient of the model is the generalization of the condition for the end of in ation. We considered a very general coupling of the two in aton elds to a water-fall eld.

Then, using the N formula, we derived an analytical expression for the curvature perturbation. Based on this expression, we obtained the curvature perturbation spectrum $\mathcal{P}_S$, the spectral index n_S, the tensor-to-scalar ratio r, and the non-Gaussian parameter $f_{NL}^{\rm local}$. We found that a large positive $f_{NL}^{\rm local}$ is possible in this model. Then, at least for a certain limited range of the parameters, we explicitly showed that it is possible to have large non-Gaussianity while keeping the values of the other quantities consistent with those of the observation. In particular, we showed that when the two in aton masses are equal, the parameters can be tuned so that they lead to a fairly large tensor-to-scalar ratio, r 0.1, as well as a large non-Gaussian parameter, $f_{NL}^{\rm local}$ 50. These values will be at a detectable level in the very near future. On the other hand, interestingly, we found that having a large mass ratio in the present model does not help in producing both r and $f_{NL}^{\rm local}$ large enough to be detected. This is in contrast to the model studied in [3].

The standard lore has been that $f_{NL}^{\rm local}$ is too small for models with large r or vice versa. We have shown, in this paper, not be the case, particularly in this model of spontaneously symmetry breaking at the end of in ation. This may be the most important conclusion of this work. At the moment, we have no clear physical explanation for this result. We hope we will be able to answer this question in the near future.

References

[1] E. Komatsu and D. N. Spergel, Phys. Rev. D **63** (2001), 063002; astro-ph/0005036.

[2] D. Babich and M. Zaldarriaga, Phys. Rev. D **70** (2004), 083005; astro-ph/0408455.

[3] M. Sasaki, Prog. Theor. Phys. **120** (2008), 159; arXiv:0805.0974 .

[4] D. H. Lyth, K. A. Malik and M. Sasaki, J. Cosmol. Astropart **0505** (2005), 004; astro-ph/0411220.

[5] L. Alabidi and D. Lyth, JCAP **0608**, 006 (2006) [arXiv:astro-ph/0604569].

[6] E. Komatsu *et al.* (WMAP Collaboration), arXiv:0803.0547.

Viscosity and Entropy Bounds from Black Hole Physics

Ishwaree P. Neupane [1]

Department of Physics and Astronomy, Rutherford Building, University of Canterbury
Private Bag 4800, Christchurch 8041, New Zealand

Abstract

The gauge theory - gravity duality has provided us a way of studying QCD at high energies or short distances from straightforward calculations in classical general relativity. Among numerous results obtained so far, one of the most striking is the universality of the ratio of the shear viscosity to the entropy density. For all gauge theories with Einstein gravity dual this ratio has been found to be $\eta/s = 1/4\pi$. In this talk, we consider higher curvature-corrected black hole solutions for which η/s can be smaller than $1/4\pi$, thus violating the conjecture bound. Here we shall argue that the Gauss-Bonnet and (Riemann)^2 gravities, in particular, provide concrete examples in which inconsistency of a theory, such as, a violation of microcausality at short distances, and a classical limit on black hole entropy are correlated.

1 Introduction

Anti de Sitter conformal field theory (CFT) correspondence [1] has proven an excellent tool to study strongly coupled gauge theories. Through AdS holography one can also study hydrodynamic properties of a certain class of boundary CFTs. Indeed, for a large class of four-dimensional CFTs, the ratio of the shear viscosity η to the entropy density s is (in units where $\hbar = k_B = 1$) given by [2],

$$\frac{\eta}{s} = \frac{1}{4\pi}. \tag{1}$$

This result is universal for all theories with Einstein gravity dual. The reason of this uniqueness is due to the fact that in pure Einstein gravity all black holes satisfy the Bekenstein-Hawking entropy law

$$\mathcal{S} = \frac{k_B c^3}{\hbar}\frac{A}{4G_N}, \tag{2}$$

where $\hbar$ is the Planck's constant, A is the area of the horizon corresponding to the surface at $r = r_+$ and G_N is the Newton's constant. However, the ratio η/s can be different from $1/4\pi$ in general gravity theories (with higher derivative or higher-curvature corrections). A violation of causality may occur in the boundary CFT when η/s is too low. This violation can be related to black hole entropy bounds.

To establish better contact with QCD via AdS holography, it is essential to understand the effect of curvature corrections to Einstein-Hilbert action in the holographic framework, see [3] and references therein. As the simplest modification to Einstein gravity, we consider the following quadratic action

$$I = \frac{1}{16\pi G_N}\int d^dx\sqrt{-g}\left[R - 2\Lambda + \alpha' L^2\left(aR^2 + bR_{\mu\nu}R^{\mu\nu} + cR_{\mu\nu\lambda\rho}R^{\mu\nu\lambda\rho}\right)\right], \tag{3}$$

where α' is a dimensionless coupling and the bulk cosmological term $\Lambda = -(d-1)(d-2)/2L^2$. We will focus our discussion to the gravity sector in AdS_5, for which we have from AdS/CFT dictionary, $G_N \equiv (\pi L^3/4N_c^2)$ and $L = (4\pi g_s N_c)^{1/4}\ell_s$, where ℓ_s is the string scale and g_s the string coupling and N_c is the number of color charges or rank of the gauge group. Since $\alpha' \sim 1/\sqrt{\lambda}$, in the dual supergravity description, a small α' corresponds to the strong coupling limit, $\lambda \equiv g_{YM}^2 N_c \gg 1$. The Gauss-Bonnet (GB) term obtained by setting $a = c = 1$ and $b = -4$ in (3), in which case the equations of motion are

[1] E-mail:ishwaree.neupane@canterbury.ac.nz

second order in the metric and there would be no need to treat α' as small. For a class of CFTs in flat space with Gauss-Bonnet gravity dual, we find [4]

$$\frac{\eta}{s} = \frac{1}{4\pi}\left(1 - \frac{2(d-1)\lambda_{GB}}{(d-3)}\right), \tag{4}$$

where $\lambda_{\rm GB} \equiv (d-3)(d-4)\alpha'$, which is smaller than $1/4\pi$ with $\lambda_{\rm GB} > 0$. Based on the bulk causal structure of an AdS_5 black brane solution, the authors of [4] found a more stronger bound for $\lambda_{\rm GB}$, i.e.

$$\lambda_{\rm GB} < \frac{9}{100}, \quad \text{or, equivalently,} \quad \frac{\eta}{s} \geq \frac{16}{25}\left(\frac{1}{4\pi}\right), \tag{5}$$

which otherwise violates a microcausality in the dual CFT defined on a flat hypersurface. Here we argue that the critical value of $\lambda_{\rm GB}$ beyond which the theory becomes inconsistent is related to the entropy bound for a large class of AdS black holes. Further, in the holographic context, we find that the AdS black hole solutions with spherical and hyperbolic event horizons allow much wider possibilities for η/s [5].

2 Entropy and Viscosity Bounds

For pure AdS GB black hole solutions, the entropy and Hawking temperature are given by [6]

$$\mathcal{S} = \frac{A}{4G_N}\left(1 + \frac{2(d-2)k\lambda_{\rm GB}}{(d-4)x^2}\right), \quad T = \frac{(d-1)x^4 + k(d-3)x^2 + (d-5)k^2\lambda_{\rm GB}}{4\pi L x(x^2 + 2k\lambda_{\rm GB})} \tag{6}$$

(in units $c = \hbar = k_B = 1$) where $x \equiv r_+/L$, $A \equiv V_{d-2} r_+^{d-2}$, with V_{d-2} being the unit volume of the base manifold or hypersurface $\mathcal{M}$. The entropy of a GB black hole depends on the curvature constant k, whose value determines the geometry of event horizon $\mathcal{M} = \mathrm{S}^{d-2}, \mathbb{R}^{d-2}$ and H^{d-2}, respectively, for $k = +1$, $k = 0$ and $k = -1$ [2]. Especially, at the $k = -1$ extremal state with zero Hawking temperature,

$$\mathcal{S}|_{T\to 0} = \frac{V_3}{G_N}\frac{L^3}{2^{7/2}}\left(1 - 12\lambda_{\rm GB}\right), \qquad E|_{T\to 0} = 0. \tag{7}$$

Thus, beyond a critical coupling $\lambda_{\rm GB} > \lambda_{\rm crit}$, the entropy $\mathcal{S}$ becomes negative, which indicates a violation of cosmic censorship or the second law of the thermodynamics. In the AdS_5 case, $\lambda_{\rm crit} = 1/12$. This critical value of $\lambda_{\rm GB}$ above which the theory is inconsistent nearly coincides with the bound $\lambda_{\rm GB} < 9/100$ required for a consistent formulation of a class of CFTs with Gauss-Bonnet gravity dual.

Next let us consider small metric fluctuations $\phi = h^1_2$ around an AdS GB black hole metric

$$ds^2 = -\frac{r_+^2}{L^2} f(z) N_*^2 dt^2 + \frac{L^2}{f(z)}\,dz^2 + \frac{r_+^2 z^2}{L^2}\left(\frac{dx_3^2}{1-kx_3^2} + x_3^2\sum_{i=1}^{2} dx_i^2 + 2\phi(t, x_3, z) dx_1 dx_2\right), \tag{8}$$

where $k = 0, \pm 1$ and $N_* \equiv a = [(1 + \sqrt{1 - 4\lambda_{\rm GB}})/2]^{1/2}$. The scalar metric fluctuation

$$\phi(t, x_3, z) = \int \frac{dw dq}{(2\pi)^3}\,\phi(z; k)\, e^{-iwt + iqx_3}, \quad \phi(z; -k) = \phi^*(z, k), \tag{9}$$

(where $k = (w, 0, 0, q)$) satisfies the following (linearized) equation of motion

$$K\partial_z^2\phi + \partial_z K \partial_z \phi + K_2 \phi = 0. \tag{10}$$

This structure is not affected by Maxwell type charges but can be affected by scalar charges. In pure GB gravity, $K = z^2\tilde{f}\,(z - \lambda_{\rm GB}\partial_z f)\,, \quad K_2 = (z^2\tilde{w}^2/N_*^2 f)\,(z - \lambda_{\rm GB}\partial_z f) - z(1 - \lambda_{\rm GB}\partial_z^2\tilde{f})\left(\tilde{q}^2 + 2\tilde{k}\right)$,

$$f(z) = \tilde{k} + \frac{z^2}{2\lambda_{\rm GB}}\left[1 - \sqrt{1 - 4\lambda_{\rm GB} + \frac{4\lambda_{\rm GB}}{z^4}\left(1 + \frac{k}{x^2} + \frac{\lambda_{\rm GB}k^2}{x^4}\right)}\right],$$

[2] The GB term is topological in $d = 4$, especially, with a constant coupling, $\alpha' L^2 = \text{const}$, so we shall take $d \geq 5$.

where $z \equiv r/r_+$, $x \equiv r_+/L$, $\tilde{k} = k/x^2$, $\tilde{w} \equiv wL/x$ and $\tilde{q} \equiv qL/x$. Equation (10) may be solved with the following incoming boundary conditions at the horizon: $\phi(z;k) = a_{\rm in}(k)\phi_{\rm in}(z;k) + a_{\rm out}(k)\phi_{\rm out}(z;k)$, $a_{\rm out} \equiv 0$ and $a_{\rm in} \equiv J(k)$, where $J(k)$ is an infinitesimal boundary source for the fluctuating field ϕ. To the leading order in $\tilde{w}$, and in the limit $\tilde{q} \to 0$, the solution is given by [5]

$$\phi(z;k) = J(k)\left[1 + \frac{i\tilde{w}}{4N_*}a^2\sqrt{1-4\lambda_{\rm GB}}\left(\frac{1}{z^4} - \frac{4\lambda_{\rm GB}\tilde{k}}{3(1+\sqrt{1-4\lambda_{\rm GB}})}\frac{1}{z^6} + \mathcal{O}(z^{-8})\right) + \mathcal{O}(\tilde{w}^2)\right]. \tag{11}$$

By identifying $\phi \sim T^2_1$, one obtains the retarded two-point Green's function

$$G^R_{12,12}(w,0) = -i\int d^4x e^{iwt}\theta(t)\langle[T_{12}(t,\vec{x}), T_{12}(0,\vec{0})]\rangle, \tag{12}$$

which satisfies $G^A(w,\vec{q}) \equiv G^R(w,\vec{q})^*$. The shear viscosity η is obtained by using the Kubo formula

$$\eta = \lim_{w\to 0}\frac{1}{2iw}\left[G^A_{12,12}(w,0) - G^R_{12,12}(w,0)\right] \equiv \lim_{w\to 0}\frac{1}{w}{\rm Im}G^R_{12,12}(w,0). \tag{13}$$

It is not difficult to see that the curvature on a boundary does not affect the result on a flat hypersurface, namely $\eta = \frac{1}{16\pi G_N}\left(\frac{r_+^3}{L^3}\right)(1-4\lambda_{\rm GB})$. However, the ratio η/s is modified to be

$$\frac{\eta}{s} = \frac{1}{4\pi}\frac{(1-4\lambda_{\rm GB})}{(1+6\tilde{k}\lambda_{\rm GB})}. \tag{14}$$

One obtains the standard result in Einstein gravity, i.e. $\eta/s = 1/4\pi$, only at a fixed $\tilde{k}$, i.e. when $k=-1$ and $x = r_+/L = \sqrt{3/2}$. The minimum of entropy density occurs at $x = \sqrt{1/2}$, implying that

$$s = \frac{1}{G_N}\frac{1}{2^{7/2}}(1-12\lambda_{\rm GB}), \quad \eta = \frac{1}{4\pi G_N}\frac{1}{2^{7/2}}(1-4\lambda_{\rm GB}). \tag{15}$$

The positivity of extremal entropy density implies $\lambda_{\rm GB} \le 1/12$ and hence $\eta/s \ge 1/6\pi$ for $k=0$ and $\eta/s \le 5/12\pi$ for $k=-1$. Quite remarkably, the lower bound $\eta/s \approx 0.66/4\pi$ is similar to a lower value of η/s anticipated at relativistic heavy ion collision experiments [7]. In the $k=+1$ case, the lower bound on η/s could be very close to that in flat space which however arises as a consequence of boundary causality, which requires that the square of local speed of graviton on a constant z-hypersurface is less than unity,

$$c_g^2 = 1 - \left(\frac{5}{2} - \frac{2}{1-4\lambda_{GB}} + \frac{1}{2\sqrt{1-4\lambda_{GB}}}\right)\frac{1}{z^4} + \mathcal{O}(z^{-8}) < 1$$

or $\lambda_{GB} < 0.09$. This limit is only very weakly affected by the Maxwell term $F_{\mu\nu}F^{\mu\nu}$ and the possible F^4 type corrections to Maxwell field [8, 9]. In $d=6$ and $d=7$, the consistency of GB gravity requires

$$\lambda^{d=6}_{\rm GB} \lesssim 0.1380, \qquad \lambda^{d=7}_{\rm GB} \lesssim 0.1905. \tag{16}$$

Next consider the (Riemann)^2 gravity which is obtained by setting $a=b=0$ in eq. (3), for which [5]

$$\eta = \frac{r_+^3 N_c^2}{4\pi^2 L^3}\left(1 - 4\lambda_{\rm Riem} + \mathcal{O}(\lambda^2_{\rm Riem})\right), \quad s = \frac{r_+^3 N_c^2}{\pi L^3}\left(1 + 4\lambda_{\rm Riem}\left(1+\frac{3}{2}\tilde{k}\right) + \mathcal{O}(\lambda^2_{\rm Riem})\right). \tag{17}$$

For a class of boundary field theories with (Riemann)^2 gravity dual in flat space ($k=0$), this yields

$$\frac{\eta}{s} = \frac{1}{4\pi}\left(\frac{1-4\lambda_{\rm Riem}}{1+4\lambda_{\rm Riem}}\right) \approx \frac{1}{4\pi}(1-8\lambda_{\rm Riem}) = \frac{1}{4\pi}\left(1-\frac{1}{N_c}\right). \tag{18}$$

The limit $\lambda_{\rm Riem} > 1/8$ is the same as implied by the positivity of extremal entropy of a (Riemann)^2 black hole. Taking into account all three possibilities for the boundary topology that $k=0$ or $k=\pm 1$, we find

$$0 < \frac{\eta}{s} \le \frac{3}{2}\left(\frac{1}{4\pi}\right). \tag{19}$$

It would be interesting to know whether either of these limits applies to nuclear matter at extreme densities and temperatures, or heavy ion collision experiments and study further a universality of the result $\eta/s \approx 1/4\pi$ through numerical hydrodynamic simulations of data from RHIC and LHC.

3 Conclusion

The Gauss-Bonnet gravity with a coupling $\lambda_{GB} < 1/4$ could be viewed as a classical limit of a consistent theory of quantum gravity. It is conceivable that the bound on the shear viscosity of any fluid in terms of its entropy density is saturated, $\eta/s = 1/4\pi$, for gauge theories at large 't Hooft coupling, which correspond to the cases where all higher-order curvature contributions are absent. But this bound is naturally in immediate threat of being violated in the presence of generic higher-order curvature corrections to the Einstein-Hilbert action. It is remarkable that by tuning of the Gauss-Bonnet and/or generic higher curvature couplings, the ratio η/s can be adjusted to a small positive value.

In this note, the limits on GB coupling are imposed by demanding the positivity of extremal black hole entropy and non-violation of boundary causality. We have not found any obvious explicit bound on λ_{GB} from the thermodynamics of spherically symmetric AdS Gauss-Bonnet black holes, which could however arise as a consequence of causality violation of a boundary CFT. The critical value of λ_{GB} beyond which the theory becomes inconsistent is found to be related to the entropy bound for an AdS GB black hole with a hyperbolic or Euclidean anti-de Sitter event horizon. This remark applies also to the $(\text{Riemann})^2$ gravity. Some other inconsistencies of higher-derivative gravity, such as an appearance of tacyonic mode, or semi-classical instability at short distances, are often related to a classical limit on black hole entropy.

Finally, we make the following remark. In the presence of a Maxwell type charge q, the ratio η/s is generally modified, which is given by $4\pi(\eta/s) = 1 - 4\lambda_{\rm GB}(1 - a/2)$, where $a \equiv q^2L^6/r_+^2$. In the extremal limit ($a \to 2$), one may restrict the coupling $\lambda_{\rm GB}$ such that $\lambda_{\rm GB} \leq 1/24$. The latter ensures that the gravitational potential of a black brane is positive and bounded. The conjecture bound $\eta/s \geq 1/4\pi$ is saturated only in the extremal limit, while in general it is violated also by charged Gauss-Bonnet black brane solutions. The bound $4\pi(\eta/s) \geq 5/6$ found in [8] with a nonzero charge is stronger than for pure EGB gravity in flat space, namely $4\pi(\eta/s) \geq 2/3$. In $d = 5$ dimensions, the entropy of a GB black hole could be negative for $\frac{1}{12} < \lambda_{\rm GB} < 1/4$, leading to a possible violation of unitarity in this range. This suggests some deeper connections between bulk causality violation and limits on black hole entropy.

Acknowledgments

This talk is based on a published work in collaboration with Naresh Dadhich. This work is supported by the New Zealand Foundation for Research, Science and Technology Grant No. E5229 and also by Elizabeth Ellen Dalton Grant No. 5393.

References

[1] O. Aharony, S. S. Gubser, J. M. Maldacena, H. Ooguri and Y. Oz, Phys. Rept. **323**, 183 (2000).

[2] P. Kovtun, D. T. Son and A. O. Starinets, Phys. Rev. Lett. **94**, 111601 (2005); D. T. Son and A. O. Starinets, Ann. Rev. Nucl. Part. Sci. **57**, 95 (2007).

[3] Y. M. Cho and I. P. Neupane, Phys. Rev. D **66**, 024044 (2002). R.-G. Cai, Phys. Rev. D **65**, 084014 (2002); M. Cvetic, S. Nojiri and S. D. Odintsov, Nucl. Phys. B **628**, 295 (2002).

[4] M. Brigante, H. Liu, R. C. Myers, S. Shenker and S. Yaida, Phys. Rev. Lett. **100**, 191601 (2008); *ibid*, Phys. Rev. D **77**, 126006 (2008); Y. Kats and P. Petrov, arXiv:0712.0743 [hep-th].

[5] I. P. Neupane and N. Dadhich, Class. Quant. Grav. **26**, 015013 (2009).

[6] I. P. Neupane, Phys. Rev. D **67**, 061501 (2003); Phys. Rev. D **69**, 084011 (2004).

[7] D. Molnar and P. Huovinen, Phys. Rev. Lett. **94**, 012302 (2005); P. Romatschke and U. Romatschke, Phys. Rev. Lett. **99**, 172301 (2007).

[8] X. H. Ge, Y. Matsuo, F. W. Shu, S. J. Sin and T. Tsukioka, arXiv:0808.2354 [hep-th].

[9] R. G. Cai, Z. Y. Nie and Y. W. Sun, Phys. Rev. D **78**, 126007 (2008).

Does the Entropy-Area Law hold for Schwarzschild-de Sitter spacetime ?

Hiromi Saida[1]

Department of Physics, Daido Institute of Technology, Minami-ku, Nagoya 457–8530, Japan

Abstract

Multi-horizon means multi-temperature unless all of the Hawking temperatures of horizons coincide. Multi-temperature system is a nonequilibrium system, and generally the equation of state in nonequilibrium is different form that in equilibrium. This may imply that the horizon entropies in multi-horizon spacetime do not satisfy the entropy-area law which is an equation of state of a horizon in thermal equilibrium. This report examines whether the entropy-area law holds for Schwarzschild-de Sitter (SdS) spacetime, which is two-temperature system due to the difference of Hawking temperatures of black hole event horizon (BEH) and cosmological event horizon (CEH). We propose a reasonable evidence of breakdown of entropy-area law for CEH in SdS spacetime. The validity of the law for BEH in SdS spacetime can not be judged, but we point out the key issue for BEH's entropy.

1 Simple question from the Nonequilibrium viewpoint

Entropy-area law, which claims the entropy of horizon is equal to one quarter of its spatial area, is the equation of state for equilibrium systems which consist of horizons and matter fields. Now this law seems accepted as the universal law of thermodynamic aspects of any horizon in thermal equilibrium. However nothing is known about nonequilibrium situations of horizons.

On the other hand, generally in nonequilibrium physics, once the system under consideration comes in a nonequilibrium state, the equation of state for nonequilibrium case takes different form in comparison with that for equilibrium case. Especially the nonequilibrium entropy deviates from the equilibrium entropy (when a nonequilibrium entropy is well defined). Indeed, although a quite general formulation of nonequilibrium thermodynamics remains unknown at present [2], the differences of nonequilibrium entropy from equilibrium one are already revealed for some restricted class of nonequilibrium systems [1].

Then, for horizon systems, a simple question arises; *does the entropy-area law of horizons hold for horizon systems in nonequilibrium states?* We try to resolve this question and discuss *to what extent the entropy-area law is universal.* The representative nonequilibrium system of horizons may be multi-horizon spacetimes whose horizons have different Hawking temperatures. As a simple example of such system, we focus our discussion on Schwarzschild-de Sitter (SdS) spacetime, which is in two-temperature nonequilibrium state due to the difference of Hawking temperatures of black hole event horizon (BEH) and cosmological event horizon (CEH). We examine the entropy-area law for SdS spacetime.

However, applying some existing nonequilibrium thermodynamics to SdS spacetime is difficult at present. Then as one trial to search for SdS horizon entropy, we make a good strategy: We construct carefully two thermal *EQUILIBRIUM* systems separately for BEH and CEH which are designed so that the origin of nonequilibrium effect of CEH (BEH) on thermodynamic state of BEH (CEH) is retained and the Euclidean action method is applicable (see next section for a more concrete explanation). The subtraction term in Euclidean action is determined with referring to Schwarzschild thermodynamics for BEH and de Sitter thermodynamics for CEH. Although our systems are in thermal equilibrium states, some implication for nonequilibrium states of SdS horizons can be extracted, because the thermal states are "fine tuned" to include the origin of nonequilibrium nature of SdS spacetime. In this report, we will propose a reasonable evidence of breakdown of entropy-area law for CEH. The validity of the law for BEH can not be judged, but we will point out the key issue for BEH's entropy.

Recall that every existing verification of entropy-area law requires the thermal equilibrium of horizons. However, strictly speaking, it is not clear whether the thermal equilibrium is the necessary and sufficient

[1]E-mail: saida@daido-it.ac.jp

[2]Or, a completely general formulation of nonequilibrium thermodynamics may not exist in our physical world.

condition for the entropy-area law. Then, if the breakdown of the law will be confirmed for our thermal systems of BEH and CEH in SdS spacetime, it implies that the thermal equilibrium is not the necessary and sufficient condition but it is just the necessary condition for the entropy-area law. The sufficient condition for the law will be also suggested by this report.

2 Nonequilibrium nature of Schwarzschild-de Sitter spacetime

In general, the clear evidence of nonequilibrium is the existence of an energy flow inside the system under consideration, since no energy flow arises in thermal equilibrium systems. In SdS spacetime, because the Hawking temperature of BEH is always higher than that of CEH [2], a net energy flow arises inevitably from BEH to CEH. SdS spacetime is obviously a two-temperature nonequilibrium system. When one tries to analyze the SdS thermodynamics with the presence of the net energy flow, there arise difficult problems of nonequilibrium physics due to the net energy flow [1]; which quantity does the net energy flow raise as a new state variable to describe the degree of nonequilibrium nature?, how does the net energy flow cause the time evolution of the two-horizon system?, and so on. Therefore, at present, we need a good strategy to research the SdS thermodynamics with avoiding such difficult problems.

Here let us dare to ask: *Is the existence of net energy flow the principal origin of the nonequilibrium nature of SdS spacetime?* This can be rephrased as: *Does the net energy flow originate from some other physical factor?* The answer to the latter question seems Yes (No for the former) at least for SdS spacetime, because the energy flow between BEH and CEH is due to the difference of Hawking temperatures of horizons [3]. Furthermore, since the Hawking temperature is given by the surface gravity, the temperature difference is produced by the gravitational interaction between BEH and CEH. Therefore we recognize the gravitational interaction between BEH and CEH as the principal origin of nonequilibrium nature of SdS spacetime. Hence, if we can construct a system including a horizon (BEH or CEH) under the influence of gravitational interaction but excluding the net energy flow, then such system may reveal the nonequilibrium properties of BEH and CEH with avoiding the difficulties due to net energy flow. Then we introduce the following setup:

Setup (Heat Wall): Place a "heat wall" at $r = r_w$ in the region, $r_b < r < r_c$, as shown in the figure below, where r is the areal radius in SdS metric, and r_b and r_c are radii of BEH and CEH respectively. This heat wall reflects perfectly Hawking radiation of each horizon, and shields BEH (CEH) from the Hawking radiation emitted by CEH (BEH). The BEH (CEH) side of heat wall is regarded as a "heat bath" of Hawking temperature of BEH (CEH), and the net energy flow from BEH to CEH disappears. Then it is obvious that the region $\mathcal{M}_b$ enclosed by BEH and heat wall ($r_b < r < r_w$) forms a thermal *EQUILIBRIUM* system for BEH which is filled with Hawking radiation emitted by BEH and reflected by heat wall. Similarly the region $\mathcal{M}_c$ enclosed by CEH and heat wall ($r_w < r < r_c$) is also regarded as a thermal *EQUILIBRIUM* system for CEH. And we place the observer at the heat wall who measures all state variables of horizons. ($\mathcal{M}_b$ and $\mathcal{M}_c$ with the observer at r_w are already used to calculate Hawking temperatures in [2].)

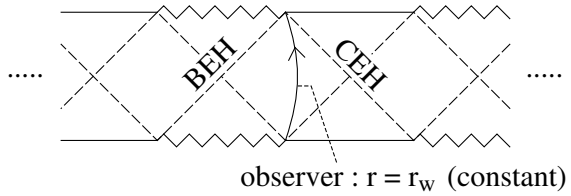

As discussed hereafter, we can regard the thermal systems $\mathcal{M}_b$ and $\mathcal{M}_c$ as the desired systems which are under the influence of gravitational interaction between BEH and CEH without the net energy flow:

To explain it, we should remark that, while the heat wall shields the energy flow between the two horizons (which is mediated by matter fields of Hawking radiation), however the heat wall does not shield the gravitational interaction between the horizons (which is not mediated by matter field but

[3]For example, for ordinary gases in laboratory, an energy flow can arise by not only temperature difference but also viscosity, differences of pressure, number density and chemical potential, and so on. Energy flow is not the "cause" but the "effect" of nonequilibrium nature.

by gravitational field). This means the following; if we find that all state variables of thermal system $\mathcal{M}_b$ depend on a parameter of such gravitational interaction, then it is reasonable to regard the system $\mathcal{M}_b$ as a thermal equilibrium system for BEH under the influence of gravitational interaction of two horizons but excluding net energy flow, and similarly for $\mathcal{M}_c$ as a thermal system for CEH. Here it seems natural that the control parameter of the gravitational interaction between BEH and CEH are the mass parameter M and the cosmological constant Λ. Furthermore, concerning the state variables, we can assume very reasonably that every state variable of BEH depends on horizon radius r_b or its surface gravity κ_b, and similarly for CEH. Here the radii r_b, r_c and surface gravities κ_b, κ_c depend on M and Λ, because, for example, $r_b(M,\Lambda)$ and $r_c(M,\Lambda)$ are the positive roots of algebraic equation $f(r)=0$, where $f(r) := -g_{tt} = 1-2M/r-\Lambda\, r^2/3$ and t is the time coordinate in the static chart of SdS metric $g_{\mu\nu}$. Then, obviously, every state variable of BEH (CEH) is under the influence of CEH's (BEH's) gravity through its dependence on horizon radii and surface gravities. Consequently, as mentioned above, we can regard the thermal systems $\mathcal{M}_b$ and $\mathcal{M}_c$ as the desired systems which are under the influence of gravitational interaction between the two horizons without the net energy flow.

Here note that the gravitational interaction on $\mathcal{M}_b$ is expressed as an external gravitational field produced by CEH which acts on BEH, and that on $\mathcal{M}_c$ is an external field by BEH acting on CEH. This situation is analogous to a magnetized gas under the influence of an external magnetic field. The magnetized gas consists of molecules possessing magnetic moment, and its thermodynamic state is characterized by three independent state variables; for example, temperature, volume and magnetization vector (response of the gas to external field), where the temperature and volume are variables required even for ordinary non-magnetized gas, and the magnetization vector is responsible for the magnetic property of the gas. The existence of three independent variables is mandatory for thermodynamic consistency of the magnetized gas. Then, as a strict thermodynamic requirement, our thermal systems $\mathcal{M}_b$ and $\mathcal{M}_c$ should also have three independent state variables to ensure thermodynamic consistency. This implies that every state variable of $\mathcal{M}_b$ and $\mathcal{M}_c$ is a function of three independent variables. Consequently, as a working hypothesis, we have to require that three parameters M, r_w and Λ are independent variables:

Working Hypothesis (three independent variables): To ensure thermodynamic consistency of our thermal systems $\mathcal{M}_b$ and $\mathcal{M}_c$, the radius of heat wall r_w, the mass parameter M and the cosmological constant Λ are regarded as three independent variables.

When one consider a non-variable Λ as a physical situation, it is obtained by setting the variation of Λ zero ($\delta\Lambda = 0$) in thermodynamics of $\mathcal{M}_b$ and $\mathcal{M}_c$ after constructing them with regarding Λ as an independent variable. In such case, the variable Λ is interpreted as a "working variable" to obtain SdS thermodynamics.

3 Entropies of horizons in Schwarzschild-de Sitter spacetime

As page space is limited, this section gives only a brief sketch of discussion of entropy-area law.

As a technique to obtain the state variables of $\mathcal{M}_b$ and $\mathcal{M}_c$, we make use of the Euclidean action method [3] which is applicable for any thermal equilibrium systems. The Euclidean action I_E is obtained by the imaginary unit i times the Wick rotation $t \to -i\tau$ of Lorentzian Einstein-Hilbert action,

$$I_E = \frac{1}{16\pi}\int_{\mathcal{M}} dx^4\,\sqrt{g_E}\,(R_E - 2\,\Lambda) + \frac{1}{8\pi}\int_{\partial\mathcal{M}} dx^3\,\sqrt{h_E}\,K_E - I_0\,, \tag{1}$$

where R_E is the scalar curvature of Euclidean spacetime region $\mathcal{M}$, $\partial\mathcal{M}$ is the boundary of $\mathcal{M}$, K_E is the trace of the extrinsic curvature of $\partial\mathcal{M}$, g_E is the determinant of Euclidean metric, h_E is the determinant of metric on $\partial\mathcal{M}$, and I_0 is the so-called *subtraction term*. I_0 is independent of the bulk metric $g_{E\mu\nu}$ of $\mathcal{M}$ and determines the integration constant of action integral with eliminating unexpected divergences of the other two integral terms. For our thermal systems for BEH and CEH in SdS spacetime, $\mathcal{M} = \mathcal{M}_b$ for BEH, $\mathcal{M} = \mathcal{M}_c$ for CEH, and $\partial\mathcal{M}$ is the heat wall for both horizons. (I_0 is determined later.)

The Euclidean spaces of $\mathcal{M}_b$ and $\mathcal{M}_c$ respectively have topology $D_2 \times S_2$, where D_2 is the time-radial part and S_2 reflects the spherical symmetry of Lorentzian SdS spacetime. The event horizon in Euclidean space is the center of D_2 and the boundary of D_2 has radius r_w. The regularity at the

center of D_2 (excluding a conical singularity) determines the temperatures T_b of BEH and T_c of CEH, $T_b = \kappa_b/(2\pi\sqrt{f_w})$ and $T_c = \kappa_c/(2\pi\sqrt{f_w})$, where $f_w = f(r_w)$ and $f(r) = -g_{tt}$. The factor $\sqrt{f(r_w)}$ is equal to the so-called *Toleman factor* which expresses the gravitational redshift on the Hawking radiation propagating from horizon to observer. Therefore, these temperatures are consistent with our setting that the observer is at the heat wall.

We determine the subtraction term I_0 to match with Schwarzschild thermodynamics for BEH and de Sitter thermodynamics for CEH. Referring to [4] which established precisely the Schwarzschild thermodynamics, it is natural to set $I_0 = I_{\rm flat}$, where $I_{\rm flat}$ is the Euclidean action for Minkowski spacetime. On the other hand, the existing formulation of de Sitter thermodynamics does not introduce any boundary, since the spacetime is closed [5]. This corresponds to considering the micro-canonical ensemble, while the introduction of the boundary (heat wall) corresponds to the canonical ensemble. We can construct the canonical ensemble for de Sitter thermodynamics with introducing an appropriate boundary term in I_E to reproduce the same equations of state which the micro-canonical ensemble gives. Then, referring to the de Sitter's canonical ensemble, we find it is natural to set $I_0 = (1 - r_c/r_w)\sqrt{f_w}\, I_{\rm flat}$. With these subtraction terms, the Euclidean actions I_b for $\mathcal{M}_b$ and I_c for $\mathcal{M}_c$ are

$$I_b = \frac{\pi}{\kappa_b}\left[\, 3M - r_b + 2r_w\left(f_w - \sqrt{f_w}\right)\right] \quad , \quad I_c = \frac{\pi}{\kappa_b}\left[\, 3M - r_c + 2r_c f_w \,\right] . \tag{2}$$

Hence, following the argument of Euclidean action method [3], the free energies F_b for BEH and F_c for CEH are given by $F_b(T_b, A_w, X_b) := -T_b\, I_b$ and $F_b(T_c, A_w, X_c) := -T_c\, I_c$, where $A_w := 4\pi r_w^2$ is the extensive state variable of system size which mimics the volume of ordinary gases (see [4] for detail of this variable), and X_b and X_c are respectively the response of thermal systems $\mathcal{M}_b$ and $\mathcal{M}_c$ to the external gravitational field. These free energies are functions of three independent state variables as discussed at the working hypothesis in previous section.

Since X_b is the response of $\mathcal{M}_b$ to the external gravitational field by CEH, X_b should be a function of the quantity which characterizes the gravity of CEH and is measured by the observer at r_w. This implies,

$$X_b = r_w^2\, \Psi_b(\Lambda\, r_w^2) \quad \text{or} \quad X_b = r_w^2\, \Psi_b(\kappa_c\, r_w)\,, \tag{3}$$

where Ψ_b is an arbitrary function of single argument, and the factor r_w^2 is due to the detail of extensive nature of state variable [4] but not an essence of present discussion. Here we can not judge which of Λ and κ_c is appropriate as the characteristic quantity of CEH's gravity. Similarly, it is natural for X_c to require $X_c = r_w^2\, \Psi_c(M/r_w)$ or $X_c = r_w^2\, \Psi_c(\kappa_b\, r_w)$, where Ψ_c is an arbitrary function. Then, following the argument of thermodynamics, the entropy of BEH S_b and that of CEH S_c are define by the partial derivatives; $S_b := -\partial F_b(T_b, A_w, X_b)/\partial T_b$ and $S_b := -\partial F_c(T_c, A_w, X_c)/\partial T_c$, which are rearranged to be first order partial differential equations of Ψ_b and Ψ_c. We can find these differential equations imply:

Result for BEH: BEH's entropy $S_b = \pi\, r_b^2$ for the choice $X_b = r_w^2\, \Psi_b(\Lambda\, r_w^2)$, but $S_b \neq \pi\, r_b^2$ for the choice $X_b = r_w^2\, \Psi_b(\kappa_c\, r_w)$. The entropy-area law for BEH holds if $\partial_M X_b = 0$, but breaks down if $\partial_M X_b \neq 0$. This denotes that the sufficient condition of entropy-area law for BEH is $\partial_M X_b = 0$. Hence it is the dependence of X_b on M that determines the validity of entropy-area law for BEH.

Result for CEH: CEH's entropy $S_c \neq \pi\, r_c^2$ for either choice $X_c = r_w^2\, \Psi_c(M/r_w)$ and $X_c = r_w^2\, \Psi_c(\kappa_b\, r_w)$. The entropy-area law seems break down for CEH in SdS spacetime.

References

[1] For example, see the list of references in; H. Saida, *Chapter 8 "Black hole evaporation as a nonequilibrium process"* (arXiv:0811.1622[gr-qc]) in the edited book by M.N. Christiansen and T.K. Rasmussen, *Classical and Quantum Gravity Research*, Nova Science Publ., 2008.

[2] G.W. Gibbons and S.W. Hawking, *Phys.Rev.***D15** (1977) 2738.

[3] See chapter 12 in: V.P. Frolov and I.D. Novikov, *Black Hole Physics*, Kluwer Academic Publ., 1998.

[4] J.W. York,Jr., *Phys.Rev.***D33** (1986) 2092.

[5] S.W. Hawking and S.F. Ross, *Phys.Rev.***D52** (1995) 5865.

Faraday Resonance in Dynamically Bar Unstable Stars

Motoyuki Saijo[1] and Yasufumi Kojima[2]

[1] *Department of Physics, Rikkyo University, Toshima, Tokyo 171–8501, Japan*
[2] *Department of Physics, Hiroshima University, Higashi-Hiroshima 739–8526, Japan*

Abstract

We investigate the nonlinear behaviour of the dynamically unstable rotating star for the bar mode by both three-dimensional hydrodynamics in Newtonian gravity and our simplified mathematical model. We find that an oscillation along the rotation axis is induced throughout the growth of the unstable bar mode, and that its characteristic frequency is twice as that of the bar mode, which oscillates mainly along the equatorial plane. We also find that, by examine several azimuthal modes, mode coupling to even modes, i.e., the bar mode and higher harmonics, significantly enhances the amplitudes of odd modes, unless they are exactly zero initially. Therefore, non-axisymmetric azimuthal modes cannot be neglected at late times in the growth of the unstable bar-mode even when starting from an almost axially symmetric state.

Dynamical bar instability in a rotating equilibrium star takes place when the ratio β ($\equiv T/W$) between rotational kinetic energy T and the gravitational binding energy W exceeds the critical value $\beta_{\rm dyn}$ (≈ 0.27 for an uniformly rotating incompressible body in Newtonian gravity [1]). Determining the onset of the dynamical bar-mode instability, as well as the subsequent evolution of an unstable star, requires a fully nonlinear hydrodynamic simulation. Recent numerical simulations also show that dynamical bar instability can occur at significantly lower β than the threshold $\beta_{\rm crt} \approx 0.27$ in some cases.

Our main concern in this paper is not to determine the onset of the instability, but to study the dynamical features of the bar. For this purpose, we numerically study the growing behaviour of the azimuthal modes in the nonlinear regime for a longer timescale. One interesting issue of nonlinear evolution is the possibility of resonant growth of other azimuthal modes triggered by the dynamical bar-mode instability. One candidate for such resonance is Faraday resonance, which is excited by the external periodic force. The dynamically unstable bar mode may work for other azimuthal oscillation modes as an external periodic force. Although the oscillation is not exactly periodic, but rather quasi-periodic, it may trigger a parametric resonance.

The other interesting issue of nonlinear evolution is to study the physical mechanism of the growth of odd modes. Are there unstable modes with odd numbers (e.g., $m = 1$ or 3) in addition to the unstable bar mode? Are the amplitudes of the odd modes enhanced by mode coupling? In order to understand the growth of odd modes, we investigate the evolution of a simplified model. The model's description of mode coupling, unstable growth, and decay mimics the realistic system very well. Moreover, the number and growth rates of the unstable modes are easily controlled. The model, therefore, deepens our understanding of the nonlinear behavior of unstable bar-mode growth in rotating stars. The physical mechanism is confirmed by comparing the model problem with a more realistic calculation of a dynamically unstable star simulated using three-dimensional hydrodynamics in Newtonian gravity.

A more detailed discussion is presented in Refs. [2, 3]. Throughout this paper, we use the geometrized units with $G = 1$ and adopt Cartesian coordinates (x, y, z) with the coordinate time t.

We study four different differentially rotating stars, which are detailed in Table 1 of Ref. [2] to investigate the nonlinear behaviour of the non-axisymmetric dynamical bar instabilities using three dimensional hydrodynamics in Newtonian gravity. We disturbed 1% of the equilibrium density by a non-axisymmetric perturbation to enhance any dynamically unstable mode.

We show the diagnostics of the model III (the weakest dynamically bar unstable system among model I – III) here, which contain both amplitude and phase in Fig. 1. The behaviours in the diagnostics

[1]E-mail: saijo@rikkyo.ac.jp
[2]E-mail: kojima@theo.phys.sci.hiroshima-u.ac.jp

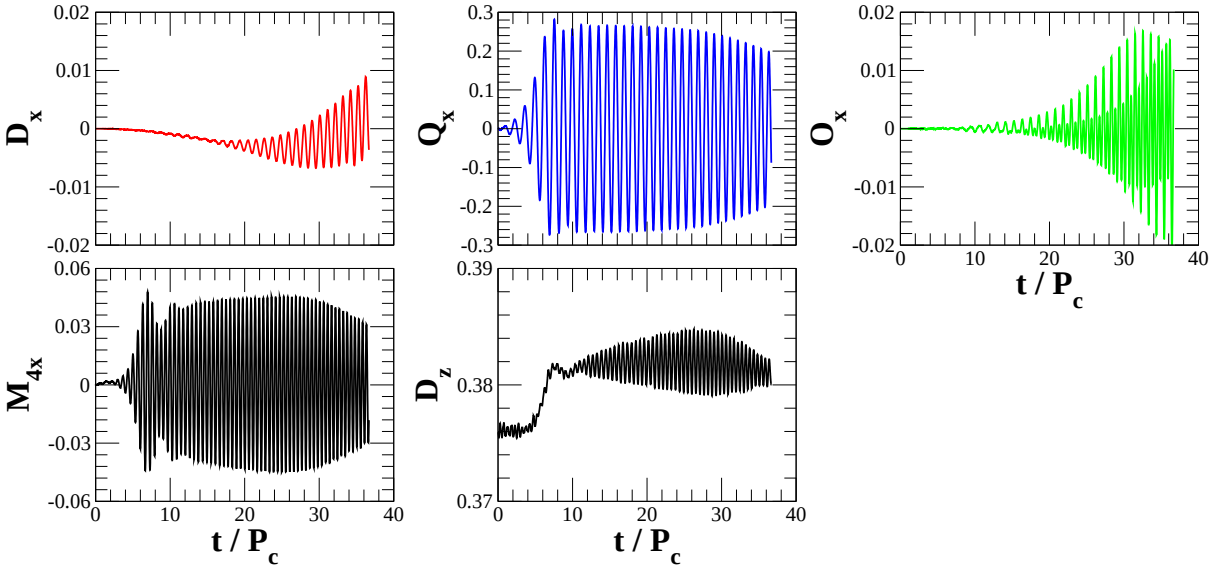

Figure 1: Diagnostics $\Re[D]$, $\Re[Q]$, $\Re[O]$, $\Re[M_4]$, and D_z as a function of $t/P_{\rm c}$ for the differentially rotating star of model III (see Table 1 of Ref. [2]). Note that the five diagnostics are defined in Ref. [2]. Hereafter, $P_{\rm c}$ is the central rotation period of the equilibrium star.

are clearly understood once we compute the spectra of the diagnostics (Fig. 2). From the spectra we find the following two remarkable features. One is that the spectra $|F_1|^2$, $|F_2|^2$, $|F_3|^2$ take a peak around $\omega_{\rm bar} \approx 5 \sim 6P_c^{-1}$ for model III, and the other is that $|F_3|^2$, $|F_4|^2$, $|F_z|^2$ take a peak around $\omega_{\rm quad} \approx 2\omega_{\rm bar} \approx 10 - 12P_c^{-1}$for bar unstable stars. Combining the present feature with the behaviour of the amplitude of the diagnostics (Fig. 1) [2], the dynamically unstable bar acts as follows.

Firstly the $m = 2$ mode grows and acts as a dominant mode of all because of the dynamical bar instability. Next the $m = 4$ mode grows because of the secondary harmonic of the $m = 2$ mode. In fact the saturation amplitude of the $m = 4$ is approximately ≈ 0.04, which is the order of the square of the saturation amplitude of the $m = 2$ ($\approx 0.2^2$). After that Faraday resonance occurs, which is clearly found in both D_z and $|F_z|^2$ from the fact $\omega_{\rm quad} \approx 2\omega_{\rm bar}$.

Note that Faraday resonance occurs in the fluid mechanics when the oscillation of the vertical direction is twice (2ω) as much as the one in the horizontal direction (ω) in the weakly nonlinear interaction [4]. Then, there is a resonance between $m = 1$ and $m = 2$, $m = 3$ and $m = 4$. The possibility of such resonances is three wave interaction: either $m = 1$ ($\omega_{\rm bar}$) and $m = 2$ ($\omega_{\rm bar}$) generates $m = 3$ ($\omega_{\rm bar} + \omega_{\rm bar}$)

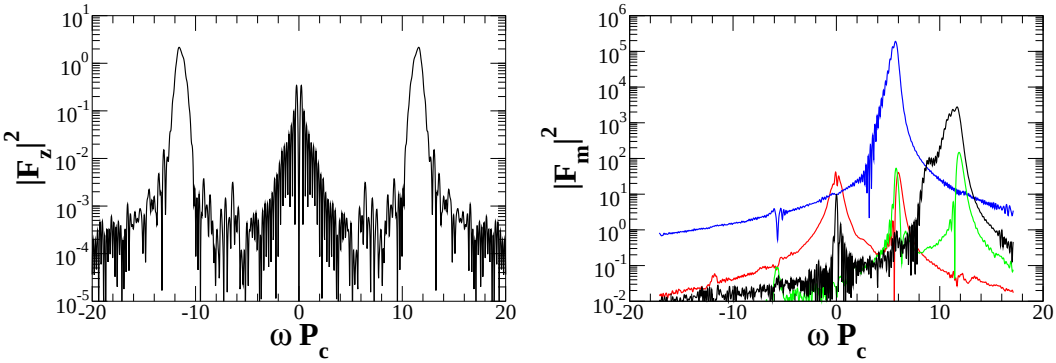

Figure 2: Spectra $|F_m|^2$ and $|F_z|^2$ as a function of $\omega P_{\rm c}$ for the differentially rotating star of model III (see Table 1 of Ref. [2]). Red, blue, green, and black line of $|F_m|^2$ denote the values of $m = 1$, 2, 3, and 4, respectively. Note that the spectra $|F_m|^2$ and $|F_z|^2$ are defined in Ref. [2].

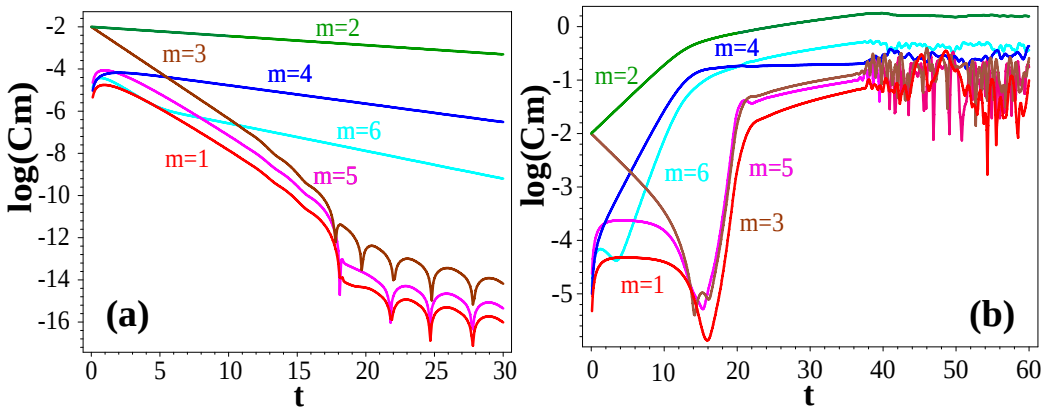

Figure 3: The time-evolution of the amplitudes of the lowest six Fourier modes ($m = 1, \cdots, 6$). Panel (a) is the result for $\nu = 0.15$ ($m = 2$ stable), (b) for $\nu = 0.05$ ($m = 2$ unstable). The initial coefficients (a_m, b_m) of the Fourier series expansion of the flow velocity $u(t, x)$ are $a_2 = a_3 = 10^{-2}$ for both cases. The behaviour of very small amplitude, say, $\log(C_m)$ ($C_m = \sqrt{{a_m}^2 + {b_m}^2}$) approximately less than -10 in panel (a), mostly comes from numerical truncation errors, and is therefore unimportant.

or $m = 3$ ($2\omega_{\rm bar}$) and $m = 2$ ($\omega_{\rm bar}$) generates $m = 1$ ($2\omega_{\rm bar} - \omega_{\rm bar}$) in the dominant part. It is the fact found in the nonlinear behaviour of the dynamically unstable bar system.

We introduce a simplified model [3] to examine the nonlinear evolution of the unstable modes, especially taking into account the nonlinearity and instability caused by an external force. Our model is Burgers' equation for a flow velocity $u(t, x)$ coupled to a scalar field $\phi(t, x)$:

$$\partial_t u + u\partial_x u = \nu\partial_x^2 u + \phi, \tag{1}$$

$$\partial_x^2 \phi + 2\phi = -u + 1, \tag{2}$$

where ν is a diffusion constant. We regard $u = 1$ and $\phi = 0$ as the background state and consider linear stability and nonlinear growth using Fourier series expansion from this uniform state.

The amplitudes of Fourier series expansion of the flow velocity $u(t, x)$ are shown in Fig. 3. Note that case (a) is stable to $m = 2$ mode, while case (b) unstable. In Fig. 3(b), the $m = 2$ mode grows exponentially until $t \sim 15$, where the amplitude of the $m = 2$ mode reaches the nonlinear regime: $10^{-2} \times \exp(0.3 \times 15) \sim 1$. All other even modes, originating from the bilinear coupling term $u\partial_x u$, also grow. The $m = 6$ mode is produced from the coupling between $m = 2$ and $m = 4$ and also from the quadric coupling of $m = 3$. Therefore, the amplitude of the $m = 6$ mode is not always smaller than that of $m = 4$. The growth of all even modes is slightly suppressed after the turning time $t \sim 15$. The turning time is also important for the odd modes. The odd modes decay for $t \lesssim 15$, but grow after that. Therefore, the nonlinearity of the amplitude of the $m = 2$ mode cannot be ignored even for the odd modes. The turning time corresponds to shock formation as will be discussed later. For Eqs. (1) and (2) all odd modes are always zero, if they are exactly zero initially. When there is at least one odd mode with a finite amplitude, the nonlinearity of the $m = 2$ mode enhances all odd modes.

The similarity can be seen in the time evolution of the Fourier components both in mathematical and three-dimensional numerical models [3]. The time evolution of the shape $u(t, x)$ is shown in Fig. 4. The $m = 2$ mode initially grows and the shape is enhanced before the turning time $t \sim 15$. The curve at $t = 4\pi$ clearly shows symmetric features due to the $m = 2$ mode. That is, the shape is the symmetry under translations $x \to x + \pi$, a "π-symmetry". The nonlinearity causes a shock as in the original Burgers' equation. After shock formation, the Gibbs phenomenon associated with Fourier series is seen at $t = 8\pi, 16\pi$. The overshoot is a numerical artifact and such behaviour always appears when a function having a sharp discontinuity is expressed as a Fourier series. Neglecting the Gibbs phenomenon, the symmetry due to the $m = 2$ mode can still be seen in the shape at $t = 8\pi$, whereas it is partially broken at $t = 16\pi$. The time $t = 16\pi$ in the mathematical model is much longer than that of nonlinear

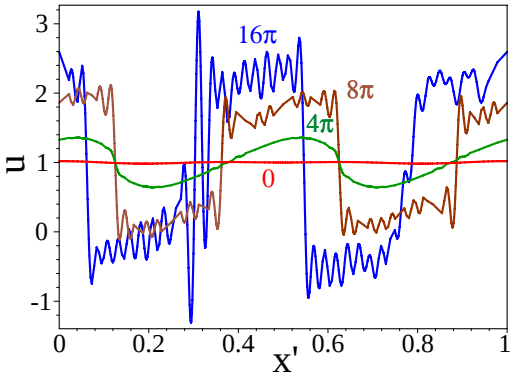

Figure 4: Snapshots of the flow velocity $u(t, x)$ are shown as a function of $x' = x/2\pi$ for $t = 0, 4\pi, 8\pi, 16\pi$ for case (b) in Fig. 3. The attached labels denote the time t.

saturation and that of growth of odd modes. Therefore, there is no counterpart in three-dimensional numerical simulations. The mathematical model suggests that a "π-symmetry" (i.e., symmetry under a 180° rotation around the z-axis) in the shape is broken in a longer timescale.

We investigate the nonlinear effects of dynamically bar unstable stars by means of both three dimensional hydrodynamic simulations in Newtonian gravity and our simplified mathematical model.

We find interesting mode coupling in the dynamically unstable system in the nonlinear regime, and that only before the destruction of the bar. The quasi-periodic oscillation mainly along the rotational axis is induced. The characteristic frequency is twice as big as that of the dynamically unstable bar mode. This feature is quite analogous to the Faraday resonance. Although our finding is only supported by the weakly nonlinear theory of fluid mechanics, we have also found the same feature of parametric resonance even in the strongly nonlinear regime [2].

We also find that our mathematically simplified model provides a concrete example showing the importance of mode coupling. The amplitudes of odd modes increase without unstable odd modes being present in the axially symmetric state; instead, they are enhanced by the bar instability with $m = 2$. We also confirmed that this physical picture is consistent with the results from a three-dimensional hydrodynamics simulation. Generally, the odd modes grow only after the bar instability reaches the nonlinear regime. The timescales of the mode coupling and the growth of unstable modes may depend on the rotation law and the strength of the initial instabilities. It is very rare that the initial perturbations in the hydrodynamics simulation should consist of purely even or odd modes only. Therefore, the unstable bar mode enhances the amplitudes of the all other modes at late times, no matter whether they are even or odd.

A similar mode coupling can be seen in numerical simulations for the one-armed spiral instability and the elliptical instability of rotating stars in Newtonian gravity. The initial models and the growth mechanism are different, but the turbulent-like behaviour appears in diagnostics of the azimuthal Fourier components at late times of nonlinear growth. The behaviour is also important for the nonlinear saturation of the unstable mode. Further study is necessary to explore the origin of the similarity seen in the development of different unstable modes. It is reasonable to assume that the nonlinearity in hydrodynamics is the source of this similarity.

References

[1] S. Chandrasekhar, *Ellipsoidal Figures of Equilibrium*, (Yale Univ. Press, New York, 1969), Chap. 5.

[2] M. Saijo and Y. Kojima, Phys. Rev. D **77**, 063002 (2008).

[3] Y. Kojima and M. Saijo, Phys. Rev. D **78**, 124001 (2008).

[4] J. Miles and D. Hederson, Ann. Rev. Fluid Mech. **22**, 143 (1990).

Gravitational-Wave Constraints on Abundance of Primordial Black Holes

Ryo Saito[1] and Jun'ichi Yokoyama[2]

[1] *Department of Physics, Graduate School of Science, The University of Tokyo, Tokyo 113-0033, Japan*
[2] *Research Center for the Early Universe, Graduate School of Science, The University of Tokyo,Tokyo 113-0033, Japan*
[3] *Institute for the Physics and Mathematics of the Universe, University of Tokyo, Chiba 277-8568, Japan*

Abstract

Formation of primordial black holes (PBHs) requires a large root-mean-square amplitude of density fluctuations, which generate second-order tensor perturbations that can be compared with observational constraints. We show that pulsar timing data essentially rules out PBHs with $10^{2-4}M_\odot$ which were previously considered as a candidate of intermediate-mass black hoes and that PBHs with mass range 10^{20-25} g which provide an astrophysical candidate for dark matter may be probed by future space-based laser interferometers.

1 Introduction

Primordial black holes (PBHs) are produced when density fluctuations with a large amplitude enters the horizon in the radiation dominated stage of the early universe with their typical mass given by the horizon mass at that epoch [1, 2]. PBHs with their mass smaller than 10^{15}g would have been evaporated away by now due to the Hawking radiation and a number of cosmological constraints have been imposed on the abundance of these light holes by big-bang nucleosynthesis (BBN) and gamma-ray background etc. Heavier PBHs can play some astrophysical roles today. For example, they may serve as the origin of the intermediate-mass black holes (IMBHs), which are considered to be the observed ultra-luminous X-ray sources, if their mass and abundance lie in the range $M_{\rm PBH} \sim 10^2 M_\odot - 10^4 M_\odot$ and $\Omega_{\rm PBH}h^2 \sim 10^{-5} - 10^{-2}$, respectively [3], while PBHs with mass $M_{\rm PBH} \sim 10^{20}{\rm g} - 10^{26}{\rm g}$ ($10^{-13}M_\odot - 10^{-7}M_\odot$) [2] and the abundance $\Omega_{\rm PBH}h^2 = 0.1$ can provide astrophysical origin of dark matter (DM) which is yet free from the constraint imposed by gravitational lensing experiments [4]. In order to produce the relevant density of PBHs, it is necessary to produce density fluctuations whose power spectrum has a high peak with an amplitude $10^{-2} - 10^{-1}$ on the corresponding scales.

Second-order effects also generate tensor fluctuations to produce stochastic background of gravitational waves (GWs) from scalar-tensor mode coupling [6, 7], whose amplitude may well exceed the first-order tensor perturbation generated by quantum effect during inflation in the current set up since the amplitude of density fluctuations required for a substantial density of PBHs is so large.

In the following sections, we show the GWs induced by scalar fluctuations as a second-order effect [6, 7] is a useful probe to investigate the abundance of the PBHs. We calculate spectrum of these second-order GWs in the case scalar fluctuations have a sufficiently large peak to realize formation of relevant numbers of PBHs. As a natural consequence we find that the spectrum of GWs has a peak on a scale approximately equal to the scale of the peak of the scalar fluctuations. We can therefore obtain information on the abundance of PBHs with the horizon mass when the scale of the peak entered the Hubble radius by observing GWs with the frequency corresponding to the same comoving scale, namely, $10^{-9}{\rm Hz} - 10^{-8}{\rm Hz}$ for IMBHs and $10^{-3}{\rm Hz} - 1{\rm Hz}$ for dark-matter PBHs. Fortunately, the former band is probed by the pulsar timing observations [8, 9] while the latter band can be observed in future by the space-based interferometers for dark matter PBHs.

[1] E-mail:r-satio@resceu.s.u-tokyo.ac.jp
[2] E-mail:yokoyama@resceu.s.u-tokyo.ac.jp

2 The induced gravitational waves

We write the perturbed metric as

$$\mathrm{d}s^2 = a(\eta)^2 \left[-e^{2\Phi}\mathrm{d}\eta^2 + e^{-2\Psi}(\delta_{ij} + h_{ij})\mathrm{d}x^i \mathrm{d}x^j\right], \tag{1}$$

including both scalar perturbations, Φ and Ψ, and tensor perturbation, h_{ij}, which satisfies $\partial_i h^i_j = h^i_i = 0$ with $h^i_j \equiv \delta^{ik}h_{kj}$. We assume the lowest-order tensor perturbation is negligible and consider that generated by the scalar mode as a second-order effect. The relevant part of the Einstein equation therefore reads

$$h^{i\,\prime\prime}_j + 2\mathcal{H}h^{i\,\prime}_j - \partial^2 h^i_j = 2\mathcal{P}^{is}_{rj}S^r_s, \tag{2}$$

where a prime denotes differentiation with respect to the conformal time, $\mathcal{P}^{is}_{rj}$ represents the projection operator to the transverse, traceless part, and $\mathcal{H} \equiv a'/a$ [6, 7]. The source term reads

$$S^r_s = 2\partial^r\Psi\partial_s\Psi - \frac{4}{3(1+w)}\partial^r(\Psi + \mathcal{H}^{-1}\Psi')\partial_s(\Psi + \mathcal{H}^{-1}\Psi'), \tag{3}$$

with $w \equiv \rho/p$ being the equation-of-state parameter of the background fluid. In practice, only the radiation dominated era is relevant, so we take $w = 1/3$ hereafter. We also neglect anisotropic stress, which is expected to give only a small correction [7], and set $\Phi = \Psi$ at linear order. In order to calculate the induced GWs up to second order, it is sufficient to use the linear scalar modes. Hence, we only need to solve the linear evolution equation,

$$\Psi''_{\boldsymbol{k}}(\eta) + \frac{4}{\eta}\Psi'_{\boldsymbol{k}}(\eta) + \frac{k^2}{3}\Psi_{\boldsymbol{k}}(\eta) = 0, \tag{4}$$

for the scalar modes where $\Psi_{\boldsymbol{k}}$ represents a Fourier mode.

For our purpose we assume the following approximate form of the power spectrum of the initial fluctuations,

$$\mathcal{P}_\Psi(k) \equiv \frac{k^3}{2\pi^2}\langle|\Psi_{\boldsymbol{k}}(0)|^2\rangle = \mathcal{A}^2\delta(\ln(k/k_p)), \tag{5}$$

where k_p and $\mathcal{A}^2$ represent the wavenumber of the peak and (amplitude)$^2 \times$ ln(peak width) of the original spectrum, respectively. With this power spectrum the fractional energy density of the region collapsing into PBHs at their formation time is estimated as

$$\beta(M_{\rm PBH}) \sim 0.1 \exp\left(-\frac{\Psi_c^2}{2\mathcal{A}^2}\right), \tag{6}$$

where $M_{\rm PBH}$ is of the order of the horizon mass when the comoving scale k_p^{-1} enters the Hubble radius and Ψ_c is the threshold value of PBH formation. Carr [5] takes the threshold value of the density contrast to be $\delta_c = 1/3$ corresponding to $\Psi_c = 1/2$. One can express the current value of the density parameter of PBHs in terms of $\beta(M_{\rm PBH})$ as

$$\Omega_{\rm PBH,0}h^2 = 2 \times 10^6 \beta(M_{\rm PBH}) \left(\frac{M_{\rm PBH}}{10^{36}\,\mathrm{g}}\right)^{-1/2} \left(\frac{g_{*p}}{10.75}\right)^{-1/3}, \tag{7}$$

where g_{*p} is the effective number of the relativistic degrees of freedom when k_p entered the Hubble radius.

We define the Fourier modes $h_{\boldsymbol{k}}$ as

$$h_{ij}(\boldsymbol{x},\eta) = \int \frac{\mathrm{d}^3k}{(2\pi)^{3/2}} e^{i\boldsymbol{k}\cdot\boldsymbol{x}} \left[h^+_{\boldsymbol{k}}(\eta)\mathrm{e}^+_{ij}(\boldsymbol{k}) + h^\times_{\boldsymbol{k}}(\eta)\mathrm{e}^\times_{ij}(\boldsymbol{k})\right], \tag{8}$$

where $\mathrm{e}^+_{ij}(\boldsymbol{k}), \mathrm{e}^\times_{ij}(\boldsymbol{k})$ are polarization tensors which are normalized as $\sum_{i,j}\mathrm{e}^\alpha_{ij}(\boldsymbol{k})\mathrm{e}_{ij}(-\boldsymbol{k}) = 2\delta^\alpha$. The Fourier transform of the source term (3) is also defined similarly. We find the source term is constant when $k_p\eta/\sqrt{3} \ll 1$, while it decreases in proportion to η^{-2} for $k_p\eta/\sqrt{3}$ 1. As a result the production of scalar-induced GWs mostly occurs around the time when k_p crosses the sound horizon. In the mass

range of the PBHs of our interest, creation of scalar-induced GWs is terminated well before the equality time. After that the energy density of GWs decreases in proportion to a^{-4}. Using the Green function method one can easily find a formal solution to (2) from which we can evaluate the density parameter of GWs contributed by a logarithmic interval of the wavenumber around k. It is formally expressed as

$$\Omega_{\rm GW}(k,\eta) = \frac{k^3}{12\pi^2\mathcal{H}^2}\left(|h_{\boldsymbol{k}}^{+\prime}|^2 + |h_{\boldsymbol{k}}^{\times\prime}|^2\right), \tag{9}$$

when k-mode is well inside the horizon. The overall feature of the spectrum of $\Omega_{\rm GW}(f,\eta_0)$ today can be estimated to be

$$\begin{aligned}\Omega_{\rm GW}(f)h^2 &= 7\times10^{-9}\left(\frac{g_{*p}}{10.75}\right)^{-1/3}\left(\frac{\mathcal{A}^2}{10^{-3}}\right)^2\left(\frac{\Omega_{\rm rad}h^2}{4\times10^{-5}}\right)\left(\frac{f}{f_p}\right)^2\left[1-\left(\frac{f}{2f_p}\right)^2\right]^2\theta\left(1-\frac{f}{2f_p}\right) \\ &\equiv A_{\rm GW}\left(\frac{f}{f_p}\right)^2\left[1-\left(\frac{f}{2f_p}\right)^2\right]^2\theta\left(1-\frac{f}{2f_p}\right),\end{aligned} \tag{10}$$

for $f \lesssim f_{\rm GW} \equiv 2f_p/\sqrt{3}$ where we have used the frequency $f \equiv 2\pi k/a_0$ instead of the wavenumber. The above expression has the peak value $\Omega_{\rm GW}(f_{\rm GW})h^2 = (16/27)A_{\rm GW}$ at $f_{\rm GW}$.

3 Constraints on the PBH abundance

We now compare our results with observational constraints. For definiteness we identify $M_{\rm PBH}$ with the horizon mass when the peak scale k_p^{-1} entered the Hubble radius. Then $M_{\rm PBH}$ is related with the peak frequency of GWs as

$$f_{\rm GW} = 1\times10^{-8}\ {\rm Hz}\left(\frac{M_{\rm PBH}}{10^{36}\,{\rm g}}\right)^{-1/2}\left(\frac{g_{*p}}{10.75}\right)^{-1/12}. \tag{11}$$

The pulsar timing observations are sensitive to GWs with $f > 1/T$ where T is the data span. The 7-year data of observation of PSR B1855+09 gives an upper limit

$$\Omega_{\rm GW}(f)h^2 < 4.8\times10^{-9}\left(\frac{f}{4.4\times10^{-9}{\rm Hz}}\right)^2, \tag{12}$$

for $f > 4.4\times10^{-9}$Hz at 90% confidence level [8]. By using this limit, we can constrain the abundance of PBHs with mass $M_{\rm PBH} \lesssim 1\times10^{37}\ {\rm g} = 5\times10^3 M_\odot$.

The space-based interferometers are sensitive to GWs with $10^{-5}{\rm Hz} \lesssim f \lesssim 10{\rm Hz}$ [10, 11], which covers the entire mass range of the PBHs which are allowed to be DM, $10^{20}{\rm g} < M_{\rm PBH} < 10^{26}{\rm g}$. LISA will have its best sensitivity $\Omega_{\rm GW}h^2 \sim 10^{-11}$ at $f \sim 10^{-2}$Hz ($M_{\rm PBH} \sim 10^{24}$g), BBO and the ultimate-DECIGO are planned to have sensitivity to $\Omega_{\rm GW}h^2 \sim 10^{-13}$ and $\Omega_{\rm GW}h^2 \sim 10^{-17}$, respectively at $f \sim 10^{-1}$Hz ($M_{\rm PBH} \sim 10^{22}$g).

Figure 1 shows the energy density of the induced GWs, whose approximate form is given by (10).

As is seen in the figure the pulsar timing constraint is so stringent that one cannot achieve $\Omega_{\rm PBH}h^2$ 10^{-5} for PBHs with $4\times10^2 M_\odot \lesssim M_{\rm PBH} \lesssim 5\times10^3 M_\odot$, ruling out the major mass range of IMBHs. On the other hand, if pulsar timing experiments should find any nontrivial modulation in near future, it might be due to the PBHs with mass around $10^2 M_\odot$ [9].

It is clear from Fig. 1 that the future space-based interferometers can test the feasibility of PBHs as the dominant constituent of the DM. The ground-based interferometers, on the other hand, have good sensitivity at $f \sim 10-10^2$Hz [12]. This frequency band corresponds to mass scale $M_{\rm PBH} \sim 10^{16}{\rm g}-10^{18}{\rm g}$. Though the sensitivity of LIGO is too low now and in near future to detect GWs from the second-order effect associated with PBH formation, we could improve the sensitivity by correlation analysis to reach the desired level to probe PBHs. Because the spectrum has a tail to lower frequencies, it may be possible to constrain the abundance of the PBHs with $M_{\rm PBH} < 7\times10^{14}$g ($f_{\rm GW} > 6\times10^2$Hz), which have evaporated by the present epoch and could contribute to cosmic rays. Further study, however, is necessary in order to obtain the conclusion because there are astronomical sources of GWs in this frequency band, too.

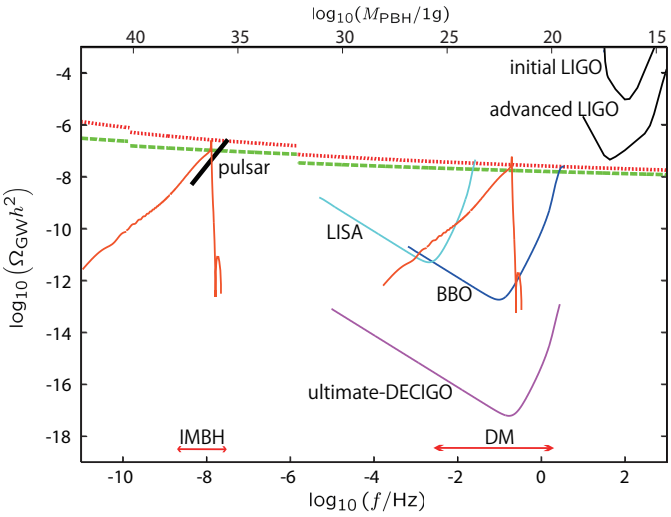

Figure 1: Energy density of scalar-induced GWs associated with PBH formation together with current pulsar constraint (thick solid line segment) and sensitivity of various GW detectors (convex curves). The planned sensitivity of the space-based interferometers depicted [10] with the instrumental parameters used in [11] as well as those of LIGO [12]. Left and right wedge-shaped curves indicate expected power spectra of GWs from two different peaked scalar fluctuations corresponding to $(\Omega_{\rm PBH}h^2, M_{\rm PBH}, g_{*p}) = (10^{-5}, 6\times10^2 M_\odot, 10.75)$ (left) and $(10^{-1}, 3\times10^{22}{\rm g}, 106.75)$ (right), respectively. The dotted (broken) line shows an envelope curve, $(16/27)A_{\rm GW}$, corresponding to $\Omega_{\rm PBH} = 10^{-1}$ (10^{-5}) obtained by moving k_p and $\mathcal{A}$.

References

[1] S. Hawking, Mon. Not. Roy. Astron. Soc. **152**, 75 (1971); B. J. Carr and S. W. Hawking, Mon. Not. Roy. Astron. Soc. **168**, 399 (1974).

[2] B. J. Carr, In Proc. 59th Yamada Conference "Inflating Horizons of Particle Astrophysics and Cosmology", (Universal Academy Press, Tokyo, 2005) p 129.

[3] T. Kawaguchi, M. Kawasaki, T. Takayama, M. Yamaguchi and J. Yokoyama, Mon. Not. Roy. Astron. Soc. **388**, 1426 (2008).

[4] C. Alcock *et al.* [MACHO Collaboration and EROS Collaboration], Astrophys. J. Lett. **499**, L9 (1998); P. Tisserand *et al.* [EROS-2 Collaboration], Astron. Astrophys. **469**, 387 (2007); G. F. Marani, R. J. Nemiroff, J. P. Norris, K. Hurley and J. T. Bonnell, Astrophys. J. Lett. **512**, L13 (1999).

[5] B. J. Carr, Astrophys. J. **201**, 1 (1975).

[6] K. N. Ananda, C. Clarkson and D. Wands, Phys. Rev. D **75**, 123518 (2007).

[7] D. Baumann, P. J. Steinhardt, K. Takahashi and K. Ichiki, Phys. Rev. D **76**, 084019 (2007).

[8] S. E. Thorsett and R. J. Dewey, Phys. Rev. D **53**, 3468 (1996).

[9] F. A. Jenet *et al.*, Astrophys. J. **653**, 1571 (2006).

[10] http://www.srl.caltech.edu/˜ shane/sensitivity/

[11] H. Kudoh, A. Taruya, T. Hiramatsu and Y. Himemoto, Phys. Rev. D **73**, 064006 (2006).

[12] http://www.ligo.caltech.edu/

Moduli fixing in Brane gas cosmology

Masakazu Sano [1]

[1] *Department of Physics, Hokkaido University, Sapporo, Hokkaido , 060–0810, Japan*

Abstract

We consider a moduli stabilization in a brane gas model based on Type II string theories. We show that gauge fields on D-branes, NS5-branes and KK5-monopoles are required in order to stabilize radial moduli fields of a six-dimensional torus as an internal space and dilaton, simultaneously.

1 Introduction

One of most interesting problems in string theories is to reveal a mechanism of a moduli fixing of higher dimensions and a dilaton field. In a higher dimensional theory like the string theories, the scales of a compactified space and the dilaton are dynamical variables. Those variables are related to gauge couplings of the theories by a Kaluza-Klein reduction. We should stabilize the moduli fields to obtain a four-dimensional theory describing a realistic universe, because the gauge coupling has a fixed value.

Brandenberger and Vafa proposed the string gas model [1]. According to this model, at a very early universe, It was assumed that fundamental strings fill the universe which has T^9 as the spatial part. In this setup, they considered an interesting mechanism of compactifications. If strings remain without annihilations in the 6-dimensions of T^9, it is expected that the internal space is stabilized by the tension of the strings. On the other hand, the 3-dimensional space decompactifies from T^9, because strings easily annihilate each other in the 3-dimensional space.

A lot of models on the moduli stabilizations have been proposed, using brane gas models [2] as well as string gas models [3, 4, 5, 6, 7, 8, 9, 10, 11, 12, 13, 14, 15, 16], since string theories neutrally include branes. However, it has been known that a simple compactification with only winding modes of branes or strings cannot stabilize radial moduli fields and the dilaton field, simultaneously [15].

The purpose of this work is to construct brane gas models with stabilized moduli fields in Type II string theories. We consider gauge fields on D-branes, NS5-branes and Kaluza-Klein monopoles (KK5) as new ingredients. It will be found that those objects are required for the stabilization of the dilaton field. This talk is based on the work in collaboration with Hisao Suzuki [17].

2 Moduli fixing with D-brane, KK5-monopole and NS5-brane in Brane gas model

2.1 Preliminaries

Before discussing a detail of the moduli stabilization in brane gas models, we give a setup of the 10-dimensional metric, the 4-dimensional Einstein frame and a bulk action. In this talk, we do not take a varying Newton constant, therefore the 4-dimensional Einstein frame is required when the Kaluza-Klein reduction is performed.

We consider a case where the 3-dimensional space has already been large and take the following homogeneous metric:

$$ds_{10}^2 = -e^{2\lambda_0(t)}dt^2 + e^{2\lambda(t)}d\mathbf{x}^2 + \sum_{m=4}^{9} e^{2\lambda_m(t)}(dy^m)^2. \tag{1}$$

The 3-dimensional space is R^3 and the internal space is T^6. The coordinate of a cycle y^m is defined as $0 \leq y^m \leq 2\pi\sqrt{\alpha'}$ where $\sqrt{\alpha'}$ is related to the string length, $l_s = \sqrt{\alpha'}$. We assume that all fields depend

[1] E-mail:sano_hokudai@mail.sci.hokudai.ac.jp

only on time and fluxes are canceled each other. This assumption implies that the dynamics of the brane gas models are decided by gases of world volume action of branes. In the system, a total action is given by $S_0 + S_{\text{brane gases}}$. S_0 is the 10-dimensional action which gives the following 4-dimensional effective action:

$$\begin{aligned} S_0 &= \frac{1}{16\pi G_{10}} \int_{M^{10}} d^{10}X\sqrt{-G}e^{-2\phi(t)}(R + 4(\nabla\phi)^2) \\ &= \frac{1}{16\pi G_4} \int_{M^4} d^4x e^{n(t)+3A(t)} \times e^{-2n(t)}\Big(-6\dot{A}^2(t) + 2\dot{\beta}^2(t) + \sum_{m=4}^{9} \dot{\lambda}_m^2(t)\Big) \end{aligned} \tag{2}$$

where we have defined the 4-dimensional Einstein frame as follows ($G_{(4)} = G_{(10)}(2\pi\sqrt{\alpha'})^{-6}$):

$$\lambda_0(t) = n(t) + \beta(t), \quad \lambda(t) = A(t) + \beta(t), \quad \beta(t) \equiv \phi(t) - \frac{1}{2}\overline{\lambda}(t), \quad \overline{\lambda}(t) \equiv \sum_{m=4}^{9} \lambda_m(t). \tag{3}$$

The new variable $\beta(t)$ is useful in order to obtain the diagonal kinetic term. Then, we can analyze a minimum condition of a potential given by the energy-momentum tensor in term of brane gases:

$$u^{(m_1\cdots m_p)}_{\text{D}p/\text{KK5}/\text{NS5}} \equiv -T^0_{\ 0} = \frac{2g^{00}}{\sqrt{-g_4(x)}} \frac{\delta\mathcal{L}^{(m_1\cdots m_p)}_{\text{D}p/\text{KK5}/\text{NS5}}}{\delta g^{00}} = -e^{-n(t)-3A(t)} \frac{\delta\mathcal{L}^{(m_1\cdots m_p)}_{\text{D}p/\text{KK5}/\text{NS5}}}{\delta n(t)}. \tag{4}$$

2.2 Brane gas

We will consider a Dp-brane which wraps over a cycle of T^6. It is known that gauge fields can be generated on the Dp-brane whose action is

$$S^{(m_1\cdots m_p)}_{\text{D}p} = -T_p \int_{R\times\Sigma_p} d^{p+1}\xi e^{-\phi(t)} \sqrt{-\det(\gamma_{ab} + 2\pi\alpha' F_{ab})} \tag{5}$$

where $\Sigma_p \subset T^6$. We have assumed the homogeneous metric and fields, and then the electric fields $F_{0i} = \dot{A}_i(t)$ flow on the Dp-brane. If fluxes are canceled each other and only brane gases dominate as ideal gases, the electric fields, $\dot{A}_m(t)$ and velocity along the internal space, $\dot{X}^m(t)$ are free. Then, we can integrate those variables once and, by Eq.(4), we obtain the potentials of brane gases ($T_p = (2\pi)^{-p}(\alpha')^{-(p+1)/2}$):

$$u^{(m_1\cdots m_p)}_{\text{D}p} = e^{-3A(t)}(2\pi\sqrt{\alpha'})^p T_p \times \left\{e^{-\overline{\lambda}(t)+2\sum_{a=1}^{p}\lambda_{m_a}(t)} + \widetilde{\mathcal{A}}(t)\right\}^{\frac{1}{2}} \tag{6}$$

where

$$\widetilde{\mathcal{A}}(t) \equiv \sum_{a=1}^{p} e^{2\beta(t)+2\lambda_{m_a}(t)} \left(\frac{f_{m_a}}{2\pi\alpha'}\right)^2 + \sum_{b=p+1}^{6} e^{2\beta(t)-2\lambda_{m_b}(t)}(v^{m_b})^2. \tag{7}$$

f_{m_a} and v^{m_b} are constants of integration of equations of motion on $\dot{A}(t)$ and $\dot{X}^m(t)$. Similarly, the potential of gases of NS5 and KK5 [18, 19, 20] whose action is

$$S^{(m_1\cdots m_5)}_{\text{NS5}} = -T_{\text{NS5}} \int_{R\times\Sigma_5} d^6\xi e^{-2\phi(t)} \sqrt{-\det\gamma_{ab}}, \tag{8}$$

$$S^{(m_1\cdots m_5)}_{\text{KK5}} = -T_{\text{KK5}} \int_{R\times\Sigma_5} d^6\xi e^{-2\phi(t)} k^2 \sqrt{-\det\widetilde{\gamma}_{ab}}, \quad \widetilde{\gamma}_{ab} \equiv \frac{\partial X^m}{\partial\xi^a}\frac{\partial X^m}{\partial\xi^a}(G_{mn} - k^{-2}k_m k_n), \tag{9}$$

($k^m \equiv \delta^{mm_6}$ is the killing vector of the S^1 isometry of the (m_6)-cycle) are given by

$$u^{(m_1\cdots m_5)}_{\text{NS5}} = e^{-3A(t)}(2\pi\sqrt{\alpha'})^5 T_{\text{NS5}} \times e^{-\beta(t)-\overline{\lambda}(t)+\sum_{a=1}^{5}\lambda_{m_a}(t)}, \tag{10}$$

$$u^{(m_1\cdots m_5)}_{\text{KK5}} = e^{-3A(t)}(2\pi\sqrt{\alpha'})^5 T_{\text{KK5}} \times e^{-\beta(t)-\overline{\lambda}(t)+2\lambda_{m_6}+\sum_{a=1}^{5}\lambda_{m_a}(t)} \tag{11}$$

where $T_{\rm NS5} = T_{\rm KK5} = T_{\rm D5}$.

We find two important facts from (6), (10) and (11). First, the energy density is proportional to $e^{-3A(t)}$ where $e^{A(t)}$ is the scale factor of the three dimensions in the 4-dimensional Einstein frame. If all moduli fields are fixed, this gives the energy density of a pressureless dust. This property result from brane gases whose all spatial parts wrap over cycles of T^6. We see those branes as gases of point particles on the 3-dimensional space. Second, It is found that the the potential of the Dp-brane cannot stabilize the dilaton field. The winding mode of the world volume action has no dilaton dependence in the 4-dimensional Einstein frame. The terms derived by electric fields and velocities have the dilaton dependence of $e^{+2\beta(t)}$ in (7). On the other hand, the potential of NS5 and KK5 has the inverse dependence of the dilaton field like Eq.(10) and Eq.(11). Therefore, It is expected that the dilaton field is stabilized by the electric fields and NS5/KK5.

2.3 D1-brane(+gauge field), KK5-monopole(IIB)

We will investigate an explicit brane gas model in Type IIB theory. This model is constructed by D1-branes wrapping over each cycle and KK5 wrapping over (45678)-cycle and its cyclic permutations. Using T-duality [17], we are able to map this system to a dual model including NS5-branes. We take the initial conditions as $v^m = 0$ and $f_m = 2\pi\alpha' f$. Then, the energy density of this system is given by

$$U^{\rm IIB} = \frac{N_{\rm D1}}{e^{3A(t)}}(2\pi\sqrt{\alpha'})T_1 \sum_{a=4}^{9} e^{-\frac{1}{2}\overline{\lambda}(t)+\lambda_a(t)}(1+f^2 e^{2\beta(t)+\overline{\lambda}(t)})^{\frac{1}{2}} + \frac{N_{\rm KK5}}{e^{3A(t)}}(2\pi\sqrt{\alpha'})^5 T_{\rm KK5} \sum_{a=4}^{9} e^{-\beta(t)+\lambda_a(t)} \tag{12}$$

where $N_{\rm D1}$ and $N_{\rm KK5}$ are constants and indicate the number density of the pressureless dust at present, $e^{A(t=t_0)} = 1$. The condition of a minimum of $U^{\rm IIB}$ is given by $\partial U^{\rm IIB}/\partial\beta = \partial U^{\rm IIB}/\lambda_m = 0$. The solution of this condition is

$$e^{2\phi_{\rm min.}} = \frac{1}{f^2}, \qquad e^{2\lambda'_{\rm min.}} = \Big(\frac{N_{\rm D1}}{N_{\rm KK5}}\Big)^{1/3}\Big(\frac{1}{2f^2}\Big)^{1/6}. \tag{13}$$

This condition shows $e^{\lambda_m} = e^{\lambda'_{\rm min.}}$ $(m = 4, 5, \cdots, 9)$, because of the isotropic initial condition for the electric fields like $f_m = 2\pi\alpha' f$.

This mechanism of the moduli stabilization is intuitively understood as follows. For example, in the 4-dimensional Einstein frame, one of the winding modes of D1-brane and KK5-monopole are $\exp[(\lambda_4 - \lambda_5 - \cdots - \lambda_9)/2]$ and $\exp[-\beta + \lambda_4]$, respectively. Those windings bind a cycle where the branes wrap around. The expanding directions are bound by another brane. The electric fields on D1-brane and KK5-monopoles stabilize the dilaton field. All forces are canceled each other, and then the radial moduli fields of T^6 and the dilaton field are stabilized, simultaneously. After the moduli stabilization, it is found that this potential gives the energy density of the pressureless dust like $U^{\rm IIB} \propto e^{-3A(t)}$.

3 Conclusions and Discussions

We have considered the mechanism of the moduli stabilization in the brane gas model based on Type II string theories. It has been found that the gauge fields on D-branes, NS5-branes and KK5-monopole are required in order to stabilize the radial moduli fields of T^6 and the dilaton, simultaneously.

Once all moduli fields are stabilized, it is expected that there is a possibility of a dark matter candidate for this wrapped brane gases, because the energy density with fixed moduli fields gives rise to $\rho \sim e^{-3A}$ which is the energy density of a pressureless dust. To realize this statement, we have to check a mass scale of wrapped branes and interactions in term of RR-flux in the 4-dimensional Einstein frame.

Acknowledgments

I would like to express my gratitude to the organizers of the JGRG18 for giving me an opportunity of this presentation. I would like to thank Hideo Kodama, Shinji Mukohyama and Misao Sasaki for useful comments and discussions.

References

[1] R. H. Brandenberger and C. Vafa: Superstrings in the Early Universe: Nucl. Phys. **B316** 391 (1989)

[2] S. Alexander, R. H. Brandenberger and D. Easson: Brane gases in the early universe: Phys.Rev.**D62**(2000) 103509: hep-th/0005212

[3] S. Watson and R. Brandenberger: Stabilization of extra dimensions at tree level: JCAP **0311**(2003)008:hep-th/0307044

[4] A. Kaya and T. Rador: Wrapped branes and compact extra dimensions in cosmology: Phys. Lett. **B565**: 19-26, (2003): hep-th/0301031

[5] B. Bassett, M. Borunda, M. Serone and S. Tsujikawa: Aspects of String-Gas Cosmology at Finite Temperature: Phys.Rev. **D67** (2003) 123506: hep-th/0301180

[6] T Batterfeld and S. Watson: Effective field theory approach to string gas cosmlogy: JCAP **0406** 001 (2004): hep-th/0403075

[7] S. Watson: Moduli Stabilization with the String Higgs Effect: Phys.Rev. **D70** (2004) 066005: hep-th/0404177

[8] S. P. Patil and R. Brandenberger: Radion stabilization by stringy effects in general relativity: Phys.Rev. **D71** (2005) 103522:hep-th/0401037

[9] S. P. Patil and R. Brandenberger: The Cosmology of massless string modes: JCAP **0601** (2006) 005:hep-th/0502069

[10] S. P. Patil: Moduli (dilaton, volume and shape) stabilization via massless F and D string modes: hep-th/0504145

[11] S. Kanno and J. Soda: Moduli Stabilization in String Gas Compactification : Phys.Rev. **D72** (2005) 104023: hep-th/0509074

[12] R. Brandenberger, Y. K. Cheung and S. Watson: Moduli stabilization with string gases and fluxes: JHEP 0605 (2006) 025: hep-th/0501032

[13] A. Chatrabhuti: Target space duality and moduli stabilization in String Gas Cosmology: Int.J.Mod.Phys. **A22** (2007) 165-180:hep-th/0602031

[14] A. J. Berndsen and J. M. Cline: Dilaton stabilization in brane gas cosmology: Int. J. Mod. Phys. **A19** (2004) 5311: hep-th/0408185

[15] A. Berndsen, T. Biswas, J. M. Cline: Moduli stabilization in brane gas cosmology with superpotentials: JCAP **0508** 012 (2005):hep-th/0505151

[16] R. J. Danos, A. R. Frey and R. H. Brandenberger: Stabilizing moduli with thermal matter and nonperturbative effects: arXiv:0802.1557

[17] M. Sano and H. Suzuki: Moduli fixing and T-duality in Type II brane gas models: Phys.Rev.**D**78 (2008) 064045: arXiv:0804.0176

[18] E. Bergshoeff, B. Janssen and T. Ortin: Kaluza-Klein monopoles and gauged sigma models: Phys. Lett. **B410**: 131-141, (1997): hep-th/9706117

[19] E. Eyras, B. Janssen and Y. Lozano: 5-branes, KK-monopoles and T-duality: Nucl. Phys. **B531** (1998) 275-301: hep-th/9806169

[20] E. Bergshoeff, Y. Lozano and T. Ortin: Massive Branes: Nucl.Phys. **B518** (1998) 363-423:hep-th/9712115

Higher Curvature Corrections to Primordial Fluctuations in Slow-roll Inflation

Masaki Satoh[1] and Jiro Soda[2]

[1,2] *Department of Physics, Kyoto University, Kyoto 606–8501, Japan*

Abstract

We study higher curvature corrections to the scalar spectral index, the tensor spectral index, the tensor-to-scalar ratio, and the polarization of gravitational waves. We find that there are cases where the higher curvature corrections can not be negligible. It turns out that the tensor-to-scalar ratio could be enhanced and the tensor spectral index could be blue due to the Gauss-Bonnet term.

1 Introduction

According to the Wilkinson Microwave Anisotropy Probe (WMAP) data [1] and other observations, it seems plausible that the large scale structure of the universe stems from quantum fluctuations during the slow-roll inflation. Considering the accuracy of future observations, it would be worth to study the corrections due to higher curvature terms to the slow-roll inflation. To the leading order, the corrections come from the Gauss-Bonnet and the axion-like parity violating coupling terms [2]. In fact, the same type of corrections can be derived from a particular superstring theory [3]. Hence, we hope the understanding of such corrections to the inflationary scenario provides a clue to the study of superstring theory.

There have been many works concerning the Gauss-Bonnet and the parity violating corrections to the Einstein gravity [3, 4, 5]. However, since no one has systematically investigated both terms simultaneously in the context of the slow-roll inflation, the combined effect on the slow-roll inflation is not so clear. Hence, we study the slow-roll inflation with higher curvature corrections and derive the formula for the observables in terms of slow-roll parameters.

The organization of the paper is as follows: In section 2, we define slow-roll parameters in the inflationary scenario with higher curvature corrections. In section 3, we obtain the scalar and tensor spectral index and the tensor-to-scalar ratio. In section 4, the concrete example is presented as an illustration. The final section is devoted to the conclusion.

2 Slow-roll inflation

We consider the gravitational action with the Gauss-Bonnet and the parity violating terms

$$S = \frac{M_{\rm Pl}^2}{2}\int \mathrm{d}^4x\sqrt{-g}R - \int \mathrm{d}^4x\sqrt{-g}\left[\frac{1}{2}\nabla\ \phi\nabla\ \phi + V(\phi)\right] - \frac{1}{16}\int \mathrm{d}^4x\sqrt{-g}\xi(\phi)R^2_{\rm GB} + \frac{1}{16}\int \mathrm{d}^4x\sqrt{-g}\omega(\phi)R\tilde{R}\ , \tag{1}$$

where $M_{\rm Pl}^2 \equiv 1/8\pi G$ denotes the reduced Planck mass and g is the metric tensor. The Gauss-Bonnet term $R_{\rm GB}$ and the parity violating term $R\tilde{R}$ are defined by

$$R^2_{\rm GB} \equiv R^{\alpha\ \ \gamma\delta}R_{\alpha\ \ \gamma\delta} - 4R^{\alpha}{}_{\ }R_{\alpha}{}_{\ } + R^2\ , \quad R\tilde{R} \equiv \frac{1}{2}\epsilon^{\alpha\ \ \gamma\delta}R_{\alpha\ \ \rho\sigma}R_{\gamma\delta}{}^{\rho\sigma}\ . \tag{2}$$

The inflaton field ϕ has the potential $V(\phi)$. We have introduced coupling functions $\xi(\phi)$ and $\omega(\phi)$. In principle, these functions should be calculated from the fundamental theory, such as superstring theory. Hence, it might be important to put constraints on these functions through observations.

[1]E-mail:satoh@tap.scphys.kyoto-u.ac.jp
[2]E-mail:jiro@tap.scphys.kyoto-u.ac.jp

Let us take the flat Friedmann-Robertson-Walker(FRW) metric

$$\mathrm{d}s^2 = -\mathrm{d}t^2 + a^2(t)\delta_{ij}\mathrm{d}x^i\mathrm{d}x^j \ , \tag{3}$$

where a is the scale factor. From the action (1), we obtain following background equations

$$3M_{\rm Pl}^2H^2 = \frac{1}{2}\dot{\phi}^2 + V + \frac{3}{2}H^3\dot{\xi} \ , \quad \ddot{\phi} + 3H\dot{\phi} + \frac{3}{2}H^2(\dot{H}+H^2)\xi_{,} \ + V_{,} \ = 0 \ , \tag{4}$$

where a dot denotes the derivative with respect to the cosmic time, and H is the Hubble parameter defined by $H \equiv \dot{a}/a$. Note that coupling function ξ works as the effective potential for the inflaton ϕ.

We consider the friction-dominated slow-roll inflation phase where the following inequalities hold:

$$\frac{\dot{\phi}^2}{M_{Pl}^2H^2} \ll 1 \ , \quad \frac{H^3\dot{\xi}}{M_{Pl}^2H^2} = \frac{H\dot{\xi}}{M_{Pl}^2} \ll 1 \ , \quad \frac{\dot{H}}{H^2} \ll 1 \ , \quad \frac{\ddot{\phi}}{H\dot{\phi}} \ll 1 \ . \tag{5}$$

Under these circumstances, Eqs.(4) read

$$H^2 = \frac{V}{3M_{\rm Pl}^2}, \quad \dot{\phi} = -\frac{V_{,}}{3H} - \frac{1}{2}H^3\xi_{,} \quad . \tag{6}$$

The inflation is driven by the potential V, whereas the dynamics of the scalar field is also determined by the Gauss-Bonnet term.

From consistency conditions, we define *five* slow-roll parameters,

$$\epsilon \equiv \frac{M_{\rm Pl}^2}{2}\frac{V_{,}^2}{V^2} \ , \quad \eta \equiv M_{\rm Pl}^2\frac{V_{,}}{V} \ , \quad \alpha \equiv \frac{V_{,}\ \xi_{,}}{4M_{\rm Pl}^2} \ , \quad \beta \equiv \frac{V\xi_{,}}{6M_{\rm Pl}^2} \ , \quad \gamma \equiv \frac{V^2\xi_{,}^2}{18M_{\rm Pl}^6} = \frac{4}{9}\frac{\alpha^2}{\epsilon} \ , \tag{7}$$

and impose that $\epsilon, |\eta|, |\alpha|, |\beta|, \gamma \ll 1$. Note that, due to the Gauss-Bonnet term, the number of parameters and accompanying conditions increased. What we want to know is the effect of new parameters α, β, γ on the cosmological fluctuations.

3 Perturbations

In this section, we show the higher curvature corrections to the scalar and tensor perturbations. We consider the scalar perturbations A, B, ψ, E and tensor perturbations h_{ij} defined by the perturbed metric

$$ds^2 = a^2(\tau)\left[-(1+2A)d\tau^2 + B_{|i}\mathrm{d}\eta\mathrm{d}x^i + (\delta_{ij} + 2\psi\delta_{ij} + 2E_{|ij} + h_{ij})\mathrm{d}x^i\mathrm{d}x^j\right] \ , \tag{8}$$

where τ is conformal time defined by $a(t)\mathrm{d}\tau = \mathrm{d}t$, the bar denotes the spatial derivative and the prime represents the derivative with respect to the conformal time. We take the gauge, $E = \delta\phi = 0$.

We can calculate perturbation quantities following same procedures in the case of ordinary slow-roll inflation. Hence we skip tedious but straightforward calculations. We define power spectrum as

$$\langle 0|\hat{\psi}^\dagger\hat{\psi}|0\rangle = \int \mathrm{d}(\log k)\mathcal{P}_\psi(k) \ , \quad \langle 0|\hat{h}_{ij}\hat{h}^{ij}|0\rangle = \sum\int \mathrm{d}(\log k)\mathcal{P}_{\rm T} \ = \int \mathrm{d}(\log k)\mathcal{P}_{\rm T} \ , \tag{9}$$

where $\pm$ denotes helicity of gravitational waves. The results are

$$\mathcal{P}_\psi(k) = \frac{1}{2\epsilon + 4\alpha/3 + \gamma/2}\left(\frac{H}{2\pi}\frac{\Gamma(\nu_\psi)}{\Gamma(3/2)}\right)^2\left(\frac{-k\tau}{2}\right)^{3-2\ \psi} \tag{10}$$

$$\mathcal{P}_{\rm T}(k) = \frac{4}{1+\epsilon-\alpha-\gamma}\left(\frac{H}{2\pi}\frac{\Gamma(\nu_{\rm T})}{\Gamma(3/2)}\right)^2\left(\frac{-C_{\rm T}k\tau}{2}\right)^{3-2\ {\rm T}}\left(1 \pm \frac{\pi}{2}\frac{H}{M_{\rm c}}\Omega\right) \ , \tag{11}$$

where we defined $\nu_\psi \equiv 3/2 + 3\epsilon - \eta - \alpha/3 - \beta$ and $\nu_{\rm T} \equiv 3/2 + \epsilon + \alpha/3$, and Ω is another small quantity, representing effect of parity violating term, defined by

$$\Omega \equiv \frac{1}{2}\frac{M_{\rm c}}{M_{\rm Pl}}\frac{\dot{\omega}}{M_{\rm Pl}} \simeq \text{const.} \ , \tag{12}$$

where $M_{\rm c}$ is the physical wave-number corresponding to the cut-off scale, *e.g.* string scale. We can read the scalar and tensor spectral indices $n_\psi, n_{\rm T}$

$$n_\psi - 1 = 3 - 2\nu_\psi = -6\epsilon + 2\eta + \frac{2}{3}\alpha + 2\beta \ , \quad n_{\rm T} = 3 - 2\nu_{\rm T} = -2\epsilon - \frac{2}{3}\alpha \ . \tag{13}$$

Of course, in the absence of the Gauss-Bonnet term, $\alpha = \beta = 0$, we recover the conventional formula.

The most impressive result is shown in Eq.(13). In the usual case, because $\epsilon > 0$, $n_{\rm T}$ takes a negative value, namely, the tensor spectrum is red. However, if we incorporate the effect of the Gauss-Bonnet term, tensor spectrum could be blue, because α takes either positive or negative value. Hence, detection of the blue spectrum in the gravitational waves through the observation of B-mode polarization might indicate the existence of the Gauss-Bonnet term.

From the scalar and tensor spectrum, we can deduce the tensor-to-scalar ratio r:

$$r \equiv \frac{\mathcal{P}_{\rm T}}{\mathcal{P}_\psi} \sim 16\epsilon + \frac{32}{3}\alpha + 4\gamma = 16\epsilon + \frac{32}{3}\alpha + \frac{16}{9}\frac{\alpha^2}{\epsilon} \quad \frac{32}{3}\left(\alpha + |\alpha|\right) \ . \tag{14}$$

For a negative α, we have the minimum, that is, $r = 0$. In the case 1 α ϵ, the last term dominates and give rise to the sizable tensor-to-scalar ratio even if ϵ is extremely small.

Another interesting observable is the circular polarization Π, which is defined as difference between left and right helicity modes

$$\Pi \equiv \frac{\mathcal{P}_{\rm T}^+ - \mathcal{P}_{\rm T}^-}{\mathcal{P}_{\rm T}^+ + \mathcal{P}_{\rm T}^-} = \frac{\pi}{2}\frac{H}{M_{\rm c}}\Omega \ . \tag{15}$$

This result for circular polarization is the same as the previous work [5], although they considered only parity violating term. Let us consider some extreme case, $H = 10^{-4}M_{\rm Pl}$, $M_{\rm c} = 10^{-3}M_{\rm Pl}$, $\Omega = 0.1$, then, the ratio becomes $\Pi \simeq 0.015$. This means we have a hope to measure the sub-percent order of polarization due to the parity violating term [6]. It should be stressed that the effect of the Gauss-Bonnet term could enhance the amplitude of the primordial gravitational waves. That also enhances the detectability.

4 Observational implications

In the previous sections, we have derived general formula for observables in slow-roll inflation with higher curvature corrections. Here, we will discuss one model as an illustration. Let us consider chaotic inflation models with higher curvature corrections. We take the functions as

$$V = \frac{1}{2}m^2\phi^2 \ , \quad \xi = \ {\rm e}^{-\kappa \ /M_{\rm Pl}} \ , \tag{16}$$

where m is the mass of the inflaton and $\ , \kappa$ are parameters of the coupling function ξ. Then, the slow-roll parameters can be calculated as

$$\epsilon = \eta = 2\frac{M_{\rm Pl}^2}{\phi^2}, \quad \alpha = -\frac{\kappa}{4}\frac{m^2\phi}{M_{\rm Pl}^3}{\rm e}^{-\kappa \ /M_{\rm Pl}}, \quad \beta = \frac{\kappa^2}{12}\frac{m^2\phi^2}{M_{\rm Pl}^4}{\rm e}^{-\kappa \ /M_{\rm Pl}}, \quad \gamma = \frac{\kappa^{2\ 2}}{72}\frac{m^4\phi^4}{M_{\rm Pl}^8}{\rm e}^{-2\kappa \ /M_{\rm Pl}} \ . \tag{17}$$

We can evaluate the spectral index and the tensor-to-scalar ratio. The results are shown in FIG.1. We have also plotted constraints from WMAP 5-year result, combined with baryon acoustic oscillations (BAO) and Type I supernova (SN). We see these observables are sensitive to higher curvature corrections. Hence, it implies that the higher curvature corrections are relevant to precision cosmology. Here, we notice that there exist parameter regions represented by blue lines which leads to the blue spectrum in tensor modes. We plotted some typical values of $n_{\rm T}$ in Fig.1.

5 Conclusion

We have studied the slow-roll inflationary scenario with the leading corrections, namely, the Gauss-Bonnet and the parity violating terms. We have obtained the higher curvature corrections to the scalar spectral

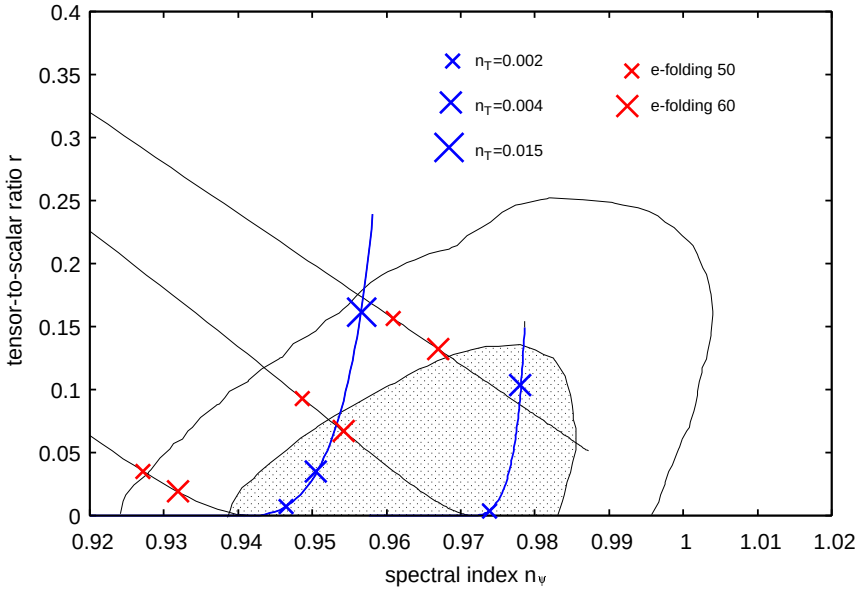

Figure 1: Expected spectral index n_ψ and tensor-to-scalar ratio r of the model (16) are shown. We have also plotted constraints from WMAP 5-year result, combined with BAO and Type I SN. The contours denote 68% and 95% confidence level. We used the out-put from Cosmological Parameters Plotter at LAMBDA [7]. Each line corresponds to the parameter (i) $m = 10^{-5} \times M_{\rm Pl}$, $\quad = 0$, $\kappa = 0$ (ordinary slow-roll), (ii) $m = 10^{-5} \times M_{\rm Pl}$, $\quad = 10^{10}$, $\kappa = 0.003$ and (iii) $m = 10^{-5} \times M_{\rm Pl}$, $\quad = 10^{10}$, $\kappa = 0.01$, from upper to lower, taking $\phi > 0$. Blue-colored lines denote the region that generate blue spectrum in tensor modes, and we plot some values of $n_{\rm T}$.

index, the tensor spectral index, and the tensor-to-scalar ratio. We found that the higher curvature corrections can not be negligible in the dynamics of the scalar field, although they are negligible in the Friedmann equation. It turned out that the tensor-to-scalar ratio could be enhanced because of the modified dynamics of the scalar field. We have found the tensor spectral index could be blue due to the Gauss-Bonnet term. We have also calculated the degree of circular polarization of gravitational waves generated during the slow-roll inflation. We discussed that the circular polarization can be observable due to the Gauss-Bonnet and parity violating terms. We revealed that the observables are sensitive to the higher curvature corrections.

References

[1] E. Komatsu *et al.*, arXiv:0803.0547[astro-ph].

[2] S. Weinberg, arXiv:0804.4291[hep-th].

[3] I. Antoniadis, J. Rizos and K. Tamvakis, Nucl. Phys. B **415**, 497 (1994) [arXiv:hep-th/9305025].

[4] S. Kawai and J. Soda, Phys. Rev. D **59**, 063506 (1999) [arXiv:gr-qc/9807060]; S. Nojiri, S. D. Odintsov and M. Sasaki, Phys. Rev. D **71**, 123509 (2005) [arXiv:hep-th/0504052]; A. Lue, L. M. Wang and M. Kamionkowski, Phys. Rev. Lett. **83**, 1506 (1999) [arXiv:astro-ph/9812088]; M. Satoh, S. Kanno and J. Soda, Phys. Rev. D **77**, 023526 (2008), arXiv:0706.3585[astro-ph].

[5] S. Alexander and J. Martin, Phys. Rev. D **71**, 063526 (2005) [arXiv:hep-th/0410230];

[6] S. Saito, K. Ichiki and A. Taruya, JCAP **0709**, 002 (2007), arXiv:0705.3701 [astro-ph]; N. Seto, Phys. Rev. Lett. **97**, 151101 (2006) [arXiv:astro-ph/0609504].

[7] `http://lambda.gsfc.nasa.gov/`

Entanglement of Universe

Shintaro Sawayama[1]

[1]*Sawayama cram school of physics, Atsuhara 328,Fuji-shi,Shizuoka-ken, 419-0201, Japan*

Abstract

By the recent study of the quantum gravity, we can solved the inhomogeneous space-time. And we quantized the enlarged Bianch I universe. As a result of quantization, we know the universe are entangled. The x,y, and z direction are entangled. So if we measure the x direction we know the information of the y and z directions.

1 Introduction

In the quantum gravity there are many difficulties i.e. problem of the time and problem of the norm and interpretation problem and problem of the inhomogeneous spacetime. One of the main difficulty comes form the Wheeler-DeWitt equation. The difficulty of the Wheeler-DeWitt still remain the Hamiltonian constraint of the loop quantum gravity. So we should remove the difficulty of the Wheeler-DeWitt equation.

So we construct the one method which called the up-to-down method. We explain what is the up-to-down method simply. Once we add an additional dimension to the usual 4-dimensional gravity. And we remove the additional dimension by using the problem of the time inversely. Then there appear the additional constraint equation. This is the up-to-down methodl.

The up-to-down method comes from the Isham's idea, that is quantum category. Imagine many world interpretation, and we assume may world is the infinitely many brane. We quantize the many brane at the same time.

In section II we write the result of the up-to-down method. In section III we quantize the enlarged Bianch I universe. And in section IV we discuss and conclude the presentation.

2 Up-to-down method

We skip the up-to-down method, because it is long. We cite the paper [5]. We start from 5-dimensional spacetime. There appear one additional constraint equation as,

$$\hat{H}_S \to -m\hat{H}_S := -\hat{K}^2 + \hat{K}^{ab}\hat{K}_{ab} - \frac{1}{2}\dot{P}. \tag{1}$$

Here, $\hat{H}_S$ is the Hamiltonian constraint of the 4+1 decomposition, and $\hat{K}_{ab}$ is the 4+1 extrinsic curvature and $\hat{K}$ is the it's trace and P is the 3+1 momentum. Now 4+1 decomposition is carried on the additional dimension s. This is the not usual decomposition. However, because we use the problem of the time inversely, the s direction vanished. We only consider the 4-dimensional quantum gravity. We obtain the next theorem.

Theorem 1. In this method, in the $\mathcal{H}_4$ additional constraint $m\hat{H}_S\Pi^3 = 0$ appears which we call static restriction, if there is no time evolution and the projection is defined by the difinition 3.

Here, Π^3 is the projection defined by $\Pi^3|g \quad\rangle = |g_s \quad = \text{const} g_{ij}\rangle$.

For example we first consider the Freedman universe as

$$g_{ab} := \begin{pmatrix} b & 0 & 0 & 0 \\ 0 & a & 0 & 0 \\ 0 & 0 & a & 0 \\ 0 & 0 & 0 & a \end{pmatrix}. \tag{2}$$

[1]E-mail:sawayama0410@gmail.com

The modified Hamiltonian constraint becomes as

$$m\hat{H}_S = 6ab\frac{\partial}{\partial a}\frac{\partial}{\partial b} + a^2\frac{\partial^2}{\partial a^2} \tag{3}$$

$$= 6\frac{\partial}{\partial \eta}\frac{\partial}{\partial \eta_b} + \frac{\partial^2}{\partial \eta^2} = 0, \tag{4}$$

And the Hamiltonian constraint becomes as well known,

$$H_S = \frac{9}{2}a^2\frac{\partial}{\partial a^2} + \Lambda \tag{5}$$

$$= \frac{9}{2}\frac{\partial}{\partial \eta^2} + \Lambda = 0. \tag{6}$$

The 4-dimensional state becomes as

$$|\Psi^4(\eta)\rangle = \exp(i\frac{\sqrt{2}}{3}\Lambda^{1/2}\eta). \tag{7}$$

And it's enlargement of 4+1 is

$$|\Psi^{5(4)}(\eta_b, \eta)\rangle = \exp\left(-i\frac{\sqrt{2}}{3}\Lambda^{1/2}\eta_b\right)\exp(i\frac{\sqrt{2}}{3}\Lambda^{1/2}\eta). \tag{8}$$

We can proof the one of the universe are appropriated to the up-to-down method. There is one enlargement and measure of the projection is not zero.

Secondary, we think about the off-diagonal metric case.

$$g_{ab} = \begin{pmatrix} -c & 0 & 0 & 0 \\ 0 & a & b & 0 \\ 0 & b & a & 0 \\ 0 & 0 & 0 & a \end{pmatrix}. \tag{9}$$

The modified Hamiltonian constraint become,

$$m\hat{H}_S = -6ac\frac{\partial}{\partial a}\frac{\partial}{\partial c} + (6a^2 - 2b^2)\frac{\partial^2}{\partial a^2} + 2(b^2 - a^2)\frac{\partial^2}{\partial b^2} = 0, \tag{10}$$

And the Hamiltonian constraint becomes as,

$$H_S = -(5a^2 - b^2)\frac{\partial}{\partial a^2} - (2b^2 - a^2)\frac{\partial^2}{\partial b^2} = 0. \tag{11}$$

This Hamiltonian constraint can not solved simply because this is the elliptic differential equation. However, if we use additional constraint as,

$$m\hat{H}_S\Pi^3 = (6a^2 - 2b^2)\frac{\partial^2}{\partial a^2} + 2(b^2 - a^2)\frac{\partial^2}{\partial b^2} = 0, \tag{12}$$

The Hamiltonian constraint can be solved.

$$|\Psi^{4(5)}(a, b)\rangle = E_1ab + E_2a + E_3b + E_4. \tag{13}$$

And the enlargement is

$$|\Psi^{5(4)}(a, b, c)\rangle = F_1ab + F_2a + F_3bc + F_4c + F_5. \tag{14}$$

This enlargement has also non zero measure of the projection.

Next we consider the Schwarzchild black holes as

$$g_{ab} = \begin{pmatrix} -f & 0 & 0 & 0 \\ 0 & f^{-1} & 0 & \\ 0 & 0 & A & 0 \\ 0 & 0 & 0 & A\sin^2\theta \end{pmatrix}. \tag{15}$$

The Hamiltonian constraint becomes as

$$H_S = \frac{1}{2}\Big(- f^2 \frac{\partial^2}{\partial f^2} + Af \frac{\partial}{\partial f}\frac{\partial}{\partial A} - 2A^2 \frac{\partial^2}{\partial A^2}\Big) + \mathcal{R} = 0, \tag{16}$$

Usually this Hamiltonian constraint does not solved. However, if we think the additional constraint equation as,

$$m\hat{H}_S \Pi^3 = -2fA\frac{\partial}{\partial f}\frac{\partial}{\partial A} + A^2 \frac{\partial^2}{\partial A^2} \tag{17}$$

$$= A\frac{\partial}{\partial A}\Big(- 2f\frac{\partial}{\partial f} + A\frac{\partial}{\partial A}\Big) = 0, \tag{18}$$

we can solve the Hamiltonian constraint equation. Although the Hamiltonian and the additional constraint equation does not commute, if we make additional constraint parameter relations, we can solve the Hamiltonian constraint. The Hamiltonian constraint become simple second order ordinal functional equations.

$$H_S = -\frac{7}{8}A^2\frac{\partial^2}{\partial A^2} + \frac{1-c^2A^2}{2A} = 0. \tag{19}$$

And this equation is solved easily by numerical method. The additional constraint or the enlargement is given by next formula.

$$m\hat{H}_S = -f^2\frac{\partial^2}{\partial f^2} + \frac{4}{7}\frac{c-cf}{f^{1/2}} = 0. \tag{20}$$

In this case the enlargement be able and measure of the projection does not zero.

3 Enlarged Bianchi I universe

Now we consider the metric diagonal case. In this case the Hamiltonian constraint becomes as,

$$\mathcal{H}_S = \sum_{ij}\frac{\delta^2}{\delta\phi_i\delta\phi_j} + \sum_{i\neq j}(\phi_{i,jj} + \phi_{i,i}\phi_{j,i})e^{\ i}. \tag{21}$$

Here, $g_{ii} = e^{\ i}$. And the commutation relation of the additional and the Hamiltonian constraint becomes as

$$[m\hat{H}_S, \mathcal{H}_4] = \delta^2\sum_{i\neq j}(\phi_{i,ii} + \phi_{i,i}^2 + \frac{1}{2}\phi_{i,i}\phi_{j,i})e^{\ i} - \frac{1}{2}\delta^2\sum_{i\neq j}\phi_{i,0}(\phi_{j,ii} - 2\phi_{i,ij} - \phi_{i,j}\phi_{i,i})e^{\ i}$$
$$-\frac{1}{2}\delta^2\sum_{i\neq j}(\phi_{i,0jj} + \phi_{i,0j}\phi_{j,j} - \phi_{i,0ji} - \phi_{i,0i}\phi_{i,j})e^{\ i}. \tag{22}$$

We know there are two case whose commutation relation is always zero. Such spacetime is following,

$$\begin{pmatrix} g_{00} & 0 & 0 & 0 \\ 0 & q_{11}(x_1) & 0 & 0 \\ 0 & 0 & q_{22}(x_2) & 0 \\ 0 & 0 & 0 & q_{33}(x_3) \end{pmatrix}. \tag{23}$$

and

$$\begin{pmatrix} g_{00} & 0 & 0 & 0 \\ 0 & q_{11}(x_2,x_3) & 0 & 0 \\ 0 & 0 & q_{22}(x_1,x_3) & 0 \\ 0 & 0 & 0 & q_{33}(x_1,x_2) \end{pmatrix}. \tag{24}$$

If we treat first metric, the Hamiltonian constraint become,

$$\mathcal{H}_S = \sum_i \frac{\delta^2}{\delta\phi_i^2} = 0. \tag{25}$$

And the additional constraint with cosmological constant becomes as

$$\mathcal{S} = \sum_{i\neq j} \frac{\delta^2}{\delta\phi_i\delta\phi_j} = \Lambda \tag{26}$$

The solution of the usual Hamilton constraint is,

$$|\Psi^4(\phi)\rangle = \prod \exp(a_i\Lambda^{1/2}\int \phi_i\delta\phi_i(x_i)). \tag{27}$$

In the a_i there are two equation as

$$a_1a_2 + a_1a_3 + a_2a_3 = 1 \tag{28}$$

$$a_1^2 + a_2^2 + a_3^2 = 1. \tag{29}$$

Because there are two equation and three parameter, there are infinitely many basis. However, if we assume the one of the norm of a_i is one, we can obtain 12 basis as follows

$$a_1 = \pm\sqrt{3}, a_2 = \pm i, a_3 = \mp i \tag{30}$$

$$a_1 = \pm i, a_2 = \pm\sqrt{3}, a_3 = \mp i \tag{31}$$

$$a_1 = \pm i, a_2 = \mp i, a_3 = \pm\sqrt{3}. \tag{32}$$

Looking these basis we can easily know that the state is entangled.

4 Conclusion and Discussions

If we only solve the usual Bianch I universe, the spacetime are entangled. The difference of the enlarged Bianch I and usual Bianch I universe are eta square or only eta. Because three direction are entangled, by the measurement of the x direction, we know y direction and z direction. And we justify the up-to-down method. the measure of the all the projection treated here has non zero measure. In this case we only consider the cosmological constant. But we can consider the Schrodinger or the Krein-Gordon field instead of the cosmological constant. Then we can know the information of the spacetime by the measurement of the field. We can answer the philosophical problem " what is existence " by the physics.

References

[1] C.J.Isham and A.Ashtekar Class. Quant. Grav. **9** 1433 (1992)

[2] C.Rovelli Quantum Gravity; Cambridge monographs on mathematical physics (2004)

[3] T.Thiemann gr-qc/0110034 (2001)

[4] C.J.Isham Adv.Theor.Math.Phys. 7 331 (2003)

[5] S.Sawayama gr-qc/0604007 (2006)

[6] B.S.DeWitt Phys. Rev. **160** 1113 (1967)

[7] J.J.Halliwell and J.B.Hartle Phys. Rev. **D 43** 1170 (1991)

[8] Quantum computation and quantum information, M.A.Nielsen and I.L.Chang, Cambridge, (2000)

[9] A.Hosoya, privet discussions

Invariances of generalized uncertainty principles

Fabio Scardigli[1]

Leung Center for Cosmology and Particle Astrophysics (LeCosPA), Department of Physics, National Taiwan University, Taipei 106, Taiwan

Abstract

In Ref.[1] we use two different generalized uncertainty principles to compute mass thresholds and lifetimes for micro black holes close to their Planck phase. Motivated by that paper, we study here in detail the conditions for the translation and rotation invariance of these two different kinds of deformed commutation relations.

1 Introduction

When we consider a high energy collision, we know that Heisenberg principle $\Delta p \Delta x \geq \hbar/2$ can be casted in the form $\Delta E \Delta x \geq \hbar c/2$ (since $\Delta E \simeq c\Delta p$). Actually, the main reason since larger and larger energies are required to explore smaller and smaller details is that the size of the smallest detail theoretically detectable with a beam of energy E is $\delta x = \hbar c/(2E)$. An equivalent argument comes from considering the resolving power of a "microscope": the smallest resolvable detail goes roughly as the wavelength of the employed photons, and therefore $\delta x \simeq \lambda = \frac{c}{\nu} = \frac{hc}{\epsilon}$.

The research on viable generalizations of the Heisenberg uncertainty principle traces back to many decades (see for early approaches [2], etc. See for a review [3] and for more recent approaches [4]). In the last 20 years, there have been seminal studies in string theory [5] suggesting that for very high energy scattering the uncertainty relation (ST GUP) should be written (in $4+n$ dimensions) as

$$\delta x \geq \frac{\hbar c}{2E} + \beta \ell_{4n} \frac{E}{\mathcal{E}_{4n}}\,, \tag{1}$$

where ℓ_{4n} is the $4+n$ dimensional Planck length and E is the energy of the colliding beams (we use the relation $\mathcal{E}_{4n}\ell_{4n} = \hbar c/2$). If however we take into account the possibility of a formation of micro black holes in the scattering, with a gravitational radius of $R_S \sim (E)^{1/(n+1)}$, then we easily see that in $4+n$ dimensions (and $n \geq 1$) the stringy principle seems to forbid the very observation of the micro hole itself. In fact, at high energy the error predicted by the stringy GUP goes like $\delta x \sim E$, while the size of the hole goes like $R_S \sim (E)^{1/(n+1)}$. For E large enough and $n \geq 1$, we always have $E > (E)^{1/(n+1)}$, thereby loosing the possibility of observing micro black holes, just when they become massive (that is, when they should approach the classicality). Also to avoid this state of affairs, and on the ground of gedanken experiments involving the formation of micro black holes, it has been proposed [6] a modification of the uncertainty principle, that in $4+n$ dimensions reads

$$\delta x \geq \frac{\hbar c}{2E} + \beta R_{4n}(E)\,, \tag{2}$$

where R_{4n} is the $4+n$ dimensional Schwarzschild radius associated with the energy E (see [7])

$$R_{4n} = \left[\frac{16\pi G_{4n} E}{(N-1)\Omega_{N-1}c^4}\right]^{\frac{1}{N-2}} = \ell_{4n}\left(\omega_n \frac{E}{\mathcal{E}_{4n}}\right)^{\frac{1}{n+1}} \tag{3}$$

and $N = 3+n$ is the number of space-like dimensions, $\omega_n = 8\pi/((N-1)\Omega_{N-1})$, $\Omega_{N-1} = 2\pi^{N/2}/\Gamma(N/2) =$ area of the unit $\mathrm{S}^{\mathrm{N}-1}$ sphere. Thus, the GUP originating from micro black hole gedanken experiments (MBH GUP) can be written as

$$\delta x \geq \frac{\hbar c}{2E} + \beta \ell_{4n}\left(\omega_n \frac{E}{\mathcal{E}_{4n}}\right)^{\frac{1}{n+1}}\,, \tag{4}$$

[1]E-mail: fabio@phys.ntu.edu.tw

where β is the deformation parameter, generally believed of $O(1)$. Remarkably, in 4 dimensions ($N = 3$, $n = 0$) the two principles coincide. The deformation parameter β, supposed independent from the dimensions N, can be therefore chosen as the same for both principles.

2 Translation and rotation invariance of the GUPs

In this section we shall prove that the GUPs previously introduced do respect the constraints posed by requiring the conventional translation and rotation invariance of the commutation relations. First, we show what these kinematic constraints imply about the structure, in $4 + n$ dimensions, of the $[x, p]$ commutations relations. In this, we follow closely Ref. [8]. As a general ansatz for the x, p commutation relation in $4 + n$ dimensions we take

$$[x_i, p_j] = i\,\hbar\;\Theta_{ij}(p) \tag{5}$$

and we require that $\Theta_{ij}(p)$ differs significantly from δ_{ij} only for large momenta. We assume also $[p_i, p_j] = 0$ and we compute the remaining commutation relation through the Jacobi identities, obtaining

$$[x_i, x_j] = i\hbar\{x_a,\ \Theta^{-1}_{ar}\Theta_{s[i}\Theta_{j]r,s}\} \tag{6}$$

where $\{\}$ are the anti-commutators and $Q_{,s} := \partial Q/\partial s$. The commutation relations (5) are translation invariant (they are preserved under the transformations $x_i \to x_i + d_i, \quad p_i \to p_i$). However, the commutation relations (6) are not invariant under translation, unless we require $\Theta_{ij}(p)$ to be such that it yields $[x_i, x_j] = 0$. Thus, in order to implement translation invariance, Θ_{ij} must satisfy the necessary and sufficient condition (read off from the (6))

$$\Theta_{ia}\partial_{p_i}\Theta_{bc} = \Theta_{ib}\partial_{p_i}\Theta_{ac} \tag{7}$$

where sum over i is understood. The rotation invariance can be implemented by requiring Θ_{ij} to have the form

$$\Theta_{ij}(p) = f(p^2)\delta_{ij} + g(p^2)p_i p_j\,. \tag{8}$$

Together, conditions (7) and (8) imply that f and g must satisfy the differential equation

$$2f'f + (2p^2 f' - f)g = 0 \tag{9}$$

where $f'(p^2) = df/d(p^2)$. Under these conditions, commutation relations do obey translation and rotation invariance. Considering, for sake of simplicity, the mono-dimensional case $i = j$, we write for the main commutator

$$[x, p] = i\hbar(f(p^2) + g(p^2)p^2)\,. \tag{10}$$

The usual Heisenberg commutator is recovered by choosing, for example, $f(p^2) = 1$. Then Eq.(9) implies $g(p^2) = 0$ and $[x, p] = i\hbar$. The stringy inspired commutator is obtained, to the first order in β, by choosing $g(p^2) = \beta$ (see [8]). Then, in fact, solving (9) (a Manfredi equation, in such case), we find

$$f(p^2) = \frac{\beta p^2}{\sqrt{1 + 2\beta p^2} - 1} \simeq 1 + \frac{\beta}{2}p^2 + O((\beta p^2)^2) \tag{11}$$

and, to the first order in β (or, equivalently, for small p) we have

$$[x, p] = i\hbar\left(1 + \frac{3}{2}\beta p^2 + O(\beta^2)\right)\,. \tag{12}$$

The MBH GUP (4) can be written in terms of momentum transferred as $p\,\delta x \gtrsim \frac{\hbar}{2}\left(1 + \gamma p^{\frac{n+2}{n+1}}\right)$ where $\gamma = \beta(\omega_n)^{\frac{1}{n+1}}\left(\frac{2\ell_{4n}}{\hbar}\right)^{\frac{n+2}{n+1}}$ and this in terms of commutators becomes

$$[x, p] = i\hbar\left(1 + \gamma p^{\frac{n+2}{n+1}}\right)\,. \tag{13}$$

To show that MBH GUP is translation and rotation invariant we must show that the commutator (13) is of the same form of commutator (10) (when $p \to 0$), with f and g satisfying (9) (in particular we would like to have $f(p^2) \to 1$ for $p \to 0$). However, the previous strategy, namely to fix a priori a given form for $g(p^2)$ and then to compute $f(p^2)$ by solving (9) (as we did for HUP, $g(p^2) = 0$, and for stringy GUP, $g(p^2) = \beta$), in this case does not work. Even if one puts $p^2 g(p^2) = \gamma p^{(n+2)/(n+1)}$, Eq.(9) becomes however rather complicated (it is an Abel equation of 2^{nd} kind), and hardly we can hope it gives $f(p^2) \to 1$ for $p \to 0$. Moreover, an explicit solution could not be so useful, since we are mainly interested in an asymptotic behaviour. Therefore we ask the following general properties to be satisfied by the functions f and g

$$\begin{cases} [f(p^2) + g(p^2)p^2] \to [1 + \gamma p^{\frac{n+2}{n+1}}] \quad \text{for} \quad p \to 0 \\ \\ 2f'f + (2f'p^2 - f)g = 0\,, \end{cases} \tag{14}$$

We shall look if there actually exist f and g such that the above two properties can be simultaneously satisfied. In this way the rotational and translational invariance of GUP (4) will result proved. In what follows such solutions are proved to exist, provided we allow g to develop poles (of course, the function f and the whole function $f + gp^2$ remain perfectly finite).

In the differential equation (9) everything is function of p^2 and $f'(p^2) = df/d(p^2)$. So, let's set $y := p^2$ ($y > 0$, $p = y^{1/2}$) and, to avoid fractionary powers, set also $y^{\frac{1}{2(n+1)}} =: \lambda$, $y = \lambda^{2(n+1)}$. Then $f'(y) = \frac{1}{2(n+1)}\lambda^{-(2n+1)}F'(\lambda)$, and the system (14) becomes

$$\begin{cases} [F(\lambda) + G(\lambda)\lambda^{2(n+1)}] \to [1 + \gamma\lambda^{n+2}] \quad \text{for} \quad \lambda \to 0 \\ \\ F'(\lambda)F(\lambda) + [\lambda F'(\lambda) - (n+1)F(\lambda)]G(\lambda)\lambda^{2n+1} = 0\,. \end{cases} \tag{15}$$

We have to see if the two conditions are compatible, and what this implies for f and g. To check this compatibility we can use power series representations of the functions $F(\lambda)$, $G(\lambda)$. We allow $G(\lambda)$ to develop poles. Since the factor $\lambda^{2(n+1)}$ multiplies $G(\lambda)$ in the boundary condition, we could allow poles until $\lambda^{-2(n+1)}$ and still the combination $[F + G\lambda^{2(n+1)}]$ would remain analytical. However, we'll show that the result can be obtained by allowing poles just until λ^{-n} only. So we write

$$F(\lambda) = \sum_{k=0}^{\infty} a_k \lambda^k \qquad \text{and} \qquad G(\lambda) = \sum_{k=-n}^{\infty} b_k \lambda^k\,. \tag{16}$$

and we look for what the two conditions imply on the coefficients a_k, b_k. We have

$$F(\lambda) + G(\lambda)\lambda^{2(n+1)} = \sum_{k=0}^{\infty} (a_k + b_{k-2(n+1)})\lambda^k \tag{17}$$

where $b_{k-2(n+1)} = 0$ for $k = 0, 1, 2, ..., n+1$ and $b_{-n} \neq 0$, $b_{-n+1} \neq 0$, etc.
At small λ we should have the matching, for $\lambda \to 0$,

$$\sum_{k=0}^{\infty} (a_k + b_{k-2(n+1)})\lambda^k \longrightarrow 1 + \gamma\lambda^{n+2}\,. \tag{18}$$

This means

$$\begin{array}{lllll} k = 0; & [a_0 + b_{-2(n+1)}] = 1 & \Rightarrow & a_0 = 1 \\ k = 1; & [a_1 + b_{1-2(n+1)}] = 0 & \Rightarrow & a_1 = 0 \\ k = 2; & [a_2 + b_{2-2(n+1)}] = 0 & \Rightarrow & a_2 = 0 \\ \ldots & \ldots & \ldots & \\ k = n+2; & [a_{n+2} + b_{-n}] = \gamma & \Rightarrow & (*) \\ k = n+3; & [a_{n+3} + b_{-n+1}] = \text{any quantity} & & \\ \ldots & \ldots & \ldots & \end{array} \tag{19}$$

(*) here at least b_{-n} is $\neq 0$, therefore at least b_{-n} can be chosen equal to γ.
Now let's see if the conditions on a_k, b_k just found above, required by the first of Eqs.(15), are compatible with those required by the differential equation (15). Since $F'(\lambda) = \sum_{k=0}^{\infty}(k+1)a_{k+1}\lambda^k$, $G(\lambda) = \sum_{k=-n}^{\infty} b_k\lambda^k = \sum_{k=0}^{\infty} b_{k-n}\lambda^{k-n}$ (with $b_{-n} \neq 0$, $b_{-n+1} \neq 0$,..., $b_0 \neq 0$), we have $F(\lambda)F'(\lambda) = \sum_{k=0}^{\infty} C_k\lambda^k$, $G(\lambda)F'(\lambda) = \sum_{k=0}^{\infty} D_k\lambda^{k-n}$, $F(\lambda)G(\lambda) = \sum_{k=0}^{\infty} E_k\lambda^{k-n}$, where $C_k = \sum_{q=0}^{k}(q+1)a_{k-q}a_{q+1}$, $D_k = \sum_{q=0}^{k}(q+1)b_{k-n-q}a_{q+1}$, $E_k = \sum_{q=0}^{k} a_{k-q}b_{q-n}$ and the differential equation (15) becomes

$$\sum_{k=0}^{\infty}\left[C_k\lambda^k + D_k\lambda^{k+n+2} - (n+1)E_k\lambda^{k+n+1}\right] = 0 \tag{20}$$

Reshuffling indexes a bit in Eq.(20) we get

$$\sum_{k=0}^{\infty}\left[C_k + D_{k-n-2} - (n+1)E_{k-n-1}\right]\lambda^k = 0 \tag{21}$$

where $D_{-n-2} = 0$, $D_{1-n-2} = 0$, ..., $D_{-1} = 0$, and $E_{-n-1} = 0$, $E_{1-n-1} = 0$, ..., $E_{-1} = 0$, and it is easy to see that these relations are direct consequences of the definitions for b_k in Eq.(17) and of relations (19). Equation (21) can be satisfied only if all the coefficients of λ^k are identically zero. We can now check explicitly that this requirement is in full agreement with conditions (19). In fact: $k = 0$; $C_0 + D_{-n-2} - (n+1)E_{-n-1} = a_0a_1 = 0 \Rightarrow a_1 = 0$ (since $a_0 = 1$) and this agrees with (19). And then $k = 1$; $C_1 + D_{1-n-2} - (n+1)E_{1-n-1} = a_1a_1 + 2a_0a_2 = 0 \Rightarrow a_2 = 0$ (since $a_0 = 1$) and this agrees with (19). Again, for $k = 2$ we have $C_2 + D_{2-n-2} - (n+1)E_{2-n-1} = 0 \Rightarrow a_3 = 0$ and so on for $k = 3, 4, ...$ For $k = n$ we find $a_{n+1} = 0$ in agreement with (19). For $k = n+1$ we have

$$C_{n+1} + D_{-1} - (n+1)E_0 = \sum_{q=0}^{n+1}(q+1)a_{n+1-q}a_{q+1} - (n+1)\sum_{q=0}^{0} a_{0-q}b_{q-n} = (n+2)a_0a_{n+2} - (n+1)a_0b_{-n} = 0$$

Since $a_0 = 1$, then $(n+2)a_{n+2} - (n+1)b_{-n} = 0$ and this equation *is* compatible with the "$k = n+2$" condition of (19). In fact, we have two equations in two unknowns

$$(n+2)a_{n+2} - (n+1)b_{-n} = 0 \qquad \text{and} \qquad a_{n+2} + b_{-n} = \gamma\,, \tag{22}$$

which allow us to compute a_{n+2} (the first non zero coefficient for $F(\lambda)$, after $a_0 = 1$) and b_{-n} (pole of order n of $G(\lambda)$). For the next case, $k = n+2$, we don't have evidently any problem, since Eq.(19) simply gives $(a_{n+3} + b_{-n+1}) =$*any quantity*. Therefore any relation between a_{n+3}, b_{-n+1} required by the differential equation in (15) is acceptable. Note moreover that if we allowed poles for $G(\lambda)$ with a degree less than n, we would find contradiction between the conditions (18)-(19), *and* the differential equation in (15). Thus, we conclude that the two conditions (15) are compatible (if we allow $G(\lambda)$ to develop poles). So the MBH GUP, as well as the ST GUP, are translational and rotational invariant. Q.E.D.

References

[1] F. Scardigli, *Glimpses on the micro black hole Planck phase*, [arXiv:0809.1832 (hep-th)]

[2] C.N. Yang, Phys. Rev. **72**, 874 (1947); F. Karolyhazy, Nuovo Cim. A **42**, 390 (1966).

[3] L.J. Garay, Int. J. Mod. Phys. A **10**, 145 (1995).

[4] M.Maggiore, Phys. Lett. B **304**, 65 (1993); F. Scardigli, Phys. Lett. B **452**, 39 (1999).

[5] D.Amati, M.Ciafaloni, G.Veneziano, Phys. Lett. B **197**, 81 (1987); D.J.Gross, P.F.Mende, Phys. Lett. B **197**, 129 (1987); K.Konishi, G.Paffuti, P.Provero, Phys. Lett. B **234**, 276 (1990).

[6] F. Scardigli, Phys. Lett. B **452**, 39 (1999); F.Scardigli, R.Casadio, Class. Quant. Grav. **20**, 3915 (2003).

[7] R.C.Myers, M.J.Perry, Annals of Physics **172**, 304 (1987).

[8] A.Kempf, J. Phys. A Math. Gen.**30**, 2093 (1997); A.Kempf, G.Mangano, Phys. Rev. D **55**, 7909 (1997).

[9] A.Kempf, G.Mangano, R.B.Mann, Phys. Rev. D **52**, 1108 (1995); Y.Himemoto, T.Tanaka, Phys. Rev. D **61**, 064004 (2000); G.Amelino-Camelia, *Quantum Gravity Phenomenology*, [arXiv:0806.0339]; G.Amelino-Camelia, M.Arzano, Y.Ling, G.Mandanici, Class. Quant. Grav. **23**, 2585 (2006); N.Sasakura, JHEP **05** 015 (2000); G.L. Alberghi, R. Casadio, A. Tronconi, Phys. Lett. B **579**, 1 (2004).

Towards clarifying the central engine of long gamma-ray bursts

Yuichiro Sekiguchi[1]

Division of Theoretical Astronomy, National Astronomical Observatory of Japan, Mitaka, Tokyo 181-8588, Japan

Abstract

Towards clarifying the formation processes of a system of black hole and massive accretion disk, we updated our full GR numerical code with microphysics (a finite temperature EOS, electron capture, local neutrino emission, and simplified treatment of neutrino cooling). Our new code shows an advanced performance that our results of spherical collapse agree quite well with those by the Boltzmann transport. We also calculate the gravitational-wave spectrum from convective activities occurred after the bounce.

1 Introduction

The observed spectroscopic connections between several SNe and long gamma-ray bursts (LGRBs) with SNe suggested that at least some LGRBs are associated with supernovae and the core collapse of massive stars. The collapsar model [1], in which the central engine of LGRBs is composed of a rotating black hole (BH) surrounded by a massive accretion disk formed after the collapse of rapidly rotating massive stellar core is currently one of the promising models of central engine of LGRBs.

To clarify the formation process of such BH-disk system, it is necessary to perform multidimensional simulations in full general relativity employing a finite temperature EOS and detailed microphysics. In this article, we briefly report our recent progress of the works.

2 Basic equations

The basic equations are the baryon conservation equation

$$\nabla_\alpha(\rho u^\alpha) = 0, \tag{1}$$

the lepton conservation equations,

$$\nabla_\alpha(\rho Y_e u^\alpha) = S_{Y_e}, \tag{2}$$

$$\nabla_\alpha(\rho Y_{\nu_i} u^\alpha) = S_{Y_{\nu_i}}, \tag{3}$$

where $\nu_i = \nu_e, \bar{\nu}_e, \nu_\mu$, and ν_τ, and the local conservation equation of the energy-momentum $\nabla_\alpha (T^{\rm Total})^\alpha_\beta = 0$. Here ρ and u^μ are the rest mass density and the 4-velocity.

The total stress-energy-momentum tensor is the sum of the fluid part ($T^{\rm (f)}_{\alpha\beta}$) and the neutrino part ($T^{(\nu)}_{\alpha\beta}$) as $(T^{\rm Tot})_{\alpha\beta} = (T^{\rm F})_{\alpha\beta} + (T^{\nu})_{\alpha\beta}$, where $(T^{\rm F})_{\alpha\beta}$ is the stress-energy-momentum tensor of the fluid assumed to take the form of the perfect fluid $(T^{\rm F})_{\alpha\beta} = (\rho + \rho\varepsilon^{\rm F} + P^{\rm F})u_\alpha u_\beta + P^{\rm F} g_{\alpha\beta}$, and $\varepsilon^{\rm F}$ and $P^{\rm F}$ denote the specific internal energy density and the pressure of the fluid. The neutrino part $(T^{\nu})_{\alpha\beta}$ is formally divided into 'trapped-neutrino' ($(T^{\nu,{\rm t}})_{\alpha\beta}$) and 'streaming-neutrino' ($(T^{\nu,{\rm s}})_{\alpha\beta}$) parts as

$$(T^{\nu})_{\alpha\beta} = (T^{\nu,{\rm t}})_{\alpha\beta} + (T^{\nu,{\rm s}})_{\alpha\beta}.$$

We assume that the stress-energy-momentum tensor of the trapped-neutrino part takes the form of the perfect fluid and is combined with the fluid part to give

$$T_{\alpha\beta} \equiv (T^{\rm F})_{\alpha\beta} + (T^{\nu,{\rm t}})_{\alpha\beta} = (\rho + \rho\varepsilon + P)u_\alpha u_\beta + P g_{\alpha\beta}.$$

[1]E-mail:sekig@th.nao.ac.jp

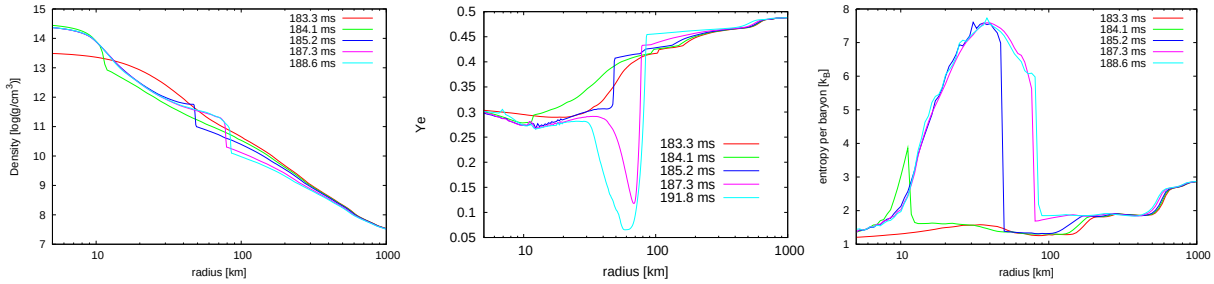

Figure 1: Radial profiles of density (the left panel), electron fraction (the middle panel), and entropy per baryon profile (the right panel) at selected time slices.

Thus, the specific internal energy density and the pressure are the sum of the contributions from the baryons (free protons, free neutrons, α-particles, and heavy nuclei), leptons (electrons, positrons, and *trapped neutrinos*), and radiation $P = P^{\rm F} + P_\nu = P_B + P_e + P_r + P_\nu$, $\varepsilon = \varepsilon^{\rm F} + \varepsilon_\nu = \varepsilon_B + \varepsilon_e + \varepsilon_r + \varepsilon_\nu$, where subscripts '$B$', '$e$', '$r$', and '$\nu$' denote the components of the baryons, electrons and positrons, radiation, and trapped neutrinos, respectively. We employ a finite temperature equation of state by Shen et al [2] for baryons. Fermions are treated as ideal Fermi gases. For radiation, we set $\varepsilon_r = a_r T^4/\rho$ $P_r = a_r T^4/3$, where a_r is the radiation constant.

On the other hand, the streaming-neutrino part is assumed to have the form

$$(T^{\nu,{\rm s}})_{\alpha\beta} = E_\nu n_\alpha n_\beta + F_\alpha n_\beta + F_\beta n_\beta + 1/3\gamma_{\alpha\beta}E_\nu,$$

where n_α and $\gamma_{\alpha\beta}$ are the unit normal and the metric of a three-dimensional hypersurface.

In terms of the above decomposition, we solve

$$\nabla_\beta T^\beta_{\ \alpha} = -Q_\alpha, \tag{4}$$
$$\nabla_\beta (T^{\nu,{\rm s}})^\beta_{\ \alpha} = Q_\alpha, \tag{5}$$

where the source term $Q_\alpha = Q u_\alpha$ is interpreted as the cooling rate due to the emission of (streaming) neutrinos. To summarize we solve Eq. (1), (2), (3), (4), and (5).

The source terms consists of the local and 'leakage' processes ($S_{Y_{\nu_i}} = S^{\rm local}_{Y_{\nu_i}} + S^{\rm leak}_{Y_{\nu_i}}$, $Q = Q^{\rm leak} = \sum Q^{\rm leak}_{Y_{\nu_i}}$). The local processes are the electron, positron, and neutrino captures [3] which is responsible to S_{Y_e} and S_{Y_i} electron-positron pair annihilation [4], plasmon decay [5], and Bremsstrahlung [6] which are to S_{Y_i}.

The leakage processes are the local emission of neutrinos according to the local diffusion timescale. In general the cross sections of neutrinos with matter can be written as $\sigma_i(\epsilon_\nu) = \tilde{\sigma}_i \epsilon_\nu^2$. The the opacity and the optical depth are similarly given by $\kappa(\epsilon_\nu) = \tilde{\kappa}\epsilon_\nu^2$ and $\tau(\epsilon_\nu) = \tilde{\tau}\epsilon_\nu^2$. We include neutrino absorption on free nucleons and heavy nuclei, neutrino scattering by electrons, free nucleons and heavy nuclei as opacity sources [6]. Then we define the diffusion timescale by

$$t^{\rm diff}_\nu(\epsilon_\nu) \equiv f^{\rm diff}\frac{\tau^2}{c\kappa} = f^{\rm diff}\frac{\tilde{\tau}^2}{c\tilde{\kappa}}\epsilon_\nu^2, \tag{6}$$

where $f^{\rm diff}$ is the constant of order unity. Then we define the local leakage rates by taking spectral average

$$S^{\rm leak}_{Y_{\nu_i}} \propto \int \frac{\hat{n}(\epsilon_\nu)}{t^{\rm diff}_\nu(\epsilon_\nu)} d\epsilon_\nu = \frac{1}{f^{\rm diff}}\frac{4\pi g_{\nu_i}}{h^3c^2}\frac{\tilde{\kappa}}{\tilde{\tau}^2}(k_B T)F_0(\eta_{\nu_i}), \tag{7}$$
$$Q_{Y_{\nu_i}} \propto \int \epsilon_\nu \frac{\hat{n}(\epsilon_\nu)}{t^{\rm diff}_\nu(\epsilon_\nu)} d\epsilon_\nu = \frac{1}{f^{\rm diff}}\frac{4\pi g_{\nu_i}}{h^3c^2}\frac{\tilde{\kappa}}{\tilde{\tau}^2}(k_B T)^2 F_1(\eta_{\nu_i}), \tag{8}$$

where $n_\nu = \int \hat{n}(\epsilon_\nu) d\epsilon_\nu$, h and k_B are the Plank constant and Boltzmann constant, g_ν is the weight factor and $F_k(x)$ is the Fermi-Dirac function.

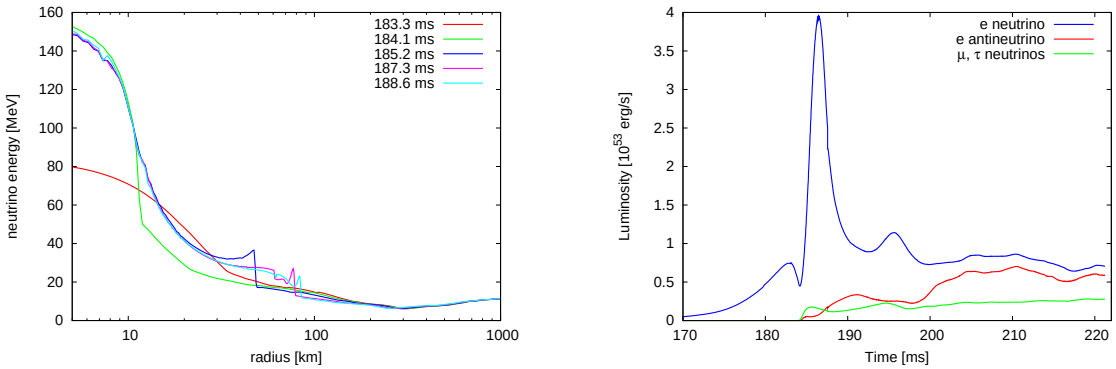

Figure 2: Radial profiles of electron-neutrino energy (the left panel) at selected time slices and time evolution of neutrino luminosities (right panel).

3 Results

First we compare the results of collapse of spherical core (model S15 [7]) with the results by Liebendöfer et al [8] in which the Boltzmann equations are solved for neutrinos. Figure 1 shows Radial profiles of density, electron fraction, and entropy per baryon profile at selected time slices after the bounce. Figure 2 shows radial profile of electron-neutrino energy and time evolution of neutrino luminosity. As the collapse proceeds, the central density exceeds the nuclear density and a bounce occurs ($t \approx 184$ ms) then a shock wave is formed and propagated outward. When the front of the shock wave pass through the neutrino sphere, a neutrino burst occur (see Fig. 2) and electron (lepton) fraction and entropy per baryon decreases rapidly ($t \approx 185$–187 ms). Note that negative gradients of electron fraction and entropy per baryon are formed in the core. Due to this neutrino burst, the shock wave eventually stalls at $r \approx 90$ km Our results shows good agreement with those by Liebendöfer et al.

It is well known that configuration with the negative gradients of lepton fraction and entropy per baryon are unstable against the Ledoux convection:

$$\left(\frac{\partial\rho}{\partial_{Y_l}}\right)_{P,s}\frac{dY_l}{dr}+\left(\frac{\partial\rho}{\partial_s}\right)_{P,Y_l}\frac{ds}{dr}>0, \qquad \text{(unstable)}. \tag{9}$$

The left panel of Fig. 3 shows contour of entropy per baryon at a time slice after the neutrino burst. As this figure clearly show, the steep negative gradients of entropy and Y_l formed above the neutrino sphere lead to the convective overturn.

We approximately estimate the energy available by the convective overturn. The gravitational energy per unit mass released as a result of convective overturn Δh is given by

$$w=-g_{\rm eff}\left[\left(\frac{\partial\ln P}{\partial s}\right)_{\rho,Y_e}\left(\frac{\partial\ln P}{\partial\ln\rho}\right)^{-1}_{s,Y_e}(ds)_{\rm amb}+\left(\frac{\partial\ln P}{\partial Y_e}\right)_{\rho,s}\left(\frac{\partial\ln P}{\partial\ln\rho}\right)^{-1}_{s,Y_e}(dY_e)_{\rm amb}\right]\Delta h, \tag{10}$$

where 'amb' and 'blob' denote ambient and convective blob fluid element, and Δh is the overturn distance.

Thus, the energy available in the convective overturn of a region of mass ΔM and thickness Δh with a value of Δs at a distance r from the center of a proto-neutron star of mass M is approximately given by $W\sim 10^{51}$ ergs $\left(\frac{\Delta M}{0.3M_\odot}\right)\left(\frac{\Delta h}{10{\rm km}}\right)\left(\frac{|\Delta s|}{s}\right)\left(\frac{50{\rm km}}{r}\right)^2\left(\frac{M}{M_\odot}\right)$, Similarly, with a value of ΔY_e, the available energy is given by $W\sim 10^{51}$ ergs $\left(\frac{\Delta M}{0.3M_\odot}\right)\left(\frac{\Delta h}{10{\rm km}}\right)\left(\frac{|\Delta Y_e|}{Y_e}\right)\left(\frac{50{\rm km}}{r}\right)^2\left(\frac{M}{M_\odot}\right)$.

We see that if $\Delta s\sim s$ and $\Delta Y_e\sim Y_e$, $W\sim 10^{51}$ ergs. These numbers are achieved in our simulations for the regions below the neutrino sphere. Since the convection timescale in the proto-neutron star seems to be $\tau_{\rm ot}\lesssim R_{\rm NS}v_{\rm ot}\sim 10$ ms the energy gain by the overturn will be $L_{\rm ot}\gtrsim 10^{53}$ ergs/s. Since this free energy compensates the energy loss due to the photo-dissociation ($L_{\rm diss}\sim 10^{53}$ ergs/s) and the neutrino emission ($L_\nu\sim 10^{53}$ ergs/s at the time when the shock wave stalls), the shock wave are pushed outward.

Associated with the convective motions, gravitational waves are emitted. The gravitational waveforms are computed using a quadrupole formula. In the left panel of Fig. 3, we show the spectra of $h_{\rm char}$ due

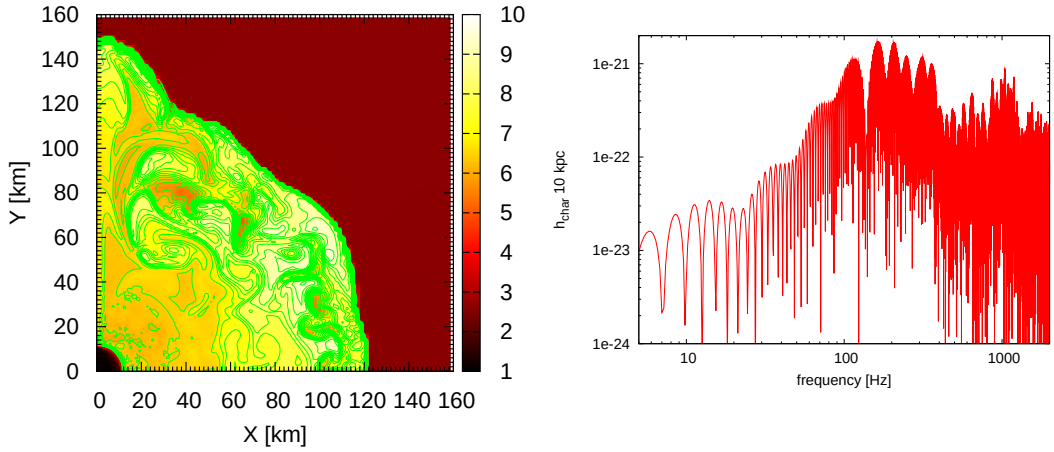

Figure 3: Contour of entropy per baryon (left panel) and gravitational-wave spectrum from convective motion (right panel).

to the convective motions. In contrast to spectra due to the core bounce, there is no dominant peak frequency in the power spectra. Instead, several maxima for the frequency range 100–500 Hz are present. This indicates that there exist a wide variety of scales of convective eddies with characteristic overturn timescales of 2–10 ms. The effective amplitude of the gravitational waves observed in the most optimistic direction is $h_{\rm char} \sim 10^{-21}$ for a event at a distance of 10 kpc, which is as large as that emitted at the bounce of rotating core collapse.

4 Summary

We perform a simulation of collapse of stellar core comparing results with those by spherical Boltzmann solver [8] and calculating spectrum of gravitational wave from convective activities. Our new code shows an advanced performance and can be used to clarify the formation process of LGRB engine. Fruitful scientific results will be reported in near future.

Numerical computations were performed on the NEC SX-9 at the data analysis center of NAOJ and on the NEC SX-8 at YITP.

References

[1] S. E. Woosley, ApJ. 405, 273 (1993); A. MacFadyen and S. E. Woosley, ApJ. 524, 262 (1999).

[2] H. Shen et al., Nucl. Phys. A 637, 435 (1998).

[3] G. M. Fuller, W. A. Fowler, and M. J. Newman, ApJ. 293, 1 (1985).

[4] J. Cooperstein, L. J. van den Horn and E. A. Baron, ApJ. 309, 653 (1986).

[5] M. Ruffert, H.-T. Janka, and G. Schaefer, Astron. Astrophys. 311, 532 (1996).

[6] A. Burrows, S. Reddy, and T. A. Thompson, ApJ. 777, 356 (2006).

[7] S. E. Woosley, A. Heger, and T. A. Weaver, Rev. Mod. Phys. 74, 1015 (2002).

[8] M. Liebendoerfer et al. ApJS. 150, 263 (2004)

The scalar field potential and the energy density of the super-in ation in Loop Quantum Cosmology

Masahiro SHIMANO[1] and Tomohiro HARADA[2]

Department of Physics, Rikkyo University, Toshima, Tokyo 171-8501, Japan

Abstract

In loop quantum cosmology there may be a super-in ation phase in the very early universe, in which a single scalar eld with a negative power-law potential $V = f\phi^{\beta}$ in Planck units plays important roles. Since the e ective horizon $\sqrt{SD}/H$ controls the behavior of quantum uctuation instead of the usual Hubble horizon, we assume the in ation scenario; the super-in ation starts when the quantum state of the scalar eld emerges into the classical regime and ends when the e ective horizon reaches the Hubble horizon, and the e ective horizon scale never gets shorter than the Planck length. From consistency with the WMAP 5-year data, we place a constraint on the parameters of the potential (β and f) and the energy density at the end of the super-in ation, depending on the volume correction parameter n, and we also determine the allowed range for n.

1 Introduction

Loop Quantum Gravity (LQG) is the candidate of the quantum gravity, and which is the canonical approach with triad variables instead of the metric. In the end of the previous century, LQG has inspired loop quantum cosmology (LQC), which is an application of loop quantization to the homogeneous universe models [5, 6, 7, 8]. This is featured with the avoidance of a big bang singularity and a super-in ation, where the Hubble parameter increases with time. If the loop quantum e ects may have been signi cant in the early universe, quantum uctuation generated in that phase must be consistent with the currently observed nearly scale-invariant power spectrum. The power spectrum for the LQC super-in ation was calculated in [11] and scale invariant conditions were obtained in [9] with the volume correction, which is one of the loop quantum e ects. The scale invariant conditions are the following: i) the scalar eld satis es a scaling condition and ii) the scalar eld has a negative potential, and iii) the potential is a power-law form and the index is in nitely large. In this paper we assume i) and ii) conditions and the following in ation scenario; the super-in ation starts when the scalar eld emerges into the classical regime from the quantum regime, and since the e ective horizon $\sqrt{SD}/H$ controls the behavior of quantum uctuation and its scale decreases with time, the super-in ation ends when the e ective horizon reaches the Hubble horizon. We need to assume that the e ective horizon never gets smaller than the order of the Planck length so that we can calculate quantum uctuation at semiclassical region. We consider the above scenario and require consistency with the WMAP 5-year data [10] to place a constraint on the parameters. In this paper we use the units in which $c = h = 1$.

2 The quantum uctuation in LQC

2.1 Loop Quantization

We rst consider the homogeneous and isotropic universe described by the FRW metric

$$ds^2 = \quad dt^2 + a(t)^2 \quad dr^2 + r^2 \quad d \ ^2 + \sin^2 \quad d \ ^2 \quad , \tag{1}$$

where a is the scale factor. In LQC the Hamiltonian for the gravitational and the single scalar elds is given by $\mathcal{H} = \mathcal{H}_{\rm grav} + \mathcal{H}_{\rm matter}$, where[1, 15] : $\mathcal{H}_{\rm grav} = \quad 3/(8 \quad G)aS(q)\dot{a}^2$, $\mathcal{H}_{\rm matter} = D(q)(2a^3)p_\phi^2 +$

[1]E-mail:shimano@rikkyo.ac.jp
[2]E-mail:harada@rikkyo.ac.jp

$a^3V(\ )$. $S(q)$ and $D(q)$ are respectively the loop correction factors for the gravitational Hamiltonian and the inverse volume in the matter Hamiltonian, and the dot denotes the derivative respect to t. The scalar eld depends only on time, i.e. $= (t)$. p_ϕ is a conjugate momentum of , de ned as $p_\phi = a^3 \dot{}/D$, and q is de ned as [2, 3, 4]: $q \quad (a/a\ )^3$, where

$$a = \frac{2j}{K}^{\frac{1}{3}} \sqrt{\frac{4}{3}} l_{\rm pl}, \quad K = \frac{2\sqrt{2}}{3\sqrt{3\sqrt{3}}}, \quad l_{\rm pl}^2 = G, \tag{2}$$

j is an SU(2) parameter which is associated with the link of the spin network state in LQG (we assume j is su ciently large), and is the Immirzi parameter which is here assumed $= \ln(2)/(\sqrt{3})$ by the black hole entropy argument in LQG [13], but see also [14]. Note that a is the characteristic scale factor in LQC: if the scale factor is smaller than a , the LQC e ects are remarkable. In the semiclassical region ($l_{\rm pl} \quad a \quad a$), $S(q)$ and $D(q)$ take the following forms [12]: $S(q) = S\ a^r$, and $D(q) = D\ a^n$, where, $S = \tilde{S}\ a\ ^r = (3/2)a\ ^r$ and $D = \tilde{D}\ a\ ^n = \{(9(9 \quad n))/(81 \quad 5n)\}^{(n \quad 9)/12} a\ ^n$, $n = 9(3 \quad l)/(1 \quad l)$ and $r = 3$. We assume $0 < l < 1$ or $9 < n < \infty$ to remove the divergence of the inverse volume factor, while, in the classical region ($a \gg a$), these are $S(q) \quad 1$, and $D(q) \quad 1$ so that the classical theory is recovered.

From the gravitational and scalar eld Hamiltonians, we can obtain the following modi ed Friedmann equation and the scalar eld equation:

$$H^2 = \frac{8 \ G}{3} S(q) \left[\frac{\dot{}^2}{2D(q)} + V(\ ) \right], \tag{3}$$

$$'' + \quad 2 \quad \frac{d\ln D}{d\ln a} \quad \frac{a'}{a} \quad ' + a^2 D V_\phi = 0, \tag{4}$$

where $V_\phi \quad dV/d$, the prime denotes the derivative with respect to (we also use the conformal time where $dt = ad$), $H \quad \dot{a}/a$ is the Hubble parameter. In the classical regime $a \gg a$, since $D(q) = S(q) = 1$, these equations reduce to the classical ones. However, in the semiclassical regime $l_{\rm pl} \quad a \quad a$, the second term acts an anti-friction term and the scalar eld may climb the potential.

More remarkably, the time derivative of the Hubble parameter

$$\dot{H} = \quad \frac{4 \ GS\dot{}^2}{D} \quad 1 \quad \frac{1}{6}\frac{d\ln D}{d\ln a} + \frac{1}{6}\frac{d\ln S}{d\ln a} \quad + \frac{4 \ GS}{3}\frac{d\ln S}{d\ln a} V, \tag{5}$$

is positive in the semiclassical regime. The in ation with this feature is called super-in ation.

2.2 The scaling solution and the power spectrum

We review the scaling solution and its stability according to Refs [11, 9]. We write the dynamics of the homogeneous system in terms of the following three variables,

$$x = \frac{\dot{}}{\sqrt{2D}}, \quad y = \frac{\sqrt{|V|}}{\sqrt{\ }}, \quad \lambda = \quad \sqrt{\frac{3D}{16 \ GS}}\frac{V_\phi}{V}, \tag{6}$$

where we use the negative potential, and we also need a constraint $x^2 \quad y^2 = 1$ to satisfy the Friedmann equation Eq. (3). Then we can derive the set of ordinary di erential equations, and we can nd the stable xed points in this equations. The one of the stable xed points correspond to the scaling solutions where the ratio of the kinetic term to the potential term is kept constant. For simplicity, we only consider a constant and then we can determine the potential from the de nition of the . For $\neq 1$, the potential is given by $V = \quad f| \ |^\beta$, where and f are constants. Moreover, we can calculate the scale factor on this xed points as $a = A(\quad)^p$, where

$$A = \left[\frac{1}{p}\sqrt{\frac{8 \ f\tilde{S}}{3(x_0^2 \quad 1)}} \left| \frac{2x_0}{n \quad r}\sqrt{\frac{3\tilde{D}}{4 \ \tilde{S}}} \right|^{\frac{\beta}{2}} \right]^p \left[\frac{2j}{K}^{\frac{1}{3}} \sqrt{\frac{4}{3}} \right]^{p+1} l_{\rm Pl}, \tag{7}$$

$$p = \quad \frac{4}{2(r+2) + (n \quad 3)}, \tag{8}$$

here x_0 is the coordinate of the xed points. As for the uctuation scale and the e ective horizon scale, for $p > 2/(n+r)$ the uctuation scale becomes longer than the e ective horizon scale, while for $p < 2/(n+r)$ the uctuation scale gets shorter than the e ective horizon scale. We assume that the horizon problem can be solved by the super-in ation in LQC, and then we impose the following condition on p,

$$p > \frac{2}{n+r} \tag{9}$$

We call this condition "the horizon problem condition". Since only scaling solution satis es this condition, we use this xed point in LQC.

We calculate the power spectrum in the same way as in [11]. However, note that we also incorporate the correction factor $S(q)$ into the matter Hamiltonian. We put the scalar eld perturbation as $= (t) + (x,t)$ into the matter Hamiltonian as

$$\mathcal{H}_{\phi+\ \phi} = \frac{1}{2}\frac{D(q)p^2_{\phi+\ \phi}}{a^3} + \frac{1}{2}aS(q)\ {}^{ab}\partial_a(+)\partial_b(+) + a^3V(+), \tag{10}$$

where $p_{\phi+\ \phi} = a^3(\dot{} + \dot{})/D$. We calculate the power spectrum with using the e ective horizon $\sqrt{SD}/H$ and $a = ( )^p$, then the tilt becomes the following

$$b = 3 \quad \frac{2\sqrt{9 \quad (6 \quad 4n \quad 3r)2p \quad (12+4n \quad 2nr \quad r^2 \quad 2n^2)p^2}}{2+(n+r)p}, \tag{11}$$

where the scale-invariant power spectrum is achieved by $p = 0$, corresponding to $\to \infty$ with $r = 3$ and xed n in Eq. (8).

3 The consistency with WMAP 5-year data

According to the WMAP 5-year data, the CMB power spectrum index is in the range $n_s = 0.963^{+0.014}_{0.015}$ [10]. Since the relation between the spectrum index n_s and the tilt b is $b = n_s \quad 1$, for inserting this data into Eq. (11) we can take two solutions of p. Because only one of these can solve the horizon problem condition (9), we take the power of potential with this p in Eq. (8).

In FIG.1, we plot the allowed region of against n. If we can specify the value for n, then we can place a rather stringent constraint on . However, if we do not have any information about n, is only weakly constrained to $15 < < 150$. In any case, is bounded from above in the present scenario and an in nitely large value is not allowed from WMAP 5-year data.

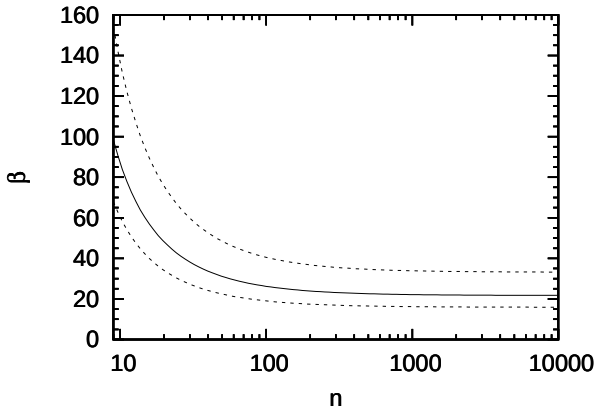

Figure 1: The allowed region of . The solid line corresponds to the best- t value, while the dashed lines denote the boundary of measurement error ranges.

Moreover, we can take the constraint on the energy density and the potential constant with the following in ation scenario: the super-in ation starts when the quantum state of the scalar eld emerges into the classical regime and ends when the e ective horizon gets equal to the Hubble horizon before the e ective horizon scale gets shorter than the square root of the smallest area element.

4 Conclusion

We have considered a single scalar eld with the negative power-law potential $V \propto f^{\beta}$ in LQC, then we have determined the allowed region of the potential power and the energy density at the end of the super-in ation, and the potential constant f, and the volume correction parameter n by using the consistency with the WMAP 5-year data.

First we have reviewed Ref [9]. Using dynamical systems theory we have found a scaling solution which is a stable xed point and satis es the horizon problem condition. Second, we have assumed the super-in ation scenario. By using this in ation scenario and the consistency with the WMAP 5-year data, we have reached the following conclusion. If we can specify the volume correction parameter n, we can determine the potential parameters and f rather stringently. Even if we only know the volume correction parameter n, then we can determine and f, and the energy density at the end of the super-in ation.

In this paper we have only considered the scalar eld perturbation. However, the CMB power spectrum is actually the temperature perturbation on the last scattering surface, so we should derive the curvature perturbations as well as matter perturbations and their evolution in di erent scales in LQC. To get more stringent constraint on the super-in ation scenario, we will need to use other independent observations: large scale structure, non-gaussianity, gravitational waves and so on. These problems will be our next work.

References

[1] A. Ashtekar, M. Bojowald, and J. Lewandowski *Adv. Theor. Math. Phys* **7** 233-268 (2003)

[2] A. Ashtekar, T. Pawlowski and P. Singh *Phys. Rev. D* **73** 124038 (2006)

[3] A. Ashtekar, T. Pawlowski and P. Singh *Phys. Rev. D* **73** 084003 (2006)

[4] A. Ashtekar, T. Pawlowski and P. Singh, and K. Vandersloot *Phys. Rev. D* **75** 024035 (2007)

[5] M. Bojowald *Class. Quant. Grav.* **17** 1489-1508 (2000)

[6] M. Bojowald *Class. Quant. Grav.* **17** 1509-1526 (2000)

[7] M. Bojowald *Class. Quant. Grav.* **18** 1055-1070 (2001)

[8] M. Bojowald *Class. Quant. Grav.* **18** 1071-1088 (2001)

[9] E. J. Copeland, D. J. Mulryne, N. J. Nunes and M. Shaeri *Phys. Rev. D* **77** 023510 (2008)

[10] E. Komatsu, et al. arXiv:0803.0547v1 [astro-ph]

[11] D. J. Mulryne and N. J. Nunes *Phys. Rev. D* **74** 083507 (2006)

[12] J. Magueijo and P. Singh *Phys. Rev. D* **74** 023510 (2007)

[13] C. Rovelli "*Quantum Gravity* " (Cambridge University Press, Cambridge, 2004)

[14] T. Tamaki and H. Nomura, Phys. Rev. D **72**, 107501 (2005).

[15] K. Vandersloot *Phys. Rev. D* **71** 103506 (2005)

Non-Gaussianity in the Curvaton Scenario

Tomo Takahashi[1]

Department of Physics, Saga University, Saga 840-8502, Japan

Abstract

We discuss the signatures of non-Gaussianity in the curvaton model where the potential includes also a non-quadratic term. In such a case the non-linearity parameter $f_{\rm NL}$ can become very small, and we show that non-Gaussianity is then encoded in the non-reducible non-linearity parameter $g_{\rm NL}$ of the trispectrum, which can be very large. Thus the place to look for the non-Gaussianity in the curvaton model may be the trispectrum rather than the bispectrum. We also show that $g_{\rm NL}$ measures directly the deviation of the curvaton potential from the purely quadratic form.

1 Introduction

The high precision of cosmological observations such as WMAP [1, 2] and the forthcoming Planck Surveyor Mission [3] will soon make it possible to probe the actual physics of the primordial perturbation rather than merely describing it. As is well known, the primordial scalar and tensor power spectra, characterized by spectral indices the and tensor-to-scalar ratio, can be used to test both models of inflation and other mechanisms for the generation of the primordial perturbation such as the curvaton [4, 5, 6]. However, many models can imprint similar features on the primordial power spectrum. Thus a possible deviation from Gaussian fluctuations, which may provide invaluable implications on the physics of the early universe, has been the focus of much attention recently.

The simplest inflation models generate an almost Gaussian fluctuation. In contrast, in the curvaton scenario there can arise a large non-Gaussianity. However, in most studies on the curvaton so far, one simply assumes a quadratic curvaton potential. Since the curvaton cannot be completely non-interacting (it has to decay), it is of interest to consider the implications of the deviations from the exactly quadratic potential, which represent curvaton self-interactions. Such self-interactions would arise e.g. in curvaton models based on the flat directions of the minimally supersymmetric standard model (MSSM). Even small deviations could be important for phenomenology, as was pointed out in [7] where it was shown that the non-Gaussianity predicted by the curvaton model can be sensitive to the shape of the potential. In particular, the nonlinearity parameter $f_{\rm NL}$ which quantifies the bispectrum of primordial fluctuation can, in contrast to the case of the quadratic curvaton potential, be very small in some cases. However, the signatures of non-Gaussianity can be probed not only with the bispectrum but also with the trispectrum. In the following, we will show that even when $f_{\rm NL}$ is negligibly small, $g_{\rm NL}$ can be very large, indicating that the first signature of the curvaton-induced primordial non-Gaussianity may not come from the bispectrum but rather from the trispectrum.

2 Non-linearity parameters

To discuss non-Gaussianity in the scenario, we make use of the non-linearity parameters $f_{\rm NL}$ and $g_{\rm NL}$ defined by the expansion

$$\zeta = \zeta_1 + \frac{3}{5} f_{\rm NL} \zeta_1^2 + \frac{9}{25} g_{\rm NL} \zeta_1^3 + \mathcal{O}(\zeta_1^4), \tag{1}$$

where ζ is the primordial curvature perturbation. Writing the power spectrum as

$$\langle \zeta_{\vec{k}_1} \zeta_{\vec{k}_2} \rangle = (2\pi)^3 P_\zeta(k_1) \delta(\vec{k}_1 + \vec{k}_2), \tag{2}$$

[1]E-mail:tomot@cc.saga-u.ac.jp

the bispectrum and trispectrum are given by

$$\langle \zeta_{\vec{k}_1} \zeta_{\vec{k}_2} \zeta_{\vec{k}_3} \rangle = (2\pi)^3 B_\zeta(k_1, k_2, k_3) \delta(\vec{k}_1 + \vec{k}_2 + \vec{k}_3). \tag{3}$$

$$\langle \zeta_{\vec{k}_1} \zeta_{\vec{k}_2} \zeta_{\vec{k}_3} \zeta_{\vec{k}_4} \rangle = (2\pi)^3 T_\zeta(k_1, k_2, k_3, k_4) \delta(\vec{k}_1 + \vec{k}_2 + \vec{k}_3 + \vec{k}_4), \tag{4}$$

where B_ζ and T_ζ are products of the power spectra and can be written as

$$B_\zeta(k_1, k_2, k_3) = \frac{6}{5} f_{\rm NL} \left(P_\zeta(k_1) P_\zeta(k_2) + P_\zeta(k_2) P_\zeta(k_3) + P_\zeta(k_3) P_\zeta(k_1) \right), \tag{5}$$

$$\begin{aligned} T_\zeta(k_1, k_2, k_3, k_4) &= \tau_{\rm NL} \left(P_\zeta(k_{13}) P_\zeta(k_3) P_\zeta(k_4) + 11 \text{ perms.} \right) \\ &\quad + \frac{54}{25} g_{\rm NL} \left(P_\zeta(k_2) P_\zeta(k_3) P_\zeta(k_4) + 3 \text{ perms.} \right). \end{aligned} \tag{6}$$

Note the appearance of the independent non-linearity parameter $\tau_{\rm NL}$. However, in the scenario we are considering in the following, $\tau_{\rm NL}$ is related to $f_{\rm NL}$ by

$$\tau_{\rm NL} = \frac{36}{25} f_{\rm NL}^2 \ . \tag{7}$$

To evaluate the primordial curvature fluctuation in the curvaton model, we need to specify a potential for the curvaton. Here we go beyond the usual quadratic approximation and consider the following potential:

$$V(\sigma) = \frac{1}{2} m_\sigma^2 \sigma^2 + \ m_\sigma^4 \left(\frac{\sigma}{m_\sigma} \right)^n \ , \tag{8}$$

which contains a higher polynomial term in addition to the quadratic term. For later discussion, we define a parameter s which represents the size of the non-quadratic term relative to the quadratic one:

$$s \equiv 2 \ \left(\frac{\sigma_*}{m_\sigma} \right)^{n-2} . \tag{9}$$

Thus the larger s is, the larger is the contribution from the non-quadratic term.

When the potential is quadratic, the fluctuation evolves exactly as the homogeneous mode. However, when the curvaton field evolves under a non-quadratic potential, the fluctuation of the curvaton evolves non-linearly on large scales. In that case the curvature fluctuation can be written, up to the third order, as [8]

$$\begin{aligned} \zeta = \delta N &= \frac{2}{3} r \frac{\sigma'_{\rm osc}}{\sigma_{\rm osc}} \delta\sigma_* + \frac{1}{9} \left[3r \left(1 + \frac{\sigma_{\rm osc} \sigma''_{\rm osc}}{\sigma'^2_{\rm osc}} \right) - 4r^2 - 2r^3 \right] \left(\frac{\sigma'_{\rm osc}}{\sigma_{\rm osc}} \right)^2 (\delta\sigma_*)^2 \\ &\quad + \frac{4}{81} \left[\frac{9r}{4} \left(\frac{\sigma^2_{\rm osc} \sigma'''_{\rm osc}}{\sigma'^3_{\rm osc}} + 3 \frac{\sigma_{\rm osc} \sigma''_{\rm osc}}{\sigma'^2_{\rm osc}} \right) - 9r^2 \left(1 + \frac{\sigma_{\rm osc} \sigma''_{\rm osc}}{\sigma'^2_{\rm osc}} \right) \right. \\ &\quad \left. + \frac{r^3}{2} \left(1 - 9 \frac{\sigma_{\rm osc} \sigma''_{\rm osc}}{\sigma'^2_{\rm osc}} \right) + 10r^4 + 3r^5 \right] \left(\frac{\sigma'_{\rm osc}}{\sigma_{\rm osc}} \right)^3 (\delta\sigma_*)^3 \ , \end{aligned} \tag{10}$$

where $\sigma_{\rm osc}$ is the value of the curvaton at the onset of its oscillation and the prime represents the derivative with respect to σ_*. r roughly represents the ratio of the energy density of the curvaton to the total density at the time of the curvaton decay. The exact definition is given by

$$r \equiv \left. \frac{3\rho_\sigma}{4\rho_{\rm rad} + 3\rho_\sigma} \right|_{\rm decay} . \tag{11}$$

Notice that $\sigma'_{\rm osc}/\sigma_{\rm osc} = 1/\sigma_*$ for the case of the quadratic potential. With this expression, we can write down the non-linearity parameter $f_{\rm NL}$ as

$$f_{\rm NL} = \frac{5}{4r} \left(1 + \frac{\sigma_{\rm osc} \sigma''_{\rm osc}}{\sigma'^2_{\rm osc}} \right) - \frac{5}{3} - \frac{5r}{6}. \tag{12}$$

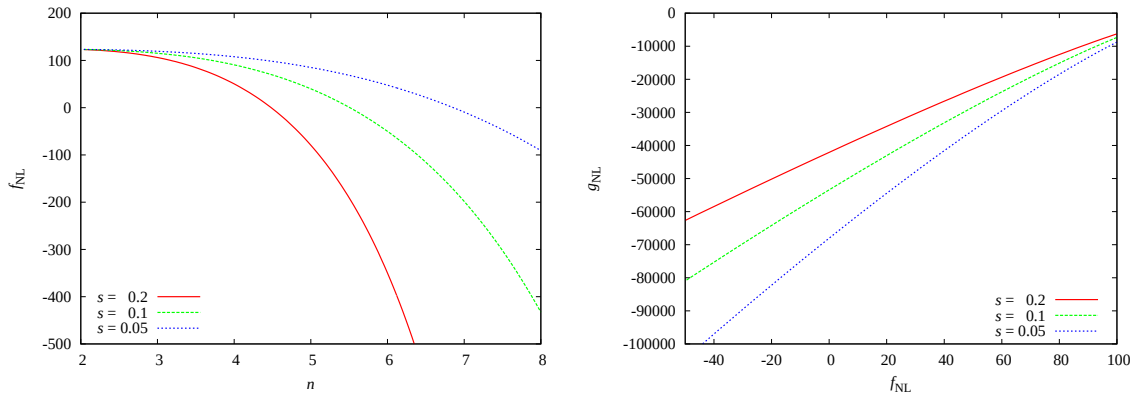

Figure 1: (Left) Plot of $f_{\rm NL}$ as a function of n for several values of s. (Right) Plot of $g_{\rm NL}$ as a function of $f_{\rm NL}$ for several values of s. Notice that $f_{\rm NL}$ and n have one-to-one correspondence. In both panels, $r = 0.01$.

Also notice that, although the curvaton scenario generally generates large non-Gaussianity with $f_{\rm NL} \gtrsim \mathcal{O}(1)$, the non-linearity parameter $f_{\rm NL}$ can be very small in the presence of the non-linear evolution of the curvaton field which can render the term $1 + (\sigma_{\rm osc}\sigma''_{\rm osc})/\sigma'^2_{\rm osc} \simeq 0$ [7, 8].

In the curvaton model, the non-linearity parameter $g_{\rm NL}$ can be written as

$$g_{\rm NL} = \frac{25}{54}\left[\frac{9}{4r^2}\left(\frac{\sigma^2_{\rm osc}\sigma'''_{\rm osc}}{\sigma'^3_{\rm osc}} + 3\frac{\sigma_{\rm osc}\sigma''_{\rm osc}}{\sigma'^2_{\rm osc}}\right) - \frac{9}{r}\left(1 + \frac{\sigma_{\rm osc}\sigma''_{\rm osc}}{\sigma'^2_{\rm osc}}\right) + \frac{1}{2}\left(1 - 9\frac{\sigma_{\rm osc}\sigma''_{\rm osc}}{\sigma'^2_{\rm osc}}\right) + 10r + 3r^2\right]. \quad (13)$$

As one can easily see, even if the non-linear evolution of σ cancels to give a very small $f_{\rm NL}$, such a cancellation does not necessarily occur for $g_{\rm NL}$. This indicates an interesting possibility where the non-Gaussian signature of the curvaton may come from the trispectrum rather than from the bispectrum.

3 Signatures of non-Gaussianity

Let us now consider non-Gaussianity in curvaton models, paying particular attention to the non-linearity parameters $f_{\rm NL}$ and $g_{\rm NL}$. We show the values of $f_{\rm NL}$ and $g_{\rm NL}$ as a function of the power n in Fig. 1. In the left panel of the figure, the value of $f_{\rm NL}$ is plotted as a function of the power n for several values of s. There we have fixed the value of r to $r = 0.01$. As can be read off from Eq. (12), when r is small, $f_{\rm NL}$ can be well approximated as

$$f_{\rm NL} \simeq \frac{5}{4r}\left(1 + \frac{\sigma_{\rm osc}\sigma''_{\rm osc}}{\sigma'^2_{\rm osc}}\right) . \quad (14)$$

Notice that the combination $\sigma_{\rm osc}\sigma''_{\rm osc}/\sigma'^2_{\rm osc}$ is zero when $n = 2$. As the value of n becomes larger, the above combination yields a negative contribution. Thus, $f_{\rm NL}$ decreases to zero as the potential deviates away from a quadratic form and then becomes zero for some values of n and s. For small values of s, which correspond to the cases where the size of the non-quadratic term is relatively small compared to the quadratic one, the power n should be large to make $f_{\rm NL}$ very small. It should also be mentioned that, for a fixed s, if we take larger values of n beyond the "cancellation point" $f_{\rm NL} = 0$, $f_{\rm NL}$ becomes negative.

However, as already discussed, even if we obtain very small values for $f_{\rm NL}$, it does not necessarily indicate that non-Gaussianity is small in the model but may show up in the higher order statistics. Indeed, this appears to be a generic feature of the curvaton model: the trispectrum cannot be suppressed and $g_{\rm NL}$ can be quite large and is always negative for small values of r. Interestingly, even if $f_{\rm NL}$ is zero, the value of $|g_{\rm NL}|$ can be very large, as can be seen Fig. 1. This is because a cancellation which can occur for $f_{\rm NL}$ does not take place for $g_{\rm NL}$, which is a smooth function of n. When r is small, $g_{\rm NL}$ is mainly

determined by the first term in Eq. (13):

$$g_{\rm NL} \simeq \frac{25}{54}\left[\frac{9}{4r^2}\left(\frac{\sigma_{\rm osc}^2\sigma'''_{\rm osc}}{\sigma'^3_{\rm osc}} + 3\frac{\sigma_{\rm osc}\sigma''_{\rm osc}}{\sigma'^2_{\rm osc}}\right)\right]. \tag{15}$$

In fact, one can show that the terms $(\sigma_{\rm osc}\sigma''_{\rm osc})/\sigma'^2_{\rm osc}$ and $(\sigma^2_{\rm osc}\sigma'''_{\rm osc})/\sigma'^3_{\rm osc}$ give negative contributions for the cases being considered here, which indicates that the cancellation between these terms never occurs [9]. Therefore $g_{\rm NL}$ is always negative for small values of r even when $f_{\rm NL}$ is very small. Thus, it may turn out that the best place to look for non-Gaussianity in curvaton models is the trispectrum and $g_{\rm NL}$ in particular.

4 Summary

We have discussed the signatures of non-Gaussianity in the curvaton model with the potential including a non-quadratic term in addition to the usual quadratic term. When the curvaton potential is not purely quadratic, fluctuations of the curvaton field evolve nonlinearly on superhorizon scales. This gives rise to predictions for the bispectrum, characterized by the non-linearity parameter $f_{\rm NL}$, which can deviate considerably from the quadratic case. However, by studying the trispectrum which is characterized by $g_{\rm NL}$ along with $f_{\rm NL}$, we find that even when $f_{\rm NL}$ is negligibly small, the absolute value of $g_{\rm NL}$ can be very large. Thus the signature of non-Gaussianity in the curvaton model may come from the trispectrum rather than from the bispectrum if its potential deviates from a purely quadratic form, as one would expect in realistic particle physics models.

Here we discussed the case where a non-quadratic term is also taken into account in the curvaton potential, however the cases where fluctuations from the inflaton can also be responsible for cosmic density perturbations today would also be interesting since such a case can arise in general. Such mixed fluctuation scenarios have been investigated in Refs. [10, 11, 12].

References

[1] E. Komatsu *et al.* [WMAP Collaboration], arXiv:0803.0547 [astro-ph].

[2] J. Dunkley *et al.* [WMAP Collaboration], arXiv:0803.0586 [astro-ph].

[3] [Planck Collaboration], arXiv:astro-ph/0604069;
Planck webpage, `http://www.rssd.esa.int/index.php?project=planck`

[4] K. Enqvist and M. S. Sloth, Nucl. Phys. B **626**, 395 (2002) [arXiv:hep-ph/0109214];

[5] D. H. Lyth and D. Wands, Phys. Lett. B **524**, 5 (2002) [arXiv:hep-ph/0110002];

[6] T. Moroi and T. Takahashi, Phys. Lett. B **522**, 215 (2001) [Erratum-ibid. B **539**, 303 (2002)] [arXiv:hep-ph/0110096].

[7] K. Enqvist and S. Nurmi, JCAP **0510**, 013 (2005) [arXiv:astro-ph/0508573].

[8] M. Sasaki, J. Valiviita and D. Wands, Phys. Rev. D **74**, 103003 (2006) [arXiv:astro-ph/0607627].

[9] K. Enqvist and T. Takahashi, JCAP **0809**, 012 (2008) [arXiv:0807.3069 [astro-ph]].

[10] K. Ichikawa, T. Suyama, T. Takahashi and M. Yamaguchi, Phys. Rev. D **78**, 023513 (2008) [arXiv:0802.4138 [astro-ph]].

[11] K. Ichikawa, T. Suyama, T. Takahashi and M. Yamaguchi, Phys. Rev. D **78**, 063545 (2008) [arXiv:0807.3988 [astro-ph]].

[12] T. Moroi and T. Takahashi, arXiv:0810.0189 [hep-ph].

Nonlinear superhorizon perturbations of non-canonical scalar field

Yu-ichi Takamizu[1] and Shinji Mukohyama[2]

[1]*Department of Physics, Waseda University, Okubo 3-4-1, Shinjuku, Tokyo 169-8555, Japan*
[2]*Institute for the Physics and Mathematics of the Universe (IPMU), The University of Tokyo, 5-1-5 Kashiwanoha, Kashiwa, Chiba 277-8582, Japan*

Abstract

We develop a theory of non-linear cosmological perturbations at superhorizon scales for a scalar field with a Lagrangian of the form $P(X, \phi)$, where $X = -\partial^\mu \phi \partial_\mu \phi$ and ϕ is the scalar field. We employ the ADM formalism and the spatial gradient expansion approach to obtain general solutions valid up to the second order in the gradient expansion. This formulation can be applied to, for example, DBI inflation models to investigate superhorizon evolution of non-Gaussianities. With slight modification, we also obtain general solutions valid up to the same order for a perfect fluid with a general equation of state $P = P(\rho)$.

1 Introduction

Generation of primordial fluctuations during inflation is one of the most interesting predictions of quantum field theory. Indeed, those quantum fluctuations are considered as seeds of the large scale structure of the present universe, and this picture has been accepted by many researchers as a standard scenario. The recent more accurate observation by WMAP has revealed deviation from exact scale invariance, with a slight red tilt. Moreover, there is a good possibility that deviation from Gaussianity can be detected by the future experiments such as PLANCK. With those current and future precision observations, deviation from the exact scale invariance and Gaussianity can be a powerful tool to discriminate many possible inflationary models. On the theoretical side, there are at least two known mechanisms to generate large non-Gaussianity: isocurvature perturbations and non-canonical kinetic terms. As for the former case, a typical example is the curvaton scenario is responsible for isocurvature perturbations during inflation. Now let us consider the later case, where non-canonical kinetic terms are responsible for large non-Gaussianity. Examples of this type include k-inflation [1] and DBI inflation [2]. In k-inflation and DBI inflation, large non-Gaussianity is expected when the non-linear nature of the non-canonical kinetic action becomes significant. To quantify the non-Gaussianity and clarify its observational signature, it is important to develop a theory that can deal with nonlinear cosmological perturbations. There are couple of methods to tackle this problem. One is a second-order perturbation theory. Another is based on spatial gradient expansion [3]. Closely related to the gradient expansion method, cosmological perturbations on superhorizon scales have been studied extensively in the so-called separate universe approach or δN formalism [4]. Actually, these approaches are essentially the leading order approximation to the gradient expansion. Including these, many of the previous studies were confined to the leading order approximation to the gradient expansion. However, higher order corrections to the leading order results can be important to get more detailed information about non-Gaussianity. One good example is the case studied by Leach et al [5]. They considered linear perturbations in single-field inflation models and supposed that there is a stage at which slow-roll conditions are violated. It has been then shown that, due to the decaying mode, the $O(\epsilon^2)$ corrections in spatial derivative expansion do affect the evolution of curvature perturbations on superhorizon scales. However, the linear perturbation theory is not capable for calculation of non-Gaussianity. Thus, it is necessary to develop nonlinear theory of cosmological perturbations valid up to $O(\epsilon^2)$ in the spatial gradient expansion. Gradient expansion formalism has been developed and used by many authors [3, 4, 6, 7]. Formulation valid up to $O(\epsilon^2)$ was developed, for example, by Tanaka and

[1]E-mail:takamizu@gravity.phys.waseda.ac.jp
[2]E-mail:shinji.mukohyama@ipmu.jp

Sasaki for a universe dominated by a perfect fluid with a specific equation of state $P/\rho = const$ [6] and that dominated by a canonical scalar field [7]. However, as far as the authors know, those works have not extended to a perfect fluid with general equation of state $P = P(\rho)$ nor to a scalar field with non-canonical kinetic action, which is essential for the second type of mechanism of generating non-Gaussianity. The purpose of this paper is to fill this gap. Namely, we shall develop a theory of nonlinear superhorizon perturbations valid up to the order $O(\epsilon^2)$ for a scalar field with non-canonical kinetic action and a perfect fluid with general equation of state.

2 Formalism

Throughout this paper we consider a minimally-coupled scalar field described by an action of the form $I = \int d^4x\sqrt{-g}P(X,\phi)$ where $X = -g^{\mu\nu}\partial_\mu\phi\partial_\nu\phi$, and suppose that $-g^{\mu\nu}\partial_\nu\phi$ is timelike and future-directed. The following relation among first-order variations of P, ρ and ϕ will be useful in the analysis below. $\delta P = c_s^2\delta\rho + \rho\Gamma\delta\phi$, where

$$c_s^2 = \frac{P_X}{2P_{XX}X + P_X}, \quad \Gamma = \frac{1}{\rho}\left(P_\phi - c_s^2\rho_\phi\right), \tag{1}$$

where the subscripts X and ϕ represent derivative with respect to X and ϕ, respectively. Note that c_s is the speed of sound for the gauge invariant scalar perturbation in the linear theory.

We shall develop a theory of nonlinear cosmological perturbations on superhorizon scales. For this purpose we employ the ADM formalism and the gradient expansion in the uniform Hubble slicing. In the (3+1)-decomposition, the metric is expressed as $ds^2 = g_{\mu\nu}dx^\mu dx^\nu = -\alpha^2dt^2 + \gamma_{ij}(dx^i + \beta^i dt)(dx^j + \beta^j dt)$ where α is the lapse function, β^i is the shift vector and Latin indices run over $1, 2, 3$. Since α and β^i represent gauge degrees of freedom for diffeomorphism and appear as Lagrange multipliers in the action, the corresponding equations of motion leads to constraint equations. Contrary to α and β, components of the spatial metric γ_{ij} are dynamical variables (subject to the constraint equations) and the corresponding equations of motion are called dynamical equations. In what follows we shall express the dynamical equations as a set of first-order differential equations with respect to the time t. For this purpose we introduce the extrinsic curvature K_{ij} defined by $K_{ij} = -\frac{1}{2\alpha}\left(\partial_t\gamma_{ij} - D_i\beta_j - D_j\beta_i\right)$ where D is the covariant derivative compatible with the spatial metric γ_{ij}. For the stress-energy tensor in the perfect fluid form, we define the 3-vector v^i as $v^i \equiv u^i/u^0$. Hereafter, we shall use γ_{ij} and its inverse γ^{ij} to raise and lower indices of K, D, v, β. In addition to the standard ADM decomposition briefly reviewed above, we further decompose the spatial metric and the extrinsic curvature as

$$\gamma_{ij} = a^2\psi^4\tilde{\gamma}_{ij}, \quad K_{ij} = a^2\psi^4\left(\frac{1}{3}K\tilde{\gamma}_{ij} + \tilde{A}_{ij}\right), \tag{2}$$

where $a(t)$ is the scale factor of a fiducial Friedmann background (specified later) and the determinant of $\tilde{\gamma}_{ij}$ is constrained to be unity: $\det\tilde{\gamma}_{ij} = 1$. Throughout this paper we adopt the uniform Hubble slicing

$$K = -3H(t), \quad H(t) \equiv \frac{\partial_t a}{a}. \tag{3}$$

In the gradient expansion approach we introduce a flat FRW universe ($a(t)$, $\phi_0(t)$) as a background and suppose that the characteristic length scale L of perturbations is longer than the Hubble length scale $1/H$ of the background, i.e. $HL \gg 1$. Therefore, we consider $\epsilon \equiv 1/(HL)$ as a small parameter and systematically expand our equations by ϵ, considering a spatial derivative acted on perturbations is of order $O(\epsilon)$. The background flat FRW universe ($a(t)$, $\phi_0(t)$) satisfies the Friedmann equation and the equation of motion. Since the FRW background is recovered in the limit $\epsilon \to 0$, we naturally have the assumptions $v^i = O(\epsilon), \beta^i = O(\epsilon)$ and $\partial_t\tilde{\gamma}_{ij} = O(\epsilon)$. Actually, following the arguments in refs. [6, 7], we assume a stronger condition $\partial_t\tilde{\gamma}_{ij} = O(\epsilon^2)$. This assumption significantly simplifies our analysis and, we believe, still allows many useful applications of the formalism. On the other hand, we consider ψ and $\tilde{\gamma}_{ij}$ (without derivatives acted on them) as quantities of order $O(1)$. We can estimate orders of magnitude of various quantities by using the above assumption and the basic equations. In summary, we have the

following estimates (including assumptions):

$$\psi = O(1), \quad \tilde{\gamma}_{ij} = O(1), \quad v^i = O(\epsilon), \quad \beta^i = O(\epsilon), \quad \chi \equiv \alpha - 1 = O(\epsilon^2),$$
$$\tilde{A}_{ij} = O(\epsilon^2), \quad \delta \equiv \frac{\rho - \rho_0}{\rho_0} = O(\epsilon^2), \quad \pi \equiv \phi - \phi_0 = O(\epsilon^2), \quad p \equiv P - P_0 = O(\epsilon^2),$$
$$\partial_t \tilde{\gamma}_{ij} = O(\epsilon^2), \quad \partial_t \psi = O(\epsilon^2), \quad v^i + \beta^i = O(\epsilon^3). \tag{4}$$

We substitute the order of magnitude shown in (4) into the conservation equations $\nabla_\mu T^\mu_{\ \nu} = 0$, the Hamiltonian and momentum constraint equations, and the evolution equations for the spatial metric and for the extrinsic curvature. By using these equations and the background conservation equation $\partial_t \rho_0 + 3H(\rho_0 + P_0) = 0$, a single equation for δ is easily obtained, $\partial_t(a^2 \rho_0 \delta) = O(\epsilon^4)$. It is intriguing to note that we have not yet specified the form of p. The form of p for the scalar field system is specified by the relation as

$$p = \rho_0(c_{s0}^2 \delta + \Gamma_0 \pi) + O(\epsilon^4), \tag{5}$$

where $c_{s0}^2 = P_{0X}/(2P_{0XX}X_0 + P_{0X})$ and $\Gamma_0 = (P_{0\phi} - c_{s0}^2 \rho_{0\phi})/\rho_0$. We can obtain another equation relating p and π, by expanding p as $p = P_{0X}(X - X_0) + P_{0\phi}\pi + O(\epsilon^4)$, where $X - X_0 = 2(\partial_t \phi_0 \partial_t \pi - \chi X_0) + O(\epsilon^4)$. Actually, this equation can be interpreted as a first-order equation for π.

3 General solution

Having written down all relevant equations up to the order $O(\epsilon^2)$ in the gradient expansion, we now seek a general solution. First, $\psi = O(1)$ and $\partial_t \psi = O(\epsilon^2)$ imply that $\psi = L^{(0)}(x^k) + O(\epsilon^2)$ where $L^{(0)}(x^k)$ is an arbitrary function of the spatial coordinates $\{x^k\}$ $(k = 1, 2, 3)$. Hereafter, the superscript (n) indicates that the corresponding quantity is of order $O(\epsilon^n)$. Similarly, $\tilde{\gamma}_{ij} = O(1)$ and $\partial_t \tilde{\gamma}_{ij} = O(\epsilon^2)$ imply that $\tilde{\gamma}_{ij} = f_{ij}^{(0)}(x^k) + O(\epsilon^2)$ where $f_{ij}^{(0)}(x^k)$ is a (3×3)-matrix with unit determinant whose components depend only on the spatial coordinates. By using these equations and background conservation equation, equations for δ and u_i are easily obtained. The traceless part of the extrinsic curvature $\tilde{A}_{ij}$ is solved by using the leading part of ψ and $\tilde{\gamma}_{ij}$. The 'constants' of integration are not independent but are related to each other by the two constraint equations. Indeed, by solving the Hamiltonian and momentum constraints, the 'constants' are expressed in terms of other integration 'constants'. Until now, we have not used (5). Therefore, the general solutions presented above are valid not only for the scalar field system but also for radiation, dust or any other sources, provided that the stress-energy tensor is of the perfect fluid form and that $p = O(\epsilon^2)$. We now use (5) to proceed further. It is easy to integrate the corresponding eqs to give the solutions of π and χ.

Solutions obtained so far are correct up to leading order in the gradient expansion. Among them, the spatial metric ψ and $\tilde{\gamma}_{ij}$ have been obtained only up to $O(1)$ while all other variables are correct at least up to $O(\epsilon^2)$. In this subsection we seek $O(\epsilon^2)$ corrections to ψ and $\tilde{\gamma}_{ij}$. For this purpose it is convenient to specify the shift vector β^i more accurately than indicated by (4) as $\beta^i = O(\epsilon^3)$. With this gauge choice, in summary we have obtained the following solutions in the gradient expansion for the scalar field

system.

$$
\begin{aligned}
\delta &= \frac{R^{(0)}}{2\kappa^2\rho_0 a^2} + O(\epsilon^4), \\
u_i &= \frac{1}{6\kappa^2(\rho_0+P_0)a^3}\partial_i\left(R^{(0)}\int_{t_0}^{t} a(t')dt' + C^{(2)}\right) + O(\epsilon^5), \\
\pi &= -\frac{\partial_t\phi_0}{6\kappa^2(\rho_0+P_0)a^3}\left(R^{(0)}\int_{t_0}^{t} a(t')dt' + C^{(2)}\right) + O(\epsilon^4), \\
\chi &= -\frac{1}{6\kappa^2(\rho_0+P_0)a^2}\left[\left(1+3c_{s0}^2 - \frac{\rho_0\Gamma_0\partial_t\phi_0}{(\rho_0+P_0)a}\int_{t_0}^{t} a(t')dt'\right)R^{(0)} - \frac{\rho_0\Gamma_0\partial_t\phi_0}{(\rho_0+P_0)a}C^{(2)}\right] \\
&\quad + O(\epsilon^4), \\
\psi &= L^{(0)}\left(1+\frac{1}{2}\int_{t_0}^{t} H(t')\chi(t')dt'\right) + O(\epsilon^4), \\
\tilde{\gamma}_{ij} &= f_{ij}^{(0)} - 2\left(F_{ij}^{(2)}\int_{t_0}^{t}\frac{dt'}{a^3(t')}\int_{t_0}^{t'} a(t'')dt'' + C_{ij}^{(2)}\int_{t_0}^{t}\frac{dt'}{a^3(t')}\right) + O(\epsilon^4), \\
\tilde{A}_{ij} &= \frac{1}{a^3}\left(F_{ij}^{(2)}\int_{t_0}^{t} a(t')dt' + C_{ij}^{(2)}\right) + O(\epsilon^4),
\end{aligned}
\tag{6}
$$

where $R^{(0)} = R\left[(L^{(0)})^4 f^{(0)}\right]$, $C^{(2)}$ in this expression is related to $\Pi^{(2)}$, and 'constants' of integration $L^{(0)}$, $f_{ij}^{(0)}$, $C^{(2)}$ and $C_{ij}^{(2)}$ depend only on the spatial coordinates $\{x^k\}$ $(k = 1, 2, 3)$.

4 Summary and discussion

We have developed a theory of nonlinear cosmological perturbations on superhorizon scales for a scalar field described by a Lagrangian of the form $P(X, \phi)$, where $X = -\partial^\mu\phi\partial_\mu\phi$ and ϕ is the scalar field, and also for a perfect fluid with a general equation of state $P = P(\rho)$. The general solutions valid up to the order $O(\epsilon^2)$ in the spatial gradient expansion have been presented for the scalar field system and in Appendix of [8] for the perfect fluid. This formalism can be applied to many interesting circumstances. Some particular examples including a scalar with shift symmetry, a canonical scalar and a DBI scalar. Thus, the formalism can be used to investigate superhorizon evolution of nonlinear cosmological perturbations in k-inflation and DBI inflation. If matching subhorizon perturbation with superhorizon perturbation occurs in enough large scale (or enough late time), the $O(\epsilon^0)$ effect becomes dominant. However, near crossing the horizon, there is the case where the $O(\epsilon^2)$ corrections need to estimate. In order to quantify the non-Gaussianity, it needs to translate curvature perturbation ψ in our solutions which has been obtained on the uniform Hubble hypersurface, into ones on the uniform density ζ, which have been discussed in the first section. Calculating three point correlation function of ζ including the $O(\epsilon^0)$ corrections will be addressed in future publication.

References

[1] C. Armendariz-Picon, T. Damour and V. F. Mukhanov, Phys. Lett. B **458**, 209 (1999).

[2] M. Alishahiha, E. Silverstein and D. Tong, Phys. Rev. D **70**, 123505 (2004).

[3] D. H. Lyth, K. A. Malik and M. Sasaki, JCAP **0505**, 004 (2005).

[4] M. Sasaki and T. Tanaka, Prog. Theor. Phys. **99**, 763 (1998).

[5] S. M. Leach, M. Sasaki, D. Wands and A. R. Liddle, Phys. Rev. D **64**, 023512 (2001).

[6] Y. Tanaka and M. Sasaki, Prog. Theor. Phys. **117**, 633 (2007).

[7] Y. Tanaka and M. Sasaki, Prog. Theor. Phys. **118**, 455 (2007).

[8] Y. Takamizu and S. Mukohyama, JCAP **0901**, 013 (2009).

Gravitating Q-balls and their stabilities

Takashi Tamaki[1] and Nobuyuki Sakai[2]

[1]*Department of Physics, Waseda University, Okubo 3-4-1, Tokyo 169-8555, Japan*
[2]*Faculty of Education, Yamagata University, Yamagata 990-8560, Japan*

Abstract

We analyze stability of gravitating Q-balls.

1 Introduction and our model

It has been argued that scalar solitons play important roles as dark matter candidates. Boson stars are one of their possibilities. Depending on their potentials and couplings, we can consider various sizes. For example, it has been argued that axidilaton star of $\sim 0.6M_\odot$ accounts for some fraction of the MACHOs (massive compact halo object) [1]. Supermassive boson stars of $10^6 - 10^9 M_\odot$ as an alternative to a black hole in the galaxy center has also been discussed [2]. For these reasons, it is important to argue their stabilities. To tackle this problem, it is instructive to consider their flat limit and examine the method which is useful for stability analysis in this case. In general, boson stars do not have a flat limit. The case having the flat limit is classified as Q-balls [3]. Kusenko showed that Q-balls are stable under the thick-wall approximation for the potential [4]

$$V_3(\phi) = \frac{m^2}{2}\phi^2 - \mu\phi^3 + \lambda\phi^4 \quad \text{with} \quad m^2,\ \mu,\ \lambda > 0\ . \tag{1}$$

The work by Pacceti Correia and Schmidt is very useful which showed that stability of Q-balls is guaranteed if and only if

$$\frac{\omega}{Q}\frac{dQ}{d\omega} < 0\ , \tag{2}$$

where Q and ω are the Q-ball charge and the phase velocity, respectively [5]. Whether or not this criterion can be extended to gravitational Q-balls is one of our interest.

We take the action described by

$$\mathcal{S} = \int d^4x\sqrt{-g}\left(\frac{{m_{\rm Pl}}^2}{16\pi}\mathcal{R} + \mathcal{L}_\phi\right), \quad \mathcal{L}_\phi \equiv \sqrt{-g}\left\{-\frac{1}{2}g^{\mu\nu}\partial_\mu\boldsymbol{\phi}\cdot\partial_\nu\boldsymbol{\phi} - V(\phi)\right\}, \tag{3}$$

where $\boldsymbol{\phi} = (\phi_1,\ \phi_2)$ is an SO(2)-symmetric scalar field and $\phi \equiv \sqrt{\boldsymbol{\phi}\cdot\boldsymbol{\phi}} = \sqrt{\phi_1^2 + \phi_2^2}$. We assume a spherically symmetric and static spacetime, $ds^2 = -\alpha^2(r)dt^2 + A^2(r)dr^2 + r^2(d\theta^2 + \sin^2\theta d\varphi^2)$. We consider spherically symmetric configurations of the field and assume homogeneous phase rotation, $(\phi_1, \phi_2) = \phi(r)(\cos\omega t, \sin\omega t)$. Then the field equations become

$$A' + \frac{A}{2r}(A^2 - 1) = \frac{4\pi r A^3}{{m_{\rm Pl}}^2}\left(\frac{{\phi'}^2}{2A^2} + \frac{\omega^2\phi^2}{2\alpha^2} + V\right), \alpha' + \frac{\alpha}{2r}(1 - A^2) = \frac{4\pi r\alpha A^2}{{m_{\rm Pl}}^2}\left(\frac{{\phi'}^2}{2A^2} + \frac{\omega^2\phi^2}{2\alpha^2} - V\right), \tag{4}$$

$$\phi'' + \left(\frac{2}{r} + \frac{\alpha'}{\alpha} - \frac{A'}{A}\right)\phi' + \left(\frac{\omega A}{\alpha}\right)^2\phi = A^2\frac{dV}{d\phi}, \tag{5}$$

where $' \equiv d/dr$. We solve (4)-(5) with boundary conditions,

$$A(0) = A(\infty) = \alpha(\infty) = 1, \quad A'(0) = \alpha'(0) = \phi'(0) = \phi(\infty) = 0. \tag{6}$$

[1]E-mail:tamaki@gravity.phys.waseda.ac.jp
[2]E-mail:nsakai@e.yamagata-u.ac.jp

Due to the symmetry there is a conserved charge,

$$Q \equiv \int d^3x\sqrt{-g}g^{\mu\nu}(\phi_1\partial_\nu\phi_2 - \phi_2\partial_\nu\phi_1) = \omega I, \quad \text{where} \quad I \equiv 4\pi\int\frac{Ar^2\phi^2}{\alpha}dr. \tag{7}$$

One finds the canonical momentum of ϕ and the matter part of the Hamiltonian density,

$$\mathcal{P}_a = \frac{\partial\mathcal{L}_\phi}{\partial\dot{\phi}_a} = \frac{\sqrt{-g}}{\alpha^2}\dot{\phi}_a, \qquad \mathcal{H}_\phi = \mathcal{P}_a\dot{\phi}_a - \mathcal{L}_\phi = \frac{\alpha^2\mathcal{P}_a^2}{2\sqrt{-g}} + \sqrt{-g}\left\{\frac{(\phi_a')^2}{2A^2} + V\right\}. \tag{8}$$

Because we will consider only virtual displacement of ϕ, we do not have to take the gravity part into account. Then the Hamiltonian is given by

$$E = \int\mathcal{H}_\phi d^3x = \frac{Q^2}{2I} + 4\pi\int r^2\alpha A\left\{\frac{(\phi')^2}{2A^2} + V\right\}dr. \tag{9}$$

We consider (1) which we call V_3 model. For V_3 model, we rescale the quantities as

$$\tilde{t} \equiv \frac{\mu}{\sqrt{\lambda}}t, \quad \tilde{r} \equiv \frac{\mu}{\sqrt{\lambda}}r, \quad \tilde{\phi} \equiv \frac{\lambda}{\mu}\phi, \quad \tilde{V}_3 \equiv \frac{\lambda^3}{\mu^4}V_3, \quad \tilde{m} \equiv \frac{\sqrt{\lambda}}{\mu}m, \quad \tilde{\omega} \equiv \frac{\sqrt{\lambda}}{\mu}\omega, \quad \kappa \equiv \frac{\mu^2}{\lambda{m_{\rm Pl}}^2}, \tag{10}$$

To estimate the parameter regions of $\tilde{\omega}^2$ where solutions exist, we consider the flat case. In this case, the field equation is

$$\frac{d^2\tilde{\phi}}{d\tilde{r}^2} = -\frac{2}{\tilde{r}}\frac{d\tilde{\phi}}{d\tilde{r}} - \tilde{\omega}^2\tilde{\phi} + \frac{d\tilde{V}}{d\tilde{\phi}}\,. \tag{11}$$

This is equivalent to the field equation for a single static scalar field with the potential $V_\omega \equiv \tilde{V} - \tilde{\omega}^2\tilde{\phi}^2/2$. For this case, solutions satisfying boundary conditions (6) exist if $\min(V_\omega) < \tilde{V}(0)$ and $d^2V_\omega/d\tilde{\phi}^2(0) > 0$, which is equivalent to

$$\tilde{\omega}^2_{\rm min} < \tilde{\omega}^2 < \tilde{m}^2 \quad \text{with} \quad \tilde{\omega}^2_{\rm min} \equiv \min\left(\frac{2\tilde{V}}{\tilde{\phi}^2}\right). \tag{12}$$

The two limits $\tilde{\omega}^2 \to \tilde{\omega}^2_{\rm min}$ and $\tilde{\omega}^2 \to \tilde{m}^2$ correspond to the thin-wall limit and the thick-wall limit, respectively. For V_3 potential, we have $\tilde{\omega}^2_{\rm min} = \tilde{m}^2 - \frac{1}{2}$. As we explain below, qualitative features of solutions change at $\tilde{m}^2 = \frac{1}{2}$.

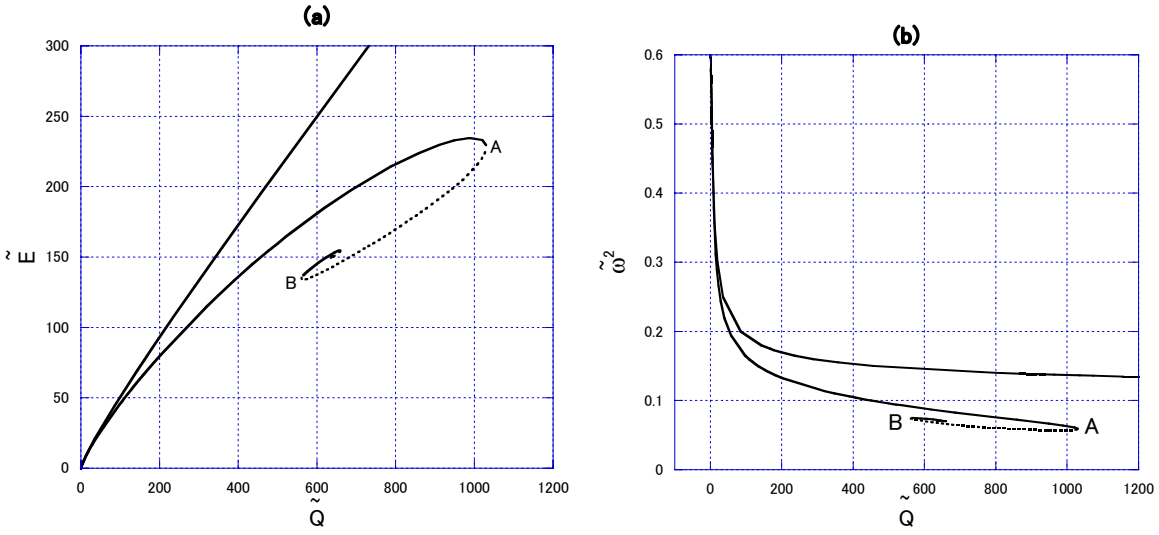

Figure 1: (a) $\tilde{Q}$-$\tilde{E}$ and (b) $\tilde{Q}$-$\tilde{\omega}^2$ for $\tilde{m}^2 = 0.6$. We compare solutions for $\kappa = 0$ with those for 0.01. Spiral structures can be seen for the case with $\kappa = 0.01$.

2 Comparison of gravitating cases with flat cases

2.1 The case for $\tilde{m}^2 > 0.5$

First, we compare $\tilde{Q}$-$\tilde{E}$ and $\tilde{Q}$-$\tilde{\omega}^2$ in the case for $\tilde{m}^2 = 0.6$ with $\kappa = 0$ (i.e., flat case), and with 0.01 in Fig. 1 (a) and (b), respectively. For the flat case, there is an one to one correspondence between $\tilde{Q}$ and $\tilde{E}$ while there is a spiral structure for the gravitating case as shown in Fig. 1 (a). As a result, we find the $\tilde{Q}$-maximum (the point A) and its local minimum (the point B). It is expected that this property would affect their stability. Actually, if we see Fig. 1 (b), we find that the stability criterion (2) is satisfied for the flat case while it is not necessarily satisfied for the gravitating case. However, since (2) is established by using the explicit form of the perturbative equation for the flat case, it is not evident whether or not it is applicable for the gravitating case.

It is natural to ask what cause these differences. To answer this question, we show the field profiles of the scalar field for $\kappa = 0$ with $\tilde{Q} = 200$ and 800 (dotted lines) and those for $\kappa = 0.01$ with $\tilde{Q} = 200$ and 800 (solid lines) in Fig. 2. If we pay attention to the case $\tilde{Q} = 200$, we notice that the scalar field is a little bit concentrated near the origin if the gravity is taken into account. This tendency becomes clear for the case $\tilde{Q} = 800$ where two solutions exist for $\kappa = 0.01$ (See, Fig. 1). The solution with more condensed configuration around the origin corresponds to that shown by a dotted line in Fig. 1. This implies that the Q-ball having larger charge than that of the point A can not support itself and will collapse or disperse. Limitation of the Q-ball size due to gravity has been pointed out in [6]. This implies that stability changes at the point A. Although we show the example $\tilde{m}^2 = 0.6$ with $\kappa = 0$ and 0.01, qualitative properties for $\tilde{m}^2 > 0.5$ and other κ do not change from these cases. The quantitative properties which are changed by other parameters are sizes of spiral structures in these diagrams. If we take large (small) κ and $\tilde{m}^2$, maximum of $\tilde{Q}$ becomes small (large).

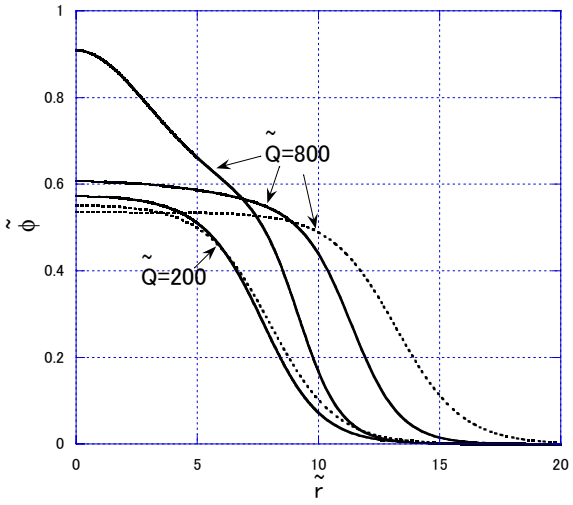

Figure 2: $\tilde{r}$-$\tilde{\phi}$ relation for $\kappa = 0$ with $\tilde{Q} = 200$ and 800 (dotted lines) and for $\kappa = 0.01$ with $\tilde{Q} = 200$ and 800 (solid lines).

2.2 The case for $\tilde{m}^2 < 0.5$

Next, we show (a) $\tilde{Q}$-$\tilde{E}$ and (b) $\tilde{Q}$-$\tilde{\omega}^2$ for $\tilde{m}^2 = 0.2$ in Fig. 3. First, we pay attention to Fig. 3 (a). We should notice that the case $\kappa = 0$ has a cusp structure and has a $\tilde{Q}$-maximum different from that for $\tilde{m}^2 > 0.5$. As a result, we have two solutions for a fixed $\tilde{Q}$ for the flat case. It has been shown that the dotted line is unstable while the solid line stable. We find that the case $\kappa = 1.0$ and 1.3 only show the slight difference from the flat case. However, there is an important difference that the cusp structure disappears. Its disappearance suggests that the catastrophe type is changed by gravity. Intrinsic differences occur for $\kappa > 1.3$ where two spiral structures appear for each κ (we call each of them lower

and higher branch corresponding to their energy, respectively). If one considers the analogy with the flat case where the solid (dotted) line is the stable (unstable), one may suppose that the lower (higher) branch is stable (unstable). However, we should suppose that two spiral structures appear for the same reason for the corresponding one for $\tilde{m}^2 > 0.5$ where gravity makes a $\tilde{Q}$-maximum. Thus, it is natural to guess that the lower branch shown by a solid (dotted) line is stable (unstable). The stability of the higher branch is more puzzling. If we compare the case $\kappa = 1.4$ with the case $\kappa = 1.3$, we may suppose that the interval between B and C is stable. However, the case $\kappa = 1.5$ does not have such an interval. Therefore, it is difficult to judge the stability without other criteria.

We also comment on the diagram (b) and the stability criterion (2). The solid (dotted) lines correspond to those in the diagram (a). For the flat case, we can confirm that the solid line satisfies (2) while the dotted line does not. For the gravitating with $\kappa < 1.4$, we also confirm it while it is not for $\kappa \geq 1.4$. In particular, the solution shown by the solid line and that by the dotted line, both satisfying (2), merge at the cusp for $\kappa = 1.4$. Since the cusp is a typical structure which suggests a stability change via a catastrophe theory, (2) would not be applicable for gravitating Q-balls.

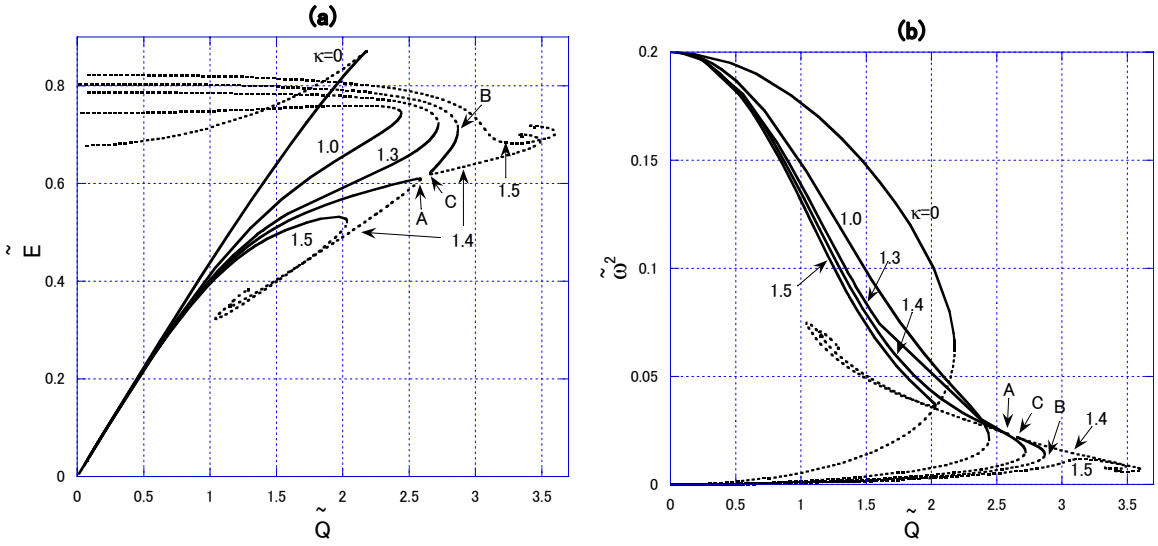

Figure 3: (a) $\tilde{Q}$-$\tilde{E}$ and (b) $\tilde{Q}$-$\tilde{\omega}^2$ for $\tilde{m}^2 = 0.2$.

3 Conclusion

We have analyzed stability of gravitating Q-balls for a V_3 model and revealed their structures.

References

[1] E. W. Mielke and F. E. Schunck, Nucl. Phys. B **564**, 185 (2000); *ibid.,* Gen. Rel. Grav. **33**, 805 (2001).

[2] F. E. Schunck and A. R. Liddle, Phys. Lett. B **404**, 25 (1997); E. W. Mielke and F. E. Schunck, Phys. Rev. D **66**, 023503 (2002).

[3] S. Coleman, Nucl. Phys. **B262**, 263 (1985).

[4] A. Kusenko, Phys. Lett. B **404**, 285 (1997).

[5] F. Paccetti Correia and M. G. Schmidt, Eur. Phys. J. **C21**, 181 (2001).

[6] T. Multamaki and I. Vilja, Phys. Lett. B **542**, 137 (2002).

Kerr black hole and rotating black string by intersecting M-branes

Makoto Tanabe[1]

[1] *Department of Physics, Waseda University, Tokyo, Japan*

Abstract

We find eleven dimensional non-BPS black M-brane solutions from Kerr solution in M-theory by using U-duality. Under the transformation four dimensional Kerr metric change to non-BPS rotating intersecting M-brane solutions. To easy application for AdS/CFT correspondence we must need a supersymmetric black brane solution, which limits special configuration of M-branes, e.g., M2-M2-M2 branes in five dimensional black brane and M5-M5-M5 brane with pp-wave in four dimensional one. In this case we may easily apply the AdS/CFT correspondence for non-BPS black hole solutions.

1 Introduction

AdS/CFT correspondence [1] is the most successful theory to describe strong coupling limit for boundary conformal field theory. There is a holographic duality between bulk quantum gravity and boundary quantum field theory. Four dimensional CFT is studied in all aspects because of CFT interests, and its dual theory is based on five dimensional supergravity black hole solutions. In recent years, Kerr/CFT correspondence are found only for the extremal limit case [2]. The paper shows the reason of the finite entropy of the extremal Kerr black hole, even the Hawking temperature is zero. AdS/CFT correspondence are very useful to show that reason. However non-extremal case we have no information about AdS/CFT correspondence, thus for non-extremal Kerr/CFT correspondence we will give the M-brane configuration about non-extremal Kerr solution.

Non BPS black ring solutions [3] using the same method we use below, but these solutions related to intersecting $M2 \perp M2 \perp M2$-brane solution in M-theory, or intersecting $F1 \perp D2 \perp D2$-brane solution in type IIA string theory with compactification on one-dimensional torus of M-Theory. These configuration in string theory is impossible to analysis for AdS/CFT correspondence [1], because we must choose typical coordinates for the compact space for near horizon limit, which is the kk-wave direction, but this solution has not any typical direction for compact spaces. Thus we show the $NS5 \perp D4 \perp D4$-brane solutions from general axisymmetric four-dimensional vacuum solution with two Killing vector, e.g., Kerr metric. We also get the general rotating black string solutions, which is rotating four-dimensional black hole with extra one dimension, by the $M2 \perp M2 \perp M2$-brane solutions from the Kerr metric.

In our previous work [4], black hole solutions with flat extra dimensions in M-theory are only exist the specific configuration of intersecting M-branes. However the earlier study for the micro state of Kerr black hole [5] using the D0⊥D6 branes, which is impossible to extension to the supersymmetric black brane solution in four dimension. The supersymmetric black brane means which have the regular event horizon with finite surface area.

Adding the new charge for the solution, we apply the boost for the ordinary metric along the extra dimension. Applying T-duality for the boost solution, we find D3-brane given by four-form field D_4, which is the self-dual field strength $dD_4 = *(d\tilde{D}_4)$. There are some technical difficulties for the Hodge dual for the stationary spacetime, since the stationary black hole remains the non-diagonal component after the boost. Such a component makes problem for integration in order to get the explicit description of the dual field $\tilde{D}_4$.

We will construct the intersecting M-brane solution consistent to the intersecting rule, and avoiding the difficulties of integration we apply the final boost after the lifting up to the eleven dimension. Thus we try to find the sequence to get the M5⊥M5⊥M5-brane soltuion, which is related to the D4⊥D4⊥NS5 brane solutions in type IIA superstring theory.

[1] E-mail:tanabe@gravity.phys.waseda.ac.jp

2 From Kerr metric to Intersecting D-branes

Before charging up the vacuum solution, we introduce the Kerr metric, which is a stationary solution of four-dimensional vacuum Einstein equation. The Kerr metric in spherical coordinate is written in

$$ds^2 = -f\left(dt + \Omega\right)^2 + \Sigma^2\left(\frac{dr^2}{\Delta} + d\theta^2\right) + \frac{\Delta}{f}\sin^2\theta d\phi^2$$

where the metric functions are defined by

$$\Sigma^2 = r^2 + a^2\cos^2\theta\,,\ \Delta = r^2 - 2mr + a^2$$
$$\Omega = \frac{2mr}{\Sigma^2 - 2mr}a\sin^2\theta d\phi\,,\ f = 1 - \frac{2mr}{\Sigma^2}\,.$$

The mass of the black hole is m and a is the specific angular momentum witch bounded for $m \quad a$. In the Kerr/CFT correspondence, we take the extremal limit $m = a$ and near horizon limit $r \to r_+$, where the event horizon r_+ is determined by $\Delta = 0$. For simplicity we denote $ds^2 = -f(dt+\Omega)^2 + ds^2_{\rm base}$ in below. The base metric $ds^2_{\rm base} = \gamma_{ij}dx^i dx^j$ are the orthogonal three-dimensional metric written by the variables r, θ, ϕ. The metric has the two Killing vector ξ_t and ξ .

Adding the extra six flat dimension, the metric change to $ds^2 + -f(dt+\Omega)^2 + ds^2_{\rm base} + \sum_{i=1}^6 dz_i^2$. This metric is also a solution of ten dimensional vacuum Einstein equation $R \quad = 0$. To add first charge (D3-brane), we apply a sequence in below;

$$B_{\alpha_2}(z_1) \to T(z_1) \to S \to T(z_2) \to T(z_3)\,,$$

then we find a $D3$-brane solution in type IIB supergravity. We denote $B_\alpha(z_1)$ is boost for z_i direction with boost parameter α, $T(z_i)$ is T-dual for z_i direction, and S is S-dual. To add second and third charges, we take next sequence in below,

$$T(z_4) \to B_{\alpha_1}(z_1) \to T(z_1) \to S \to T(z_5) \to T(z_6) \to T(z_2) \to B(z_6) \to T(z_6) \to S \to T(z_5)\,,$$

then we find a $D2 \perp D2 \perp D2$ intersecting brane solution as

$$ds^2 = -\xi^{-1/2}f(dt + c_1c_2c_3\Omega)^2 + \xi^{1/2}ds^2_{\rm base} + \xi^{1/2}\left[h_1^{-1}\sum_{i=1}^2 dz_i^2 + h_2^{-1}\sum_{i=3}^4 dz_i^2 + h_3^{-1}\sum_{i=5}^6 dz_i^2\right]\,,$$

where $\xi = h_1h_2h_3 - \beta_t^2$, $\beta_t = s_1s_2s_3\frac{ma\cos\theta}{\Sigma^2}$. The dilaton field is $e^{-2\varphi} = \xi^{-3/2}h_1h_2h_3$ and the gauge fields are

$$B_{z_iz_j} = h_\alpha^{-1}\frac{c_\alpha}{s_\alpha}\beta_t\,,\ \tilde{A}_t = -\xi^{-1}\beta_t f\,,\ \tilde{A} \quad = -\xi^{-1}\beta_t f\omega$$
$$\tilde{C}_{z_iz_jt} = \frac{2}{3}h_\alpha^{-1}s_\alpha c_\alpha(f-1)\,,\ \tilde{C}_{z_iz_j} \quad = \frac{2}{3}h_\alpha^{-1}fc_\alpha^{-1}s_\alpha\omega\,.$$

where the pair of indices $(i,j) = (1,2),(3,4),(5,6)$ are corresponding to $\alpha = 1,2,3$, and $\omega = c_1c_2c_3\Omega$.

For the first example of a black hole solution, we continue to apply the U-duality for the charging up the four-dimensional Kerr solutions. Next we try to apply another example related to the rotating black string, which can be described by the Kerr metric with another one extra dimension, and these solutions must possess the Gregory-Laflamme instability [6].

In order to get M5⊥M5⊥M5 brane solution, we must apply the sequence in following as

$$T(z_1) \to T(z_3) \to T(z_5) \to T(z_2) \to T(z_4) \to T(z_6)\,,$$

then we find the $D4 \perp D4 \perp D4$-brane solutions and we lift up the z^7 direction and boost for the same direction z^7, then we find the $M5 \perp M5 \perp M5$-brane with pp-wave solutions in M-theory;

$$ds^2 = \Xi^{1/3}\left[\bar{h}_1^{-1}\sum_{i=1}^2 dz_i^2 + \bar{h}_2^{-1}\sum_{i=3}^4 dz_i^2 + \bar{h}_3^{-1}\sum_{i=5}^6 dz_i^2\right]$$
$$+ \Xi^{1/3}\left[-\xi^{-1}f(dt+\omega d\phi)^2 + ds^2_{\rm base}\right] + \Xi^{-2/3}\xi\left(dz_7 + \hat{A}_t dt + \hat{A} \ d\phi\right)^2\,, \qquad (1)$$

where the conformal factor can be written by $\Xi = \bar{h}_1\bar{h}_2\bar{h}_3$ and $\bar{h}_i = \xi\hat{h}_i^{-1}$ with $\hat{h}_i = -s_i^2 f + c_i^2 g_i^{-1}$. The function g_i is determined by $g_i = 1 + (h_1h_2h_3)^{-1}h_i^{-1}s_2^{-2}\beta_t^2$. The three-form fields related to $M5$-brane are given by

$$\hat{C}_7^{(\alpha)} \equiv C_{z_iz_jz_7} = \frac{2}{3}\bar{h}_\alpha^{-1}s_\alpha^{-1}c_\alpha\beta_t\,, \quad \hat{C}_a^{(\alpha)} \equiv \tilde{C}_{z_iz_ja} = \frac{8}{3}\hat{D}_a^{(\alpha)} + \bar{h}_\alpha^{-1}s_\alpha^{-1}c_\alpha\beta_t\hat{A}_a\,,$$

where the component of M5-brane fields and the metric components are given by

$$\begin{aligned}
&\hat{D}_t^{(1)} = -\xi^{-1}h_2s_1c_2c_3\tilde{D}_t\,, \quad \hat{D}^{(1)} = s_2c_2\left[\tilde{D} \ + (1-\xi^{-1}h_2c_1^2c_3^2)\tilde{D}_t\Omega \ \right]\\
&\hat{D}_t^{(2)} = -\xi^{-1}h_1c_1s_2c_3\tilde{D}_t\,, \quad \hat{D}^{(2)} = s_1c_1\left[\tilde{D} \ + (1-\xi^{-1}h_1c_2^2c_3^2)\tilde{D}_t\Omega \ \right]\\
&\hat{D}_t^{(3)} = -\xi^{-1}h_3c_1c_2s_3\tilde{D}_t\,, \quad \hat{D}^{(3)} = s_3c_3\left[\tilde{D} \ + (1-\xi^{-1}h_3c_1^2c_2^2)\tilde{D}_t\Omega \ \right]\\
&\hat{A}_t = s_1c_1s_2c_2s_3c_3\frac{ma^2\cos^2\theta}{\Sigma^4}\\
&\hat{A} \ = -s_1s_2s_3\left(c_1^2c_2^2c_3^2 + \frac{2r\Sigma^2h_1h_2h_3}{r^2-a^2\cos^2\theta}\right)\frac{ma^3\sin^2\theta\cos^2\theta}{\Sigma^4}\,.
\end{aligned}$$

We note that Kerr metric with flat dimensions has no Chern-Simons term, but there are exist in eleven dimension after the charging up sequence, e.g., $\hat{C}_7^{(1)} \wedge d\hat{C}_t^{(2)} \wedge \hat{C}^{(3)}$ or like that combinations. The Chern-Simons terms gives the non-trivial effect of the topology for BPS black ring solutions, and this effect change the Laplace equation for the harmonic function h_i to the Poisson equation for the non-harmonic function $\bar{h}_i$. Because of non conformally flat base space, supersymmetrie breaks for ϕ direction, thus in the ordinary base space configuration we took maximally charge for three.

Finally we apply the boost for the z_7 direction, then we find non-BPS four charge solution. However if we took same special value for physical parameters, we find supersymmetric solution with conformally flat base space. To Compactify extra seven dimensions $(z_1, \cdots, z_7)$ on torus, we find the four dimensional charged solution as

$$ds^2 = -\Upsilon f(dt + \bar{\omega}d\phi)^2 + \Upsilon^{-1}ds^2_{\text{base}}\,, \tag{2}$$

where $\bar{\omega}$ and Υ are determined by

$$\begin{aligned}
&\bar{\omega} = c_4\omega + s_4(\omega\hat{A}_t - \hat{A} \ )\\
&\Upsilon^{-2} = \Xi\left(-\xi^{-1}fs_4^2 + \Xi^{-1}\xi(c_4 + s_4\hat{A}_t)^2\right)\,,
\end{aligned}$$

In the Kerr metric case, the regularity condition for the rotating axis are the same as before, thus the metric has no conical singularity at the ordinary event horizon $r_+ = m + \sqrt{m^2 - a^2}$.

In the asymptotic region ($r \to \infty$) the metric becomes flat and the ADM mass $M = m(1+\sum_{i=1}^4 s_i^2/2)$, the conserved charge $Q = \sqrt{2}m\sum_{i=1}^4 s_ic_i/2$ and the angular momentum $J = c_1c_2c_3c_4a$ are given in the asymptotic metric form. The surface gravity change as below

$$\kappa = \frac{1}{\beta_{t+}^2(c_4 + s_4\hat{A}_{t+})}\frac{r_+^2 - a^2}{4mr_+^2}\,, \tag{3}$$

where β_{t+} and $\hat{A}_{t+}$ are defined by the substitution for $r = r_+$. The surface area of the outer event horizon

$$\begin{aligned}
\mathcal{A} &= \int d\theta d\phi \left.\sqrt{\Sigma^2\left(\Upsilon^{-2}\gamma \quad - f\bar{\omega}^2\right)}\right|_{r=r_+}\\
&= 8\pi mr_+c_1c_2c_3\left[c_4 - \frac{1}{2}a^3s_4\left(\frac{\pi}{4} - \frac{a}{r_+}\arctan\,\frac{r_+}{a}\right)\right]\,,
\end{aligned}$$

and we can show the thermodynamics with the physical parameter as the charge and angular momentum and the temperature, but the dilaton fields does not contribute.

The extremal solution ($\kappa = 0$) is given by $m = a$, which is as the same as ordinary Kerr metric. The area surface is vanishing in the extremal limit of the ordinary Kerr metric, however the area surface in M-theoretical Kerr metric doesn't vanishing ($\mathcal{A} = 8\pi m^2 c_1 c_2 c_3 c_4$). Since c_α is related to the charge of M-brane (or D-brane), this non-vanishing area surface gives the microstate of M-brane.

Sen gave the rotating charged black hole solution [7], which metric is given in

$$ds^2 = -h_\alpha^{-1} f \left(dt + c_\alpha^2 \Omega\right)^2 + h_\alpha ds^2_{\rm base}\,, \tag{4}$$

where $h_\alpha = -s_\alpha^2 f + c_\alpha^2$. Sen's solution is included in our solution with the parameter $c_1 = c_2 = c_\alpha$ and $c_3 = c_4 = 1$, and this case the action is changing as $\phi_1 = \phi_2$ and $\phi_3 = \phi_4 = 0$ and $\rho_\alpha = 0$ and only $\mathcal{A}_a^{(1)} = \mathcal{A}_a^{(2)}$ are exist.

3 Concluding remark

In this paper we have presented the charging up Kerr solution using the U-duality method. Black hole solutions are presented by intersecting M-brane, and we have construct the intersecting M-brane solution, which consistent to the supersymmetrical black hole solution given by our previous work [4]. The four-dimensional black hole solution is given by M5⊥M5⊥M5 brane solution with traveling wave, and the five-dimensional black string solution is given by M2⊥M2⊥M2 brane solution. Both of the solution exist the non-vanishing Chern-Simons term in M-theory, although the Chern-Simons term in the ordinary Kerr metric with additional flat extra dimensions must be vanishing. The Chern-Simons terms change the metric function given by Laplece equation to the function given by Poisson equation.

The four-dimensional solution is represented by the charged dilaton black hole. The Maxwell charge and the dilatons are coupled to each other, and the angular momentum are represented by the charges. Thus we are only possible to take the limit to vanishing the charges with the trivial dilaton, and this limit gives static black brane solution [**?**]. The black hole has the regular extremal limit to the BPS solution in four dimension with non-vanishing are surface, and the area surface are represented by the micro state of M- or D-branes.

Since there are kk-wave mode in the ten-dimensional metric, the D-brane configuration of this metric is suitable to apply the AdS/CFT correspondence. We will show the micro state of these solutions in the context of AdS/CFT correspondence, and we will also show the regular solutions with the specific physical parameters in subsequent paper, witch we are writing now. In the limit for the CFT, we compare the micro state of Kerr black hole by $D0 \perp D6$-brane solutions given by Horowitz et. al., [5].

By the way of this paper we only consider from the vacuum solutions, but adding the extra dimension we can extend to the Einstein manifold with the constant gauge field, which satisfy the Einstein and Maxwell equation in lower and higher dimension. In this formalism, including the one rotating black ring case, we can apply the more interesting case, especially cosmology and black hole dynamics.

References

[1] O. Aharony, S. S. Gubser, J. M. Maldacena, H. Ooguri and Y. Oz, Phys. Rept. 323, 183 (2000) [arXiv:hep-th/9905111].

[2] M. Guica, T. Hartman, W. Song, A. Strominger, [arXiv:0809.4266].

[3] H. Elvang, R Emparan and P. Figueras, JHEP 0502 (2005) 031, [arXiv:hep-th/0412130].

[4] K. Maeda and M Tanabe, Nucl. Phys. B738 (2006) 184, [arXiv:hep-th/0510082].

[5] G. T. horowitz and M. M. Roberts, [arXiv:0708.1346].

[6] R. Gregory and R. Laflamme, Phys. Rev. D 37 (1988) 305.

[7] A. Sen, Phys.Rev.Lett. 69 (1992) 1006, [arXiv:hep-th/9204046].

[8] , G. W. Gibbons and K. Maeda, Nucl. Phys. B 298 (1998) 741.

Initial data of black hole localized on Karch-Randall brane

Norihiro Tanahashi[1] and Takahiro Tanaka[2]

Department of Physics, Kyoto University, Kyoto 606–8502, Japan

Abstract

Based on the conjectured duality in the Karch-Randall braneworld models, it is suggested that a static brane-localized black hole larger than bulk curvature length does exist in this model. It is also suggested that the Hawking-Page transition of the four-dimensional black hole may be reproduced as a change in the shape of five-dimensional black hole in the bulk. In order to test these suggestions, we try to construct time-symmetric initial data of brane-localized black hole in the Karch-Randall braneworld model and study its properties. I will explain the method of the analysis and illustrate expected results.

1 Introduction

The Randall-Sundrum II (RS-II) model [1] is a brane world model, which provides a way to realize our four-dimensional world in a higher-dimensional spacetime. This model is composed of five-dimensional bulk spacetime with negative cosmological constant and a four-dimensional brane with positive tension. Weak gravitational field on the brane obeys the usual four-dimensional Newton law with a correction suppressed at a large distance from the gravitational source [1, 2], though the extra-dimension extends infinitely in this model. If we weaken the brane tension a little, a small negative cosmological constant appears in the effective Einstein gravity on the four-dimensional brane, and the spacetime on the brane becomes AdS_4. It is known that there is an "almost" massless graviton even in this model, and four-dimensional gravity is realized if length scale of interest is shorter than the curvature scale on the brane. This model with an AdS brane is called the Karch-Randall (KR) model [3]. Since four-dimensional gravity is realized effectively in these models, it is difficult to distinguish them from ordinary four-dimensional models as long as we investigate only in the weak gravity regime. Essential features of these models will appear in strong gravitation phenomena on them. In order to assess viability of these models observationally, we should study how these models behave when strongly gravitation exists in them.

Now, consider a gravitational collapse on the brane in each of these models for an example of such strong gravitation phenomena. Naively thinking, a static black hole (BH) whose horizon is localized near the brane will form as a final state of this collapse, since ordinary four-dimensional gravity is realized on the brane. There are exact static solutions of black objects, which are black strings (BS) in those models [4,5], and they also are candidates of the black object which is formed after the collapse. However, it seems unlikely that a BS is formed as a result of gravitational collapse, since it is singular at the bulk AdS horizon and also unstable due to so-called Gregory-Laflamme instability [6]. Thus, a brane-localized BH seems to be most likely to form after the collapse on the brane.

Contrary to this expectation of brane-localized BH formation, such an exact static solution has not been discovered yet though much effort has been devoted into this issue (e.g. Ref. [7]). Numerical solution of a static brane-localized BH was constructed when the horizon size is not much larger than the bulk curvature scale, but the construction becomes harder as the horizon size becomes larger [8, 9]. A work on brane-localized BH issue [10] reports that there are some problems in numerical solution construction even when the brane-localized BH is smaller than the bulk curvature scale. These facts do not exclude the possibility that a static solution of brane-localized BH larger than the bulk curvature scale does exist, but we do not have any strong evidence of its existence. As an explanation of the lack of static solution, there is a conjecture that brane-localized static BHs larger than bulk curvature scale do not exist in RS-II model based on the AdS/CFT correspondence in this model [11, 12].

[1]E-mail:tanahashi@tap.scphys.kyoto-u.ac.jp
[2]E-mail:tama@scphys.kyoto-j.ac.jp

There are several works related to this conjecture (e.g. [13,14]), but no definite conclusion is obtained yet. It is desirable to investigate the properties of static BH solution directly in order to test the validity of this conjecture, but it is technically difficult to construct a static large BH solution numerically. Thus, we consider time-symmetric initial data which have a brane-localized apparent horizon (AH), expecting that their properties may give some insight into the brane-localized BH.

We have done this initial data construction and analysis of their properties in [15]. It was confirmed in this work that there exists an initial data with an arbitrariry large blane-localized BH. We analyzed their themodynamic properties by comparing this initial data with a black string solution which have the same four-dimensional ADM mass. This analysis revealed that such a large brane-localized BH have smaller entopy than than the black string of the same mass has, and thus it seems to be unstable and tend to evolve into some other black object. This tendency changes as we decrease the size of the brane-localized BH; when it is smaller than the bulk curvature scale, it have more entropy than the black string has. This result is consistent that a static stable brane-localized BH does exists when it is smaller than the bulk curvature scale, and it becomes unstable when it is larger than that scale.

This time, we do a similar analysis on the KR model. One of the differences from the RS-II model is the behavior of warp factor in the bulk; in the RS-II model, it just decreases down to zero as we move into the bulk from the brane; in KR model, it first decreases, but it begins to grow again after we passed over a critical point which is at a distant of the bulk curvature scale. The effective potential for a small particle behaves in a similar manner to the warp factor. If we put a small black hole at that minimum point of the effective potential, it will stay there stably. At this stage, no black object is visible from an observer on the brane; radiation field of nonzero temperature is induced on the brane by that BH, and the brane observer will see only a lump of this thermal radiation.

Now, let us gradually increase the size of that BH which sits at that potential minimum. It will keep to stay there as long as its size is smaller than the bulk curvature scale. A curious phase transition occurs when its size become comparable to the bulk curavature scale: the BH touches the brane, and it becomes observable from an observer on the brane. By the way, in the four-dimensional AdS spacetime, it is known that such a phase transition occurs between thermal AdS phase and AdS BH phase. This phenomenon is known as the Hawking-Page transition [16]. We conjecture that the transition of the bulk BH shape to be a holographic dual of the Hawking-Page transition on the brane [11]. In order to check this conjecture, we construct initial data of bulk BHs and brane-localized BHs in the KR model, and test the thermodynamic property of those BHs.

2 Initial data construction method

In this section, we introduce a construction method of time-symmetric initial data with a BH in the KR model. This model is composed of two copies of five-dimensional empty bulk with negative cosmological constant Λ, and they are separated by a $\mathbb{Z}_2$-symmetric positive tension brane. The tension of the brane is given by $= 3k(1+\delta)/4\pi G_5$ with $k = \sqrt{-\Lambda/6}$, where G_5 is the five-dimensional gravitational constant. The parameter δ describes how a brane tension is detuned from that of the RS-II model; when $\delta = 0$, this model reduce to the RS-II model with a Minkowski brane. Four-dimensional cosmological constant is given by $\Lambda_{4\mathrm{D}} = 3k^2\left(2\delta + \delta^2\right)$, thus a negative cosmological constant appears when $\delta < 0$. In this work, we assume $\delta < 0$. The initial data we consider have $O(3)$-symmetry in the spacelike dimension as well as the symmetry with respect to time reversal. These symmetries are property shared with static brane-localized BH solutions. Hence, we think it appropriate to restrict our attention to this class of initial data.

The starting point of our construction procedure is to choose an asymptotically AdS vacuum solution of the Einstein equations with negative cosmological constant Λ. In this study, we use the well-known AdS-Schwarzschild solution. The metric is given by

$$ds^2 = -U(r)dt^2 + \frac{dr^2}{U(r)} + r^2\left(d\chi^2 + \sin^2\chi d\Omega_{\mathrm{II}}\right), \quad U(r) = 1 + k^2r^2 - \frac{}{r^2}, \tag{1}$$

where $d\Omega_{\mathrm{II}}$ is the line element on a unit S^2, and is the mass parameter of the AdS-Schwarzschild BH. The spacetime described by this metric is asymptotically AdS, and has an spherical event horizon

at $r = r_g$ where $U(r)$ vanishes. In the following discussion, we set k to unity by rescaling the unit of length. In this sense, this background spacetime has only one free parameter , which becomes one of free parameters of the initial data.

We put a vacuum brane with $\mathbb{Z}_2$-symmetry in this AdS BH bulk. We denote the unit normal of the brane by $\tilde{s}$, and take this $\tilde{s}$ in the direction toward the bulk from the brane. We introduce the induced metric $\tilde{\gamma}$ $\equiv g$ $- \tilde{s}$ $\tilde{s}$ on the brane. The extrinsic curvature $\tilde{K}_{ab}$ on the brane is defined by $\tilde{K}_{ab} = -\tilde{\gamma}_a$ $\tilde{\gamma}_b$ ∇ $\tilde{s}$. Here Latin indices starting from the beginning of the alphabet $(a, b, \cdots)$ run the four-dimensional coordinates on the brane. A vacuum brane has the four-dimensional energy-momentum tensor localized on the brane given by $T_{ab} = -$ $\tilde{\gamma}_{ab}$. Israel's junction condition [17] on the brane is given by $\tilde{K}_{ab} - \tilde{K}\tilde{\gamma}_{ab} = \frac{1}{2} \cdot 8\pi G_5 T_{ab}$, where we used $\mathbb{Z}_2$-symmetry across the brane. At the moment of the time-reversal symmetry, we only have to solve the Hamiltonian constraint, which is the (t, t)-component of the junction condition. Using the normal vector $\tilde{s}$, this equation is written as

$$D_i \tilde{s}^i = -3k\,(1 + \delta)\,, \tag{2}$$

where D_i is a covariant differenciation with respect to the induced metric $\tilde{\gamma}_{ij}$. Assuming $O(3)$-symmetry of the brane, we specify the brane trajectory by $(r, \chi) = (r_b(\xi), \chi_b(\xi))$, where ξ is the proper radial length along the brane. The spacelike unit normal $\tilde{s}$ is given by

$$\tilde{s} = \left(\sqrt{U} r_{\rm b} \chi'_{\rm b}, -\frac{r'_{\rm b}}{\sqrt{U} r_{\rm b}}\right). \tag{3}$$

Then the Hamiltonian constraint (2) becomes a second order ODE of $r_b(\xi)$ and $\chi_b(\xi)$. We solve Eq. (2) numerically to obtain the brane trajectory. In this way, we can construct a system of a brane and a BH which floats on it. We can change the brane position with respect to the bulk BH, and also we can change the mass parameter of the bulk BH as well as the detune paramter δ of the brane tension. Namely, we can construct a three-parameter family of the initial data. We note here that we can construct an initial data which have a BH localized on the brane, not one floating in the bulk.

3 Analysis method

In order to study thermodynamic properties of these BHs in the KR model, we have to calculate mass and entropy of them. When we studied the system with a flat brane, we calculated four-dimensional ADM mass measured on the brane and five-dimensional BH horizon area, and conducted a thermodynamic analysis using them. We obtained some pieces of evidence that brane-localized BHs larger than the bulk curvature scale are unstable. We would like to do a similar analysis using BH initial data on the KR model, but there is a difficulty in the calculation of mass. In the RS-II model, the localization of the four-dimensional graviton is perfect, and the four-dimensional ADM mass is expected to be an appropriate quantity to characterize the system. On the other hand, the bulk of the KR model largely opens up to the AdS boundary, and then the localization of the graviton is not perfect; the lowest Kaluza-Klein mode have very small mass, and since it behaves differently from zero mass graviton when it propagates a long length. In order to calculate mass in this system with imperfectly localized gravitation, we have to calculate five-dimensionally defined mass, not the mass which is four-dimensionally defined on the brane. However, there are no definite way to define five-dimensional mass in the KR model.

In [18], a way to define mass in AdS spacetime is proposed. They construct a conserved quantity which is expressed as a surface integral of metric perturbation. Our proposal is to use this definition to calculate mass in the KR model. We regard pure AdS_5 spacetime as background spacetime, calculate metric perturbation which is induced by the brane and the BH, and then calculate mass by integrating the metric perturbation on some surface which is located near spatial infinity.

When we applied this Abbott-Deser definition of mass to the KR model, we found that the mass defined in this way is conserved only when we keep to take the Gaussian-Normal coordinates. Thus, the mass defined in this way is coordinate dependent. It is not so clear that this mass satisfies the laws of thermodynamics, but we expect that we can obtain some information of the system using mass defined in this way.

Consider a family of initial data for a fixed value of mass. There are initial data of two types in this family: one with a BH floating in the bulk, and one with a BH localized on the brane. In this two-parameter family of the initial data for a fixed mass, we can find one which extremizes the entropy. We expect this initial data to be one with a floating BH in the bulk when the temperature on the brane is low, and to be one with a brane-localized BH when the temperature is above a critical temperature which is determined by the curvature scale on the brane.

From this analysis, we will obtain useful information about the holography in RS-II and KR models. Based on this result, we would like to tackle more difficult problems toward proof of the classical evaporation conjecture. Especially, we would like to simulate a time-evolving brane-localized black hole using numerical relativity technique. This analysis will clarify the behavior of BH solutions on these models, and will provide essential knowledge about the holography on these braneworld models.

References

[1] L. Randall and R. Sundrum, Phys. Rev. Lett. **83**, 4690 (1999)

[2] J. Garriga and T. Tanaka, Phys. Rev. Lett. **84**, 2778 (2000)

[3] A. Karch and L. Randall, Phys. Rev. Lett. **87**, 061601 (2001) [arXiv:hep-th/0105108].

[4] A. Chamblin and A. Karch, Phys. Rev. D **72**, 066011 (2005) [arXiv:hep-th/0412017].

[5] A. Chamblin, S. W. Hawking and H. S. Reall, Phys. Rev. D **61**, 065007 (2000)

[6] R. Gregory, Class. Quant. Grav. **17**, L125 (2000)

[7] D. Karasik, C. Sahabandu, P. Suranyi and L. C. R. Wijewardhana, Phys. Rev. D **69**, 064022 (2004)

[8] H. Kudoh, T. Tanaka and T. Nakamura, Phys. Rev. D **68**, 024035 (2003)

[9] H. Kudoh, Phys. Rev. D **69**, 104019 (2004) [Erratum-ibid. D **70**, 029901 (2004)]

[10] H. Yoshino, JHEP **0901**, 068 (2009) [arXiv:0812.0465 [gr-qc]].

[11] T. Tanaka, Prog. Theor. Phys. Suppl. **148**, 307 (2003)

[12] R. Emparan, A. Fabbri and N. Kaloper, JHEP **0208**, 043 (2002)

[13] P. R. Anderson, R. Balbinot and A. Fabbri, Phys. Rev. Lett. **94**, 061301 (2005)

[14] T. Tanaka, arXiv:0709.3674 [gr-qc].

[15] N. Tanahashi and T. Tanaka, arXiv:0712.3799 [gr-qc].

[16] S. W. Hawking and D. N. Page, Commun. Math. Phys. **87**, 577 (1983).

[17] W. Israel, Nuovo Cim. B **44S10**, 1 (1966) [Erratum-ibid. B **48**, 463 (1967 NUCIA,B44,1.1966)].

[18] L. F. Abbott and S. Deser, Nucl. Phys. B **195**, 76 (1982).

Black hole entropy for the general area spectrum

Tomo Tanaka[1] and Takashi Tamaki[2]

[1] *Department of Physics, Waseda University, Okubo 3-4-1, Tokyo 169–8555, Japan*
[2] *Department of Physics, Waseda University, Okubo 3-4-1, Tokyo 169–8555, Japan and Department of Physics, Rikkyo University, Toshima, Tokyo 171–8501, Japan*

Abstract

We consider the possibility that the horizon area is expressed by the general area spectrum in loop quantum gravity and calculate the black hole entropy by counting the degrees of freedom in spin-network states related to its area. Although the general area spectrum has a complex expression, we succeeded in obtaining the result that the black hole entropy is proportional to its area as in previous works where the simplified area formula has been used. This gives new values for the Barbero-Immirzi parameter ($\gamma = 0.5802\cdots$ or $0.7847\cdots$) which are larger than that of previous works.

1 Introduction

Statistical mechanics in a self-gravitating system is quite different from that without gravity. For example, particles in the box have maximal entropy when they spread out uniformly in the box if gravity is not taken into account. On the other hand, if particles are self-gravitating, we can suppose that clusters appear as an entropically favorable state. Then, if the pressure of particles can be neglected, it is likely that a black hole appears as a maximal entropy state. Thus, black hole entropy would be the key for understanding statistics in a self-gravitating system.

One of the most mysterious things about black holes is their entropy S which is *not* proportional to its volume *but* to its horizon area A. This was first pointed out related to the first law of black hole thermodynamics. The famous relation $S = A/4$ has been established by the discovery of the Hawking radiation. Recently, its statistical origin has been discussed in the candidate theories of quantum gravity, such as string theory, or loop quantum gravity (LQG) [1], etc. It has been discussed that LQG can describe its statistical origin independent of black hole species because of its background independent formulation [2]. For this reason, we concentrate on LQG here.

Quantum states in LQG are described by spin-network [3], and basic ingredients of the spin-network are edges, which are lines labeled by spin $j (j = 0, 1/2, 1, 3/2, \cdots)$ reflecting the SU(2) nature of the gauge group, and vertices which are intersections between edges. For three edges having spin $j_1, j_2,$ and j_3 that merge at an arbitrary vertex, we have following conditions.

$$j_1 + j_2 + j_3 \in \mathbb{N}, \tag{1}$$

$$j_i \leqq j_j + j_k, \ (i, j, k \text{ different from each other.}). \tag{2}$$

These conditions guarantee the gauge invariance of the spin-network.

Using this formalism, general expressions for the spectrum of the area and the volume operators can be derived [4, 5]. For example, the area spectrum A_j is

$$A_j = 4\pi\gamma \sum_i \sqrt{2j_i^u(j_i^u + 1) + 2j_i^d(j_i^d + 1) - j_i^t(j_i^t + 1)} \ , \tag{3}$$

where γ is the Barbero-Immirzi parameter related to an ambiguity in the choice of canonically conjugate variables. The sum is added up all intersections between a surface and edges. Here, the indices u, d, and t mean edges upper side, down side, and tangential to the surface, respectively (We can determine which side is upper or down side arbitrarily).

[1] E-mail:tomo@gravity.phys.waseda.ac.jp
[2] E-mail:tamaki@gravity.phys.waseda.ac.jp

In [1], it was proposed that black hole entropy is obtained by counting the number of degrees of freedom about j when we fix the horizon area where a simplified area formula is used. This simplified area formula is obtained by assuming that there are no tangential edges on black hole horizon, that is $j_i^t = 0$. We obtain $j_i^u = j_i^d := j_i$ by using the condition (2). Then, we consider the degrees of freedom about j satisfying

$$A_j = 8\pi\gamma \sum_i \sqrt{j_i(j_i+1)} = A. \tag{4}$$

The standard procedure is to impose the Bekenstein-Hawking entropy-area law $S = A/4$ for large black holes in order to fix the value of γ. Ashtekar et al. in [2] extended this idea using the isolated horizon framework (ABCK framework) [6]. Error in counting in this original work has been corrected in [7, 8]. Similar works appear related to how to count the number of freedom in [9, 10].

However, should we restrict to the simplified area spectrum (4) ? Thiemann in [11] used the boundary condition that there is no other side of the horizon, i.e., $j_i^d = 0$. Then, by using (2), we obtain $j_i^u = j_i^t := j_i$ which gives $A_j = 4\pi\gamma \sum_i \sqrt{j_i(j_i+1)}$. Based on this proposal, the number counting has been performed in [12] which gives $\gamma = 0.323\cdots$.

Another interesting possibility is to use (3) motivated by the hypothesis that a black hole is a maximal entropy state in a self-gravitating system. If we agree that the origin of the black hole entropy is related to degrees of freedom in j (or $m = -j, -j+1, \cdots, j$ considered in [2]), it is evident that (3) can gain larger number of states than (4) for the fixed area. See, also [13] which also discuss using (3) as expressing the horizon area. Of course, it is speculative and the typical objection to the idea is that since the black hole evaporates, it is not the maximal entropy state. However, the black hole we consider is the limit $A \to \infty$ where the evaporation process can be negligible. The second objection is that if we require the entropy-area law $S = A/4$, the black hole entropy does not depend on what types of area formula we use, so it is not relevant to the above hypothesis. This is a delicate question to be answered carefully. From the view point that the Barbero-Immirzi parameter is determined *a priori*, the formula $S = A/4$ only provides us the method to *know* the value of γ. If this is the case, using (3) would enhance the entropy. Therefore, we concentrate on evaluating the number of states using (3) by adopting this view point. To answer whether this view point is true or not, we need independent discussion to *know* the value of γ through, e.g., cosmology [14] or quasinormal modes of black holes [15, 16, 17].

Our strategy is as follows [18]. Based on the observation that the value of γ in [2] is qualitatively same as that inferred in [1] which counts the degrees of freedom of j without imposing the horizon conditions for the case (4), we restrict counting the corresponding j freedom for (3) as a first step. We can perform it by carefully reanalyzing the case (4). This paper is organized as follows. In section 2, we count the degrees of freedom for (3). In section 3, we mention concluding remarks.

2 Consideration of the general area spectrum

In the case for (4), horizon conditions does not affect entropy formula. Therefore in the case for (3) we consider only degrees of freedom about area. In this case, we also denote number of states as $N(A)$ which is defined as

$$N(A) := \left\{ (j_1^u, j_1^d, j_1^t, \cdots, j_n^u, j_n^d, j_n^t) | 0 \neq j_i^u, j_i^d \in \frac{\mathbb{N}}{2}, \quad 0 \neq j_i^t \in \mathbb{N}, \quad j_i^u, j_i^d, j_i^t \text{ should satisfy (1) and (2).} \right.$$
$$\left. \sum_i \sqrt{2j_i^u(j_i^u+1) + 2j_i^d(j_i^d+1) - j_i^t(j_i^t+1)} = \frac{A}{4\pi\gamma} \right\} . \tag{5}$$

We adopt the condition $j^t \in \mathbb{N}$ motivated by the ABCK framework where the "classical horizon" is described by $U(1)$ connection. This is, of course, not verified in the present situation and should be reconsidered in future.

Then, we perform counting as follows. If we use the condition $j^t \in \mathbb{N}$, we have $j^u + j^d := n \in \mathbb{N}$ by (1). If we fix n, we can classify the possible j^u, j^d, j^t as follows, which is one of the most important parts in this paper. First, we have $(j^u, j^d) = (\frac{n}{2} \pm \frac{s}{2}, \frac{n}{2} \mp \frac{s}{2})$ (double-sign corresponds) for $0 \leqq s \leqq n$, $s \in \mathbb{N}$ to

satisfy (2). Then, for each s, possible value of j^t is $j^t = s, s+1, \cdots, n$ to satisfy (2). For any eigenvalue $x := 4\pi\gamma\sqrt{2j^u_x(j^u_x+1)+2j^d_x(j^d_x+1)-j^t_x(j^t_x+1)}$ $(0 < x \leqq A)$ of the area operator, we have

$$(\mathbf{j}_1, \cdots, \mathbf{j}_n) \in N(A-x) \Rightarrow (\mathbf{j}_1, \cdots, \mathbf{j}_n, \mathbf{j}_x) \in N(A), \tag{6}$$

where we used the abbreviation as $\mathbf{j}_i = (j^u_i, j^d_i, j^t_i)$. We have $(\mathbf{j}_1, \cdots, \mathbf{j}_n, \mathbf{j}_x) \neq (\mathbf{j}_1, \cdots, \mathbf{j}_n, \mathbf{j}_{x'})$, if $\mathbf{j}_x \neq \mathbf{j}_{x'}$. Therefore, as for the case in (4), if we consider all $0 < x \leqq A$ and $(\mathbf{j}_1, \cdots, \mathbf{j}_n) \in N(A-x)$, $(\mathbf{j}_1, \cdots, \mathbf{j}_n, \mathbf{j}_x)$ form the entire set $N(A)$.

Then, if we use the notation $j^u = \frac{n}{2}+\frac{s}{2}, j^d = \frac{n}{2}-\frac{s}{2}, j^t = t$, we have $x(n,s,t) = 4\pi\gamma\sqrt{n^2+2n+s^2-t(t+1)}$ and

$$N(A) = \sum_{n=1}^{\infty}\left[\sum_{s=1}^{n}\sum_{t=s}^{n} 2N(A-x(n,s,t)) + \sum_{t=0}^{n} N(A-x(n,s=0,t))\right], \tag{7}$$

where the factor 2 in front of $N(A-x(n,s,t))$ for $s \neq 0$ corresponds to the fact that same $x(n,s,t)$ appears twice for the exchange of j^u and j^d. For $A \to \infty$, by assuming $N(A) = Ce^{\frac{A\gamma_M}{4\gamma}}$, where C is a constant and substituting to the recursion relation (7), we obtain the beautiful formula as a generalization of the case (4) as,

$$1 = \sum_{n=1}^{\infty}\left[\sum_{s=1}^{n}\sum_{t=s}^{n} 2\exp(-\gamma_M x(n,s,t)/4\gamma) + \sum_{t=0}^{n}\exp(-\gamma_M x(n,s=0,t)/4\gamma)\right]. \tag{8}$$

If we require $S = A/4$, we have $\gamma = \gamma_M = 0.5802\cdots$. This means that even if we use (3) as the horizon spectrum, we can reproduce the entropy formula $S = A/4$ by adjusting the Barbero-Immirzi parameter. This is nontrivial and is our main result in this paper.

Let us turn back to our assumptions. Although we obtained γ satisfying $S = A/4$ for the case (3), there may be a criticism that the result is underestimated by only counting j freedom. To answer it, we consider the following counting. When the simplified area formula was used, there is an proposal that we should count not only j but also $m = -j, -j+1, \cdots, j$ freedom based on the ABCK framework [9]. Although it is nontrivial whether this framework can be extended to the general area formula, let us count also the m freedom for each j^u to maximize the estimate. Counting only m related to j^u is reasonable from the point of view of the entanglement entropy or the holography principle.

If we notice that there are $(n+s+1)$ and $(n-s+1)$ freedoms for m (total $2(n+1)$) corresponding to $(j^u, j^d) = (\frac{n}{2}+\frac{s}{2}, \frac{n}{2}-\frac{s}{2})$ and $(\frac{n}{2}-\frac{s}{2}, \frac{n}{2}+\frac{s}{2})$, respectively, the factor 2 in the first term of the right-hand side of (8) is replaced by $2(n+1)$ in this case. For $s = 0$, the factor 1 in the second term is replaced by $(n+1)$. Then, we obtain

$$1 = \sum_{n=1}^{\infty}\left[\sum_{s=1}^{n}\sum_{t=s}^{n} 2(n+1)\exp(-\gamma_M x(n,s,t)/4\gamma) + \sum_{t=0}^{n}(n+1)\exp(-\gamma_M x(n,s=0,t)/4\gamma)\right], \tag{9}$$

which gives $\gamma = \gamma_M = 0.7847\cdots$. Thus, we confirm that the black hole entropy is proportional to the area again. Naively speaking, we expect that there is no qualitative deviation from these two values of γ even if we take into account the ABCK framework for (3) appropriately.

3 Conclusion and Discussion

In this paper, we obtained the black hole entropy by considering the general area formula. It is surprising that we succeeded in obtaining the black hole entropy proportional to the horizon area even in this case. Then, it is natural to ask what the area formula should be in describing the horizon area. There are many possibilities examining the area spectrum. For example, we have not yet established the black hole thermodynamics in LQG which is one of the most important topics to be investigated. There is an idea that black hole evaporation process should also be described by using the general area formula [13]. Therefore, whether we can establish the generalized second law of black hole thermodynamics might be one of the criteria in judging which area formula is appropriate. For this purpose, it is desirable to extend

the ABCK framework for the general area formula since the exact counting is required. Though we do not take care of the topology of the horizon, discussing the difference caused by the topology is important as considered for the simplified area formula [19].

Of course, as we mentioned in the introduction, we should check the value of the Barbero-Immirzi parameter in several independent discussions. Therefore, we should also take care of cosmology [14] and quasinormal modes of black holes [15, 16, 17] in determining the Barbero-Immirzi parameter. Confirming LQG in many independent methods would be the holy grail of the theory.

Acknowledgements

We would like to thank Tomohiro Harada and Kei-ichi Maeda for useful comments and continuous encouragement.

References

[1] C. Rovelli, Phys. Rev. Lett. **77**, 3288 (1996).

[2] A. Ashtekar, J. Baez, A. Corichi, and K. Krasnov, Phys. Rev. Lett. **80**, 904 (1998); A. Ashtekar, J. Baez, and K. Krasnov, Adv. Theor. Math. Phys. **4**, 1 (2000).

[3] C. Rovelli and L. Smolin, Phys. Rev. D **52**, 5743 (1995).

[4] C. Rovelli and L. Smolin, Nucl. Phys. B **442**, 593 (1995); Erratum, *ibid.*, **456**, 753 (1995).

[5] A. Ashtekar and J. Lewandowski, Class. Quantum Grav. **14**, A55 (1997).

[6] A. Ashtekar, A. Corichi, and K. Krasnov, Adv. Theor. Math. Phys. **3**, 419 (1999).

[7] M. Domagala and J. Lewandowski, Class. Quant. Grav. **21**, 5233 (2004).

[8] K. A. Meissner, Class. Quant. Grav. **21**, 5245 (2004).

[9] A. Ghosh and P. Mitra, Phys. Lett. B **616**, 114 (2005); Int. J. Mod. Phys. **80**, 867 (2006); Phys. Rev. D **74**, 064026 (2006).

[10] T. Tamaki and H. Nomura, Phys. Rev. D **72**, 107501 (2005).

[11] T.Thiemann, gr-qc/0110034, Modern Canonical Quantum General Relativity (Cambridge University Press, Cambridge, 2007).

[12] T. Tamaki, Class. Quant. Grav. **24**, 3837 (2007).

[13] M. H. Ansari, Nucl. Phys. B **783**, 179 (2007); *ibid.*, **795**, 635 (2008).

[14] M. Bojowald, Living. Rev. Rel. **8**, 11 (2005); A. Ashtekar, T. Pawlowski, P. Singh, Phys. Rev. D **74**, 084003, (2006).

[15] For review, see, e.g., J. Natario and R. Schiappa, hep-th/0411267.

[16] O. Dreyer, Phys. Rev. Lett. **90**, 081301 (2003).

[17] S. Hod, Phys. Rev. Lett. **81**, 4293 (1998).

[18] T. Tanaka and T. Tamaki, arXiv:0808.4056.

[19] S. Kloster, J. Brannlund, and A. DeBenedictis, Class. Quant. Grav. **25**, 065008 (2008).

Nonlinear supersymmetric general relativity and origin of mass

Kazunari Shima[1] and Motomu Tsuda[2]

Laboratory of Physics, Saitama Institute of Technology
Fukaya, Saitama 369-0293, Japan

Abstract

We explain the relation between the large scale structure (the cosmology) and the low energy particle physics, e.g. the observed mysterious relation between the (dark) energy density of the universe and the neutrino mass, which gives a new insight into the origin of mass, based upon nonlinear supersymmetric general relativity towards the unity of nature beyond (behind) the standard model.

Nonlinear supersymmetric general relativity (NLSUSY GR) [1], which is based upon the general relativity (GR) principle and the nonlinear (NL) representation [2] of supersymmetry (SUSY) [3, 4], proposes a new paradigm called the SGM (*superon-graviton model*) scenario [1, 5, 6] for the unified description of space-time and matter beyond (behind) the standard model.

The NLSUSY [2] is known as a symmetry which represents a priori *spontaneous SUSY breaking (SSB)* and the basic NLSUSY action [2] is described in terms of only spin-1/2 Nambu-Goldstone (NG) massless fermions. Also, the NLSUSY model is recasted (related) rigorously to various linear (L) SUSY theories with the SSB (*NL/L SUSY relation*), which has been shown by many authors in the various cases [7]-[12].

In NLSUSY GR, a new (generalized) space-time, *SGM space-time* [1], is introduced, where the tangent space-time has the NLSUSY structure, i.e. it is specified not only by the $SO(3,1)$ Minkowski coodinates x_a but also by $SL(2,C)$ Grassmann coordinates ψ^i_α $(i = 1, 2, \cdots, N)$ for NLSUSY. The new Grassmann coordinates in the new (SGM) space-time means the coset parameters of $\frac{superGL(4R)}{GL(4R)}$ which can be interpreted as the NG fermions (*superons*) associated with the spontaneous breaking of super-$GL(4R)$ down to $GL(4R)$. The fundamental action in NLSUSY GR is given in the Einstein-Hilbert (EH) form in SGM space-time by extending the geometrical arguments of GR in Riemann space-time, which has a priori promising large symmetries isomorphic to $SO(10)$ ($SO(N)$) super-Poincaré (SP) group [5].

The SSB in NLSUSY GR due to the NLSUSY structure is interpreted as the phase transition of SGM space-time to Riemann space-time with massless superon (fermionic matter), i.e. *Big Decay* [6, 11] which subsequently ignites the Big Bang and the inflation of the present universe. In the SGM scenario all (observed) particles are assigned uniquely into a single irreducible representation of $SO(N)$ ($SO(10)$) SP group as an on-shell supermultiplet of N LSUSY. And they are considered to be realized as (massless) eigenstates of $SO(N)$ SP composed of N NG fermion-superons through the NL/L SUSY relation after Big Decay.

Since the cosmological term in NLSUSY GR gives the NLSUSY model [2] in *asymptotic* Riemann-flat (an ordinary vierbein $e^a{}_\mu \to \delta^a{}_\mu$) space-time, the scale of the SSB in NLSUSY GR induces (naturally) a fundamental mass scale depending on the cosmological constant and through the NL/L SUSY relation it gives a simple explanation of the mysterious (observed) numerical relation between the (four dimensional) dark energy density of the universe and the neutrino mass [6] in the vacuum of the $N = 2$ SUSY QED theory (in two-dimensional space-time ($d = 2$) for simplicity) [13].

In order to explain the above low energy physics in NLSUSY GR, i.e. *the relation between the large scale structure and the low energy particle physics*, let us begin with the fundamental EH-type action of NLSUSY GR in SGM space-time given by [1]

$$L_{\rm NLSUSYGR}(w) = \frac{c^4}{16\pi G}|w|\{\Omega(w) - \Lambda\}, \tag{1}$$

[1]E-mail:shima@sit.ac.jp
[2]E-mail:tsuda@sit.ac.jp

where G is the Newton gravitational constant, Λ is a (*small*) cosmological constant, $\Omega(w)$ is the the unified scalar curvature in terms of the unified vierbein $w^a{}_\mu(x)$ (and the inverse $w_a{}^\mu$) defined by

$$w^a{}_\mu = e^a{}_\mu + t^a{}_\mu(\psi), \quad t^a{}_\mu(\psi) = \frac{\kappa^2}{2i}(\bar{\psi}^i\gamma^a\partial_\mu\psi^i - \partial_\mu\bar{\psi}^i\gamma^a\psi^i), \tag{2}$$

and $|w| = \det w^a{}_\mu$. In Eq.(2), $e^a{}_\mu$ is the ordinary vierbein of GR for the local $SO(3,1)$, $t^a{}_\mu(\psi)$ is the stress-energy-momentum tensor (i.e. the mimic vierbein) of the NG fermion $\psi^i(x)$ for the local $SL(2,C)$ and κ is an arbitrary constant of NLSUSY with the dimemsion $(\text{mass})^{-2}$. Note that $e^a{}_\mu$ and $t^a{}_\mu(\psi)$ contribute equally to the curvature of space-time, which may be regarded as the Mach's principle in ultimate space-time.

The NLSUSY GR action (1) possesses promissing large symmetries isomorphic to $SO(N)$ ($SO(10)$) SP group [5]; namely, $L_{\text{NLSUSYGR}}(w)$ is invariant under

$$\text{[new NLSUSY]} \otimes \text{[local GL(4,R)]} \otimes \text{[local Lorentz]} \otimes \text{[local spinor translation]} \otimes \text{[global SO(N)]} \otimes \text{[local U(1)}^N\text{]}.$$

Note that the no-go theorem is overcome (circumvented) in a sense that the nontivial N-extended SUSY gravity theory with $N > 8$ has been constructed in the NLSUSY invariant way.

The SGM (*empty*) space-time for *everything* described by the (*vacuum*) EH-type NLSUSY GR action (1) is unstable due to NLSUSY structure of tangent space-time and decays spontaneously to Riemann space-time with the NG fermion-superons (matter) described by the ordinary EH action with the cosmological term, the NLSUSY action for the N NG fermions and their gravitational interactions, i.e. by the following SGM action;

$$L_{\text{SGM}}(e,\psi) = \frac{c^4}{16\pi G}e|w_{\text{VA}}|\{R(e) - \Lambda + T(e,\psi)\}, \tag{3}$$

where $R(e)$ is the scalar curvature of ordinary EH action, $T(e,\psi)$ represents highly nonlinear gravitational interaction terms of ψ^i, and $|w_{\text{VA}}| = \det w^a{}_b = \det(\delta^a_b + t^a{}_b)$ is the determinant in the NLSUSY model [2]. The second cosmological term in the action (3) reduces to the NLSUSY action [2], $L_{\text{NLSUSY}}(\psi) = -\frac{1}{2\kappa^2}|w_{\text{VA}}|$, i.e. the arbitrary constant κ of NLSUSY is now fixed to

$$\kappa^{-2} = \frac{c^4\Lambda}{8\pi G} \tag{4}$$

in Riemann-flat $e_a{}^\mu(x) \to \delta^\mu_a$ space-time. Note that the NLSUSY GR action (1) and the SGM one (3) possess different asymptotic flat space-time, i.e. SGM-flat $w_a{}^\mu \to \delta^\mu_a$ space-time and Riemann-flat $e_a{}^\mu \to \delta_a{}^\mu$ space-time, respectively. The scale of the SSB in NLSUSY GR (Big Decay) induces a fundamental mass scale depending on the Λ through the relation (4).

It is interesting and important to investigate the low energy physics of NLSUSY GR through the NL/L SUSY relation. In asymptotic Riemann-flat space-time, we focus below on the relation between the NLSUSY model and a LSUSY QED theory for the minimal and realistic $N = 2$ [10] SUSY (in the $d = 2$ case for simplicity) [11, 12]; namely,

$$L_{N=2\text{SGM}}(e,\psi) \overset{e^a{}_\mu \to \delta^a_\mu}{\longrightarrow} L_{N=2\text{NLSUSY}}(\psi) = L_{N=2\text{SUSYQED}}(V,\Phi) + \text{[tot. der. terms]}. \tag{5}$$

In the relation (5), the $N = 2$ NLSUSY action $L_{N=2\text{NLSUSY}}(\psi)$ for the two (Majorana) NG-fermion superons ψ^i $(i = 1, 2)$ is written in $d = 2$ as follows;

$$\begin{aligned} L_{N=2\text{NLSUSY}}(\psi) &= -\frac{1}{2\kappa^2}|w_{\text{VA}}| = -\frac{1}{2\kappa^2}\left\{1 + t^a{}_a + \frac{1}{2!}(t^a{}_a t^b{}_b - t^a{}_b t^b{}_a)\right\} \\ &= -\frac{1}{2\kappa^2}\left\{1 - i\kappa^2\bar{\psi}^i\partial\!\!\!/\psi^i - \frac{1}{2}\kappa^4(\bar{\psi}^i\partial\!\!\!/\psi^i\bar{\psi}^j\partial\!\!\!/\psi^j - \bar{\psi}^i\gamma^a\partial_b\psi^i\bar{\psi}^j\gamma^b\partial_a\psi^j)\right\}, \end{aligned} \tag{6}$$

where κ is a constant with the dimension $(\text{mass})^{-1}$, which satisfies the relation (4) in the $d = 4$ case.

On the other hand, in Eq.(5), the $N = 2$ LSUSY QED action $L_{N=2\text{SUSYQED}}(V,\Phi)$ is constructed from a $N = 2$ minimal off-shell vector supermultiplet V and a $N = 2$ off-shell scalar one Φ. Indeed, the

most general $L_{N=2\text{SUSYQED}}(V,\Phi)$ in $d=2$ with a Fayet-Iliopoulos D term and Yukawa interactions, is given in the explicit component form as follows for the massless case;

$$
\begin{aligned}
L_{N=2\text{SUSYQED}}(V,\Phi) \;=\; & -\frac{1}{4}(F_{ab})^2+\frac{i}{2}\bar{\lambda}^i\partial\!\!\!/\lambda^i+\frac{1}{2}(\partial_a A)^2+\frac{1}{2}(\partial_a\phi)^2+\frac{1}{2}D^2-\frac{\xi}{\kappa}D \\
& +\frac{i}{2}\bar{\chi}\partial\!\!\!/\chi+\frac{1}{2}(\partial_a B^i)^2+\frac{i}{2}\bar{\nu}\partial\!\!\!/\nu+\frac{1}{2}(F^i)^2 \\
& +f(A\bar{\lambda}^i\lambda^i+\epsilon^{ij}\phi\bar{\lambda}^i\gamma_5\lambda^j-A^2D+\phi^2D+\epsilon^{ab}A\phi F_{ab}) \\
& +e\Big\{iv_a\bar{\chi}\gamma^a\nu-\epsilon^{ij}v^aB^i\partial_aB^j+\bar{\lambda}^i\chi B^i+\epsilon^{ij}\bar{\lambda}^i\nu B^j \\
& -\frac{1}{2}D(B^i)^2+\frac{1}{2}A(\bar{\chi}\chi+\bar{\nu}\nu)-\phi\bar{\chi}\gamma_5\nu\Big\}+\frac{1}{2}e^2({v_a}^2-A^2-\phi^2)(B^i)^2. \qquad (7)
\end{aligned}
$$

where (v^a,λ^i,A,ϕ,D) ($F_{ab}=\partial_a v_b-\partial_b v_a$) is the V containing v^a for a $U(1)$ vector field, λ^i for doublet (Majorana) fermions and A for a scalar field in addition to ϕ for another scalar field and D for an auxiliary scalar field, while (χ, B^i, ν, F^i) is the Φ containing (χ,ν) for two (Majorana) are fermions, B^i for doublet scalar fields and F^i for auxiliary scalar fields. Also ξ is an arbitrary dimensionless parameter giving a magnitude of SUSY breaking mass, and f and e are Yukawa and gauge coupling constants with the dimension (mass)^1 (in $d=2$), respectively. The $N=2$ LSUSY QED action (7) can be rewritten as the familiar manifestly invariant form under the local ($U(1)$) gauge transformation in the superfield formulation (for further details see Ref.[12]).

In the relation (equivalence) of the two theories (5), the component fields of (V,Φ) in the $N=2$ LSUSY QED action (7) are expanded as composites of the NG fermions ψ^i, i.e. as *SUSY invariant relations*,

$$
(V,\Phi)\sim\xi\kappa^{n-1}(\psi^i)^n|w_{\text{VA}}|+\cdots\ (n=0,1,2), \qquad (8)
$$

where $(\psi^i)^2=\bar{\psi}^i\psi^j,\epsilon^{ij}\bar{\psi}^i\gamma_5\psi^j,\epsilon^{ij}\bar{\psi}^i\gamma^a\psi^j$, which are very promissing features for SGM scenario. The explicit form [11] of the SUSY invariant relations (8) are obtained *systematically* in the superfield formulation (for example, see Refs.[7, 9, 12]) and the familiar LSUSY transformations on the component fields of the supermultiplet are reproduced in terms of the NLSUSY transformations on the ψ^i contained. Note that *a four NG-fermion self-interaction term (i.e. the condensation of ψ^i)* appears only in the auxiliary fields F^i of the scalar supermultiplet Φ as the origin of the familiar local $U(1)$ gauge symmetry of LSUSY theory [11, 12]. Is the condensation of NG-fermion superons the origin of the local $U(1)$ gauge interaction? The relation (5) are shown explicitly (and systematically) by substituting Eq.(8) into the LSUSY QED action (7) [11, 12].

Now we briefly show the (physical) vacuum structure of $N=2$ LSUSY QED action (7) related (equivalent) to the $N=2$ NLSUSY action (6) [13]. The vacuum is determined by the minimum of the potential $V(A,\phi,B^i,D)$ in the action (7), which is given by using the equation of motion for the auxiliary field D as

$$
V(A,\phi,B^i)=\frac{1}{2}f^2\left\{A^2-\phi^2+\frac{e}{2f}(B^i)^2+\frac{\xi}{f\kappa}\right\}^2+\frac{1}{2}e^2(A^2+\phi^2)(B^i)^2\geq 0, \qquad (9)
$$

In the potential (9) the configurations of the fields corresponding to vacua in (A,ϕ,B^i)-space, which are $SO(1,3)$ or $SO(3,1)$ invariant, are classified according to the signatures of the parameters e,f,ξ,κ. The particle (mass) spectra are obtained by expanding the field (A,ϕ,B^i) around the vacua. We have found that two different vacua appear in the $SO(3,1)$ isometry [13], one of which are described by means of the resulting (physical) model with

one charged Dirac fermion ($\psi_D{}^c\sim\chi+i\nu$), one neutral (Dirac) fermion ($\lambda_D{}^0\sim\lambda^1-i\lambda^2$),
one massless vector (a photon) (v_a),
one charged scalar ($\phi^c\sim\theta+i\varphi$), one neutral complex scalar ($\phi^0\sim\rho+i\omega$),

which are the composites of NG-fermion superons and the vacuum breaks SUSY spontaneously (the local $U(1)$ is not broken) (for further detailes, e.g. mass spectra, $\cdots$ etc., see [13]).

As for the cosmological significances of $N=2$ SUSY QED in SGM scenario, the (physical) vacuum for the above model simply explains the observed mysterious (numerical) relation between *the (dark) energy density of the universe* ρ_D ($\sim\frac{c^4\Lambda}{8\pi G}$) and *the neutrino mass* m_ν,

$$\rho_D^{\rm obs} \sim (10^{-12} GeV)^4 \sim (m_\nu)^4 \sim \frac{\Lambda}{G}\ (\sim {g_{\rm sv}}^2),$$

provided $-\xi f \sim O(1)$ and λ^i is identified with neutrino ($m^2_{\lambda^i} = \frac{-4\xi f}{\kappa}$), which gives a new insight into the origin of mass [6, 13]. ($g_{\rm sv}$ is the superon-vacuum coupling constant.) Furthermore, the neutral scalar field ρ ($\sim m_\nu$) of the radial mode in the vacuum may be a candidate of *the dark matter*, provided the $N = 2$ LSUSY QED structure is preserved in the realistic large N SUSY GUT model. (Note that ω in the model is a NG boson and disappears provided the corresponding local gauge symmetry is introduced as in the standard model.)

Recently, we have been shown that *the magnitude of the bare electromagnetic coupling constant e (i.e. the fine structure constant $\alpha = \frac{e^2}{4\pi}$) is determined* in the NL/L SUSY relation (i.e. the over-all compositness condition) between the $N = 2$ NLSUSY model and the $N = 2$ LSUSY QED theory (in $d = 2$) from the *general* auxiliary-field structure in the *general* off-shell vector supermultiplet [14].

The similar investigations in $d = 4$ are urgent, and the extension to $N = 5$ is important in SGM scenario and to $N = 4$ is suggestive for the anomaly free nontrivial $d = 4$ field theory. Also NLSUSY GR with extra space-time dimensions equipped with the Big Decay is an interesting problem, which can give the framework for describing all observed particles as elementary *à la* Kaluza-Klein. Linearizing the SGM action (3), $L_{\rm SGM}(e, \psi)$, on curved space-time, which elucidates the topological structure of space-time, is a challenge. The corresponding NL/L SUSY relation will give the supergravity (SUGRA) [15, 16] analogue with the vacuum breaking SUSY spontaneously. The physical and mathematical meanings of the black hole as a singularity of space-time and the role of the equivalence principle are to be studied in detail in NLSUSY GR and SGM scenario. Finally we just mention that NLSUSY GR and the subsequent SGM scenario for spin-3/2 NG fermions [5, 17] is in the same scope.

References

[1] K. Shima, *European Phys. J.* **C7** (1999) 341; *Phys. Lett.* **B501** (2001) 237.

[2] D.V. Volkov and V.P. Akulov, *JETP Lett.* **16** (1972) 438; *Phys. Lett.* **B46** (1973) 109.

[3] J. Wess and B. Zumino, *Phys. Lett. B* **49** (1974) 52.

[4] Yu. A. Golfand and E.S. Likhtman, *JETP Lett.* **13** (1971) 323.

[5] K. Shima and M. Tsuda, *Phys. Lett.* **B507** (2001) 260; *Class. Quant. Grav.* **19** (2002) 5101.

[6] K. Shima and M. Tsuda, *PoS HEP2005* (2006) 011.

[7] E.A. Ivanov and A.A. Kapustnikov, *J. Phys.* **A11** (1978) 2375; *ibid* **G8** (1982) 167.

[8] M. Roček, *Phys. Rev. Lett.* **41** (1978) 451.

[9] T. Uematsu and C.K. Zachos, *Nucl. Phys.* **B201** (1982) 250.

[10] K. Shima, Y. Tanii and M. Tsuda, *Phys. Lett.* **B525** (2002) 183; *ibid* **B546** (2002) 162.

[11] K. Shima and M. Tsuda, *Mod. Phys. Lett.* **A22** (2007) 1085; *ibid* **A22** (2007) 3027.

[12] K. Shima and M. Tsuda, *Phys. Lett.* **B666** (2008) 410; $N = 2$ SUSY QED in nonlinear/linear SUSY relation, *Mod. Phys. Lett.* **A**, at press, arXiv:0810.2015 [hep-th].

[13] K. Shima and M. Tsuda, *Phys. Lett.* **B645** (2007) 455; K. Shima, M. Tsuda and W. Lang, *ibid* **B659** (2008) 741, Erratum *ibid* **B660** (2008) 612, *ibid*, at press, arXiv:0710.1680 [hep-th].

[14] K. Shima and M. Tsuda, Gauge coupling constant, compositeness and supersymmetry, arXiv:0810.5006 [hep-th].

[15] D. Z. Freedman, P. van Nieuwenhuisen and S. Ferrara, *Phys. Rev. D* **13**, 3214 (1976).

[16] S. Deser and B. Zumino, *Phys. Lett. B* **62**, 335 (1976).

[17] N. S. Baaklini, *Phys. Lett. B* **67**, 335 (1977).

Solution to IR divergence problem of interacting inflaton field

Yuko Urakawa[1] and Takahiro Tanaka[2]

[1] *Department of Physics, Waseda University, Okubo 3-4-1, Shinjuku, Tokyo 169-8555, Japan*
[2] *Yukawa Institute for Theoretical Physics, Kyoto University, Kyoto 606–8502, Japan*

Abstract

In the direct computation of the fluctuations generated during inflation, we will easily find the logarithmic divergence in the infrared(IR) limit. We focus on the fact that the usual gauge invariant perturbation theory cannot describe the fluctuations that we actually observe. This is because we can observe the fluctuations only within the causally connected region to us. In this paper, we show that, taking an appropriate gauge, we can compute the evolution of fluctuations which better correspond to what we actually observe. In this gauge we no longer encounter the IR divergence.

1 Introduction

Inflation has become the leading paradigm to explain the initial condition of the universe as seen in the Cosmic Microwave Background (CMB) anisotropies. Despite its attractive aspects, there are still many unknowns about the inflation theory When we discuss the primordial fluctuations within linear analysis, many inflation models predict almost the same results, which are compatible with the observational data, although the underlying models are quiet different. To discriminate between different inflationary models, it is important to take into account nonlinear effects However, it is widely known that we encounter the divergence coming from the infrared (IR) corrections in computing the non-linear perturbations generated during inflation This divergence is due to the massless (or quasi massless) fields including the inflaton which gives the almost scale invariant power spectrum, i.e., $\mathcal{P}(k) \propto k^{-3}$. In the gauge-invariant treatment, the curvature perturbation in the comoving gauge, ζ, is often used to describe fluctuations of the inflaton field. Fluctuations in ζ are directly related to the observed CMB anisotropies, and ζ is not free from the IR divergence problem, either.

We can easily observe the appearance of the logarithmic divergence in the IR limit from the direct computation of the loop corrections under the assumption of scale invariant power spectrum. As the simplest example, let us consider the one loop diagram containing only one four-point vertex, in which the end points of the loop are connected to the same four-point vertex. Therefore the factor coming from the integral of this loop becomes $\int d^3k\,\mathcal{P}(k)$. Substituting the scale invariant power spectrum into $\mathcal{P}(k) \propto k^{-3}$, we find that the integral is logarithmically divergent in the IR limit like $\int d^3k/k^3$. As is seen also in this simple example, the IR divergence on the primordial perturbation is typically logarithmic To be a little more precise, we also need to care about UV divergence, since the loop integral is also UV divergent in general. However, since the fluctuation modes whose wavelength is well below the horizon scale (sub-horizon modes) do not feel the cosmic expansion, they are expected to behave as if in Minkowski spacetime. Namely, the quantum state of sub-horizon modes is approximately given by the one in the adiabatic vacuum. Hence, the sub-horizon modes will not give any time-dependent cumulative contribution to the loop integral after appropriate renormalization. They are therefore irrelevant for the discussions in this paper.

As a practical way to make the loop corrections finite, we often introduce the IR cut-off at the comoving scale corresponding to the Hubble horizon scale at the initial time, $a_i H_i$ This kind of artificial IR cut-off is not fully satisfactory because it leads to the logarithmic amplification of the loop corrections as we push the initial time to the past like $\int_{a_i H}^{aH} d^3k\,k^{-3} \propto \log(a/a_i)$ where a_i is the scale factor at the initial time and we neglected the time dependence of the Hubble parameter. Due to the non-vanishing IR contribution, the choice of the IR cut-off affects the amplitude of loop corrections. Furthermore, the

[1] E-mail:yuko@gravity.phys.waseda.ac.jp
[2] E-mail:tanaka@yukawa.kyoto-u.ac.jp

reason why we select a specific IR cut-off is not clear. This means that, in order to obtain a reliable estimate for the IR corrections, we need to derive a scheme to make the corrections finite from physically reasonable requirements. This is what we wish to discuss in this paper.

To begin with, we point out that the usual gauge invariant perturbation theory cannot describe the fluctuations that we actually observe. This is because we can observe the fluctuations only within the causally connected region to us. [1] To discuss the so-called observable quantities in the framework of the gauge invariant perturbation, in general, it is necessary to fix the gauge in all region of the universe. However, in reality it is impossible for us to make observations imposing the gauge conditions in the region causally disconnected from us. We need to be careful in defining what is the observable fluctuation. We usually define the fluctuation by the deviation from the background value which is the averaged value over the whole universe. However, since we can observe only a finite volume of the universe, the fluctuations evaluated in such a way are inevitably influenced by the information contained in the unobservable region. In general, the deviation from the global average is much larger than the deviation from the local average, which leads to the over-estimation of the fluctuations due to the contribution from long wavelength fluctuations. In this paper, we show that, taking an appropriate gauge, we can compute the evolution of fluctuations which better correspond to what we actually observe. It is often the case to adapt the flat gauge or the comoving gauge in computing non-linear quantum effects.

2 A Solution to IR problem

2.1 Setup of the problem

We first define the setup that we study in this paper. We consider the single field inflation model with the conventional kinetic term. The total action is given by $S = \frac{1}{2}\int\sqrt{-g}\ [R - (\nabla\phi)^2 - V(\phi)]$. where $m_{\rm pl}^{-2} \equiv 8\pi G = 1$. In order to discuss the non-linearity, it is convenient to use the ADM formalism, where the line element is expressed in terms of the lapse function N, the shift vector N^i, and the purely spatial metric h_{ij}: $ds^2 = -N^2dt^2 + h_{ij}(dx^i + N^i dt)(dx^j + N^j dt)$. Using this metric ansatz, we can denote the action as

$$S = \frac{1}{2}\int\sqrt{h}\Big[N\ {}^{(3)}R - 2NV(\phi) + \frac{1}{N}(E_{ij}E^{ij} - E^2) + \ \frac{1}{N}(\dot\phi - N^i\partial_i\phi)^2 - Nh^{ij}\partial_i\phi\partial_j\phi\Big] \tag{1}$$

where $E_{ij} = N\kappa_{ij} = \frac{1}{2}\{\dot h_{ij} - D_iN_j - D_jN_i\}$ and $E = h^{ij}E_{ij}$. In the ADM formalism, we can obtain the constraint equations easily by varying the action with respect to N and N^i, which can be though of as Lagrange multipliers. Hereafter, neglecting the vector perturbation, we denote the shift vector as $N_i = \partial_i\chi$. In this paper, we work in the flat gauge, defined by $h_{ij} = e^{2\rho}\delta_{ij}$ where $a = e^\rho$ is the background scale factor, and we focused on the scalar perturbation, in which the IR divergence of our interest arises . In this gauge, we find two constraint equations as

$$2N^2\sum_{n=0}\frac{1}{n!}(\partial_\phi^n V(\phi))\varphi^n - 6\dot\rho^2 + 4\dot\rho e^{-2\rho}\partial^2\chi + e^{-4\rho}\{\partial^i\partial^j\chi\partial_i\partial_j\chi - (\partial\chi)^2\}$$
$$+(\dot\phi + \dot\varphi - e^{-2\rho}\partial^i\chi\partial_i\varphi)^2 + N^2e^{-2\rho}(\partial\varphi)^2 = 0 \tag{2}$$
$$(\partial_iN)\{2\dot\rho\delta^i{}_j + e^{-2\rho}(\partial^i\partial_j\chi - \delta^i{}_j\partial^2\chi)\} - (\partial_j\varphi)N\ (\dot\phi + \dot\varphi - e^{-2\rho}\partial^i\chi\partial_i\varphi) = 0\ . \tag{3}$$

Expanding N and χ as $N = 1 + \delta N_1 + \frac{1}{2}\delta N_2 + \cdots$ and $\chi = \chi_1 + \frac{1}{2}\chi_2 + \cdots$, for instance, we find that the first order constraint equations are written as

$$V_\phi\varphi + 2V\delta N_1 + 2\dot\rho e^{-2\rho}\partial^2\chi_1 + \dot\phi\ \dot\varphi = 0\ , \qquad \partial_i(2\dot\rho\ \delta N_1 - \dot\phi\ \varphi) = 0\ . \tag{4}$$

Taking the variation of the action with respect to φ, we can derive the equation of motion for φ, which includes the Lagrange multipliers δN and χ. Solving the constraint equations for the lapse function and shift vector at each order, we can express N and χ as functions of φ.

To compute n-point functions of $\varphi(x)$, we expand the Heisenberg field $\varphi(x)$ in terms of the interaction picture field $\varphi_I(x)$. Here we shall adopt the expansion in which we take the full advantage of using

the retarded Green function $G_R(x,x')$. It is because the retarded Green function has a finite non-vanishing support for fixed t and t', its three dimensional Fourier transform becomes regular in the IR limit, while the other Green functions behave like k^{-3}. Let us denote the equation of motion for φ schematically as $(\ \nabla^2 - m_{\rm eff}^2\ )\varphi = \Gamma_{\rm int}[\varphi]$. The left hand side is identical to the linear equation for φ. $\Gamma[\varphi]$ represents the non-linear interaction terms. Using the retarded Green function $G_R(x,x')$ that satisfies $(\ \nabla^2 - m_{\rm eff}^2\ )G_R(x,x') = e^{-3\rho}\delta(x-x')$, we can solve the equation of motion for φ as

$$\varphi(x) = \varphi_I(x) + \int d^4x'\, G_R(x,x')e^{3\rho}\Gamma_{\rm int}[\varphi](x'). \tag{5}$$

Substituting this expression for $\varphi(x)$ iteratively into $\varphi(x)$ on the R.H.S., we obtain the Heisenberg field $\varphi(x)$ expanded in terms of $\varphi_I(x)$ to any order using the retarded Green function $G_R(x,x')$.

When we compute the expectation value for n-point functions of the Heisenberg field, the interaction picture fields φ_I are contracted to make pairs. Then, when we evaluate the expectation value, the pairs of φ_I are replaced with Wightman functions, $G^+(x,x')$ or $G^-(x,x')$. As these propagators are IR singular in contrast to $G_R(x,x')$, they are the possible origin of IR divergence in momentum integrations.

2.2 Gauge degree of freedom in flat gauge

On the most computation of non-linear quantum effects, either the flat gauge or the comoving gauge (in which $\varphi = 0$ and $h_{ij} = e^{2(\rho+\zeta)}\delta_{ij}$) has been adapted. It is partly because these gauges do not have any residual gauge degrees of freedom. However, we claim that this statement is not strictly correct. For instance, in the flat gauge we have to solve the constraint equations to determine the lapse function and the shift vector. As is shown in Eqs. (4), these equations are differential equations which are not hyperbolic. The solutions of these equations depend on the boundary conditions when they are solved within a finite volume. At the linear order, these extra degrees of freedom appears as arbitrary time-dependent integration constants. Indeed, we can solve the first order momentum constraint equation as $\delta N_1(x) = f_1(t) + \frac{\dot\phi}{2\dot\rho}\varphi_1(x)$ where an arbitrary function $f_1(t)$ was introduced. Substituting this into the Hamiltonian constraint, we can solve it to obtain $\chi_1(x) = -\frac{\dot\phi^2}{2\dot\rho^2}e^{2\rho}\partial^{-2}\partial_t\left(\frac{\dot\rho}{\dot\phi}\varphi_1\right) - \frac{V}{6\dot\rho}f_1(t)e^{2\rho}x_ix^i$. The last term proportional to x^ix_i cannot be expanded in terms of the spatial harmonics ($\approx e^{i\boldsymbol{kx}}$), we do not have this residual gauge degree of freedom in the standard cosmological perturbation scheme.

The degree of freedom $\alpha(t)$ introduced above corresponds to scale transformation: $x^i \longrightarrow \tilde x^i = e^{\dot\rho\alpha(t)}x^i$. Such a scale transformation is compatible with the perturbative expansion only when our interest is concentrated on a finite region of spacetime. Once we consider an infinite volume, this transformation does not remain to be a small change of coordinates irrespective of the amplitude of $\alpha(t)$. Simultaneously, we apply the temporal coordinate transformation $t \to \tilde t$ such that $\tilde t$ satisfies $\rho(\tilde t) = \rho(t) - \dot\rho\alpha(t)$. Under this transformation, (i,j) component of the metric transforms as $\tilde h_{ij}(\tilde x) = e^{-2\dot\rho\alpha(t)}\ h_{ij}(x) = e^{2\rho(\tilde t)}\delta_{ij}$. Thus we find that this scale transformation keeps the flat gauge conditions that we imposed on the spatial metric unchanged, and therefore it is in fact a residual gauge degree of freedom. Under the same coordinate transformation with the identification $f_1 = \dot\alpha - \frac{\dot\phi^2}{2\dot\rho}\alpha$, we can easily confirm that the first order lapse function and the shift vector transform as given above. Here we have explained only for the first order lapse function and the shift vector, the corresponding degree of freedom also exists in the higher order. In this paper we focus on the flat gauge, but a similar discussion applies for the comoving gauge, too.

2.3 Local gauge condition

As is mentioned in Sec. 1, our final goal is to define finite observable quantities in place of the naively divergent quantum correlation functions. Here, we propose a minimum necessary regularization scheme which naturally requires to control the residual gauge degree of freedom discussed in the preceding subsection as is explained immediately below.

We consider the time evolution for $t \in [t_i,\ t_f]$, where t_f represents the observation time. We denote the region which is causally connected to us by $\mathcal{O}$. On a final time slice Σ_{t_f}, where we evaluate the n-point functions, we evaluate the fluctuation at $x \in \mathcal{O} \cap \Sigma_{t_f}$. We require that the fluctuation at $x \in \mathcal{O} \cap \Sigma_{t_f}$

not to be affected by the evolution of the field in $\mathcal{O}^c$. Thus, we fix the residual gauge only using the information within the observable region $\mathcal{O}$. We impose the gauge condition:

$$W_t \cdot \varphi(t) \equiv \frac{1}{L_t^3} \int d^3\boldsymbol{x}\ W_t(\boldsymbol{x})\ \varphi(t,\ \boldsymbol{x}) = 0 \tag{6}$$

where $W_t(\boldsymbol{x})$ is the window function, whose non-vanishing support is limited to the finite region $\mathcal{O}_t \equiv \mathcal{O} \cap \Sigma_t$. We assume that $W_t(\boldsymbol{x})$ is almost a step function except in the region near the boundary of $\mathcal{O}_t$. Near the boundary $W_t(\boldsymbol{x})$ is supposed to smoothly continue to zero so as to avoid artificial UV contribution due to sharp cutoff. L_t, an approximate radius of the region $\mathcal{O}_t$, is defined by the normalization condition $W_t \cdot 1 = 1$. By construction, φ represents the deviation from the local average value in $\mathcal{O}_t$. By choosing the corresponding function $f(t)$ on each time slice, we can adapt this local gauge condition. The detailed explanation will be described in [2]. In addition, to be completely determined by the information in $\mathcal{O}_t$, we define ∂^{-2} by $\partial^{-2}F(x) = -(4\pi)^{-1}\int_{\mathcal{O}_t} d^3\boldsymbol{y}/|\boldsymbol{x}-\boldsymbol{y}|\ F(t,\boldsymbol{y})$ where $F(x)$ is an arbitrary function. As the observable fluctuation, inserting the window function, we compute the Fourier mode of φ : $\varphi^{obs}_{\boldsymbol{k}}(t) = \int d^3\boldsymbol{x}\ W_\tau(\boldsymbol{x})\ e^{i\boldsymbol{k}\cdot\boldsymbol{x}}\varphi(x)$.

2.4 IR regularity

In this subsection, we show that once we impose the local gauge condition, the n-point functions for φ become IR regular for the most of inflation models. Thanks to the gauge condition Eq.(6), $\varphi(x)$ does not include the long wave-length modes such that $k < 1/L_t$. Indeed, $\varphi(x)$ is rewritten as $\varphi(x) = (1-W_t\cdot)\varphi(x)$ The long wave-length modes with $k < 1/L_t$ in φ is also included in $W_{\mathcal{O}_t}\cdot\varphi$ and they are canceled with each other. Here, appealing the intuitive understanding, we briefly describe how the n-point function for $\varphi^{obs}_{\boldsymbol{k}}(t)$ is regularized. The IR divergence can appear both from the temporal and the spatial(or momentum) integrals. To assure their regularity, the preservation of the causal evolution is necessary. All the interaction vertexes, mediated by the retarded Green function, are confined within the causal past $\mathcal{O}$. In addition, thanks to the local gauge condition, the integral region of ∂^{-2} in δN and χ is set to the causal past $\mathcal{O}$. Therefore, all the interaction vertexes which contribute to $\varphi^{obs}_{\boldsymbol{k}}(t_f)$ are limited only within the finite region $\mathcal{O}$. Furthermore, in this gauge the IR modes of φ_I are removed. Therefore, the momentum integrals no longer give IR divergence. Similarly, since the IR modes of $G_R\cdot\Gamma[\varphi]$ are removed, the temporal integrals are also regularized. It is because the logarithmically increasing terms appear from the temporal integrals of these IR corrections. More accurate proof will be given in [2].

3 Conclusion

In this paper, we have showed that adapting the local gauge in which the fluctuation mimics to what we actually observe, we can regularize the IR corrections. Nevertheless, since we have only one residual gauge degree of freedom, our argument is not enough to regularize more than one IR divergent fields.

Acknowledgments
YU would like to thank Kei-ichi Maeda for his continuously encouragement. YU is supported by JSPS. TT is supported by Monbukagakusho Grant-in-Aid for Scientific Research Nos. 17340075 and 19540285.

References

[1] D. H. Lyth, JCAP **0712**, 016 (2007) [arXiv:0707.0361 [astro-ph]].

[2] Y. Urakawa and T. Tanaka, in preparation

Classification of dynamical intersecting brane solutions

Kunihito Uzawa*

[1] *Osaka City University Advanced Mathematical Institute Sumiyoshi-ku, Osaka-shi 558-8585, Japan*

Abstract

We present general intersecting dynamical brane solutions in higher-dimensional gravitational theory coupled to dilaton and several forms. The dynamical solutions give rise to a static geometry in a certain spacetime region.

1 Introduction

Recently there have been works on dynamical solutions of supergravity which are of cosmological interest. The dynamical solution of supergravity has a number of important applications. In the original version [1], one considers a time-dependent solution with five-form flux and gravity in the ten-dimensional type IIB supergravity. In the presence of the time dependence in the background metric, one finds, even for the general black p-brane system, that the structure of warp factor which depends on the time is different from the usual "product type" ansatz.

In addition to time-dependent solutions in higher-dimensional supergravity, there are several analysis of lower-dimensional effective theory after compactifying the internal space [2]. Since the four-dimensional cosmology can be understood in terms of the dynamics of the original higher-dimensional theory, the same considerations apply to the string theories which are of much interest as an approach to behavior of the early universe. However, there can be four-dimensional effective theories for warped compactification of ten-dimensional type IIB supergravity that cannot be obtained from solutions in the original higher-dimensional theories [2]. These remarks can be generalized in various p-brane solutions [3]. Another, equally significant fact is that the dynamical solutions arise if the gravity are coupled not only to single gauge field but to several combination of the scalar and gauge fields, as intersecting brane solutions in the supergravity. For instance, in a supergravity theory with several antisymmetric tensor fields, one can obtain the solution to the equations of motion. The intersecting brane solutions were originally found by Güven in eleven-dimensional supergravity. After that, many authors investigated related solutions such as intersecting membranes, and they constructed static new solutions of intersecting branes. At the same time, the concepts in string theory such as dualities and discovery of D-branes led to the relation between several types of superstring theory. Among others, dynamical solutions which depend both on time and space coordinates have been found in [4], and special intersecting dynamical solutions of D4-D8 are given in [3].

In the proceeding, we give general dynamical solutions for intersecting brane systems in D-dimensional theory, which may have more general applications to cosmology.

2 Dynamical intersecting p-branes solutions

In this section, we consider dynamical intersecting p-brane systems in D dimensions. We write down the Einstein equations under a certain ansatz on the metric, which is a generalization of that of known static intersecting p-brane solutions. We then solve the Einstein equations and present the solutions explicitly.

Let us consider a gravitational theory with the metric g_{MN}, dilaton ϕ, and an anti-symmetric tensor field of rank $(p_I + 2)$, $I = 1, \cdots m$. The most general action for the p_I-brane system is written as

$$S = \frac{1}{2\kappa^2} \int \left[R * \mathbf{1}_D - \frac{1}{2} d\phi \wedge *d\phi - \sum_I \frac{1}{2(p_I+2)!} e^{c_I \phi} F_{(p_I+2)} \wedge *F_{(p_I+2)} \right], \tag{2.1}$$

*E-mail:uzawa@sci.osaka-cu.ac.jp

where κ^2 is the D-dimensional gravitational constant, $*$ is the Hodge dual operator in the D-dimensional spacetime, c_I is a constant given by $c_I^2 = 4 - 2(p_I+1)(D-p_I-3)(D-2)^{-1}$. The expectation values of fermionic fields are assumed to be zero.

The field equations are given by

$$R_{MN} = \frac{1}{2}\partial_M\phi\partial_N\phi + \frac{1}{2}\sum_I \frac{1}{(p_I+2)!}e^{\epsilon_I c_I \phi}\left[(p_I+2)F_{MA_2\cdots A_{p_I+2}}F_N{}^{A_2\cdots A_{p_I+2}} - \frac{p_I+1}{D-2}g_{MN}F^2_{(p_I+2)}\right],$$
$$\triangle\phi = \frac{1}{2}\sum_I \frac{\epsilon_I c_I}{(p_I+2)!}e^{c_I\phi}F^2_{(p_I+2)}, \qquad d\left(e^{c_I\phi} * F_{(p_I+2)}\right) = 0, \tag{2.2}$$

where $\triangle$ is the D-dimensional D'Alambertian.

To solve the field equations, we assume the D-dimensional metric of the form

$$\begin{aligned} ds^2 &= -B(t,y)dt^2 + \sum_{\mu=1}^{p} C^\mu(t,y)(dx^\mu)^2(\mathrm{X}) + A(t,y)u_{ij}(\mathrm{Y})dy^i dy^j \\ &= -\prod_I h_I^a(t,y)dt^2 + \sum_{\mu=1}^{p}\prod_I h_I^{\frac{\delta_I^\mu}{D-2}}(t,y)(dx^\mu)^2(\mathrm{X}) + \prod_I h_I^b(t,y)u_{ij}(\mathrm{Y})dy^i dy^j, \end{aligned} \tag{2.3}$$

where u_{ij} is the $(D-p-1)$-dimensional metric which depends only on the $(D-p-1)$-dimensional coordinates y^i, which are also written as a vector $\boldsymbol{y}$. The parameters a, δ_I^μ and b are given by

$$a = -\frac{D-p_I-3}{D-2}, \qquad b = \frac{p_I+1}{D-2}, \qquad \delta_I^\mu = \begin{cases} -(D-p_I-3) & \text{for } \mu \parallel I \\ p_I+1 & \text{for } \mu \perp I \end{cases} \tag{2.4}$$

The metric (2.3) is a straightforward generalization of a static p-brane system with a dilaton coupling. We also assume that the scalar field ϕ and the gauge field strength $F_{(p+2)}$ are given by

$$e^\phi = \prod_I h_I^{\epsilon_I c_I/2}, \qquad F_{(p_I+2)} = d(h_I^{-1}) \wedge \Omega(\mathrm{X}_I), \tag{2.5}$$

where ϵ_I is defined by

$$\epsilon_I = \begin{cases} + & \text{if } p_I\text{−brane is electric} \\ - & \text{if } p_I\text{−brane is magnetic} \end{cases} \tag{2.6}$$

and $\Omega(\mathrm{X}_I)$ denotes the volume (p_I+1)-form $\Omega(\mathrm{X}_I) = dt \wedge dx^{p_1} \wedge \cdots \wedge dx^{p_I}$. The form (2.5) is written for electric ansatz, but the final results are basically the same for magnetic ansatz. In what follows, we write our formulae mainly for electric case with comments on modifications for magnetic case.

Let us assume $B^{1/2}\left(\sum_\mu C^\mu\right)^{1/2} A^{(D-p-3)/2} = 1$, and define V_I, $V_I^\perp$ as $V_I = B^{1/2}\left(\prod_{\mu||I} C^\mu\right)^{1/2}$, $V_I^\perp = \left(\prod_{\mu\perp I} C^\mu\right)^{1/2}$. We also make the following ansatz $V_I^{-2}e^{\epsilon_I c_I\phi} = h_I^2$, where B, C^μ, A are given by $B = \prod_I h_I^{-\frac{D-p_I-3}{D-2}}$, $C^\mu = \prod_I h_I^{\frac{\delta_I^\mu}{D-2}}$, $A = \prod_I h_I^{\frac{p_I+1}{D-2}}$. The Einstein equations (2.2) then reduce to

$$\begin{aligned} &\frac{1}{2}\sum_{I,I'}\left[M_{II'} - 2\delta_{II'} + \frac{2}{D-2}\left\{(p_I+1) - \delta_{II'}(p_{I'}+1)\right\}\right]\partial_t \ln h_I \partial_t \ln h_{I'} \\ &\quad + \sum_I \frac{(D+p_I-1)}{(D-2)}h_I^{-1}\partial_t^2 h_I + 2\prod_I h_I^{-1}\sum_{I'}\frac{D-p_{I'}-3}{D-2}h_{I'}^{-1}\triangle_{\mathrm{Y}}h_{I'} = 0, \end{aligned} \tag{2.7}$$

$$2\sum_I h_I^{-1}\partial_t\partial_i h_I + \sum_{I,I'}\left(M_{II'} - 2\delta_{II'}\right)\partial_t \ln h_I \partial_i \ln h_{I'} = 0, \tag{2.8}$$

$$\delta_{ab}\prod_{J'}h_{J'}^{\frac{D-p_{J'}-3}{D-2}}\sum_{\mu}\prod_{J}h_J^{\frac{\delta_J^\mu}{D-2}}\sum_{I}\left[\delta_I^\mu h_I^{-1}\partial_t^2 h_I-\left(\delta_I^\mu\partial_t\ln h_I-\sum_{I'}\delta_{I'}^\mu\partial_t\ln h_{I'}\right)\partial_t\ln h_I\right]$$
$$-\delta_{ab}\prod_{J'}h_{J'}^{-\frac{p_{J'}+1}{D-2}}\sum_{\mu}\prod_{J}h_J^{\frac{\delta_J^\mu}{D-2}}\sum_{I}\delta_I^\mu h_I^{-1}\triangle_{\rm Y}h_I=0, \tag{2.9}$$

$$R_{ij}({\rm Y})+\frac{1}{2}u_{ij}\prod_{J}h_J\sum_{I}\left[(p_I+1)h_I^{-1}\partial_t^2 h_I+\left\{(p_I+1)\partial_t\ln h_I-\sum_{I'}(p_{I'}+1)\partial_t\ln h_{I'}\right\}\partial_t\ln h_I\right]$$
$$-\frac{1}{2}u_{ij}\sum_{I}h_I^{-1}\frac{p_I+1}{D-2}\triangle_{\rm Y}h_I-\frac{1}{4}\sum_{I,I'}\left(M_{II'}-2\delta_{II'}\right)\partial_i\ln h_I\partial_j\ln h_{I'}=0, \tag{2.10}$$

and $R_{ij}({\rm Y})$ is the Ricci tensor of the metric u_{ij}, $M_{II'}$ is given by

$$M_{II'}\equiv\frac{1}{(D-2)^2}\left[(D-p_I-3)(D-p_{I'}-3)+\sum_{\mu}\delta_I^\mu\delta_{I'}^\mu+(d-2)(p_I+1)(p_{I'}+1)\right]+\frac{1}{2}\epsilon_I\epsilon_{I'}c_Ic_{I'} \tag{2.11}$$

Let us consider Eq. (2.8). We can rewrite this as

$$\sum_{I,I'}\left[M_{II'}+2\delta_{II'}\frac{\partial_t\partial_i\ln h_I}{\partial_t\ln h_I\partial_i\ln h_I}\right]\partial_t\ln h_I\partial_i\ln h_{I'}=0. \tag{2.12}$$

In order to satisfy this equation for arbitrary coordinate values and independent functions h_I, the second term in the square bracket must be constant

$$\frac{\partial_t\partial_i\ln h_I}{\partial_t\ln h_I\partial_i\ln h_I}=c. \tag{2.13}$$

Then in order for (2.12) to be satisfied identically, we must have $M_{II'}+2c\delta_{II'}=0$. Using the expression c_I, (2.4) and (2.11), we get

$$M_{II}=\frac{1}{(D-2)^2}[(p_I+1)(D-p_I-3)^2+(p-p_I)(p_I+1)^2+(d-2)(p_I+1)^2]+\frac{1}{2}c_I^2=2. \tag{2.14}$$

This means that the constant c in (2.13) is $c=-1$, namely $M_{II'}=2\delta_{II'}$. It then follows from Eq. (2.13) that $\partial_i\partial_t[h_I(t,y)]=0$, and hence the warp factor h_I must be in the form $h_I(t,y)=H_I(t)+K_I(y)$.

For $I\neq I'$, the equation $M_{II'}=2\delta_{II'}$, gives a restriction on the dimension $\bar{p}$ of the intersection for each pair of branes I and I' ($\bar{p}\leq p_I,p_{I'}$) : $2\bar{p}=2(p_I+1)(p_{I'}+1)(D-2)^{-1}-2-\epsilon_Ic_I\epsilon_{I'}c_{I'}$.

Let us next consider the gauge field. Under the ansatz (2.5) for electric background, we find $dF_{(p_I+2)}=0$. Thus, the Bianchi identity is automatically satisfied. Also the equation of motion for the gauge field becomes $d\left[e^{-c_I\phi}*F_{(p_I+2)}\right]=0$. Hence we again find the condition $h_I(t,y)=H_I(t)+K_I(y)$, and $\triangle_{\rm Y}h_I=0$. We note that the roles of the Bianchi identity and field equations are interchanged for magnetic ansatz but the net result is the same.

Let us finally consider the scalar field equation. Substituting the scalar field, the gauge field (2.5), and the warp factor $h_I(t,y)=H_I(t)+K_I(y)$ into the equation of motion for the scalar field (2.2), we obtain

$$-\prod_{J}h_J^{(D-p_J-3)/(D-2)}\sum_{I,I'}\epsilon_Ic_I\left[h_I^{-1}\partial_t^2H_I+\left(-\delta_{II'}\delta_I^\mu+\delta_{I'}^\mu\right)\partial_t\ln h_I\partial_t\ln h_{I'}\right]$$
$$+\prod_{J}h_J^{-(p_J+1)/(D-2)}\sum_{I}h_I^{-1}\epsilon_Ic_I\triangle_{\rm Y}K_I=0. \tag{2.15}$$

This equation is satisfied by

$$\partial_t^2H_I=0,\quad \triangle_{\rm Y}K_I=0,\qquad \sum_{I,I'}\epsilon_Ic_I\left(-\delta_I^\mu+\delta_{II'}\delta_{I'}^\mu\right)\partial_t\ln h_I\partial_t\ln h_{I'}=0. \tag{2.16}$$

Equation (2.16) can be satisfied *only if there is only one function h_I depending on both y^i and t and other functions depend either on y^i or constant.* The Einstein equations (2.7)- (2.10) now reduce to

$$\sum_{I,I'} [(p_I+1) - \delta_{II'}(p_{I'}+1)]\, \partial_t \ln h_I \partial_t \ln h_{I'} = 0, \quad \sum_{I,I'} (-\delta^\mu_I + \delta_{II'}\delta^\mu_{I'})\, \partial_t \ln h_I \partial_t \ln h_{I'} = 0, \tag{2.17}$$

$$R_{ij}(\mathrm{Y}) = 0, \qquad h_I(t,y) = H_I(t) + K_I(y), \tag{2.18}$$

where Eq. (2.18) is valid only for one I, and other h's can depend on either on y or constant only and must satisfy $\triangle_{\mathrm{Y}} h_I = 0$. Obviously the first two sets of equations (2.17) are automatically satisfied for our solutions in which there is only one function h_I depending on both t and y^i. Given the set of solutions to Eq. (2.18), (2.16), and $\triangle_{\mathrm{Y}} h_I = 0$, we have thus derived general intersecting dynamical brane solutions (2.3). For static (time-independent) case, our solutions are consistent with the harmonic function rule, but are more general with time-dependent functions. Note that the internal space is not warped [2] if the function K_I is trivial.

As a special example, we consider the case $u_{ij} = \delta_{ij}$, where δ_{ij} is the $(D-p-1)$-dimensional Euclidean metric. In this case, the solution for h_I can be obtained explicitly as

$$h_I(t,y) = At + B + \sum_\alpha \frac{M_{\alpha,I}}{|\boldsymbol{y} - \boldsymbol{y}_\alpha|^{D-p-3}}, \tag{2.19}$$

where A, B and M_α are constant parameters and $\boldsymbol{y}_\alpha$ represent the positions of the branes in Y. For $A = 0$, the metric describes the known extremal multi-black hole solution with black hole masses $M_{\alpha,I}$.

Here let us point out an important fact on the nature of the dynamical solutions described in the above. In general, we consider the (p_I+1)-dimensional spacetime to contain our four-dimensional universe while the remaining space is assumed to be compact and sufficiently small in size. Then one would expect that an effective (p_I+1)-dimensional description of the theory should be possible at low energies. However, the dynamical solutions of the above type have the warp factor which is a sum of time-dependent and internal space parts. This means that they are genuinely D-dimensional so that one can never neglect the dependence on the internal space Y in h_I.

3 Summary

In this proceeding, we have derived general intersecting dynamical brane solutions and discussed the dynamics of the higher-dimensional model. The solutions we have found are the time-dependent solutions. These solutions were obtained by replacing a constant A in the warp factor $h = A + h_1(y)$ of a supersymmetric solution by a function $h_0(x)$ of the coordinates x^μ [4, 3]. Our solutions can contain only one function depending on both time and transverse space coordinates.

In the viewpoint of higher-dimensional theory, the dynamics of four-dimensional background are given by the solution of higher-dimensional Einstein equations. For instance, in the black p-brane system, the solution tells us that the $(p+1)$-dimensional spacetime X is Ricci flat. The $(p+1)$-dimensional spacetime is then similar to the Kasner solution for the $(p+1)$-dimensional background [3]. Although the examples considered in the present paper do not provide realistic cosmological models, this feature may be utilised to investigate a cosmological analysis in a realistic higher-dimensional cosmological model.

References

[1] G. W. Gibbons, H. Lu and C. N. Pope, Phys. Rev. Lett. **94** (2005) 131602 [arXiv:hep-th/0501117].

[2] H. Kodama and K. Uzawa, JHEP **0603** (2006) 053 [arXiv:hep-th/0512104].

[3] P. Binetruy, M. Sasaki and K. Uzawa, arXiv:0712.3615 [hep-th].

[4] H. Kodama and K. Uzawa, JHEP **0507** (2005) 061 [arXiv:hep-th/0504193].

Deformed phase space and canonical quantum cosmology

Babak Vakili[1]

Department of Physics, Islamic Azad University of Chalous, P. O. Box 46615-397, Chalous, Iran

Abstract

The effects of noncommutativity and deformed Heisenberg algebra on the evolution of a two dimensional minisuperspace quantum cosmological model are investigated.

1 Introduction

We study the effects of noncommutativity and deformed Heisenberg algebra on the evolution of a two dimensional minisuperspace quantum cosmological model. The phase space variables turn out to correspond to the scale factor and the anisotropic parameter of a magnetized Bianchi type I model with a cosmological constant. The exact quantum solutions in commutative and noncommutative cases are presented. We also obtain some approximate analytical solutions for the corresponding quantum cosmology in the presence of the deformed Heisenberg relations between the phase space variables, in the limit where the minisuperspace variables are small. These results are compared with the standard commutative and noncommutative cases and similarities and differences of these solutions are discussed.

2 The model

Let us consider a cosmological model in which the spacetime is assumed to be of Bianchi type I whose metric can be written, working in units where $c = \hbar = 16\pi G = 1$, as

$$ds^2 = -N^2(t)dt^2 + e^{2u(t)}e^{2\beta_{ij}(t)}dx^i dx^j, \tag{1}$$

where $N(t)$ is the lapse function, $e^u(t)$ is the scale factor of the universe and $\beta_{ij}(t)$ determine the anisotropic parameters $v(t)$ and $w(t)$ as follows

$$\beta_{ij} = \mathrm{diag}\left(v + \sqrt{3}w, v - \sqrt{3}w, -2v\right). \tag{2}$$

To simplify the model we take $w = 0$. The Lagrangian in the minisuperspace $\{u, v\}$ can be written as [1]

$$\mathcal{L} = \frac{6e^{3u}}{N}\left(-\dot{u}^2 + \dot{v}^2\right) - \Lambda N e^{3u}. \tag{3}$$

Thus, with the choice of the harmonic time gauge $N = e^{3u}$, the Hamiltonian takes the form

$$\mathcal{H} = \frac{1}{24}\left(-p_u^2 + p_v^2\right) + \Lambda e^{6u}, \tag{4}$$

where Λ is a cosmological constant and p_u and p_v denote the momenta conjugate to u and v respectively.

3 Quantization of the model

Let us now proceed to quantize the model. In ordinary canonical quantum cosmology, use of the usual commutation relations $[x_i, p_j] = i\delta_{ij}$, , results in the well-known representation $p_i = -i\partial/\partial x_i$, from which the WD equation can be constructed as

$$\left[\frac{\partial^2}{\partial u^2} - \frac{\partial^2}{\partial v^2} + 24\Lambda e^{6u}\right]\Psi(u, v) = 0. \tag{5}$$

[1] E-mail: bvakili45@gmail.com, b-vakili@sbu.ac.ir

It is easy to obtain the eigenfunctions of the above equation in terms of Bessel functions as

$$\Psi_\nu(u,v) = e^{-3\nu v} J_\nu\left(2\sqrt{\frac{2\Lambda}{3}}e^{3u}\right), \quad \Lambda > 0, \quad \Psi_\nu(u,v) = e^{3i\nu v} K_{i\nu}\left(2\sqrt{\frac{2|\Lambda|}{3}}e^{3u}\right), \quad \Lambda < 0, \tag{6}$$

where ν is a separation constant. We may now write the general solutions to the WD equations as a superposition of the eigenfunctions

$$\Psi(u,v) = \int_{-\infty}^{+\infty} C(\nu)\Psi_\nu(u,v)d\nu, \tag{7}$$

where $C(\nu)$ can be chosen as a shifted Gaussian weight function $e^{-a(\nu-b)^2}$.

Let us now concentrate on the noncommutativity concepts in this cosmological model. Noncommutativity in physics is described by a deformed product, also known as the Moyal product law between two arbitrary functions of position and momenta as [2]

$$(f *_\alpha g)(x) = \exp\left[\frac{i}{2}\alpha^{ab}\partial_a^{(1)}\partial_b^{(2)}\right] f(x_1)g(x_2)|_{x_1=x_2=x}, \tag{8}$$

such that

$$\alpha_{ab} = \begin{pmatrix} \theta_{ij} & \delta_{ij}+\sigma_{ij} \\ -\delta_{ij}-\sigma_{ij} & \beta_{ij} \end{pmatrix}, \tag{9}$$

where the $N \times N$ matrices θ and β are assumed to be antisymmetric with $2N$ being the dimension of the phase space and represent the noncommutativity in coordinates and momenta, respectively. With this product law, the deformed commutators can be written

$$[f,g]_\alpha = f *_\alpha g - g *_\alpha f. \tag{10}$$

A simple calculation shows that

$$[x_i,x_j]_\alpha = i\theta_{ij}, \quad [x_i,p_j]_\alpha = i(\delta_{ij}+\sigma_{ij}), \quad [p_i,p_j]_\alpha = i\beta_{ij}. \tag{11}$$

Here we consider a noncommutative phase space in which $\beta_{ij} = 0$ and so $\sigma_{ij} = 0$, i.e. the commutators of the phase-space variables are as follows

$$[u_{nc},v_{nc}] = i\theta, \quad [x_{inc},p_{jnc}] = i\delta_{ij}, \quad [p_{inc},p_{jnc}] = 0. \tag{12}$$

With the noncommutative phase space defined above, we consider the Hamiltonian of the noncommutative model as having the same functional form as equation (4), but in which the dynamical variables satisfy the above-deformed commutation relations, that is

$$\mathcal{H}_{nc} = \frac{1}{24}\left(-p_{u_{nc}}^2 + p_{v_{nc}}^2\right) + \Lambda e^{6u_{nc}}. \tag{13}$$

The corresponding WD equation can be obtained by the modification of the operator product in (5) with the Moyal deformed product

$$\left[-p_u^2 + p_v^2 + 24\Lambda e^{6u}\right] * \Psi(u,v) = 0. \tag{14}$$

Using the definition of Moyal product (8), it is easy to show that

$$f(u,v) * \Psi(u,v) = f(u_{nc},v_{nc})\Psi(u,v), \tag{15}$$

where the relations between the noncommutative variables u_{nc}, v_{nc} and commutative variables u, v are given by

$$p_{u_{nc}} = p_u, \quad p_{v_{nc}} = p_v, \quad u_{nc} = u - \frac{1}{2}\theta p_v, \quad v_{nc} = v + \frac{1}{2}\theta p_u, \tag{16}$$

Therefore, the noncommutative version of the WD equation can be written as

$$\left[\frac{\partial^2}{\partial u^2}-\frac{\partial^2}{\partial v^2}+24\Lambda e^{6(u-\frac{1}{2}\theta p_v)}\right]\Psi(u,v)=0. \tag{17}$$

We separate the solutions into the form $\Psi(u,v)=e^{3i\nu v}U(u)$. Noting that

$$\begin{aligned} e^{6(u-\frac{1}{2}\theta p_v)}\Psi(u,v) &= e^{6u}\Psi(u,v+3i\theta) \\ &= e^{6u}U(u)e^{3i\nu(v+3i\theta)} \\ &= e^{6u}e^{-9\nu\theta}\Psi(u,v), \end{aligned} \tag{18}$$

equation (17) takes the form

$$\left[\frac{\partial^2}{\partial u^2}-\frac{\partial^2}{\partial v^2}+24\Lambda e^{6u}e^{-9\nu\theta}\right]\Psi(u,v)=0. \tag{19}$$

The eigenfunctions of the above equation can be written as

$$\Psi_\nu(u,v)=e^{-3\nu v}J_\nu\left(2\sqrt{\frac{2\Lambda}{3}}e^{3(u-\frac{3}{2}\nu\theta)}\right),\quad \Lambda>0,\qquad \Psi_\nu(u,v)=e^{3i\nu v}K_{i\nu}\left(2\sqrt{\frac{2|\Lambda|}{3}}e^{3(u-\frac{3}{2}\nu\theta)}\right),\quad \Lambda<0. \tag{20}$$

The general solutions of equation (19) may be find as a superposition of these eigenfunctions like expression (7).

A general predictions of any quantum theory of gravity is that there exists a minimal length below which no other length can be observed. An important feature of the existence of a minimal length is the modification of the standard Heisenberg commutation relation in the usual quantum mechanics [3]. Such relations are known as the Generalized Uncertainty Principle (GUP). In one dimension, the simplest form of such relations can be written as

$$[x,p]=i\hbar\left(1+\beta p^2\right), \tag{21}$$

where β is positive and independent of $\triangle x$ and $\triangle p$, but may in general depend on the expectation values $<x>$ and $<p>$. In more than one dimensions a natural generalization of (21) is defined by the following commutation relations [3]

$$[x_i,p_j]=i\left(\delta_{ij}+\beta\delta_{ij}p^2+2\beta p_i p_j\right). \tag{22}$$

Now, it is easy to show that the following representation of momentum operator in position space fulfills the relations (22) in the first order in β

$$p_i=-i\left(1-\frac{\beta}{3}\frac{\partial^2}{\partial x_i^2}\right)\frac{\partial}{\partial x_i}. \tag{23}$$

Let us focus attention on the study of the quantum cosmology of the model described by the Hamiltonian (4) in GUP framework. With representation (23) the corresponding WD equation reads

$$\left\{\frac{\partial^2}{\partial u^2}-\frac{2}{3}\beta\frac{\partial^4}{\partial u^4}-\frac{\partial^2}{\partial v^2}+\frac{2}{3}\beta\frac{\partial^4}{\partial v^4}+24\Lambda e^{6u}\right\}\Psi(u,v)=0. \tag{24}$$

Taking $\beta=0$ in this equation yields the ordinary WD equation where its solutions are given in equation (6). In the case when $\beta\neq 0$, we cannot solve equation (24) exactly, but we can provide an approximate method which in its validity domain we need to solve a second order differential equation. To this end, note that the effects of β are important in Planck scales, *i. e.* in cosmology language in the very early universe, that is, when the scale factor is small, $e^{3u}\to 0$. Thus if we use the solutions (6) in the β- term of (24), we may obtain some approximate analytical solutions in the region $e^{3u}\to 0$. The results up to first order in β are

$$\Psi_\nu(u,v)=e^{-3\nu(1+3\beta\nu^2)v}J_{\nu(1+3\beta\nu^2)}\left(2\sqrt{\frac{2\Lambda}{3}}e^{3u}\right),\quad \Lambda>0, \tag{25}$$

$$\Psi_\nu(u,v)=e^{3i\nu(1-3\beta\nu^2)v}K_{i\nu(1-3\beta\nu^2)}\left(2\sqrt{\frac{2|\Lambda|}{3}}e^{3u}\right),\quad \Lambda<0. \tag{26}$$

Again, the general solutions can be written as a superposition of these eigenfunctions.

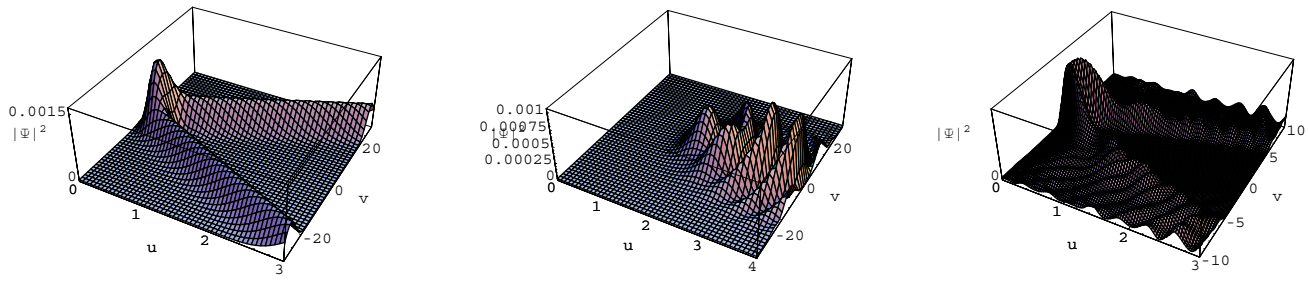

Figure 1: From left to right, the figures show the square of the commutative, noncommutative and GUP wave function. The figures are plotted in the case of a negative cosmological constant.

4 Summary and comparison of the results

In general, one of the most important features in quantum cosmology is the recovery of classical cosmology from the corresponding quantum model, or in other words, how can the WD wavefunctions predict a classical universe. In figure 1 we have plotted the square of the wave functions obtained in the previous section. As we can see from this figure, in the commutative case the peaks follow a path which can be interpreted as the classical trajectories. The crests are symmetrically distributed around $v = 0$ which may correspond to the different classical paths. Thus, it is seen that there is an almost good correlations between the quantum patterns and classical trajectories in the $u - v$ plane. In this case we have only one possible universe around a nonzero value of u and $v = 0$, which means that the universe in this case approaches a flat FRW one. On the other hand, we see that noncommutativity causes a shift in the minimum value of u corresponding to the spatial volume. The emergence of new peaks in the noncommutative wave packet may be interpreted as a representation of different quantum states that may communicate with each other through tunneling. This means that there are different possible universes (states) from which our present universe could have evolved and tunneled, from one state to another. Therefore, the noncommutative wavefunction predicts the emergence of the universe from a state corresponding to one of the peaks. We see that the correlation with classical trajectories is missed, i.e. the noncommutativity implies that the universe escapes the classical trajectories and approaches a stationary state. Finally, in the GUP case as is clear from the figure the wave function has a single peak. Although there are some small peaks in this figure, as u and v grow, their amplitude are suppressed. Compare to the commutative wave function, here we have no wave packet with peaks following the classical trajectories. We see that instead of a series of peaks in the ordinary WD approach, we have only a single dominant peak. This means that, similar to the noncommutative case and within the context of the GUP framework, the wave function also shows a stationary behavior. One may then conclude that from the point of view adopted here, noncommutativity and GUP may have close relations with each other. However, there is an important difference, namely, that the noncommutative wave function not only peaks around $v = 0$, but appear symmetrically around a nonzero value of v, which is the characteristic of an anisotropic universe. On the other hand, the GUP wave function as is seen in the figure, has many peaks around the value $v = 0$ and therefore from the point of predicting an isotropic universe the GUP wave packet behaves like the ordinary commutative case.

References

[1] B. Vakili and H.R. Sepangi, *Phys. Lett.* B **651** (2007) 79

[2] J.E. Moyal, *Proc. Cambridge Phil. Soc.* **45** (1949) 99

[3] A. Kempf, G. Mangano, R.B. Mann, *Phys. Rev.* D **52** (1995) 1108

Stringent Constraints on Brans-Dicke Parameter using deci-Hz Gravitational Wave Interferometers

Kent Yagi[1], Takahiro Tanaka[2] and Naoki Seto[3]

[1,3] *Department of Physics, Kyoto University, Kyoto, 606–8502, Japan*
[2] *Yukawa Institute for Theoretical Physics, Kyoto University, Kyoto 606–8502, Japan*

Abstract

We calculate how strong one can put constraints on Brans-Dicke parameter $\omega_{\rm BD}$ using 0.1Hz space laser interferometers such as DECIGO and BBO. We consider situations where neutron stars inspiral into small mass black holes whilst radiating gravitational waves. Compared to General Relativity, gravitational waves in Brans-Dicke theory have dipole radiation. For the amplitudes of the waveforms, we only take the leading quadrupole term and for the phases, we take subleading terms up to 2PN including spin-spin coupling term. For simplicity, we assume that the orbits are circular and we neglect the effect of spin precessions. We find that we can put 100 times stronger constraints on $\omega_{\rm BD}$ than the Cassini bound $\omega_{\rm BD} > 40000$, which is the current greatest constraint found by solar system experiments. This certainly gives a big scientific significance for DECIGO/BBO projects.

1 Introduction

One of the approaches to solve dark energy problem is to modify gravitational thoery from general relativity. The simplest modification is to add scalar degree of freedom to gravity. This theory is called scalar-tensor theory. This theory also appears in inflation problem and superstring theory. A prototype of scalar-tensor theory is Brans-Dicke theory. This theory is characterised by a parameter $\omega_{\rm BD}$ and by taking the limit $\omega_{\rm BD} \to \infty$, it reduces general relativity. The current strongest bound on $\omega_{\rm BD}$ is the Cassini bound obtained in the solar system experiment [1]; $\omega_{\rm BD,Cassini} > 40000$.

The aim of our work is to investigate how strongly we can constrain $\omega_{\rm BD}$ in the strong field regime by detecting gravitational waves from NS/BH binaries. Berti *et al.* [2] estimated this by using space interferometer LISA [3] and we estimated this by using deci-Hz interferometer DECIGO [4]. We take spin-spin coupling effect into account which Berti *et al.* [2] does not include. We find, by using DECIGO, we can put at least 100 times stronger constraint on $\omega_{\rm BD}$ than the Cassini bound.

2 Binary Gravitational Waveforms in Brans-Dicke Theory

Gravitational waveforms in general depend on the orientations of the binaries and the orbital angular momentum, but here, we average over these orientations. We adopt the restricted 2nd post-Newtonian (2PN) waveforms in which the amplitude is expressed to the leading order in a post-Newtonian expansion whilst the phase is taken up to 2PN order. (Post-Newtonian approximation is an expansion for slow-motion, weak-field systems in powers of binary velocity v.) For point masses, the phase evolution is calculated up to 3.5PN order but spin terms are known only up to 2PN order. Therefore to be consistent, we take the phase up to 2PN. Under the stationary phase approximation, the Fourier component of the waveform is [2]

$$\tilde{h}(f) = \frac{\sqrt{3}}{2}\mathcal{A} f^{-7/6} e^{i\Psi(f)}. \tag{1}$$

Here, f is the frequency of the gravitational waves. The amplitude is given by

[1]E-mail:kent@tap.scphys.kyoto-u.ac.jp
[2]E-mail:tanaka@yukawa.kyoto-u.ac.jp
[3]E-mail:seto@tap.scphys.kyoto-u.ac.jp

$$\mathcal{A} = \frac{1}{\sqrt{30}\pi^{2/3}} \frac{\mathcal{M}^{5/6}}{D}, \tag{2}$$

where $\mathcal{M} = \eta^{3/5} M$ is the chirp mass, with total mass $M = m_1 + m_2$ and dimensionless mass parameter $\eta = m_1 m_2 / M^2$, and D is the luminosity distance to the source.

The phase is given by

$$\begin{aligned} \Psi(f) =& 2\pi f t_c - \phi_c + \frac{3}{128}(\pi \mathcal{M} f)^{-5/3} \left[1 - \frac{5}{84} \mathcal{S}^2 \bar{\omega} x^{-1} + \left(\frac{3715}{756} + \frac{55}{9}\eta \right) x \right. \\ & \left. - 4(4\pi - \beta) x^{3/2} + \left(\frac{15293365}{508032} + \frac{27145}{504}\eta + \frac{3085}{72}\eta^2 - 10\sigma \right) x^2 \right], \end{aligned} \tag{3}$$

where $x = v^2 = (\pi M f)^{2/3} = \eta^{-2/5} (\pi \mathcal{M} f)^{2/3}$. The first two terms are related to the time t_c and phase ϕ_c of coalescence. The first term ("1") inside the brackets corresponds to the leading quadrupole approximation of general relativity. The second term represents the dipole gravitational radiation in Brans-Dicke theory. $\bar{\omega} \equiv \omega_{\rm BD}^{-1}$ is the inverse of the Brans-Dicke parameter. $\mathcal{S} = s_2 - s_1$ where s_i is called the *sensitivity* of the i-th body defined as

$$s_i \equiv \left(\frac{\partial(\ln m_i)}{\partial(\ln G_{\rm eff})} \right)_0 . \tag{4}$$

Here, $G_{\rm eff}$ is the gravitational constant at the location of the body and is proportional to the inverse of the Brans-Dicke scalar field there. The subscript 0 denotes that we evaluate s_i at infinity. This sensitivity roughly equals to the binding energy of the body per unit mass. For example, $s_{\rm WD} \sim 10^{-3}$ and $s_{\rm NS} \sim 0.2$. Because of No Hair Theorem, black holes cannot have scalar charges and $s_{\rm BH} = 0.5$. From Eq. (3), larger the $\mathcal{S}$, greater the contribution of dipole radiation. Binaries with large $\mathcal{S}$ are the ones with bodies of different types. Here, we consider NS/BH binaries. The event rate of NS/BH mergers is still uncertain, but it seems that it is considerably small for LISA, so only a lucky detection can constrain Brans-Dicke parameter. In contrast, for DECIGO, it is said to be around 10^4 merger events per year so NS/BH binaries should be the definite sources [5]. The rest of the terms in brackets are usual higher order PN terms in general relativity.

The quantities β and σ represent spin-orbit and spin-spin contributions to the phase respectively, given by

$$\beta = \frac{1}{12} \sum_{i=1}^{2} \chi_i \left(113 \frac{m_i^2}{M^2} + 75\eta \right) \hat{\boldsymbol{L}} \cdot \hat{\boldsymbol{S}}_i, \tag{5}$$

$$\sigma = \frac{\eta}{48} \chi_1 \chi_2 (-247 \hat{\boldsymbol{S}}_1 \cdot \hat{\boldsymbol{S}}_2 + 721 (\hat{\boldsymbol{L}} \cdot \hat{\boldsymbol{S}}_1)(\hat{\boldsymbol{L}} \cdot \hat{\boldsymbol{S}}_2)), \tag{6}$$

where $\hat{\boldsymbol{L}}$ and $\hat{\boldsymbol{S}}_i$ are unit vectors in the direction of the orbital angular momentum and spin angular momenta respectively. The spin angular momenta are given by $\boldsymbol{S}_i = \chi_i m_i^2 \hat{\boldsymbol{S}}_i$ where χ_i are the dimensionless spin parameters. For black holes, they must be smaller than unity, and for neutron stars, they are generally much smaller than unity. It follows that $|\beta| \lesssim 9.4$ and $|\sigma| \lesssim 2.5$.

3 Parameter Estimation

The detected signal $s(t)$ is the sum of the gravitational wave signal $h(t; \boldsymbol{\theta})$ and the noise $n(t)$. We use the matched filtering analysis to estimate the binary parameters $\boldsymbol{\theta}$. We assume that the noise is stationary and Gaussian. Then, the probability that the GW parameters are $\boldsymbol{\theta}$ given by [2]

$$p(\boldsymbol{\theta}|s) \propto p^{(0)}(\boldsymbol{\theta}) \exp\left[-\frac{1}{2} \Gamma_{ij} \Delta\theta^i \Delta\theta^j \right], \tag{7}$$

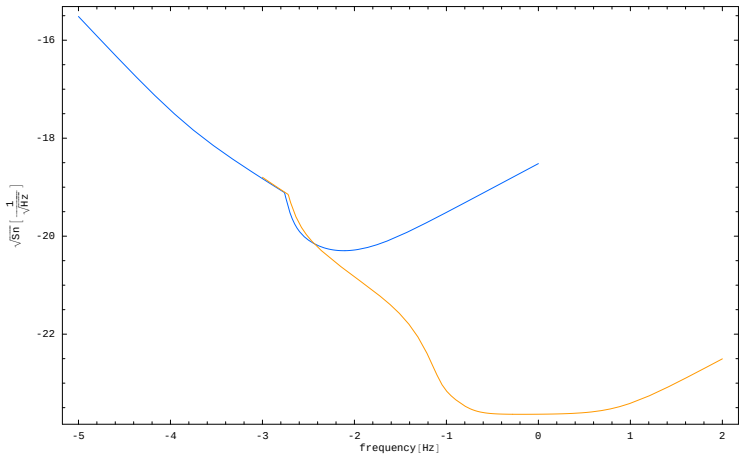

Figure 1: Noise curves for LISA(blue) [2] and DECIGO(red). Both horizontal and vertical axes are in log scales. Horizontal axis represents frequency[Hz] and vertical axis shows noise spectral density[$\mathrm{Hz}^{-1/2}$].

where the Fisher matrix Γ_{ij} is given by

$$\Gamma_{ij} = \left(\frac{\partial h}{\partial \theta^i} \middle| \frac{\partial h}{\partial \theta^i} \right). \tag{8}$$

Here, we define the inner product as

$$(A|B) = 4\mathrm{Re} \int_0^\infty df \, \frac{\tilde{A}^*(f)\tilde{B}(f)}{S_n(f)}, \tag{9}$$

where $S_n(f)$ is the noise spectral density. LISA and DECIGO noise strain sensitivity $\sqrt{S_n(f)}$ are shown in Fig.1. We denote estimates of rms errors as $\Delta\theta^i = \theta^i - \hat{\theta}^i$ where $\hat{\theta}^i$ is the fitted parameters. Then, $\Delta\theta^i$ can be calculated by taking the square root of the diagonal elements of the covariant matrix Σ_{ij}, which is the inverse of the Fisher matrix Γ_{ij};

$$\left\langle \Delta\theta^i \Delta\theta^j \right\rangle = \Sigma^{ij}, \qquad \Sigma^{ij} \equiv (\Gamma^{-1})^{ij}. \tag{10}$$

We take into account our prior information on the maximum spin by assuming

$$p^{(0)}(\boldsymbol{\theta}) \propto \exp\left[-\frac{1}{2}\left(\frac{\beta}{9.4}\right)^2 - \frac{1}{2}\left(\frac{\sigma}{2.5}\right)^2 \right]. \tag{11}$$

The signal to noise ratio(SNR) for a given h is given by $\rho[h] \equiv \sqrt{(h|h)}$.

4 Numerical Calculations and Results

4.1 Set Up

We think of detecting NS/BH inspiralling gravitational waves by LISA and DECIGO, and calculate how accurately we can deterimine the binary parameters, especially ω_{BD}. We assume that the orbit is circular and observation lasts 1 year. Also, we neglect spin precessions for simplicity.

The binary parameters are as follows; chirp mass $\ln \mathcal{M}$, dimensionless mass parameter $\ln \eta$, coalescence time t_c, coalescence phase ϕ_c, distance to the source $\ln D$, spin-orbit coupling β, spin-spin coupling σ, and reciprocal of Brans-Dicke parameter $\bar{\omega}$. We assume $t_c = 0, \phi_c = 0, \beta = 0, \sigma = 0, \bar{\omega} = 0$ and $\mathcal{S} = 0.3$. We fix $m_{\mathrm{NS}} = 1.4 M_\odot$. We also fix the distance to be the one that gives SNR $\rho = 10$. We change m_{BH} and see how the constraints on ω_{BD} change. Berti *et al.* did not take σ into binary parameters. We

Table 1: Constraints on $\omega_{\rm BD}/10^4$ with different $m_{\rm BH}$ by using DECIGO and LISA. 1st row shows the constraints with σ taken into parameters, and 2nd row shows the ones without σ.

	DECIGO				LISA			
	$3M_\odot$	$10M_\odot$	$50M_\odot$	$400M_\odot$	$400M_\odot$	$1000M_\odot$	$5000M_\odot$	$10^4M_\odot$
parameters without σ	539.5	269.8	81.72	10.22	3.891	2.110	0.6432	0.3048
parameters with σ	429.4	162.9	35.94	4.254	2.472	0.8154	0.1916	0.0854

evaluate the constraints on $\omega_{\rm BD}$ in both cases where σ is not taken into binary parameters and where σ is taken into parameters, and compare both results.

4.2 Results

Table 1 shows the estimated constraints on $\omega_{\rm BD}/10^4$ with different $m_{\rm BH}$ by using DECIGO and LISA. The 1st row shows the constraints in the case where we do not take σ into binary parameters, and the 2nd row shows the ones where we do take σ into binary parameters.

From the table, including σ into parameters reduces the constraint by a factor of a few. Generally, the more the number of parameters increases, the worse the parameter determination accuracies are. You can also see that DECIGO can put about 200 times stronger constraint than LISA. There are mainly 2 reasons for this. First reason is because the number of GW cycles $\mathcal{N}_{\rm GW} = \int_{f_{\rm in}}^{f_{\rm fin}} df\ (f/\dot{f})$ are larger for DECIGO sources than LISA sources. Another reason is that the sensitivity of DECIGO is much better than that of LISA. Again from the table, you can see the constraint becomes more stringent as the BH mass decreases. This is because the bodies of the binaries become slower, which makes the dipole contribution greater. Even if we include σ as binary parameters, DECIGO can put at least 100 times stronger constraint than the current strongest one ($\omega_{\rm BD,Cassini} > 40000$).

5 Conclusions

We estimate how strongly we can put constraint on $\omega_{\rm BD}$ by detecting gravitational waves from inspiralling NS/BH binaries using LISA and DECIGO. We found that including σ as binary parameters reduces the constraint by a factor of a few. We also found that DECIGO can put at least 100 times stronger constraint than the current strongest one.

We have also calculated the constraint including eccentricity of the orbit and the effect of spin precessions [6]. We took the source orientation dependence into account. We performed following Monte Carlo simulation. We randomly distribute 10^4 binaries, evaluate the parameter estimation accuracies for each binary, and take the average. We found that for binaries with $\rho = 10$, DECIGO can put at least 10 times stronger constraint than the Cassini bound. For binaries with $D = 200$Mpc, whose event rate is thought to be roughly 1 merger per year, DECIGO can put 1000 times stronger constraint than Cassini bound. This certainly gives a big scientific significance to DECIGO project.

References

[1] B. Bertotti, L. Iess and P. Tortora, Nature **425**, 374 (2003)

[2] E.Berti, A.Buonanno and C.M.Will, Phys.Rev.**D71**, 084025 (2005)

[3] K.Danzmann, Class.Quant.Grav.**14**, 1399 (1997)

[4] S.Kawamura *et al.*, Class. Quantum Grav. **23**, S125 (2006)

[5] R.Voss and T.M.Tauris, Mon.Not.Roy.Astron.Soc.**342**,1169 (2003)

[6] K.Yagi, T.Tanaka and N.Seto (to be published)

Open Inflation in String Landscape

Daisuke Yamauchi[†,1], Andrei Linde[††,2], Misao Sasaki[†,3], Takahiro Tanaka[†,4] and Atsushi Naruko[†,5]

[†] *Yukawa Institute for Theoretical Physics, Kyoto University, Kyoto 606–8502, Japan*
[††] *Department of Physics, Stanford University, Stanford, CA 94305-4060, USA*

Abstract

The recent observational data indicate that the universe is almost spatially flat. Nevertheless, the open inflationary scenario is attracting a renewed interest in the context of string landscape. Since there are a large number of metastable de Sitter vacua in string landscape, tunneling transitions to lower metastable vacua through the bubble nucleation occur quite naturally, which leads to a natural realization of open inflation. Recently, it was argued anthropically that string landscape would lead to an estimate of the density parameter in the range $\Omega_0 \approx 0.998 \sim 0.9996$. Although the deviation of Ω_0 from unity, the effect of this small deviation on the CMB anisotropies might be significant. If their estimate of the value of Ω_0 is correct, although yet there is no consensus about the problem of the probability measure, we might be able to discriminate the string landscape scenario from others. We argue that although the deviation of Ω_0 from unity may be small, the effect of this small deviation on the large angle CMB anisotropies may be significant for large angle mode in tensor-type perturbation. We found that the large amplification of power spectrum occurs when the difference of false and true vacuum potential energy is exponentially large.

1 Introduction

The recent observational data indicate that the universe is almost spatially flat. Nevertheless, the open inflationary scenario is attracting a renewed interest in the context of "string landscape" [2]. It realized that inflation may divide our universe into many exponentially large domains corresponding to different metastable vacuum, so-called "inflationary multiverse". Since in this context there are a enormous number of metastable de Sitter vacua in the range of 10^{100} or 10^{1000} and the global universe is an eternally inflating "megaverse" that is continually producing small pocket universes, the tunneling transitions to a lower metastable vacuum and the bubble nucleation occurs quite naturally, which leads to a natural realization of the open inflation scenario.

The basic idea of the one-bubble open inflationary scenario is following. Initially the scalar field is trapped in the false vaccum during the sufficiently long period such that it solve the homogeneity problem and the our universe becomes well-approximated by a pure de Sitter space. Then, bubble nucleation occurs through quantum tunneling. The process is described by a Euclidean $O(4)$-symmetric bounce solution called Coleman-De Luccia (CDL) instanton [3]. The expanding bubble after nucleation is described by analytic continuation of the bounce solution to Lorentzian regime. The bubble formed by CDL instanton looks from the inside like an infinite open universe [3, 2]. If we assume that the vacuum energy inside the bubble is nonzero, the second stage of inflation inside the bubble occurs and it solves entropy problem and is necessary to avoid the curvature dominant universe.

Although the open inflation scenario, by definition, predicts nonzero spatial curvature of the universe, as long as the curvature is sufficiently small, this scenario will not contradict with observations. Recently, string theorists are interested in this kind of scenario [2] in context of string landscape by means of anthropic argument. The most important cosmological consequence they claimed was that there was a tunneling event in our past. Especially Freivogel et al. have estimated the present value of density parameter Ω_0 by using their landscape measure and the estimated value is given by $\Omega_0 \approx 0.998 \sim 0.9996$

[1] E-mail:yamauchi@yukawa.kyoto-u.ac.jp
[2] E-mail:alinde@stanford.edu
[3] E-mail:misao@yukawa.kyoto-u.ac.jp
[4] E-mail:tanaka@yukawa.kyoto-u.ac.jp
[5] E-mail:naruko@yukawa.kyoto-u.ac.jp

by means of anthropic argument. Although the deviation of Ω_0 from unity, the effect of this small deviation on the CMB anisotropies might be significant. If their estimate of the value of Ω_0 is correct, although yet there is no consensus about the problem of the probability measure, we might be able to discriminate the string landscape scenario from others.

We also have to comment the another distinct feature for the string landscape. Almost inflationary model inspired by string theory are formulated in the context of type IIB string theory with the Kachru-Kallosh-Linde-Trivedi(KKLT) stabilization mechanism [5]. There exists strong constraints on particle phenomenology and on inflation model and one can expect that the final slow-roll inflation must be low-scale inflation. Also, one can naively expect that the shape of the global potential for landscape is decided only by fundamental scale corresponding to Planck scale. Thus, the distinctive feature for string landscape is expected as the large difference of the hight of potential between false and true vacua. In this paper, we will consider the possibility that "open inflation scenario" can realize in "string landscape". Especially, we will focus on the power spectrum and power spectrum in open inflation scenario under the condition one can expect that it is satisfied in string landscape [1].

2 Power spectrum for one-bubble open inflation model

We consider the system that consists of a minimally coupled scalar field, ϕ with the Einstein gravity. We denote the potential of the scalar field by $V(\phi)$. Let us consider the $O(4)$-symmetric bubble solution. We are, in particular, interested in the wall fluctuation mode, which will show up a distinctive feature of open inflation in the context of string landscape. An $O(4)$-symmetric bubble nucleation is described by the Euclidean solution (instanton). The metric is given by

$$ds^2 = d\tau_E^2 + a_E^2(\tau_E)(d\chi_E^2 + \sin^2\chi_E d\Omega^2)\,, \tag{1}$$

and the background scalar field is denoted by $\phi = \phi(\tau)$. The Euclidean background equations are

$$\left(\frac{\dot{a}_E}{a_E}\right)^2 - \frac{1}{a_E^2} = \frac{\kappa}{3}\left(\frac{1}{2}\dot{\phi}^2 - V(\phi)\right)\,,\quad \left(\frac{\dot{a}_E}{a_E}\right)^{\cdot} + \frac{1}{a_E^2} = -\frac{\kappa}{2}\dot{\phi}^2\,,\quad \ddot{\phi} + 3\frac{\dot{a}_E}{a_E}\dot{\phi} - V'(\phi) = 0\,, \tag{2}$$

where a dot " $\dot{}$ " represents differentiation with respect to τ_E. The background geometry and the field configuration in the Lorentzian regime are obtained by the analytic continuation of the bounce solution. Sometimes it is convenience to use the coordinate η defined by $d\tau = a(\eta)d\eta$. The coordinates in the Lorentzian regime are given by $\eta_E = \eta_C = -\eta_R - \frac{\pi}{2}i = \eta_L + \frac{\pi}{2}i\,, \chi_E = -i\chi_C + \frac{\pi}{2}i = -i\chi_R = -i\chi_L\,, a_E = a_C = ia_R = ia_L$.

From a gauge-invariant method developed by Garriga, Motes, Sasaki, Tanaka [4] in the one-field model of one-bubble open inflation, the tensor-type perturbation is conveniently described by a variable $\mathbf{w}$, which is related to the transverse-traceless metric perturbation in the open universe. When we expand this mode function in terms of the sherical harminics and spatial eigenfunction $\mathbf{w}^p$ with eigenvalue p^2, the equation for $\mathbf{w}^p$ is given by

$$\left[-\frac{d^2}{d\eta_E^2} + U_T(\eta_E) - p^2\right]\mathbf{w}^p = 0\,, \tag{3}$$

where η_E denotes Euclidean conformal time defined by $\eta_E = \int d\tau_E/a_E$ and $U_T(\eta_E) = \kappa\phi'^2/2$.

In order to compute the power spectrum at the end of inflation, we will define "tansfer function" given by In order to compute the power spectrum at the end of inflation, we will define an auxiliary "transfer function" given by

$$\mathcal{T}_T^p = \lim_{\eta_R \to \eta_R^{\rm end}} -\frac{\kappa}{a^2(p^2+1)}\frac{d}{d\eta_R}\left(a\tilde{\mathbf{w}}^p\right)\,, \tag{4}$$

where $\eta_R^{\rm end}$ denotes the value of the conformal time η_R for which $a \to \infty$ and $\tilde{\mathbf{w}}^p$ is the solution of the equation which analytic continuation of Eq. (3) to region-R which satisfies the appropriate boundary

condition, i.e., behaves as $\tilde{\mathbf{w}}^p \to e^{ip\eta_R}$ when $\eta_R \to -\infty$. Then, the power spectrum for tensor-type perturbation can be expressed as [4]

$$\left\langle \ U_p \ ^2 \right\rangle = 2\frac{|\mathcal{T}_T^p|^2(p^2+1)\coth \pi p}{\kappa p}\Big[1 - y_{\rm eff}\Big]\,, \tag{5}$$

where $y_{\rm eff}$ represents the effects of the bubble wall and the phase factor of the transfer function.

3 CMB anisotropy in string landscape

3.1 Assumption

Before calculating the CMB anisotropy in the string landscape, we take the some assumption: As one can expect naively, almost all information about the string landscape can be determined only by the fundamental scale (at least this is valid at sufficiently high energy region), i.e. Planck scale and/or string scale, which leads that the shape and width of the potential for the scalar field are also determined only by fundamental scale. Futhermore, we assume that the final tunneling transition occurs through CDL instanton. Typically, CDL instantons exists only if $m^2 \equiv V'' > H_L^2 \equiv \kappa V_{\rm false}/3$ during tunneling. Therefore we have to consider the steep potential after the tunneling. From the approximated equations of motion, e.g., $H_L^2 \sim V_{\rm false}/M_{pl}^2\,, m^2 \sim V_b/(\triangle\phi)^2$, we have the condition for the CDL instanton as

$$\frac{H_L^2}{m^2} \sim \frac{V_{\rm false}}{V_b}\frac{(\triangle\phi)^2}{M_{pl}^2} \lesssim 1\,. \tag{6}$$

In this paper, we will assume this CDL condition Eq. (6).

Under these condition, one can show that the thin-wall approximation in region-C is almost valid, i.e. the effective potential U_T of the mode function $\mathbf{w}^p$ in Eq. (3) has only local and small contribution in region-C : $U_T \approx \triangle s\delta(\eta_C - \eta_W)$ where $\triangle s = \int d\eta_C U_T(\eta_C)$ and η_W denotes the value of the conformal time at the bubble wall. However, the tunneling transition through CDL instanton in our setup is not approximated by exact thin wall since one can expect that the energy scale of the final inflation is pretty lower than the fundamental scale due to the strong constrants from the particle phenomenology, i.e. there exists very large difference of the potential hight at the nucleation point of the bubble and at true vacuum. Thus, we find that the evolutionary behavior of scalar field inside the bubble is significant due to the large potential gap.

3.2 Evolutionary behavior of scalar eld inside bubble

Since the amplitude for the open inflation Eq. (5) is almost determined by the transfer function Eq. (4). The transfer function becomes constant for $p^2+1 \ll H^2$ except for the decaying mode. Then the transfer function is approximated at the froze-in time $t_{\rm froze}(p)$ s.t. $(p^2+1) \approx a^2H^2(t_{\rm froze})$:

$$\mathcal{T}_T^p \approx -\frac{\kappa}{p^2+1}H\mathbf{w}^p{}_{\,t=t_{\rm froze}(p)}\,, \tag{7}$$

If one can neglect the effects of the evolution inside the bubble, mode function becomes the plane wave solution in the all range and the transfer function is given by $\mathcal{T}_T^p \approx -\kappa H_R/(p^2+1)$ where $H_R^2 = \kappa V_{\rm true}$. However, in general the scale factor in Eq. (7) is no longer exactly de Sitter space and can evolve through the evolution of the scalar field. Also the mode function is no longer plane wave solution. Especially when we consider the large effects of the evolution or small p mode, i.e. $(\kappa\phi')_{\max} \quad p^2$, the mode function is well-approximated by WKB solution from Eq. (3). In this case, one can see that the norm of $\mathbf{w}^p$ can be exponentially enhanced. Reminding the boundary condition and the connection formulas at the turning point $\eta = \eta_{\rm crit}(p)$ such that $p^2 = U_T(\eta_{\rm crit})$, one can obtain the WKB solution at $\eta \to \eta_{\rm froze}(p)$ as follow:

$$\ln\,\mathbf{w}^p(\eta_{\rm froze}(p)) = \mathcal{A}(\text{small } p) \sim \int_{\eta_{\rm crit}(p)}^{\eta_{\rm froze}(p)} d\eta'\sqrt{U_T(\eta')} - \frac{1}{4}\ln\left[\frac{U_T(\eta_{\rm froze}(p))}{U_T(\eta_{\rm crit}(p))}\right], \tag{8}$$

Thus, in this case the amplitude becomes exponentially larger than usual ones.

3.3 Power spectrum and multipole moment

Under these consideration in Sec. 3.1, 3.2, one can calculate the power spectrum by using the general formula Eq. (5). In order to investigate the feature of the power spectrum, we assume that the energy density of the scalar field at the nucleation point is not exponentially smaller than the wall tension. This condition is naturally valid under the assumption in Sec. 3.1. One can see that the power spectrum for tensor-type perturbation is sharply peaked around $p \approx 0$ mode, so-called "wall fluctuation mode". Note that the amplitde can be larger than the usual ones in exact thin wall approximation due to the evolution inside the bubble as we already mentioned in Sec. 3.2. For the large p mode, the amplitude becomes scale invariant spectrum : $|U_p|^2 p^3 \to \kappa H_R^2$.

Here we study how severely the revised open inflation scenarios based on the string landscape are constrained after more detailed comparison with the observed CMB anisotropies. Although the observational date indicate that our universe is almost spatially flat, the deviation of Ω_0 from unity might be significant in string landscape. Expanding all the quantities with respect to $|1-\Omega_0|$, one can calculate the approximateed multipole moment:

$$C_\ell^{(T)} \approx f_\ell \frac{\kappa H_R^2 e^{2\mathcal{A}_0}}{\triangle s}(1-\Omega_0)^\ell \,;\; f_\ell = \frac{(\ell+1)(\ell+2)}{100\pi}\left(\frac{\Gamma(\ell+1)}{\Gamma(\ell+3/2)}\right)^2 \left(1+\ell \times z_{\rm LSS}^{1/2}\right)^2 . \tag{9}$$

where $z_{\rm LSS} \approx 1100$ and $\mathcal{A}_0$ denotes the amplification factor due to the evolution of the scalar field inside the bubble. By a certain fine-tunining of parameters one can obtain Eq. (8) as amplification factor.

4 Summary

In this paper we considered the possibility that "open inflation scenario" can realize in "string landscape". We focused on the power spectrum and power spectrum in open inflation scenario under the condition one can expect that it is satisfied in string landscape. We find that the multipole moment is in proportion to $|1-\Omega_0|^\ell$. This means that the wall fluctuation mode corresponding to small p modes affects only small ℓ mode in CMB fluctuations, especially when Ω is close to unity. An interesting observation is that there can exist the enhancement factor $\mathcal{A}(p)$ due to the evolution inside the bubble. We found that the wall fluctuation mode is significant even in string landscape and the evolutionary behavior of scalar field inside the bubble is sufficiently important the due to large difference of false and true potential energy. If the potential energy at the nucleation point becomes pretty higher than the true one, the power spectrum becomes amplified. The multipole moment for higher ℓ modes are highly suppressed by the deviation of the density parameter $|1-\Omega_0|$. Thus, the wall fluctuation mode affects only small ℓ mode in CMB fluctuations. From these interesting oservations, we might be able to discriminate the string landscape scenario from others.

References

[1] D. Yamauchi, A. Linde, M. Sasaki, T. Tanaka, A. Naruko, in preparation

[2] L. Susskind, arXiv:hep-th/0302219 , B. Freivogel and L. Susskind, Phys. Rev. D **70**, 126007 (2004) [arXiv:hep-th/0408133] , B. Freivogel, M. Kleban, M. Rodriguez Martinez and L. Susskind, JHEP **0603**, 039 (2006) [arXiv:hep-th/0505232].

[3] S. R. Coleman, Phys. Rev. D **15**, 2929 (1977) [Erratum-ibid. D **16**, 1248 (1977)] , S. R. Coleman and F. De Luccia, Phys. Rev. D **21**, 3305 (1980).

[4] J. Garriga, X. Montes, M. Sasaki and T. Tanaka, Nucl. Phys. B **551**, 317 (1999) [arXiv:astro-ph/9811257] , J. Garriga, X. Montes, M. Sasaki and T. Tanaka, Nucl. Phys. B **513**, 343 (1998) [arXiv:astro-ph/9706229].

[5] S. Kachru, R. Kallosh, A. Linde and S. P. Trivedi, Phys. Rev. D **68**, 046005 (2003) [arXiv:hep-th/0301240].

Solving the Inverse Problem with Inhomogeneous Universes
— Toward a test of the Copernican principle —

Chul-Moon Yoo[1], Tomohiro Kai[2] and Ken-ichi Nakao[2]

[1]*Asia Pacific Center for Theoretical Physics,*
Pohang University of Science and Technology, Pohang 790-784, Korea
[2]*Department of Physics, Graduate School of Science, Osaka City University, Osaka 558-8585, Japan*

Abstract

We construct the Lemaître-Tolman-Bondi (LTB) dust universe whose distance-redshift relation is equivalent to that in the concordance Λ cold dark matter (ΛCDM) cosmological model. In our model, the density distribution and velocity field are not homogeneous, whereas the big-bang time is uniform, which implies that the universe is homogeneous at its beginning. We also study the temporal variation of the cosmological redshift and show that, by the observation of this quantity, we can distinguish our LTB universe model from the concordance ΛCDM model, even if their redshift-distance relations are equivalent to each other.

1 Introduction

Λ cold dark matter (ΛCDM) models have achieved wide acceptance as concordance models due to the results of observations over the last decade. The isotropy of our universe is strongly supported by the CMB observations. Thus, if we assume that our universe is homogeneous, results from SNe observation suggest that the volume expansion of our universe is accelerating. The accelerating expansion of a homogeneous and isotropic universe means the existence of exotic energy components, the so-called dark energy, within the framework of general relativity (GR). However, there are several crucial problems regarding the existence of the cosmological constant or other dark energy candidates (see, for example, Ref.[1]). No one knows the origin of dark energy and there has not yet been a conclusive illustration of dark energy.

There are other possibilities that explain the observations. The basic idea is that we are in a large underdense region, i.e., a large void; we reject the Copernican principle, which states that we live at a typical position in the universe. For inhomogeneous universe models, Lemaître-Tolman-Bondi (LTB) solutions[10, 11, 12] are often employed. At present, the Copernican principle is not based on sufficient observational facts. However, by virtue of the recently improved observational technologies, we might reach the stage at which we are able to investigate through observation whether our location in the universe is unusual or not . In order to test inhomogeneous universe models by observations, it is important to know the types of inhomogeneous universe models that can be used to explain current observations, and to reveal what predictions are given by these universe models. This is the subject of this paper.

The inverse problem using LTB universe models is a useful method for investigating the possibility of explaining observational results with inhomogeneities in the universe [15, 6, 7, 16]. LTB dust solutions contain three arbitrary functions of the radial coordinate: the mass function M, the big-bang time $t_{\rm B}$ and the curvature function k, and the inverse problem means determining M, $t_{\rm B}$ and k so that a given distance-redshift relation is realized on the past light-cone of an observer. In order to specify the three arbitrary functions, we need three conditions. One of these conditions corresponds to the choice of the radial coordinate and thus has no physical meaning. Hence, one more condition in addition to the distance-redshift relation is necessary.

In terms of perturbation theory, the inhomogeneity of the big-bang time corresponds to the decaying mode. The condition of uniform big-bang time might guarantee the consistency of the present model with the inflationary scenario, since a universe that experiences inflation is almost homogeneous immediately after the inflationary period is over.

The time derivative of the cosmological redshift is a very important observable quantity in distinguishing LTB models from concordance ΛCDM universe models. We study it and show that it gives a criterion for observationally deciding whether the universe is described by an LTB model with uniform big-bang time.

Throughout this paper, we use the unit of $c = G = 1$, where c and G are the speed of light and the gravitational constant, respectively.

2 LTB dust universe and conditions to fix the model

LTB solutions are exact solutions to the Einstein equations, which describe the dynamics of a spherically symmetric dust fluid and whose line element is written in the form

$$ds^2 = -dt^2 + \frac{\left(\partial_r R(t,r)\right)^2}{1-k(r)r^2}dr^2 + R^2(t,r)d\Omega^2, \tag{1}$$

where $k(r)$ is an arbitrary function of the radial coordinate r. The LTB solutions include homogeneous and isotropic universes as special cases; in this case, k is a constant called the curvature parameter in the appropriate gauge, and thus we call it the curvature function. The stress-energy tensor of the dust is given by $T^{\mu\nu} = \rho(t,r)u^\nu u^\nu$, where $\rho(t,r)$ is the rest mass density of the dust and $u^\mu = \delta^\mu_0$ is the 4-velocity of a dust particle. The Einstein equations lead to the equations for the areal radius $R(t,r)$ and the rest mass density $\rho(t,r)$,

$$\left(\partial_t R\right)^2 = -k(r)r^2 + \frac{2M(r)}{R} \tag{2}$$

and

$$4\pi\rho = \frac{\partial_r M(r)}{R^2\partial_r R}, \tag{3}$$

where $M(r)$ is an arbitrary function of the radial coordinate r. We assume that ρ is nonnegative and that R is monotonic with respect to r, i.e., $\partial_r R > 0$.

Following Tanimoto and Nambu [17], the solution to Eqs. (2) and (3), which represents the expanding universe, is written in the form

$$R(t,r) = (6M(r))^{1/3}(t - t_{\rm B}(r))^{2/3}\mathcal{S}(x), \tag{4}$$

$$x = k(r)r^2\left(\frac{t-t_{\rm B}(r)}{6M(r)}\right)^{2/3}, \tag{5}$$

where $t_{\rm B}(r)$ is an arbitrary function of the radial coordinate r and $\mathcal{S}(x)$ is the function defined in Ref. [17].

Following Refs.[8] and [9], we define the local Hubble function by

$$H(t,r) = \frac{\partial_t R}{R} \tag{6}$$

and the density-parameter function of dust as

$$\Omega_{\rm M}(t,r) = \frac{2M(r)}{H(t,r)^2R(t,r)^3}. \tag{7}$$

In LTB universes, we can define another expansion rate of the spatial length scale, the so-called longitudinal expansion rate, by

$$H^L(t,r) = \frac{\partial_t\partial_r R}{\partial_r R}. \tag{8}$$

In the case of homogeneous and isotropic universes, H^L agrees with H. Thus, if we can measure the difference between H and H^L, it can be used as an indicator of the inhomogeneity in the universe[13].

3 Numerical results

The two physical functional degrees of freedom are fixed by imposing the following conditions.

- Uniform big-bang time $t_{\rm B} = 0$.
- The angular diameter distance $D(z)$ is equivalent to that in the ΛCDM universe in all the redshift domain except in the vicinity of the symmetry center in which D is appropriately set so that the regularity of the spacetime geometry is guaranteed.

We have obtained the solution of the inverse problem by using the numerical procedure described in Ref.[20]. First, we express $\Omega_{\rm M}(t_0, r(z))$, $H(t_0, r(z))$, $H^L(t_0, r(z))$ as functions of the cosmological redshift z. We can see from these figures that the resultant inhomogeneity is a large-scale void structure. We

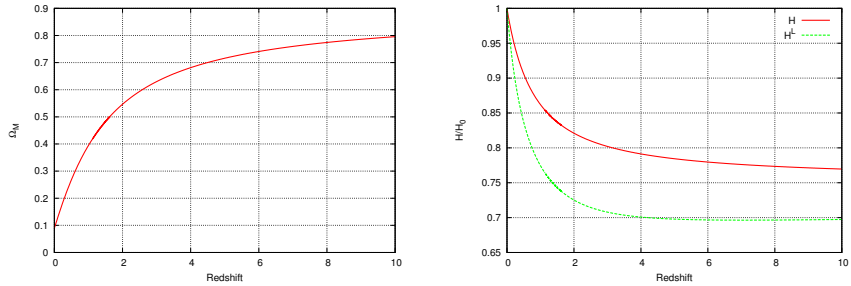

Figure 1: (left figure)Density-parameter functions $\Omega_{\rm M}(t_0, r(z))$ depicted as functions of the cosmological redshift. (right figure)Local Hubble function $H(t_0, r(z))$ and longitudinal expansion rate $H^L(t_0, r(z))$ depicted as functions of the cosmological redshift.

note that $H(t_0, r(z)) = H^L(t_0, r(z))$ in homogeneous and isotropic universes, whereas $H(t_0, r(z))$ and $H^L(t_0, r(z))$ are different from each other by about 10% for $2 \lesssim z < 10$ in the inhomogeneous case. This result means that, in order to fit the distance-redshift relation of the LTB model with observations that agree with that predicted by the concordance ΛCDM universe with $(\Omega_{\rm M0}, \Omega_{\Lambda 0}) = (0.3, 0.7)$, the scale of the inhomogeneity should be at least a few Gpc.

It is very important to study how to observationally distinguish these two models from each other. Here, we show that the temporal variation of the cosmological redshift is a useful observational quantity. In Fig. 2, we depict the derivative dz/dt_0 of the cosmological redshift with respect to the time t_0 of the observer at the symmetry center $r = 0$ as a function of the cosmological redshift itself. As can be seen

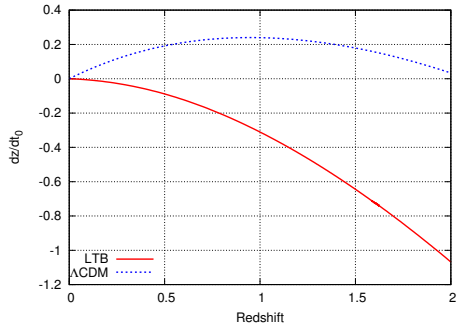

Figure 2: Time derivatives of the cosmological redshift depicted as functions of the cosmological redshift.

from this figure, dz/dt_0 is positive for $0 < z \lesssim 2$ in the case of the concordance ΛCDM model, while it is negative for all z in the LTB universe models with the uniform big-bang time. Therefore, if we observe whether dz/dt_0 is positive or negative for $z \lesssim 2$, we can distinguish our LTB model from the concordance ΛCDM model.

4 Summary and discussion

We have solved the inverse problem to construct an LTB universe model that has the same distance-redshift relation as that of the concordance ΛCDM model with $(\Omega_{\rm M0}, \Omega_{\Lambda 0}) = (0.3, 0.7)$, and we obtained solutions by numerical integration. Our results imply that it is possible to construct an inhomogeneous but isotropic universe model with a distance-redshift relation that agrees quite well with the observational data of the distance-redshift relation.

Our LTB universe model is regarded as an unnatural model from the viewpoint of the Copernican principle, because the observer stands exactly at the center of the isotropic universe. However, no observational data has yet been reported that entirely excludes inhomogeneous universe models. Therefore, it is important to know the type of inhomogeneous universes that can explain current observations and to propose observational methods for testing inhomogeneous universe models.

In this paper, we have also studied the temporal variation of the distance-redshift relation in our LTB universe model whose distance-redshift relation is the same as the concordance ΛCDM model with $(\Omega_{\rm M0}, \Omega_{\Lambda 0}) = (0.3, 0.7)$. The result implies that if we can observe the time derivative of the cosmological redshift with sufficient accuracy, we can distinguish our LTB model from the concordance ΛCDM universe model. We have $dz/dt_0|_{z=1} \sim 0.24 H_0$ for the concordance ΛCDM model, and thus, the variation of the cosmological redshift in one year is $\Delta z|_{z=1} \sim 1.8 \times 10^{-11} (H_0/75 \text{ km/s/Mpc})$. Thus, over ten years, $\Delta z|_{z=1}$ is larger than 10^{-10} for the concordance ΛCDM universe model, and this value will become observable in the near future as a result of technological innovations[18, 19].

References

[1] E. W. Kolb, arXiv:0709.3102.

[2] I. Zehavi, A. G. Riess, R. P. Kirshner and A. Dekel, Astrophys. J. **503** (1998), 483.

[3] K. Tomita, Astrophys. J. **529** (2000), 38.

[4] K. Tomita, Mon. Not. R. Astron. Soc. **326** (2001), 287.

[5] K. Tomita, Prog. Theor. Phys. **106** (2001), 929.

[6] H. Iguchi, T. Nakamura and K. Nakao, Prog. Theor. Phys. **108** (2002), 809.

[7] D. J. H. Chung and A. E. Romano, Phys. Rev. D **74** (2006), 103507.

[8] K. Enqvist and T. Mattsson, J. Cosmol. Astropart. Phys. **02** (2007), 019.

[9] K. Enqvist, Gen. Rel. Grav. **40** (2008), 451.

[10] G. Lemaitre, Gen. Rel. Grav. **29** (1997), 641.

[11] R. C. Tolman, Proc. Nat. Acad. Sci. **20** (1934), 169.

[12] H. Bondi, Mon. Not. R. Astron. Soc. **107** (1947), 410.

[13] C. Clarkson, B. A. Bassett and T. H.-C. Lu, Phys. Rev. Lett. **101** (2008), 011301.

[14] J.-P. Uzan, C. Clarkson and G. F. R. Ellis, Phys. Rev. Lett. **100** (2008), 191303.

[15] N. Mustapha, C. Hellaby and G. F. R. Ellis, Mon. Not. R. Astron. Soc. **292** (1997), 817.

[16] R. A. Vanderveld, E. E. Flanagan and I. Wasserman, Phys. Rev. D **74** (2006), 023506.

[17] M. Tanimoto and Y. Nambu, Class. Quantum Grav. **24** (2007), 3843.

[18] C.-H. Li *et al.*, Nature **452** (2008), 610.

[19] Liske, J. *et al.*, Mon. Not. R. Astron. Soc. **386** (2008), 1192.

[20] C. M. Yoo, T. Kai and K. Nakao, Prog. Theor. Phys. **120**, 937 (2008).

Black string perturbations and the Gregory-Laflamme instability

Alexander Zhidenko[1]

Instituto de Física, Universidade de São Paulo
C.P. 66318, 05315-970, São Paulo-SP, Brazil

Abstract

We study evolution of gravitational perturbations of black strings. Using numerical methods, we find the quasinormal modes and time-domain profiles of the black string perturbations in the stable sector and also show the appearance of the Gregory-Laflamme instability in the time domain. We observe the static solution of the wave equation at the threshold point of instability. The presented results were obtained together with R.A. Konoplya, Keiju Murata and Jiro Soda in [1].

1 Introduction

Unlike four dimensional Einstein gravity, which allows existence of black holes, higher dimensional theories, such as the brane-world scenarios and string theory, allow existence of a number of "black" objects: higher dimensional black holes, black strings and branes, black rings and saturns, D-branes and others. In higher than four dimensions we lack the uniqueness theorem, so that stability may be that criteria which will select physical solutions among this variety of solutions.

It is well known that the such black strings suffer from the so-called Gregory-Laflamme instability, which is the long wavelength gravitational instability of the scalar type of the metric perturbations [2, 3]. The threshold values of the wave vector k at which the instability appears are known [4]. We study the evolution of linear perturbations of D-dimensional black strings: quasi-normal ringing and late-time tales. We consider what happen on the edge of instability of black strings and how the perturbation develop in time in the stable and unstable sectors.

2 Perturbations of black strings

According to the brane-world scenarios, after a gravitational collapse of brane-localised matter, black objects with the horizon extended to the transverse extra direction will form. The simplest of such objects is black string, which looks like a black hole on the brane, being a direct product of a black hole and a circle.

$$ds^2 = -\left(1-\left(\frac{r_+}{r}\right)^n\right)dt^2 + \frac{dr^2}{1-\left(\frac{r_+}{r}\right)^n} + r^2 d\Omega_{n+1} + dz^2,$$

where

$$D = n+4, \qquad z \to z + 2\pi R,$$

and $d\Omega^2_{n+1}$ is the metric on a unit $(n+1)$-sphere.

The equations of the $(n+1)$-spherically symmetric perturbations of this metric can be reduced to the wave-like equations

$$\left(\frac{\partial^2}{\partial t^2} - \frac{\partial^2}{\partial r_\star^2} + V(r)\right)\Psi = 0, \tag{1}$$

where $dr_\star = \frac{dr}{f(r)}$ is the tortoise coordinate and the effective potential $V(r)$ is given by

$$V(r) = \frac{f(r)}{4r^2}\frac{U(r)}{\left(2k^2r^2 + n(n+1)(r_+/r)^n\right)^2},$$

[1]E-mail:zhidenko@fma.if.usp.br

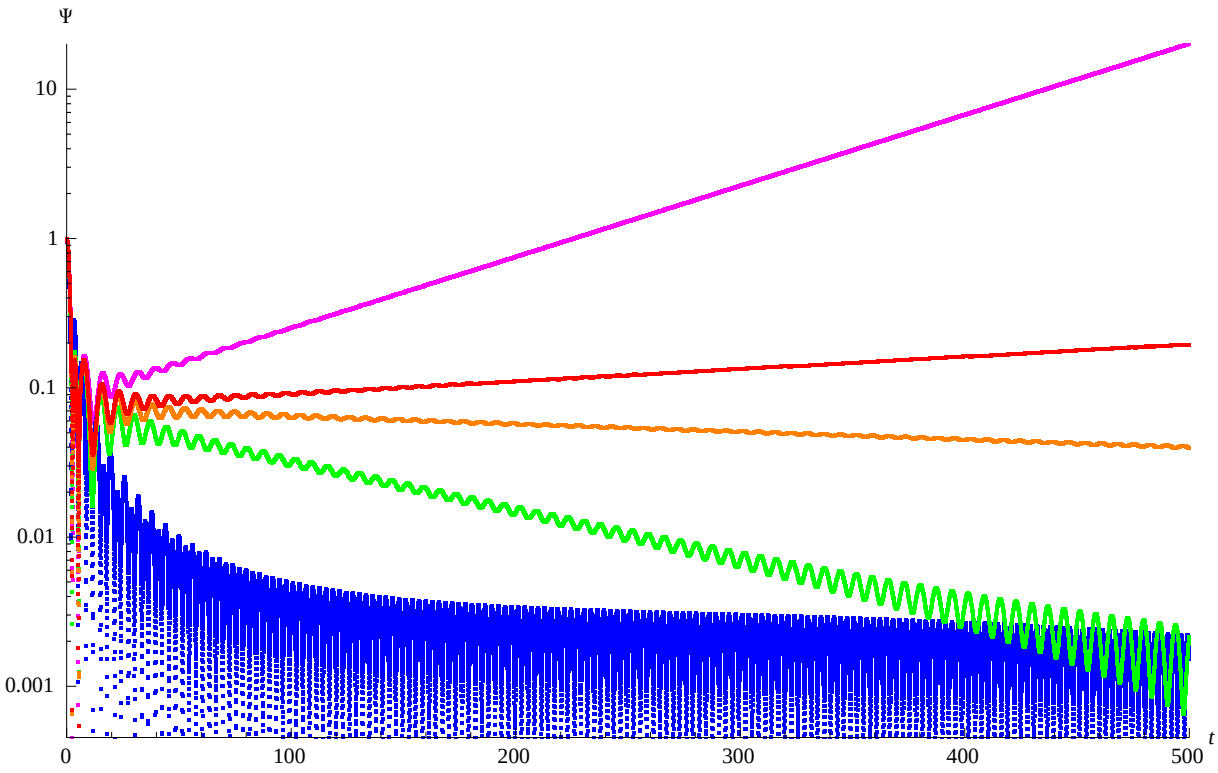

Figure 1: Time-domain profiles of black string $(n+1)$-spherically symmetric perturbations for $n=1$ $k=0.84$ (magenta, top), $k=0.87$ (red), $k=0.88$ (orange), $k=0.9$ (green), $k=1.1$ (blue, bottom). We can see two concurrent modes: for large Kaluza-Klein momentum k the oscillating mode dominates, near the critical value of k the dominant mode does not oscillate, for unstable values of k the dominant mode grows. The plot is logarithmic, so that strict lines correspond to an exponential decay. All quantities are measured in units of the radius of the event horizon r_+.

$$\begin{aligned} U(r) &= 16k^6r^6 + 4k^4r^4(n+5)(3f(r) - 2n + 3nf(r)) - \\ &\quad -4k^2r^2n(n+1)\left(n(n+5) + f(r)(2n^2+7n+9)\right)\left(\frac{r_+}{r}\right)^n - \\ &\quad -n^2(n+1)^3\left(f(r) - 2n + nf(r)\right)\left(\frac{r_+}{r}\right)^{2n}, \end{aligned}$$

k is the Kaluza-Klein momentum.

The equation (1) can be integrated using the Gundlah-Price-Pullin method [5].

On the figure 1 one can see the time-domain profiles of black string perturbations for various values of the Kaluza-Klein momentum.

- At large values of k, far from instability, the profile has qualitatively the same form as that for massive fields.
- When approaching the instability point, the non-oscillating mode becomes dominant.
- For low values of k (unstable regime), this non-oscillating mode is unstable.
- Exactly in the threshold point of instability we can find the non-oscillating and non-growing mode which correspond to a static solution of the perturbation equations of motion.

From the figure 2, we see that at the asymptotically late time the behavior is qualitatively the same as for massive fields. The Kaluza-Klein momentum k plays the role of the effective mass [6]

$$\Psi \propto t^{(D+2)/2} sin(kt), \qquad D \geq 7.$$

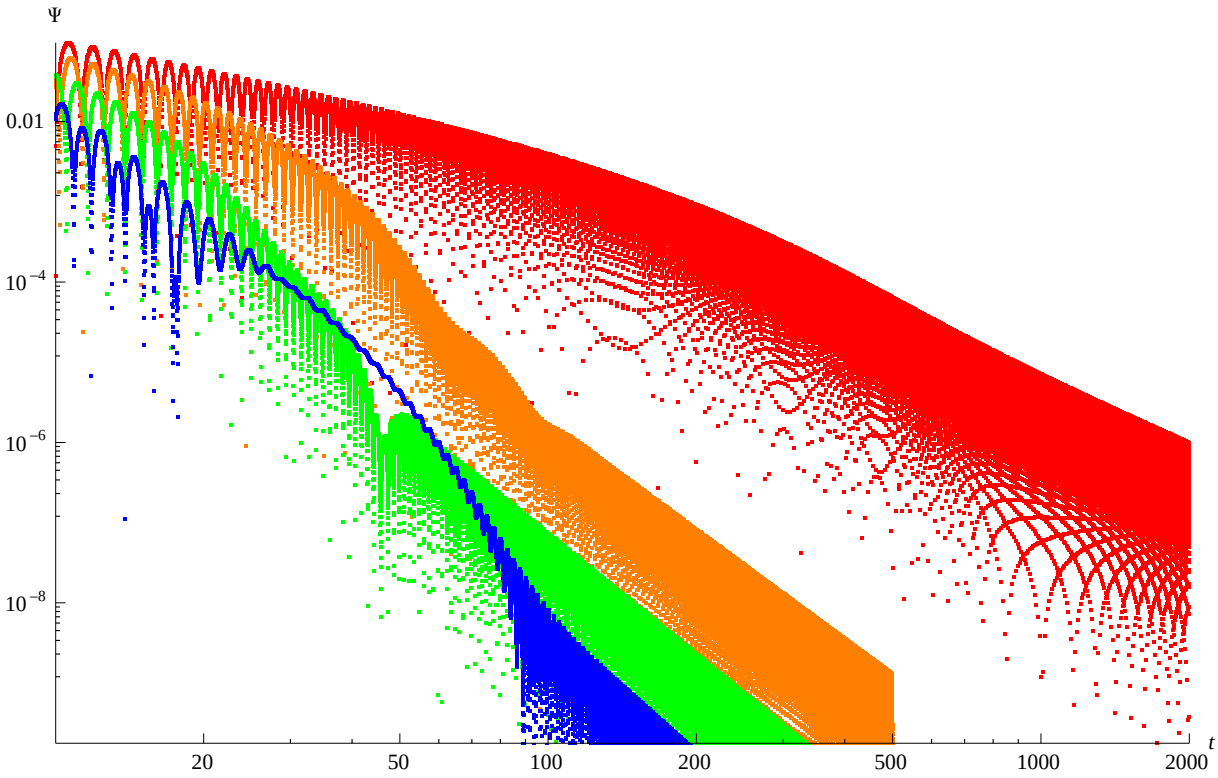

Figure 2: Time-domain profiles of black string $(n+1)$-spherically symmetric perturbations for $k = 2.5$ $n = 2$ (red, top), $n = 3$ (orange), $n = 4$ (green), $n = 5$ (blue, bottom). Late-time decay of perturbations for $n \geq 3$ is $\propto t^{-(n+6)/2}$. All quantities are measured in units of the radius of the event horizon r_+.

The first overtone's behavior is qualitatively similar to that of the fundamental mode for massive fields of higher-dimensional Schwarzschild black holes [7, 8]:

- For $D = 5$, as k grows, the imaginary part of the first overtone quickly decreases and vanishes for some threshold value of k, while its real part stays smaller than the threshold value of k. After the threshold value is reached, the first overtone "disappears".
- For $D \geq 6$, the imaginary part of the first overtone becomes small for large k, while the real part asymptotically approaches k.

3 Conclusions

1. We have found the quasinormal modes and late-time tails for scalar type of gravitational perturbations of D-dimensional black strings, that is for the type of perturbations where the Gregory-Laflamme instability forms.
2. In the stable sector the behavior of the perturbations evolution is qualitatively similar to the behavior of the scalar field in the Schwarzschild background.
3. The time domain profiles indicate that the threshold instability value of k corresponds to dominance of some static solution.

References

[1] R. A. Konoplya, K. Murata, J. Soda and A. Zhidenko, Phys. Rev. D **78**, 084012 (2008) [arXiv:0807.1897 [hep-th]].

[2] R. Gregory and R. Laflamme, Phys. Rev. Lett. **70**, 2837 (1993) [arXiv:hep-th/9301052].

[3] R. Gregory and R. Laflamme, Nucl. Phys. B **428** (1994) 399 [arXiv:hep-th/9404071].

[4] J. L. Hovdebo and R. C. Myers, Phys. Rev. D **73** (2006) 084013 [arXiv:hep-th/0601079].

[5] C. Gundlach, R. H. Price and J. Pullin, Phys. Rev. D **49**, 883 (1994) [arXiv:gr-qc/9307009].

[6] R. A. Konoplya, C. Molina and A. Zhidenko, Phys. Rev. D **75** (2007) 084004 [arXiv:gr-qc/0602047].

[7] A. Zhidenko, Phys. Rev. D **74** (2006) 064017 [arXiv:gr-qc/0607133].

[8] R. A. Konoplya and A. Zhidenko, Phys. Lett. B **609** (2005) 377 [arXiv:gr-qc/0411059].

Deparametrized Quantum Cosmology with Phantom Dust

Fumitoshi Amemiya[1] and Tatsuhiko Koike[2]

Faculty of Science and Technology, Keio University
3-14-1 Hiyoshi, Kohoku-ku, 223-8522 Yokohama Japan

Abstract

We study a canonical, reduced phase space quantization of the at Friedmann-Robertson-Walker universe which is formulated as a gauge invariant fashion in the classical theory. We construct a wave packet as the wave function of the universe and compute the expectation value of the scale factor. As a results, it is shown that the initial singularity of the universe is avoided in our models.

1 Introduction

The modern cosmolgy is mainly based on General Relativity (GR). However, since GR breaks down at the singularity, one must construct a quantum theory of gravity in order to understand what is occuring near the singularity. Because we still do not have a complete quantum theory of gravity, a number of works for this purpose have been done by rst carrying out a symmetry reduction, e.g. homogeneous and isotropic one, and then quantizing the resulting models. Although various interesting results are suggested so far, these previous works seem imcomplete at least in the sense that there are not enough considerarions for the problem of time, which is inevitable when one tries to quantize GR canonically. Roughly speaking, the problem of time is that the time evolution of a wave function is lost in canonical quantum gravity because time has no physical meaning in GR.

Recently Dittrich developed Rovelli's relational formalism [1] for constructing gauge invariant quantities [2, 3]. The application of this formalism to the Friedmann-Robertson-Walker (FRW) universe with dynamical dust [4] provide a possible resolultion to the problem of time. We assume that this dynamical dust has negative energy in order for the physical Hamiltonian to become positive di nite, and this dust is called Phantom dust [5]. In our study, we canonically quantize this gauge-invariantly reformulated FRW universe with Phantom dust by using a reduced phase space quantization method [6].

2 Relational formalism for deparametrized theories

In this section we summarize the relational formalism especially for deparametrized theories, which is enough to treat the FRW universe. Here, "deparametrized theory" means that one can nd phase space coordinates $\{q^a, T; p_a, P\}$ such that the constraints can be written in the form $C = P + h(q^a, p_a)$.

We consider the system which contains only one constraint for simplisity. In the relational formalism, the key observation to de ne gauge invariant quantities is as follows: Take two functions F and T. Then the value of F when $T =$ is gauge invariant even if F and T themselves are gauge variant respectively. We can interpret the function T as a clock. The mathematical de nition of the gauge invariant quantity $O_F(\ )$ is given by

$$O_F(\ ) := \ {}^t_C(F)|_{\ {}^t_C(T)=} \ . \tag{1}$$

Here, ${}^t_C(F)$ denotes the action of the gauge transformation generated by C on the function F, which is de ned as

$$\begin{aligned} {}^t_C(F) &:= \sum_{n=0}^{\infty} \frac{t^n}{n!} \{C, F\}_{(n)}, \\ \{C, F\}_{(0)} &:= F, \ \{C, F\}_{(n+1)} := \left\{C, \{C, F\}_{(n)}\right\}, \end{aligned} \tag{2}$$

[1] E-mail:famemiya@rk.phys.keio.ac.jp
[2] E-mail:koike@phys.keio.ac.jp

where t is a gauge parameter. In other words, $O_F(\ )$ can be interpreted as the gauge invariant extention of F along gauge orbits.

In order to reduce the phase space, we consider the map $O\ : F \mapsto O_F(\ )$ on the phase space coordinates $\{q^a, T; p_a, P\}$. The homomorphism property of the map O is used in the calculation below. The gauge invariant quantity associated to T,

$$O_T(\ ) = \ {}^{t}_{C}(T)|_{\ {}^{t}_{C}(T)=} \ = \ , \tag{3}$$

becomes simply a constant value . Then the same calculation associated to P on the constraint surface yields

$$O_P(\ ) = \ O_h(\ ) = h\left(O_{q^a}(\ ), O_{p_a}(\ )\right) =: \ H. \tag{4}$$

Thus $O_P(\ )$ is expressed in terms of $O_{q^a}(\ )$ and $O_{p_a}(\ )$ on the constraint surface. Finally, the Poisson bracket of $O_{q^a}(\ )$ and $O_{p_a}(\ )$ is given by

$$\{O_{q^a}(\ ), O_{p_a}(\ )\} = O_{\{q^a, p_b\}}(\ ) = O\ {}^{a}_{b}(\ ) = \ {}^{a}_{b}. \tag{5}$$

The above discussion shows that the reduced phase space is coordinatized by a conjugate pair $(O_{q^a}(\ ), O_{p_a}(\ ))$ and the symplectic structure has a simple expression in terms of them. Moreover, it is shown that the function H becomes a true physical Hamiltonian which generates the time evolution of the gauge invariant quantities:

$$\frac{\partial O_F(\ )}{\partial} = \{H, O_F(\ )\}. \tag{6}$$

Thus we now have the time evolution of the gauge invariant quantity, so that the problem of time has completely been resolved in the present case. Since the reduced phase space is characterized by (5) and (6), we can quantize the system by the ordinary quantization method with no constraints.

3 FRW universe with Phantom dust

In order to use the reduced phase space quantization method to the FRW universe, we must rst deparametrize the system. It is known that the system is completely deparametrized by adding the pressure free dust Lagrangian to the usual Einstein-Hilbert action [4]. We add the dust with negative energy, which is called Phantom dust as mentioned above.

The action of Phantom dust is given by

$$S_{\rm dust} = \ \frac{1}{2}\int_M d^4x\sqrt{\ g}\ \ (g^{\mu\nu}U_\mu U_\nu + 1). \tag{7}$$

Here, g is the determinant of the metric tensor $g_{\mu\nu}$ on the spacetime manifold M, is the energy density and the 1-form U is de ned by $U = \ dT + W_i dS^i$, where the vector eld $U^\mu = g^{\mu\nu}U_\nu$ is tangent to an a nely parametrized geodesic, T de nes the proper time along each geodesic and W_i and S^i are constants along geodesics. The variable S^i labels the geodesics along the uid particles. Phantom dust lls the spacetime, so that (T, S^i) can be used as coordinates on M.

In the case of the FRW universe, the Einstein-Hilbert action with Phantom dust is written as

$$S = \int dt\ \ p_a\dot{a} + PT_{,t} \quad NC^{\rm tot}\ \ , \tag{8}$$

$$C^{\rm tot} = C + P, \tag{9}$$

$$C = \ \ c^2\frac{p_a^2}{12a} + \frac{a^3}{\ } + \ {}_m a^3 \quad \frac{3ka}{\ }. \tag{10}$$

Here, a is the scale factor, p_a is its conjugate momentum, c is the speed of light, is the cosmological constant, ${}_m$ is the energy density of the matter except Phantom dust and the constant $k = \ 1, 0$ determine the curvature of the three dimensional space. In this work, we consider the $k = 0$ case which

corresponds to the at universe. In general, since the volume of the three-space and the Hamiltonian will diverge in the at case, we must get rid of this divergence. In the present work, we solve this problem by assuming that the topology of the universe is compact. For simplisity, we only consider the case of three-dimensional torus where the ducial cell is a cube. We shall interpret the scale factor as the length of an edge of the cube, which in fact represent the physical size of the universe.

The reduced phase space are coordinatized by

$$A(\ ) := O_a(\ ),\ P_A(\ ) := O_{p_a}(\ ) \tag{11}$$

and the symplectic structure is given by

$$\{A(\ ), P_A(\ )\} = 1. \tag{12}$$

The Hamiltonian which generates time evolution of gauge invariant variables becomes

$$\begin{aligned} H :&= h'(A, P_A) \\ &= \quad c^2 \frac{P_A^2}{12A} + \frac{A^3}{\quad} + \ {}_m A^3. \end{aligned} \tag{13}$$

4 Quantization of the model

In order to quantize the previously derived system, we simply replace the classical Poisson bracket relation and the Hamilton equation,

$$\{A, P_A\} = 1\ ,\ \frac{dF}{d} = \{H, F\}\ ,\ F = F(A, P_A), \tag{14}$$

with the quantum commutation relation and the Heisenberg equation,

$$[\hat{A}, \hat{P}_A] = i\hbar\ ,\ \frac{d\hat{F}}{d} = \frac{1}{i\hbar}[\hat{H}, \hat{F}]. \tag{15}$$

We choose the Schrodinger representation,

$$|\ \rangle \to \ \ (A),\ \hat{A}|\ \rangle \to A\ \ (A),\ \hat{P}_A|\ \rangle \to \ \ i\hbar\frac{\partial}{\partial A}\ \ (A). \tag{16}$$

Since we would like to restrict the range of the scale factor as $A \geq 0$, it is necessary to consider a condition to ensure the self-adjointness of the Hamiltonian in the space $L^2(0, \infty)$.

To this end, we choose the operator ordering of the Hamiltonian as

$$\hat{H} = \quad c^2 \frac{1}{12\hat{A}} \hat{P}_A^2 + \frac{\hat{A}^3}{\quad} + \ {}_m(\hat{A})\hat{A}^3 \tag{17}$$

and de ne the inner product by

$$\langle\ \ ,\ \ \rangle := \int_0^\infty \quad (A)\ \ (A) A dA. \tag{18}$$

Then, it can be shown that the following boundary conditions to a wave function ensure the self-adjointness of the Hamiltonian [7]:

$$(1)\quad (0, t) = 0, \quad \text{or} \quad (2)\ \frac{d}{dt}(0, t) = 0. \tag{19}$$

The Schrodinger-Wheeler-DeWitt equation (time-dependent Schrodinger equation) is

$$i\hbar\frac{\partial}{\partial} = \frac{c^2\hbar^2}{12A}\frac{\partial^2}{\partial A^2} + \quad \frac{A^3}{\quad} + \frac{R}{A} \quad , \tag{20}$$

where R is a constant which corresponds to the total energy of a radiation in the universe.

In this proceeding, we consider only the case $= R = 0$ in which one can analytically solve the di erential equation (20). The energy eigenvalue equation is

$$\frac{1}{4x}\frac{d^2 \ (x)}{dx^2} = E \ \ (x). \tag{21}$$

Here, we have introduced the dimensionless variables $x := \frac{A}{A_0}$ and $t := H_0$, where $A_0 := \frac{\hbar H_0}{_{c0}}$, $_{c0} = \frac{3H_0^2}{c^2}$ and H_0 is the present value of Hubble's constant. The general solution of this equation takes the form

$$\begin{aligned} (x) &= C_1 \mathrm{Ai}(\ \ y) + C_2 \mathrm{Bi}(\ \ y) \\ &= \sqrt{y} \ \ C_3 J_{\frac{1}{3}} \ \ \frac{2}{3} y^{\frac{3}{2}} \ \ + C_4 J \ _{\frac{1}{3}} \ \ \frac{2}{3} y^{\frac{3}{2}} \ \ , \end{aligned} \tag{22}$$

where y is given by $y := [4(\ _{\mathrm{m}} \ \ E)]^{\frac{1}{3}} x$, Ai and Bi are Airy functions, $J_{\pm\frac{1}{3}}$ are Bessel functions and C_j's are arbitrary constants. We can construct the following wave packets by superposing the energy eigenstates,

$$^{(1)}(x,t) = \frac{x}{(2 \ )^{\frac{4}{3}}} e^{\ \frac{x^3}{4\alpha} \ \ i\Omega_{\mathrm{m}} t}, \tag{23}$$

$$^{(2)}(x,t) = \frac{1}{(2 \ )^{\frac{2}{3}}} e^{\ \frac{x^3}{4\alpha} \ \ i\Omega_{\mathrm{m}} t}, \tag{24}$$

where $\quad := \quad i\frac{9}{16}t$. These wave packets correspond to the two types of boundary conditions (19). The expectation value of x is given by

$$\langle x \rangle = \frac{\int_0^\infty x \quad (x,t) x \quad (x,t) dx}{\int_0^\infty x \quad (x,t) \quad (x,t) dx}. \tag{25}$$

The calculation of the right hand side for the wave packets above leads to

$$\langle x \rangle^{(1)} = \frac{2 \quad \frac{5}{3}}{3 \quad \frac{7}{3}} \quad \frac{^2 + \ \frac{9}{16}t \ ^2}{2} \Bigg)^{\frac{1}{3}}, \tag{26}$$

$$\langle x \rangle^{(2)} = \frac{4}{3 \ \ 2^{\frac{1}{3}} \quad \frac{5}{3}} \quad \frac{^2 + \ \frac{9}{16}t \ ^2}{2} \Bigg)^{\frac{1}{3}}. \tag{27}$$

These solutions represent a bounsing universe with no singularity because the expectation value of x never goes to zero in both cases.

References

[1] C.Rovelli, Phys.Rev.D **42**, 2638 (1990)

[2] B.Dittrich, gr-qc/0411013

[3] B.Dittrich, Class.Quant.Grav. **23**, 6155 (2006)

[4] J.D.Brown and K.V.Kuchař, Phys.Rev.D **51**, 5600 (1995)

[5] K.Giesel, T.Thiemann, arXiv:0711.0119[gr-qc]

[6] T.Thiemann, Class.Quant.Grav. **23**, 1163 (2006)

[7] F.G.Alvarenga and N.A.Lemos, Gen.Rel.Grav. **30**, 681 (1998)

Influence of Dark Matter on Light Propagation in Solar System Experiment

Hideyoshi Arakida[1]

School of Education, Waseda University
1-6-1, Nishiwaseda, Shinjuku, Tokyo 169-8050 JAPAN

Abstract

We investigated the influence of dark matter on light/signal propagation in the solar system. We concentrated on the gravitational time delay and relative frequency shift and took the effect of solar system-bound dark matter into consideration. As the application of results, we considered the secular increasing of the astronomical unit reported by Krasinsky and Brumberg (2004).

1 Introduction

It is considered the dark matter is the essential component of the Universe, then it is worth to investigate the possibility to detect and estimate its abundance in our Solar System. Especially, recent astronomical/astrophysical measurements in the solar system have been grown drastically. Due to such a context, till now, the gravitational influence of dark matter on the planetary motion, such as the additional perihelion advance, has aroused interest and studied by several authors. The effect of galactic dark matter on the planetary dynamics are considered by [6, 12, 14, 15]. On the other hand, the upper limit of density of dark matter bound in the solar system has been estimated by [3, 8, 11, 9, 17, 10, 7]. Also planet-bound dark matter is evaluated by [1, 2].

While its contribution to the light/signal propagation has hardly been examined in disregard of the fact the current accurate observations are archived by the improvement of observational of light/signal and perhaps this advance will go on. Then from these situations, it is interesting to examine how the existence of dark matter bound in solar system affects the light/signal propagation and whether we can detect its traces from the observations of light/signal.

We will study the influence of dark matter on the light/signal propagation in the solar system. First, under the spherical symmetry, we derive the approximate solution of Einstein equation which consists of gravitational field due to the central celestial body as the Sun and the thin distributed dark matter surrounding to the external region of central body. Then we will concentrate on the light/signal propagation and calculate the additional effects due to the dark matter on the gravitational time delay and the relative frequency shift. As the application of results, we consider the problem of secular increase of astronomical unit (of length) AU reported by Krasinsky and Brumberg (2004) [13].

2 Approximate Solution of Einstein Equation

We seek the spherically symmetric form of spacetime as,

$$ds^2 = -e^{\quad} c^2 dt^2 + e^{\quad} dr^2 + r^2(d\theta^2 + \sin^2\theta d\phi^2), \tag{1}$$

where $\quad, \nu$ are the function of time t and radius r, and c is the speed of light in vacuum. As the stress-energy tensor T^{α}, we suppose as,

$$T^0_0 = -\varrho(t,r)c^2, \quad T^1_0 = \sigma(t,r)c, \quad T^i_j = 0. \tag{2}$$

T^0_0 is due to the dark matter density $\varrho(t,r)$ and let us choose the form of $\varrho(t,r)$ as,

$$\varrho(t,r) = \rho(t)\left(\frac{\ell}{r}\right)^k, \tag{3}$$

[1]E-mail:arakida@edu.waseda.ac.jp

in which ℓ is the normalizing factor and we put $\ell \simeq r_{\rm E}$ where $r_{\rm E}$ is the orbital radius of Earth, k is the exponent characterising r-dependence of $\varrho(t,r)$, and $\rho(t)$ represents the time variation of dark matter density, which is considered as the dark matter density around the Earth since $\ell \sim r_{\rm E}$. We retain time-dependence of $\rho(t)$ in order to formulate as general as possible and to apply to secular increase of astronomical unit discussed in Section 5. Nonetheless for the sake of simplicity, we specify $\rho(t)$ as, presuming the time variation of dark matter density in solar system is much slower,

$$\rho(t) \simeq \rho_0 + \left.\frac{d\rho}{dt}\right|_0 (t - t_0). \tag{4}$$

here subscript 0 denotes the initial epoch of ephemerides.

From Einstein equation $G \equiv R - (1/2)g R = (8\pi G/c^4)T$, as the approximate solution, we have,

$$ds^2 = -\left[1 - \frac{2}{c^2}U(t,r)\right]c^2dt^2 + \left[1 + \frac{2}{c^2}V(t,r)\right]dr^2 + r^2d\Omega^2, \tag{5}$$

where

$$U(t,r) = \frac{GM}{r} - \frac{4\pi G\rho(t)\ell^k}{(2-k)(3-k)}r^{2-k}, \quad V(t,r) = \frac{GM}{r} + \frac{4\pi G\rho(t)\ell^k}{3-k}r^{2-k}. \tag{6}$$

3 Gravitational Time Delay

In this section, we calculate the additional time delay due to the existence of dark matter. To begin with, we transform (5) into rectangular coordinates by the coordinate transformation $x = r\sin\theta\sin\phi, y = r\sin\theta\cos\phi, z = r\cos\theta$. And as the first approximation of light/signal path, we suppose the rectilinear motion along x-direction, $y = b =$ constant, $z = 0, r = \sqrt{x^2 + b^2}$. Then we have,

$$ds^2 = -\left(1 - \frac{2}{c^2}U\right)c^2dt^2 + \left(1 + \frac{2}{c^2}V\frac{x^2}{r^2}\right)dx^2. \tag{7}$$

World line of the light/signal is the null geodesic $ds^2 = 0$, hence we have from (7),

$$c\frac{dt}{dx} = 1 + \frac{1}{c^2}\left[\frac{GM}{r}\left(1 + \frac{x^2}{r^2}\right) - \frac{4\pi G\ell^k\rho(t)}{(2-k)(3-k)}r^{2-k} + \frac{4\pi G\ell^k\rho(t)}{3-k}\frac{x^2}{r^k}\right]. \tag{8}$$

As the $\rho(t)$ we adopt (4) and from (8) we reckon the time lapse. We assume the lapse time Δt is the linear combination of each effect as,

$$\Delta t = \Delta t_{\rm pN} + \Delta t_{{\rm dm}_0} + \Delta t_{{\rm dm}_t} \tag{9}$$

here $\Delta t_{\rm pN}$ corresponds to the Shapiro time delay in 1st post-Newtonian approximation, $\Delta t_{{\rm dm}_0}$ is due to the static part of dark matter density (ρ_0 of (4)) and $\Delta t_{{\rm dm}_t}$ is the contribution of time dependent part of dark matter density ($d\rho/dt|_0 t$ of (4)). The round-trip time in the coordinate time, ΔT is given by,

$$\begin{aligned}
\Delta T &= 2\frac{a_{\rm E} + a_{\rm R}}{c} + \frac{2GM}{c^3}\left[2\ln\frac{(a_{\rm E} + \sqrt{a_{\rm E}^2 + b^2})(a_{\rm R} + \sqrt{a_{\rm R}^2 + b^2})}{b^2}\right. \\
&\quad \left. - \left(\frac{a_{\rm E}}{\sqrt{a_{\rm E}^2 + b^2}} + \frac{a_{\rm R}}{\sqrt{a_{\rm R}^2 + b^2}}\right)\right] + \frac{2\pi G}{c^3}\left(\rho_0 + \left.\frac{d\rho}{dt}\right|_0 T\right)\mathcal{H}(a_{\rm E}, a_{\rm R}; k). \\
\mathcal{H}(a_{\rm E}, a_{\rm R}; k) &= H(0, a_{\rm E}; k) + H(0, a_{\rm R}; k)
\end{aligned} \tag{10}$$

$$H(x_1, x_2; k) = \begin{cases}
-2\ell b^2 \ln\frac{x_2 + \sqrt{x_2^2 + b^2}}{x_1 + \sqrt{x_1^2 + b^2}} & (k = 1) \\
\frac{2}{3}\left[\frac{1}{3}(x_2^3 - x_1^3) - b^2(x_2 - x_1)\right] & (k = 0) \\
-\frac{1}{12\ell}\left[3b^4 \ln\frac{x_2 + \sqrt{x_2^2 + b^2}}{x_1 + \sqrt{x_1^2 + b^2}}\right. & \\
\quad -2(x_2\sqrt{x_2^2 + b^2}^3 - x_1\sqrt{x_1^2 + b^2}^3) & \\
\quad \left. + 3b^2(x_2\sqrt{x_2^2 + b^2} - x_1\sqrt{x_1^2 + b^2})\right] & (k = -1)
\end{cases} \tag{11}$$

Let us estimate the extra time delay $\Delta T_{\rm dm}$. In this estimation, we set $\rho_0 \simeq 10^{-16}$ [g/cm^3] which is the largest upper limit from the dynamical perturbation on planetary motion. Since the part of $d\rho/dt|_0 T$ is anticipated to be much smaller than the dominant part of ρ_0, then we drop the $d\rho/dt|_0 T$ term here and evaluate,

$$\Delta T_{\rm dm} \simeq \frac{2\pi G\rho_0}{c^3}\mathcal{H}(a_{\rm E}, a_{\rm R}; k). \tag{12}$$

$\Delta T_{\rm dm}$ is approximately order of 10^{-20} [s] in the inner planetary region, while in the outer planetary region, $10^{-19} < \Delta T_{\rm dm} < 10^{-17}$ [s] for $k = 0$ and $10^{-16} < \Delta T_{\rm dm} < 10^{-14}$ [s] for $k = -1$. However, the current observational limit in the solar system is $\sim 10^{-8}$[s] or a few 100 [m] for planetary radar, 10^{-11}[s] or a few [m] for spacecraft ranging, and synchronization (internal) error of atomic clocks is $\sim 10^{-9}$ [s]. Then at this time, it is hard to extract the trace of dark matter from the existing observational data.

4 Relative Frequency Shift

Next using (11), we derive the relative frequency shift of light/signal y which is defined as,

$$y = \frac{\delta\nu}{\nu} \equiv -\frac{d\Delta T}{dt}. \tag{13}$$

When the light/signal passes near the limb of the Sun as the Cassini experiment [5], the conditions $a_{\rm E}, a_{\rm R} \quad b, da_{\rm E}/dt, da_{\rm R}/dt \ll db/dt$ hold, here $b = \sqrt{b_0^2 + (vt)^2}$. Then the relative frequency shift due to the gravitational field of the Sun $y_{\rm pN}$ and dark matter $y_{\rm dm}$ are obtained as,

$$y_{\rm pN} = \frac{8GM}{c^3 b}\frac{db}{dt} \tag{14}$$

$$y_{\rm dm} = \frac{\pi G}{c^3}\left(\rho_0 + \frac{d\rho}{dt}T\right)\mathcal{K}(a_{\rm E}, a_{\rm R}; k) \tag{15}$$

$$\mathcal{K}(a_{\rm E}, a_{\rm R}; k) = \begin{cases} 8b\ell\left(\ln\frac{4a_{\rm E}a_{\rm R}}{b^2} - 1\right)\frac{db}{dt} & (k=1) \\ \frac{8}{3}b(a_{\rm E}+a_{\rm R})\frac{db}{dt} & (k=0) \\ \frac{2}{\ell}b\left[b^2\ln\frac{4a_{\rm E}a_{\rm R}}{b^2} - (a_{\rm E}^2 + a_{\rm R}^2)\right]\frac{db}{dt} & (k=-1) \end{cases} \tag{16}$$

Approximately, the order of magnitude of $y_{\rm dm}$ is $\sim 10^{-25}$ but current threshold of relative frequency shift measurement is around 10^{-15} or better. Therefore expected frequency shift due to the dark matter is about 10 order of magnitude smaller than the present observational limit of relative frequency shift.

5 Application to Secular Increase of Astronomical Unit

In this section, we apply our result to the secular increase of astronomical unit (of length) AU reported by Krasinsky and Brumberg (2004) [13]. Astronomical unit AU is one of the important and fundamental astronomical constants which gives the relation of two length unit; 1 [AU] of astronomical system of units and 1 [m] of SI ones. Presently the astronomical unit AU is determined by using the planetary radar and spacecraft ranging data (the round-trip time of light/signal), and the latest value is, 1 [AU] = $1.495978706960 \times 10^{11} \pm 0.1$ [m] [16]. From the planetary ephemerides (the solution of equation of motion of planet), the theoretical value of round-trip time $t_{\rm theo}$ is calculated as, $t_{\rm theo} = d_{\rm theo}{\rm AU}/c$ [sA] where $d_{\rm theo}$ [AU] is the interplanetary distance calculated from the planetary ephemerides. Then $t_{\rm theo}$ [s] is compared with the observed round-trip time $t_{\rm obs}$ [s], and AU is optimized by the least square method. See e.g. Section 5 of [4] for more detail.

However, when Krasinsky and Brumberg set $t_{\rm theo}$ as,

$$t_{\rm theo} = \frac{d_{\rm theo}}{c}\left({\rm AU} + \frac{d{\rm AU}}{dt}T\right), \tag{17}$$

and fit to observational data, they found non-zero and positive value $d{\rm AU}/dt = 15\pm4$[m/century], where T is the time interval counted off from some initial epoch. The evaluated value $d{\rm AU}/dt = 15\pm4$ [m/century]

is about 100 times larger than the current determination error of AU. Here it is worth to note the observed $d\mathrm{AU}/dt$ does not mean the expansion of planetary orbit and/or increase of orbital period of planet. As a matter of fact, the determination error of the latest planetary ephemerides is much smaller than the reported $d\mathrm{AU}/dt$. The recent orbital determination error of lunar and planetary ephemerides is shown e.g. in Table 4. of [16]. Hence, $d\mathrm{AU}/dt$ may be caused not by dynamical perturbation on planetary motion but by the some influences on light/signal propagation.

Then, let us investigate whether the time variation of dark matter density in (11) explains the observed $d\mathrm{AU}/dt$. If we assume $d\mathrm{AU}/dt$ is related with $d\rho/dt|_0$, it follows,

$$\frac{d_{\mathrm{theo}}}{c}\frac{d\mathrm{AU}}{dt}T \sim \frac{2\pi G}{c^3}\left.\frac{d\rho}{dt}\right|_0 TR^3, \tag{18}$$

where approximately we set $\mathcal{H}(a_{\mathrm{E}}, a_{\mathrm{R}}; k) \sim R^3$ and R is the radius of sphere in which the light/signal propagates. Taking Earth–Mars ranging into account, we put $R \sim 1.52$ [AU] (the orbital radius of Mars). To cause the observed $d\mathrm{AU}/dt$, $d\rho/dt|_0$ must be the order of 10^{-9} [g/(cm^{3}s)] and we have $d\rho/dt|_0 T \sim 1$[g/cm^3] for $T \sim 100$ [y]. But this value corresponds to the density of water, thus this possibility is made an exception.

Krasinsky and Brumberg (2004) [13], and Arakida (2008) [4] attempted to explain $d\mathrm{AU}/dt$ in terms of the cosmological expansion. Further Krasinsky and Brumberg (2004) also considered the effect of solar mass loss and variation of gravitational constant, G. However it is shown that these effect is too small to give an explanation of observed $d\mathrm{AU}/dt$.

References

[1] Adler, S., 2008, arXiv:0808.0899

[2] Adler, S., 2008, arXiv:0808.2823

[3] Anderson, J. D., Lau, E. L., Taylor, A. H., Dicus, D. A., Teplitz, D. C., Teplitz, V. L., 1989, ApJ, **342**, 539.

[4] Arakida, H. 2009, New Astron., **14**, 264, arXiv:0808.3828

[5] Bertotti, B., Iess, L., and Tortora, P., 2003, Nature, 425, 374.

[6] Braginsky, V. B., Gurevich, A. V., and Zybin, K. P., 1992, Phys. Lett. A, **171**, 275.

[7] Frére, J.-M., Ling, F.-S., and Vertongen, G., Phys. Rev. D, 2008, **77**, id. 083005.

[8] Grøn, Ø., and Soleng, H, H. 1996, ApJ, **456**, 445.

[9] Iorio, L. 2006, J. Cosm. Astr Phys., **05**, 2.

[10] Khriplovich, I. B., 2007, Int. J. Mod. Phys. D, **16**, 1475.

[11] Khriplovich, I. B. and Pitjeva, E. V., 2006, Int. J. Mod. Phys. D, **15**, 616.

[12] Klioner, S. S., and Soffel, M. H., 1993, **184**, 41.

[13] Krasinsky, G. A. and Brumberg, V. A., 2004, Celest. Mech. Dyn. Astron., **90**, 267.

[14] Nordtvedt, K., 1994, ApJ, **437**, 529.

[15] Nordtvedt, K., and Soffel, M. H., 1995, A&A, **293**, L73.

[16] Pitjeva, E. V., 2005. Solar Syst. Res., 39, 176.

[17] Sereno, M., and Jetzer, Ph., 2006, MNRAS, **371**, 626.

Bound geodesics in Kerr space time

Ryuichi Fujita[1] and Wataru Hikida[2]

[1] *Theoretical Physics, Raman Research Institute, Bangalore 560 080, India*
[2] *Department of Earth and Space Science, Graduate School of Science, Osaka University, Toyonaka, Osaka 560-0043, Japan*

Abstract

We derive the analytical solutions of the bound timelike geodesic orbits in Kerr spacetime. The analytical solutions are expressed in terms of the elliptical integrals using Mino time λ. Mino time is useful to understand physical properties of Kerr geodesics since it decouples radial and polar motion of a particle. Then, we can estimate the fundamental frequencies of the orbits such as radial, polar and azimuthal motion, and the Fourier series of arbitrary functions of particle's orbits. In this paper, we derive the analytical expression of both the fundamental frequencies and the orbits in terms of the elliptical integrals using Mino time. We can use these analytical expressions to investigate physical properties of Kerr geodesics and immediately apply them to the estimation of gravitational waves from the extreme mass ration inspirals.

1 Introduction

One of the main subjects to understand the properties of Kerr black hole spacetime is the geodesic motion. A lot of studies of the geodesic motion in black hole spacetime are summarized in the classical text book of Chandrasekhar[1]. In the weak eld regime, the orbits of a particle is almost same as that of Newton gravity. In the strong eld regime, however, the orbits show quite complicated trajectories. For the case of bound geodesics, this can be explained by mismatches between fundamental frequencies of radial, $_r$, polar, and azimuthal-motion, $_\phi$. $_\phi$ shows the precession of orbital plane and $_\phi$ $_r$ shows the precession of orbital ellipse. These mismatches become larger as the particle goes to strong gravity region around black hole horizon or separatrix, which is the boundary between stable and unstable orbits. These relativistic e ects are studied for some cases and some sorts of extreme phenomena, such as horizon-skimming orbits[2, 3, 4] and zoom-whirl orbits[5], are found.

Therefore the fundamental frequencies play important roles to understand geodesic orbits. However, the coupling of both r and motions in geodesics equation has been preventing us from deriving the fundamental frequencies, $_r$, and $_\phi$, for bound geodesic orbits until recently. Using elegant Hamilton-Jacobi formalism, Schmidt[6] derived the fundamental frequencies without discussing the coupling of both r and motions. Mino[7] decoupled both r and motions introducing a new time parameter λ, which is called Mino time. Then Drasco and Hughes[8] rederived the fundamental frequencies using Mino time and showed how to compute the Fourier components of arbitrary functions of orbits. These facts enable us to compute gravitational waves from extreme mass ratio inspirals(EMRIs) in the case of bound geodesics.

In this paper, we derive the analytical expression of both the fundamental frequencies and the orbits in Kerr spacetime. This analytical expressions help us to discuss bound geodesics in Kerr spacetime. Moreover, it enables us to compute gravitational waves from EMRIs more accurately since we can compute the orbits with the arbitrary accuracy in principle. This paper is organized as follows. In Sec. 2, we review Kerr geodesics in Mino time. In Sec. 3, we brie y show how to derive the analytical expressions of the fundamental frequencies of bound geodesics in terms of the elliptic integrals. And we summarize this paper in Sec. 4. Throughout this paper, we use units with $G = c = 1$.

[1] E-mail:draone@rri.res.in
[2] E-mail:hikida@vega.ess.sci.osaka-u.ac.jp

2 Geodesic Orbits in Kerr Spacetime

The geodesic equations that describes particle's orbits in Kerr spacetime are given by

$$\left(\frac{dr}{d\lambda}\right)^2 = R(r), \qquad \left(\frac{d\cos}{d\lambda}\right)^2 = (\cos),$$
$$\frac{dt}{d\lambda} = T_{\rm r}(r) + T(\cos) + a\mathcal{L}_z, \qquad \frac{d}{d\lambda} = {}_{\rm r}(r) + (\cos) \quad a\mathcal{E}, \tag{1}$$

where the functions $R(r)$, $(\cos)$,$T_{\rm r}(r)$, $T(\cos)$, ${}_{\rm r}(r)$ and $(\cos)$ are de ned by

$$\begin{aligned} R(r) &= [P(r)]^2 \quad [r^2 + (a\mathcal{E} \quad \mathcal{L}_z)^2 + \mathcal{C}], \\ (\cos) &= \mathcal{C} \quad (\mathcal{C} + a^2(1 \quad \mathcal{E}^2) + \mathcal{L}_z^2)\cos^2 \quad + a^2(1 \quad \mathcal{E}^2)\cos^4 \quad , \\ T_r(r) &= \frac{r^2 + a^2}{\quad} P(r), \quad T(\cos) = \quad a^2\mathcal{E}(1 \quad \cos^2 \quad), \\ {}_r(r) &= \frac{a}{\quad} P(r), \qquad (\cos) = \frac{\mathcal{L}_z}{1 \quad \cos^2}, \end{aligned}$$

with $P(r) = \mathcal{E}(r^2 + a^2) \quad a\mathcal{L}_z$, $= r^2 + a^2\cos^2$ and $= r^2 \quad 2Mr + a^2$. Here M and a are the mass and the angular momentum of the black hole, respectively. λ is Mino time de ned by $\lambda = \int d \ / \ $, where is proper time along geodesics. There are three constants of motion, $\mathcal{E}$, $\mathcal{L}_z$ and $\mathcal{C}$, which are the energy, the z-component of the angular momentum and the Carter constant per unit mass, respectively.

In Eq. (1), $dr/d\lambda$ depends only on r and $d\cos \ /d\lambda$ depends only on $\cos$. Thus, for the bound orbits, $r(\lambda)$ and $\cos$ (λ) become periodic functions which are independent of each other. The fundamental periods for the radial and polar motion, ${}_r$ and , with respect to λ are given by

$${}_r = 2\int_{\rm r_{min}}^{\rm r_{max}} \frac{dr}{\sqrt{R(r)}}, \qquad = 4\int_0^{\cos \ {}_{\rm min}} \frac{d\cos}{\sqrt{\ (\cos \ )}}, \tag{2}$$

where

$$r_{\rm min} = \frac{pM}{1+e}, \quad r_{\rm max} = \frac{pM}{1 \quad e}, \qquad {}_{\rm inc} + (\mathrm{sgn}\,\mathcal{L}_z) \ {}_{\rm min} = \frac{}{2}. \tag{3}$$

Here $r_{\rm min}$ and $r_{\rm max}$ is periapsis and apoapsis for the radial motion respectively, and ${}_{\rm inc}$ is the inclination angle from the equatorial plane of black hole. Of course, $(\mathcal{E}, \mathcal{L}_z, \mathcal{C})$ are described by these orbital parameters $(p, e, \ {}_{\rm inc})$ and given in Ref.[6, 8].

Then the angular frequencies of the radial and the polar motion become

$${}_r = \frac{2}{r}, \qquad = \frac{2}{\quad}. \tag{4}$$

Integral forms of $t(\lambda)$ and (λ) sre given by

$$t(\lambda) = \ \lambda + t^{(r)}(\lambda) + t^{(\ )}(\lambda), \qquad (\lambda) = \ {}_\phi\lambda + \ {}^{(r)}(\lambda) + \ {}^{(\ )}(\lambda), \tag{5}$$

where and ${}_\phi$ are the frequencies of coordinate time t and with respect to λ respectively, which are given by

$$= \ {}_{t^{(r)}} + \ {}_{t^{(\theta)}} + a\mathcal{L}_z, \qquad {}_\phi = \ {}_{\phi^{(r)}} + \ {}_{\phi^{(\theta)}} \quad a\mathcal{E}, \tag{6}$$

where

$$\begin{aligned} {}_{t^{(r)}} &= \tfrac{2}{\Lambda_r}\textstyle\int_{r_{\rm min}}^{r_{\rm max}} \frac{T_r(r)}{\sqrt{R(r)}}dr, \qquad {}_{t^{(\theta)}} = \tfrac{4}{\Lambda_\theta}\textstyle\int_0^{\cos \ {}_{\rm min}} \frac{T_\theta(\cos \ )}{\sqrt{\Theta(\cos \ )}}d\cos \ , \\ {}_{\phi^{(r)}} &= \tfrac{2}{\Lambda_r}\textstyle\int_{r_{\rm min}}^{r_{\rm max}} \frac{{}_r(r)}{\sqrt{R(r)}}dr, \qquad {}_{\phi^{(\theta)}} = \tfrac{4}{\Lambda_\theta}\textstyle\int_0^{\cos \ {}_{\rm min}} \frac{{}_\theta(\cos \ )}{\sqrt{\Theta(\cos \ )}}d\cos \ , \end{aligned} \tag{7}$$

and $t^{(r)/(\ )}$ and ${}^{(r)/(\ )}$ are given by

$$t^{(r)}(\lambda) \quad = \quad \int_{r_{\rm min}}^{r[\ ]} \frac{T_{\rm r}(r) \qquad {}_{t^{(r)}}}{\sqrt{R(r)}}dr, \quad t^{(\ )}(\lambda) = \int_0^{\cos \ [\ ]} \frac{T(\cos \ ) \qquad {}_{t^{(\theta)}}}{\sqrt{\ (\cos \ )}}d\cos \ ,$$

$$^{(r)}(\lambda) \quad = \quad \int_{r_{\min}}^{r[\ ]} \frac{_{\mathrm{r}}(r) \quad ^{\phi(r)}}{\sqrt{R(r)}} dr, \qquad ^{(\ )}(\lambda) = \int_0^{\cos\ [\ ]} \frac{(\cos\ ) \quad ^{\phi(\theta)}}{\sqrt{\ (\cos\ )}} d\cos\ . \tag{8}$$

Eq. (5) shows that both $t(\lambda)$ and (λ) are decomposed into two parts, in which the rst term represents accumulation over λ-time and the last two terms represent oscillation from it with periods $2\ /\ _r$ and $2\ /\ $. We note that the frequencies with respect to λ are related to the frequencies with distant observer time as[8]

$$_r = \frac{r}{}, \qquad = —, \qquad _\phi = \frac{\phi}{}. \tag{9}$$

3 Analytical solutions of bound geodesics

Since both $R(r)$ and $(\cos\ )$ are forth order polynomials, Eq. (2) can be expressed in terms of the elliptic integrals. It is useful if we know the four zero points of both $R(r)$ and $(\cos\ )$. We rewrite $R(r)$ and $(\cos\ )$ as[8]

$$\begin{array}{rcl} R(r) & = & (1 \quad \mathcal{E}^2)(r_1 \quad r)(r \quad r_2)(r \quad r_3)(r \quad r_4), \\ (\cos\ ) & = & \mathcal{L}_z^2\ _0(z \quad \cos^2\ )(z_+ \quad \cos^2\ ), \end{array} \tag{10}$$

where

$$\begin{array}{rcl} r_1 = \dfrac{pM}{1 \quad e}, \quad r_2 & = & \dfrac{pM}{1+e}, \quad r_3 = \dfrac{(A+B) + \sqrt{(A+B)^2 \quad 4AB}}{2}, \quad r_4 = \dfrac{AB}{r_3}, \\ A+B & = & \dfrac{2M}{1 \quad \mathcal{E}^2} \quad (r_1+r_2), \quad AB = \dfrac{a^2\mathcal{C}}{(1 \quad \mathcal{E}^2)\, r_1 r_2}, \end{array} \tag{11}$$

and where $_0 = a^2(1 \quad \mathcal{E}^2)/\mathcal{L}_z^2$, $z \ = \cos^2\ _{\min}$ and $z_+ = \mathcal{C}/(\mathcal{L}_z^2\ _0 z\ )$. We note that two zero points, r_1 and r_2, of $R(r)$ are apoapsis and periapis respectively and two zero point, z and z , of $(\cos\ )$ are $_{\min}$ and $_{\min}$ respectively. These zero points correspond to turning points, de ned in Eq. (3), of radial and polar motion. But the other two zero points of both $R(r)$ and $(\cos\ )$, r_3, r_4 and z_+, do not correspond to turning points of radial and polar motion, but represent zero points of them.

Using Eq. (10), we can express Eq. (2) in terms of the elliptic integrals as

$$\begin{array}{rcl} \displaystyle\int_{r_2}^{r} \frac{dr}{\sqrt{R(r)}} & = & \dfrac{2}{\sqrt{(1 \quad \mathcal{E}^2)(r_1 \quad r_3)(r_2 \quad r_4)}} F(\arcsin y_r, k_r), \\ \displaystyle\int_0^{\cos} \frac{d\cos}{\sqrt{\ (\cos\ )}} & = & \dfrac{1}{\mathcal{L}_z\sqrt{\ _0 z_+}} F(\arcsin y\ , k\ ), \end{array} \tag{12}$$

where

$$\begin{array}{rcl} y_r & = & \sqrt{\dfrac{r_1 \quad r_3}{r_1 \quad r_2}\dfrac{r \quad r_2}{r \quad r_3}}, \quad k_r = \sqrt{\dfrac{r_1 \quad r_2}{r_1 \quad r_3}\dfrac{r_3 \quad r_4}{r_2 \quad r_4}}, \\ y & = & \dfrac{\cos}{\sqrt{z}}, \quad k \ = \sqrt{\dfrac{z}{z_+}}, \end{array} \tag{13}$$

and $F(\varphi, k)$ is the incomplete elliptic integral of the rst kind.

Therefore orbital frequencies of radial and polar motion with respect to λ are given by

$$_r = \frac{\sqrt{(1 \quad \mathcal{E}^2)(r_1 \quad r_3)(r_2 \quad r_4)}}{2K(k_r)}, \qquad = \frac{\mathcal{L}_z\sqrt{\ _0 z_+}}{2K(k\ )}. \tag{14}$$

Here $K(k)$ is the complete elliptic integral of the rst kind de ned by $K(k) = F(\ /2, k)$. Using Eq. (13), it is straightforward to express and $_\phi$ in terms of the complete elliptic integrals. Explicit forms of and $_\phi$ will be given in elsewhere. Basically, geodesic orbits are derived by replacing the complete elliptic integrals of the fundamental frequencies with the elliptic integrals. Again, explicit forms of geodesic orbits will be given in elsewhere. We compare our analytical results of bound geodesics with that of numerical integration method as a consistency check in Fig. 1. This gure shows that the analytical solutions of geodesic equation in this paper exactly represent the solutions of bound geodesics in Kerr spacetime.

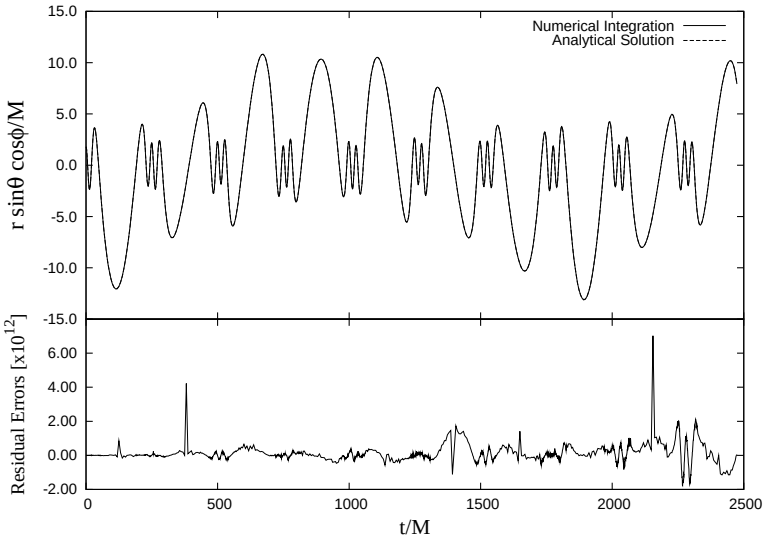

Figure 1: Plots of function $x(t) = r(t)\sin\ (t)\cos\ (t)$ using both analytical expressions and numerical integration method. In this gure, we set orbital elements as $a = 0.9M$, $p = 4M$, $e = 0.7$ and $_{\rm inc} = 40$. Upper gure shows plots of both analytical solution, $x_{\rm A}(t)$, and numerical integration method, $x_{\rm N}(t)$. Lower gure shows the residual errors, $x_{\rm A}(t)$ $x_{\rm N}(t)$.

4 Summary

We derived the analytical solutions of the bound timelike geodesics in Kerr spacetime. We expressed these solutions in terms of the elliptic integrals using Mino time. Since Mino time decouples both r and -motion, it is straightforward to express the orbits in terms of the elliptic integrals if we suitably transform variables, r and .

We can apply these solutions to the computation of gravitational waves from extreme mass ratio inspirals, which are one of the main targets for space-based gravitational waves antenna LISA[9]. Using the analytical solution in this paper, we can compute the orbits arbitrary accuracy in principle. Thus it is very useful to compute gravitational waves from EMRI. We may also apply these solutions to investigate the properties of timelike and null geodesics in the case of both bound and unbound orbits. All of them will be discussed in future work.

References

[1] S. Chandrasekhar, *Mathematical theory of black holes*, Oxford University Press, 1983.

[2] D. C. Wilkins, Phys. Rev. D **5**, 814 (1972).

[3] S.A. Hughes, Phys. Rev. D **63**, 064016 (2001).

[4] E. Barausse, S. A. Hughes and L. Rezzolla, Phys. Rev. D **76**, 044007 (2007).

[5] K. Glampedakis and D. Kenne ck, Phys. Rev. D **66**, 044002 (2002).

[6] W. Schmidt, Class. Quantum Grav.**19**, 2743 (2002).

[7] Y. Mino, Phys. Rev. D **67**, 084027 (2003).

[8] S. Drasco and S. A. Hughes, Phys. Rev. D **69**, 044015 (2004).

[9] LISA web page : *http://lisa.jpl.nasa.gov/*

Cosmology of multigravity

Teruki Hanada[1], Kazuhiko Shinoda[2] and Kiyoshi Shiraishi[3]

Graduate School of Science and Engineering, Yamaguchi University, Yoshida, Yamaguchi-shi, Yamaguchi 753–8512, Japan

Abstract

We have constructed a nonlinear multi-graviton theory. An application of this theory to cosmology is discussed. We found that scale factors in a solution for this theory repeat acceleration and deceleration.

1 Introduction

We have constructed a nonlinear multi-graviton theory [1] so far. The features of our model are following: (i) Gravitons as the fluctuation from Minkowski spacetime have a Fierz-Pauli (FP) type mass [2]. (ii) This model based on dimensional deconstruction method. So, we can tune the mass spectrum more easily than Kaluza-Klein theory. (iii) The mass term has a reflection symmetry at each vertex and a exchange symmetry at each edge of a graph.

In this article, beginning with graph theory, dimensional deconstruction [3, 4] and our model are reviewed (see also [5, 6]). Next, we consider the vacuum cosmological solutions of the case with the four-site star graph and the four-site path graph. Finally, we summarize our work and remark about the outlook.

2 A review of graph theory and dimensional deconstruction

2.1 Graph theory

We consider the matrix representation of graph theory.[4] A graph G is a pair of V and E, where V is a set of vertices while E is a set of edges. An edge connects two vertices; two vertices located at the ends of an edge e are denoted as $o(e)$ and $t(e)$. Then, we introduce two matrices, an incidence matrix and a graph Laplacian, associated with a specific graph. The incidence matrix represents the condition of connection or structure of a graph, and the graph Laplacian Δ can be obtained by EE^T . By use of these matrices, a quadratic form of vectors $a^T\Delta a(= a^T EE^T a)$ can be written as a sum of $(a_i\Delta_{ij}a_j)$. If all $a_i(i = 1, 2, ..., \sharp V)$, components of a, take the same value, $E^T a = 0$ and then $a = 0$.

2.2 Dimensional deconstruction

It is assumed that we put fields on vertices or edges. An idea that there are four dimensional fields on the sites (vertices) and links (edges), dubbed as dimensional deconstruction, is introduced by Arkani-Hamed *et al.*. In this scheme, the square of mass matrix is proportional to the Laplacian of the associated graph. In the case of a cycle graph (a 'closed circuit') with N sites (C_N), when N becomes large, the model on the graph corresponds to the five-dimensional theory with S^1 compactification. In other words, the mass scale of the model f over N corresponds to the inverse of the compactification radius $L/(2\pi)$:

$$M_\ell^2 = 4f^2(\sin \pi\ell/N)^2 \quad \rightarrow \quad M_\ell^2 = (2\pi\ell/L)^2 \qquad (f/N \rightarrow 1/L).$$

For a cycle graph, the linear graviton model presented in the previous work [1] coincides with the FP model proposed in [2]. The model is a most general linear graviton theory on a generic graph.

[1]E-mail:k004wa@yamaguchi-u.ac.jp
[2]E-mail:k009vc@yamaguchi-u.ac.jp
[3]E-mail:shiraish@yamaguchi-u.ac.jp
[4]Please see [7] for a review of application of graph theory to field theory.

3 Nonlinear multi-graviton theory on a graph

We consider a nonlinear multigravity on a graph. Following Nibbelink *et al.* [8, 9], we introduce the important 'tool':

$$\langle ABCD\rangle \equiv -\varepsilon_{abcd}\varepsilon^{\mu\nu\rho\sigma}A^a_\mu B^b_\nu C^c_\rho D^d_\sigma,$$

where ε is the totally antisymmetric tensor. Using this tool, we have the Einstein-Hilbert term replacing A and B by vierbeins and C and D by a curvature 2-form. In addition, because fourth power of vierbein in the angle brackets is equal to the determinant of vierbeins, the use of this tool illuminates that the Einstein-Hilbert term and the cosmological term have the same structure.

We assume the following term for each edge of a graph form;

$$\langle (e_1e_1 - e_2e_2)^2\rangle,$$

where e_1 and e_2 are vierbeins at two ends of one edge. This term has a reflection symmetry $e \leftrightarrow -e$ at each vertex and an exchange symmetry $e_1 \leftrightarrow e_2$ at each edge.

In the weak-field limit, $e_1 = \eta + f_1, e_2 = \eta + f_2$,

$$\langle (e_1e_1 - e_2e_2)^2\rangle = 8\left(([f_1]-[f_2])^2 - \left[(f_1-f_2)^2\right]\right) + O(f^3),$$

where η is Minkowski metric, and $[f] = \mathrm{tr}f$ for notational simplicity. This quadratic term corresponds to the FP mass term [5] . On the other hand, $\frac{1}{2}|e|R$ contains the kinetic terms of a graviton in the leading order.

Therefore, in the case of the tree graph, we have the nonlinear Lagrangian of multi-graviton theory without higher derivertive and non-local terms,

$$L_0 = \frac{1}{2}\exp\Phi\sum_{v\in V}|e^v|\,R^v + M^2\sum_{e\in E}\left\langle \left(e_{o(e)}e_{o(e)} - e_{t(e)}e_{t(e)}\right)^2\right\rangle,$$

where $M^2 \equiv m^2/16$ and we assume $\phi_1 = \phi_2 = \cdots = \phi_N = \Phi$.

4 Vacuum cosmological solution

Now we consider two vacuum cosmological models, based on the four-site star graph and the four-site path graph. We assume the following metric;

$$g_{\mu\nu}dx^\mu dx^\nu = -e^{\Phi(t)}dt^2 + e^{\Phi(t)+2a_i(t)}(dr^2 + r^2d\Omega^2)$$

where $\Phi(t)$ is a scalar field and $a_i (i = 1, \cdots, 4)$ are scale factors. Then,

$$\left\langle (e_ie_i - e_je_j)^2\right\rangle = e^{-2\Phi(t)}(e^{2a_i(t)} - e^{2a_j(t)})^2.$$

In the case of the star graph, the Lagrangian is following;

$$L = \frac{1}{2}\exp\Phi(t)\sum_{i=1}^{4}|e^i|R^i + M^2\sum_{i=2}^{4}\left\langle (e_1e_1 - e_ie_i)^2\right\rangle,$$

where, a_1 is on the center of the graph. On the other hand, the Lagrangian of the case of the path graph is

$$L = \frac{1}{2}\exp\Phi(t)\sum_{i=1}^{4}|e^i|R^i + M^2\sum_{i<j}\left\langle (e_ie_i - e_je_j)^2\right\rangle,$$

where, a_1 and a_4 are on each end of the graph.

We show the results of numerical calculations of the two models on the same initial conditions in Figure 1 and Figure 2. Both scalar fields behave similarly and each scale factor repeats the increase and

[5] It is known that the asymmetric part of f can be omitted. [10]

the decrease. However, the scalar field in the star graph case changes slightly slower than the other. The oscillation of the scale factors in the path graph case include more modes of different frequencies than that of the scale factors in the star graph case.

The star graph model has more symmetries than the path graph model. A lot of modes in the star graph case degenerate. In the path graph case, increase of the number of sites gives the more complicated behaviors of the scale factors. On the other hand, in the star graph case, the symmetries are preserved if the number of sites are inceased. Therefore, the behaviors of the scale factors are the same as the four-site model, essentially.

5 Summary and prospects

We considered the four-site star and path graph model and found that vacuum cosmological solutions with the scale factors show the repeated accelerating and decelerating expansions. The differences between these two models were discussed from a viewpoint about symmetries.

As the future works, we should investigate the case that the matter fields exist. We also should investigate the models based on arbitrary tree graphs.

Acknowledgements

The authors would like to thank N. Kan and K. Kobayashi for useful comments, and also the organizers of JGRG18.

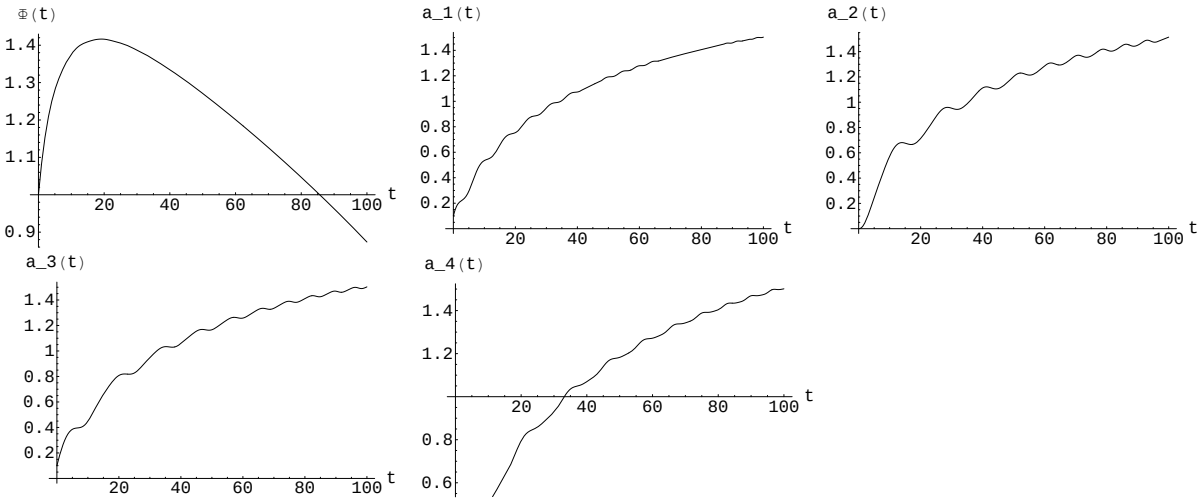

Figure 1: A numerical solutions of the scale factors in the case of the four-site star graph.

References

[1] T. Hanada, K. Shinoda and K. Shiraishi, to appear in Proceedings of the Seventeenth Workshop on General Relativity and Gravitation (Nagoya University, Nagoya, December 2-6, 2007) arXiv:0801.2641[gr-qc].

[2] M. Fierz and W. Pauli, Proc. Roy. Soc. Lond. **A173** (1939) 211.

[3] N. Arkani-Hamed, A. G. Cohen and H. Georgi, Phys. Rev. Lett. **86** (2001) 4757; Phys. Lett. **B513** (2001) 232.

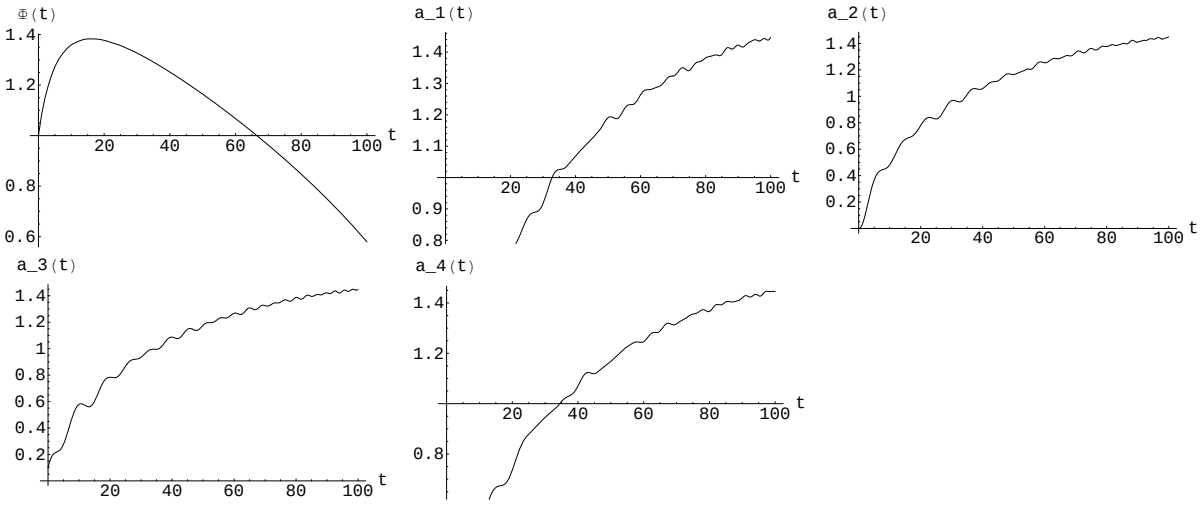

Figure 2: A numerical solutions of the scale factors the case of the four-site path graph.

[4] C. T. Hill, S. Pokorski and J. Wang, Phys. Rev. **D64** (2001) 1050050.

[5] S. Hamamoto, Prog. Theor. Phys. **97** (1997) 327, hep-th/9611141.

[6] N. Kan and K. Shiraishi, Class. Quant. Grav. **20** (2003) 4965, gr-qc/0212113.

[7] N. Kan and K. Shiraishi, J. Math. Phys. **46** (2005) 112301.

[8] S. G. Nibbelink, M. Peloso and M. Sexton, Eur. Phys. J. **C51** (2007) 741, hep-th/0610169.

[9] S. G. Nibbelink and M. Peloso, Class. Quant. Grav. **22** (2005) 1313, hep-th/0411184.

[10] C. Bizdadea et al., JHEP **02** (2005) 016; C. Bizdadea et al., Eur. Phys. J. **C48** (2006) 265.

The distance-redshift relation for the inhomogeneous and anisotropic universe

Kazuhiro Iwata[1], Yasusada Nambu[2] and Masayuki Tanimoto[3]

[1,2,3] *Department of Physics, Graduate School of Science, Nagoya University, Chikusa, Nagoya 464-8602, Japan*

Abstract

Recently, there have been a indication that the universe is in a state of accelerated expansion. This accelerated expansion is supposed to be caused by unidentified dark energy as a result of fitting the observations of type Ia supernovae to a distance-redshift relation of homogeneous and isotropic universe model. But the universe is not perfectly homogeneous and isotropic because of structures such as galaxies or groups of galaxies. In this work, by taking into account effects of such inhomogeneities and anisotropies of the matter distribution, we explain the distance-redshift relation suggested by the observations of type Ia supernovae without dark energy. First, we show that after averaging the optical scalar equation of an inhomogeneous and anisotropic spacetime over the sphere, we can obtain a simplified optical scalar equation, which coincides with that in the Lemaître-Tolman-Bondi spacetime with a Dyer-Roeder-like extention. Then, we show that the distance-redshift relation obtained from our equation provides better fitting of the observational data than the ΛCDM model and the void model.

1 Introduction

Conparisons of reliable distance-redshift relation obtained from Type Ia supernova (SNIa) observations(e.g. [1]) with the predictions from Friedmann-Lemaître (FL) homogeneous and isotropic universe models suggest that the Universe is in a phase of accelerated expansion, and there must exist undefined dark energy that causes the acceleration.

On the other hand, the possibilities have been discussed that the distance-redshift relations provided by the SNIa observations could be reproduced by taking account of the inhomogeneties in the matter distibution and geometry even without dark energy. One of such models is the so-called void model, in which existence of a large scale underdense region (void). Alnes *et al.* [2] showed that there exists a model that provides a good fit to the SNIa observations, assuming that the outside if a spherical region is homogeneous and isotropic but the inside of it is described by the Lemaître-Tolman-Bondi (LTB) spherically symmetric dust solution (e.g. see [2]).

In reality, however, the matter distribution in the Universe is not isotropic, and the distance-redshift relation inferred by the observational data should be considered as an average over all the directions of sight. This point seems to have been mostly ignored in the literature. To take into account the effect caused by these anisotropies, we start with the optical scalar equation in general inhomogeneous and anisotropic spacetimes, and then take an average of a form of this equation (distance equation) over the spheres on the past light cone. With this averaged distance equation, we numerically investigate a void model.

[1]E-mail:iwata@gravity.phys.nagoya-u.ac.jp
[2]E-mail:nambu@gravity.phys.nagoya-u.ac.jp
[3]E-mail:tanimoto@gravity.phys.nagoya-u.ac.jp

2 The distance equation for inhomogeneous and anisotropic spacetime

2.1 The distance equation in general spacetime

Let us consider a null geodesic congruence which arrive at the observer. We start with the optical scalar equation [3], which determines the variations of the cross sectional area of a null geodesic congruence. For simplicity, let us assume the spacetime which there is no the shear and rotation of the congruence. The optical scalar equation in this case becomes

$$\frac{2}{\sqrt{A}}\frac{d^2\sqrt{A}}{d\ ^2} + R\quad k\ k\ = 0, \tag{1}$$

where A is the cross sectional area of the congruence, k the null geodesic generator, the affine parameter, and R the Ricci tensor. With the relation $D_A \propto \sqrt{A}$ for the angular diameter distance D_A, we obtain

$$\frac{1}{D_A}\frac{d^2D_A}{d\ ^2} + 4\pi GT\quad k\ k\ = 0, \tag{2}$$

from Eq.(1) and Einstein's equation. The only energy content we consider is dust, so that $T\quad = \rho u\ u\ $, where ρ is the energy density for dust, u the 4-velocity of dust. The frequency of the light observed by the comoving observer at a given with 4-velocity u is given by $\omega(\ ) = -u\ k\ $.Therefore the second term in the left hand side of Eq.(2) yields $T\quad = \omega(0)(1+z)^2\rho$, where we have used the definition of redshift z, $z \equiv \omega(\ )/\omega(0) - 1$. Thus, Eq.(2) can be written as

$$\mathcal{L}^2 D_A + 4\pi G\rho D_A = 0, \tag{3}$$

where $\mathcal{L}^2$ is the second order linear derivative operator defined by $\mathcal{L}^2 = \frac{1}{\omega^2(0)(1+z)^2}\frac{d^2}{d\lambda^2}$. We stress that this equation is valid for any dust universem, as long as the shear and rotation of the congruence can be ignored. Note also that solving this equation requires another equation (geodesic equation) to relate with z, for a given ρ.

2.2 Averaging of anisotropies

In this subsection, we take a spherical average of Eq.(3).

For our purpose, it is most convenient to take a particular coordinate system that is based on a foliation of spacetime by past light cones of a timelike curve. We employ a spherical null coordinate system (t, z, θ, ϕ) such that on each light cone $t =$ constant, that $z = 0$ corrsponds to the vertex of each light cone, that the timelike curve the vertices $z = 0$ comprise coincides with the orbit of matter flow there, and that the angular coordinates (θ, ϕ) are constant along every null geodesic that reaches the vertex $z = 0$. (This choice of angular coordinates is possible each other.) The radial null coordinate z is chosen to give the redshift along each null geodesic labeled by (t, θ, ϕ). Our observation is supposed to be done at the coordinate center $z = 0$ at a certain instant $t = t_0$.

Let $D_A(z; \theta, \phi)$ be the angular-diameter distance to an object observed in the direction (θ, ϕ) with redshift z. This is a function of z, θ, ϕ, but we will often regard this as a function of z with θ and ϕ being parameters, since we mostly consider its variations along the null geodesic, in which situation θ and ϕ are constant. We will therefore use d/dz instead $\partial/\partial z$ when it acts on $D_A(z; \theta, \phi)$. The same rule will be applied to other functions as well.

Let us define the spherical average of function $f(z; \theta, \phi)$ by

$$\bar{f}(z) \equiv \langle f(z; \theta, \phi)\rangle \equiv \frac{1}{4\pi}\int f(z; \theta, \phi)d\Omega, \tag{4}$$

where $d\Omega = \sin\theta d\theta d\phi$. Then, then spherical average of Eq.(3) can be written as

$$\langle \mathcal{L}^2 D_A(z; \theta, \phi)\rangle + 4\pi G\langle \rho(z; \theta, \phi)D_A(z; \theta, \phi)\rangle = 0. \tag{5}$$

Here, the derivative operator $\mathcal{L}^2$ becomes under our coordinates

$$\mathcal{L}^2 = \frac{1}{\omega^2(0)(1+z)^2}\left(\frac{d}{d}\right)^2 = H(z;\theta,\phi)\frac{d}{dz}\left[H(z;\theta,\phi)(1+z)^2\frac{d}{dz}\right], \tag{6}$$

where the function $H(z;\theta,\phi)$ is defined by $H(z;\theta,\phi) \equiv \frac{1}{\omega(0)(1+z)^2}\frac{dz}{d\lambda}$.

Note that in the averaged equation (5), each term in the left hand side depends only on z. We wish to estimate how much different the averaged distance function $\bar{D}_A(z) = \langle D_A(z;\theta,\phi)\rangle$ is from an spherically symmtetric LTB distance function $D_A^{(\mathrm{LTB})}(z)$. To this, we match an LTB solution with the given inhomogeneous and anisotropic universe according to the following correspondence: $\bar{\rho}(z) = \rho_{\mathrm{LTB}}(z)$, $\bar{H}(z) = H_{\mathrm{LTB}}(z)$. Since the LTB solution possesses two arbitrary physical functions, it is natural to expect that these two conditions are satisfied for a suitable choice of these functions.

Keeping this correspondence in mind, we formally rewrite Eq.(5) in the form

$$\beta(z)\mathcal{L}^2_{\mathrm{LTB}}\bar{D}_A(z) + 4\pi G\alpha(z)\rho_{\mathrm{LTB}}(z)\bar{D}_A(z) = 0, \tag{7}$$

where

$$\alpha(z) \equiv \frac{\langle\rho(z;\theta,\phi)D_A(z;\theta,\phi)\rangle}{\rho_{\mathrm{LTB}}(z)\bar{D}_A(z)}, \quad \beta(z) \equiv \frac{\langle\mathcal{L}^2 D_A(z;\theta,\phi)\rangle}{\mathcal{L}^2_{\mathrm{LTB}}\bar{D}_A(z)}, \quad \mathcal{L}^2_{\mathrm{LTB}} \equiv H_{\mathrm{LTB}}(z)\frac{d}{dz}\left[H_{\mathrm{LTB}}(z)(1+z)^2\frac{d}{dz}\right]. \tag{8}$$

To estimate the magnitude of the ratio function $\alpha(z)$ and $\beta(z)$, let us decompose physical function as

$$\rho(z;\theta,\phi) = \rho_{\mathrm{LTB}}(z) + \delta\rho(z;\theta,\phi), \tag{9}$$
$$H(z;\theta,\phi) = H_{\mathrm{LTB}}(z) + \delta H(z;\theta,\phi), \tag{10}$$
$$D_A(z;\theta,\phi) = \bar{D}_A(z) + \delta D_A(z;\theta,\phi), \tag{11}$$

where $\langle\delta\rho\rangle = \langle\delta H\rangle = \langle\delta D_A\rangle = 0$. Then α can be calculated as

$$\alpha(z) = 1 + \langle\frac{\delta\rho(z;\theta,\phi)}{\rho_{\mathrm{LTB}}(z)}\frac{\delta D_A(z;\theta,\phi)}{\bar{D}_A(z)}.\rangle \tag{12}$$

In general, the emptier the region the light we observe travels, the longer the distance, which implies that $\delta\rho$ and δD_A have opposite signs each other. This in turn implies $\alpha(z) \quad 1$ with equality being satisfied only in the LTB isotropic universe.

For β, we can roughly estimate as

$$\beta(z) \sim 1 + \langle\left(\frac{\delta H(z;\theta,\phi)}{H_{\mathrm{LTB}}(z)}\right)^2\rangle, \tag{13}$$

where we have used $\delta D_A/\bar{D}_A \sim \delta H/H_{\mathrm{LTB}}$ because the perturbation of distance is mainly caused by the perturbation of the expansion rate. According to the CMB observation, however, the perturbation of the expansion rate is about 0.1 on scales of $z \sim 0.1$. This implies that $\Delta\beta \equiv |\beta - 1|$ is much smaller and can be neglected as compared to $\Delta\alpha \equiv |\alpha - 1|$.

Putting $\beta \sim 1$ in Eq.(7), we finally obtain

$$\mathcal{L}^2_{\mathrm{LTB}}\bar{D}_A(z) + 4\pi G\alpha(z)\rho_{\mathrm{LTB}}(z)\bar{D}_A(z) = 0 \tag{14}$$

This is the distance equation the averaged distance function $\bar{D}_A(z)$ should satisfy. We obtained this equation for a given inhomogeneous and anisotropic universe, but in practice, we will use it to determine a matched LTB solution and $\alpha(z)$ so that the solution $\bar{D}_A(z)$ well describes observational data.

3 Numerically Analysis

Using Eq.(14), we numerically seek in a space of control parameters the best confuguration that can explain observational data of SNIa. For inhomogeneity, we employ the same void model considered by

Alnes *et al.* [2] as the parametrization of the LTB solution. In their model, the arbitrary functions $t_B(r)$, $M(r)$, $E(r)$ are chosen to be

$$t_B(r) = 0, \quad M(r) = \frac{1}{2}H_0^2 r^3 \left[1 - \frac{\Delta M}{2}\left(1 - \tanh\frac{r - r_0}{2\Delta r}\right)\right], \quad E(r) = \frac{1}{4}H_0^2 r^2 \Delta M \left(1 - \tanh\frac{r - r_0}{2\Delta r}\right). \tag{15}$$

The model represents FL universe near the center, since $M(r) \propto r^3$, $E(r) \propto r^2$ there. From this fact, we can define the following density parameters at the center: $\Omega_k \equiv -\frac{E''(0)}{H_0^2}$, $\Omega_m \equiv \frac{M'''(0)}{3H_0^2} = 1 - \Omega_k$. These equation allow us to use observational value Ω_m instead of ΔM.

For anisotropy, we define the function $\alpha(z)$ as

$$\alpha(z) = 1 - \frac{1 - \alpha_0}{2}\left(1 - \tanh\frac{r(z) - r_{\alpha 0}}{2\Delta r_\alpha}\right) \tag{16}$$

Thus, our paramter space consists of $(\Omega_m, r_0, \Delta r, \alpha_0, r_{\alpha 0}, \Delta r_\alpha)$. But, for simplicity, we set $\Delta r_\alpha = 0.001$. As for the observational data to consider, we use the so-called gold samples of Riess *et al.* [4].

The best-fit parameters for our model are summarized in Table 1. Our best-fit value $\chi^2 = 174.046$ is smaller than $\chi^2_{\Lambda\mathrm{CDM}} = 174.046$ in the ΛCDM model [4] and $\chi^2_{\mathrm{void}} = 176.5$ in the void model of Alnes *et al.* [2]. From the value $\alpha = 0.42 (z < 2)$, we can estimate the characteristic magnitude of density fluctuation on the scale $z \sim 1$ as $\delta\rho/\rho \sim 5.8$, since $\delta H/H$ is of the magnitude about 0.1 on this scale. Our value $\Omega_m = 0.31$ coincides with the galaxy survey. The scale $z_0 = 0.199$ corresponds to large-scale structure of the Universe.

Table 1: Our best-fit parameters.

$(\Omega_m,\ r_0,\ \Delta r,\ \alpha_0)$	χ^2	z_0	$z_{\ 0}$
$(0.31, 0.18, 0.085, 0.42)$	174.046	0.199	$z_{\ 0} > 2$

4 Conclusion

Since SNIae are observed in various directions in the sky, the distance-redshift relation inferred by a collective data of them should be considered as an averaged over the solid angle. On the other hand, the distance-redshift relation $D_A(z)$ for a given direction of sight can theoretically be determined by a distance equation that is equivalent to the optical scalar equation. To obtain an effective equation for the spherically averaged distance $\bar{D}_A$, with which the observed distance-redshift relation can directly be compared, we took an average of the distance equation.

The function $\alpha(z)$ introduced in our effective equation represents the degree to which the Universe fluctuates from an isotropic configulation. This newly introduced freedom enabled us to obtain a better fit to the observation, and our best-fit value of α suggests that the dark matter fluctuation $\delta\rho/\bar{\rho} \sim 6$. Although it is very rough, this is perhaps the first estimation of the fluctuation determined from the observational data of SNIae.

References

[1] Supernova Search Team, A. G. Riess *et al.*, Astron. J. **116**, 1009 (1998), astro-ph/9805201.

[2] H. Alnes, M. Amarzguioui, and O. Grøn, Phys. Rev. **D73**, 083519 (2006), astro-ph/0512006.

[3] R. K. Sachs, Proc. Roy. Soc. Lond. **A264**, 309 (1961).

[4] Supernova Search Team, A. G. Riess *et al.*, Astrophys. J. **607**, 665 (2004), astro-ph/0402512.

Cancellation of long-range forces in Einstein-Maxwell-dilaton system

Nahomi Kan*[1], Koichiro Kobayashi†[2], Teruki Hanada†[3] and Kiyoshi Shiraishi†[4]

* *Yamaguchi Junior College, Hofu-shi, Yamaguchi 747–1232, Japan*
† *Yamaguchi University, Yamaguchi-shi, Yamaguchi 753–8512, Japan*

Abstract

We examine cancellation of long-range forces in Einstein-Maxwell-Dilatonic system. Several conditions of the equilibrium of two charged masses in general relativity is found by many authors. These conditions are altered by taking account of dilatonic field. Under the new condition, we show cancellation of $1/r^2$ potential using Feynman diagrams.

1 Introduction

The interaction between two charged massive particles is described by the Newton and the Coulomb potential:

$$V(r) = -G\frac{Mm}{r} + \frac{1}{4\pi}\frac{Qq}{r}, \tag{1}$$

where G is the Newton constant. If $Qq = 4\pi GMm$, $V(r) = 0$ and long-range forces are canceled each other at the classical level. In general relativity, the static exact solution for the equilibrium of two charged masses was found by Majumdar and Papapetrou [1]. The solution requires a condition: $\sqrt{4\pi G}M_i = Q_i$. The static exact solution with dilaton was found by Shiraishi [2]. The solution stands for the case with the balance condition: $(M_i : Q_i : \Sigma_i) = (1 : \sqrt{1+a^2} : a)$, where Σ is a dilatonic charge. In this work, we examine cancellation of long-range forces in the Einstein-Maxwell-Dilatonic system using Feynman diagrams under the balance condition, $Q = \sqrt{1+a^2}M$.

2 Feynman rules for dilaton

We start with the Lagrangian including a dilaton field ϕ:

$$\mathcal{L} = \frac{\sqrt{-g}}{4}(R - e^{-2a\phi}F^2 + 2g^{\mu\nu}\nabla_\mu\phi\nabla_\nu\phi) \ , \tag{2}$$

where $4\pi G = 1$, R is Ricci scalar, $F_{\mu\nu} = \partial_\mu A_\nu - \partial_\nu A_\mu$, $\nabla_\mu\phi = \partial_\mu\phi$, and a is the coupling constant between the dilaton field and other fields. In order to extract the interactions coupled with the dilaton field, we use a complex scalar boson φ as a probe. The Lagrangian of complex Klein-Gordon field is [3]

$$\mathcal{L}_{KG} = \sqrt{-g}\,[e^{-a\phi}g^{\mu\nu}(D_\mu\varphi)^* D_\nu\varphi - m^2 e^{a\phi}\varphi^*\varphi] \ , \tag{3}$$

where $D_\mu\varphi = \partial_\mu\varphi + iqA_\mu\varphi$. We decompose the metric $g_{\mu\nu}$ into the flat background field $\eta_{\mu\nu}$ and the graviton field $h_{\mu\nu}$:

$$g_{\mu\nu} = \eta_{\mu\nu} + \kappa h_{\mu\nu}, \tag{4}$$

where $\kappa = \sqrt{32\pi G}$ and $\eta_{\mu\nu} = diag(1,-1,-1,-1)$. In this decomposition, we read

$$g^{\mu\nu} = \eta^{\mu\nu} - \kappa h^{\mu\nu} + \kappa^2 h^{\mu\lambda}h^\nu_\lambda - \kappa^3 h^{\mu\lambda}h_{\lambda\alpha}h^{\alpha\nu} + \cdots \ , \tag{5}$$

[1] E-mail:kan@yamaguchi-jc.ac.jp
[2] E-mail:m004wa@yamaguchi-u.ac.jp
[3] E-mail:k004wa@yamaguchi-u.ac.jp
[4] E-mail:shiraish@yamaguchi-u.ac.jp

and

$$\sqrt{-g} = \sqrt{-\det g_{\mu\nu}} = 1 + \frac{\kappa}{2}h + \frac{\kappa^2}{8}(h^2 - 2h^{\mu\nu}h_{\mu\nu}) + \frac{\kappa^3}{48}(h^3 - 6hh^{\mu\nu}h_{\mu\nu} + 8h^{\mu}_{\nu}h^{\nu}_{\lambda}h^{\lambda}_{\mu}) + \cdots \ , \quad (6)$$

where $h^{\mu\nu} \equiv \eta^{\mu\alpha}h_{\alpha\beta}\eta^{\beta\nu}$ and $h \equiv \eta^{\mu\nu}h_{\mu\nu}$. Using these expansions, we obtain the Einstein-Hilbert action:

$$\begin{aligned}
\mathcal{L}_{EH} &= \frac{1}{16\pi G}\sqrt{-g}R = \frac{2}{\kappa^2}\sqrt{-g}R & (7)\\
&= \frac{1}{2}\left(\partial^{\mu}h^{\nu\lambda}\partial_{\mu}h_{\nu\lambda} - \frac{1}{2}\partial^{\mu}h\partial_{\mu}h\right) + \kappa\left(\frac{1}{2}h^{\alpha}_{\beta}\partial^{\mu}h^{\beta}_{\alpha}\partial_{\mu}h - \frac{1}{2}h^{\alpha}_{\beta}\partial_{\alpha}h^{\mu}_{\nu}\partial^{\beta}h^{\nu}_{\mu} - h^{\alpha}_{\beta}\partial_{\mu}h^{\nu}_{\alpha}\partial^{\mu}h^{\beta}_{\nu}\right.\\
&\quad \left. + \frac{1}{4}h\partial^{\alpha}h^{\mu}_{\nu}\partial_{\alpha}h^{\nu}_{\mu} + h^{\beta}_{\mu}\partial_{\nu}h^{\alpha}_{\beta}\partial^{\mu}h^{\nu}_{\alpha} - \frac{1}{8}h\partial^{\mu}h\partial_{\mu}h\right) + \cdots \ , & (8)
\end{aligned}$$

where we use the de Donder gauge, $\partial_{\mu}h^{\mu}_{\nu} = \frac{1}{2}\partial_{\nu}h$. This expression involves a kinetic term as well as terms for an infinite number of interactions among gravitons. The Lagrangian of Maxwell theory coupled with gravitons becomes

$$\begin{aligned}
\mathcal{L}_{M} &= -\frac{\sqrt{-g}}{4}F^2 = -\frac{\sqrt{-g}}{4}g^{\alpha\beta}g^{\mu\nu}F_{\alpha\mu}F_{\beta\nu} & (9)\\
&= -\frac{1}{4}\eta^{\alpha\beta}\eta^{\mu\nu}F_{\alpha\mu}F_{\beta\nu} - \frac{\kappa}{2}h^{\mu\nu}\left[-\eta^{\alpha\beta}F_{\alpha\mu}F_{\beta\nu} - \eta_{\mu\nu}\left(-\frac{1}{4}\eta^{\gamma\delta}\eta^{\lambda\sigma}F_{\gamma\lambda}F_{\delta\sigma}\right)\right]\\
&\quad + \frac{\kappa^2}{4}\left[\frac{1}{2}(h^2 - 2h^{\mu\nu}h_{\mu\nu})\left(-\frac{1}{4}\eta^{\gamma\delta}\eta^{\lambda\sigma}F_{\gamma\lambda}F_{\delta\sigma}\right)F_{\alpha\beta}F_{\mu\nu}(hh^{\alpha\mu}\eta^{\beta\nu} - 2h^{\alpha\lambda}h^{\mu}_{\lambda}\eta^{\beta\nu} - h^{\alpha\mu}h^{\beta\nu})\right] + \cdots & (10)
\end{aligned}$$

where we choose the Lorenz gauge, $\partial^{\mu}A_{\mu} = 0$. We also find the coupling between the massive scalar boson and the dilaton as follows:

$$\begin{aligned}
\mathcal{L}_{KG} &= \mathcal{L}_0 - a\phi(D_{\mu}\varphi)^*D^{\mu}\varphi - am^2\phi\varphi^*\varphi - \frac{\kappa}{2}h^{\mu\nu}\left(\partial_{\mu}\varphi^*\partial_{\nu}\varphi - \eta_{\mu\nu}\mathcal{L}_0\right)\\
&\quad + \frac{\kappa^2}{2}\left[\frac{1}{4}(h^2 - 2h^{\mu\nu}h_{\mu\nu})\mathcal{L}_0 + \left(h^{\mu}_{\lambda}h^{\lambda\nu} - \frac{1}{2}hh^{\mu\nu}\right)\partial_{\mu}\varphi^*\partial_{\nu}\varphi\right] + \cdots \ , & (11)
\end{aligned}$$

where $\mathcal{L}_0$ is the Lagrangian in flat spacetime,

$$\mathcal{L}_0 \equiv \frac{1}{2}(\eta^{\mu\nu}\partial_{\mu}\varphi^*\partial_{\nu}\varphi - m^2\varphi^*\varphi) \, . \quad (12)$$

3 Elementary processes : gravitation

Following Ref. [4], we use a classical source of gravitation: $T^{\mu\nu}(x) = M\delta^{\mu}_0\delta^{\nu}_0\delta^{(3)}(\mathbf{x})$. According to the equation of motion, this source creates an external field $h^{ext}_{\mu\nu}(\mathbf{k})$:

$$h_{\mu\nu}(k) = \frac{\kappa M}{4\mathbf{k}^2}(\eta_{\mu\nu} - 2\eta_{\mu 0}\eta_{\nu 0})2\pi\delta(k_0) \equiv h^{ext}_{\mu\nu}(\mathbf{k})2\pi\delta(k_0) \ , \quad (13)$$

where $k = p' - p$, $k_0 = 0$ and $h^{ext}_{\mu\nu}(\mathbf{k})$ is shown in Fig. 1 (a). We call amplitudes including the external field as "semiclassical" amplitudes. The "Newton" potential is evaluated from the semiclassical amplitude including the graviton-scalar boson interaction. Up to $\mathcal{O}(1/r^2)$, the potential becomes

$$V(r)_{Newton} \approx -\frac{GMm}{r} - \frac{3GM\mathbf{p}^2}{2mr} + \frac{G^2M^2m}{2r^2} + \cdots \, . \quad (14)$$

The first term in (14) is recognized as the attractive Newton potential.

4 Elementary process : electromagnetism

We use a static charge as a classical source: $J^\mu(x) = Q\delta^\mu_0\delta^{(3)}(\mathbf{x})$, as usual. This source creates an external field A^{ext}_μ:

$$A^\mu(k) = \frac{Q}{\mathbf{k}^2}\delta^\mu_0 2\pi\delta(k_0) \equiv A^{ext\ \mu}(\mathbf{k})2\pi\delta(k_0)\ , \tag{15}$$

where $k = p' - p$, $k_0 = 0$ and $A^{ext\ \mu}$ is shown in Fig. 1 (b). We obtain "Coulomb" potential from the semiclassical amplitude, where several interactions between photons, scalar bosons and gravitons, as well as between photons and scalar bosons, are included. Up to $\mathcal{O}(1/r^2)$, the potential becomes

$$V(r)_{Coulomb} \approx \frac{Qq}{4\pi r} + \frac{GmQ^2}{8\pi r^2} - \frac{GMQq}{4\pi r^2} + \cdots\ . \tag{16}$$

Note that the first term in (16) is the Coulomb potential with no dependence on the momentum $\mathbf{p}$.

5 Elementary process : Dilaton

Now, we introduce a dilaton field and employ a dilatonic charge $\rho_\Sigma = \Sigma\,\delta^{(3)}(\mathbf{x})$, as a classical source. This source creates an external field $\phi^{ext}(\mathbf{k})$, which is shown in Fig. 1 (c):

$$\phi^{ext}(\mathbf{k}) \equiv -\frac{aM}{\mathbf{k}^2} \equiv -\frac{\Sigma}{\mathbf{k}^2}\ . \tag{17}$$

The diagrams for the first and second order of interactions are gathered in Fig. 2. These amplitudes include the gravitational, the electrical and the dilatonic sources.

We finally evaluate the semiclassical amplitudes of the scalar boson including the dilatonic force and interactions between gravitons, photons and dilatons. The sum of the contributions of the diagrams gives the additional potential due to the dilatonic interaction. The potential of the dilatonic force can be read as

$$V(r)_{dilaton} \approx -\frac{a^2Mm}{4\pi r} + \frac{a^2M\mathbf{p}^2}{8\pi mr} + \frac{a^2Q^2m}{2(4\pi)^2r^2} + \frac{a^2M^2m}{(4\pi)^2r^2} - \frac{a^2MQq}{(4\pi)^2r^2} + \frac{a^4M^2m}{2(4\pi)^2r^2}\,. \tag{18}$$

6 Cancellation of potential

We consider a static case. If we set $\mathbf{p} = \mathbf{0}$ and impose balance conditions, $Q = \sqrt{1+a^2}M$, $q = \sqrt{1+a^2}m$, in (14), (16) and (18), the static potentials are cancelled each other up to $\mathcal{O}(1/r^2)$:

$$V_{Newton} + V_{Coulomb} + V_{dilaton} = 0\,. \tag{19}$$

7 Summary and Outlook

We evaluated the potential of long-range forces coupled with the dilaton field from Feynman diagrams. Up to $\mathcal{O}(1/r^2)$, we showed cancellation of the static potential under the balance condition, $Q = \sqrt{1+a^2}M$. In future, we wish to study the following subjects; higher-derivative theories, calculation on the classical curved background which realizes a three-body system, loop corrections as in Ref. [5, 6], higher-dimensional theories, $\cdots$ and much more !

Acknowledgements

The authors would like to thank K. Shinoda for comments, and also the organizers of JGRG18.

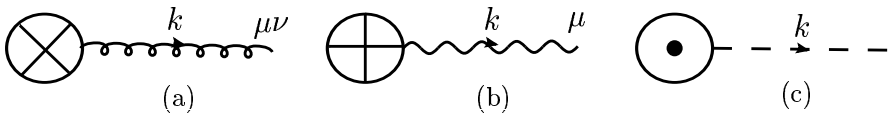

Figure 1: The external field of graviton, photon and dilaton with momentum **k** in (a), (b) and (c), respectively.

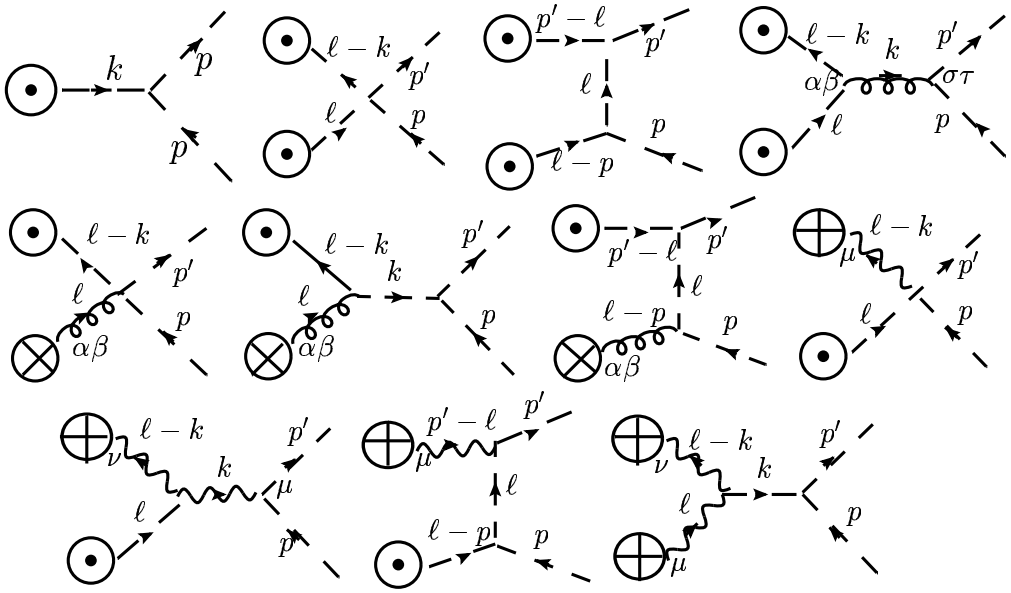

Figure 2: The diagrams for the first and second order of interactions between gravitons, photons and dilatons. These diagrams include the classical sources shown in Fig. 1.

References

[1] S. D. Majumdar, Phys. Rev. **72** (1947) 930; A. Papapetrou, Proc. R. Irish Acad. **A51** (1947) 191.

[2] K. Shiraishi, J. Math. Phys. **34** (1993) 1480.

[3] Y. Degura and K. Shiraishi, Class. Q. Grav. **17** (2000) 4031.

[4] R. Paszko, arXiv:0801.1835v2 [gr-qc]

[5] S. Faller, Phys. Rev. **D77** (2008) 124039.

[6] N. E. J. Bjerrum-Bohr, hep-th/0206236v3 (2007).

The correlation of black hole mass with metallicity index of host spheroid

Shota Kisaka[1], Yasufumi Kojima[2] and Yosuke Otani

[1,2] *Department of Physics, Hiroshima University, Higashi-hiroshima, 739–8526, Japan*

Abstract

We investigate the correlation between the mass of the supermassive black holes (SMBHs) and metal abundance, using existing data sets. The SMBH mass $M_{\rm bh}$ is well correlated with integrated stellar feature of Mgb. For 28 galaxies, the best-fitting $M_{\rm bh}$-Mgb relation has a small scatter, which is an equivalent level with other well-known relation, such as a correlation between the stellar velocity dispersion and the mass. An averaged iron index $\langle {\rm Fe} \rangle$ also positively correlates with $M_{\rm bh}$, but the best-fitting $M_{\rm bh}$-$\langle {\rm Fe} \rangle$ relation has a larger scatter. The difference comes from the synthesis and evolution mechanisms, and may be important for the SMBH and star formation history in the host spheroid.

1 Introduction

Recent observations of nearby massive spheroids (ellipticals, lenticular and spiral bulges) have established that supermassive black holes (SMBHs) are present in the nuclei of galaxies. The mass $M_{\rm bh}$ of SMBHs ranges from 10^6 to 10^9 $M_\odot$. Several statistical correlations between supermassive black hole mass and characteristic parameter of host spheroid (e.g., the luminosity, L; the stellar velocity dispersion, σ) have been explored (e.g., [1], [2]). If the fitting models are good, the correlations may provide some clues to the co-evolution of SMBHs and the host spheroids.

The galaxies have some aspect as an assemble of stars, gases and dark matters. The quantity σ represents the dynamical aspect, while L represents the photometrical one, although they are closely related to each other. Very little attention is paid to the chemical one. Both the metal abundance and black hole mass increase with time and we therefore expect some correlations between them. It is important to clarify the correlation, and the extent, if any. The chemical parameter using Lick/IDS absorption line indices, for example [3], especially Mg and Fe are systematically studied in literatures (e.g., [4]) for the galaxies in which presence of SMBH is reliable. Using the published data, we investigate the correlation with SMBH mass.

2 The sample

Our sample consists of 28 neargy galaxies. We put two criteria to pick up the sample from literatures. First, the black hole masses are measured by good spatial resolution. The sources are limited to $M_{\rm bh} > \sigma^2 r_{\rm res}/(2G)$, where σ^2 is stellar velocity dispersion, $r_{\rm res}$ is the instrumental spatial resolution. Secondly, metal indices of Mg or Fe are measured. For the chemical parameter of spheroids, we use spectral absorption line indices in the visual as defined by the Lick group, for example [5]. Lick indices have proven to be a useful tool for the derivation of ages and metallicity of unresolved stellar population ([6]). In this paper, we use Mgb, Fe5270, Fe5335 indices, measuring, respectively, the strength of $\rm Mg_I$ at $\simeq$ 5156-5197 Å, $\rm Fe_I$ at $\simeq$ 5246-5286 Å and $\simeq$ 5312-5352 Å. These indices in mag are calculated by the standard equations:

$$\mathrm{EW_{mag}} = -2.5 \log \left\{ \frac{\int_{\lambda_1}^{\lambda_2} [F(\ )/C(\ )] d}{{}_2 - {}_1} \right\}, \tag{1}$$

[1] E-mail:kisaka@theo.phys.sci.hiroshima-u.ac.jp
[2] E-mail:kojima@theo.phys.sci.hiroshima-u.ac.jp

where

$$C(\ ) = F_{\rm b}\frac{{}_{\rm r}-}{{}_{\rm r}-{}_{\rm b}} + F_{\rm r}\frac{-\ {}_{\rm b}}{{}_{\rm r}-{}_{\rm b}} \tag{2}$$

and ${}_{\rm b}$ and ${}_{\rm r}$ are the mean wavelength in the blue and red pseudo-continuum intervals, respectively. We have adopted the spectral pseudocontinua and band passes of the Mgb, Fe5270, Fe5335 Lick/IDS indices defined in [3]. We use a combined "iron" index, $\langle$Fe$\rangle$ defined by

$$\langle {\rm Fe}\rangle \equiv \frac{1}{2}({\rm Fe5270} + {\rm Fe5335}). \tag{3}$$

This index has smaller random error than either that of Fe5270 or that of Fe5335. These index values used from the literatures, are the measurements within the central region $r < r_{\rm e}/8$, where $r_{\rm e}$ is effective radius of the spheroids. The details of galaxy parameters uesd in the fits are listed in [7].

3 Results

In order to fit the data to the linear relation $y = a + bx$, we use a version of the routine FITEXY [8] modified by [9].

3.1 Dynamical and photometric properties

In order to check the dependence on the sampling data, we derive $M_{\rm bh}$-σ and $M_{\rm bh}$-$M_{\rm B}$ relations from our sample. First, for the dynamical aspect, we show a relation between the SMBH mass and the stellar velocity dispersion. Our result of $M_{\rm bh}$-σ relation is given by

$$\log(M_{\rm bh}/M_\odot) = (3.98 \pm 0.35)\log(\sigma/200) + 8.23 \pm 0.06 \tag{4}$$

with $\epsilon = 0.25^{+0.06}_{-0.03}$dex in $\log M_{\rm bh}$. This relation is consistent with previous relations. For example, recent updated one by [2] using a sample of 23 galaxies is

$$\log(M_{\rm bh}/M_\odot) = (3.79 \pm 0.32)\log(\sigma/200) + 8.16 \pm 0.06 \tag{5}$$

with $\epsilon = 0.23$ dex. Figure 1 shows our M_{bh}-σ relation (4) in comparison with (5).

Next, for the photometric aspect, we derive the $M_{\rm bh}$-$M_{\rm B}$ relation. Our result is

$$\log(M_{\rm bh}/M_\odot) = (-0.42 \pm 0.05)(M_{\rm B} + 19.5) + 8.14 \pm 0.08 \tag{6}$$

with $\epsilon = 0.36^{+0.07}_{-0.05}$dex. Graham obtained

$$\log(M_{\rm bh}/M_\odot) = (-0.40 \pm 0.05)(M_{\rm B} + 19.5) + 8.27 \pm 0.08 \tag{7}$$

with $\epsilon = 0.30^{+0.04}_{-0.05}$dex. Although intrinsic scatter in our relation is a little high, both two relations agree within the uncertainties. Both relations (6) and (7) are plotted in Figure 2. By comparing with previous results, we may say that there is no serious bias in our sampling data.

3.2 Chemical property

In Figure 3, we plot $M_{\rm bh}$ as a function of the integrated stellar feature of Mgb for the 28 galaxies. It is found that the mass $M_{\rm bh}$ significantly correlates with the index Mgb. The best fit relation is obtained as

$$\log(M_{\rm bh}/M_\odot) = (27.23 \pm 3.00)({\rm Mgb} - 0.16) + 8.13 \pm 0.07 \tag{8}$$

with $\epsilon = 0.32^{+0.06}_{-0.04}$dex. The scatter is not so bad as that of well-fitted $M_{\rm bh}$-σ and $M_{\rm bh}$-$M_{\rm B}$ relations. The index Mgb is a good indicator, but other indicator of the metal abundance is not so good. We have tested the correlation with different index. For instance, we show $M_{\rm bh}$ as a function of $\langle$Fe$\rangle$ index in Figure 4. The best fit relation is

$$\log(M_{\rm bh}/M_\odot) = (60.25 \pm 26.01)(\langle {\rm Fe}\rangle - 0.083) + 8.34 \pm 0.13 \tag{9}$$

with $\epsilon = 0.58^{+0.12}_{-0.07}$ dex. This relation has much larger scatter than that of eqs.(5)-(9). It is clear from Figure 4 that the index $\langle$Fe$\rangle$ is not good one. Summarizing the relationships obtained in our own study, we find that $M_{\rm bh}$-σ is the best, $M_{\rm bh}$-Mgb and $M_{\rm bh}$-$M_{\rm B}$ are moderate, and $M_{\rm bh}$-$\langle$Fe$\rangle$ is the worst.

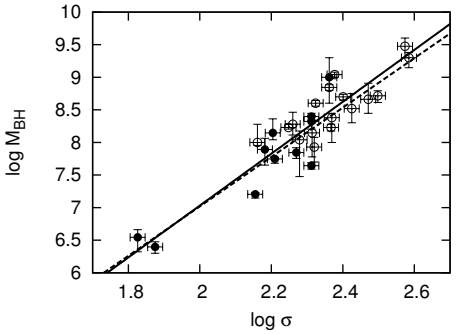

Figure 1: Relationship between SMBH mass and effective stellar velocity dispersion for 28 galaxy samples. The solid line represents our best fit relation (4). For a comparison, the relation by [2] is shown by a dashed line. Elliptical galaxies are denoted by open circles, lenticulars and spirals by filled circles.

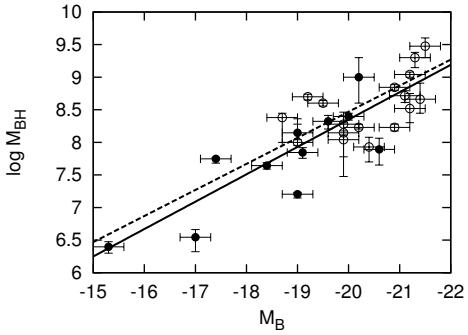

Figure 2: Relationship between SMBH mass and absolute B-band luminosity of the spheroid for 28 galaxy samples. The solid line represents our best fit relation (6). For a comparison, the relation found by [1] is shown by a dashed line. The symbols are the same as Figure 1.

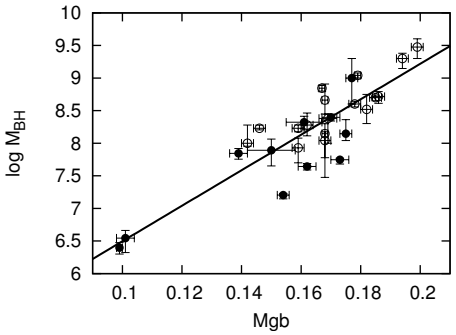

Figure 3: Relationship between SMBH mass and Mgb index value within a circular aperture of $r_e/8$ for our samples. The symbols and line are the same as in Figure 1.

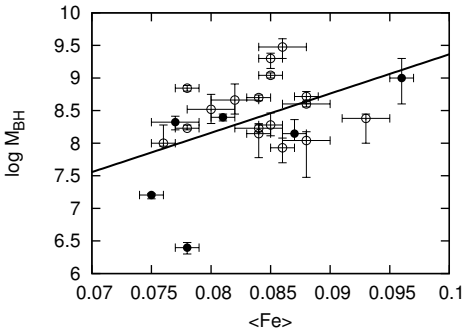

Figure 4: Relationship between SMBH mass and $\langle$Fe$\rangle$ index within $r_e/8$ for our samples. The symbols and line are the same as in Figure 1.

4 Discussion

We have shown that a good correlation between SMBH mass and Mgb index value. The best-fitting $M_{\rm bh}$-Mgb relation has small intrinsic scatter 0.32 dex which is comparable one in other strong correlations found so far. Such a new correlation in the chemical aspect is expected through other relations in dynamical/photometric aspects. The metal abundance is roughly correlated with total stellar mass, absolute magnitudes etc. e.g., [10]. In particular, there is a remarkably tight relation between $\rm Mg_2$ and the central velocity dispersion of stars[11]. The positive correlations have been found between some quantities characterizing the hosts and SMBH mass. A positive correlation is also suggested between the SMBH mass and the metallicity derived from emission line ratios in 578 AGNs spanning a wide range in redshifts[12]. Our result of Mgb for nearby galaxies is more tight. Thus, positive correlation is expected, but the degree was not clear beforehand. It was not clear which indicators of the metal abundance strongly correlate with the SMBH mass. The index $\langle \rm Fe \rangle$ correlates with it, but the intrinsic scatter is not so small as that of Mgb. Heavy elements Mg and Fe are synthesized by two different types of supernovae (Type Ia and II), with different time scales. This evolutionary difference causes the scatter in the correlations.

The growth of black hole mass is mainly determined by the accretion rate and the lifetime of the activity. The environmental factors near the central region of galaxies may partially be affected by some global quantities, such as the mass and size of the host. If the mass $M_{\rm bh}$ of SMBH is determined solely by the spheroid mass $M_{\rm s}$ as $M_{\rm bh} = \varepsilon M_{\rm s}$ ($\varepsilon \sim 10^{-3}$), then we have $M_{\rm bh} \propto M_{\rm s} \propto {\rm L} \propto \sigma^4$, where we assume that a constant mass-to-light ratio and the Faber-Jackson relation in elliptical galaxies hold in the spheroids. The features in the host spheroids are transferred to the relations with the black hole mass, $M_{\rm bh}$-L and $M_{\rm bh}$-σ relations. Other features in the hosts, binding energy, light concentration and so on also give some relations with $M_{\rm bh}$. Bender et al. discuss that the strength of $\rm Mg_2$ is determined not only by the global mass $M_{\rm s}$, but also by the local stellar density, which is related with the star-formation rate etc. It is therefore important to examine the correlation of $M_{\rm bh}$ with the other physical quantities of the spheroid, in addition to $M_{\rm s}$. The metal abundance is a tracer for integrated stellar populations. The tight relation $M_{\rm bh}$-Mgb, which is discovered here but is still tentative, may be useful for the better understanding of the coevolution of SMBH and host spheroid, if it is not accidental. Further work is needed to clarify whether this relation is fundamental or not.

References

[1] Graham, A. W. 2007, MNRAS, 379, 711

[2] Aller, M. C., & Richstone, D. O. 2007, ApJ, 665, 120

[3] Worthey, G., Faber, S. M., & González, J. J., Burstein, D. 1994, ApJS, 94, 687

[4] Trager, S. C., Faber, S. M., Worthey, G., & González, J. J. 2000, AJ, 119, 1645

[5] Burstein, D., Faber, S. M., Gaskell, C. M., & Krumm, N. 1984, ApJ, 287, 586

[6] Denicoló, G., et al. 2005, MNRAS, 356, 1440

[7] Kisaka, S., Kojima, Y., & Otani, Y. 2008, MNRAS, 390, 814

[8] Press, W. H., Teukolsky, S. A., Vetterling, W. T., & Flannery, B. P. 1992, Numerical Recipes (2nd ed.; Cambridge: Cambridge Univ. Press)

[9] Tremaine, S., et al. 2002, ApJ, 574, 740

[10] Pagel, B. E. J. 1997, Nucleosynthesis and Chemical Evolution of Galaxies (Cambridge: Cambridge Univ. Press)

[11] Bender, R., Burstein, D. & Faber, S. M., 1993, ApJ, 411, 153

[12] Warner, C., Hamann, F., & Dietrich, M. 2003, ApJ, 596, 72

Integrability of strings with a symmetry in the Minkowski spacetime

Hiroshi Kozaki[1], Tatsuhiko Koike[2] and Hideki Ishihara[3]

[1]*Department of General Education, Ishikawa National College of Technology, Tsubata, Ishikawa 929–0392, Japan*
[2]*Department of Physics, Keio University, Yokohama 223–8522, Japan*
[3]*Department of Mathematics and Physics, Graduate school of Science, Osaka City University, Osaka 558–8585, Japan*

Abstract

We investigate the integrability of Nambu-Goto strings with a cohomogeneity-one symmetry in the Minkowski spacetime. By virtue of the symmetry, the equations of motion reduce to the geodesic equations in a three dimensional orbit space. The orbit space inherits the Killing vectors from the Minkowski spacetime, which help us to integrate the geodesic equations. The cohomogeneity-one strings are fallen into seven families (Type I $\sim$ VII) in the Minkowski spacetime. We find that the strings of Type I $\sim$ VI are integrable due to the existence of two or more inherited Killing vectors. We also find that the strings of Type VII are integrable due to the existence of an inherited Killing vector and a Killing tensor.

1 Introduction

Recently, cosmic strings gather much attention in the context of the superstring theories, since it was pointed out that the fundamental strings and other string-like solitons such as D-strings could exist in the universe as cosmic strings [1]. In the brane inflation models, these cosmic superstrings are produced at the end of inflation [2, 3] and stretched by the expansion of the universe. Existence of the cosmic superstrings is a strong evidence of the superstring theories.

Jackson *et al.* showed that the reconnection probability of the cosmic superstrings can be much more suppressed than that of the gauge theoretic cosmic strings [4]. If the reconnection probability is much suppressed, the cosmic superstrings exist stably in the universe. When the cosmic superstrings stay in isolation in effect, they must have gone through some kind of relaxation process such as gravitational radiations. Then, they are considered to be in stationary motions.

The stationary string has a world surface which is tangent to a timelike Killing vector field. Existence of the tangential Killing vector reduces the equations of motions of the string to ordinary differential equations, which are much more tractable than partial differential equations. Stationary strings in various spacetimes have been studied so far, and many non-trivial solutions were found even in the Minkowski spacetime [5, 6, 7].

The notion of stationary strings is generalized to that of cohomogeneity-one strings. A cohomogeneity-one string is defined as a string whose world surface is tangent to a Killing vector field which is not restricted to being timelike. The cohomogeneity-one string is characterized by the Killing vector to which the world surface is tangent. When the spacetime admits multiple independent Killing vectors, there are infinitely various Killing vectors in the form of linear combination of the independent Killing vectors. Hence, correspondingly various cohomogeneity-one strings are possible. However, all of the cohomogeneity-one strings do not have equal importance. For example, two stationary rotating strings with equal angular velocity but different rotational axis, e.g. x-axis and y-axis, are physically equivalent. This kind of equivalence are generalized as follows: two strings are equivalent if their world surfaces, say

[1]E-mail:kozaki@ishikawa-nct.ac.jp
[2]E-mail:koike@phys.keio.ac.jp
[3]E-mail:ishihara@sci.osaka-cu.ac.jp

Σ_1 and Σ_2, are mapped by an isometry $\varphi : \Sigma_1 \to \Sigma_2$. In terms of the Killing vectors of the cohomogeneity-one strings, we identify the strings if the tangential Killing vectors, say ξ_1 and ξ_2, are mapped by the isometry $\varphi_* : \xi_1 \to \xi_2$.

In the Minkowski spacetime, the Killing vectors are classified into seven families (Type I $\sim$ VII) under the identification by the isometries, and then, the cohomogeneity-one strings are fallen into seven families [8]. The Type I family includes stationary rotating strings. The Nambu-Goto equations of motion for this class are exactly solved and various configurations are found. By using the exact solutions, the energy momentum tensors are calculated and the properties of the stationary rotating strings are clarified [7]. The gravitational perturbations are also studied in detail and the wave form of the gravitational waves are obtained [9].

The studies of Type I family show that exact solutions are useful for investigating the gravitational phenomena such as gravitational lensing and gravitational waves, which are indispensable to verifying the existence of cosmic strings. Furthermore, exact solutions provide us a deeper insight to the string dynamics. In this article, we clarify the integrability of the remaining families (Type II $\sim$VII). We assume that the motions of the strings are governed by the Nambu-Goto action.

2 Integrability of the cohomogeneity-one string

A trajectory of the string is a two-dimensional surface, say Σ, embedded in a spacetime $(\mathcal{M}, g)$. We denote the embedding

$$\zeta^a \to x^\mu = x^\mu(\zeta^a), \tag{1}$$

where $\zeta^a (\zeta^0 = \tau, \zeta^1 = \sigma)$ are the coordinate on Σ and x^μ $(\mu = 0, 1, 2, 3)$ are the coordinate in $\mathcal{M}$. The Nambu-Goto action is written as

$$S = \int_\Sigma \sqrt{-\gamma} d^2\zeta, \tag{2}$$

where γ is the determinant of the induced metric γ_{ab} on Σ which is given by

$$\gamma_{ab} = g_{\mu\nu} \frac{\partial x^\mu}{\partial \zeta^a} \frac{\partial x^\nu}{\partial \zeta^b}. \tag{3}$$

Let us consider the case that the spacetime $\mathcal{M}$ admits a Killing vector field ξ. We denote the one-parameter isometry group generated by ξ as H. The group action on a point in $\mathcal{M}$ makes an orbit of H, or an integral curve of ξ. If the string world surface Σ is foliated by the orbits of H, the string is called cohomogeneity-one associated with the Killing vector ξ. It is obvious that Σ is tangent to ξ. Stationary strings are examples of cohomogeneity-one strings, where the Killing vectors are timelike.

When we identify all the points in $\mathcal{M}$ which are connected by the action of H, we have the orbit space $\mathcal{O} := \mathcal{M}/H$. Under this identification, the cohomogeneity-one world surface Σ turns out to be a curve in $\mathcal{O}$. This curve is shown to be a spacelike geodesic in $\mathcal{O}$ with the norm-weighted metric

$$\tilde{h}_{\mu\nu} = -f h_{\mu\nu}, \tag{4}$$

where f is the norm of ξ and $h_{\mu\nu}$ is a naturally induced metric on $\mathcal{O}$:

$$h_{\mu\nu} = g_{\mu\nu} - \xi_\mu \xi_\nu / f. \tag{5}$$

Therefore, the problem of solving the equations of motion for the cohomogeneity-one string is reduced to solving the geodesic equations in $(\mathcal{O}, \tilde{h})$.

Integrability of the geodesic equations is related to the existence of the Killing vectors. The geodesic equations in $(\mathcal{O}, \tilde{h})$, where $\dim \mathcal{O} = 3$, are integrable if $(\mathcal{O}, \tilde{h})$ admits two or more linearly independent Killing vectors which commute with each other. In the orbit space $(\mathcal{O}, \tilde{h})$, we can investigate such Killing vectors without solving the Killing equations. Let us consider a Killing vector X in $(\mathcal{M}, g)$ which

commutes with ξ. We can easily find that the projection of X, say $\pi_* X$, where $\pi : \mathcal{M} \to \mathcal{O}$ is the projection, is a Killing vector in $(\mathcal{O}, \tilde{h})$:

$$\begin{aligned}\mathcal{L}_{\pi_* X}\tilde{h} &= \mathcal{L}_X(-fg \quad + \xi\ \xi\ ) = \mathcal{L}_X\ \ (-g_\alpha\ g \quad + g\ _\alpha g \quad)\xi^\alpha \xi \\ &= (-g_\alpha\ g \quad + g\ _\alpha g \quad)\ \ (\mathcal{L}_X \xi^\alpha)\xi \ \ + \xi^\alpha \mathcal{L}_X \xi \\ &= (-g_\alpha\ g \quad + g\ _\alpha g \quad)\ \ [X, \xi]^\alpha \xi \ \ + \xi^\alpha [X, \xi] \quad = 0. \end{aligned} \tag{6}$$

Killing vectors which commute with ξ constitute a Lie subalgebra, called centralizer of ξ which we denote $C(\xi)$. Let $X, Y \in C(\xi)$ commute with each other. We see that the projections of them on $\mathcal{O}$ also commutes;

$$[\pi_* X, \pi_* Y] = \pi_*[X, Y] = 0. \tag{7}$$

Therefore, if there are two or more linearly independent and commuting Killing vectors in $C(\xi)$ except for ξ itself, $(\mathcal{O}, \tilde{h})$ inherits the same number of commuting Killing vectors, and then the geodesic equations in $(\mathcal{O}, \tilde{h})$ are integrable. In the Minkowski spacetime, all of the cohomogeneity-one strings are classified into seven families (Type I $\sim$ VII). For each type, we list the Killing vector ξ, basis of $C(\xi)$ and the number of commuting basis of $C(\xi)$ except for ξ in Table 1. For type I $\sim$ VI, there are two or more commuting Killing vectors in $C(\xi)$, hence, the geodesic equations in $(\mathcal{O}, \tilde{h})$ are integrable. For the strings of Type VII, there is only one Killing vector in $(\mathcal{O}, \tilde{h})$ which is inherited from $(\mathcal{M}, g)$. Nevertheless, the geodesic equations are solved exactly. This is due to the existence of a nontrivial conserved quantity which is related to a Killing tensor field. In the next section, we solve the geodesic equation in $(\mathcal{O}, \tilde{h})$, and show the existence of the Killing tensor.

Type	tangential Killing vector ξ	basis of $C(\xi)$	n
I	$P_t + aL_z\ (a \neq 0)$	P_t, P_z, L_z	2
I	P_t	$P_t, P_x, P_y, P_z, L_x, L_y, L_z$	3
I	L_z	P_t, P_z, L_z, K_z	3
II	$(P_t + P_z) + aL_z\ (a \neq 0)$	P_t, P_z, L_z	2
II	$P_t + P_z$	$P_t, P_x, P_y, P_z, K_y + L_x, K_x - L_y, L_z$	3
III	$P_z + aL_z\ (a \neq 0)$	P_t, P_z, L_z	2
III	P_z	$P_t, P_x, P_y, P_z, L_z, K_x, K_y$	3
IV	$P_z + a(K_y + L_z)$	$P_t - P_x, P_z, P_y + a(K_z - L_y), K_y + L_z$	2
V	$P_z + aK_y\ (a \neq 0)$	P_x, P_z, K_y	2
V	K_y	P_x, P_z, L_y, K_y	2
VI	$K_y + L_z + aP_x\ (a \neq 0)$	$K_y + L_z + aP_x, P_t - P_x, P_z$	2
VII	$K_z + aL_z\ (a \neq 0)$	L_z, K_z	1

Table 1: Inherited symmetry of $(O, \tilde{h})$ from the Minkowsiki space. P_α is the generator of translation along α-direction. L_i $(i = x, y, z)$ are the generators of rotation around i-axis. K_i $(i = x, y, z)$ are the generators of Lorentz boosts along i-directions. n is the number of commuting basis in $C(\xi)$.

3 Integrability of Type VII strings

For the conventional cylindrical coordinate $(\bar{t}, \bar{\rho}, \bar{\phi}, \bar{z})$, we take a new coordinate (t, ρ, ϕ, z);

$$(\bar{t}, \bar{\rho}, \bar{\phi}, \bar{z}) = (z \sinh t, \rho, \phi + at, z \cosh t). \tag{8}$$

In this coordinate, the tangential Killing vector ξ is written as $\xi = K_z + aL_z = \partial_t$, i.e., t is a coordinate along the orbits of H. The metric is represented as

$$g = (-z^2 + a^2\rho^2)dt^2 + 2a\rho^2 d\phi dt + d\rho^2 + \rho^2 d\phi^2 + dz^2, \tag{9}$$

then, the norm weighted metric $\tilde{h}$ is

$$\tilde{h} = (z^2 - a^2\rho^2)(d\rho^2 + dz^2) + z^2\rho^2 d\phi^2. \tag{10}$$

We solve the geodesic equation for this metric. Let σ be a parameter of the geodesic curve; $(\rho(\sigma), \phi(\sigma), z(\sigma))$. The cohomogeneity one string solution, i.e., embedding $(\tau, \sigma) \to (t, \rho, \phi, z)$, is given as

$$(\tau, \sigma) \to (\tau, \rho(\sigma), \phi(\sigma), z(\sigma)). \tag{11}$$

In order to solve the geodesic equation in $(\mathcal{O}, \tilde{h})$, we start from the action

$$S = \int \left[\frac{1}{N} \ \ (z^2 - a^2\rho^2)(\rho'^2 + z'^2) + z^2\rho^2\phi'^2 \ \ + N \right] d\sigma, \tag{12}$$

where the prime represents the differentiation with σ and N is a function of σ. N determines the parameter choice of the geodesic curve. For example, when we set $N(\sigma) = 1$, σ becomes an affine parameter. Fixing the re parametrization freedom by taking the function N as $N = z^2 - a^2\rho^2$, we can solve the geodesic equations as

$$z^2 = C + \sqrt{C^2 - a^2L^2}\cosh 2(\sigma + \sigma_0), \tag{13}$$

$$a^2\rho^2 = C + \sqrt{C^2 - a^2L^2}\cos 2a\sigma, \tag{14}$$

$$\phi = \tan^{-1}\left\{ \frac{C - \sqrt{C^2 - a^2L^2}}{aL} \tan a\sigma \right\} - a\tanh^{-1}\left\{ \frac{C - \sqrt{C^2 - a^2L^2}}{aL} \tanh(\sigma + \sigma_0) \right\}. \tag{15}$$

where L, σ_0 and $C > 0$ are constants. The constant L is related to ϕ-independence of $\tilde{h}$ which is the result of the inherited Killing. The constant C is related to the Killing tensor

$$K = a^2\rho^2(z^2 - a^2\rho^2)dz^2 + z^2(z^2 - a^2\rho^2)d\rho^2 + z^2\rho^2(z^2 + a^2\rho^2)d\phi^2. \tag{16}$$

4 Conclusion

We have found that the equation of motion for the cohomogeneity-one Nambu-Goto strings in the Minkowski spacetime are integrable. The equations of motion for the cohomogeneity-one strings are reduce to the geodesic equations in the orbit space. For the Type I $\sim$ VI, integrability of the geodesic equations comes from two or more inherited Killing vectors. For the Type VII, integrability comes from an inherited Killing vector and a non-trivial Killing tensor.

References

[1] E. J. Copeland, R. C. Myers and J. Polchinski, JHEP **0406**, 013 (2004)

[2] S. Sarangi and S. H. H. Tye, Phys. Lett. B **536**, 185 (2002)

[3] G. Dvali and A. Vilenkin, JCAP **0403**, 010 (2004)

[4] M. G. Jackson, N. T. Jones and J. Polchinski, JHEP **0510**, 013 (2005)

[5] C. J. Burden and L. J. Tassie, Austral. J. Phys. **35**, 223 (1982).
C. J. Burden and L. J. Tassie, Austral. J. Phys. **37**, 1 (1984).

[6] V. P. Frolov, V. Skarzhinsky, A. Zelnikov and O. Heinrich, Phys. Lett. B **224**, 255 (1989).
V. P. Frolov, S. Hendy and J. P. De Villiers, Class. Quant. Grav. **14**, 1099 (1997)

[7] K. Ogawa, H. Ishihara, H. Kozaki, H. Nakano and S. Saito,

[8] H. Ishihara and H. Kozaki, Phys. Rev. D **72**, 061701 (2005)

[9] K. Ogawa, H. Ishihara, H. Kozaki and H. Nakano, arXiv:0811.2846 [gr-qc].

Primordial magnetic fields from second-order cosmological perturbations: Tight coupling approximation

Satoshi Maeda[1], Satoshi Kitagawa[2], Tsutomu Kobayashi[3] and Tetsuya Shiromizu[4]

[1] *Department of Physics, Tokyo Institute of Technology, Tokyo 152-8551, Japan*
[2,3] *Department of Physics, Waseda University, Tokyo 169-8555, Japan,*
[4] *Department of Physics, Kyoto University, Kyoto 606–8502, Japan*

Abstract

We explore the possibility of generating large-scale magnetic fields from second-order cosmological perturbations during the pre-recombination era [1]. The key process for this is Thomson scattering between the photons and the charged particles within the cosmic plasma. To tame the multi-component interacting fluid system, we employ the tight coupling approximation. It is shown that the source term for the magnetic field is given by the vorticity, which signals the intrinsically second-order quantities, and the product of the first order perturbations. The vorticity itself is sourced by the product of the first-order quantities in the vorticity evolution equation. The magnetic fields generated by this process are estimated to be $\sim 10^{-29}$ Gauss on the horizon scale.

1 Introduction

Magnetic fields are known to be present on various scales in the universe [2, 3]. For example, magnetic fields are observed in galaxies and clusters, with intensity ~ 1 Gauss. Only an upper limit has been given for magnetic fields on cosmological scales, $< 10^{-9}$ Gauss. Primordial large-scale magnetic fields may be present and serve as seeds for the magnetic fields in galaxies and clusters, which are amplified through the dynamo mechanism after galaxy formation [4].

A number of models have been proposed for generating large-scale magnetic fields in the early universe. However, they rely more or less on some unknown physics. In the present paper, we discuss magnetogenesis in the pre-recombination era using only the conventional physics that has been established. The generation of magnetic fields in this era has been studied in Refs. [5, 6, 7, 8]. Now it is widely accepted that large-scale cosmological perturbations, generated from inflation in the early universe, evolve into a variety of structures such as the cosmic microwave background anisotropies and galaxies. However, inflation produces only density fluctuations (scalar perturbations) and gravitational waves (tensor perturbations); vector perturbations, and hence large-scale magnetic fields, are quite unlikely to be generated in the context of standard inflationary scenarios. Even if they were generated due to some mechanism, they only decays without any sources. This argument is based on *linear* perturbation theory, and so we will be studying second-order perturbations to overcome this difficulty. We consider a multi-fluid system composed of photons, electrons, and protons, which are tightly coupled via Thomson and Coulomb scattering but slightly deviate from each other [9]. Thomson scattering is important for the generation of large-scale magnetic fields in the pre-recombination era, because a rotational current will be produced by the momentum transfer due to the Thomson interaction. We shall see how this process occurs by doing the tight coupling expansion.

[1]E-mail:maeda"at"th.phys.titech.ac.jp
[2]E-mail:satoshi"at"gravity.phys.waseda.ac.jp
[3]E-mail:tsutomu"at"gravity.phys.waseda.ac.jp
[4]E-mail:shiromizu"at"tap.scphys.kyoto-u.ac.jp

2 Basic equations in second-order cosmological perturbation theory

The background spacetime is given by the spatially flat Friedmann-Lemaitre-Robertson-Walker metric. We write the perturbed metric in the Poisson gauge as

$$ds^2 = a^2(\eta)\left[-\left(1+2\phi^{(1)}+2\phi^{(2)}\right)d\eta^2 + 2\chi_i^{(2)}d\eta dx^i + \left(1-2\mathcal{R}^{(1)}-2\mathcal{R}^{(2)}\right)\delta_{ij}dx^i dx^j\right], \tag{1}$$

where a is the scale factor and η is the conformal time We have dropped the first order vector perturbations $\chi_i^{(1)}$ since they are not generated from inflation in the standard scenarios. We also neglect the tensor perturbations (gravitational waves) for simplicity.

We consider a multi-fluid system composed of photons (γ), electrons (e), and protons (p). We assume that the energy-momentum tensor for each fluid component is given by that of a perfect fluid (i.e., we neglect anisotropic stresses):

$$T_{(I)} = (\rho_I + p_I)u_{(I)}\ u_{(I)} + p_I\delta \qquad (I=\gamma,p,e), \tag{2}$$

where $p_I = w_I\rho_I$ ($w_p = w_e = 0, w_\gamma = 1/3$) and $u_{(I)}$ is the 4-velocity of the fluid satisfying $g\ \ u_{(I)}\ u_{(I)} = -1$. We define $\delta v_{(IJ)i} \equiv v_{(I)i} - v_{(J)i}$, $\beta \equiv m_e/m_p$ and $v_{(b)i}$ as the center of baryon's mass velocity.

The equations of motion governing the present 3-fluid system are given by

$$\nabla\ T_{(\gamma)i} = \kappa_i^{\gamma p} + \kappa_i^{\gamma e}, \tag{3}$$
$$\nabla\ T_{(p)i} = en_pE_i + \kappa_i^{pe} + \kappa_i^{p\gamma}, \tag{4}$$
$$\nabla\ T_{(e)i} = -en_eE_i + \kappa_i^{ep} + \kappa_i^{e\gamma}, \tag{5}$$

where we neglected the Lorentz force from the magnetic field because it will give rise to higher order contributions and scattering term is

$$\kappa_i^{\gamma e} = -\kappa_i^{e\gamma} = -\sigma_T n_e\rho_\gamma\left(u_{(\gamma)i} - u_{(e)i}\right), \tag{6}$$
$$\kappa_i^{\gamma p} = -\kappa_i^{p\gamma} = -\frac{m_e^2}{m_p^2}\sigma_T n_p\rho_\gamma\left(u_{(\gamma)i} - u_{(p)i}\right), \tag{7}$$

where σ_T, ρ_γ, n_e, n_p and m_e, m_p are the Thomson cross section, the energy density of photons, the number density and mass of electrons and protons [6, 8]. The momentum transfer due to Coulomb scattering is written as

$$\kappa_i^{pe} = -\kappa_i^{ep} = -e^2n_pn_e\eta_C\left(u_{(p)i} - u_{(e)i}\right), \tag{8}$$

where η_C is a electric resistivity which comes from Coulomb scattering.

We get "Ohm's law" from Eq.(4) and Eq.(5):

$$E_i = \frac{1-\beta^3}{1+\beta}\frac{\sigma_T}{e}a\rho_\gamma(1-2\mathcal{R})\delta v_{(\gamma b)i}. \tag{9}$$

where we neglect $\delta v_{(pe)i}$ because $\delta v_{(pe)i} \ll \delta v_{(\gamma b)i}$ in our case [8]. This equation may be regarded as "Ohm's law" in some sense. In the standard Ohm's law, the electric field is proportional to the electric current density $\sim e\delta v_{(pe)i}$. It is reminded that the contribution from the electric current gives us the diffusion term in the evolution equation for the magnetic field, and then the source for the magnetic field cannot be induced. However, the electric field is proportional to $\delta v_{(\gamma b)i}$ in the above formula. The current in our "Ohm's law"is originated from the velocity difference between protons and electrons through the interaction with photons. Indeed, if one takes the same mass limit of $\beta \to 1$ (though it is not realized in the nature), the electric field cannot be generated.

Maxwell equation, $\nabla_{[\lambda}F\ \ _{]} = 0$, is

$$\left(a^3B^i\right)' = -\epsilon^{ijk}\partial_j\left[a\left(1+\phi\right)E_k\right] - \epsilon^{ijk}\left(av_jE_k\right)'. \tag{10}$$

Thus we substitute Eq.(9) into Eq.(10) and get

$$\left(a^3 B^i\right)' = -\frac{1-\beta^3}{1+\beta}\frac{\sigma_T}{e}\epsilon^{ijk}a^2\left[\partial_j\left(\rho_\gamma \delta v_{(\gamma b)k}\right) + \rho_\gamma \partial_j(\phi - 2\mathcal{R})\delta v_{(\gamma b)k} + \frac{1}{a^2}\left(\rho_\gamma v_j a^2 \delta v_{(\gamma b)k}\right)'\right]. \tag{11}$$

Our remaining task is to evaluate $\delta v_{(\gamma b)i}$. The evolution equation of $\delta v_{(\gamma b)i}$ is $(4\rho_\gamma/3)^{-1} \times (3) - [m_p\,(1+\beta)\,n]^{-1} \times [(4)+(5)]$:

$$\frac{\rho_\gamma'}{\rho_\gamma}\left(v_{(\gamma)i} + \chi_i\right) - \frac{n'}{n}\left(v_{(b)i} + \chi_i\right) + \left(\delta v_{(\gamma b)i}\right)' + 4\mathcal{H}\delta v_{(\gamma b)i} - (\phi + 2\mathcal{R})\left[\frac{\rho_\gamma'}{\rho_\gamma}v_{(\gamma)i} - \frac{n'}{n}v_{(b)i} + \left(\delta v_{(\gamma b)i}\right)' + 4\mathcal{H}\delta v_{(\gamma b)i}\right]$$
$$-5\mathcal{R}'\delta v_{(\gamma b)i} + \frac{1}{4}\frac{\partial_i \rho_\gamma}{\rho_\gamma} + \partial_j\left(v_{(\gamma)i}v^j_{(\gamma)}\right) - \frac{1}{1+\beta}\partial_j\left(v_{(p)i}v^j_{(p)} + \beta v_{(e)i}v^j_{(e)}\right) = -\alpha(1-2\mathcal{R})\delta v_{(\gamma b)i}, \tag{12}$$

where α is defined as

$$\alpha := \frac{1+\beta^2}{1+\beta}(1+R)\frac{a\sigma_T\rho_\gamma}{m_p}\left(= \frac{\beta(1+\beta^2)}{1+\beta}(1+R)\frac{1}{\tau_T}\right) \tag{13}$$

with $R := 3m_p\,(1+\beta)\,n/4\rho_\gamma$ and τ_T is the timescale of Thomson scattering for electrons.

3 Tight coupling approximation

We are to solve Eq. (12) using the tight coupling approximation (TCA) [9]. In this approximation the time scale of Thomson scattering, τ_T, is assumed to be much smaller than the wavelengths of the perturbations (k^{-1}). Thus, the small expansion parameter of the TCA is $k\tau_T$, which is dimensionless. During the pre-recombination era, photons, protons, and electrons are strongly coupled via Thomson scattering, and hence the TCA will be a good approximation.

At zeroth order in the TCA, all fluid components have the same velocity v_i and the density fluctuations are adiabatic. Following Ref. [8], we define the deviation from the adiabatic distribution for baryons by $n_b = \bar{n}_b\,(1+\Delta_b)$. Then, we expand various quantities such as Δ_b and $v_{(I)i}$ in terms of the tight coupling parameter $k\tau_T$:

$$\Delta_b = \Delta_b^{(I)} + \Delta_b^{(II)} + \cdots, \tag{14}$$
$$v_{(\gamma)i} = v_i, \qquad v_{(b)i} = v_i + v^{(I)}_{(b)i} + v^{(II)}_{(b)i} + \cdots, \tag{15}$$
$$\delta v_{(\gamma b)i} = \delta v^{(I)}_{(\gamma b)i} + \delta v^{(II)}_{(\gamma b)i} + \cdots, \tag{16}$$

where v_i is the common velocity of photons and baryons in the tight coupling limit. Our notation is that Roman and Arabic numerals stand for the order of TCA and that in cosmological perturbation theory, respectively. Here, we adopt the photon frame, so that $\Delta_\gamma^{(I)} = \Delta_\gamma^{(II)} = 0$. In other words, the quantities associated with photons give the "background" in the TCA. Note that we consider cosmological perturbation theory and the TCA simultaneously. The following analysis includes cosmological perturbations up to second-order and the tight coupling expansion up to TCA(II), where TCA(n) denotes the tight coupling approximation at n-th order.

4 Generation of magnetic fields

We solve Eq.(12) for $\delta v_{(\gamma b)i}$ using TCA and substitute the results into Eq.(11). When we consider up to TCA(I), the equation of the magnetic field is

$$(a^3 B^i)' = 2\frac{1-\beta^3}{1+\beta}\frac{\sigma_T}{e}a^4\bar{\rho}_\gamma^{(0)}\frac{\mathcal{H}}{\bar{\alpha}^{(0)}}\omega^{(2)i}. \tag{17}$$

where $\omega^{(2)i}$ is photon's vorticity, $\omega^i \equiv -\frac{1}{2}\varepsilon^{i\ \rho\lambda}u_{(\gamma)\lambda}\nabla\ u_{(\gamma)\rho}$. The evolution equation of the vorticity is obtained by taking the curl of the total momentum conservation:

$$\left(2a^2\bar{\rho}_T^{(0)}\omega^{i(2)}\right)' + 8a^2\mathcal{H}\bar{\rho}_T^{(0)}\omega^{i(2)} = 0. \tag{18}$$

It is important to note here that there is no source for the vorticity at TCA(I). Therefore, the vorticity decays and the magnetic field is not generated at TCA(I).

Next we consider up to TCA(II). Then the equation of the magnetic field is

$$(a^3 B^i)' = \frac{1-\beta^3}{1+\beta}\frac{\sigma_T}{e}a^2\bar{\rho}_\gamma^{(0)}\left[\frac{2a^2\mathcal{H}}{\bar{\alpha}^{(0)}}\omega^{(2)i} + \epsilon^{ijk}\frac{\bar{R}^{(0)}}{1+\bar{R}^{(0)}}\partial_j\Delta_b^{(I,1)}\delta v_{(\gamma b)k}^{(I,1)}\right]. \tag{19}$$

In the same way the evolution equation of the vorticity is

$$(a^2\omega^{(2)i})' + \frac{\mathcal{H}\bar{R}^{(0)}}{1+\bar{R}^{(0)}}a^2\omega^{(2)i} = \frac{\bar{R}^{(0)}}{2(1+\bar{R}^{(0)})^2}\epsilon^{ijk}\partial_j\Delta_b^{(I,1)}\delta v_{(\gamma b)k}^{(I,1)}. \tag{20}$$

Since the right hand side in Eq. (20) contain the source term for the vorticity at TCA(II), the vorticity can be generated at this order. Thus the magnetic field is generated. We estimate roughly the value of the generated magnetic field at the recombination epoch. When we consider the horizon scale, $B \sim 10^{-29}$ Gauss. According to [4], this will be amplified enough to explain the present observed magnetic fields.

5 Summary and future works

We have derived an analytic formula for the magnetic fields generated from second-order cosmological perturbations in the pre-recombination era. Photons and charged particles are strongly coupled via Thomson scattering within the cosmic plasma, and hence the system behaves almost as a single fluid. In this single-fluid description magnetic fields are never generated, and therefore the tiny deviation from the single-fluid description is crucial here. Using the tight coupling approximation (TCA) to treat the small difference between photons and charged particles, we have seen how magnetic fields are generated from cosmic inhomogeneities. It was found that magnetic fields are not generated at first order in the TCA. Therefore, we conclude that magnetogenesis requires both the second-order cosmological perturbations and the second-order TCA. The resultant magnetic fields are expressed in terms of the vorticity and the product of the first-order perturbations. The latter can be computed by solving the linear Einstein equations, while the former is governed by the vorticity evolution equation, with the source term given by the product of the first order terms.

We have not included the effect of anisotropic stresses of photon fluids and the recombination process, though they will be equally important for magnetogenesis on small scales [7]. Taking into account these effects and computing the power spectrum of the generated magnetic fields require detailed numerical calculations, which are left for future works.

References

[1] S. Maeda, S. Kitagawa, T. Kobayashi and T. Shiromizu , arXiv:0805.0169 [astro-ph].

[2] L. M. Widrow, Rev. Mod. Phys. **74**, 775 (2002).

[3] D. Grasso and H. R. Rubinstein, Phys. Rep. **348**, 163 (2001).

[4] See, e.g., A. C. Davis, M. Lilley and O. Tornkvist, Phys. Rev. D **60**, 021301 (1999).

[5] S. Matarrese, S. Mollerach, A. Notari and A. Riotto, Phys. Rev. D **71**, 043502 (2005).

[6] T. Kobayashi, R. Maartens, T. Shiromizu and K. Takahashi, Phys. Rev. D **75**, 103501 (2007).

[7] K. Ichiki, K. Takahashi, N. Sugiyama, H. Hanayama and H. Ohno, Science **311**, 827 (2006).

[8] K. Takahashi, K. Ichiki and N. Sugiyama, Phys. Rev. D **77**, 124028 (2008).

[9] P. J. E. Peebles, The Large Scale structure of the Universe (Princeton University Press, Princeton, NJ, 1980).

Dilatonic Universe in Arbitrary Dimensions

Takuya Maki[1] and Kiyoshi Shiraishi[2]

* *Japan Women's College of Physical Education, Setagaya, Tokyo 157-8565, Japan*

† *Faculty of Science, Yamaguchi University, Yoshida,Yamaguchi-shi, Yamaguchi 753-8512, Japan*

Abstract

The solutions of dilaton gravity theory is investigated in arbitrary dimensions. We find a class of the solutions depending only on one space-like or time-like co-ordinate for Einstein-Dilaton theory with cosmological constant. Also the configurations and behaviors of these solutions are illustrated for typical cases.

1 Introduction

Motivated by higher dimensional unified theories and the related cosmologies[1]-[3], we study the one-parameter solutions of dilaton gravity in arbitrary dimensions. The action of Einstein-dilaton theory with cosmological constant is given by

$$S = \int dx^{N+1}\sqrt{-g}\left\{R - \frac{4}{N-1}\left(\partial\phi\right)^2 - e^{4b\phi/(N-1)}\Lambda\right\}, \tag{1}$$

where R is the scalar curvature and Λ is the cosmological constant. The scalar ϕ is the dilaton field. The constant b represents the dilaton coupling constant to Λ[4].
We find a class of static solutions which depend only on a space-like or a time-like co-ordinate of Einstein-dilaton theory with finite cosmological constant and Maxwell field.

2 Field Equations and Solutions

First we consider one-parameter solutions of the action.(1). We describe the metric by

$$ds^2 = \mp e^{\rho_0}dx_0^2 \pm e^{\rho_1}dz^2 + \sum_{i=2}^{N} e^{\rho_i}dx_i^2, \tag{2}$$

Note that we can study two cases of one-parameter solutions of dilaton gravity theory. For the upper sign of (2) z is a space-like co-ordinate(Case(A)). while for the lower sign z are time-like co-ordinates (Case(B)).
Suppose that all metric components and the dilaton field ϕ depend only on z.
Furthermore we choose the following ansatz:

$$\rho_1 = \rho_0 + \sum_{i=2}^{N}\rho_i. \tag{3}$$

The field equations can be obtained as the following simple form:

$$\ddot{\rho}_\mu = \mp\frac{2}{N-1}\Lambda e^{\psi_1}, \quad \ddot{\phi} = \pm\frac{b}{2}\Lambda e^{\psi_1} \tag{4}$$

[1]E-mail:maki@jwcpe.ac.jp
[2]E-mail:shiraish@sci.yamaguchi-u.ac.jp

where $\mu = 0, 2, \cdots, N$ and the dot denotes the derivative with respect to z. Hereafter the upper sign corresponds to the case(A) in equations and the lower sign is the case(B).

Defining a variable $\psi_1(z)$ as

$$\psi_1 := \rho_0 + \sum_{i=2}^{N} \rho_i + 4b\phi/(N-1), \tag{5}$$

we obtain the equation of motion for the variable ψ_1 as

$$\ddot{\psi}_1 = \pm \frac{2(b^2 - N)}{N-1} \Lambda e^{\psi_1}, \tag{6}$$

where $i, j, k = 2, 3, \cdots, N$.
Also we obtain the Hamiltonian constraint

$$\frac{1}{2} \sum_{\nu \neq \mu} \sum_{\mu} \dot{\rho}_\mu \dot{\rho}_\nu = -\frac{8}{N-1} \dot{\phi}^2 \mp 2\Lambda e^{\psi_1}. \tag{7}$$

(6) is the Liouville equation for ψ_1 when $b \neq 2$ and can be analytically integrable:

$$e^{\psi_1} = \left(\frac{2c_1(N-1)}{\mid \pm (b^2 - N)\Lambda \mid} \right) \Big/ \left(e^{\sqrt{c_1/2}(z - z_{01})} - \varepsilon e^{-\sqrt{c_1/2}(z - z_{01})} \right)^2, \tag{8}$$

where c_1 and z_{01} are integration constants and the symbol ε denotes the sign of $\pm(b^2 - N)\Lambda$, i.e. when $\pm(b^2 - N)\Lambda > 0$, $\varepsilon = +1$ and then $-\infty < c_1 < \infty$, while $\pm(b^2 - N)\Lambda < 0$ corresponds to $\varepsilon = -1$ and $0 < c_1 < \infty$.
Substituting this solution into the $r.h.s$ of Eq.(4), one can obtain the general solutions:

$$\rho_1 = \pm \frac{2N}{(b^2 - N)} \ln \left(e^{\sqrt{c_1/2}(z - z_{01})} - \varepsilon e^{-\sqrt{c_1/2}(z - z_{01})} \right) + d_1 z + d_1', \tag{9}$$

$$\rho_\mu = \pm \frac{2}{(b^2 - N)} \ln \left(e^{\sqrt{c_1/2}(z - z_{01})} - \varepsilon e^{-\sqrt{c_1/2}(z - z_{01})} \right) + d_\mu z + d_\mu', \tag{10}$$

$$\phi = \pm \frac{b(N-1)}{2(b^2 - N)} \ln \left(e^{\sqrt{c_1/2}(z - z_{01})} - \varepsilon e^{-\sqrt{c_1/2}(z - z_{01})} \right) + d_\phi z + d_\phi', \tag{11}$$

where d_μ, d_μ' $(\mu = 0, 2, 3, \cdots, N)$, d_ϕ and d_ϕ' are the integration constants which satisfy

$$d_1 = \sum_{\mu} d_\mu = -\frac{4b}{N-1} d_\phi, \tag{12}$$

$$d_1' = \sum_{\mu} d_\mu' = \ln \frac{2c_1(N-1)}{\mid (b^2 - N)\Lambda \mid}. \tag{13}$$

The Hamiltonian constraint (7) gives the relation between the constants of integration:

$$\frac{c_1(N-1)}{2(N - b^2)} = \frac{4(b^2 - N + 1)}{(N-1)^2} d_\phi^2 - \frac{1}{4} \sum_{\mu} d_\mu^2. \tag{14}$$

Some Special Solutions
The case of upper sign of (2)-(7) corresponds to the universe described by a space-like co-ordinate(case(A)). The other one describes the time development of the universe(case(B)). We demonstrate some special solutions. In Figure 1 we show the case(A) when $N = 4$, $b = 1$, $d_\mu' = 0$, $d_\mu = 1/4$, $z_{01} = 0$. In Figure 2 the case(B) is illustrated which $N = 4$, $b = 1$, $d_\mu' = 0$, $d_\mu = 1/4$, $z_{01} = 0$. The horizontal axis corresponds to z and the variables are rescaled.in these figures.

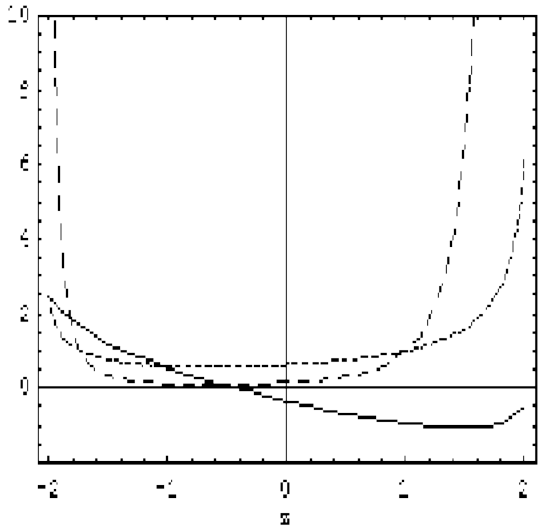

Figure 1: case(A) The solid line is dilaton ϕ, the doted line is $g_{00} = e^{\rho_0}$ and the dashed line is $g_{11} = e^{\rho_1}$.

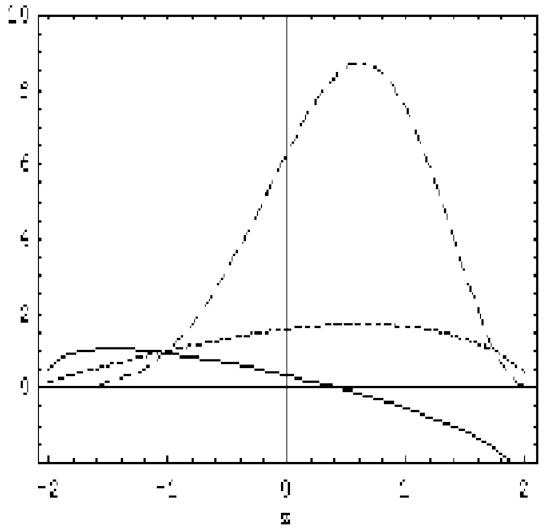

Figure 2: case(A) The solid line is dilaton ϕ, the doted line is $g_{00} = e^{\rho_0}$ and the dashed line is $g_{11} = e^{\rho_1}$.

3 Charged Dilatonic Universe

Next we consider the case of Einstein-Maxwell-Dilaton system given by the action

$$S = \int dx^{N+1}\sqrt{-g}\left\{R - \frac{4}{N-1}\left(\partial\phi\right)^2 - e^{-4a\phi/(N-1)}F^2\right\}, \tag{15}$$

where F is the strength of Maxwell field, and $a = 1$ corresponds to the low energy string action in Einstein frame.

Define a set of the variables ψ_μ where $\mu = 0, 2, ...N$ as

$$\psi_\mu = \rho_\mu + \frac{4a}{N-1}\phi. \tag{16}$$

For the case(A) the field equations are described by ψ's as

$$\ddot{\psi}_\mu = 4\sum_\alpha \eta^{\mu\alpha} q_\alpha q_\mu e^{\psi_\mu} + \frac{4(a^2-1)}{N-1}\sum_{\alpha,\beta}\eta^{\alpha\beta} q_\alpha q_\beta e^{\psi_\alpha}, \tag{17}$$

$$\ddot{\phi} = a\sum_{\mu,\nu}\eta^{\mu\nu} q_\mu q_\nu e^{\psi_\mu}, \tag{18}$$

where $\eta^{\mu\nu} = diag(-1, +1, +1, ..., +1)$ and $q_\mu = (q_e, q_{mj})$ are the constants of integration with respect to Maxwell field:

$$F_{1\mu} = \dot{A}_\mu = q_\mu e^{\psi_\mu}. \tag{19}$$

The Hamiltonian constraint is

$$\frac{1}{2}\sum_{\nu\neq\mu}\sum_{\mu}\dot{\rho}_\mu\dot{\rho}_\nu = \frac{-8}{N-1}\dot{\phi}^2 - 4\sum_{\alpha,\beta}\eta^{\alpha\beta} q_\alpha q_\beta e^{\psi_\alpha} \tag{20}$$

From (μ,ν)-components($\mu \neq \nu$) of the Einstein equations

$$q_\mu q_\nu = 0, \qquad (q_\mu \neq q_\nu). \tag{21}$$

For the case(B) we obtained the equation of motion by exchanging $\eta_{\mu\nu}$ to $\delta_{\mu\nu}$ in (17)-(20) This result means that only one of q_μ is not zero.

The electric solutions with vanishing cosmological constant
In this case, *i.e.* $q_\mu = (q_e, 0, 0, \cdots, 0)$ and $\Lambda = 0$, the field equations are

$$\ddot{\psi}_0 = \mp 4\left(1 + \frac{a^2-1}{N-1}\right) q_e^2 e^{\psi_0}, \quad \ddot{\psi}_j = \mp 4\left(\frac{a^2-1}{N-1}\right) q_e^2 e^{\psi_0}, \tag{22}$$

$$\ddot{\rho}_0 = \mp 4(1 \pm \frac{1}{N-1}) q_e^2 e^{\psi_0} \qquad \ddot{\rho}_j = \pm \frac{4}{N-1} q_e^2 e^{\psi_0}, \tag{23}$$

$$\ddot{\phi} = -a q_e^2 e^{\psi_0}, \tag{24}$$

$$F_{10} = \dot{A}_0 = q_e e^{\psi_0}. \tag{25}$$

The Hamiltonian constraint is

$$\frac{1}{2}\sum_{\nu\neq\mu}\sum_{\mu} \dot{\rho}_\mu \dot{\rho}_\nu = \frac{-8}{N-1}\dot{\phi}^2 \mp 4 q_e e^{\psi_0} \tag{26}$$

One can integrate these equations and obtain the 'electric solutions':

$$\rho_0 = \frac{2(N-2)}{N+a^2-2} \ln\cosh\sqrt{\frac{c_1}{2}}(z - z_{01}) + d_0 z + d_0', \tag{27}$$

$$\rho_1 = \frac{2(2N-3)}{N+a^2-2} \ln\cosh\sqrt{\frac{c_1}{2}}(z - z_{01}) + d_1 z + d_1', \tag{28}$$

$$\rho_i = \frac{2}{N+a^2-2} \ln\cosh\sqrt{\frac{c_1}{2}}(z - z_{01}) + d_i z + d_i', \tag{29}$$

$$\phi = \frac{-a(N-1)}{N+a^2-2} \ln\cosh\sqrt{\frac{c_1}{2}}(z - z_{01}) + d_\phi + d_\phi', \tag{30}$$

$$F_{10} = \cdot\frac{(c/4q_e)(N-1)}{N+a^2-2} \frac{1}{\cosh^2\sqrt{\frac{c_1}{2}}(z - z_{01})}. \tag{31}$$

The configurations of the solution are researching now and will be studied in a separate publication.

4 Summary and Outlook

We have investigated the universe of the dilaton gravity in arbitrary dimensions. The metric given in this paper describes two type solutions, i.e. the static dilatonic universe depending only on a space-like co-ordinate and the universe which behaves by a time-like co-ordinate. A class of the solutions have been found for finite cosmological constant and Maxwell field. We have shown some special configurations of the solutions.

References

[1] N. Arkani-Hamed, S. Dimpooulos and G. Dvali, *Phys.Lett.* **B429** (1998) 263.

[2] L. Randall and R. Sundrum, *Phys.Rev.Lett.* **83** (1999) 3370.

[3] C. Charmousis, *Class. Quant. Grav.* **19** (2002) 83.

[4] M. Cadoni, *Phys. Rev.* **D54**, 7378 (1996)

Thick de Sitter brane solutions in higher dimensions

Vladimir Dzhunushaliev, [1] Vladimir Folomeev [2] and Masato Minamitsuji [3]

[1] *Department of Physics and Microelectronic Engineering, Kyrgyz-Russian Slavic University, Bishkek, Kievskaya Str. 44, 720021, Kyrgyz Republic,*
[2] *Institute of Physics of National Academy of Science Kyrgyz Republic, 265 a, Chui Street, Bishkek, 720071, Kyrgyz Republic,*
[3] *Center for Quantum Spacetime, Sogang University, Shinsu-dong 1, Mapo-gu, 121-742 Seoul, South Korea*

Abstract

We present thick de Sitter brane solutions which are supported by two interacting *phantom* scalar fields in five-, six- and seven- dimensional spacetime. It is shown that for all cases regular solutions with anti-de Sitter asymptotic (5D problem) and a flat asymptotic far from the brane (6D and 7D cases) exist. We also discuss the stability of our solutions.

1 Introduction

In recent years, there is growing interest in higher-dimensional cosmological models inspired by the recent progresses in string theory. In these models, branes which are submanifolds embedded into the higher-dimensional spacetime play an important (even essential) role, for instance, in a description of the confinement of the nongravitational interactions and/or stabilization of the extra dimensions. Much effort to reveal cosmology on the brane has been given in the context of five-dimensional spacetime (see the review [1]). But of course there is no particular reason to restrict the number of dimensions to be five. In recent years, the focus has been turned to higher-dimensional braneworld models.

It is still unclear how the gravity and cosmology on the brane embedded in the higher-dimensional spacetime behave. In higher dimensions, there would be many kinds of classes of possible braneworld models. Here we focus on the generic feature of higher-dimensional braneworld models and from this we deduce the subject to be revealed in this paper.

It is commonly assumed that a brane is an infinitely thin object. In five dimensions, this is a good approximation as long as one is interested in the scales larger than the brane thickness. Then, the cosmology on the brane in five dimensions, i.e., dynamics of the brane in one bulk spacetime, is uniquely determined by the Israel junction conditions once the matter on the brane is specified. But, in higher dimensions the situation is quite different. It happens because self-gravity of an infinitesimally thin three-brane in a higher-dimensional spacetime develops a severe singularity and one cannot put any kind of matter on the brane if the number of codimensions is larger than 2. Also in the case of a codimension-two brane, one cannot put any kind of matter on the brane other than the pure tension. The cosmology on such a brane must be investigated under some prescription of the singular structure of the brane. The well-motivated prescription is to regularize the brane by taking its microscopic structure into consideration. However, in the case of six-dimensional models, the cosmology on the brane strongly depends on the way of regularization. This implies that there is no unique brane cosmology in the case of higher codimensions.

Thus, in this paper we take a different point of view. We shall take the brane thickness into account *from the beginning* and look for the regular braneworld solutions with finite thickness, called *thick brane solutions*, in a field theory model. The thickness of the brane may be very close to the length scale of the quantum gravitational theory, e.g., the string length scale. As we mentioned, the brane thickness must be more essential in higher-dimensional spacetimes, than in the five-dimensional one. Thus, we look for the thick brane solutions in higher dimensions as well as in five dimensions. Bearing the cosmological

[1] Email:vdzhunus"AT"krsu.edu.kg
[2] Email: vfolomeev"AT"mail.ru
[3] Email: minamituzi"AT"sogang.ac.kr

applications, we focus on the thick brane solutions which have de Sitter geometry in the ordinary four-dimensions.

The thick brane solutions and their properties in five dimensions have been explored in the literatures (see Ref. 3 and 4 in [2]). In this paper, we consider thick brane solutions supported by two interacting scalar fields ϕ and χ, whose potential is given by

$$V(\phi,\chi)=\frac{\lambda_1}{4}(\phi^2-m_1^2)^2+\frac{\lambda_2}{4}(\chi^2-m_2^2)^2+\lambda_3\phi^2\chi^2+\Lambda. \tag{1}$$

A stronger interaction between two scalar fields develops the local metastable vacua, which may be able to support our brane universe, other than the global one. Several works on thick brane solutions in such a setup have already been performed. Minkowski brane solutions were derived in [3]. Bearing cosmological applications in mind, our goal in this work is to find thick de Sitter brane solutions.

In Ref. [4] there are some arguments in favor of the fact that the scalar fields, used in [3], are a quantum nonperturbative condensate of a SU(3) gauge field. Briefly these arguments consist of the following: components of the SU(3) gauge field can be divided in some natural way into two parts. The first group contains those components which belong to a subgroup $SU(2)\in SU(3)$. The remaining components belong to a factor space $SU(3)/SU(2)$. Following Heisenberg's idea [5] about the nonperturbative quantization of a nonlinear spinor field the nonperturbative quantization for the SU(3) gauge field is being carried out as follows. It is supposed that two-point Green functions can be expressed via the scalar fields. The first field ϕ describes two-point Green functions for SU(2) components of a gauge potential, and the second scalar field χ describes two-point Green functions for $SU(3)/SU(2)$ components of the gauge potential. It is supposed further that four-point Green functions can be obtained as some bilinear combination of the two-point Green functions. Consequently, the Lagrangian of the SU(3) gauge field takes the form (2). It allows us to regard such sort of thick brane solutions as some defect in a spacetime filled by a condensate of the gauge field living in the bulk.

2 Basic theory

Our interest is in the $D=(4+n)$-dimensional Einstein-scalar theory whose action is given by

$$S=\int d^Dx\sqrt{-g}\left\{-\frac{M_{n+4}^{n+2}}{2}R+\epsilon\left[\frac{1}{2}\partial_A\phi\partial^A\phi+\frac{1}{2}\partial_A\chi\partial^A\chi-V(\phi,\chi)\right]\right\}\ , \tag{2}$$

where M_{n+4} is the gravitational energy scale in the spacetime with n extra dimensions. The potential energy V is defined by Eq. (1). $\epsilon=+1(-1)$ corresponds to the case of normal (phantom) scalar fields and Λ is an arbitrary constant. As we mentioned in the introduction, in Ref. [4], it was argued that such a theory composed of two interacting scalar fields coupled to the remaining $U(1)$ degrees of freedom appears as a result of the gauge condensation in the original $SU(3)$ gauge theory. In this case, the scalar fields ϕ and χ correspond to the vacuum expectation values of the $SU(2)$ and $SU(3)/(SU(2)\times U(1))$ gauge sectors, respectively.

We assume that the generalized D-dimensional metric has the static form

$$ds^2=a^2(r)\gamma_{\alpha\beta}(x^\nu)dx^\alpha dx^\beta-\lambda(r)(dr^2+r^2d\Omega_{n-1}^2)\ , \tag{3}$$

where $d\Omega_{n-1}^2$ is the solid angle for the $(n-1)$ sphere. $\gamma_{\alpha\beta}$ is the metric of the four-dimensional de Sitter space whose scalar curvature is given by $R_{\mu\nu}[\gamma]=3H^2\gamma_{\mu\nu}$. The detailed forms of Einstein and scalar field equations for our ansatz can be found in Ref. [2].

The extremum of the bulk potential are located at the following four points

$$\begin{gathered}\left(\phi=\pm\phi_0:=\pm\sqrt{\tfrac{2\lambda_3\lambda_2m_2^2-\lambda_1\lambda_2m_1^2}{4\lambda_3^2-\lambda_1\lambda_2}},\chi=\pm\chi_0:=\pm\sqrt{\tfrac{2\lambda_3\lambda_1m_1^2-\lambda_1\lambda_2m_2^2}{4\lambda_3^2-\lambda_1\lambda_2}}\right)\\(\phi:=0,\chi:=0)\\(\phi:=\pm m_1,\chi:=0)\\(\phi:=0,\chi:=\pm m_2)\end{gathered}\ . \tag{4}$$

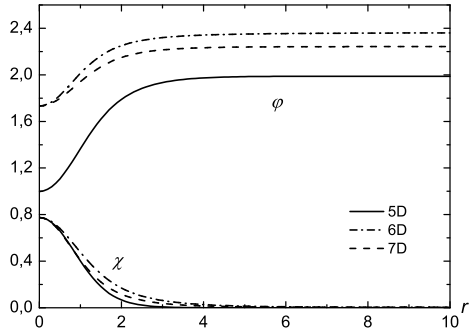

Figure 1: The scalar field configurations ϕ and χ are shown as functions of the dimensionless r.

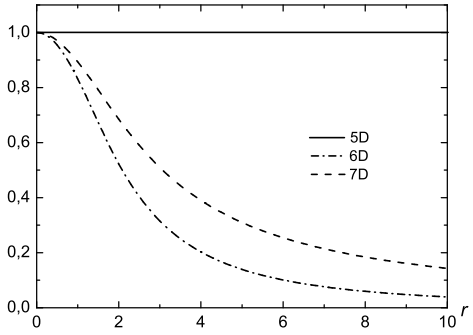

Figure 2: The metric function $\lambda(r)$ is shown as functions of dimensionless r.

We call these points 0, 1, 2 and 3, respectively, with correspoding potentials V_i $(i = 0, 1, 2, 3)$. Clearly, $\max(V_2, V_3) \leq V_1$. The potential (1) has two global minimums 3 and two local minima 2 at values of the parameters λ_1, λ_2 used in this paper. The conditions for existence of local minima are $\lambda_1 > 0, m_1^2 > \lambda_2 m_2^2/(2\lambda_3)$, and for global minima $\lambda_2 > 0, m_2^2 > \lambda_1 m_1^2/(2\lambda_3)$. From comparison of the values of the potential in global and local minima we have (taking into account that $V_{loc} = 0$ at $V_0 = \lambda_2 m_2^4/4$, see below for the six- and seven-dimensional cases) $V_{gl} < V_{loc} \Longrightarrow V_{gl} < 0$, i.e. $\lambda_2 m_2^4 > \lambda_1 m_1^4$. Besides two local and two global minima, four unstable saddle points (0) and the local maximum (1) exist. In the next sections, we look for thick brane solutions starting and finishing in one of local minima 2 of the potential (1).

For our purpose, in the following sections the bulk coordinate and scalar field variables are rescaled to made them dimensionless as $r \to H^{-1} r$, $\phi \to M_{n+4}^{-(n+2)/2} \phi$ and $\chi \to M_{n+4}^{-(n+2)/2} \chi$. Correspondingly, the potential and its parameters are also rescaled as $V \to H^2 M_{n+4}^{n+2} V$, $\lambda_i \to \lambda_i H^2 / M_{n+4}^{n+2}$ and $m_j^2 \to M_{n+4}^{n+2} m_j^2$, where $i = 1, 2, 3$ and $j = 1, 2$.

Then, the boundary conditions at $r \to 0$ are given by $a'(0) = 0$, $\phi' = 0$ and $\chi' = 0$. And from the constraint relation of Einstein equations, we find the boundary value of scale factor $a(0) = \sqrt{6\epsilon/V(0)}$. At the asymptotic infinity, the scalar fields approach the local minimum where $\phi'(\infty) = \chi'(\infty) = 0$. Also at the asymptotic infinity, the bulk geometry is assumed to be anti-de Sitter (AdS) for the five-dimensional model and Minkowki for the six- and seven-dimensional models.

3 Solutions

We present the numerical examples of thick de Sitter brane solutions for the case of phantom scalar field $\epsilon = -1$. We solved the coupled Einstein-scalar system by the iteration method. The detailed descriptions of the method can be found in Ref. [2, 3].

We set the parameters as: $\lambda_1 = 0.1$, $\lambda_2 = 1.0$, $\lambda_3 = 1.0$. For the five-dimensional case we have chosen $\phi(0) = 1.0$, $\chi(0) = \sqrt{0.6}$ and $\Lambda = -3.6$. For these parameters we solved the nonlinear eigenvalue problem for m_1 and m_2. After 11 iterations the following eigenvalues $m_1 \approx 1.989512$ and $m_2 \approx 1.964764$ were found. In Figs. 1-4 we showed our numerical solutions. The spacetime is an asymptotically anti-de Sitter one: the asymptotic value of the potential (1) $\epsilon V_\infty = \epsilon(\lambda_2 m_2^4/4 + \Lambda) < 0$ plays the role of a negative cosmological constant.

For the six-dimensional case we take the boundary condition $\phi(0) = \sqrt{3} \approx 1.73205$ and $\chi(0) = \sqrt{0.6} \approx 0.774597$. We also choose the bulk cosmological constant as $\Lambda = -\lambda_2 m_2^4/4$, in order for our solutions to be asymptotically flat in the bulk. After 10 iterations, we find the eigenvalues $m_1 \approx 2.3590$ and $m_2 \approx 3.0599$. In Figs. 1-4 we showed our numerical solution for a given set of parameters.

For the case of the seven-dimensional case, we also choose the bulk cosmological constant as $\Lambda =$

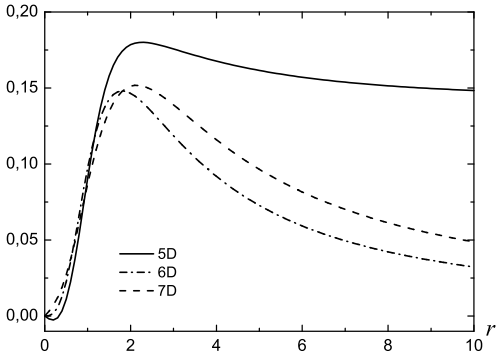

Figure 3: The function a'/a is shown as functions of dimensionless r.

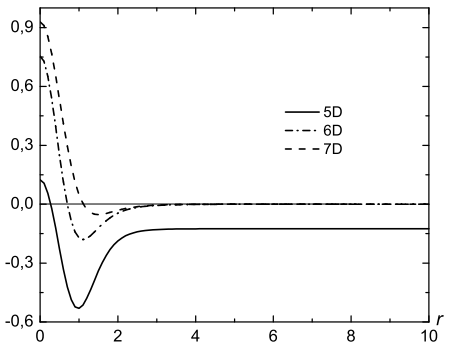

Figure 4: The energy density $T_0^0 = \epsilon\left[\frac{1}{2\lambda}\left(\phi'^2+\chi'^2\right)+V\right]$ is shown as functions of dimensionless r.

$-\lambda_2 m_2^4/4$. After 10 iterations, we find the eigenvalues $m_1 \approx 2.24633$ and $m_2 \approx 3.11911$. The obtained solutions for this case are presented in Fig. 1-4.

4 Summary and Discussions

In this presentation, we have presented five-, six- and seven-dimensional thick de Sitter brane solutions supported by two interacting (*phantom*) scalar fields. The special form of the potential (1) allows us to find regular solutions with finite energy density. It was shown that asymptotically there exist anti-de Sitter spacetime for the five-dimensional case and flat spacetime for the six- and seven-dimensional cases.

Also we have confirmed that our solutions in five-dimensional spacetime are stable. It is also quite reasonable to expect that our thick brane solutions in higher dimensions are also stable since the spacetime and vacuum structures are essentially the same as in the case of five spacetime dimensions. For more details, see [2].

References

[1] R. Maartens, Living Rev. Rel. **7**, 7 (2004) [arXiv:gr-qc/0312059]l P. Brax, C. van de Bruck and A. C. Davis, Rept. Prog. Phys. **67**, 2183 (2004) [arXiv:hep-th/0404011].

[2] V. Dzhunushaliev, V. Folomeev and M. Minamitsuji, arXiv:0809.4076 [gr-qc], to be published in PRD.

[3] V. Dzhunushaliev, Grav. Cosmol. **13**, 302 (2007) [arXiv:gr-qc/0603020]; V. Dzhunushaliev, V. Folomeev, S. Myrzakul and R. Myrzakulov, arXiv:0804.0151 [gr-qc]; V. Dzhunushaliev, V. Folomeev, K. Myrzakulov and R. Myrzakulov, arXiv:0705.4014 [gr-qc]; V. Dzhunushaliev, V. Folomeev, D. Singleton and S. Aguilar-Rudametkin, Phys. Rev. D **77**, 044006 (2008) [arXiv:hep-th/0703043].

[4] V. Dzhunushaliev, arXiv:hep-ph/0605070.

[5] W. Heisenberg, *Introduction to the unified field theory of elementary particles.*, (Max - Planck - Institut für Physik und Astrophysik, Interscience Publishers London, New York-Sydney, 1966).

Informational interpretation on volume operator and physical bound on information

Yoshiyuki Morisawa[1]

Faculty of General Arts and Sciences, Osaka University of Economics and Law, Gakuonji 6-10, Yao, Osaka, 581–8511, Japan

Abstract

From informational viewpoint on volume operator in loop quantum gravity, following conjecture is suggested: a logic gate must occupy finite volume which has the minimum value, and number of logic gates contained within a region of space are bounded by the volume of the region.

1 Introduction

Since information is registered and processed by physical system, it is necessarily restricted by physical law. Several physical bounds on information are well-known. The most famous example is causality: information cannot travel faster than the speed of light. As for thermodynamics, it must consume free energy $kT\ln 2$ to erase a bit [1, 2]. In addition, entropy (or information) that can be contained within a region of a space are bounded by the area of the region as $S \leq A/4$, so-called holographic bound (see *e.g.* [3]). Margolus-Levitin theorem gives the bound on the maximum speed of dynamical evolution (*i.e.* bound on information processing rates) [4]. This bound depends on the energy of the system. Using this, Lloyd estimated the bound for the total number of elementary operations in the universe [5].

In this article, a new physical bound on information is conjectured: a logic gate must occupy finite volume and this volume has the minimum value. Then, number of logic gates contained within a region of a space are bounded by the volume of the region.

2 Informational viewpoint on loop quantum gravity

At the beginning, we review some facts about loop quantum gravity (for detail, see *e.g.* [6]). Loop quantum gravity is the nonperturbative quantization of the general relativity as a diffeomorphism-invariant gauge theory. Its quantum states are gauge invariant and diffeo-invariant. The spin network states satisfy such invariances, and they span the state space of loop quantum gravity as the ortho-normal bases. A spin network state is labeled by a spin network. A spin network is a graph with edges labeled by half-integer spin and can be interpreted as a linear combination of some loops. As a functional of connection field, a spin network state takes value of the trace of the holonomy along its spin network.

In loop quantum gravity, area and volume are defined as operators. These operators geometrically operate on spin network states, and spin network states are eigen states of area and volume operators. Area operator for a surface is constructed from area integral with regularization. Its discrete eigenvalue is the form of $A = 8\pi\gamma l^2_{\text{Planck}} \sum_{n=1}^{N} \sqrt{j_n(j_n+1)}$. Where $n = 1 \ldots N$ labels the edges (of the spin network) crossing the surface, and each edge has spin j_n. The area of the surface is sum over the area of the edges crossing the surface. Volume operator for a region is also constructed from volume integral with regularization. The volume of the region is sum over the volume of vertices within the region. It has also discrete eigenvalues: 3-valent vertex has 0 volume, and 4(or more)-valent vertex has finite volume.

Now, let us see the loop quantum gravity from informational viewpoint. Consider a spin network state with spin 1/2 edge. How is this state different from the state without such edge as a functional of connection? The difference is (trace of) holonomy along that edge. By existence of the edge, this state can probe the connection there like as spin 1/2 degree of freedom. It seems there is 1 bit information along spin 1/2 edge.

[1]E-mail:morisawa@keiho-u.ac.jp

Then, consider the situation that the spin 1/2 edge across some surface. There is 1 bit information along the spin 1/2 edge and this edge produces area on the surface. It seems that a channel where 1 bit information can pass must have the area $\frac{\sqrt{3}}{4}l_0^2$ where $l_0^2 = 8\pi\gamma l_{\text{Planck}}^2$. This is a kind of holographic bound.

Finally, let us reinterpret the volume operator from informational viewpoint. The spin 1/2 edges can be regarded as 1 bit channels and an invertible logic gate such as controlled-NOT has at least 2 inputs and 2 outputs. Then, can 4-valent vertices be regarded as invertible logic gates? 4-valent vertices produce finite volumes under operation of the volume operator. Thus, the logic gate must occupy finite volume at least $\sqrt{\frac{\sqrt{3}}{8}}l_0^3$.

3 Summary and discussion

A new kind of physical bound on information is conjectured. A logic gate must occupy finite volume and this volume has the minimum value. Then, number of logic gates contained within a region of a space are bounded by the volume of the region.

Roughly estimation shows that computation with only 10^{183} logic gates can be executed in the universe. Of course this bound is not so severe on present CPUs. They have about 10^9 gates in about $10^{-6}m^3$ volume. It takes about 600 years to become effective even if "Moore' s law" is correct.

It should be mentioned that the dynamical feature is not treated here. The spin foam model might show the bound for executable operations in a finite spacetime region.

References

[1] R. Landauer, "Irreversibility and Heat Generation in the Computing Process," IBM Journal of Research and Development **5**, 183 (1961).

[2] C. H. Bennett, "Logical Reversibility of Computation," IBM Journal of Research and Development **17**, 525 (1973).

[3] R. Bousso, "The holographic principle," Rev. Mod. Phys. **74**, 825 (2002) [arXiv:hep-th/0203101].

[4] N. Margolus and L. B. Levitin, "The maximum speed of dynamical evolution," Physica D **120**, 188 (1998) [arXiv:quant-ph/9710043].

[5] S. Lloyd, "Computational capacity of the universe," Phys. Rev. Lett. **88**, 237901 (2002) [arXiv:quant-ph/0110141].

[6] C. Rovelli, "*Quantum Gravity*," Cambridge University Press, (2004).

Consistency relations between the source terms in the second-order Einstein equations for cosmological perturbations

Kouji NAKAMURA[1],

Department of Astronomical Science, the Graduate University for Advanced Studies, Mitaka, Tokyo 181-8588, Japan.

Abstract

In addition to the second-order Einstein equations on four-dimensional homogeneous isotropic background universe filled with the single perfect fluid, we also derived the second-order perturbations of the continuity equation and the Euler equation for a perfect fluid in gauge-invariant manner without ignoring any mode of perturbations. The consistency of all equations of the second-order Einstein equation and the equations of motion for matter fields is confirmed. Due to this consistency check, we may say that the set of all equations of the second-order are self-consistent and they are correct in this sense.

1 Introduction

The general relativistic second-order cosmological perturbation theory is one of topical subjects in the recent cosmology. By the recent observation[1], the first order approximation of the fluctuations of our universe from a homogeneous isotropic one was revealed. The observational results also suggest that the fluctuations of our universe are adiabatic and Gaussian at least in the first order approximation. We are now on the stage to discuss the deviation from this first order approximation from the observational[2] and the theoretical side[3] through the non-Gaussianity, the non-adiabaticity, and so on. To carry out this, some analyses beyond linear order are required. The second-order cosmological perturbation theory is one of such perturbation theories beyond linear order.

In this article, we confirm the consistency of all equations of the second-order Einstein equation and the equations of motion for matter fields, which are derived in Refs. [4, 5]. Since the Einstein equations include the equation of motion for matter fields, the second-order perturbations of the equations of motion for matter fields are not independent equations of the second-order perturbation of the Einstein equations. Through this fact, we can check whether the derived equations of the second order are self-consistent or not. This confirmation implies that the all derived equations of the second order are self-consistent and these equations are correct in this sense.

2 Metric perturbations

The background spacetime for the cosmological perturbations is a homogeneous isotropic background spacetime. The background metric is given by

$$g_{ab} = a^2 \left\{ -(d\eta)_a (d\eta)_b + \gamma_{ij} (dx^i)_a (dx^j)_b \right\}, \tag{1}$$

where $\gamma_{ab} := \gamma_{ij} (dx^i)_a (dx^j)_b$ is the metric on the maximally symmetric three-space and the indices $i, j, k, ...$ for the spatial components run from 1 to 3. On this background spacetime, we consider the perturbative expansion of the metric as $\bar{g}_{ab} = g_{ab} + \lambda \overset{1}{h}_{ab} + \frac{\lambda^2}{2} \overset{2}{l}_{ab} + O(\lambda^3)$, where λ is the infinitesimal parameter for perturbation and h_{ab} and l_{ab} are the first- and the second-order metric perturbations, respectively. As shown in Ref. [6], the metric perturbations h_{ab} and l_{ab} are decomposed as

$$h_{ab} =: \mathcal{H}_{ab} + \pounds_X g_{ab}, \quad l_{ab} =: \mathcal{L}_{ab} + 2 \pounds_X h_{ab} + \left(\pounds_Y - \pounds_X^2 \right) g_{ab}, \tag{2}$$

[1]E-mail:kouchan@th.nao.ac.jp

where $\mathcal{H}_{ab}$ and $\mathcal{L}_{ab}$ are the gauge-invariant parts of h_{ab} and l_{ab}, respectively. The components of $\mathcal{H}_{ab}$ and $\mathcal{L}_{ab}$ can be chosen so that

$$\mathcal{H}_{ab} = a^2\left\{-2\overset{(1)}{\Phi}(d\eta)_a(d\eta)_b + 2\overset{(1)}{\nu}_i(d\eta)_{(a}(dx^i)_{b)} + \left(-2\overset{(1)}{\Psi}\gamma_{ij} + \overset{(1)}{\chi}_{ij}\right)(dx^i)_a(dx^j)_b\right\}, \tag{3}$$

$$\mathcal{L}_{ab} = a^2\left\{-2\overset{(2)}{\Phi}(d\eta)_a(d\eta)_b + 2\overset{(2)}{\nu}_i(d\eta)_{(a}(dx^i)_{b)} + \left(-2\overset{(2)}{\Psi}\gamma_{ij} + \overset{(2)}{\chi}_{ij}\right)(dx^i)_a(dx^j)_b\right\}. \tag{4}$$

In Eqs. (3) and (4), the vector-mode $\overset{(p)}{\nu}_i$ and the tensor-mode $\overset{(p)}{\chi}_{ij}$ $(p = 1, 2)$ satisfy the properties

$$D^i\overset{(p)}{\nu}_i = \gamma^{ij}D_p\overset{(p)}{\nu}_j = 0, \quad \overset{(p)}{\chi}{}^i{}_i = 0, \quad D^i\overset{(p)}{\chi}_{ij} = 0, \tag{5}$$

where γ^{kj} is the inverse of the metric γ_{ij}.

3 Background, First-, and Second-order Einstein equations

The Einstein equations of the background, the first order, and the second order on the above four-dimensional homogeneous isotropic universe are summarized as follows.

The Einstein equations for this background spacetime filled with a perfect fluid are given by

$$\overset{(0)}{(p)}E_{(1)} := \mathcal{H}^2 + K - \frac{8\pi G}{3}a^2\epsilon = 0, \quad \overset{(0)}{(p)}E_{(2)} := 2\partial_\eta\mathcal{H} + \mathcal{H}^2 + K + 8\pi G a^2 p = 0, \tag{6}$$

where $\mathcal{H} = \partial_\eta a/a$, K is the curvature constant of the maximally symmetric three-space, ϵ and p are energy density and pressure, respectively.

On the other hand, the second-order perturbations of the Einstein equation are summarized as

$$\overset{(2)}{(p)}E_{(1)} := (-3\mathcal{H}\partial_\eta + \Delta + 3K)\overset{(2)}{\Psi} - 3\mathcal{H}^2\overset{(2)}{\Phi} - 4\pi G a^2\overset{(2)}{\mathcal{E}} - \Gamma_0 = 0, \tag{7}$$

$$\overset{(2)}{(p)}E_{(2)} := \left(\partial_\eta^2 + 2\mathcal{H}\partial_\eta - K - \frac{1}{3}\Delta\right)\overset{(2)}{\Psi} + \left(\mathcal{H}\partial_\eta + 2\partial_\eta\mathcal{H} + \mathcal{H}^2 + \frac{1}{3}\Delta\right)\overset{(2)}{\Phi} - 4\pi G a^2\overset{(2)}{\mathcal{P}} - \frac{1}{6}\Gamma_k{}^k = 0, \tag{8}$$

$$\overset{(2)}{(p)}E_{(3)} := \overset{(2)}{\Psi} - \overset{(2)}{\Phi} - \frac{3}{2}(\Delta + 3K)^{-1}\left(\Delta^{-1}D^iD^j\Gamma_{ij} - \frac{1}{3}\Gamma_k{}^k\right) = 0, \tag{9}$$

$$\overset{(2)}{(p)}E_{(4)i} := \partial_\eta D_i\overset{(2)}{\Psi} + \mathcal{H}D_i\overset{(2)}{\Phi} - \frac{1}{2}D_i\Delta^{-1}D^k\Gamma_k + 4\pi G a^2(\epsilon + p)D_i\overset{(2)}{v} = 0, \tag{10}$$

$$\overset{(2)}{(p)}E_{(5)i} := (\Delta + 2K)\overset{(2)}{\nu}_i + 2\left(\Gamma_i - D_i\Delta^{-1}D^k\Gamma_k\right) - 16\pi G a^2(\epsilon + p)\overset{(2)}{\mathcal{V}}_i = 0, \tag{11}$$

$$\overset{(2)}{(p)}E_{(6)i} := \partial_\eta\left(a^2\overset{(2)}{\nu}_i\right) - 2a^2(\Delta + 2K)^{-1}\left\{D_i\Delta^{-1}D^kD^l\Gamma_{kl} - D^k\Gamma_{ik}\right\} = 0, \tag{12}$$

$$\begin{aligned}\overset{(2)}{(p)}E_{(7)ij} := {} & \left(\partial_\eta^2 + 2\mathcal{H}\partial_\eta + 2K - \Delta\right)\overset{(2)}{\chi}_{ij} - 2\Gamma_{ij} + \frac{2}{3}\gamma_{ij}\Gamma_k{}^k \\ & + 3\left(D_iD_j - \frac{1}{3}\gamma_{ij}\Delta\right)(\Delta + 3K)^{-1}\left(\Delta^{-1}D^kD^l\Gamma_{kl} - \frac{1}{3}\Gamma_k{}^k\right) \\ & - 4\left(D_{(i}(\Delta + 2K)^{-1}D_{j)}\Delta^{-1}D^lD^k\Gamma_{lk} - D_{(i}(\Delta + 2K)^{-1}D^k\Gamma_{j)k}\right) = 0,\end{aligned} \tag{13}$$

where we denote $\Gamma_i{}^j = \gamma^{jk}\Gamma_{ik}$. In these equations, $\overset{(2)}{\mathcal{E}}$ and $\overset{(2)}{\mathcal{P}}$ are the second-order perturbations of the energy density and the pressure, respectively. Further, $D_i\overset{(2)}{v}$ and $\overset{(2)}{\mathcal{V}}_i$ are the scalar- and the vector-parts

of the spatial components of the covariant fluid four-velocity, in these equations. Γ_0, Γ_i, and Γ_{ij} are the collections of the quadratic terms of the linear-order perturbations in the second-order Einstein equations and these can be regarded as the source terms in the second-order Einstein equations. The explicit form of these source terms are given in Refs. [4, 7]. First-order perturbations of the Einstein equations are given by the replacements $\overset{(2)}{\Phi}\to\overset{(1)}{\Phi}$, $\overset{(2)}{\Psi}\to\overset{(1)}{\Psi}$, $\overset{(2)}{\nu_i}\to\overset{(1)}{\nu_i}$, $\overset{(2)}{\chi_{ij}}\to\overset{(1)}{\chi_{ij}}$, $\overset{(2)}{\mathcal{E}}\to\overset{(1)}{\mathcal{E}}$, $\overset{(2)}{\mathcal{P}}\to\overset{(1)}{\mathcal{P}}$, $D_i\overset{(2)}{v}\to D_i\overset{(1)}{v}$, $\overset{(2)}{\mathcal{V}_i}\to\overset{(1)}{\mathcal{V}_i}$, and $\Gamma_0=\Gamma_i=\Gamma_{ij}=0$.

4 Consistency with the equations of motion for matter field

Now, we consider the second-order perturbation of the energy continuity equation and the Euler equations. In terms of gauge-invariant variables, the second-order perturbations of the energy continuity equation and the Euler equation for a single perfect fluid are given by[5]

$$a^{(2)}\mathcal{C}_0^{(p)} := \partial_\eta \overset{(2)}{\mathcal{E}} + 3\mathcal{H}\left(\overset{(2)}{\mathcal{E}} + \overset{(2)}{\mathcal{P}}\right) + (\epsilon+p)\left(\Delta \overset{(2)}{v} - 3\partial_\eta \overset{(2)}{\Psi}\right) - \Xi_0 = 0, \tag{14}$$

$$^{(2)}\mathcal{C}_i^{(p)} := (\epsilon+p)\left\{(\partial_\eta+\mathcal{H})\left(D_i \overset{(2)}{v} + \overset{(2)}{\mathcal{V}_i}\right) + D_i \overset{(2)}{\Phi}\right\} + D_i \overset{(2)}{\mathcal{P}} + \partial_\eta p\left(D_i \overset{(2)}{v} + \overset{(2)}{\mathcal{V}_i}\right) - \Xi_i^{(p)} = 0, \tag{15}$$

where Ξ_0 and $\Xi_i^{(p)}$ are the collection of the quadratic terms of the linear order perturbations and its explicit forms are given in Ref. [5, 7].

To confirm the consistency of the background and the perturbations of the Einstein equation and the energy continuity equation (14), we first substitute the second-order Einstein equations (6)–(8), and (10) into Eq. (14). For simplicity, we first impose the first-order version of Eq. (9) on all equations. Then, we obtain

$$\begin{aligned} 4\pi G a^{3\,(2)}\mathcal{C}_0^{(p)} &= -\partial_\eta\, {}^{(p)}\overset{(2)}{E}_{(1)} - \mathcal{H}\, {}^{(p)}\overset{(2)}{E}_{(1)} - 3\mathcal{H}\, {}^{(p)}\overset{(2)}{E}_{(2)} + D^i\, {}^{(p)}\overset{(2)}{E}_{(4)i} + \frac{3}{2}\left(3\, {}^{(p)}\overset{(0)}{E}_{(1)} - {}^{(p)}\overset{(0)}{E}_{(2)}\right)\partial_\eta \overset{(2)}{\Psi} \\ &\quad -\partial_\eta\Gamma_0 - \mathcal{H}\Gamma_0 - \frac{1}{2}\mathcal{H}\Gamma_k{}^k + \frac{1}{2}D^k\Gamma_k - 4\pi G a^2\Xi_0. \end{aligned} \tag{16}$$

This equation shows that the second-order perturbation (14) of the energy continuity equation is consistent with the second-order and the background Einstein equations if the equation

$$4\pi G a^2\Xi_0 + (\partial_\eta+\mathcal{H})\,\Gamma_0 + \frac{1}{2}\mathcal{H}\Gamma_k{}^k - \frac{1}{2}D^k\Gamma_k = 0 \tag{17}$$

is satisfied under the background, the first-order Einstein equations. Actually, through the background Einstein equations (6) and the first-order version of the Einstein equations (7)–(13), we can easily see that Eq. (17) is satisfied under the Einstein equations of the background and of the first order[7].

Next, we consider the second-order perturbations of the Euler equations. For simplicity, we first impose the first-order version of Eq. (9) on all equations, again. Through the background Einstein equations (6) and the Einstein equations of the second order (8)–(10), we can obtain

$$\begin{aligned} 8\pi G a^{2\,(2)}\mathcal{C}_i^{(p)} &= -8\pi G a^3\, \overset{(0)}{C_0^{(p)}}\left(D_i \overset{(2)}{v} + \overset{(2)}{\mathcal{V}_i}\right) - D_i \overset{(2)}{\Phi}\left(3\, {}^{(p)}\overset{(0)}{E}_{(1)} - {}^{(p)}\overset{(0)}{E}_{(2)}\right) - 2D_i\, {}^{(p)}\overset{(2)}{E}_{(2)} \\ &\quad -\frac{2}{3}D_i\,(\Delta+3K)\, {}^{(p)}\overset{(2)}{E}_{(3)} + \frac{1}{2}(\partial_\eta+2\mathcal{H})\left(+4\, {}^{(p)}\overset{(2)}{E}_{(4)i} - {}^{(p)}\overset{(2)}{E}_{(5)i}\right) \\ &\quad +\frac{1}{2a^2}(\Delta+2K)\, {}^{(p)}\overset{(2)}{E}_{(6)i} - 8\pi G a^2\Xi_j^{(p)} + (\partial_\eta+2\mathcal{H})\,\Gamma_j - D^l\Gamma_{jl}. \end{aligned} \tag{18}$$

This equation shows that the second-order perturbations of the Euler equations is consistent with the Einstein equations of the background and the second order if the equation

$$(\partial_\eta+2\mathcal{H})\,\Gamma_j - D^l\Gamma_{jl} - 8\pi G a^2\Xi_j^{(p)} = 0 \tag{19}$$

is satisfied under the Einstein equations of the background and the first order. Actually, we can easily confirm Eq. (19) due to the background Einstein equations and the first-order perturbations of the Einstein equations[7], and implies that the second-order perturbation of the Euler equation is consistent with the set of the background, the first-order, and the second-order Einstein equations.

The consistency of equations for perturbations shown here is just a well-known result, i.e., the Einstein equation includes the equations of motion for matter field due to the Bianchi identity. However, the above verification of the identities (17) and (19) implies that our derived second-order perturbations of the Einstein equation, the equation of continuity, and the Euler equation are consistent. In this sense, we may say that the derived second-order Einstein equations, especially, the derived formulae for the source terms Γ_0, Γ_i, Γ_{ij}, Ξ_0, and Ξ_i in Ref. [7] are correct.

5 Summary

In summary, we show the all components of the second-order perturbation of the Einstein equation without ignoring any modes of perturbation in the case of a perfect fluid. The derivation is based on the general framework of the second-order gauge-invariant perturbation theory developed in Refs. [8]. In this formulation, any gauge fixing is not necessary and we can obtain any equation in the gauge-invariant form which is equivalent to the complete gauge fixing. In other words, our formulation gives complete gauge fixed equations without any gauge fixing. Therefore, equations which are obtained in gauge-invariant manner cannot be reduced without physical restrictions any more. In this sense, these equations are irreducible. This is one of the advantages of the gauge-invariant perturbation theory.

We have also checked the consistency of the set of equations of the second-order perturbation of the Einstein equations and the evolution equation of the matter field in the cases of a perfect fluid. Therefore, in the case of the single matter field, we may say that we have been ready to clarify the physical behaviors of the second-order cosmological perturbations. The physical behavior of the second-order perturbations in the universe filled with a single matter field will be instructive to clarify those of the second-order perturbations in more realistic cosmological situations. We leave these issues as future works.

References

[1] C.L. Bennett et al., Astrophys. J. Suppl. Ser. **148**, (2003), 1.

[2] E. Komatsu et al., arXiv:0803.0547 [astro-ph], (2008).

[3] V. Acquaviva, N. Bartolo, S. Matarrese, and A. Riotto, Nucl. Phys. B **667** (2003), 119; J. Maldacena, JHEP, **0305** (2003), 013; K. A. Malik and D. Wands, Class. Quantum Grav. **21** (2004), L65; N. Bartolo, S. Matarrese and A. Riotto, Phys. Rev. D **69** (2004), 043503; N. Bartolo, S. Matarrese and A. Riotto, JHEP **0404** (2004), 006; D.H. Lyth and Y. Rodríguez, Phys. Rev. D **71** (2005), 123508; F. Vernizzi, Phys. Rev. D **71** (2005), 061301R; N. Bartolo, S. Matarrese and A. Riotto, JCAP **0401** (2004), 003; N. Bartolo, S. Matarrese and A. Riotto, Phys. Rev. Lett. **93** (2004), 231301; N. Bartolo, E. Komatsu, S. Matarrese and A. Riotto, Phys. Rept. **402** (2004), 103; N. Bartolo, S. Matarrese, and A. Riotto, [arXiv:astro-ph/0512481].

[4] K. Nakamura, *Proceedings of 17th General Relativity and Gravitation in Japan*, "Inclusion of the first-order vector- and tensor-modes in the second-order gauge-invariant cosmological perturbation theory".

[5] K. Nakamura, preprint (arXiv:0804.3840 [gr-qc]).

[6] K. Nakamura, Phys. Rev. D **74** (2006), 101301(R); K. Nakamura, Prog. Theor. Phys. **117** (2007), 17.

[7] K. Nakamura, preprint (arXiv:0812.4865 [gr-qc]).

[8] K. Nakamura, Prog. Theor. Phys. **110**, (2003), 723; K. Nakamura, Prog. Theor. Phys. **113** (2005), 481.

Comparison of Post-Newtonian and Numerical Evolutions of Black-Hole Binaries

Hiroyuki Nakano[1], Manuela Campanelli[2], Carlos O. Lousto[3], and Yosef Zlochower[4]

Center for Computational Relativity and Gravitation, and School of Mathematical Sciences, Rochester Institute of Technology, Rochester, New York 14623, USA

Abstract

In this paper, we compare the waveforms from the post-Newtonian (PN) approach with the numerical simulations of generic black-hole binaries which have mass ratio $q \sim 0.8$, arbitrarily oriented spins with magnitudes $S_1/m_1^2 \sim 0.6$ and $S_2/m_2^2 \sim 0.4$, and orbit 9 times from an initial orbital separation of $r \approx 11M$ prior to merger. We observe a reasonably good agreement between the PN and numerical waveforms, with an overlap of over 98% for the first six cycles of the $(\ell = 2, m = \pm 2)$ mode and over 90% for the $(\ell = 2, m = 1)$ and $(\ell = 3, m = 3)$ modes.

1 Introduction

In 2005, two complementary and independent methods were discovered that allowed numerical relativists to completely solve the black-hole binary problem in full strong-field gravity [1, 2, 3]. On the other hand, there are currently major experimental and theoretical efforts underway to measure these gravitational wave signals. Therefore, one of the most important tasks of numerical relativity (NR) is to assist gravitational wave observatories in detecting gravitational waves and extracting the physical parameters of the sources. Given the demanding resources required to generate these black-hole binary simulations, it is necessary to develop various techniques in order to model arbitrary binary configuration based on numerical simulations in combination with post-Newtonian (PN) and perturbative (e.g. black-hole perturbation) calculations.

In this paper, we compare the NR and PN waveforms for the challenging problem of a generic black-hole binary, i.e., a binary with unequal masses and unequal, non-aligned, and precessing spins. Comparisons of numerical simulations with post-Newtonian ones have several benefits aside from the theoretical verification of PN. From a practical point of view, one can directly propose a phenomenological description and thus make predictions in regions of the parameter space still not explored by numerical simulations. From the theoretical point of view, an important application is to have a calibration of the post-Newtonian error in the last stages of the binary merger.

The paper is organized as follows. In Sec. II we present our method to derive the PN gravitational waveforms from generic black-hole binaries, and in III we compare the NR and PN waveforms. Finally in Sec. IV we summarize this paper and discuss remaining problems. The detailed numerical method and PN calculation presented here have been given in [4].

2 Gravitational waveforms in the PN approach

In order to calculate PN gravitational waveforms, we need to calculate the orbital motion of binaries in the post-Newtonian approach. Here we use the ADM-TT gauge, which is the closest to our quasi-isotropic numerical initial data coordinates. In this paper, we use the PN equations of motion (EOM) based on [5, 6, 7]. The Hamiltonian is given in [5], with the additional terms, i.e., the next-to-leading

[1]E-mail:hxnsma@rit.edu
[2]E-mail:manuela@astro.rit.edu
[3]E-mail:colsma@rit.edu
[4]E-mail:yrzsma@rit.edu

order gravitational spin-orbit and spin-spin couplings provided in [6, 7], and the radiation-reaction force given in [5]. The Hamiltonian which we used here is given by

$$\begin{aligned} H &= H_{\rm O,Newt} + H_{\rm O,1PN} + H_{\rm O,2PN} + H_{\rm O,3PN} \\ &\quad + H_{\rm SO,1.5PN} + H_{\rm SO,2.5PN} + H_{\rm SS,2PN} + H_{\rm S_1S_2,3PN}\,, \end{aligned} \tag{1}$$

where the subscript O, SO and SS denote the pure orbital (non-spinning) part, spin-orbit coupling and spin-spin coupling, respectively, and Newt, 1PN, 1.5PN, etc., refer to the perturbative order in the post-Newtonian approach. From this Hamiltonian, the conservative part of the orbital and spin EOM is derived using the standard techniques of the Hamiltonian formulation. For the dissipative part, we use the non-spinning radiation reaction results up to 3.5PN (which contributes to the orbital EOM at 6PN order), as well as the leading spin-orbit and spin-spin coupling to the radiation reaction [5].

The above PN evolution is used both to produce very low eccentricity orbital parameters at $r \approx 11M$ from an initial orbital separation of $50M$, and to evolve the orbit from $r \approx 11M$. We use these same parameters at $r \approx 11M$ to generate the initial data for our numerical simulations. The initial binary configuration at $r = 50M$ had the mass ratio $q = m_1/m_2 = 0.8$, $\vec{S}_1/m_1^2 = (-0.2, -0.14, 0.32)$, and $\vec{S}_2/m_2^2 = (-0.09, 0.48, 0.35)$.

We then construct a hybrid waveform from the orbital motion by using the following procedure. First we use the 1PN accurate waveforms derived by Wagoner and Will [8] (WW waveforms) for a generic orbit. By using these waveforms, we can introduce effects due to the black-hole spins, including the precession of the orbital plane. On the other hand, Blanchet *et al.* [9] recently obtained the 3PN waveforms (B waveforms) for non-spinning circular orbits. We combine these two waveforms to produce a hybrid waveform. In order to combine the WW and B waveforms, we need to take into account differences in the definitions of polarization states and the angular coordinates. The WW waveforms use the standard definition of GW polarization states, which are the same as those derived from the Weyl scalar, but the B waveforms use an alternate definition. The angular coordinates in the B waveforms are derived from circular orbits in the equatorial (xy) plane. To directly compare the NR and PN waveforms, we must add a time dependent inclination to the B waveforms because in the generic case the orbital planes are inclined with respect to the xy plane.

We note that since there is no gauge ambiguity for combining the two waveforms, the combination of the WW and B waveforms is unique. Also, it should be noted that we calculate the spin contribution to the waveforms through its effect on the orbital motion directly in the WW waveforms and indirectly in B waveforms through the inclination of the orbital plane.

For the NR simulations we calculate the Weyl scalar ψ_4 and then convert the (ℓ, m) modes of ψ_4 into (ℓ, m) modes of $h = h_+ - ih_\times$.

3 Comparison of the NR and PN waveforms

To compare PN and numerical waveforms, we need to determine the time translation δt between the numerical time and the corresponding point on the PN trajectory. That is to say, the time it takes for the signal to reach the extraction sphere ($r = 100M$ in our numerical simulation). We determine this by finding the time translation near $\delta t = 100M$ that maximizes the agreement of the early time waveforms in the $(\ell = 2, m = \pm 2)$, $(\ell = 2, m = \pm 1)$, and $(\ell = 3, m = \pm 3)$ simultaneously. We find $\delta t \sim 112$, in good agreement with the expectation for our observer at $r = 100M$. Since our PN waveforms are given uniquely by a binary configuration, i.e., an actual location of the PN particle, we do not have any time shift or phase modification other than this retardation of the signal. It is noted that other methods which are not based on the particle locations, have freedom in choosing a phase factor.

In the left panel of Fig. 1, we show the real part of the $(\ell = 2, m = 2)$ mode of the strain h with this time translation. (The other modes are shown in [4].) We note that the reasonable agreement of the numerical and PN waveforms for $700M$.

From the analysis of the amplitudes of each mode, we see that the precession and eccentricity of the orbit impart signatures on the modes of the waveform at the orbital frequency. However, the long-time oscillations in the amplitudes, here apparent only in the ($\ell = 2$, $m = \pm 1$) modes, seem to be due purely to

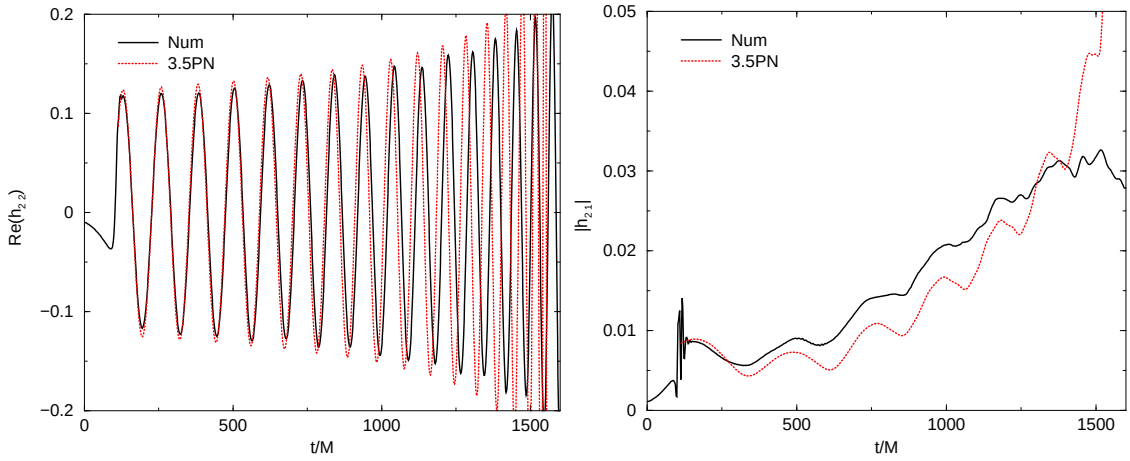

Figure 1: **Left:** The real part of the $(\ell = 2, m = 2)$ mode of h from the numerical and 3.5PN simulations. Here 3.5PN predicts an early merger and has a higher frequency than the numerical waveform. **Right:** The amplitude of the $(\ell = 2, m = 1)$ mode of h from the numerical and 3.5PN simulations. The secular oscillation in the numerical amplitude occurs at roughly the precessional frequency. The timescale is of order $1000M$. Here the shorter-timescale oscillations correspond roughly to the orbital period.

precession, and occur at the precessional frequency. In the right panel of Fig. 1, we show the amplitudes of the $(\ell = 2, m = 1)$ mode of h.

Next, in order to quantitatively compare the modes of the PN waveforms with the numerical waveforms we define the overlap, or matching criterion, for the real and imaginary parts of each mode as

$$M^{\Re}_{\ell m} = \frac{< R^{\rm Num}_{\ell m}, R^{\rm PN}_{\ell m} >}{\sqrt{< R^{\rm Num}_{\ell m}, R^{\rm Num}_{\ell m} >< R^{\rm PN}_{\ell m}, R^{\rm PN}_{\ell m} >}}, \quad M^{\Im}_{\ell m} = \frac{< I^{\rm Num}_{\ell m}, I^{\rm PN}_{\ell m} >}{\sqrt{< I^{\rm Num}_{\ell m}, I^{\rm Num}_{\ell m} >< I^{\rm PN}_{\ell m}, I^{\rm PN}_{\ell m} >}}, \tag{2}$$

where $R_{\ell m}$ and $I_{\ell m}$ are defined by the real and imaginary parts of the waveform mode $h_{\ell m}$, respectively, and the inner product is calculated by $< f, g >= \int_{t_1}^{t_2} f(t)g(t)dt$. Hence, $M^{\Re}_{\ell m} = M^{\Im}_{\ell m} = 1$ indicates that the given PN and numerical mode agree. The results of these matching studies are summarized in Table 1.

Table 1: The match of the real and imaginary parts of the modes of h of the G3.5 configuration for the 3.5 PN waveforms and the numerical waveforms with the time translation $\delta t = 112.5$.

Integration Time	600	800	1000
$M^{\Re}_{22}$	0.986	0.964	0.895
$M^{\Im}_{22}$	0.987	0.962	0.900
$M^{\Re}_{2-2}$	0.986	0.964	0.895
$M^{\Im}_{2-2}$	0.987	0.962	0.901
$M^{\Re}_{21}$	0.904	0.912	0.843
$M^{\Im}_{21}$	0.916	0.901	0.820
$M^{\Re}_{2-1}$	0.920	0.908	0.833
$M^{\Im}_{2-1}$	0.917	0.903	0.816
$M^{\Re}_{33}$	0.938	0.891	0.738
$M^{\Im}_{33}$	0.919	0.868	0.721
$M^{\Re}_{3-3}$	0.931	0.880	0.733
$M^{\Im}_{3-3}$	0.906	0.857	0.721

We also determine an alternate time translation, one wavelength in the $(\ell = 2, m = 2)$ mode, that increases the matching of the $(\ell = 2, m = 2)$ mode over longer integration periods. On the other hand, this new time translation, $\delta t = 233$, causes the $(\ell = 3)$ modes to be out of phase, leading to negative overlaps. Thus by looking at the $(\ell = 2)$ and $(\ell = 3)$ modes simultaneously, we can reject this false match.

4 Conclusion and discussion

We analyzed the first long-term generic waveform produced by the merger of unequal mass, unequal spins, precessing black holes. It is found that a good initial agreement of waveforms for the first six cycles, with overlaps of over 98% for the $(\ell = 2, m = \pm 2)$ modes, over 90% for the $(\ell = 2, m = \pm 1)$ modes, and over 90% for the $(\ell = 3, m = \pm 3)$ modes. These agreement degrades as we approach the more dynamical region of the late merger and plunge.

There are some remaining problems. The PN gravitational waveforms used here do not include direct spin effects. We considered the spin contribution to the waveform only through its effect on the orbital motion. Recently, the direct spin effects have been discussed in [10]. And also in the PN approach, the waveforms are derived from binaries whose each body is considered as a point particle. The finite size effects of the bodies is also important in the late-inspiral region. Furthermore, we will need higher-order post-Newtonian calculations of both spin-orbit and spin-spin terms, especially for the phase evolution of gravitational waves.

We also have a important issue. In order to detect the gravitational waves from binaries, it is necessary to study the data analysis. (For example, the Numerical INJection Analysis (NINJA) project [11].) Here, we must treat a very large parameter space for intrinsic parameters of black-hole binaries, The development of effective GW templates for the whole history of binaries, i.e., the inspiral, merger and ringdown should be done.

Acknowledgments

We would like to thank H. Tagoshi and R. Fujita for useful discussions.

References

[1] F. Pretorius, Phys. Rev. Lett. **95**, 121101 (2005) [arXiv:gr-qc/0507014].

[2] M. Campanelli, C. O. Lousto, P. Marronetti and Y. Zlochower, Phys. Rev. Lett. **96**, 111101 (2006) [arXiv:gr-qc/0511048].

[3] J. G. Baker, J. Centrella, D. I. Choi, M. Koppitz and J. van Meter, Phys. Rev. Lett. **96**, 111102 (2006) [arXiv:gr-qc/0511103].

[4] M. Campanelli, C. O. Lousto, H. Nakano and Y. Zlochower, arXiv:0808.0713 [gr-qc].

[5] A. Buonanno, Y. Chen and T. Damour, Phys. Rev. D **74**, 104005 (2006) [arXiv:gr-qc/0508067].

[6] T. Damour, P. Jaranowski and G. Schaefer, Phys. Rev. D **77**, 064032 (2008) [arXiv:0711.1048 [gr-qc]].

[7] J. Steinhoff, S. Hergt and G. Schaefer, Phys. Rev. D **77**, 081501 (2008) [arXiv:0712.1716 [gr-qc]].

[8] R. V. Wagoner and C. M. Will, Astrophys. J. **210** (1976) 764 [Erratum-ibid. **215** (1977) 984].

[9] L. Blanchet, G. Faye, B. R. Iyer and S. Sinha, arXiv:0802.1249 [gr-qc].

[10] K. G. Arun, A. Buonanno, G. Faye and E. Ochsner, arXiv:0810.5336 [gr-qc].

[11] Numerical INJection Analysis (NINJA) Project Home Page, http://www.gravity.phy.syr.edu/dokuwiki/doku.php?id=ninja:home

Damping of the baryon acoustic oscillations in the matter power spectrum as a probe of the growth factor[1]

Hidenori Nomura[2]

Department of Physics, Hiroshima University, Higashi-Hiroshima, 739–8526, Japan

Abstract

We investigate damping of the baryon acoustic oscillations (BAO) in the matter power spectrum due to quasi-nonlinear clustering of density perturbations. On the basis of third order perturbation theory, we construct a fitting formula of the damping in an analytic way. This demonstrates that the damping is closely related with the growth factor and the amplitude of the matter power spectrum. Then, we investigate the feasibility of constraining the growth factor through a measurement of the BAO damping. An extension of our formula based on the Lagrangian perturbation theory is also discussed.

1 Introduction

The Baryon Acoustic Oscillations (BAO) imprinted in galaxy clustering has recently attracted remarkable attention, as a powerful probe for exploring the nature of mysterious dark energy component commonly believed to be responsible for the accelerated expansion of the universe [2]. The usefulness of the BAO to constrain the dark energy has been demonstrated, and a lot of the BAO survey projects are in progress or planned.

Even though the BAO surveys will precisely measure the galaxy power spectrum, but we also need precise theoretical templates, in order to obtain a useful cosmological constraint from observational data. In practice, the observed galaxy power spectrum is contaminated by nonlinear evolution of the density perturbations, redshift-space distortions and galaxy clustering bias. These uncertainties might yield some systematic effects on the BAO signature. Therefore the comparison of theoretical templates with observation is complicated.

We examine one of the above uncertainties about the nonlinear correction due to the gravitational clustering. This effect cause shift of peaks (troughs) and damping of the amplitude of the BAO signature. In this work, we focus on the BAO damping, and investigate the nonlinear correction in an analytic way. As a result, we construct a fitting formula of the BAO damping in weakly nonlinear regime. We also discuss the feasibility of constraining the growth factor of density fluctuations using a measurement of the BAO damping.

2 Damping of the baryon acoustic oscillations

In this section, we examine the BAO damping due to the nonlinear gravitational clustering with employing the third order perturbation theory. The BAO signature in the matter power spectrum can be extracted as follows:

$$B(k,z) \equiv \frac{P(k,z)}{\tilde{P}(k,z)} - 1, \tag{1}$$

where $P(k,z)$ is the matter power spectrum including the BAO, but $\tilde{P}(k,z)$ is the matter power spectrum without the BAO, which is calculated using the no-wiggle transfer function in [3]. Hereafter, the quantity with the 'tilde' implies the quantity calculated using the no-wiggle transfer function.

[1]This work is based on a collaboration with Kazuhiro Yamamoto and Takahiro Nishimichi, which is published in Ref.[1].

[2]E-mail:hide@theo.phys.sci.hiroshima-u.ac.jp

2.1 Analytic approach

Within the standard perturbation theory (SPT) up to the third order of density perturbation, the second order power spectrum is expressed by

$$P_{\rm SPT}(k,z) = D_1^2(z)P_{\rm lin}(k) + D_1^4(z)P_2(k), \tag{2}$$

with

$$P_2(k) = P_{22}(k) + 2P_{13}(k), \tag{3}$$

where $D_1(z)$ is the growth factor of the density perturbation, $P_{\rm lin}(k)$ is the linear power spectrum, and $P_{22}(k)$ and $2P_{13}(k)$, which describe mode-couplings of density perturbations, are explicitly given by

$$P_{22}(k) = \frac{k^3}{392\pi^2}\int_0^\infty dr P_{\rm lin}(kr)\int_{-1}^1 dx P_{\rm lin}\left[k(1+r^2-2rx)^{1/2}\right]\frac{(3r+7x-10rx^2)^2}{(1+r^2-2rx)^2}, \tag{4}$$

$$2P_{13}(k) = \frac{k^3}{1008\pi^2}P_{\rm lin}(k)\int_0^\infty dr P_{\rm lin}(kr)\left[\frac{12}{r^2} - 158 + 100r^2 - 42r^4 + \frac{3}{r^3}(r^2-1)^3(7r^2+2)\ln\left|\frac{1+r}{1-r}\right|\right]. \tag{5}$$

From Eq.(1), we have

$$B_{\rm SPT}(k,z) = \frac{P_{\rm SPT}(k,z)}{\tilde{P}_{\rm SPT}(k,z)} - 1 = \frac{P_{\rm lin}(k) + D_1^2(z)P_2(k)}{\tilde{P}_{\rm lin}(k) + D_1^2(z)\tilde{P}_2(k)} - 1. \tag{6}$$

One of the aim of this work is to understand the BAO damping in detail. To this end, we here adopt the following approximations;

$$P_{22}(k) \simeq \tilde{P}_{22}(k), \tag{7}$$

$$2P_{13}(k) \simeq 2\tilde{P}_{13}(k)\left[1 + B_{\rm lin}(k)\right]. \tag{8}$$

Using these approximations and taking up to the second order of $D_1(z)$, Eq.(6) yields

$$B_{\rm SPT}(k,z) \simeq \left[1 - D_1^2(z)\frac{\tilde{P}_{22}(k)}{\tilde{P}_{\rm lin}(k)}\right]B_{\rm lin}(k), \tag{9}$$

where $B_{\rm lin}(k) \equiv P_{\rm lin}(k)/\tilde{P}_{\rm lin}(k) - 1$. This expression indicates that the leading effect of the nonlinear mode-coupling on the damping is described by the factor $-D_1^2(z)\tilde{P}_{22}(k)/\tilde{P}_{\rm lin}(k)$, and that the sign of the term clearly shows that this effect is a damping.

From a detailed analysis of $\tilde{P}_{22}(k)/\tilde{P}_{\rm lin}(k)$ as a function of k, we find that the following fitting formula works well,

$$\frac{\tilde{P}_{22}(k)}{\tilde{P}_{\rm lin}(k)} = \sigma_8^2\left(\frac{k}{k_n}\right)^2\left(1 - \frac{\gamma}{k}\right), \tag{10}$$

where σ_8 is the rms matter density fluctuations averaged over the sphere with the radius of $8h^{-1}$Mpc, k_n and γ are fitting parameters which depend on $\Omega_m h^2$, $\Omega_b h^2$ and n_s,

$$k_n = -1.03(\Omega_m h^2 + 0.077)(\Omega_b h^2 - 0.24)(n_s + 0.92) \ \ h{\rm Mpc}^{-1}, \tag{11}$$

$$\gamma = -11.4(\Omega_m h^2 - 0.050)(\Omega_b h^2 - 0.076)(n_s - 0.34) \ \ h{\rm Mpc}^{-1}. \tag{12}$$

Though these dependence on the cosmological parameter might have to be investigated more carefully, but the validity is guaranteed in the following narrow range: $0.13 \lesssim \Omega_m h^2 \lesssim 0.15$, $0.022 \lesssim \Omega_b h^2 \lesssim 0.024$, $0.94 \lesssim n_s \lesssim 0.98$.

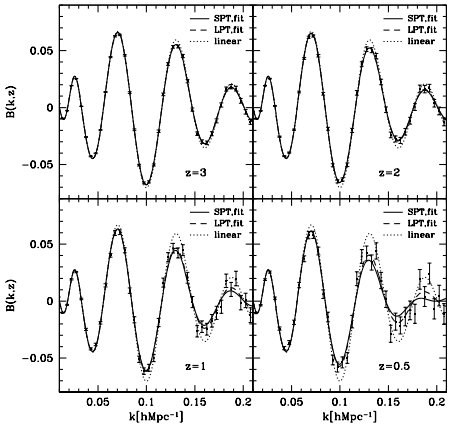

Figure 1: The square with the error bar is the result of N-body simulation. The solid curve is the fitting formula based on the SPT, Eq.(9), while the dotted curve is the linear theory. The dashed curve is the result of an extended fitting formula, Eq.(15).

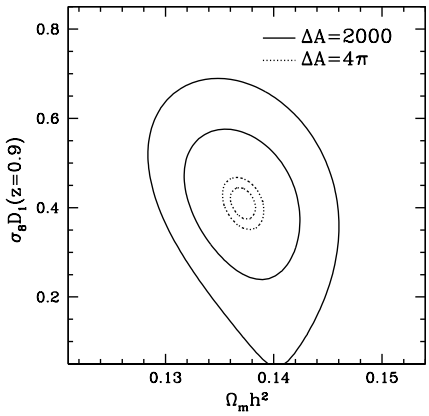

Figure 2: Constraint on $\sigma_8 D_1(z)$ and $\Omega_m h^2$. The solid and the dotted circle correspond to $\Delta A = 2000\mathrm{deg}^2$ and $\Delta A = 4\pi$, respectively. Inner and our circle indicate 1σ and 2σ confidence level, respectively.

2.2 Possible extension

The SPT formula is useful to analyse the BAO damping in an analytic way, however, it is not enough for precise predictions that match with result of N-body simulations in the regime where the nonlinear effect becomes significant. Recently, several authors have developed new formalism beyond the SPT.As an alternative to the SPT, we here consider the work proposed by [4], which uses the technique of resumming infinite series of higher order perturbations on the basis of the Lagrangian perturbation theory (LPT). One of the advantage of this approach is the simplicity of the resulting expression of the nonlinear power spectrum, which enable us to incorporate the result into our formula.

In the framework of the LPT[4], the matter power spectrum is given by

$$P_{\rm LPT}(k,z) = e^{-D_1(z)^2 g(k)}\left[D_1(z)^2 P_{\rm lin}(k) + D_1(z)^4 P_2(k) + D_1(z)^4 P_{\rm lin}(k) g(k)\right], \tag{13}$$

where

$$g(k) = \frac{k^2}{6\pi^2}\int dq P_{\rm lin}(q). \tag{14}$$

With an approximation $g(k) \simeq \tilde{g}(k)$ in addition to Eq.(7) and Eq.(8), we can obtain the leading correction of the BAO,

$$B_{\rm LPT}(k,z) \simeq \left[1 - \frac{D_1^2(z)}{1 + D_1^2(z)\tilde{g}(k)}\frac{\tilde{P}_{22}(k)}{\tilde{P}_{\rm lin}(k)}\right] B_{\rm lin}(k). \tag{15}$$

Comparing Eq.(15) and Eq.(9), the difference is the contribution from $D_1^2(a)\tilde{g}(k)$ in the denominator in front of $\tilde{P}_{22}(k)/\tilde{P}_{\rm lin}(k)$. Since $\tilde{g}(k)$ is positive, this correction make the BAO damping weaker compared with Eq.(9).

Figure 1 shows an example to show the agreement of our fitting formula with the result of N-body simulation. As one can see from this figure, the fitting formula of $B_{\rm LPT}$ (dashed curve) better reproduces the result from N-body simulation (square with error bar) compared with the case of the SPT (solid curve), especially for larger wavenumber even at lower redshift.

3 Future feasibility of constraining the growth factor

As shown in the previous section, the BAO damping is closely related with the amplitude of the power spectrum, which is determined by $\sigma_8 D_1(z)$. In this section, we discuss the feasibility of constraining $\sigma_8 D_1(z)$ by measuring the BAO damping in the power spectrum in quasi-nonlinear regime. To this end, the formula developed in the previous section is useful.

As mentioned in section 1, the redshift-space distortions and the clustering bias might be additionally influential to the BAO damping[6]. However, we here assume an optimistic case that the damping is determined by the quasi-nonlinear clustering effect and neglect the effects of the redshift-space distortions and the clustering bias. Then, we study how a measurement of the damping is useful to determine $\sigma_8 D_1(z)$. Very recently, it is recognized that a measurement of the growth factor of the density perturbations is a key to distinguish between the dark energy model and modified gravity model for the cosmic accelerated expansion (e.g., [5], and references therein). Our investigation is the first step to investigate if a measurement of the BAO damping is useful to measure the growth factor.

In our investigation, we adopt a simple Monte Carlo simulation (for detail, [1]) of the galaxy power spectrum assuming the ΛCDM model and assess χ^2 as

$$\chi^2 = \sum_i \frac{\left[B(k_i,z)^{th} - B(k_i,z)^{obs}\right]^2}{\triangle B^2(k_i,z)}, \tag{16}$$

where $B(k_i,z)^{th}$ is the theoretical one of a fiducial target model at the wavenumber k_i, which corresponds to the cosmological model of $h = 0.7$, $\Omega_m = 0.28$, $\Omega_b = 0.046$, $\sigma_8 = 0.82$ and $n_s = 0.96$, while $B(k_i,z)^{obs}$ is the corresponding observational one which obtained through a Monte Carlo simulation.

Figure 2 shows an example of the constraint of $\sigma_8 D_1(z)$. Solid curves show the contour of $\triangle\chi^2 = 2.3$ (inner curve) and $\triangle\chi^2 = 6.17$ (outer curve), which corresponds to the 1 σ and the 2 σ confidence level, respectively, in the $\Omega_m h^2$ and $\sigma_8 D_1(z = 0.9)$ plane, for the WFMOS-like galaxy sample of $\Delta A = 2000$ deg^2. The dotted curves show the same but with the sample of the survey area $\Delta A = 4\pi$ steradian.

4 Summary

In this work, we examined the effect of the nonlinear gravitational clustering on the BAO signature in the matter power spectrum. In particular, we focus on the BAO damping in the weakly nonlinear regime. With the analytic approach based on the third order perturbation theory, we found a simple expression that describe the BAO damping. We showed that the leading correction for the damping is in proportional to the amplitude of the power spectrum. On the basis of the result, we construct a fitting formula for the BAO damping in weakly nonlinear regime and discussed a possible extension of our formula by using the Lagrangian perturbation theory. This formula was compared with a result of N-body simulation, which showed the validity of the extended formula. A measurement of the BAO damping might be useful as an unique probe of the growth factor of the density perturbations. As a first step to investigate such a possibility, we assessed the feasibility of constraining $\sigma_8 D_1(z)$ by measuring the BAO damping. We need a very wide survey area of the sky. For a definite conclusion, however, we must include the effect redshift-space distortion on the BAO damping. More detailed discussions are given in Ref.[6].

References

[1] Nomura H, Yamamoto K & Nishimichi T, J. Cosmol. Astropart. Phys. **0810** (2008) 031

[2] Albrecht A *et al*, 2006 arXiv:astro-ph/0609591

[3] Eisenstein D J and Hu W, 1998 Astrophys. J. 496 605

[4] Matsubara T, 2008 Phys. Rev. D 77 063530

[5] Yamamoto K, Sato T and Hütsi G, 2008 Prog. Theor. Phys. 120 609

[6] Nomura H, Yamamoto K, Hütsi G & Nishimichi T, in preparation.

Quasinormal Modes of Black Holes Localized on the Randall-Sundrum 2-brane

Masato Nozawa[1] and Tsutomu Kobayashi[2]

Department of Physics, Waseda University, Okubo 3-4-1, Shinjuku, Tokyo 169-8555, Japan

Abstract

We explore the quasinormal modes of a black hole localized on the Randall-Sundrum 2-brane against the test field perturbations [1]. The background metric admits a conformal Killing tensor, which allows us to obtain tractable–indeed separable–field equations for the conformally coupled scalar, the massless Dirac and the Maxwell fields. We find that each radial equation obeys the same equation as the corresponding equation in the Schwarzschild background with the same horizon radius. The angular equation reflects the impact of brane tension, resulting in a distinct quasinormal mode prediction.

1 Exact description of a braneworld black hole

The Randall-Sundrum scenario has attracted much attention for intriguing phenomenological prediction in particle physics and cosmological scenario [2]. In order to further validate this model, the strong gravity test is imperative. Black holes are the best experimental fields for this purpose. Despite that a lot of effort has been devoted toward finding an exact solution describing a black hole localized on the Randall-Sundrum 3-brane, none of them are successful yet. Some authors discussed based on the AdS/CFT correspondence that the static (and large) back holes fail to exist [3, 4]. Under the present circumstances, it is very illustrative to look in a bird's-eye view. We consider a simple toy model and extract useful information. Emparan, Horowitz and Myers succeeded in constructing the desired black hole solution in a 3+1-dimensional Randall-Sundrum model [5], on which we will focus hereafter.

The Randall-Sundrum braneworld has a negative cosmological constant in the bulk, so as to reproduce a Newtonian gravity on the brane. An important point to notice is the fact that the brane undergoes a uniform acceleration in the background AdS. So the repelling acceleration is required to obtain a static black hole. In 4-spacetime dimensions, the C-metric in AdS is the desired solution. For the Z_2-symmetry across the brane, the metric describing a localized black hole is given by

$$g_{ab}\mathrm{d}x^a\mathrm{d}x^b=\frac{\ell^2}{(|x|-y)^2}\left[F(y)\mathrm{d}t^2-\frac{\mathrm{d}y^2}{F(y)}+\frac{\mathrm{d}x^2}{G(|x|)}+G(|x|)\mathrm{d}\varphi^2\right], \tag{1}$$

where

$$F(y)=-y^2-2\mu y^3, \qquad G(x)=1-x^2-2\mu x^3. \tag{2}$$

The metric (1) solves Einstein's equations with a negative cosmological constant, $R_{ab}=-(3/\ell^2)g_{ab}$, for $|x|>0$. The brane locus is $x=0$, across which the bulk has a mirror symmetry. Israel's junction condition shows that the brane tension is proportional to $1/\ell$. The x and y-coordinates are the direction cosine $x=\cos\theta$ and the radial coordinate $y=-\ell/r$. x ranges from the brane $x=0$ to the axis $x=x_2$–the largest root of $G(x_2)$–and y from the horizon $y=-1/2\mu$ to infinity $y=x$. Observe that in order to avoid conical singularities on the axis $x=x_2$, the period of φ is fixed by $\Delta\varphi=2\pi\beta$, where $\beta^{-1}=-G'(x_2)/2$.

The parameter μ corresponds to the mass of the black hole, hence we take $\mu\geq 0$. The black hole with small μ mimics the isolated black hole. Indeed, one can confirm easily that the $\mu\to 0$ limit with $r_h=2\mu\ell$ fixed recovers the Schwarzschild black hole with the horizon radius $r_h(\ll\ell)$. On the other hand, the horizon will become flattened in the $\mu\gg 1$ limit (see Fig. 1). In the latter case, the brane tension has a distinguished effect on the properties of black holes from the isolated ones.

[1]Email:nozawa“ at”gravity.phys.waseda.ac.jp
[2]Email:tsutomu“ at”gravity.phys.waseda.ac.jp

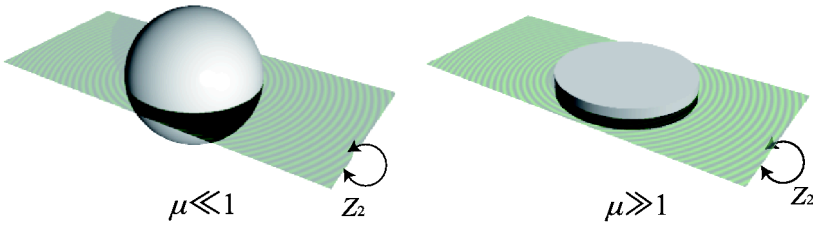

Figure 1: Schematic picture of a black hole localized on the brane. For $\mu \ll 1$, the horizon is round (left). As μ increases, the horizon tends to deform into a flattened pancake (right).

The induced metric on the brane reads

$$\mathrm{d}s^2 = -\left(1-\frac{r_h}{r}\right)\mathrm{d}\tilde{t}^2 + \left(1-\frac{r_h}{r}\right)^{-1}\mathrm{d}r^2 + r^2\mathrm{d}\varphi^2, \tag{3}$$

where $\tilde{t} = \ell t$. Since $\Delta\varphi$ is less than 2π, the 2+1 dimensional gravity is recovered on the brane, as we desired.

2 Quasinormal frequencies

Since the black hole metric (1) is so involved, little is known about the quantitative properties of the solution. Quasinormal modes of black holes are the highly suggestive quantities to identify the intrinsic properties black holes.

At first glance, the background metric would not allow a separation of variables. Indeed, the massless scalar field equation are not separable, due to the overall factor $(x-y)^{-2}$ in front of the metric. We will circumvent this difficulty by restricting ourselves to conformally invariant field equations–the conformally coupled scalar field, the massless Dirac field and the Maxwell fields. For these fields, we can discard the annoying factor $(x-y)^{-2}$ from the equations of motion via the simple conformal transformation

$$\hat{g}_{ab} = \Omega^2 g_{ab}, \qquad \Omega = x - y. \tag{4}$$

In this article, only the conformally coupled scalar field is discussed. But we can proceed analogously for the Dirac and Maxwell fields, the behavior of which are qualitatively the same. A more detailed analysis can be found in Ref. [1].

A conformally coupled scalar field evolves according to

$$\left(\nabla_a\nabla^a - \frac{1}{6}R\right)\Phi = 0, \tag{5}$$

which is form-invariant under the conformal transformation (4) with $\Phi \to \hat{\Phi} = \Omega^{-1}\Phi$. Let us assume the separable form $\hat{\Phi} = e^{-i\omega t + im\varphi/\beta}R_0(y)S_0(x)$. Noticing that the Ricci scalar of the conformally related metric $\hat{g}_{ab}$ is $\hat{R} = 12\mu(x-y)$ and working in the $x > 0$ region, we can reduce the field equation to "angular" and "radial" equations as

$$\frac{\mathrm{d}}{\mathrm{d}x}\left[G(x)\frac{\mathrm{d}}{\mathrm{d}x}S_0\right] + \left[\nu(\nu+1) - 2\mu x - \frac{m^2/\beta^2}{G(x)}\right]S_0 = 0, \tag{6}$$

$$\frac{\mathrm{d}}{\mathrm{d}y}\left[F(y)\frac{\mathrm{d}}{\mathrm{d}y}R_0\right] + \left[\nu(\nu+1) - 2\mu y + \frac{\omega^2}{F(y)}\right]R_0 = 0, \tag{7}$$

where ν is the separation constant. Taking into account the Z_2-symmetry across the brane, equation (6) gives rise to the Neumann boundary condition at the brane, $\mathrm{d}S_\mathrm{s}/\mathrm{d}x|_{x=0} = 0$. The boundary condition at

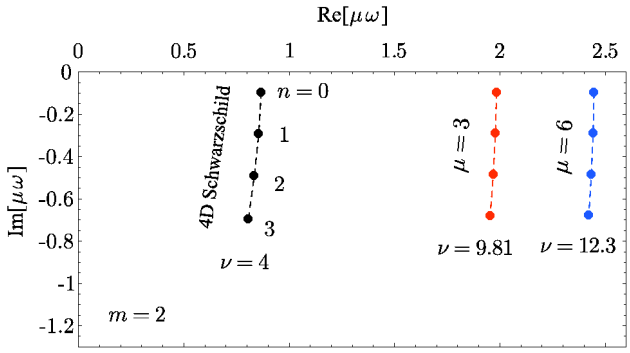

Figure 2: Quasinormal modes of a conformally coupled scalar for $m = 2$. The plots are for the second lowest ν modes.

$x = x_2$, on the other hand, is read off by defining $\tilde{S}_0 := (x_2 - x)^{-|m|/2} S_0$ and requiring the regularity for $\tilde{S}_0$ at $x = x_2$. The angular eigenvalue is obtained numerically [1]. The numerical result shows that as μ increases, the angular eigenvalue ν will become large. This tendency is also found for the codimension-two brane (see, e.g., [6]). For $\mu \ll 1$, $\nu - m$ is approximated by an even integer, recovering the (even mode) spectrum in the Schwarzschild background.

Let us move on to the analysis of equation (7). This equation can be written in a familiar form using $r = -\ell/y$ and $\mathrm{d}r_* = (1 - 2\mu\ell/r)^{-1}\mathrm{d}r$. The black hole horizon is mapped to $r_* = -\infty$ ($r = 2\mu\ell$), while the acceleration horizon $y = 0$ corresponds to $r_* = +\infty$. In terms of r_*, equation (7) is translated into the Schrödinger-type equation

$$\frac{\mathrm{d}^2}{\mathrm{d}r_*^2} R_0 + [\tilde{\omega}^2 - V_0(r)] R_0 = 0, \qquad V_0(r) = \left(1 - \frac{2\mu\ell}{r}\right)\left(\frac{\nu(\nu+1)}{r^2} + \frac{2\mu\ell}{r^3}\right), \tag{8}$$

where $\tilde{\omega} := \omega/\ell$. It is important to note that equation (8) is apparently identical to the radial equation for the (conformally coupled) scalar field perturbation in the four dimensional Schwarzschild background with the horizon radius $r_h = 2\mu\ell$. *The only distinction arises from the different angular eigenvalues.*

We impose the following quasinormal boundary conditions for the radial equation

$$R_0 \to e^{+i\tilde{\omega} r_*} \quad (r_* \to \infty), \qquad R_0 \to e^{-i\tilde{\omega} r_*} \quad (r_* \to -\infty). \tag{9}$$

having only an incoming wave at the black hole horizon and an outgoing wave at the acceleration horizon. These boundary conditions give rise to a discrete frequency, corresponding to the quasinormal modes of black holes. We employ the third order WKB method developed by Iyer and Will [7] in order to evaluate the quasinormal modes. We show the result in Fig. 2. We have normalized the frequencies by (half of) the horizon radius: $\mu\ell \cdot \tilde{\omega} = \mu\omega$. As μ increases, the real part of quasinormal modes are likely to enlarge, as expected from the results in Ref. [6].

The WKB approximation will fail for higher overtones with $n > \nu$. The asymptotic quasinormal modes ($n \gg 1$) are obtained using the monodromy method [8] as

$$\mu\omega_n \approx \frac{\ln 3}{8\pi} - \frac{\mathrm{i}}{4}\left(n + \frac{1}{2}\right), \tag{10}$$

where one takes $n \to \infty$. This is independent of the angular eigenvalue and therefore the leading order behavior will be the same for the brane-localized and braneless black holes.

3 Summary

In this article we explored the quasinormal modes of black holes localized on the Randall-Sundrum 2-brane. The background is the exact black hole solution found in Ref. [5]. Taking advantage the fact that

the background metric allows a conformal Killing tensor, which is a direct consequence of Petrov type D, we have investigated the behavior of conformally invariant field perturbations around the brane-localized black hole.

For all types of fields we considered, we found that each radial equation is identical to the corresponding field equation in the four Schwarzschild background. However, the angular equations differ from their Schwarzschild counterparts. We have determined the angular eigenfunctions and eigenvalues numerically. In the case of the conformal scalar field, the angular eigenvalues ν are given by $\nu \simeq l = 0, 1, 2, ...$ for a small black hole ($\mu \ll 1$), recovering the Schwarzschild result. As the size of the black hole increases, ν becomes larger ($\nu > l$) and hence become sensitive to the magnetic quantum number m. Accordingly, each quasinormal modes of the large localized black hole (with the horizon radius $2\mu\ell$ on the brane) behaves like the mode having a larger angular mode number in the four dimensional Schwarzschild background with the same horizon radius $r_h = 2\mu\ell$. The situation is basically the same for electromagnetic and massless Dirac field perturbations. In particular, we have found no unstable modes for any types of fields we investigated.

It has been widely known that the Randall-Sundrum braneworlds have a rich structure concerning the AdS/CFT correspondence [3, 4]. It would be also interesting to discuss the implications of our result from the viewpoint of the AdS/CFT correspondence.

Acknowledgements. MN and TK are supported by the JSPS under Contract Nos. 19-204 and 19-4199.

References

[1] M. Nozawa and T. Kobayashi, Phys. Rev. D. 78 064006 (2008) [arXiv:0803.3317 [hep-th]].

[2] L. Randall and R. Sundrum, Phys. Rev. Lett. **83**, 3370 (1999) [arXiv:hep-ph/9905221]; L. Randall and R. Sundrum, Phys. Rev. Lett. **83**, 4690 (1999) [arXiv:hep-th/9906064].

[3] T. Tanaka, Prog. Theor. Phys. Suppl. **148**, 307 (2003) [arXiv:gr-qc/0203082].

[4] R. Emparan, A. Fabbri and N. Kaloper, JHEP **0208**, 043 (2002) [arXiv:hep-th/0206155].

[5] R. Emparan, G. T. Horowitz and R. C. Myers, JHEP **0001**, 007 (2000).

[6] T. Kobayashi, M. Nozawa and Y. i. Takamizu, Phys. Rev. D **77**, 044022 (2008) [arXiv:0711.1395 [hep-th]].

[7] S. Iyer and C. M. Will, Phys. Rev. D **35**, 3621 (1987).

[8] L. Motl, Adv. Theor. Math. Phys. **6**, 1135 (2003) [arXiv:gr-qc/0212096].

Classicality of the stochastic approach to inflation

Yuji Ohsumi[1] and Yasusada Nambu[2]

Department of Physics, Nagoya University, Nagoya, 464–8602, Japan

Abstract

The stochastic approach to the inflationary universe is the method which treats quantum time evolution of long wave length mode of an inflaton field as a stochastic process. In this presentation, we discuss the conditions for the probability distribution to behave as classical one by using the bipartite entanglement, or quantum correlation among two regions.

1 Introduction

The inflationary scenario indicates that the large scale structure in the present universe originated from the quantum fluctuation of a field in the early universe. There is a conventional method to calculate this fluctuation, called stochastic approach [1, 2]. In this approach, by coarse-graining the quantum field in the inflationary universe over the super-horizon scale, the quantum stochastic behavior of the field is represented by a classical distribution function. Classical distribution means a positive definite normalized function. This method is based on the naive assumption in the inflationary scenario that the quantum field becomes classical when their wave length exceeds to the super-horizon scale by the inflationary expansion. And this is used to calculate various quantities including the non-Gaussian fluctuations.

However, it is in general impossible to describe the quantum mechanical nature by using a classical distribution. For example, let us consider two particles with spin half in the follwing state.

$$|\psi\rangle = \frac{1}{\sqrt{2}}(|\uparrow\uparrow\rangle + |\downarrow\downarrow\rangle),$$

where the first arrow in each term is the state of one spin, and the second is that of the other spin. Note that the direction of one particle fluctuates and is not fixed. If we observe this direction and obtain the result "↑", then that of the other spin also becomes "↑". In other words, the observation on one degree of freedom affects the other degree of freedom. Such a correlation between two degrees of freedom is called entanglement, which is known as purely quantum correlation and does not exist in classical mechanics. J. S. Bell showed that the the classical distribution function cannot reproduce the correlations in the system under this state [3]. Cavalcanti *et al.* showed that this theorem is valid for general bipartite systems [4]. Thus general bipartite systems in entangled state do not have the classical distribution function. Therefore, if the coarse-grained region has entanglement with another region, there does not exist the classical distribution function describing the stochastic nature of the field. Then the stochastic approach is not valid.

Nambu showed that, if the entanglement in the system disappear, the classical distribution for the system appears [5]. We investigated the classicality condition for the stochastic approach by applying Nambu's result to the quantum field in inflaionary universe. In conclusion, we find that the system can be treat as classical if the coarse-graining scale is sufficiently large.

2 Classicality condition

2.1 The entanglement measure

In this section, we introduce the entanglement measure λ which is necessary to represent the classicality condition. Let us consider a bipartite system $(q,\ p)$, $(Q,\ P)$ in Gaussian state. We introduce the

[1]E-mail:osumi@gravity.phys.nagoya-u.ac.jp
[2]E-mail:nambu@gravity.phys.nagoya-u.ac.jp

correlation matrix $A,\ B,\ V$ for this system as follows:

$$A := \begin{pmatrix} \langle\{\Delta q,\ \Delta q\}\rangle & \langle\{\Delta q,\ \Delta p\}\rangle \\ \langle\{\Delta p,\ \Delta q\}\rangle & \langle\{\Delta p,\ \Delta p\}\rangle \end{pmatrix} \qquad A' = \begin{pmatrix} \langle\{\Delta Q,\ \Delta Q\}\rangle & \langle\{\Delta Q,\ \Delta P\}\rangle \\ \langle\{\Delta P,\ \Delta Q\}\rangle & \langle\{\Delta P,\ \Delta P\}\rangle \end{pmatrix}$$
$$B := \begin{pmatrix} \langle\{\Delta q,\ \Delta Q\}\rangle & \langle\{\Delta q,\ \Delta P\}\rangle \\ \langle\{\Delta p,\ \Delta Q\}\rangle & \langle\{\Delta p,\ \Delta P\}\rangle \end{pmatrix} \qquad V := \begin{pmatrix} A & B \\ B & A \end{pmatrix},$$

where $\{X,\ Y\} := (XY + YX)/2$, $\langle\ \rangle$ is the quantum average value of some quantity, and $\Delta q := q - \langle q \rangle$ is the deviation of the quantity q. The matrices A and A' are the auto correlation for each degree of freedom respectively; the matrix B is the correlation between these degrees of freedom; the matrix V is the correlation matrix for the bipartite system. We assume that $A = A'$ here. This assumption does not make any problem on the description of the quantum fluctuation in inflation. Now, let us define the entanglement measure λ using these quantities as follows:

$$\lambda = \sqrt{\det A - \det B - \sqrt{(\det A - \det B)^2 - \det V}}$$

This is real quantity with the dimension of $\hbar$. If $\lambda < \hbar$, the system is entangled and the smaller λ is, the stronger the degree of entanglement is. If $\lambda > \hbar$, entanglement is zero.

We can state the classicality condition using this λ as follows:

Classicality condition

> For a bipartite system in Gaussian state, if $\lambda \gg \hbar$, the stochastic proparty of the variables in this system is described using a classical distribution function.

Note that the condition is not $\lambda > \hbar$ but $\lambda \gg \hbar$. This statement is stronger than the disappearence of the entanglement (figure 1).

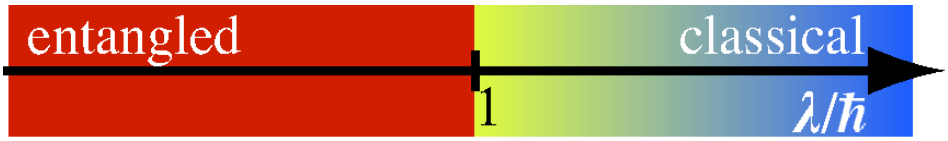

Figure 1: The schematic picture of the relation between entanglement and classicality. If $\lambda \gg \hbar$, the system is classical, and there exists a classical distribution.

With in our mind this, we can construct the strategy for finding the classicality condition as follows: First, we introduce the coarse-grained field in the method of the stochastic approach; second, we calculate the second order correlations of the field between 2 points, and find λ; finally, we investigate whether the way of coarse-graining such that $\lambda \gg \hbar$ exists or not in the regime of stochastic approach. Under this procedure, we consider the classicality condition in the next section.

3 Model and Results

3.1 Model

Now, let us investigate the quantum fluctuation of the scalar field. As the expansion law of the universe, we assume the de Sitter spacetime ($a \propto \exp Ht$), the power law model ($a \propto t^n$), and the Minkowski spacetime. We use the minimally coupling massless real scalar field, and assume that the back reaction to the gravitational field can be neglegible.

In the stochastic approach, the coarse-grained field is obtained by using the ultra-violet cut off $k_S := \varepsilon aH$; ε is a dimensionless parameter; a is the scale factor; H is the Habble parameter. Then the coarse-graining scale in physical scale is $a/k_S = 1/\varepsilon H$ (figure 2). This is constant in time. Note that this scale is determined by ε. The smaller value it takes, the larger the scale becomes. Futhermore, we insert another

cut off $k_0 := \alpha\varepsilon a_0 H$ to prevent the infra-red divergence; a_0 is the scale factor at the initial time. And we have inserted another parameter α so that these cut off do not coinside at the initial time.

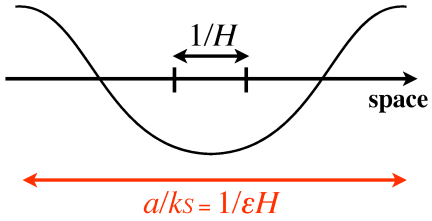

Figure 2: The schematic image of the ultra-violet cut off. The field is coarse-grained with the physical scale $a/k_S = 1/\varepsilon H$. This scale is constant in time.

Then the coarse-grained field operators are follows.

$$\chi = \int_{k_0 \leq |\mathbf{k}| \leq k_S} (a_{\mathbf{k}} f_\chi e^{i\mathbf{k}\cdot\mathbf{x}} + \text{h.c.}) d\mathbf{k}^3, \qquad \pi = \int_{k_0 \leq |\mathbf{k}| \leq k_S} (a_{\mathbf{k}} f_\pi e^{i\mathbf{k}\cdot\mathbf{x}} + \text{h.c.}) d\mathbf{k}^3,$$

where χ and π are the quantities corresponding to the field coordinate and its canonical conjugate momentum, respectively; f_χ and f_π are the mode functions of the Fourier expansions of χ and π; $a_{\mathbf{k}}$ is the annihilation operator of $\mathbf{k}$ -mode saticefying the usual commutation relation

$$[a_{\mathbf{k}}, {a_{\mathbf{l}}}^\dagger] = \delta^{(3)}(\mathbf{k} - \mathbf{l}).$$

Due to the insertion of cut off, the commutation relation between χ and π becomes

$$[\chi(\mathbf{x}), \pi(\mathbf{y})] = \frac{2i}{(2\pi)^2} \int_{k_0}^{k_S} k^2 \frac{\sin kR}{kR} dk. \qquad R := |\mathbf{x} - \mathbf{y}|$$

We must require this commutation relation to be zero for $\mathbf{x} \neq \mathbf{y}$. And this leads to the equation for the comoving distance R,

$$k_0 R \cos k_0 R - \sin k_0 R = k_s R \cos k_s R - \sin k_s R. \tag{1}$$

From now on, we consider the minimum value of R which saticefies 1. This means that we compare the neighbering regions in coarse-grained regions. Because k_S depends on time, R is also time dependent.

3.2 Results

We calculated λ for the considering models. The results are shown in figure 3. Here, figure 3(a), (b), (c) are the case of de Sitter, power law with $n = 6$, and Minkowski, respectively. The vartical axes are $\lambda/\hbar$, the horizontal axes are k_0/k_S. The different lines are the results for the different values of ε, What we would like to pay attention to firstly is the lowest lines in each models. These lines are $\varepsilon \to \infty$, and coinside with the line of Minkowski case. Current coarse-graining scale is $1/\varepsilon H$, and this limit correponds to the limit in which we take the "resolution" of the field infinitly high. On the other hand, since we are comparing the neighbering regions, this means that we are comparing the two spacial points for which the effect of the cosmic expansion is negeligeble.

As we have said, the smaller we take ε, the larger λ gets its value. Since the classicality condition was $\lambda \gg \hbar$, this condition can be replaced with how large λ becomes by taking ε small. By investigating the analytical expression of λ in the limit of $\varepsilon \ll 1$, we find

$$\lambda_{\text{de Sitter}} \propto \frac{1}{\varepsilon} \qquad \lambda_{\text{Power law}} \propto \frac{1}{\varepsilon^{1+2/(n-1)}}$$

Since $n > 1$ for accelerating universe model, both of them diverge in the limit of $\varepsilon \to 0$. In other words, the larger we take the coarse-graining scale, the more the system become classical. Therefore, if we take the coarse-graining scale sufficiently large, the stochastic approach is valid.

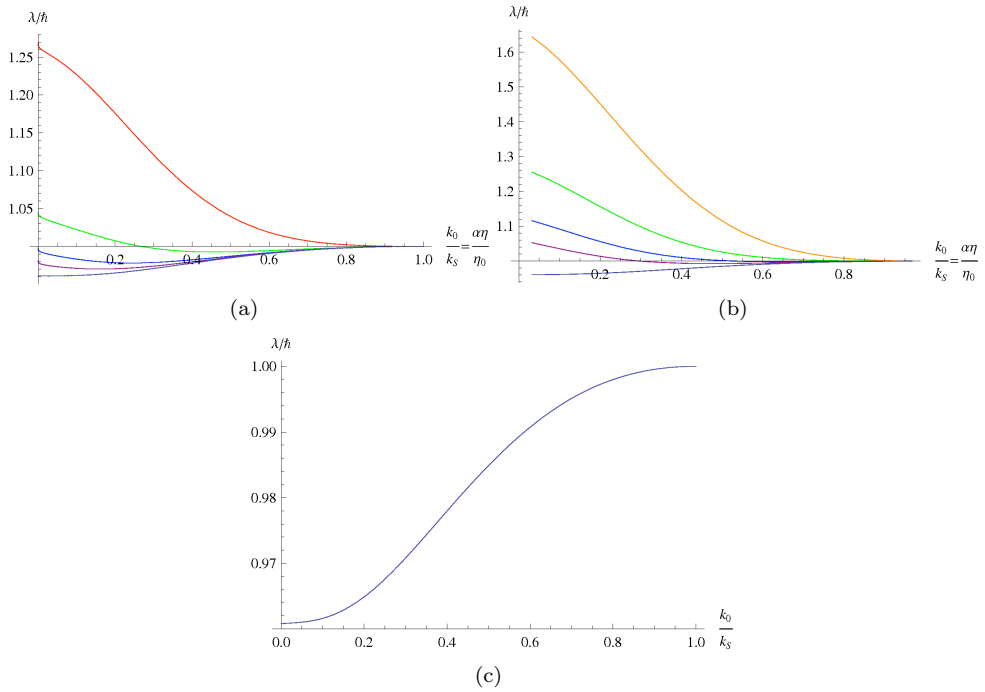

Figure 3: Entanglement measure λ in each model. The horizontal axes are k_0/k_S, which is $\alpha\eta/\eta_0$ in expanding universe models. (a) de Sitter model case : Red, green, blue, purple, and pale-purple lines are $\varepsilon = 1,\ 2,\ 3,\ 4$, and $\varepsilon \to \infty$, respectively. (b) Power law model case ($n = 6$) : Orange, green, blue, purple, and pale-purple lines are $\varepsilon = 1,\ 3/2,\ 2,\ 5/2$, and $\varepsilon \to \infty$, respectively. (c)Minkowski model case.

4 Summary and future works

In this article, we have shown that the stochastic approach is valid from the view point of entanglement. Since we treat only the Gaussian fluctuation, we must investigate the non-Gaussian fluctuation next. Since the classical condition derived by Nambu is valid for only Gaussian state, some extension is necessary. And, we neglected the back reaction to the gravitational field. Since the stochastic approach is also used to investigate the case with the back reaction , it is important problem to extend for involving the back reaction.

On the other hand, the consideration for λ itself is interesting problem. In this investigation, we inserted the infra-red cut off for preventing the infra-red divergence. But, as you can see from figure 3, λ is infra-red divergence free. This suggests that λ itself has some clear physical meaning. Making use of this property of λ, we might predict any other quantity.

References

[1] A. A. Starobinsky, *Current Topics in Field Theory, Quantum Gravity, and Strings*, 107

[2] S. Habib, Phys. Rev. D 46, 2408(1992)

[3] J. S. Bell, Physics 1, 195(1964) ; *Speakable and Unspeakable in Quantum Mechanics*(Cambridge University Press, 1987)

[4] E. G. Cavalcanti *et al.* Phys.Rev.Lett 99, 210405(2007)

[5] Y. Nambu, Phys. Rev. D 78, 044023(2008)

Testing general relativity on the scales of cosmology using the redshift-space distortion[1]

Takahiro Sato[2],

Department of Physical Sciences, Hiroshima University, Higashi-hiroshima, 739–8526, Japan

Abstract

As a test of general relativity on cosmological scales, we measure the γ parameter for the growth rate of density perturbations using the redshift-space distortion of the luminous red galaxies (LRG) in the Sloan Digital Sky Survey (SDSS). Assuming the cosmological constant model, which matches the results of the WMAP experiment, we find $\gamma = 0.63 + 2.0 \times (\sigma_8 - 0.8) \pm 0.09$ at 1σ confidence level, which is consistent with the prediction of general relativity, $\gamma \simeq 0.55 \sim 0.56$. Rather high value of σ_8 (> 0.85) is required to be consistent with the prediction of the cosmological GDP model, γ ($\simeq 0.68$).

1 Introduction

Modified gravity models, e.g., $f(R)$ gravity, TeVeS theory, DGP model, have been proposed as possible alternatives to the dark energy model. Measurement of the growth of density perturbations will be the key for testing the gravity theory [4]. Several authors have already investigated the growth of density perturbations as a way of constraining these theories [11, 12, 13]. In the future weak lensing statistics will be a promising probe of the density perturbations, while the redshift-space distortions may also be useful for constraining the growth rate of perturbations. Recently, Guzzo et al. have reported a constraint on the growth rate by evaluating the anisotropic correlation function of the galaxy sample from the VIMOS-VLT Deep Survey (VVDS) [14]. The characteristic redshift of the VVDS galaxy sample is rather large. However, the survey area of the VVDS sample is small. This is a disadvantage in detecting the linear redshift-space distortions.

In this work, we used the Sloan Digital Sky Survey (SDSS) luminous red galaxy (LRG) sample from the Data Release 6, whose survey area is around 6,000deg^2. We present the results of the multipole power spectrum analysis for the SDSS LRG sample, and use it to measure the γ parameter for the growth rate of density perturbations.

2 Measurement of the quadrupole spectrum

The peculiar velocity of galaxies contaminates the observed redshift. It leads to the difference in the radial position if the redshift is taken as the indicator of the distance. This causes the difference in the spatial clustering between redshift space and real space, which is called the redshift-space distortion. The power spectrum including the redshift-space distortion can be modeled as (e.g., [8])

$$P(k,\mu) = \left(b(k) + f\mu^2\right)^2 P_{mass}(k)\, D(k,\mu),$$

where μ is the directional cosine between the line of sight direction and the wave number vector, $b(k)$ is the bias factor, $P_{mass}(k)$ is the mass power spectrum, $D(k,\mu)$ describes the damping factor due to the finger of God effect.

Thus, the redshift-space distortion causes the anisotropy of the clustering amplitude depending on μ. The multipole power spectra are defined by the coefficients of the multipole expansion [9, 10], $P(k,\mu) = \sum_{l=0,2,\cdots} P_l(k)\,\mathcal{L}_l(\mu)\,(2l+1)$, where $\mathcal{L}_l(\mu)$ are the Legendre polynomials. The monopole

[1] In collaboration with K. Yamamoto, G. Nakamura and G. Hütsi (see also [1])

[2] E-mail:sato@theo.phys.sci.hiroshima-u.ac.jp

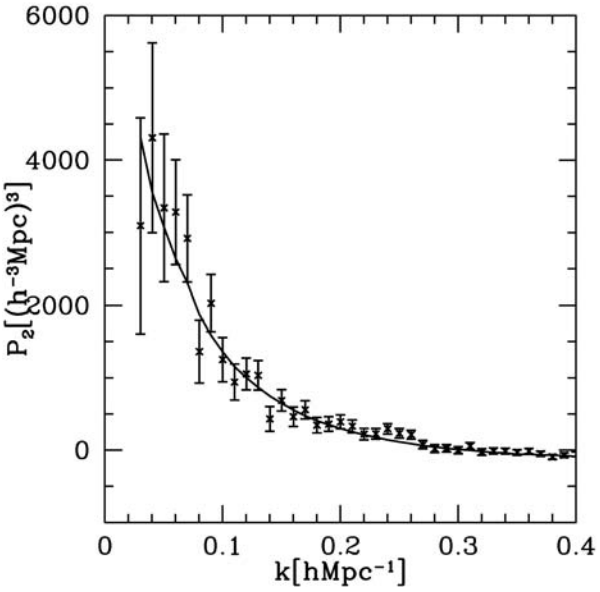

Figure 1: Quadrupole power spectrum. The solid curve is the theoretical curve of the ΛCDM model.

$P_0(k)$ represents the angular averaged power spectrum and is usually what we mean by the power spectrum. $P_2(k)$ is the quadrupole spectrum, which gives the leading anisotropic contribution. The usefulness of the quadrupole spectrum for the dark energy is discussed in [7].

Within the linear theory of density perturbations, the quadrupole spectrum is given by $P_2(k) = \left[4b(k)f/3 + 4f^2/7\right] P_{mass}(k)/5$. Thus, we can measure the growth rate from the quadrupole spectrum. However, we need other independent information for the clustering bias $b(k)$.

By using the quadrupole spectrum, we perform a simple test of the gravity theory. We focus on the γ parameter, which is introduced to parameterise the growth rate as $f \equiv d\ln D_1(a)/d\ln a = \Omega_m(a)^\gamma$, where $\Omega_m(a) = H_0^2\Omega_m a^{-3}/H(a)^2$, $H(a) = \dot{a}/a$, $H_0(= 100h\mathrm{km/s/Mpc})$ is the Hubble parameter. Measurement of γ provides a simple test of the gravity theory. Within general relativity, even with the dark energy component, γ takes the value around $\gamma \simeq 0.55$ [4]. However, γ may take different values in modified gravity models. For example, $\gamma \simeq 0.68$ in the cosmological DGP model including a self-acceleration mechanism. Thus, the measurement of γ is a simple test of general relativity.

In the present work we measured the monopole and quadrupole power spectra in the clustering of the SDSS DR6 luminous red galaxy sample. The galaxy sample used in our analysis consists of 82,000 galaxies overs the survey area of 6,000deg^2 and redshift range $0.16 \leq z \leq 0.47$ [3]. We have excluded the southern survey stripes since these just increase the sidelobes of the survey window without adding much of the extra volume. We have also removed some minor parts of the LRG sample to obtain more continuous and smooth chunk of volume.

We need to take the clustering bias and the finger of God effect into account. For the finger of God effect we adopt the following form of $D(k,\mu)$, the damping due to the nonlinear random velocity, $D(k,\mu) = 1/[1 + (k\mu\sigma_v/H_0)^2/2]$, where σ_v is the one dimensional pairwise velocity dispersion. (e.g., [6]). This form of damping assumes an exponential distribution function for the pairwise peculiar velocity. In order to determine the clustering bias, we use the monopole spectrum. If σ_8 is fixed, and the cosmological parameters and the bias are given, we can compute the monopole spectrum $P_0^{theor}(k)$, where we use the Peacock and Dodds formula for the mass power spectrum $P_{mass}(k)$ [8]. We determine the clustering bias $b(k)$ through the condition $P_0^{obs}(k) = P_0^{theor}(k)$ using a numerical method. Here $P_0^{obs}(k)$ is the measured value of the monopole, and $P_0^{theor}(k)$ is the corresponding theoretical value. We used the monopole spectrum to determine the bias, and the quadrupole spectrum to obtain constraints on γ and σ_v. Since the galaxy sample covers rather broad redshift range, $0.16 \leq z \leq 0.47$, the effect of the time-evolution should be considered properly [2]. However, for simplicity, we here evaluated the theoretical spectra at

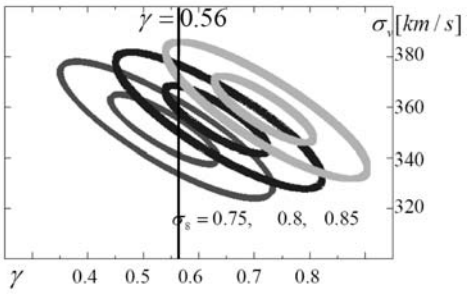

Figure 2: The contour of $\Delta\chi^2$ in the $\gamma - \sigma_v$ plane. We fixed the normalization of the mass power spectrum as $\sigma_8 = 0.75$, 0.80, 0.85. The contour levels are 1-sigma and 2-sigma confidence levels. The other parameters are $h = 0.7$, $n_s = 0.96$, $\Omega_m = 0.28$.

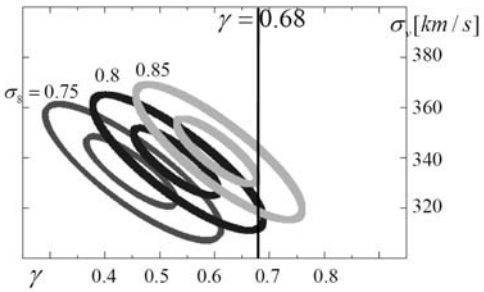

Figure 3: Same as the Figure 2, except here we used the expansion history of the DGP model.

the mean redshift of $z = 0.31$.

Figure 1 plots the quadrupole spectrum. The solid curve is the theoretical curve for the ΛCDM model with $h = 0.7$, $n_s = 0.96$(initial spectral index), Ω_m=0.28, $\sigma_8 = 0.8$, $\gamma = 0.63$, $\sigma_v = 355$km/s.

Figure 2 demonstrates the contour of $\Delta\chi^2$ in the γ versus σ_v parameter plane. We compute χ^2 as $\chi^2 = \sum_i [P_2^{obs}(k_i) - P_2^{theor}(k_i)]/[\Delta P_2^{obs}(k_i)]^2$. Where $P_2^{obs}(k_i)$ and $\Delta P_2^{obs}(k_i)$ are the measured values and errors as plotted in Figure 1. $P_2^{theor}(k_i)$ are the corresponding theoretical value. The curves assume $\sigma_8 = 0.75$, $\sigma_8 = 0.8$, $\sigma_8 = 0.85$. The other parameters are fixed as $h = 0.7$, $n_s = 0.96$, $\Omega_m = 0.28$. In Figure 2 we plot the contour levels in 1-sigma and 2-sigma confidence levels of the χ^2 distribution. We find $\gamma = 0.63 + 2.0 \times (\sigma_8 - 0.8) \pm 0.09$ at 68 percent confidence level, respectively. The value of γ is consistent with general relativity. The result is not sensitive to the inclusion of baryon oscillation in the theoretical power spectrum.

The relation of γ and σ_8 can be understood as the degeneracy between σ_8 and the growth rate f in the following way. As the observed power spectra can be roughly written as $P_0^{obs} \propto b^2(k){\sigma_8}^2 D_1^2(z)/D_1^2(z=0)$ and $P_2^{obs} \propto b(k) f {\sigma_8}^2 D_1^2(z)/D_1^2(z=0)$. The degeneracy between σ_8 and the growth rate f(or γ) in our method is given by $f\sigma_8 D_1(z)/D_1(z=0) =$ constant.

Figure 3 is the analogue of Figure 2, with the expansion history now taken to be that of the spatially flat DGP model, which follows $H^2(a) - H(a)/r_c = 8\pi G\rho/3$, where ρ is the matter density and $r_c = 1/H_0(1-\Omega_m)$ is the crossover scale related to the 5-dimensional Planck mass. the expansion history in this model can be well approximated by the dark energy model with the equation of state parameter $w(a) = w_0 + w_a(1-a)$, where $w_0 = -0.78$ and $w_a = 0.32$, as long as $\Omega_m \sim 0.3$ [4]. However the Poisson equation is modified, and the growth history is approximated by the formula with $\gamma \simeq 0.68$. In order to be consistent with $\gamma = 0.68$, Figure 3 requires higher value of σ_8 as compared to the ΛCDM case. We find $\gamma(\simeq 0.68)$ at 68 percent confidence level, which requires $\sigma_8 \geq 0.85$.

3 Conclusion

We measured the monopole and quadrupole spectra in the spatial clustering of the SDSS LRG sample from DR6. Using the spectra, we measured the γ parameter for the linear growth rate and the pairwise peculiar velocity dispersion. The measured value of γ is consistent with general relativity as long as $0.72 \leq \sigma_8 \leq 0.81$. However, it is inconsistent with the cosmological DGP model, $\gamma \simeq 0.68$, as long as $\sigma_8 < 0.85$. If a constraint on σ_8 from other independent sources, we would be able to obtain tighter constraint on the DGP model. The constraint on γ can be applied to other modified gravity models, given that the value of γ which characterises a particular model is found, as discussed by Linder and Cahn [5].

References

[1] K. Yamamoto, T. Sato and G. Hütsi, Prog. Theor. Phys. 120 (2008), 609

[2] K. Yamamoto and Y. Suto, Astrophys. J. 517 (1999), 1.

[3] G. Hütsi, Astron. Astrophys. 449 (2006), 891; Astron. Astrophys. 459 (2006), 375.

[4] E. V. Linder, Phys. Rev. D 72 (2005), 043529.

[5] E. V. Linder and R. N. Cahn, Astropart. Phys. 28 (2007),481

[6] H. J. Mo, Y. P. Jing and G. Boerner, Mon. Not. R. Astron. Soc. 286 (1997), 979

[7] K. Yamamoto, B. A. Bassett and H. Nishioka Phys. Rev. Lett. 94 (2005), 051301.

[8] J. A. Peacock and S. J. Dodds, Mon. Not. Not. R. Astron. Soc. 280 (1996), L19; Mon. Not. R. Astron. Soc. 267 (1994), 1020

[9] A. N. Taylor and A. J. S. Hamilton, Mon. Not. R. Astron. Soc. 282 (1996), 767.

[10] K. Yamamoto et al., Publ. Astron. Soc. Jpn. 58 (2006), 93.

[11] Y. Wang, J. Cosmol. Astropart. Phys. 05 (2008), 021.

[12] C. di Porto and L. Amendola, Phys. Rev. D 77 (2008), 083508.

[13] S. Nesseris and L. Perivolaropoulos, Phys. Rev. D77 (2008), 023504.

[14] L. Guzzo et al., Nature 451 (2008), 541

Higher curvature theories of gravity in the ADM canonical formalism

Yuuiti Sendouda[1,a], Nathalie Deruelle[b], Misao Sasaki[a] and Daisuke Yamauchi[a]

[a] *Yukawa Institute for Theoretical Physics, Kyoto University, Kyoto 606–8502, Japan*
[b] *APC, UMR 7164 (CNRS, Université Paris 7, CEA, Observatoire de Paris), 75205 Paris Cedex 13, France*

Abstract

We present a canonical formulation for higher-curvature theories of gravity whose action is a generic function of Riemann tensor. The Arnowitt–Deser–Misner canonical formalism is employed to identify the extra gravitational dynamical degrees of freedom other than metric. We also find a surface term that gives Dirichlet boundary conditions for the dynamical degrees of freedom.

1 Introduction

Quantum theories of gravity, such as string theories, predict the conventional Einstein–Hilbert action, $S_{\rm g} = (2\kappa)^{-1}\int_{\mathcal{M}}\sqrt{-g}R$, is necessarily supplemented by higher-order terms in curvature, which, even at the classical level, may come into play in the regime of strong gravity. Studies on higher-order gravity can open a window to the fundamental theory and it is therefore interesting to investigate its possible imprints on cosmological and/or astrophysical phenomena.

Our start-up strategy is to abstract essential properties of higher-order gravity and examine whether each class of theories can qualify basic requirements as viable gravity theory. In order to serve such phenomenological studies, one should keep as much generality as possible. We treat generic actions on D-dimensional spacetime $(\mathcal{M}, g)$ such as

$$S_{\rm g} = \frac{1}{2\kappa}\int_{\mathcal{M}}\sqrt{-g}f(R_{abcd}, g_{ab}), \tag{1}$$

where f is an arbitrary scalar-valued (non-linear) function of the Riemann tensor.

Since the equation of motion stemming from the above action contains fourth-order derivatives, gravity involves extra dynamical degrees of freedom other than metric. To have a clear view on such aspect, we employ the Arnowitt–Deser–Misner (ADM) [1] canonical formalism to describe the theory. We will at the same time find a relevant surface action by which existence of extra gravitational degrees of freedom is taken into account.

The main body of this article consists of identification of a Dirichlet surface term necessary in constructing a first-order action (section 2) and ADM canonical formulation (section 3).

2 Dirichlet surface term

Appearance of higher derivatives is avoided by considering an equivalent theory which is linear in second derivative of the metric

$$S_{\rm g} = \frac{1}{2\kappa}\int_{\mathcal{M}}\sqrt{-g}[\ {}^{abcd}(R_{abcd} - {}_{abcd}) + f({}_{abcd}, g_{ab})], \tag{2}$$

where the auxiliary field ${}_{abcd}$ and the Lagrange multiplier ^{abcd} are independent of g_{ab}. The variation of the action reads

$$\begin{aligned} S_{\rm g} = \frac{1}{2\kappa}\int_{\mathcal{M}}\sqrt{-g}\quad & E^{ab}\ \delta g_{ab} + ({}^{}R_{abcd} - {}_{abcd})\ \delta{}^{abcd} + \frac{\partial f}{\partial\ {}_{abcd}}\ \delta{}_{abcd} \\ & + \frac{1}{2\kappa}\int_{\mathcal{M}}\sqrt{-g}\nabla_d(\ \delta g_{ab}\nabla_c\ {}^{acbd} - {}^{acbd}\nabla_c\ \delta g_{ab}), \end{aligned} \tag{3}$$

[1] E-mail:sendouda(a)yukawa.kyoto-u.ac.jp

where

$$E^{ab} \quad R^{(a}{}_{cde}{}^{b)cde} + 2\nabla_c\nabla_d{}^{(a|c|b)d} + 2\,{}^{(a}{}_{cde}\frac{\partial f}{\partial{}^{b)cde}} \quad \frac{1}{2}[{}^{cdef}(R_{cdef} \quad {}_{cdef}) + f]g^{ab}. \tag{4}$$

It is understood that fourth derivative has been splitted into two second derivatives R_{abcd} and $\nabla_c\nabla_d{}^{acbd}$.

We are to impose Dirichlet boundary conditions on the (propagating components of) metric at the spacetime boundary $\partial\mathcal{M}$. To do so, the second term in the surface integral in (3) has to be cancelled by some suitable term localised on the boundary. It is here worth mentioning that the existence of the normal derivative in that term indicates the action involves second derivatives of the metric.

De ne here n^a to be the unit normal for boundaries whose orientation is outward-pointing for timelike boundaries whereas inward-pointing for spacelike ones. The induced metric on the boundary is given by ${}_{ab} = g_{ab} \quad n_a n_b$, where $n^a n_a$ is the sign of the normal (1 for timelike and +1 for spacelike, respectively). We take the following surface term

$$S_{\rm g} = \frac{2}{} \oint_{\partial\mathcal{M}} \sqrt{|\ |}\, n_c n_d \ {}^{acbd} K_{ab}, \tag{5}$$

where $K_{ab} \quad {}^{c}{}_{a}\nabla_c n_b$ is the extrinsic curvature of the boundary. This is a generalisation of the York–Gibbons–Hawking surface term [2] in General Relativity. Indeed, variation of the total action, $S_{\rm g} + S_{\rm g}$, on-shell now reads

$$(S_{\rm g} + S_{\rm g})|_{\text{on-shell}} = \frac{1}{} \oint_{\partial\mathcal{M}} \sqrt{|\ |}(P^{ab} \quad {}_{ab} + 2\ K_{ab}\ (n_c n_d \ {}^{acbd})), \tag{6}$$

where P^{ab} is some function. This result implies that the Dirichlet boundary conditions

$${}_{ab}|_{\partial\mathcal{M}} = \ (n_c n_d \ {}^{acbd})|_{\partial\mathcal{M}} = 0 \tag{7}$$

gives well-posed initial-value problems. In other words, second derivatives have been get rid of from the action by virtue of the surface term.

3 ADM canonical formalism

In the ADM formalism, the bulk spacetime is foliated by $(D \quad 1)$-dimensional non-null hypersurfaces labeled by t, $\{ \ {}_t\}$. For simplicity, we consider the case where ${}_t$ is compact and there exists two constant-t surfaces as the spacetime boundary, namely, ${}_0$ at $t = t_0$ and ${}_1$ at $t = t_1$.

Here we introduce a 'future-pointing' unit vector eld normal to the hypersurfaces by $n_a = N(\mathrm{d}t)_a$, where $N\,(>0)$ is the lapse function and $= n^a n_a = 1$ the signature. We also introduce the shift vector ^{a} together with the notion of the ' ow' vector eld $t^a = Nn^a + {}^a$ satisfying $t^a\nabla_a t = 1$.

We decompose the action (2) in a $(D \quad 1)+1$ manner. In particular, the Gauss and Codazzi relations are employed to yield

$$\begin{aligned} {}^{abcd}R_{abcd} = {}_\perp \ {}^{abcd}(R_{abcd} \quad 2\ K_{ac}K_{bd}) + 8\ {}_\perp \ {}^{abc\mathbf{n}}\nabla_a K_{bc} \\ + 4{}_\perp \ {}^{a\mathbf{n}b\mathbf{n}}(KK_{ab} \quad K_{ac}K_b{}^c \quad N \ {}^1\nabla_a\nabla_b N) \\ + 4K_{ab}n^c\nabla_c{}_\perp \ {}^{a\mathbf{n}b\mathbf{n}} \quad 4\nabla_c(n^c{}_\perp \ {}^{a\mathbf{n}b\mathbf{n}}K_{ab}). \end{aligned} \tag{8}$$

Here the bar denotes $(D \quad 1)$-dimensional intrinsic quantities: ∇_a is the covariant derivative associated with the induced metric ${}_{ab}$ and R_{abcd} the Riemann tensor of ${}_{ab}$. The $\perp$ symbol denotes projection onto ${}_t$ by the orthogonal projector ${}_a{}^b$, and the $\mathbf{n}$ index means contraction with n^a (before $\perp$-projection). We recognise, e.g., as ${}_\perp \ {}^{a\mathbf{n}b\mathbf{n}} = {}^a{}_c n_d \ {}^b{}_e n_f \ {}^{cdef}$. As the second derivative has been casted into the form of a divergence by the Leibniz rule, normal derivative of ${}_\perp \ {}^{a\mathbf{n}b\mathbf{n}}$ has shown up. The divergence is cancelled by the surface action $S_{\rm g}$. Consequently this decomposition has revealed that the extra dynamical degrees of freedom are con ned in the symmetric tensor ${}_\perp \ {}^{a\mathbf{n}b\mathbf{n}}$. For this distinctive feature, we shall hereafter denote ${}^{ab} \quad 2\ {}_\perp \ {}^{a\mathbf{n}b\mathbf{n}}$.

Terms in the action are all decomposed in this manner. We may see f as a function of projected components of $\ _{abcd}$ and of metric g^{ab}. We de ne 'velocities' of the dynamical variables in terms of Lie derivatives as $\dot{}_{ab}\quad \pounds_t\ _{ab} = 2NK_{ab} + 2\nabla_{(a\ \ b)}$ and $\dot{}^{ab}\quad \pounds_t\ ^{ab}$, respectively. Then we arrive at the action totally represented with the following set of quantities (and their derivatives on $\ _t$):

$$\{\ _{ab},\ \ ^{ab},\ \dot{}_{ab},\ \dot{}^{ab}, N,\ \ ^{a}, {}_{\perp}\ _{abcd}, {}_{\perp}\ _{abc\mathbf{n}}, {}_{\perp}\ _{a\mathbf{n}b\mathbf{n}}, {}_{\perp}\ ^{abcd}, {}_{\perp}\ ^{abc\mathbf{n}}\}. \tag{9}$$

This form of action is suitable for canonical formulation. Canonical momenta conjugate to each variable are de ned by

$$_{q_i}\quad \frac{(S_{\mathrm{g}} + S_{\mathrm{g}})}{\dot{q}_i}. \tag{10}$$

Then the total action is rewritten in terms of canonical variables $\{q_i,\ \ _{q_i}\}$ via Legendre transformation

$$S_{\mathrm{g}} + S_{\mathrm{g}} = \int_{t_0}^{t_1} \mathrm{d}t \ \int_{\ t} (\ \ ^{ab}\dot{}_{ab} + \ \ _{ab}\dot{}^{ab})\quad H_{\mathrm{g}}\ \ , \tag{11}$$

where H_{g} is the Hamiltonian.

At this stage, Dirac's prescription [3] tells how to obtain canonical equations of motion and constraints. Here we illustrate the procedure and outcomes, the whole of which will be presented in a forthcoming paper [4]. Each variable whose velocity is missing in the action gives a primary constraint

$$_i\quad\ _i\quad 0, \tag{12}$$

where $\lambda_i = N,\ \ ^{a}, {}_{\perp}\ _{abcd}, {}_{\perp}\ _{abc\mathbf{n}}, {}_{\perp}\ _{a\mathbf{n}b\mathbf{n}}, {}_{\perp}\ ^{abcd}, {}_{\perp}\ ^{abc\mathbf{n}}$ represents those non-dynamical variables and the weak equality $\quad$ means modulo constraints. The total Hamiltonian is constructed as

$$H_{\mathrm{t}} = H_{\mathrm{g}} + \sum_i \int_t u\ _i\quad\ _i, \tag{13}$$

where $u\ _i$'s are multipliers. Evolution of the variables is described by Poisson bracket. t-derivative of each quantity is determined by Poisson bracket with the total Hamiltonian

$$\dot{Q}\qquad \{H_{\mathrm{t}}, Q\}. \tag{14}$$

The canonical equations of motion for dynamical variables are therefore given as

$$\dot{}_{ab}\quad \frac{H_{\mathrm{g}}}{\ _{ab}},\quad \dot{}\ _{ab}\qquad \frac{H_{\mathrm{g}}}{\ _{ab}},\quad \dot{}^{ab}\quad \frac{H_{\mathrm{g}}}{\ _{ab}},\quad \dot{}\ ^{ab}\qquad \frac{H_{\mathrm{g}}}{\ _{ab}}. \tag{15}$$

They correspond to the de nitions of velocities and the dynamical part of the Euler–Lagrange equations of motion, i.e., those two normal components containing second derivatives. On the other hand, as the constraints must preserve, consistency of the theory demands derivatives of primary constraints $_i$ vanish thereby leading to secondary constraints $\dot{}_i\quad 0$. One can check that the rest of Euler–Lagrange equations is indeed recovered by them. Consequently equivalence between the Euler–Lagrange and Hamilton formulations has been con rmed at the level of equations of motion.

To guarantee that those secondary constraints preserve, we have to pay attention to what $\ _i$ brings about. When $\ _i\quad 0$ is not automatically satis ed, i.e., it is independent of known secondary constraints, we have two possibilities; If the equality contains some multiplier $u\ _i$ yet undetermined, then the equation is used to x, or constrain, the multiplier. On the other hand, if the equality does not contain multipliers, then we add it to the set of constraints. In the latter case, we have to continue to take derivatives of those new secondary constraints until derivatives will automatically vanish by virtue of other constraints. The number of collected secondary constraints in turn tells how many dynamical degrees of freedom can survive and this is where the detailed form of f plays an essential role. This aspect will be discussed elsewhere [4].

Focusing on rather basic properties, derivatives of the momenta of lapse and shift are analogues of the Hamiltonian and momentum constraints in General Relativity,

$$\mathcal{C}^N\quad \frac{H_{\mathrm{g}}}{N}\quad 0,\quad \mathcal{C}^{\beta}_{a}\quad \frac{H_{\mathrm{g}}}{\ _a}\quad 0. \tag{16}$$

The Hamiltonian can be represented as

$$H_{\rm g} = \int_{t} (N\mathcal{C}^N + \ {}^a\mathcal{C}_a^\beta). \tag{17}$$

up to divergence on $_t$. Derivatives of the Hamiltonian and momentum constraints does not arise further secondary constraints leaving corresponding multipliers u_N and u^a_β undetermined.

4 Conclusion

We presented a basic framework of ADM canonical formulation for higher-curvature theories of gravity whose Lagrangian is a generic function of Riemann tensor. Two auxiliary elds, $_{abcd}$ and ^{abcd}, were introduced to make the action linear in second derivative. Further, in order to cast the theory into a rst-order form, the action (2) was supplemented by a Dirichlet surface term (5). Then the rst-order action was Legendre transformed to the canonical form. We showed all the possible dynamical degrees of freedom other than metric were con ned in $^{ab} = 2 \ ^{a\mathbf{n}b\mathbf{n}}$. Emergence of new dynamical degrees of freedom is all due to non-linearity of $R_{a\mathbf{n}b\mathbf{n}}$ in f, which exclusively contains second derivative of the metric among projected components of the Riemann tensor.

Then Dirac's procedure was employed to derive canonical equations of motion and constraints. The equivalence between Euler–Lagrange and Hamilton formulations were seen at the level of equations of motion. The resultant number of the extra degrees of freedom is controlled by the detailed form of f via secondary constraints.

Our results can be applied in various contexts. Surface action will play an inevitable role in gravitational systems with boundary (e.g., construction of new braneworld models, AdS/CFT correspondence, and so on). As a theoretical problem, there have long been claims that spin-2 elds coupled to gravity tend to appear ghost [5], which can cause serious inconsistency in quantum theory as well as instabilities at the classical level. Possibilities of such pathology should be taken care of in applications.

Acknowledgements

Two of the authors were supported by Grant-in-Aid for JSPS Fellows No. 19-7852 (YS) and No. 20-1117 (DY). MS was supported in part by JSPS Grant-in-Aid for Scienti c Research (B) No. 17340075 and (A) No. 18204024, and by JSPS Grant-in-Aid for Creative Scienti c Research No. 19GS0219. This work was also supported by Grant-in-Aid for the Global COE Program "The Next Generation of Physics, Spun from Universality and Emergence" from the Ministry of Education, Culture, Sports, Science and Technology of Japan.

References

[1] R. Arnowitt, S. Deser, and C.W. Misner, in *Gravitation: an introduction to current research*, ed. L. Witten (John Wiley & Sons, Inc., New York, 1962), pp. 227–265, gr-qc/0405109.

[2] J.W. York, Jr., Phys. Rev. Lett. **28** (1972) 1082–1085; G.W. Gibbons and S.W. Hawking, Phys. Rev. **D15** (1977) 2752–2756.

[3] P.A.M. Dirac, *Lectures on Quantum Mechanics* (Dover Publications, Inc., New York, 2001).

[4] N. Deruelle, M. Sasaki, Y. Sendouda, and D. Yamauchi, in preparation.

[5] K.S. Stelle, Gen. Rel. Grav. **9** (1978) 353–371.

Towards the dynamics in Einstein-Gauss-Bonnet gravity: Initial Value Problem[1]

Takashi Torii[2] and Hisa-aki Shinkai[3]

[1] *General Education of Science, Osaka Institute of Technology, Omiya, Asahi-ku, Osaka 535-8585*
[2] *Dept. of Information Systems, Osaka Institute of Technology, Kitayama, Hirakata, Osaka 573-0196*

Abstract

Towards the investigation of the full dynamics in higher-dimensional and/or stringy gravitational model, we present the basic equations of the Einstein-Gauss-Bonnet gravity theory. We show $(N+1)$-dimensional version of the Arnowitt-Deser-Misner decomposition including the Gauss-Bonnet term, which shall be the standard approach to treat the space-time as a Cauchy problem. Due to the quasi-linear property of the Gauss-Bonnet gravity, we find that the evolution equations can be in a treatable form in numerics. We also show the conformally-transformed constraint equations for constructing an initial data. Our equations can be used both for timelike and spacelike foliations.

1 Introduction

General relativity (GR) has been tested with many experiments and observations both in the strong and weak gravitational field regimes, and none of them are contradictory to GR. However, the theory also predicts the appearance of the spacetime singularities under natural conditions, which also indicates that GR is still incomplete as a physics theory that describes whole of the gravity and the spacetime structure.

We expect that the true fundamental theory will resolve these theoretical problems. Up to now, several quantum theories of gravity have been proposed. Among them superstring/M-theory, formulated in higher dimensional spacetime, is the most promising candidate. The Gauss-Bonnet (GB) term is the next leading order of the α'-expansion (α' is the inverse string tension) of type IIB superstring theory[2, 3], and has nice properties such that it is ghost-free combinations[4] and does not give higher derivative equations but an ordinary set of equations with up to second derivative in spite of the higher curvature combinations.

The models with the GB term and/or other higher curvature terms have been intensively studied in the high energy physics, in the contexts both in string cosmology and in black hole physics (see references in [1]). All the analysis so far are performed on the assumption of highly symmetric spacetime because the system is much more complicated than that in GR. To obtain deeper understanding of the early stage of the universe, singularity, and/or black holes, we should consider less symmetric and/or dynamical spacetime; the analyses require the direct numerical integration of the equations. None of the fully dynamical simulations in GB gravity has been performed.

In this article, we present the basic equations of the Einstein-GB gravity theory. We show $(N+1)$-dimensional version of the ADM decomposition, which is the standard approach to treat the spacetime as a Cauchy problem. The topic was first discussed by Choquet-Bruhat [5], but the full set of equations and the methodology have not yet been presented. Therefore, as the first step, we in this paper just present the fundamental space-time decomposition of the GB equations, focusing on the GB term.

The ADM decomposition is supposed to construct the spacetime with foliations of the constant-time hypersurfaces. This method can be also applied to study the brane-world model. We think these expressions are useful for future dynamical investigations.

[1] Please refer the details in [1].

[2] E-mail: torii@ge.oit.ac.jp
[3] E-mail: shinkai@is.oit.ac.jp

2 $(N+1)$-decomposition in Einstein-Gauss-Bonnet gravity

We start from the Einstein-Gauss-Bonnet action in $(N+1)$-dimensional spacetime $(\mathcal{M}, g\quad)$ which is described as [4]:

$$S = \int_{\mathcal{M}} d^{N+1}X\sqrt{-g}\left[\frac{1}{2\kappa^2}\left(\mathcal{R} - 2\Lambda + \alpha_{GB}\mathcal{L}_{GB}\right) + \mathcal{L}_{\rm matter}\right], \tag{1}$$

with $\mathcal{L}_{GB} = \mathcal{R}^2 - 4\mathcal{R}\quad\mathcal{R}\quad{}_{\rho\sigma}\mathcal{R}\quad{}^{\rho\sigma}$,where κ^2 is the $(N+1)$-dimensional gravitational constant, $\mathcal{R}$, $\mathcal{R}\quad{}_{\rho\sigma}$ and $\mathcal{L}_{\rm matter}$ are the $(N+1)$-dimensional scalar curvature, Ricci tensor, Riemann curvature and the matter Lagrangian, respectively. This action reproduces the standard $(N+1)$-dimensional Einstein gravity, if we set the coupling constant α_{GB} (0) equals to zero.

The action (1) gives the gravitational equation as

$$\mathcal{G}\quad + \alpha_{GB}\mathcal{H}\quad = \kappa^2\,\mathcal{T}\quad, \tag{2}$$

$$\text{where}\ \ \mathcal{G}\quad = \mathcal{R}\quad - \frac{1}{2}g\quad\mathcal{R} + g\quad\Lambda, \quad \mathcal{T}\quad = -2\frac{\delta\mathcal{L}_{\rm matter}}{\delta g} + g\quad\mathcal{L}_{\rm matter}, \tag{3}$$

$$\mathcal{H}\quad = 2\Big(\mathcal{R}\mathcal{R}\quad - 2\mathcal{R}\ {}_{\alpha}\mathcal{R}^{\alpha} - 2\mathcal{R}^{\alpha}\ \mathcal{R}\ {}_{\alpha}\quad + \mathcal{R}\ {}^{\alpha}\ {}^{\gamma}\mathcal{R}\ {}_{\alpha}\ {}_{\gamma}\Big) - \frac{1}{2}g\quad\mathcal{L}_{GB}. \tag{4}$$

In order to investigate the space-time structure as the foliations of the N-dimensional (spacelike or timelike) hypersurface Σ, we introduce the projection operator to Σ as

$$\perp\quad = g\quad - \varepsilon n\ n\ , \tag{5}$$

where $n\quad$ is the unit-normal vector to Σ with $n\ n\quad = \varepsilon$, with which we define $n\quad$ is timelike (if $\varepsilon = -1$) or spacelike (if $\varepsilon = 1$). Therefore, Σ is spacelike (timelike) if $n\quad$ is timelike (spacelike).

The projections of the gravitational equation (2) give the following three equations:

$$\left(\mathcal{G}\quad + \alpha_{GB}\mathcal{H}\quad\right) n\ \ n\quad = \kappa^2\,\mathcal{T}\quad n\ \ n\quad = \kappa^2\rho, \tag{6}$$

$$\left(\mathcal{G}\quad + \alpha_{GB}\mathcal{H}\quad\right) n\ \perp_{\rho} = \kappa^2\,\mathcal{T}\quad n\ \perp_{\rho} = -\kappa^2 J_{\rho}, \tag{7}$$

$$\left(\mathcal{G}\quad + \alpha_{GB}\mathcal{H}\quad\right) \perp_{\rho}\perp_{\sigma} = \kappa^2\,\mathcal{T}\quad \perp_{\rho}\perp_{\sigma} = \kappa^2 S_{\rho\sigma}, \tag{8}$$

where we defined the components of the energy-momentum tensor as $\mathcal{T}\quad = \rho n\ \ n\quad + J\ \ n\quad + J\ \ n\quad + S\quad$, and we also define $\mathcal{T} = \varepsilon\rho + S^{\alpha}_{\ \alpha}$ for later convenience.

Following the standard procedure of the ADM formulation, we find that the equations (6)–(8) correspond to (a) the Hamiltonian constraint equation:

$$M + \alpha_{GB}\left(M^2 - 4M_{ab}M^{ab} + M_{abcd}M^{abcd}\right) = -2\varepsilon\kappa^2\rho_H + 2\Lambda\,, \tag{9}$$

(b) the momentum constraint equation:

$$N_i + 2\alpha_{GB}\left(MN_i - 2M_i{}^a N_a + 2M^{ab}N_{iab} - M_i{}^{cab}N_{abc}\right) = \kappa^2 J_i\,, \tag{10}$$

and (c) the evolution equations for γ_{ij}:

$$\begin{aligned} &M_{ij} - \frac{1}{2}M\gamma_{ij} - \varepsilon\left(-K_{ia}K^a_{\ j} + \gamma_{ij}K_{ab}K^{ab} - \pounds_n K_{ij} + \gamma_{ij}\gamma^{ab}\pounds_n K_{ab}\right) \\ &\quad + 2\alpha_{GB}\Big[H_{ij} + \varepsilon\left(M\pounds_n K_{ij} - 2M_i{}^a\pounds_n K_{aj} - 2M_j{}^a\pounds_n K_{ai} - W_{ij}{}^{ab}\pounds_n K_{ab}\right)\Big] = \kappa^2 S_{ij} - \gamma_{ij}\Lambda\,, \end{aligned} \tag{11}$$

respectively, where

$$M_{ijkl} = \quad R_{ijkl} - \varepsilon(K_{ik}K_{jl} - K_{il}K_{jk}), \tag{12}$$

$$N_{ijk} = \quad D_i K_{jk} - D_j K_{ik}, \tag{13}$$

[4]The Greek indices move $0, 1, \cdots, N$, while the Latin indices move $1, \cdots, N$.

$$
\begin{aligned}
H_{ij} = \quad & MM_{ij} - 2(M_{ia}M^{a}_{\ j} + M^{ab}M_{iajb}) + M_{iabc}M_{j}^{\ abc} \\
& -2\varepsilon\Big[-K_{ab}K^{ab}M_{ij} - \frac{1}{2}MK_{ia}K^{a}_{\ j} + K_{ia}K^{a}_{\ b}M^{b}_{\ j} + K_{ja}K^{a}_{\ b}M^{b}_{\ i} + K^{ac}K_{c}^{\ b}M_{iajb} \\
& \qquad + N_iN_j - N^a(N_{aij} + N_{aji}) - \frac{1}{2}N_{abi}N^{ab}_{\ \ j} - N_{iab}N_{j}^{\ ab}\Big] \\
& -\frac{1}{4}\gamma_{ij}\big(M^2 - 4M_{ab}M^{ab} + M_{abcd}M^{abcd}\big) \\
& -\varepsilon\gamma_{ij}\big(K_{ab}K^{ab}M - 2M_{ab}K^{ac}K_{c}^{\ b} - 2N_aN^a + N_{abc}N^{abc}\big), \qquad (14) \\
W_{ij}^{\ \ kl} = \quad & M\gamma_{ij}\gamma^{kl} - 2M_{ij}\gamma^{kl} - 2\gamma_{ij}M^{kl} + 2M_{iajb}\gamma^{ak}\gamma^{bl}. \qquad (15)
\end{aligned}
$$

and these contracted variables; $M_{ij} = \gamma^{ab}M_{iajb}$, $M = \gamma^{ab}M_{ab}$, and $N_i = \gamma^{ab}N_{aib}$. We remark that the terms of $\pounds_n K_{ij}$ appear only in the linear form in (11). This is due to the quasi-linear property of the GB gravity.

3 Conformal Approach to solve the Constraints

In order to prepare an initial data for dynamical evolution, we have to solve two constraints, (9) and (10). The standard approach is to apply a conformal transformation on the initial hypersurface [6]. The idea is that introducing a conformal factor ψ between the initial trial metric $\hat{\gamma}_{ij}$ and the solution γ_{ij}, as

$$
\gamma_{ij} = \psi^{2m}\hat{\gamma}_{ij}, \quad \gamma^{ij} = \psi^{-2m}\hat{\gamma}^{ij}, \qquad (16)
$$

where m is a constant, and solve for ψ so as to the solution satisfies the constraints.

Regarding to the extrinsic curvature, we decompose K_{ij} into its trace part, $K = \gamma^{ij}K_{ij}$, and the traceless part, $A_{ij} = K_{ij} - \frac{1}{N}\gamma_{ij}K$, and assume the conformal transformation [5] as $A_{ij} = \psi^{\ell}\hat{A}_{ij}, A^{ij} = \psi^{\ell-4m}\hat{A}^{ij}, K = \psi^{\tau}\hat{K}$,where ℓ and τ are constants. For the matter terms, we also assume the relations $\rho = \psi^{-p}\hat{\rho}$ and $J^i = \psi^{-q}\hat{J}^i$, where p and q are constants, while we regard the cosmological constant is common to the both flames, $\Lambda = \hat{\Lambda}$.

Up to here, the powers of conformal transformation, ℓ, m, τ, p and q are not yet specified. Note that in the standard three-dimensional initial-data construction cases, the combination of $m = 2$, $\ell = -2$, $\tau = 0$, $p = 5$ and $q = 10$ is preferred since this simplifies the equations. We also remark that if we chose $\tau = \ell - 2m$, then the extrinsic curvature can be transformed as $K_{ij} = \psi^{\ell}\hat{K}_{ij}$ and $K^{ij} = \psi^{\ell-4m}\hat{K}^{ij}$.

- **Hamiltonian constraint:** Using these equations, (9) turns to be

$$
\begin{aligned}
& 2(N-1)m\hat{D}_a\hat{D}^a\psi - (N-1)\big[2-(N-2)m\big]m(\hat{D}\psi)^2\psi^{-1} \\
& \quad = \hat{R}\psi - \frac{N-1}{N}\varepsilon\psi^{2m+2\tau+1}\hat{K}^2 + \varepsilon\psi^{-2m+2\ell+1}\hat{A}_{ab}\hat{A}^{ab} + 2\varepsilon\kappa^2\hat{\rho}\psi^{-p} - 2\hat{\Lambda} + \alpha_{GB}\hat{\Theta}\psi^{2m+1}.
\end{aligned}
$$

  The explicit form of the GB part $\hat{\Theta} = M^2 - 4M_{ab}M^{ab} + M_{abcd}M^{abcd}$ is shown in [1].

- **Momentum constraint:** By introducing the transverse traceless part and the longitudinal part of $\hat{A}^{ij}$ as $\hat{D}_j\hat{A}^{ij}_{TT} = 0, \hat{A}^{ij}_{L} = \hat{A}^{ij} - \hat{A}^{ij}_{TT}$, respectively, then (10), can be written as

$$
\psi^{\ell-2m}\hat{D}_a\hat{A}_{i\ L}^{\ a} + \big[\ell + (N-2)m\big]\psi^{\ell-2m-1}\hat{A}_{i\ L}^{\ a}\hat{D}_a\psi - \frac{N-1}{N}\hat{D}_i(\psi^{\tau}\hat{K}) + 2\alpha_{GB}\hat{\Xi}_i = \kappa^2\psi^{2m-q}\hat{J}_i
$$

  The explicit form of the GB part $\hat{\Xi}_i$ is shown in [1].

In [1], we discussed how the equations turn to be in two sets of parameter choices, together with the version of momentarily static situation.

[5] In the strict sense this is not the conformal transformation but just the relation between the values with and without a caret.

4 Dynamical equations

The Einstein evolution equation in general N-dimensional ADM version is presented in [7]. With the GB terms, the evolution equation (11) cannot be expressed explicitly for each $\pounds_n K_{ij}$. That is, (11) is rewritten as

$$\begin{aligned}(1+2\alpha_{GB}M)\pounds_n K_{ij} - (\gamma_{ij}\gamma^{ab} + 2\alpha_{GB}W_{ij}{}^{ab})\pounds_n K_{ab} - 8\alpha_{GB}M_{(i}{}^{a}\pounds_n K_{|a|j)} \\ = -\varepsilon\left(M_{ij} - \frac{1}{2}M\gamma_{ij}\right) - K_{ia}K^{a}_{\ j} + \gamma_{ij}K_{ab}K^{ab} + \varepsilon\kappa^2 S_{ij} - \varepsilon\gamma_{ij}\Lambda - 2\varepsilon\alpha_{GB}H_{ij}\,, \end{aligned} \tag{17}$$

and the second and the third terms in r.h.s include the linearly-coupled terms between $\pounds_n K_{ij}$. Therefore, in an actual simulation, we have to extract each evolution equation of K_{ij} using a matrix form of Eq. (17) like

$$\mathbf{k} = A\mathbf{k} + \mathbf{b} \tag{18}$$

where $\mathbf{k} = (\pounds_n K_{11}, \pounds_n K_{12}, \cdots, \pounds_n K_{NN})^T$ and A, $\mathbf{b}$ are appropriate matrix and vector derived from Eq. (17).

The procedure of the inverting the matrix $(1 - A)$ is technically available, but the invertibility of the matrix is not generally guaranteed at this moment. In the case of the standard ADM foliation in four-dimensional Einstein equations, the continuity of the time evolutions depends on the models and the choice of gauge conditions for the lapse function and shift vectors. If the combination is not appropriate, then the foliation hits the singularity which stops the evolution. The similar obstacle may exist also for the GB gravity. Actually, Deruelle and Madore [8] gave an explicit example in a simple cosmological model where the equation corresponding to (18) is not invertible. We expect that in the most cases Eq. (18) is invertible for K_{ij} but we cannot deny the pathological cases which depend on the models and gauge conditions. Such a study must be done together with actual numerical integrations in the future.

5 Discussion

In summary, we show the $(N+1)$-dimensional decomposition of the basic equations, in order to treat the space-time as a Cauchy problem. The equations can be separated to the constraints (the Hamiltonian constraint and the momentum constraint) and the evolution equations.

Two constraints should be solved for constructing an initial data, and we show how the actual equations turn to be. If we have the GB term, however, the equations still remain in a complicated style.

For the evolution equations, we find that $\pounds_n K_{ij}$ components are coupled. However, this mixture is only up to the linear order due to the quasi-linear property of the GB term, so that the equations can be in a treatable form in numerics.

We are now developing our numerical code and hope to present some results elsewhere near future.

References

[1] T. Torii and H. Shinkai, Phys. Rev. **D 78**, 084037 (2008).

[2] D. J. Gross and E. Witten, Nucl. Phys. **B277**, 1 (1986);
D. J. Gross and J. H. Sloan, Nucl. Phys. **B291**, 41 (1987).

[3] M. C. Bento and O Bertolami, Phys. Lett. B **368**, 198 (1996).

[4] B. Zwiebach, Phys. Lett. B **156**, 315 (1985).

[5] Y. Choquet-Bruhat, J. Math. Phys. **29**, 1891 (1988).

[6] N. ÓMurchadha and J. W. York, Jr., Phys. Rev. D **10**, 428 (1974).

[7] H. Shinkai and G. Yoneda, Gen. Rel. Grav. **36**, 1931 (2004).

[8] N. Deruelle and J. Madore, arXiv:gr-qc/0305004.

Revisiting chameleon gravity–thin-shells and no-shells with appropriate boundary conditions

Takashi Tamaki[1] and Shinji Tsujikawa[2]

[1]*Department of Physics, Waseda University, Okubo 3-4-1, Tokyo 169-8555, Japan*
[2]*Department of Physics, Faculty of Science, Tokyo University of Science, 1-3, Kagurazaka, Shinjuku-ku, Tokyo 162-8601, Japan*

Abstract

We derive analytic solutions of a chameleon scalar field ϕ that couples to a non-relativistic matter in the weak gravitational background of a spherically symmetric body, paying particular attention to a field mass m_A inside of the body.

1 Introduction

Recently there have been a lot of efforts to understand the origin of dark energy under the framework of modified gravity theories (see Refs. [1] for reviews). In modified gravity models of dark energy, it is crucially important to appropriately study the compatibility of couplings with local gravity experiments as well as with a late-time acceleration of the Universe preceded by a standard matter era. Interesting attempt to reconcile large coupling models with local gravity constraints is to use "chameleon" scalar fields whose masses depend on the environment they are in [2, 3]. The analysis in Refs. [2, 3] assumes that the field is frozen ($\phi = \phi_A$) in the regime $0 < r < r_1$ without explicitly taking into account the field mass m_A. Here and [4], we consider m_A.

The action we study is given by

$$S = \int \mathrm{d}^4x\sqrt{-g}\left[\frac{M_{\rm pl}^2}{2}R - \frac{1}{2}(\nabla\phi)^2 - V(\phi)\right] - \int \mathrm{d}^4x\,\mathcal{L}_m(\Psi_m^{(i)}, g_{\mu\nu}^{(i)})\,, \tag{1}$$

where $\Psi_m^{(i)}$ are matter fields that couple to a metric $g_{\mu\nu}^{(i)}$ related with the Einstein frame metric $g_{\mu\nu}$ via $g_{\mu\nu}^{(i)} = e^{2Q_i\phi}g_{\mu\nu}$. Here Q_i are the strength of couplings for each matter field. An example is

$$V(\phi) = M^{4+n}\phi^{-n}\,, \tag{2}$$

where M has a unit of mass and n is a constant. In the context of $f(R)$ gravity, Hu and Sawicki [5] and Starobinsky [6] proposed models that can be consistent with cosmological and local gravity constraints. We consider

$$V(\phi) = V_0\left[1 - C(1 - e^{-2Q\phi})^p\right]\,, \tag{3}$$

where $V_0 > 0,\ C > 0,\ 0 < p < 1$ as a generalization of the potential in $f(R)$ gravity.

2 Chameleon mechanism

The trace of the i-th matter is given by $T^{(i)} \equiv g_{(i)}^{\mu\nu}T_{\mu\nu}^{(i)} = -\tilde{\rho}_i$ for a non-relativistic fluid, where $\tilde{\rho}_i$ is an energy density. It is more convenient to introduce the quantity $\rho_i = \tilde{\rho}_i\, e^{3Q_i\phi}$, which is conserved in the Einstein frame. In a spherically symmetric background, we obtain

$$\frac{\mathrm{d}^2\phi}{\mathrm{d}r^2} + \frac{2}{r}\frac{\mathrm{d}\phi}{\mathrm{d}r} = \frac{\mathrm{d}V_{\rm eff}}{\mathrm{d}\phi}\,, \tag{4}$$

[1]E-mail:tamaki@gravity.phys.waseda.ac.jp
[2]E-mail:shinji@rs.kagu.tus.ac.jp

where $V_{\rm eff}(\phi) \equiv V(\phi) + \sum_i \rho_i e^{Q_i \phi}$. In the following, we shall consider the case $Q_i = Q$ and $\rho_i = \rho$. We assume that the body has a homogeneous density $\rho = \rho_A$ and that the density is homogeneous with a value $\rho = \rho_B$ outside of the body. The mass of this body is given by $M_c = (4\pi/3)\rho_A r_c^3$, where r_c is a radius of the body. The effective potential $V_{\rm eff}$ has minima at field values ϕ_A and ϕ_B. The former corresponds to the interior of the body that gives $m_A^2 \equiv \frac{{\rm d}^2 V_{\rm eff}}{{\rm d}\phi^2}(\phi_A)$, whereas the latter to the exterior of the body with $m_B^2 \equiv \frac{{\rm d}^2 V_{\rm eff}}{{\rm d}\phi^2}(\phi_B)$. We impose $\frac{{\rm d}\phi}{{\rm d}r}(r=0) = 0\,, \quad \phi(r \to \infty) = \phi_B$.

In the region $0 < r < r_1$, the solution is

$$\phi(r) = \phi_A + \frac{A(e^{-m_A r} - e^{m_A r})}{r} \qquad (0 < r < r_1). \tag{5}$$

This automatically satisfies the boundary condition: $\frac{{\rm d}\phi}{{\rm d}r}(r=0) = 0$.

In the region $r_1 < r < r_c$, we obtain

$$\phi(r) = \frac{1}{6} Q \rho_A r^2 - \frac{C}{r} + D \qquad (r_1 < r < r_c), \tag{6}$$

where C and D are constants. In the limit $r_1 \to 0$ the coefficient C is required to be zero.

In the region outside of the body, the solution is given by

$$\phi(r) = \phi_B + E \frac{e^{-m_B(r-r_c)}}{r} \qquad (r > r_c). \tag{7}$$

We match three solutions (5), (6) and (7) by imposing continuous conditions for ϕ and ${\rm d}\phi/{\rm d}r$ at $r = r_1$ and $r = r_c$. Especially when the conditions, $m_B r_c \ll 1$ and $m_A \gg m_B$, are satisfied so that the contribution of the m_B-dependent terms are negligible, we have

$$\phi(r) = \phi_A - \frac{1}{m_A(e^{-m_A r_1} + e^{m_A r_1})} \left[\phi_B - \phi_A + \frac{1}{2} Q \rho_A (r_1^2 - r_c^2) \right] \frac{e^{-m_A r} - e^{m_A r}}{r} \qquad (0 < r < r_1), \tag{8}$$

$$\phi(r) = \phi_B + \frac{1}{6} Q \rho_A (r^2 - 3 r_c^2) + \frac{Q \rho_A r_1^3}{3r} - \left[1 + \frac{e^{-m_A r_1} - e^{m_A r_1}}{m_A r_1 (e^{-m_A r_1} + e^{m_A r_1})} \right] \left[\phi_B - \phi_A + \frac{1}{2} Q \rho_A (r_1^2 - r_c^2) \right] \frac{r_1}{r} \qquad (r_1 < r < r_c), \tag{9}$$

$$\phi(r) = \phi_B - \left[r_1 (\phi_B - \phi_A) + \frac{1}{6} Q \rho_A r_c^3 \left(2 + \frac{r_1}{r_c} \right) \left(1 - \frac{r_1}{r_c} \right)^2 + \frac{e^{-m_A r_1} - e^{m_A r_1}}{m_A (e^{-m_A r_1} + e^{m_A r_1})} \left\{ \phi_B - \phi_A + \frac{1}{2} Q \rho_A (r_1^2 - r_c^2) \right\} \right] \frac{e^{-m_B(r-r_c)}}{r} \qquad (r > r_c) \tag{10}$$

The radius r_1 is determined by the following condition $m_A^2 [\phi(r_1) - \phi_A] = Q \rho_A$, which translates into

$$\phi_B - \phi_A + \frac{1}{2} Q \rho_A (r_1^2 - r_c^2) = \frac{6 Q \Phi_c}{(m_A r_c)^2} \frac{m_A r_1 (e^{m_A r_1} + e^{-m_A r_1})}{e^{m_A r_1} - e^{-m_A r_1}}\,, \tag{11}$$

where $\Phi_c = M_c/(8\pi r_c) = \rho_A r_c^2/6$ is a gravitational potential at the surface of the body. Under this relation the field profile (10) outside of the body can be written as

$$\phi(r) = \phi_B - 2 Q \Phi_c r_c \left[1 - \frac{r_1^3}{r_c^3} + 3 \frac{r_1}{r_c} \frac{1}{(m_A r_c)^2} \left\{ \frac{m_A r_1 (e^{m_A r_1} + e^{-m_A r_1})}{e^{m_A r_1} - e^{-m_A r_1}} - 1 \right\} \right] \frac{e^{-m_B(r-r_c)}}{r} \qquad (r > r_c)\,. \tag{12}$$

3 Thin-shell and no-shell solutions

3.1 Thin-shell solutions ($(r_c - r_1) \ll r_c$)

3.1.1 The massive case ($m_A r_c \gg 1$)

As we see below, thin-shell solutions originally derived in Refs. [2, 3] can be recovered by taking the limit $m_A r_1 \gg 1$, together with the thin-shell condition given by $\Delta r_c \equiv r_c - r_1 \ll r_c$. Expanding Eq. (11) in terms of small parameters $\Delta r_c/r_c$ and $1/m_A r_c$, we obtain $\epsilon_{\rm th} \simeq \frac{\Delta r_c}{r_c} + \frac{1}{m_A r_c}$.

From Eq. (12) the field profile outside of the body is given by

$$\phi(r) \simeq \phi_B - 2Q_{\rm eff}\frac{GM_c}{r}e^{-m_B(r-r_c)}\,, \tag{13}$$

where $Q_{\rm eff}$ is the effective coupling given by $Q_{\rm eff} \simeq 3Q\left(\frac{\Delta r_c}{r_c}+\frac{1}{m_A r_c}\right) = 3Q\epsilon_{\rm th}$. As long as both $\Delta r_c/r_c$ and $1/(m_A r_c)$ are much smaller than unity so that $\epsilon_{\rm th} \ll 1$, it is possible to satisfy local gravity constraints.

3.1.2 The light mass case ($m_A r_c \ll 1$)

From Eq. (11) we get $\epsilon_{\rm th} \simeq \frac{\Delta r_c}{r_c}+\frac{1}{(m_A r_c)^2} \simeq \frac{1}{(m_A r_c)^2}$, which gives the relation $\epsilon_{\rm th} \gg 1$. Even if the body has a thin-shell, the parameter $\epsilon_{\rm th}$ is much larger than unity under the condition $m_A r_c \ll 1$. The field profile (12) in the region $r > r_c$ reduces to

$$\phi(r) \simeq \phi_B - 2Q\left[1-\frac{1}{15}(m_A r_c)^2\right]\frac{GM_c}{r}e^{-m_B(r-r_c)}\,. \tag{14}$$

This means that the coupling is of the order of Q as in the thick-shell case. Hence it is not possible to be compatible with local gravity constraints for $|Q| = \mathcal{O}(1)$.

3.2 No-shell solutions ($r_1 = r_c$)

We require $m_A^2\left[\phi(r_c)-\phi_A\right] \le Q\rho_A$, which is equivalent to

$$\epsilon_{\rm th} \le \frac{e^{m_A r_c}+e^{-m_A r_c}}{m_A r_c(e^{m_A r_c}-e^{-m_A r_c})}\,. \tag{15}$$

3.2.1 The massive case ($m_A r_c \gg 1$)

If the field ϕ is massive such that $m_A r_c \gg 1$, the solution outside of the body is

$$\phi(r) \simeq \phi_B - 6Q\frac{GM_c}{r}\epsilon_{\rm th}\left(1-\frac{1}{m_A r_c}\right)e^{-m_B(r-r_c)}\,. \tag{16}$$

This shows that the effective coupling is given by $Q_{\rm eff} \simeq 3Q\epsilon_{\rm th}$. It is possible to satisfy local gravity constraints provided that $\epsilon_{\rm th} \ll 1$. Equation (15) gives the following constraint

$$\epsilon_{\rm th} \le \frac{1}{m_A r_c}\,. \tag{17}$$

The opposite inequality, $\epsilon_{\rm th} > 1/(m_A r_c)$, holds for the thin-shell case in the massive limit ($m_A r_c \gg 1$).

3.2.2 The light mass case ($m_A r_c \ll 1$)

When the field is almost massless such that $m_A r_c \ll 1$, the solution in the region $r > r_c$ is

$$\phi(r) \simeq \phi_B - 2Q\frac{GM_c}{r}\epsilon_{\rm th}(m_A r_c)^2 e^{-m_B(r-r_c)}\,. \tag{18}$$

From Eq. (15) we get $\epsilon_{\rm th} \le \frac{1}{(m_A r_c)^2}$. As long as $\epsilon_{\rm th}$ is much smaller than $1/(m_A r_c)^2$, it is possible to make the effective coupling $Q_{\rm eff} = Q\,\epsilon_{\rm th}(m_A r_c)^2$ small. However, the mass m_A is generally heavy to satisfy the condition $\epsilon_{\rm th}(m_A r_c)^2 \gg 1$ in concrete models that satisfy local gravity constraints.

4 Concrete models

The fifth force induced by the field $\phi(r)$ leads to the acceleration of a point particle given by $a_\phi = |Q_{\rm eff}\phi(r)|$ [3]. This then gives rise to a difference for free-fall accelerations of the moon ($a_{\rm Moon}$) and the Earth ($a_\oplus$) toward the Sun. Using the present experimental bound, $2|a_{\rm Moon}-a_\oplus|/(a_{\rm Moon}+a_\oplus) < 10^{-13}$, we obtain

$$|\phi_{B,\oplus}| < 3.7\times 10^{-15}\,. \tag{19}$$

4.1 Inverse-power law potential

Let us consider the inverse power-law potential (2). In this case we have

$$\phi_{B,\oplus} = \left[\frac{n}{Q} \frac{M_{\rm pl}^4}{\rho_B} \left(\frac{M}{M_{\rm pl}} \right)^{n+4} \right]^{\frac{1}{n+1}} M_{\rm pl} \,. \tag{20}$$

On using the bound (19) with n and Q of the order of unity, we get the following constraint

$$M \lesssim 10^{-\frac{15n+130}{n+4}} M_{\rm pl} \,. \tag{21}$$

This shows that $M \lesssim 10^{-2}\,{\rm eV}$ for $n = 1$ and $M \lesssim 10^{-4}\,{\rm eV}$ for $n = 2$, which are consistent with the bound derived in Ref. [3].

4.2 The potential motivated by $f(R)$ gravity

The next example is the potential (3), which covers viable $f(R)$ models that satisfy local gravity constraints [5, 6]. The field value $\phi_{B,\oplus}$ is given by

$$|\phi_{B,\oplus}| = \frac{1}{2|Q|} \left(\frac{2pCV_0}{\rho_B} \right)^{\frac{1}{1-p}} M_{\rm pl} \,. \tag{22}$$

Employing (19), one can derive the bound $p > 14/9$.

The quantity $(m_A r_c)^2$ for the Earth is

$$(m_A r_c)^2 = 6|Q|(1-p) \frac{\Phi_{c,\oplus}}{|\phi_{B,\oplus}|} \left(\frac{\rho_A}{\rho_B} \right)^{\frac{1}{1-p}} \,. \tag{23}$$

Under the constraint (19) we get

$$m_A r_c \gtrsim [|Q|(1-p)]^{1/2} \cdot 10^{\frac{31-6p}{2(1-p)}} \,. \tag{24}$$

When $p > 0.65$ this condition correspond to $m_A r_c \gtrsim 10^{39}$, which means that the field is extremely massive inside of the body.

5 Conclusions

In this paper we have derived analytic solutions of a chameleon scalar field ϕ in the background of a spherically symmetric body by taking into account a field mass m_A about the potential minimum at $\phi = \phi_A$ inside of the body. We have shown that the chameleon mechanism works in a robust way provided that the field mass inside of the body satisfies the condition $m_A r_c \gg 1$ with appropriate boundary conditions.

References

[1] E. J. Copeland, M. Sami and S. Tsujikawa, Int. J. Mod. Phys. D **15**, 1753 (2006); S. Nojiri and S. D. Odintsov, Int. J. Geom. Meth. Mod. Phys. **4**, 115 (2007); T. P. Sotiriou and V. Faraoni, arXiv:0805.1726 [gr-qc].

[2] J. Khoury and A. Weltman, Phys. Rev. Lett. **93**, 171104 (2004).

[3] J. Khoury and A. Weltman, Phys. Rev. D **69**, 044026 (2004).

[4] T. Tamaki and S. Tsujikawa Phys. Rev. D **78**, 084028 (2008).

[5] W. Hu and I. Sawicki, Phys. Rev. D **76**, 064004 (2007).

[6] A. A. Starobinsky, JETP Lett. **86**, 157 (2007).

Squashed Kerr-Gödel Black Holes

Shinya Tomizawa,[1] Hideki Ishihara,[2] Ken Matsuno[3] and Toshiharu Nakagawa[4]

[1] *Cosmophysics Group, Institute of Particle and Nuclear Studies, KEK, Tsukuba, Ibaraki, 305-0801, Japan*

[2,3,4] *Department of Mathematics and Physics, Graduate School of Science, Osaka City University, 3-3-138 Sugimoto, Sumiyoshi, Osaka 558-8585, Japan*

Abstract

Applying *squashing transformation* to Kerr-Gödel black hole solutions, we present a new type of a rotating Kaluza-Klein black hole solution to the five-dimensional Einstein-Maxwell theory with a Chern-Simonss term. The new solutions generated via the squashing transformation have no closed timelike curve everywhere outside the black hole horizons. The spacetime is asymptotically locally flat. One of the remarkable features is that the solution has two independent rotation parameters along an extra dimension associated with the black hole's rotation and the Gödel's rotation. The space-time also admits the existence of two disconnected ergoregions, an inner ergoregion and an outer ergoregion. These two ergoregions can rotate in the opposite direction as well as in the same direction.

1 Summary

In recent years, some non-BPS black hole solutions have also been found in addition to supersymmetric black hole solutions. Although no one has found higher-dimensional Kerr-Newman solutions in Einstein-Maxwell theory yet, Cvetič *et al* [1] found a non-extremal, charged and rotating black hole solution with asymptotic flatness in the five-dimensional Einstein-Maxwell theory with a Chern-Simons term. In the neutral case, the solution reduces to the same angular momenta case of the Myers-Perry black hole solution [2]. Exact solutions of non-BPS Kaluza-Klein black hole solutions are found in neutral case [3, 4] and charged case [5]. These solutions have a non-trivial asymptotic structure, i.e., the spacetime is asymptotically locally flat and approaches a twisted S^1 metric over a four-dimensional Minkowski spacetime, topologically not a direct product. The horizons are deformed due to this non-trivial asymptotic structure and have a shape of a squashed S^3, where S^3 is regarded as a S^1 bundle over a S^2 base space. The ratio of the radius S^2 to that of S^1 is always larger than one.

As was proposed by Wang, a kind of Kaluza-Klein black hole solutions can be generated by the *squashing transformation* from black holes with asymptotic flatness [6]. In fact, he regenerated the five-dimensional Kaluza-Klein black hole solution found by Dobiasch and Maison [3, 4] from the five-dimensional Myers-Perry black hole solution with two equal angular momentum (The solution generated by Wang coincides with the solution in Ref.[3, 4].). In the previous work [7], applying the squashing transformation to the Cvetič *et al*'s charged rotating black hole solution [1] in vanishing cosmological constant case, we obtain the new Kaluza-Klein black hole solution in the five-dimensional Einstein-Maxwell theory with a Chern-Simons term. This is the generalization of the Kaluza-Klein black hole solutions in Ref. [3, 4, 5]. This solution has four parameters, the mass, the angular momentum in the direction of an extra dimension, the electric charge and the size of the extra dimension. The solution describes the physical situation such that in general a non-BPS black hole is boosted in the direction of the extra dimension. As the interesting feature of the solution, unlike the static solution [5], the horizon admits a prolate shape in addition to a round S^3. The solution has the limits to the supersymmetric black hole solution and a new extreme non-BPS black hole solutions and a new rotating black hole solution with a constant S^1 fiber.

[1] E-mail:tomizawa@post.kek.jp
[2] E-mail:ishihara@sci.osaka-cu.ac.jp
[3] E-mail:matsuno@sci.osaka-cu.ac.jp
[4] E-mail:tosiharu@sci.osaka-cu.ac.jp

Applying this squashing transformation to Kerr-Gödel black hole solutions [8], we have constructed [9] a new type of rotating Kaluza-Klein black hole solutions to the five-dimensional Einstein-Maxwell theory with a Chern-Simons term. We also have investigated the features of the solutions. Though the Gödel black hole solutions have closed timelike curves in the region away from the black hole, the new Kaluza-Klein black hole solutions generated by the squashing transformation have no closed timelike curve everywhere outside the black hole horizons. At the infinity, the space-time is asymptotically a Kaluza-Klein spacetime. The solution has four independent parameters, the mass parameter, the size of an extra dimension and two kinds of rotations parameters in the same direction of the extra dimension. These two independent parameters are associated with the rotations of the black hole and the universe. In the case of the absence of a black hole, the solution describes the Gross-Perry-Sorkin (GPS) monopole which is boosted in the direction of an extra dimension and has an ergoregion by the effect of the rotation of the universe.

2 Squashed Kerr-Gödel black hole solution

The action is given by

$$S = \frac{1}{16\pi}\int\left(R*1 - 2F\wedge *F - \frac{8}{3\sqrt{3}}F\wedge F\wedge A\right). \tag{1}$$

The metric and the gauge potential for the squashed Kerr-Gödel black hole solution are given by

$$ds^2 = -f(r)dt^2 - 2g(r)\sigma_3 dt + h(r)\sigma_3^2 + \frac{k(r)^2dr^2}{V(r)} + \frac{r^2}{4}[k(r)(\sigma_1^2+\sigma_2^2)+\sigma_3^2], \tag{2}$$

and

$$\mathcal{A} = \frac{\sqrt{3}}{2}jr^2\sigma_3, \tag{3}$$

respectively, where the functions in the metric are

$$f(r) = 1 - \frac{2m}{r^2}, \tag{4}$$

$$g(r) = jr^2 + \frac{ma}{r^2}, \tag{5}$$

$$h(r) = -j^2r^2(r^2+2m) + \frac{ma^2}{2r^2}, \tag{6}$$

$$V(r) = 1 - \frac{2m}{r^2} + \frac{8jm(a+2jm)}{r^2} + \frac{2ma^2}{r^4}, \tag{7}$$

$$k(r) = \frac{V(r_\infty)r_\infty^4}{(r^2-r_\infty^2)^2} \tag{8}$$

and the 1-forms on S^3 are given by

$$\sigma_1 = \cos\psi d\theta + \sin\psi\sin\theta d\phi, \tag{9}$$

$$\sigma_2 = -\sin\psi d\theta + \cos\psi\sin\theta d\phi, \tag{10}$$

$$\sigma_3 = d\psi + \cos\theta d\phi. \tag{11}$$

The coordinates r, θ, ϕ and ψ run the ranges of $0 < r < r_\infty$, $0 \le \theta < \pi$, $0 \le \phi < 2\pi$, $0 \le \psi < 4\pi$, respectively. m, a, j and r_∞ are constants. The space-time has the timelike Killing vector fields ∂_t and two spatial Killing vector fields with closed orbits, ∂_ϕ and ∂_ψ. Note that this metric can be obtained from the Kerr-Gödel black hole solution [8] by the transformation $\sigma_1 \to \sqrt{k(r)}\sigma_1$, $\sigma_2 \to \sqrt{k(r)}\sigma_2$, $\sigma_3 \to \sqrt{k(r)}\sigma_3$ and $dr \to k(r)dr$, which is called squashing transformation. In the limit of $k(r) \to 1$, i.e., $r_\infty \to \infty$ with the other parameters kept finite, the metric coincides with that of the original Kerr-Gödel

black hole solution [8] with CTCs. Here we assume that the parameters j, m, a and r_∞ appearing in the solutions satisfy the following inequalities

$$m > 0, \tag{12}$$

$$\frac{r_\infty^2}{m} > 1 - 4j(a + 2jm) > \sqrt{\frac{2}{m}}|a|, \tag{13}$$

$$r_\infty^4 - 2m(1 - 4j(a + 2jm))r_\infty^2 + 2ma^2 > 0, \tag{14}$$

$$-4j^2 r_\infty^6 + (1 - 8j^2 m)r_\infty^4 + 2ma^2 > 0. \tag{15}$$

These are the necessary and sufficient conditions that there are two horizons and no CTCs outside the horizons. Eqs. (12)-(14) are conditions for the presence of two horizons, and Eq.(15) is the condition for the absence of CTCs outside the horizons. It is noted that in the limit of $r_\infty \to \infty$ with the other parameters finite, Eq.(15) can not be satisfied. Let us normalize the parameters a, j and r_∞ as $A = a/\sqrt{m}, J = \sqrt{m}j$ and $R_\infty = r_\infty/\sqrt{m}$, respectively and furthermore, we fix the value of R_∞. Then, in the cases of $R_\infty^2 < 2$, $R_\infty^2 = 2$ and $R_\infty^2 > 2$, the quadratic curve $R_\infty^4 - 2(1-4J(A+2J))R_\infty^2 + 2A^2 = 0$ in the condition (14) becomes an ellipse, a line and a hyperbola, respectively. The curve $R_\infty^2 = 1 - 4J(A + 2J)$ in the condition (13) has different shapes in the cases of $R_\infty^2 < 1$, $R_\infty^2 = 1$ and $R_\infty^2 > 1$. Hence we consider the cases of (i) $0 < R_\infty^2 < 1$, (ii) $R_\infty^2 = 1$ (iii) $1 < R_\infty^2 < 2$ (iv) $R_\infty^2 = 2$ and (v) $R_\infty^2 > 2$. The shaded regions in Figure1-5 show the parameter region (12)-(15) for a given R_∞ in each case of (i)-(v), respectively. Thus, applying the squashing transformation to the Kerr-Gödel black hole solution, we can obtain such a Kaluza-Klein black hole solution without CTCs everywhere outside the black hole.

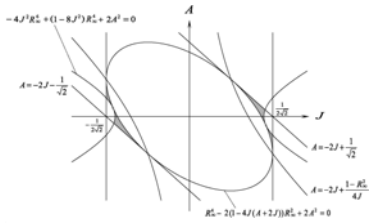

Figure 1: The parameter region in the (J, A)-plane in the case of $0 < R_\infty^2 < 1$.

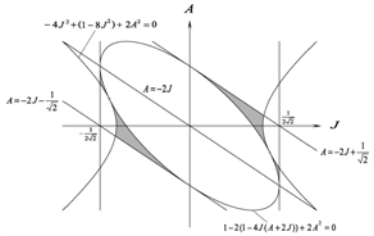

Figure 2: The parameter region in the (J, A)-plane in the case of $R_\infty^2 = 1$.

References

[1] M. Cvetič and D. Youm, Nucl. Phys. B **476**, 118 (1996).
M. Cvetič, H. Lü and C.N. Pope, Phys. Lett B **598**, 273 (2004).

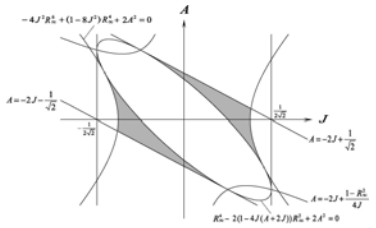

Figure 3: The parameter region in the (J, A)-plane in the case of $1 < R_\infty^2 < 2$.

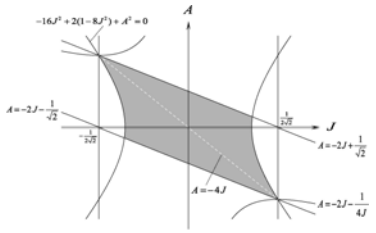

Figure 4: The parameter region in the (J, A)-plane in the case of $R_\infty^2 = 2$.

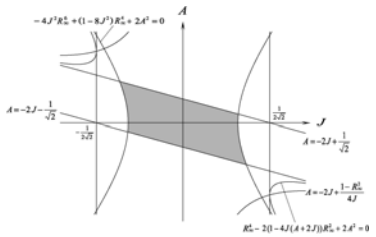

Figure 5: The parameter region in the (J, A)-plane in the case of $2 < R_\infty^2$.

Z.-W. Chong, M. Cvetič, H. Lü and C.N. Pope, Phys. Rev. Lett. **95** 161301 (2005).

[2] R.C. Myers and M.J. Perry, Annals Phys. **172**, 304 (1986).

[3] P. Dobiasch and D. Maison, Gen. Rel. Grav. **14**, 231 (1982).

[4] G.W. Gibbons and D.L. Wiltshire, Ann. Phys. **167**, 201 (1986).

[5] H. Ishihara and K. Matsuno, Prog. Theor. Phys. **116**, 417 (2006).

[6] T. Wang, Nucl. Phys. B, **756**, 86 (2006).

[7] T. Nakagawa, H. Ishihara, K. Matsuno and S. Tomizawa, Phys. Rev. D **77**, 044040 (2008).

[8] E. Gimon and A. Hashimoto, Phys. Rev. Lett. **91**, 021601 (2003).

[9] S. Tomizawa, H. Ishihara, K. Matsuno and T. Nakagawa, e-Print: arXiv:0803.3873 [hep-th], to be published in Prog. Theor. Phys.

Dilatonic Black Holes in Gauss-Bonnet Gravity in Various Dimensions

Takashi Torii[1], Zong-Kuan Guo[2], and Nobuyoshi Ohta[3]

[1]*Department of General Education, Osaka Institute of Technology, Asahi-ku, Osaka 535-8585, Japan*
[2,3]*Department of Physics, Kinki University, Higashi-Osaka, Osaka 577-8502, Japan*

Abstract

We study asymptotically AdS topological black hole solutions with $k = 0$ (planar symmetric) in the Einstein gravity with Gauss-Bonnet term, the dilaton and a "cosmological constant" in various dimensions. We derive the field equations for suitable ansatz for general D dimensions. We determine the parameter regions including dilaton couplings where such solutions exist and construct black hole solutions of various masses numerically in $D = 4, 5, 6$ and 10 dimensional spacetime with $(D-2)$-dimensional hypersurface of zero curvature.

1 Introduction

One of the most important problems in theoretical physics is the formulation of the quantum theory of gravity and its application to physical system to understand physics at strong gravity. There has been interest in the application of string theory to the cosmology and black hole physics. The first attempt at understanding black holes in the Einstein-Maxwell-dilaton system was made in Refs. [1], in which a static spherically symmetric black hole solution with dilaton hair was found. After this, many solutions were discussed in various models. On the other hand, it is known that there are correction terms of higher orders in the curvature to the lowest effective supergravity action coming from superstrings. The simplest correction is the Gauss-Bonnet (GB) term coupled to the dilaton field in the low-energy effective heterotic string [2]. It is then natural to ask how the black hole solutions are affected by the higher order terms in these effective theories.

There has been recently a renewed interest in these solutions as the application to the calculation of shear viscosity in strongly coupled gauge theories using black hole solutions in five-dimensional Einstein-GB theory via AdS/CFT correspondence [3]. Almost all these studies consider a pure GB term without a dilaton, or assume a constant dilaton, which is not a solution of the heterotic string. It is, however, expected that AdS/CFT correspondence is valid within the effective theories of superstring. It is thus important to investigate how the properties of black holes are modified when the dilaton is present.

It may appear odd to add a cosmological constant in a low-energy effective theory of the superstring theories, but actually it may be present in such theories. For example, it is known that type IIA theories have a 10-form whose expectation value may give rise to such a cosmological constant [4]. Other possible sources include generation of such a term at one-loop in non-supersymmetric heterotic string [5]. There are also various forms in superstrings which could produce similar terms with various dilaton dependences, so we will simply suppose that such terms are present.

2 Dilatonic Einstein-Gauss-Bonnet theory

We consider the following low-energy effective action for a heterotic string

$$S = \frac{1}{2\kappa_D^2}\int d^Dx\sqrt{-g}\left[R - \frac{1}{2}(\partial_\mu\phi)^2 + \alpha_2 e^{-\gamma\phi}R^2_{\rm GB} - \Lambda e^{\lambda\phi}\right], \tag{1}$$

[1]E-mail:torii@ge.oit.ac.jp
[2]E-mail:guozk@physik.uni-bielefeld.de
[3]E-mail:ohtan@phys.kindai.ac.jp

where κ_D^2 is a D-dimensional gravitational constant, ϕ is a dilaton field, $\alpha_2 = \alpha'/8$ is a numerical coefficient given in terms of the Regge slope parameter α', and $R^2_{\rm GB} = R_{\mu\nu\rho\sigma}R^{\mu\nu\rho\sigma} - 4R_{\mu\nu}R^{\mu\nu} + R^2$ is the GB correction. In this paper we leave the coupling constant of dilaton γ arbitrary as much as possible, while the ten-dimensional critical string theory predicts $\gamma = 1/2$. We have also included the negative cosmological constant $\Lambda = -(D-1)(D-2)/\ell^2$ with possible dilaton coupling λ. The RR 10-form in type IIA theory can produce "cosmological constant" in the string frame, but that will carry such dilaton couplings with $\lambda = 5/2$ in the Einstein frame [4]. Note that this "cosmological term" gives a Liouville type of potential. If this is the only potential, there is no stationary point and the dilaton cannot have a stable asymptotic value. However, for asymptotically AdS solutions, the Gauss-Bonnet term produces an additional potential in the asymptotic region, and we will see that it is possible to have the solutions where the dilaton takes finite constant value at infinity. There may be other possible sources of "cosmological terms" with different dilaton couplings, so we leave λ arbitrary and specify it in the numerical analysis.

We parametrize the metric as

$$ds_D^2 = -Be^{-2\delta}dt^2 + B^{-1}dr^2 + r^2 h_{ij}dx^i dx^j, \tag{2}$$

where $h_{ij}dx^i dx^j$ represents the line element of a $(D-2)$-dimensional hypersurface with constant curvature $k = 0$ and volume Σ_0.

It is useful to consider several symmetries of our field equations (or our model). Firstly the field equations are invariant under the transformation: $(\gamma \to -\gamma,\ \lambda \to -\lambda,\ \phi \to -\phi)$. By this symmetry, we can restrict the parameter range of γ to $\gamma \geq 0$. For $k = 0$, the field equations are invariant under the scaling transformation $(B \to a^2 B,\ \tilde{r} \to a\tilde{r})$, with an arbitrary constant a. If a black hole solution with the horizon radius $\tilde{r}_H$ is obtained, we can generate solutions with different horizon radii but the same $\tilde{\Lambda}$ by this scaling transformation. The field equations have a shift symmetry: $(\phi \to \phi - \phi_*,\ \tilde{\Lambda} \to e^{(\lambda-\gamma)\phi_*}\tilde{\Lambda},\ B \to e^{-\gamma\phi_*}B)$, where ϕ_* is an arbitrary constant. This changes the magnitude of the cosmological constant. Hence this may be used to generate solutions for different cosmological constants but with the same horizon radius, given a solution for some cosmological constant and $\tilde{r}_H$. The final one is another shift symmetry under $(\delta \to \delta - \delta_*,\quad t \to e^{-\delta_*}t)$ with an arbitrary constant δ_*, which may be used to shift the asymptotic value of δ to zero. The model (1) has several parameters D, α_2, Λ, γ, and λ. The black hole solutions have also physical independent parameters such as the horizon radius $\tilde{r}_H$ and the value of δ at infinity. However, owing to the above symmetries (including the scaling by α_2), we can reduce the number of the parameters and are left only with D, $\gamma \geq 0$, λ, and $\tilde{r}_H$.

Let us first examine the boundary conditions of the black hole spacetime. We assume the following boundary conditions for the metric functions:

1. The existence of a regular horizon $\tilde{r}_H$: $B(\tilde{r}_H) = 0,\ \ |\delta_H| < \infty,\ \ |\phi_H| < \infty\,.$
2. The nonexistence of singularities outside the event horizon: $B(\tilde{r}) > 0,\ \ |\delta| < \infty,\ \ |\phi| < \infty\,.$

Here and in what follows, the values of various quantities at the horizon are denoted with subscript H. At infinity we assume the condition that the leading term of the metric function B comes from AdS radius $\tilde{\ell}_{AdS}$, i.e.,

3. "AdS asymptotic behavior" $(\tilde{r} \to \infty)$:

$$B \sim \tilde{b}_2\tilde{r}^2 - \frac{2\tilde{M}}{\tilde{r}^\mu},\quad \delta(r) \sim \delta_0 + \frac{\delta_1}{\tilde{r}^\sigma},\ \ \phi \sim \phi_0 + \frac{\phi_1}{\tilde{r}^\nu}\,, \tag{3}$$

with finite constants $\tilde{b}_2 > 0$, $\tilde{M}$, δ_0, δ_1, ϕ_0, ϕ_1 and positive constant μ, σ, ν.

The coefficient of the first term $\tilde{b}_2$ is related to the AdS radius as $\tilde{b}_2 = \ell_{\rm AdS}^{-2}$.

Substituting Eqs. (3) into the field equations, one finds the conditions that the leading terms ($\tilde{r}^2$ and constant terms in each equation) balance with each other are given by

$$\tilde{b}_2{}^2 = \frac{-\lambda\tilde{\Lambda}}{(D)_3\gamma}\left[\frac{D(D-3)}{(D-1)_2}(-\tilde{\Lambda})\frac{\gamma}{\lambda}\left(1 + \frac{(D-4)\lambda}{D\gamma}\right)^2\right]^{\frac{\gamma+\lambda}{\gamma-\lambda}}, \tag{4}$$

$$e^{\phi_0} = \left[\frac{D(D-3)}{(D-1)_2}(-\tilde{\Lambda})\frac{\gamma}{\lambda}\left(1 + \frac{(D-4)\lambda}{D\gamma}\right)^2\right]^{\frac{1}{\gamma-\lambda}}, \tag{5}$$

for $\lambda \neq \gamma$, where $(D-m)_n = (D-m)(D-m-1)\cdots(D-n)$.

From the next leading terms, we find

$$\nu = \nu_\pm = \frac{D-1}{2}\left[1 \pm \sqrt{1 - \frac{4(D)_2\lambda\gamma(\lambda-\gamma)\big[(D-4)\lambda + D\gamma\big]}{(D-1)^2\big[(D-4)^2\lambda^2 - D^2\gamma^2 - 8(D-1)_2\lambda^2\gamma^2\big]}}\,\right]. \tag{6}$$

and $\sigma = \mu + 2 = \nu$. The power indices ν, μ and σ do not depend on $\tilde{\Lambda}$. We rewrite the indices $\nu_\pm$ as

$$\nu_\pm = \frac{D-1}{2}\left[1 \pm \sqrt{1 - \frac{\tilde{m}^2}{\tilde{m}^2_{BF}}}\right], \tag{7}$$

where the mass square of Breitenlohner and Freedman (BF) bound [6] is defined by $\tilde{m}^2_{BF} = -(D-1)^2/4\tilde{\ell}^2_{AdS}$, and we define the mass square of the dilaton field as

$$\tilde{m}^2 = -\frac{(D)_2\lambda(\lambda-\gamma)\big[(D-4)\lambda + D\gamma\big]}{(D-4)^2\lambda^2 - D^2\gamma^2 - 8(D-1)_2\lambda^2\gamma^2}\tilde{b}_2. \tag{8}$$

by the analogy with the discussion in BF bound. This mass is considered to be the second derivative of the "effective potential" of the dilaton field. Note that these equations hold even for the $\gamma = \lambda$ case.

Using the above results, we discuss the parameter regions which give desirable black hole solutions. We impose that the mass of the dilaton field $\tilde{m}$ should satisfy the conditions

$$\tilde{m}^2_{BF} \leq \tilde{m}^2 < 0, \tag{9}$$

which comes from that the stability of the asymptotic structure of the solution against time-dependent perturbations. We find that there are two separate allowed regions in the parameter space (λ, γ). This is shown in Fig. 1.

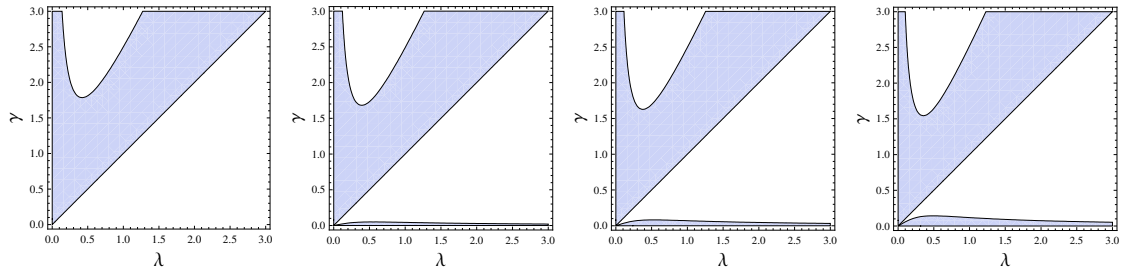

(a) (b) (c) (d)

Figure 1: The allowed regions from the conditions (9) for (a) $D = 4$, (b) $D = 5$, (c) $D = 6$, and (d) $D = 10$.

3 Black hole solutions

The basic equations do not have analytical solutions, so we have to resort to the numerical method. In the numerical analysis, we have to first choose the parameters for our black hole solutions from the allowed regions of γ and λ, and other parameters. Considering the results in the previous section, we choose the following parameters and conditions as a typical example in various dimensions:

$$\gamma = \frac{1}{2}, \quad \lambda = \frac{1}{3}, \quad \tilde{\Lambda} < 0, \quad \phi_- = 0, \quad \delta_0 = 0, \tag{10}$$

and expect that this choice gives the typical solutions.

We present the configurations of the field functions of the black hole solutions for $D = 5$ in Figs. 2, where the variable $\tilde{m}_g$ is the gravitational mass defined by

$$-g_{tt} = \tilde{b}_2\tilde{r}^2 - \frac{2\tilde{m}_g(\tilde{r})}{\tilde{r}^{D-3}}. \tag{11}$$

By the numerical analysis we also find the relation between the mass and horizon radius of the black holes:

$$\tilde{M}_0 = 0.28014\big(2|\tilde{\Lambda}|/3\big)^3 \tilde{r}_H^{\,3}, \quad (D=4), \qquad \tilde{M}_0 = 3.7819\big(|\tilde{\Lambda}|/3\big)^3 \tilde{r}_H^{\,4}, \quad (D=5), \tag{12}$$

$$\tilde{M}_0 = 19.933\big(|\tilde{\Lambda}|/5\big)^3 \tilde{r}_H^{\,5}, \quad (D=6), \qquad \tilde{M}_0 = 771.68\big(|\tilde{\Lambda}|/18\big)^3 \tilde{r}_H^{\,9}, \quad (D=10). \tag{13}$$

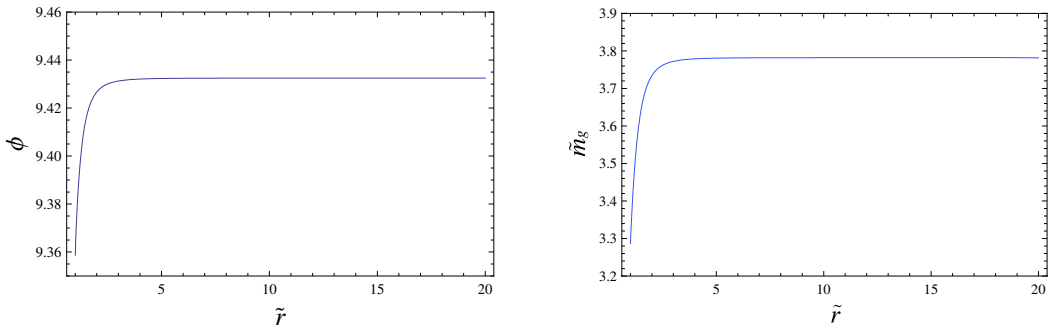

(a) (b)

Figure 2: The configurations of (a) ϕ and (b) $\tilde{m}_g$ in five dimensions for $\tilde{r}_H = 1$ and $\tilde{\Lambda} = -3$.

4 Conclusions

We have studied the black hole solutions in dilatonic Einstein-GB theory with the negative cosmological constant. The cosmological constant introduces the Liouville type of potential for the dilaton field. We have taken the planar symmetric spacetime, i.e., the $(D-2)$-dimensional hypersurface spanned by the angular coordinates with vanishing constant curvature ($k = 0$). The basic equations have some symmetries which are used to generate the black hole solutions with different horizon radius and the cosmological constant.

There are some remaining issues left for future works such as thermodynamics of our black holes, stability, formulation of the canonical mass, spherically symmetric solutions (k=1), and the properties of field theories via AdS/CFT correspondence.

References

[1] G. W. Gibbons and K. Maeda, Nucl. Phys. **B298** (1988) 741; D. Garfinkle, G. T. Horowitz, and A. Strominger, Phys. Rev. D **43** (1991) 3140.

[2] D. J. Gross and J. H. Sloan, Nucl. Phys. B **291** (1987) 41; M. C. Bento and O. Bertolami, Phys. Lett. B **368** (1996) 198.

[3] A. Buchel and J. T. Liu, Phys. Rev. Lett. **93** (2004) 090602; P. Kovtun, D. T. Son and A. O. Starinets, Phys. Rev. Lett. **94** (2005) 111601; M. Brigante, H. Liu, R. C. Myers, S. Shenker and S. Yaida, Phys. Rev. Lett. **100** (2008) 191601.

[4] J. Polchinski, "String theory," *Cambridge Univ. Pr. (1998).*

[5] L. Alvarez-Gaume, P. H. Ginsparg, G. W. Moore and C. Vafa, Phys. Lett. B **171** (1986) 155.

[6] P. Breitenlohner and D. Z. Freedman, Annals Phys. **144** (1982) 249.

Apparent Horizon Formation in Five-dimensional Spacetime

Yuta Yamada[1] and Hisa-aki Shinkai[2]

Dept. of Information Science and Technology,Osaka Institute of Technology, Hirakata, Osaka 573-0196

Abstract

We numerically investigated the formation of an apparent horizon in ve-dimensional spacetime in the context of the cosmic censorship hypothesis. We modeled the matter by distributing collisionless particles both in spheroidal and toroidal con gurations under the momentarily static assumption, and obtained the sequence of initial data by solving the Hamiltonian constraint equation. We found both S^3 and S^2 S^1 horizons, only when the matter con guration is not steep. By monitoring the location of the maximum Kretchmann invariant, we guess an appearance of 'naked singularity' or 'naked ring' under the special situations.

1 Introduction

In general relativity, there are two famous conjectures concerning the gravitational collapse. One is the cosmic censorship hypothesis which states collapse driven singularities will always be clothed by event horizon and hence can never be visible from the outside. The other is the hoop conjecture [1] which states that black holes will form when and only when a mass M gets compacted into a region whose circumference in every direction is $C \leq 4 \ M$. These two conjectures have been extensively searched in various methods, among them we believe the numerical works by Shapiro and Teukolsky [2] showed the most exciting results; (a tendency of) the appearance of a naked singularity. This was reported from the fully relativistic time evolution of collisionless particles in a highly prolate initial shape; and the results of time evolutions are agree with those of the sequence of their initial data [3].

In recent years, on the other hand, gravitation in higher-dimensional spacetime is much getting a lot of attention. This is from an attempt to unify fundamental forces including gravity at TeV scale, and if so, it is suggested that small black-holes might be produced at the CERN Large Hadron Collider (LHC). The four-dimensional black-holes are known to be S^1 from the topological theorem, while in higher-dimensional spacetime quite rich structures are available including a torus black-hole ("black ring").

We, therefore, plan to reproduce the earlier numerical works in higher-dimensional spacetime, and this report shows our rst trials to obtain the sequence of the initial data. As for the hoop conjecture, the modi ed version called *hyper-hoop* was proposed by Ida and Nakao [4] for the higher-dimensional spacetime, which was consistent with semi-analytic works [5]. We used the results of [5] as our code checks, and developed the code as we can investigate in more general situations.

2 Basic Equations

2.1 The Hamiltonian constraint equation

We consider the initial data sequence on a four-dimensional space-like hypersurface. A solution of the Einstein equations is obtained by solving the Hamiltonian constraint equation if we assume the moment of time symmetry. Applying a conformal transformation,

$$_{ij} = \ ^{2\hat{}}{}_{ij}, \tag{1}$$

from conformally- at base metric $\hat{}_{ij}$, the Hamiltonian constraint equation becomes

$$\hat{} \quad = \quad 4 \ ^2G_5 \ , \tag{2}$$

[1]E-mail:m1m08a26@info.oit.ac.jp
[2]E-mail:shinkai@is.oit.ac.jp

where is the mass density, G_5 is the gravitational constant in ve dimensional theory of gravity. We solve (2) using the Cartesian coordinates, $ds^2 = \hat{}_{ij}dx^i dx^j = dx^2 + dy^2 + dz^2 + dw^2$, with various matter con gurations (spheroidal and toroidal) by distributing 10^6 collisionless particles. We numerically solve (2) in the upper-half region ($x \geq 0,\ y \geq 0,\ z \geq 0,\ w \geq 0$) with 50^4 grids by setting the boundary conditions as

$$\nabla \quad = 0\,(\text{at } r = 0), \qquad = 1 + \frac{M}{2r^2}\,(\text{at } r \to \infty), \quad \text{where } r = \sqrt{x^2 + y^2 + z^2 + w^2}, \tag{3}$$

where M can be interpreted the total mass of the matter.

2.2 Apparent Horizons

For nding an apparent horizon, we follow [4] and [5]. Since we assume the matter is axially symmetrical distribution, the horizon will also be axially symmetric. Using the coordinate and , where

$$= \arctan\frac{\sqrt{x^2 + y^2 + w^2}}{z}, \qquad = \arctan\frac{\sqrt{x^2 + y^2}}{w}, \tag{4}$$

the axisymmetric apparent horizon is identi ed by solving

$$\begin{aligned} & r_m \quad \frac{4\dot{r}_m^2}{r_m} \quad 3r_m + \frac{r_m^2 + \dot{r}_m^2}{r_m} \qquad \frac{2\dot{r}_m}{r_m}\cot \qquad \frac{3}{-}(\dot{r}_m \sin \quad + r_m \cos \ )\frac{\partial}{\partial z} \\ & + \frac{3}{-}(\dot{r}_m \cos \qquad r_m \sin \ ) \quad \frac{\partial}{\partial z}\sin \quad \cos \ + \frac{\partial}{\partial y}\sin \quad \sin \ + \frac{\partial}{\partial w}\cos \qquad = 0, \end{aligned} \tag{5}$$

with the boundary condition

$$\dot{r}_m = 0 \quad \text{at} \quad = \frac{-}{2}. \tag{6}$$

On the other hand, for the torus of the ring radius C, additional $S^2 \quad S^1$ apparent horizon may exist. This marginal surface is obtained by solving the equation for $r(\ )$, satisfying

$$r \quad \frac{3\dot{r}^2}{r} \quad 2r \quad \frac{r^2 + \dot{r}^2}{r} \quad \frac{\dot{r}\sin \quad + r\cos}{r\cos \quad + C} \quad \frac{\dot{r}}{r}\cot \ + \frac{3}{-}(\dot{r}\sin \quad + r\cos \ )\frac{\partial}{\partial x} \quad \frac{3}{-}(\dot{r}\cos \qquad r\sin \ )\frac{\partial}{\partial z} \quad = 0, \tag{7}$$

with the boundary condition

$$\dot{r} = 0 \quad \text{at} \quad = 0, \tag{8}$$

3 Results

3.1 Spheroidal configurations

First, we show the cases with homogeneous spheroidal matter con gurations,

$$\frac{x^2}{a^2} + \frac{y^2}{a^2} + \frac{w^2}{a^2} + \frac{z^2}{b^2} \leq 1. \tag{9}$$

where a and b are constants. In Figure 1, we show particle distributions and shape of the apparent horizon on our numerical grid. When $a = b$, the horizon is spherically symmetric and located at Schwarzschild radius. When $b = 3a$, the horizon becomes prolate. When $b = 5a$, on the other hand, we can not nd an apparent horizon. The behavior is the same with [3] and [5]. The asterisk in Fig.1 is the location of the largest Kretchmann invariant, $I_{\max} = \max\{R_{abcd}R^{abcd}\}$, where R_{abcd} is the four-dimensional Riemann tensor. For all cases, we see the location of $I_{\max}$ is always outside the matter on the axis. We show the contours of $I = R_{abcd}R^{abcd}$ in Figure 2.

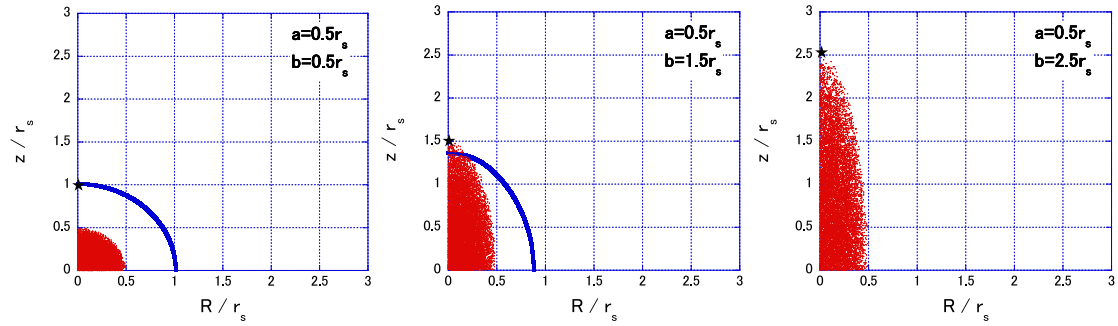

Figure 1: Matter distributions and apparent horizons for spheroidal matter distributions. We can not nd an apparent horizon for highly spindle cases.

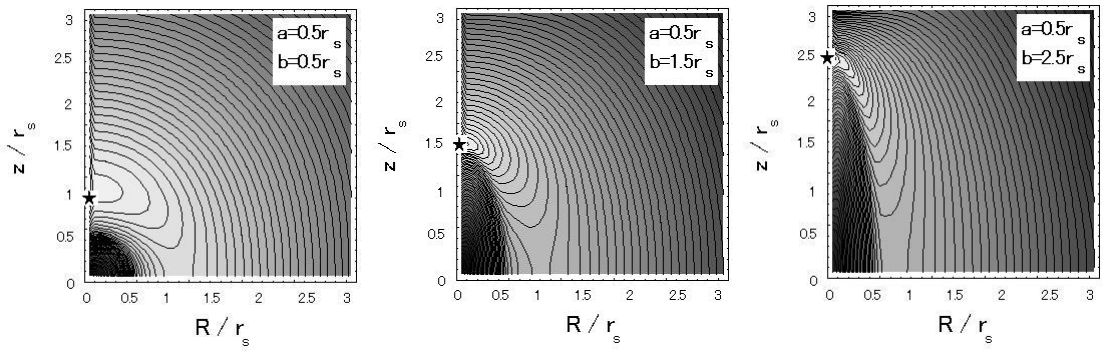

Figure 2: Contours of Kretchmann invariant, $I = R_{abcd}R^{abcd}$, corresponding to Fig.1.

In Figure 3, we plot $I_{\max}$ as a function of b/a. Fig.3 shows that the spindle cases have larger $I_{\max}$, that suggests the possibility of appearance of a naked singularity as in the four-dimensional case.

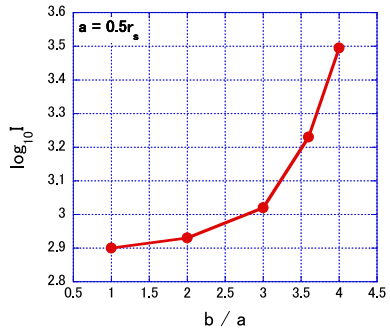

Figure 3: $I_{\max}$ as a function of b/a.

3.2 Toroidal configurations

Next, we consider homogeneous toroidal matter con gurations as

$$\left(\sqrt{x^2+y^2} - C\right)^2 + \left(\sqrt{w^2+z^2}\right)^2 \leq r^2, \tag{10}$$

where C is the circle radius of torus, and r is ring radius of torus. Figure 4 shows the results of searches for apparent horizons. When C is $1.65r_s$, both S^3 and S^2 S^1 apparent horizons exist. On the other hand, when C is larger ($C = 1.78r_S$), only the S^2 S^1 ring horizon is observed. The value of $I_{\max}$ appears

at the outside as well as spheroidal cases. Interestingly, $I_{\max}$ is not hidden inside the ring horizon when C is $2.55r_s$.

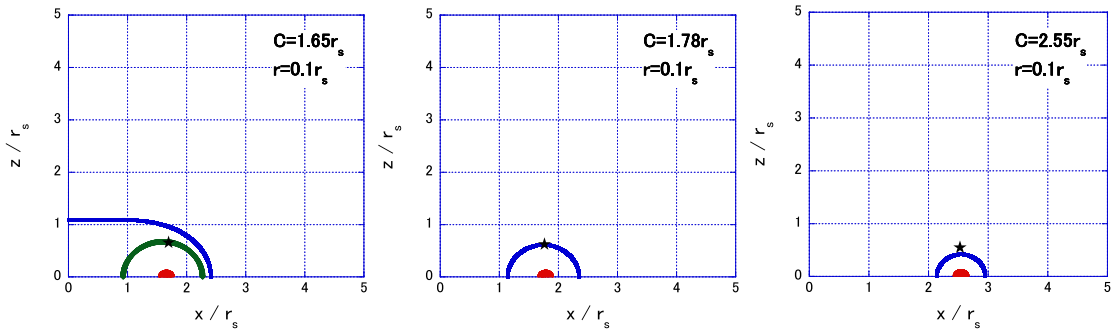

Figure 4: Matter distributions and apparent horizons for toroidal matter distributions.

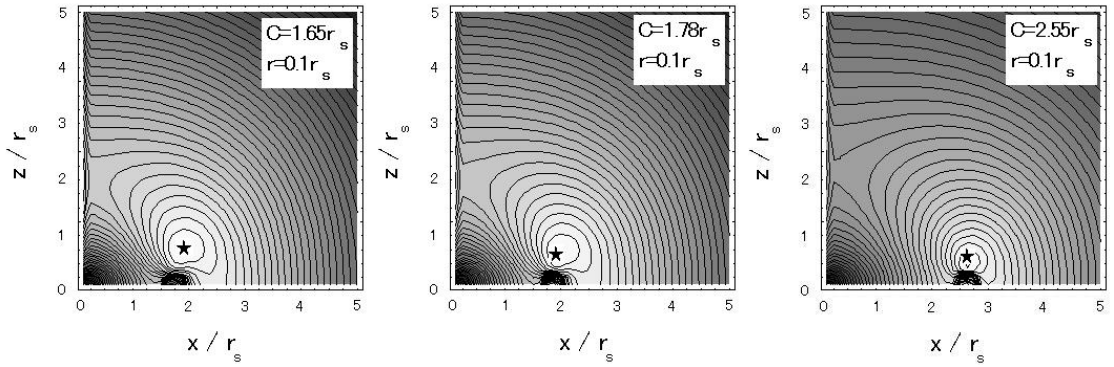

Figure 5: Contours of $I = R_{abcd}R^{abcd}$, corresponding to g.4.

4 Future works

We showed our preliminary results of constructing initial-data in ve-dimensional spacetime. We developed our code for solving the Hamiltonian constraint equation and searching for apparent horizons. Sequences of initial data both for spherical and toroidal matter con gurations are obtained, and we searched when apparent horizons are formed.

We are now examining the validity of the hyper-hoop conjecture, and also preparing the con gurations with rotations. In the future, we plan to report the fully general relativistic dynamical process in ve-dimensional space-time.

References

[1] K. S. Thorne, *Nonspherical gravitational collapse: A short review*, in *Magic Without Magic*, ed. by J. R. Klauder (Freeman, San. Francisco), 231-258 (1972).

[2] S. L. Shapiro and S. A. Teukolsky, Phys. Rev. Lett. 66, 994 (1991).

[3] T. Nakamura, S. L. Shapiro and S. A. Teukolsky, Phys. Rev. D38, 2972 (1988).

[4] D. Ida and K. Nakao, Phys. Rev. D66, 064026(2002)

[5] C. M. Yoo, K. Nakao and D. Ida, Phys. Rev. D71, 104014(2005)